ISSN 1318-0207

Pages 1–266 ■ Year 2017, Vol. 64, No. 1

Slovensko kemijsko društvo
Slovenian Chemical Society

Acta Chimica Slovenica

1

64/2017

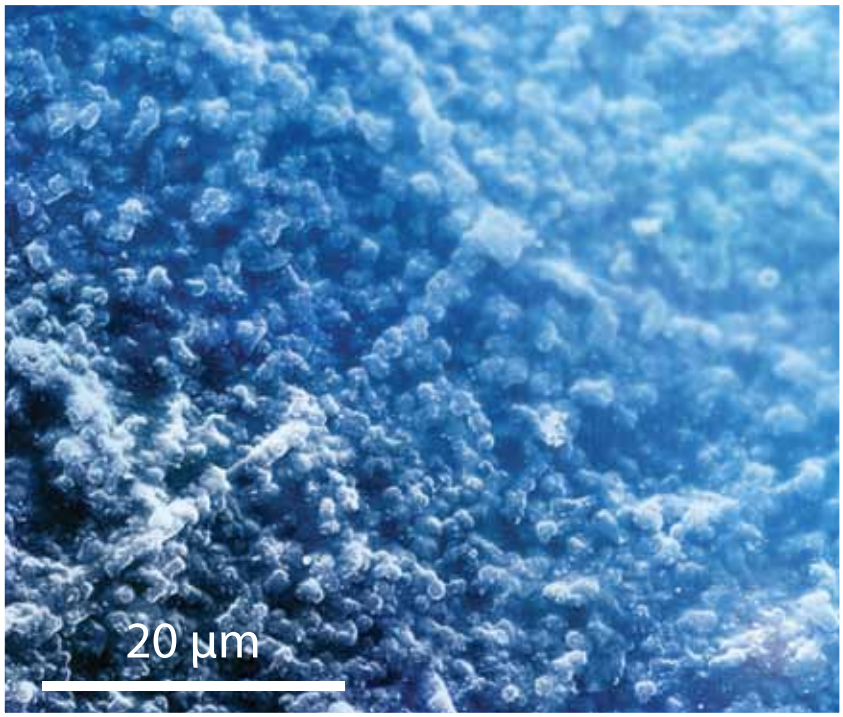

Review: Theoretical Purge Factor Determination as a Control Strategy for Potential Mutagenic Impurities in the Synthesis of Drug Substances ■ The Lock is the Key: Development of Novel Drugs through Receptor Based Combinatorial Chemistry

Scientific papers: Forward Osmosis in Wastewater Treatment Processes ■ Influence of Thermal and Bacterial Pretreatment of Microalgae on Biogas Production in Mesophilic and Thermophilic Conditions ■ Monodispersed Gold Nanoparticles as a Probe for the Detection of Hg^{2+} Ions in Water

http://acta.chem-soc.si

Acta Chimica Slovenica is indexed in: *Chemical Abstracts Plus, Current Contents (Physical, Chemical and Earth Sciences), PubMed, Science Citation Index Expanded* and *Scopus.* Impact factor for 2015 is IF = 1,167.

Izdaja – Published by:
SLOVENSKO KEMIJSKO DRUŠTVO – SLOVENIAN CHEMICAL SOCIETY
Naslov redakcije in uprave – Address of the Editorial Board and Administration
Hajdrihova 19, SI-1000 Ljubljana, Slovenija
Tel.: (+386)-1-476-0252; Fax: (+386)-1-476-0300; E-mail: chem.soc@ki.si

Slovensko kemijsko društvo
Slovenian Chemical Society

Izdajanje sofinancirajo – Financially supported by:
Slovenian Research Agency, Ljubljana, Slovenia
National Institute of Chemistry, Ljubljana, Slovenia
Jožef Stefan Institute, Ljubljana, Slovenia
Faculty of Chemistry and Chemical Technology at University of Ljubljana, Slovenia
Faculty of Chemistry and Chemical Engineering at University of Maribor, Slovenia
Faculty of Pharmacy at University of Ljubljana, Slovenia
University of Nova Gorica, Nova Gorica, Slovenia
Chamber of Commerce and Industry of Slovenia – Chemical and Rubber Industry Association, Slovenia

Članom je revija na voljo brezplačno. Za nečlane in pravne osebe znaša letna naročnina 50 EUR, za inozemstvo 110 EUR vključno s poštnino.
Annual subscription: 110 EUR including postage.

Transakcijski račun: 02053-0013322846
Bank Account No.: SI56020530013322846-Nova Ljubljanska banka d. d., Trg republike 2, SI-1520 Ljubljana, Slovenia, SWIFT Code: LJBA SI 2X

Na podlagi Zakona o davku na dodano vrednost sodi revija Acta Chimica Slovenica med proizvode, od katerih se obračunava DDV po stopnji 9,5 %.

Acta Chimica Slovenica izhaja štirikrat letno v 200 izvodih – Acta Chimica Slovenica appears quarterly in 200 copies

Oblikovanje ovitka – Design cover: KULT, oblikovalski studio, Simon KAJTNA, s. p. Grafična priprava za tisk: Majanafin, d. o. o. Tisk – Printed by: Tiskarna Skušek, Ljubljana

Graphical Contents

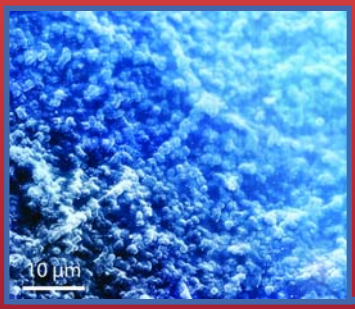

Acta Chimica Slovenica

Year 2017, Vol. 64, No. 1

REVIEW

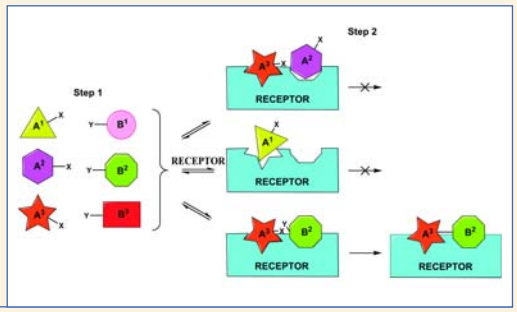

SCIENTIFIC PAPER

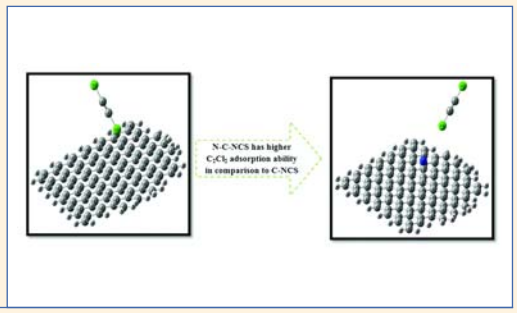

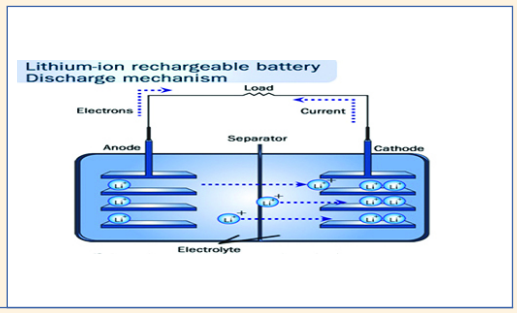

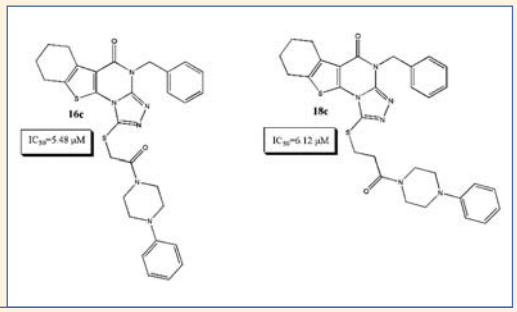

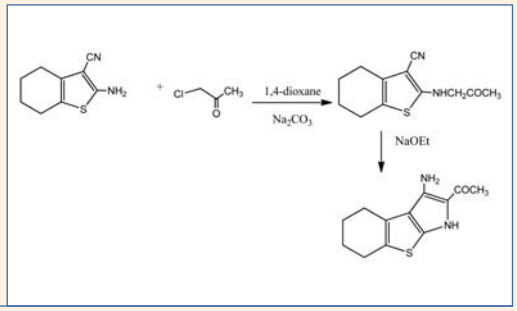

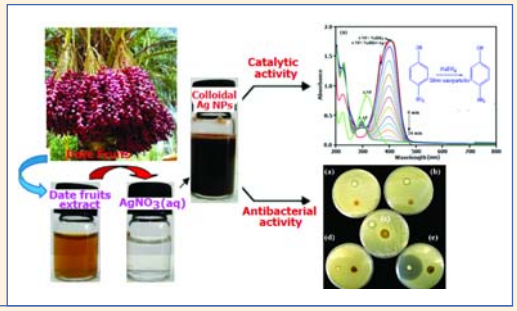

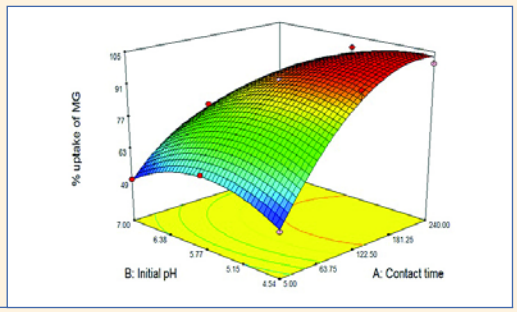

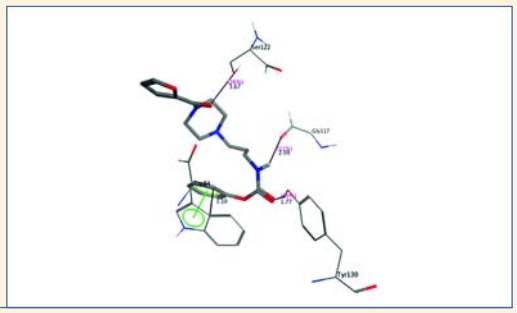

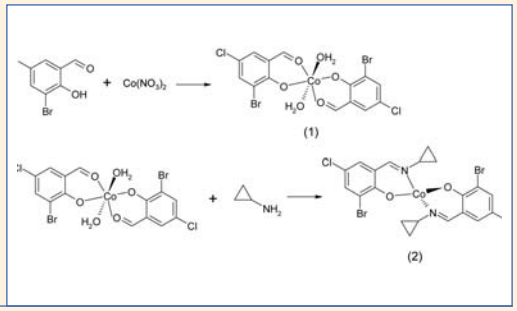

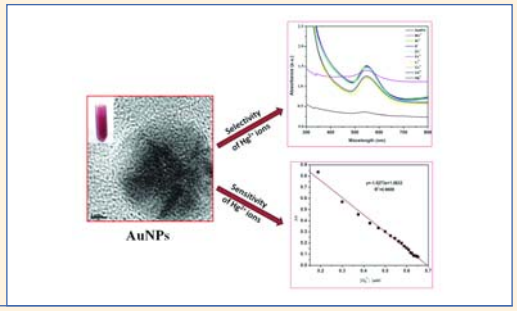

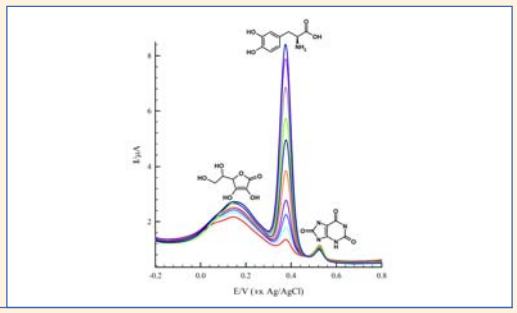

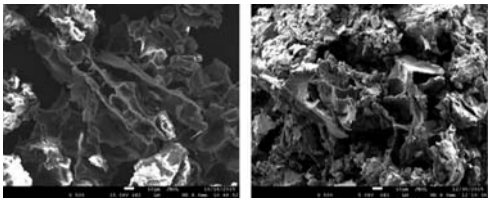

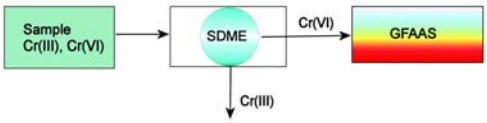

SHORT COMMUNICATION

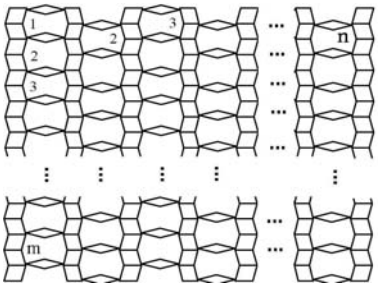

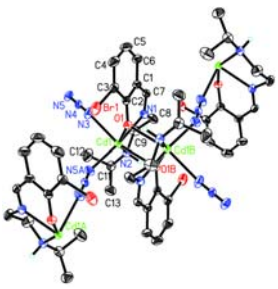

Review

Theoretical Purge Factor Determination as a Control Strategy for Potential Mutagenic Impurities in the Synthesis of Drug Substances

Nevenka Kragelj Lapanja,[1,*] Renata Toplak Časar,[1] Sabina Jurca[1] and Bojan Doljak[2]

[1] *Lek Pharmaceuticals d.d., Verovškova 57, 1526 Ljubljana, Slovenia*

[2] *Faculty of Pharmacy, Aškerčeva 7, 1000 Ljubljana, Slovenia*

* *Corresponding author: E-mail: nevenka.lapanja@sandoz.com*
Tel: +386 1 5803443

Received: 24-08-2016

Abstract

Mutagenic impurities (MIs) are of serious concern for pharmaceutical industry, regulatory agencies and public health. The first guideline addressing the control of genotoxic impurities (GTIs) dates back to 2006. Since then there have been several updates and refinements, which eventually resulted in the guideline, published by the International Conference on Harmonisation (ICH) in June 2014. The ICH M7 guideline, compared to previous ones, offers greater flexibility in terms of control strategies for GTIs in drug substances. More specifically, it describes a control strategy that relies on process controls *in lieu* of analytical testing which is based on understanding the process chemistry and process parameters that impact the levels of GTIs. This principle is adopted in the theoretical purge factor determination tool proposed by Teasdale et al. Several case studies applying the proposed theoretical purge factor determination tool were published in recent years. The results confirm the tool's good predictability of the extent to which the impurity is removed by the process. Hopefully, this approach will soon be released as an *in-silico* tool, generally accepted by the regulatory agencies.

Keywords: Drug substance, mutagenic impurity, purge factors

1. Introduction

The need to investigate the potential genotoxicity of drugs resulted from several incidents in the past and is nowadays a serious matter of concern for pharmaceutical industry. According to the definition given in the International Conference on Harmonisation (ICH) M7 guideline,[1] *genotoxicity* refers to any deleterious change in the genetic material regardless of the mechanism by which the change is induced, whereas the term *mutagen* refers to a substance that induces mutation which is a heritable change in cells or organisms.[2] It should be stressed that not all DNA damage results in mutation. However, many mutagens have the ability to induce cancer since there is a strong correlation between mutagenicity and carcinogenicity.[2] Without a doubt, mutagenicity and consequently potential carcinogenicity are strongly undesirable in relation to the use of medicines. However, in some cases, e.g., for treating life-threatening conditions, the use of drugs with higher risk may be acceptable. While a safe medicinal product is one with acceptable risk/benefit ratio, the same is not true for impurities found in drug substances and drug products; as impurities convey only risk with no associated benefit. Genotoxic impurities (GTIs) in drug substances are mainly the consequence of using electrophilic reagents for building up the molecular structure. If they don't react completely, they can persist in the reaction mixture and may be carried onward in the synthesis. Due to their high reactivity they can also react with the DNA and potentially induce genetic mutations. For this reason regulatory agencies established standards which assure that unavoidable impurities are limited to have no or acceptable levels of risk.[3] Identification and control of potential mutagenic/genotoxic impurities in drug substances or drug products is still a challenging task for pharmaceutical companies. Hence, an overview of regulatory guide-

lines will be presented in this review article, together with identification and control strategies, especially the theoretical purge factor determination approach and its practical application.

2. Historical Background

As already mentioned in the introduction, the risk related to the potential presence of GTIs emerged from various events in the past. In 2000 a first article regarding GTIs' related concern was published, i.e. an enquiry by the European Directorate for the Quality of Medicines and Healthcare (EDQM) on alkyl mesylate impurities in mesylate salts.[4] This publication was the first that revealed the potential risk of formation of sulfonate esters during a salt formation process with sulfonic acids in alcoholic solutions and it is now considered as a milestone indicating a beginning of genotoxicity risk awareness.[4,5] Two years later, in December 2002, the Committee for Proprietary Medicinal Products (CPMP) which was later renamed to Committee for Human Medicinal Products (CHMP), published a position paper on the limits of GTIs.[6] The position paper was, after being significantly revised, released as a draft guideline in June 2004.[7] The awareness of genotoxic risk was significantly increased by the prominent incident of Viracept® in 2007. In June of that year excess levels of ethyl methane sulfonate (EMS) were detected in the nelfinavir mesylate active substance, manufactured by Roche Registration Ltd. EMS is a process-related impurity that was formed during manufacture of Viracept due to an inadvertent reaction between methane sulfonic acid used in the active pharmaceutical ingredient (API) salt formation and the solvent ethanol which was used to clean the acid storage tank. Since EMS is a potential human carcinogen, Roche had to recall the product from the European Union markets immediately.[8]

3. Regulatory Guidelines

3. 1. EMA Guideline on the Limits of Genotoxic Impurities

The first guideline that addressed the control of GTIs in marketing applications for pharmaceuticals was the European Medicines Agency (EMA, formerly EMEA) guideline,[9] finalized in 2006 (draft published in June 2004). Before its implementation, the issue of impurities with genotoxic potential was not specifically covered by the existing guidelines for qualification of impurities (ICH Q3A (R2)[10]/Q3B(R2)[11]/Q3C (R5)[12]/Q3D[13]). In the context of the EMA guideline,[9] the term *genotoxic impurity* refers to positive findings in established *in vitro* or *in vivo* genotoxicity tests with the main focus on DNA reactive substances. GTIs may be classified as those with sufficient or those without sufficient (experimental) evidence for a threshold-related mechanism of genotoxicity. For compounds with clear evidence for threshold genotoxicity, exposure levels that are without considerable risk of genotoxicity can be established based on calculation of a permitted daily exposure (PDE), which is derived from the no-observed-effect level (NOEL), or the lowest-observed-effect level (LOEL) in the most relevant animal study using uncertainty factors. For compounds without sufficient evidence for threshold-related mechanism the as low as reasonably practicable' (ALARP) principle should be followed, where avoiding is not possible. However, it is often impossible to define a safe exposure level for genotoxic carcinogens without a threshold or completely eliminate GTIs from the drug substance. This has led to the need of a pragmatic approach that would recognize an acceptable risk exposure level. For this purpose a threshold of toxicological concern (TTC) has been developed. A TTC value of 1.5 μg/person/day, corresponding to a 10^{-5} lifetime risk of cancer, defines a common exposure level for any unstudied chemical that will not pose a risk of significant carcinogenicity or other toxic effects.[14,15] The limit was set based on the analysis of 343 carcinogens,[16] expanded to more than 700 carcinogens from a carcinogenic potency database.[17–19] A simple linear extrapolation from 50 % tumor incidence (TD50) data for the most sensitive species and most sensitive site to a 1 in 10^6 incidence was used, which makes the principle very conservative.[14] Some high potency genotoxic carcinogens like aflatoxin-like-, N- nitroso-, and azoxy- compounds have to be excluded from the TTC approach.[19] Compound-specific toxicity data is needed for the risk assessment of such compounds. A TTC value higher than 1.5 μg/day may be acceptable for short term-exposure drugs, for treatment of life-threatening conditions, when life expectancy is less than 5 years, or where the impurity is a known substance and human exposure will be much greater from other sources, e.g. food. For the calculation of concentration limits in ppm of genotoxic impurity in drug substance the following equation is used, where dose applies to expected daily dose to the patient:

$$\text{concentration limit (ppm)} = \frac{\text{TTC [μg/day]}}{\text{dose[g/day]}} \quad (1)$$

The guideline on the limits of GTIs [9] left certain concerns unaddressed. Besides that, industry struggled to fully understand how to interpret and apply it in its entirety.[5] For this reason significant clarifications of several key topics have been issued in the Question and Answers (Q&A) on the 'Guideline on the limits of genotoxic impurities',[20] published by the Safety Working Party (SWP) in September 2010. The Q&A document clarified that no genotoxicity testing or the ALARP principle application is needed when a potential GTI is controlled at the TTC level unless the impurity belongs to a class of very potent

genotoxic carcinogens, e.g., N-nitroso-, aflatoxin-like- and azoxy- compounds. It was also clarified that a negative bacterial mutagenicity test (Ames test) overrules a structural alert which means that no further studies are required providing the level remains below ICH Q3A[10]/Q3B[11] limits. If the quantitative structure-activity relationship (QSAR) assessment gives no structural alerts it can be concluded that the impurity has no genotoxicity concern and no further qualification studies or justification will be required. It has also been clarified and confirmed that durational adjustments to the TTC limit are acceptable for investigational studies. The proposal of a staged TTC was first described by the Pharmaceutical Research and Manufacturers of America (PhRMA) cross-industry workgroup led by Mueller et al.[21] However, the SWP incorporated a dose rate correction factor of 2 to account for deviations from the linear extrapolation model which gives slightly different values than those from the original PhRMA proposal. The acceptable limits for daily intake of GTI according to the SWP are 5, 10, 20 and 60 µg/day for duration of exposure of 6–12 months, 3–6 months, 1–3 months, and less than 1 month, respectively. For a single dose an intake of up to 120 µg is acceptable. With regards to the control of multiple GTIs, SWP stated that the TTC value of 1.5 µg/day can be applied to each individual impurity present in the drug substance only if the impurities are structurally unrelated. This is based on the assumption that the impurities act by the same genotoxic mode of action and have the same molecular target and thus might exert its effect in an additive manner. A limitation of the sum of the GTIs at 1.5 µg/day is recommended in such cases. The SWP document states that if a GTI is formed or introduced in a step before the final synthetic step, it is acceptable to not include the impurity in the drug substance specification if it is controlled to a suitable limit in a process intermediate. However, it has to be demonstrated by analysis results that the presence of this impurity does not exceed 30 % of the acceptable limit in the drug substance, otherwise it has to be included in the drug substance specification and the test has to be carried out on a routine basis. When a GTI is formed or introduced in the final synthesis step, it should be included in the specifications. However, skip testing can be applied if the level of the impurity does not exceed 30% of the acceptable limit in the drug substance. Data for at least 6 consecutive pilot scale or 3 consecutive production scale batches should be presented to support this approach.

3. 2. FDA Draft Guidance: Genotoxic and Carcinogenic Impurities in Drug Substances and Products: Recommended Approaches

In December 2008, the Food and drug administration (FDA) published their draft guidance addressing the issue of GTIs.[22] The guidance contained nonbinding recommendations to the pharmaceutical industry and never reached its finalization. FDA considers the approach taken in the EMA guideline[9] for setting an exposure limit for genotoxic or carcinogenic impurities reasonable. However, the EMA guideline addresses the exposure limits only to products for marketing applications. Therefore, the FDA draft guidance provides recommendations on evaluation and acceptable exposure thresholds of genotoxic and carcinogenic impurities during clinical development as well as for marketing applications. According to the guidance, the potential lifetime cancer risk associated with genotoxic and carcinogenic impurities can be reduced by changing the synthetic and/or purification route to minimize the formation and/or maximize the removal of the impurity of concern. Following the EMA guideline,[9] a maximum daily exposure of 1.5 µg/day was proposed, allowing higher levels for products during clinical development.[22]

3. 3. ICH M7 Guideline: Assessment and Control of DNA Reactive (Mutagenic) Impurities in Pharmaceuticals to Limit Potential Carcinogenic Risk

In June 2014 the ICH M7 guideline: Assessment and control of DNA reactive (mutagenic) impurities in pharmaceuticals to limit potential carcinogenic risk[1] reached Step 4 of the ICH process, meaning that the final draft became recommended for adoption to the three regulatory bodies of the ICH: European Union, Japan and USA. Implementation of ICH M7 was encouraged after publication; however, its application was not expected prior to 18 months after the publication. The purpose of the ICH M7 guideline is to provide a practical framework that is applicable to the identification, categorization, qualification, and control of mutagenic impurities (MIs) to limit potential carcinogenic risk. It applies to new drug substances and new drug products during their clinical development and subsequent applications for marketing. It also applies to post-approval submissions of marketed products, and to new marketing applications for products with a drug substance that is present in an already approved product. This is only valid when (1) changes that result in new impurities are made or (2) increased limits for existing impurities are implemented or (3) when changes in indication or dosing regimen are made which significantly affect the acceptable cancer risk level. As previously already proposed by the EMA[9] and FDA guideline,[22] the ICH M7 also finds it justified to use the TTC approach in the assessment of acceptable limits for any unstudied chemical. Higher acceptable intakes of impurities for less-than-lifetime (LTL) exposures are also allowed. Moreover, it is stressed that the TTC concept is a highly hypothetical concept that should not be regarded as a realistic indication of the actual risk and that exceeding the

TTC is not necessarily associated with an increased cancer risk. The impurity assessment according to the ICH M7 should include all actual and potential impurities that are likely to arise during the synthesis and storage of a drug substance, and during manufacturing and storage of a drug product. All these should then be evaluated for mutagenic potential by conducting database and literature searches for carcinogenicity and bacterial mutagenicity data. Based on the obtained data the impurities are classified as one of the following classes:

Class 1: Impurities that are known mutagenic carcinogens.

Class 2: Impurities that are known mutagens with unknown carcinogenic potential.

Class 3: Impurities with alerting structure, unrelated to the structure of the drug substance; no mutagenicity data.

Class 4: Impurities with alerting structure, same alert in drug substance or compounds related to the drug substance which have been tested and are non-mutagenic.

Class 5: Impurities with no structural alerts, or alerting structure with sufficient data to demonstrate lack of mutagenicity or carcinogenicity.

If data for carcinogenicity and bacterial mutagenicity are not available, a (Q)SAR assessment that focuses on bacterial mutagenicity predictions should be performed. Two (Q)SAR computational methodologies that complement each other are required according to the ICH M7. One methodology should be expert rule-based and the second one should be statistical-based. If none of the methods give structural alerts, it is sufficient to conclude that the impurity is non-mutagenic (Class 5). In case of an identified structural alert, a bacterial mutagenicity assay, e.g., Ames test, can be conducted. Negative result will overrule any structural alert, meaning that no further genotoxicity assessment is needed (Class 5). In case of positive bacterial mutagenicity assay, a further assessment and/or control strategy is needed (Class 2). *In vivo* genotoxicity assays could also be performed, for example when levels of the impurity cannot be controlled at an acceptable limit and the relevance of the bacterial mutagenicity under *in vivo* conditions needs to be understood. If an impurity has the same structural alert as the drug substance or related compounds, this impurity can be considered as non-mutagenic if the bacterial mutagenicity assays of the drug substance or related compounds were negative. For class 1 impurities with positive carcinogenicity data a compound-specific acceptable intake calculated based on carcinogenic potency and linear extrapolation can be used. Other established risk assessment practices or already existing values used by regulatory bodies may also be applied. For impurities which are chemically similar to a known carcinogen compound class, class specific acceptable intakes can be applied when justified. For MIs with non-linear dose response or practical threshold a PDE can be calculated based on NOEL and uncertainty factors. When treatment duration is less than lifetime, the acceptable cumulative lifetime dose is uniformly distributed over the total number of exposure days during treatment. Acceptable intakes for LTL to lifetime exposures for clinical development and marketing are presented in Table 1. The TTC-based acceptable intakes should be applied to each individual impurity. However, when there are three or more Class 2 or Class 3 impurities present in the drug substance, total mutagenic impurities should be limited as presented in the Table 1. Class 1 impurities with compound-specific or class-related acceptable intakes limits should be excluded from this total limits. Degradation impurities originating from drug products also need to be controlled individually.

Table 1. Acceptable intakes for less-than-lifetime (LTL) to lifetime exposures for a) an individual impurity and b) for multiple impurities (based on ICH M7[1])

Treatment duration	Maximum daily dose [µg/day]	
	a)	b)
≤ 1 month	120	120
> 1–12 months	20	60
> 1–10 years	10	30
> 10 years to lifetime	1.5 (TTC limit)	5

Besides the described acceptable intakes ICH M7 also lists some exceptions and flexibilities in approaches, e.g., higher acceptable intakes for impurities which are more abundant in other sources e.g., food, or products of endogenous metabolism (e.g., formaldehyde), than in pharmaceuticals. Exceptions can also be made in cases of severe disease, reduced life expectancy, late onset but chronic disease, or when there are limited therapeutic alternatives. Impurities with high carcinogenic potency (aflatoxin-like, N-nitroso, and alkyl-azoxy structures) need to be controlled with tighter limits, based on carcinogenicity data. For classes 2 and 3 the TTC approach would usually be used. When an impurity has been identified as Class 1, 2 or 3, a control strategy needs to be developed; assuring that the level of this impurity in the drug substance and drug product is below the acceptable limit. ICH M7 lists 4 potential approaches for development of a control strategy for drug substance:

Option 1: Test for the MI is included in the drug substance specification. Acceptance criterion is set at or below the acceptable limit using a suitable analytical method. When it can be shown that levels of the impurity in at least 6 consecutive pilot scale or 3 consecutive production scale batches of drug substance are less than 30 % of the acceptable limit, it is justified to apply periodic verification testing.

Option 2: Test for the MI is included in the specification for raw material, starting material or intermediate, or as an in-process control. Acceptance criterion is set at or below the acceptable limit using a suitable analytical method.

Option 3: Test for the MI is included in the specification for raw material, starting material or intermediate, or as an in-process control. Acceptance criterion is set

above the acceptable limit of the impurity in drug substance, using a suitable analytical method coupled with demonstrated understanding of fate and purge and associated process controls that assure the level in the drug substance is below the acceptable limit without the need for any additional testing later in the process. Option 3 can be justified when the level of the impurity will be less than 30 % of the acceptable limit by review of laboratory scale experiments data (e.g., spiking studies).

Option 4: The MI does not need to be included on any specification when it can be demonstrated that the level of the impurity in the drug substance will be below the acceptable limit such that no analytical testing is required. Option 4 control strategy relies on understanding process chemistry and process parameters and their impact on residual impurity levels, including fate and purge knowledge. According to the ICH M7, justification of this control approach based on scientific principles alone is sufficient

Table 2: A brief history of development of GTIs guidelines (based on Teasdale[5] and Szekely et al.[24]).

Year	Issue	Key points
March 1995	ICH Q3A: Impurities in New Drug substances	The term 'unusually toxic' is used to address GTIs.
2000	PharmEuropa Enquiry: Alkyl mesylate (methane sulfonate) impurities in mesylate salts	The first article regarding the GTIs related concern published (potential risk of formation of sulfonate esters during a salt formation process).
December 2002	CPMP: Position paper on the limits of genotoxic impurities	Wherever possible, alternative routes that avoid GTIs should be used. Otherwise they should be reduced to 'as low as technically feasible' level. Safety tests, including *in vivo* studies are required to determine a NOEL or to carry out a quantitative risk assessment.
June 2004	CHMP: Guidelines on the limits of genotoxic impurities – Draft	'As low as technically feasible' terminology is replaced with the ALARP (As low as reasonably practical) principle. Requirement to introduce an alternative route is omitted. The need to provide justification of selected route remains. TTC concept is introduced.
January 2006	PhRMA (Mueller) White paper	A 'staged TTC' approach is introduced. A classification system, defining five separate classess of impurities, is defined.
June 2006	CHMP: Guidelines on the limits of genotoxic impurities – Finalized	The note that the guideline doesn't need to be applied retrospectively to authorised products unless there is specific cause for concern is added. Excipients are excluded from the finalized guideline.
December 2008	FDA draft guidance: Genotoxic and carcinogenic impurities in drug substances and products: recommended approaches	It is suggested to introduce lower limits for different patient populations (e.g. pediatric). Genotoxicity testing should be performed for any impurity above the ICH qualification threshold. Different staged TTC values for short term studies are proposed.
September 2010	SWP: Questions and Answers on the CHMP Guideline on the limits of genotoxic impurities	Durational adjustments to the TTC limit are acceptable for investigational studies. A 'cause of concern' terminology is explained. If a substance is controlled to an appropriate safety based limit, then no further actions are required.
June 2014	ICH M7: Assessment and control of DNA reactive (mutagenic) impurities in pharmaceuticals to limit potential carcinogenic risk	Two (Q)SAR computational methodologies that complement each other are required (one expert rule-based and the second one statistical-based). Four potential approaches to development of a control strategy for drug substance are proposed, including a control strategy that relies on understanding process chemistry and process parameters and their impact on residual impurity levels, including fate and purge knowledge.
June 2015	ICH M7 Addendum: Application of the principles of the ICH M7 guideline to calculation of compound-specific acceptable intake	Acceptable intakes have been derived for substances that are considered to be mutagens and carcinogens and are commonly used in the manufacture of drug substances.

in many cases. The scientific risk assessment used to justify this approach can be based on physicochemical properties and process factors that influence the fate and purge of an impurity. This includes chemical reactivity, solubility, volatility, ionizability and any physical process steps designed to remove impurities. The result of this risk assessment can be shown as an estimated purge factor for clearance of the impurity by the process. When justification based on scientific principles alone is not considered sufficient, analytical data to support the control approach is expected. If option 4 approach (and also option 3 approach) cannot be justified, a test for the impurity should be included on the specification of a drug substance, raw material, starting material, intermediate, or as an in-process control.

ICH M7 guideline also clarifies that the application of ALARP principle is not necessary if the level of the MI is below acceptable limits. It is also not necessary to demonstrate that alternative routes of synthesis have been explored which was required by EMA guideline[9] before the implementation of ICH M7.

ICH M7 guideline addresses many issues that were left unclear in the previous guidelines. The guideline is still very complex and its application in the pharmaceutical industry and regulatory agencies is quite challenging. To complement the harmonized guideline finalized in June 2014, an Addendum to ICH M7 was proposed in June 2015 (Step 2): Application of the principles of the ICH M7 guideline to calculation of compound-specific acceptable intakes.[23] The purpose of this document is to provide useful information regarding the acceptable limits of known mutagenic/carcinogenic impurities commonly found or used in drug synthesis and supporting monographs. The development of the guidelines toward the ICH M7 publication is presented in Table 2.

Pharmaceutical industry can apply different approaches to mitigate the risk of GTIs in the synthesis of APIs. While the preferred approach (especially augmented by the regulatory agencies in early guidelines) is to avoid the use of genotoxic synthetic pathways by modifying the existing synthetic routes, this is not always possible since the use of highly reactive reagents is often required for the production of APIs.[25] Therefore, a strategy based on elimination or reduction of GTI can be applied. This can be achieved by adjusting the process conditions (i.e., reaction time, pH, temperature, solvent matrix etc.). Furthermore, a Quality by Design (QbD) approach can also be applied to control GTI formation.[26]

Many purification steps (i.e. crystallization, solvent liquid-liquid extraction, precipitation, distillation, column chromatography, etc.) have the ability to remove GTIs along with other process impurities. Purging of impurities was previously addressed by Pierson et al.[27] The risk of GTI carry over was defined considering the number of synthetic steps between the point of GTI appearance and final production step. If the GTI appears more than four steps before the final step, chemical rationale could be used to assess the need of GTI removal. The purging approach was later upgraded as it will be presented in the following section.

4. Theoretical Purge Factor Determination Approach

Since publishing the guidelines covering the control of GTIs, regulatory authorities have requested evidence that any GTI is controlled in line with the acceptable limits. For this reason pharmaceutical companies had to present extensive analytical data. To avoid unnecessary analytical testing, Teasdale et al.[28] took the challenge to develop an approach that would allow the likelihood of potential carryover of a GTI to be assessed ahead of performing analyses. In line with the ICH M7

Table 3. Physicochemical parameters and associated purge factors (adapted from Teasdale et al.[8])

Physicochemical parameter	Purge factors 100	10	3	1
reactivity	highly reactive	moderately reactive	–	low reactivity/unreactive
solubility	–	freely soluble	moderately soluble	sparingly soluble
volatility	–	boiling point > 20 °C below that of the reaction/process solvent	boiling point ± 10 °C that of the reaction/process solvent	boiling point > 20 °C above that of the reaction/ process solvent
ionizability	ionization potential of GTI significantly different from that of the desired product (a specific purge factor is assigned where such an approach is specifically applied)			
physical processes – chromatography	GTI elutes prior to desired product	GTI elutes after desired product	–	–
physical processes – recrystallization*	freely soluble			sparingly soluble

* In the original approach the recrystallization process was described within the solubility term; however, based on the under-prediction of the purge factor tool in case of crystallization steps, it was proposed to describe it as an individual physical process with a scale from 1 to 100.[29]

option 4 control strategy, the scientific approach proposed by Teasdale[28] is based on physicochemical properties and process factors that influence the fate and purge of an impurity. In order to assess the carryover of potential GTIs into API, AstraZeneca developed a tool based on the assessment of key physicochemical properties of the agent of concern, relating them to the downstream processing conditions. A score is assigned for each of them to establish a 'purge factor'. The approach has been applied to various processes with available data. In order to assess the potential carry-over of a GTI, the following parameters are defined: reactivity, solubility, volatility, ionizability, and any physical process designed to remove impurities (e.g., chromatography). For each of the parameter a score is assigned as presented in Table 3. The scores are then multiplied together to give a purge factor for each stage of the process. Multiplying the purge factors for individual stages yields an overall purge factor. Teasdale et al.[28] provided a case study, presenting both the outcome of the predictive purge factor and the real measured values. Theoretical purge factors were calculated for three potentially genotoxic impurities in the synthesis of AZD9056 (Scheme 1). Experimental purge factors were also determined for each of them by tracking the residual levels of impurities at successive stages. Results are summarized in Table 4.

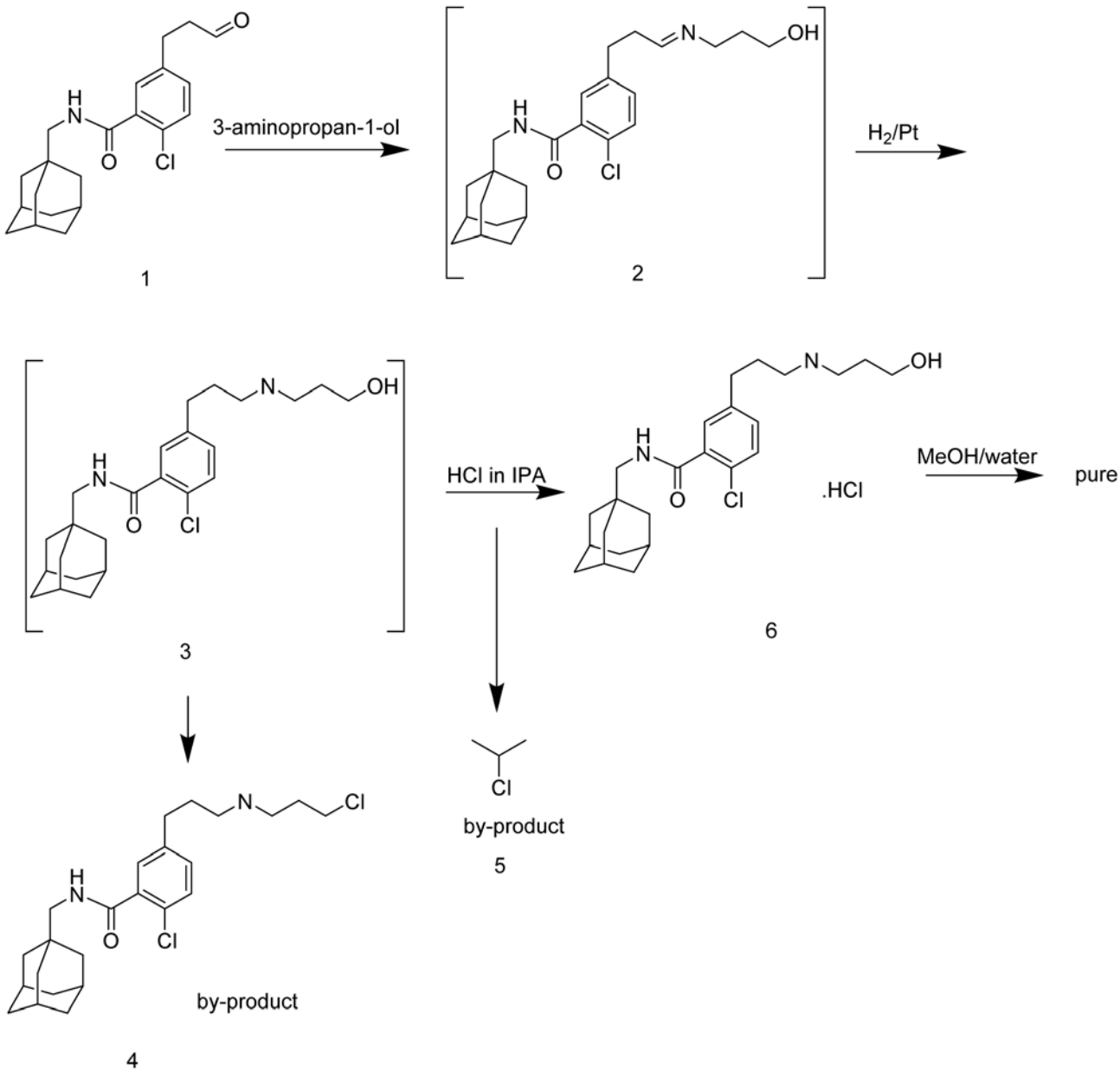

Scheme 1: Synthesis of AZD9056 (adapted from Teasdale et al.[28]).

Authors also noted that in the case of the impurity 1, the predicted purge factor in the isolated crude stage differed significantly from the experimental purge factor (10 versus 560, respectively). Based on this it could be argued that the scale for the solubility factor could be extended to 1–100 instead of 1-10. However, authors decided to retain the more conservative scale of 1–10 in order to compensate for any variance in processes such as uncontrolled crystallization, poor washing and/or inefficient deliquoring of the isolated product. Moreover, underprediction of the purge capacity of the process is preferable to an overprediction.

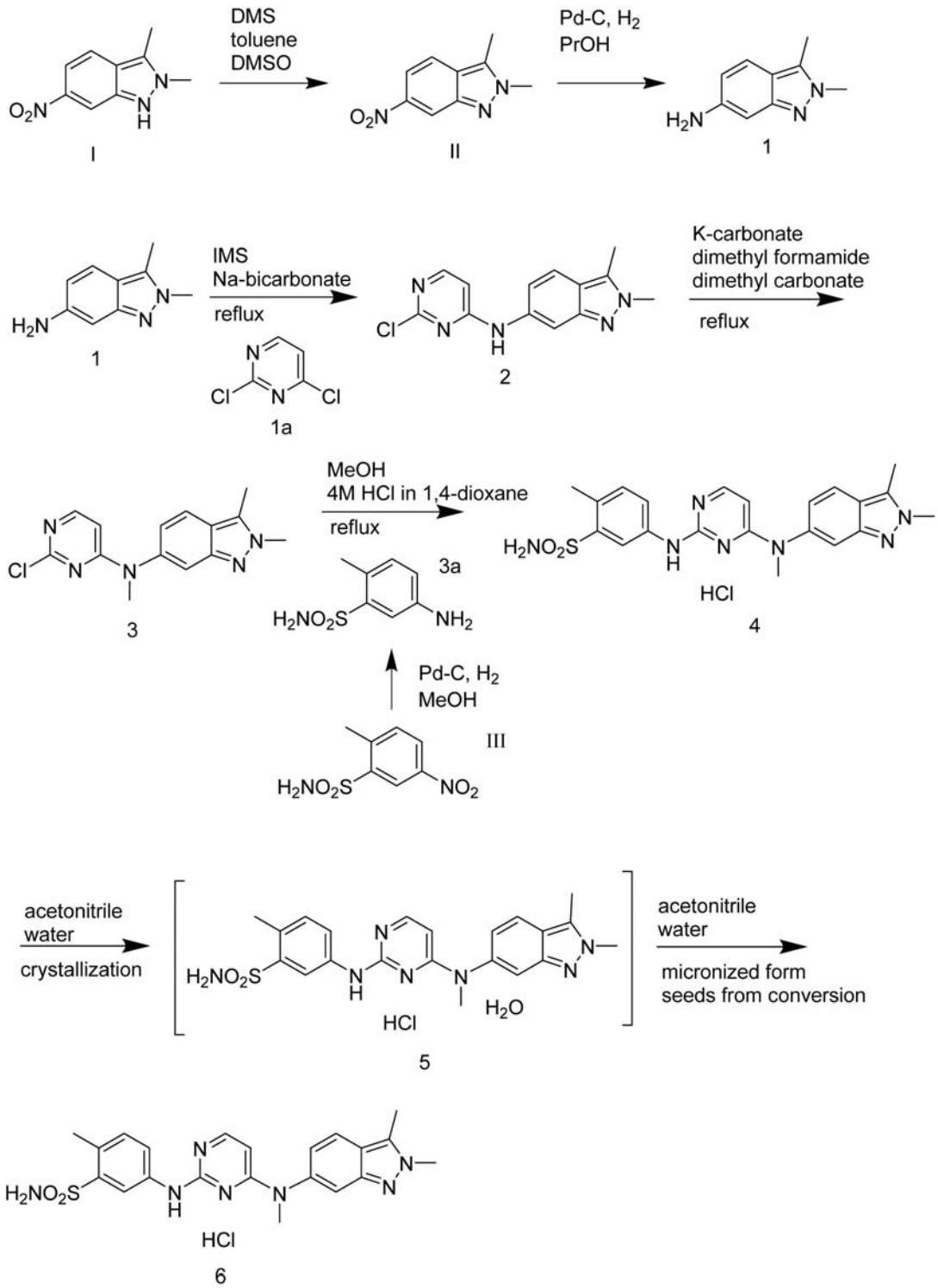

Scheme 2: Synthesis of pazopanib hydrochloride (adapted from Elder et al.[31]).

Table 4. Summarized results of the case study for the synthesis of AZD9056 (based on Teasdale et al.[28]).

Impurity of concern	Theoretical purge factor	Experimental purge factor	Interpretation of the results
Impurity 1 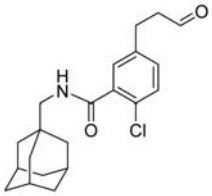	10 000	112 000	The calculated purge factor underpredicts the purge capacity of the process by a factor of 10. Even a conservatively calculated purge factors predicts that the risk of carryover of significant levels of this impurity into the API is low.
Impurity 4 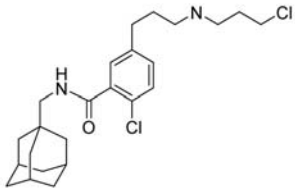	3	10	The calculated purge factor of 3 accurately predicts that the process has limited capacity of effectively removing this impurity.
Impurity 5 	10 000	38 500	The calculated purge factor accurately predicts the efficient removal of the impurity by the process.

Table 5. Summarized results of the case study for the synthesis of pazopanib hydrochloride (based on Elder et al.[31]).

Impurity of concern	Theoretical purge factor	Experimental purge factor	Interpretation of the results
DMS 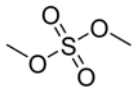	30 000	29 411	The tool very accurately predicts the purging capacity for DMS.
Impurity II 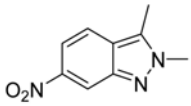	8 100	30 044	The calculated purge factor underpredicts the purge capacity of the process by a factor of 3.
Impurity 1 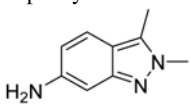	2 700	7 700	The calculated purge factor and experimental purge factor agree reasonably well.
Impurity 3 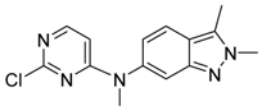	9	52-174	Theoretical and experimental purge factor are in reasonable agreement, however a control strategy needs to be implemented due to a low factor.
Impurity III 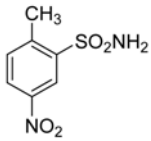	900	17 647	The calculated purge factor underpredicts the purge capacity of the process by a factor of 20.

In 2013 Teasdale et al.[30] published further and more detailed information about the determination of theoretical purge factors, alongside various case studies. Instructions are given on how to assign values for different physicochemical parameters, how to calculate the factors and how to evaluate the results.

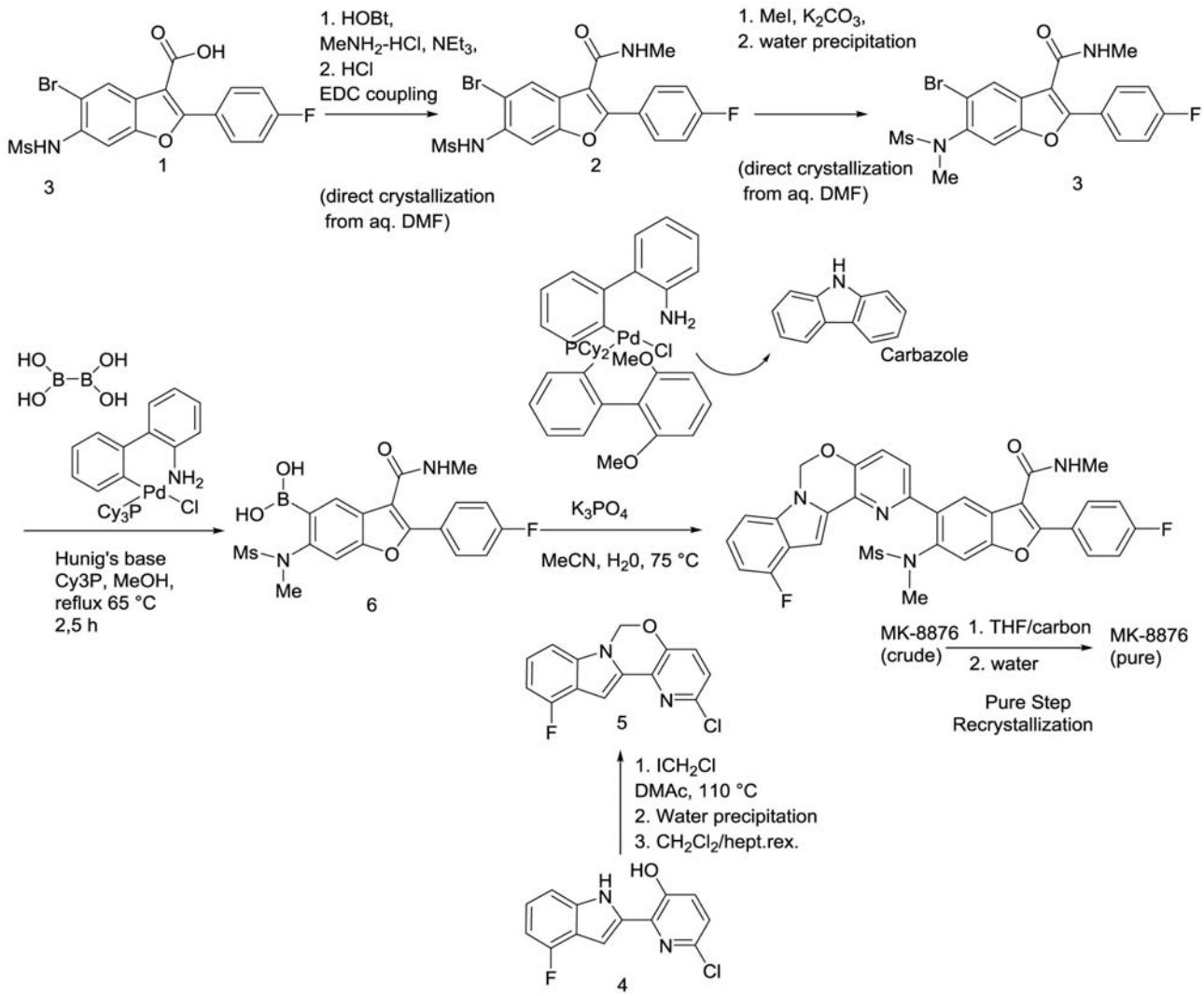

Scheme 3: Synthesis of MK-8876 (adapted from McLaughlin et al.[33]).

Another case study was described by Elder et al.[31] in 2013, using the same approach to assess the ability to purge impurities in the synthesis of pazopanib hydrochloride (Scheme 2). The theoretical purge factor assessment tool was applied to five mutagenic impurities (Table 5). The measured purge factor for each of the MI has been previously determined,[32] therefore the authors were able to compare theoretical and experimental purge factors in order to assess the reliability of the proposed tool. Compared to the original approach, Elder et al.[31] decided to include isolation steps within the physical process parameter, whereas a factor 3 was used if the isolation step was present and 1 if not. According to their results the tool very accurately predicted the purging capacity for the most reactive MIs. For less reactive MIs, measured and predicted values agreed reasonably well.

In 2015 two additional practical applications of the proposed tool were published, i.e. by McLaughlin et al.[33] and by Lapanja et al.[29] McLaughlin et al.[33] applied purge factor assessment tool to six MIs in the synthesis of a development compound MK-8876 (Scheme 3). Theoretical purge factors were compared with the analytically determined purge factors. Results are summarized in Table 6. It was emphasized that the proposed tool tends to underpredict the likely purge capacity of a process, thus staying on the safe / more conservative side.

Lapanja et al.[29] also used the same approach for assessing the presence of four potential MIs in the vortioxetine synthetic process (Scheme 4). Additionally, one minor modification regarding the physical process parameter was proposed, i.e. a recrystallization step was included within the physical process parameter, while according to Teasdale et al.[28] recrystallization would be described within the solubility parameter. The theoretical purge factors were then compared with measured values and with the results of depletion studies. Results are summarized in Table 7. In conclusion it was noted that by assigning a va-

Table 6. Summarized results of the case study for the synthesis of MK-8876 (based on McLaughlin et al.[33]).

Impurity of concern	Theoretical purge factor	Experimental purge factor	Interpretation of the results
EDC 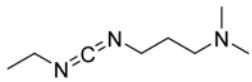	1[10]	> 50 000	The tool very accurately predicted the purging capacity for EDC.
methyl iodide 	1 000 000	100 000	The calculated purge factor overrpredicts the purge capacity of the process by a factor of 10. However, theoretical purge factor is in agreement with the actual analytical value of < 10 ppm of methyl iodide at intermediate stage.
Chloroiodomethane 	10 000 (crude) 100 000 (pure)	20 000 (crude) > 200 000 (pure)	The calculated purge factor and experimental purge factors agree reasonably well.
Arylboronic acid	10 000 (crude) 30 000 (pure)	143 000 (crude) > 1 000 000 (pure)	Measured purge factors at the crude API stage and at the pure API stage are much higher than the theoretical purge factor.
Bis boronic acid (BBA)	100 (crude) 1 000 (pure)	> 3 333 (crude) > 250 000 (pure)	Measured purge factors at the crude API stage and at the pure API stage are much higher than theoretical purge factor.
Carbazole 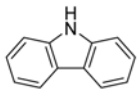	100	> 375	The calculated and experimental purge factors agree reasonably well.

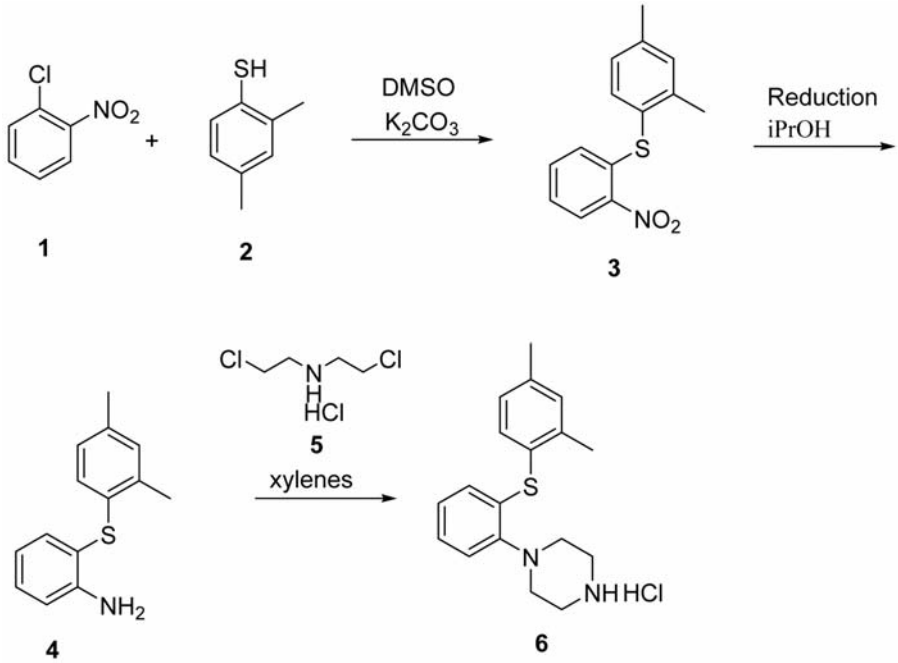

Scheme 4: Synthesis of vortioxetine hydrochloride (adapted from Lapanja et al.[29]).

lue of 3 for the recrystallization process the ability of the process to eliminate impurities was clearly underpredicted. However, Teasdale et al.[28] suggested retaining a more conservative scale in order to compensate for any variance in processes.

5. Conclusion

Several updates and refinements were done since the first guideline covering the issue of GTIs in pharmaceuticals was finalized by EMA in 2006. The ICH M7 guideli-

Table 7. Summarized results of the case study for the synthesis of vortioxetine (based on Lapanja et al.[29]).

Impurity of concern	Theoretical purge factor	Experimental purge factor	Interpretation of the results
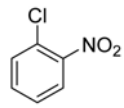 (1)	8.1×10^6	4.9×10^{10}	The calculated purge factor underpredicts the purge capacity of the process by a factor of 6 000. Underprediction is especially significant in the case of recrystallization step (theoretical value of 9 versus 4 000).
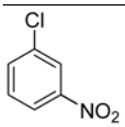	8 100	–	Ames test for this compound was negative; however a theoretical purge factor has been calculated to assess the impact of reactivity parameter on the purge factor determination. The theoretical purge factor is clearly lower than the factor for compound I due to the different position of substituent and thus different reactivity.
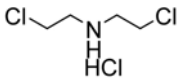 (5)	300	297 738	The experimental purge factor is approximately 1000-times higher than the theoretical purge factor.
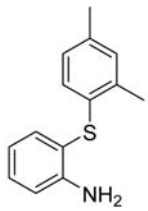 (4)	3 000	20	The calculated purge factor overpredicts the purge capacity of the process.

ne which was released in June 2014 addressed many issues that were left unclear in the previous guidelines. Moreover, it offers greater flexibility in terms of mechanisms to demonstrate absence of MIs in drug substances. The use of theoretical purge factor determination tool which is in line with ICH M7 Option 4 control approach is very promising and allows avoiding analytical testing where not necessary. Many pharmaceutical companies have applied this semi quantitative approach using purge factors as described by Teasdale et al.[28] and some of them published their results. Authors noted that the calculated purge factors agree very well or reasonably well with the experimental purge factors. In several cases it was noted that the purge factor tool tends to underpredict the purging capacity of the process. This underprediction was especially significant in the case of isolation steps during synthesis. While one could argue that the theoretically determined purge factors differ too much from the measured values, it must be emphasized that the underprediction is intentional in order to gain acceptance of the approach. When relating the theoretically determined purge factors to the required purge, it is expected that the theoretical purge would be preferably 100-times greater than the required purge. This makes the approach even more conservative and assures that we always stay on the safe side. Taking into account the conservatism of the approach, this tool should provide satisfactory evidence to the regulatory agencies for the absence of MIs above determined limits. It is to be hoped that this approach will become a regular practice benefiting the pharmaceutical industry, while not increasing any risk for the patients whatsoever.

6. Associated Content

Author Contributions

The manuscript was written through contributions of all authors. All authors have given approval to the final version of the manuscript.

Funding Sources

Lek Pharmaceuticals d.d., Verovškova 57, 1526 Ljubljana, Slovenia

Faculty of Pharmacy, Aškerčeva 7, 1000 Ljubljana, Slovenia

Abbreviations

ALARP, as low as reasonably practicable; API, active pharmaceutical ingredient; CHMP, Committee for Human Medicinal Products; CPMP, Committee for Proprietary Medicinal Products; DMSO, dimethyl sulphoxide; DNA, deoxyribonucleic acid; EDQM, European Directorate for the Quality of Medicines and Healthcare; EMA, European Medicines Agency; EMS, ethyl methane sulfonate; FDA, Food and Drug Administration; GTI, genotoxic impurity; ICH, International Conference on Harmonisation; LOEL, lowest-observed effect level; LTL, Less than lifetime; MI, mutagenic impurity; NOEL, no-obser-

ved-effect level; PDE, permitted daily exposure; PhRMA, Pharmaceutical Research and Manufacturers of America; QbD, Quality by Design; Q&A, Questions and answers; QL, quantitation limit; (Q)SAR , (Quantitative) Structure-Activity Relationships; SWP, Safety Working Party; TTC, Threshold of Toxicological Concern.

7. References

1. ICH: Guidance for industry, M7 Assessment and Control of DNA Reactive (Mutagenic) Impurities in Pharmaceuticals to Limit Potential Carcinogenic Risk, ICH, **2014**.
2. R. W. Tennant, Mutagens and carcinogens, in AccessScience **2014** http://dx.doi.org/10.1036/1097-8542.441100
3. D. Jacobson-Kram, T. McGovern, *Adv. Drug Delivery Rev.* **2007**, *59*, 38–42. https://doi.org/10.1016/j.addr.2006.10.007
4. European Directorate for the Quality of Medicines and Healthcare: Enquiry: Alkyl mesylate (methane sulfonate) impurities in mesylate salts, *PharmEuropa 12:27*, **2000**.
5. A. Teasdale (Ed.): Genotoxic impurities: Strategies for identification and control, Wiley, New Jersey, United States, **2010**, pp. 3-4.
6. EMEA/CPMP: Position paper on the limits of genotoxic impurities, EMEA, **2001**.
7. EMEA/CHMP: Guidelines on the limits of genotoxic impurities, EMEA, **2004**.
8. EMEA/CHMP: CHMP assessment report for Viracept, EMEA, **2007**.
9. EMEA/CHMP: Guidelines on the limits of genotoxic impurities, EMEA, **2006**.
10. ICH: Guidance for industry, Q3A (R2) Impurities in new drug substances, ICH, **2006**.
11. ICH: Guidance for industry, Q3B (R2) Impurities in new drug products, ICH, **2006**.
12. ICH: Guidance for industry, Q3C (R5) Guidelines for residual solvents, ICH, **2011**.
13. ICH: Guidance for industry, Q3D Guideline for elemental impurities, ICH, **2014**.
14. I. C. Munro, E. Kennepohl, R. Kroes, *Food Chem. Toxicol.* **1999**, *37*, 207–232. https://doi.org/10.1016/S0278-6915(98)00112-4
15. R. Kroes, G. Kozianowski, *Toxicol. Lett.* **2002**, *127*, 43–46. https://doi.org/10.1016/S0378-4274(01)00481-7
16. L. S. Gold, C. B. Sawyer, R. Magaw, G. M. Backman, M. de Veciana, R. Levinson, N. K. Hooper, W. R. Havender, L. Bernstein, R. Peto, M. C. Pike, B. N. Ames, *Environ. Health Perspect.* **1984**, *58*, 9–319. https://doi.org/10.1289/ehp.84589
17. I. C. Munro, *Regul. Toxicol. Pharmacol.* **1990**, *12*, 2–12. https://doi.org/10.1016/S0273-2300(05)80042-X
18. M. A. Cheeseman, E. J. Machuga, A. B. Bailey, *Food Chem. Toxicol.* **1999**, *37*, 387–412. https://doi.org/10.1016/S0278-6915(99)00024-1
19. R. Kroes, A. G. Renwick, M. Cheeseman, J. Kleiner, I. Mangelsdorf, A. Piersma, B. Schilter, J. Schlatter, F. van Schothorst, J. G. Vos, G. Würtzen, *Food Chem. Toxicol.* **2004**, *42*, 65–83. https://doi.org/10.1016/j.fct.2003.08.006
20. EMEA/CHMP: Questions and Answers on the CHMP Guideline on the Limits of Genotoxic Impurities, EMEA, **2010.**
21. L. Muller, R. J. Mauthe, C. M. Riley, M. M. Andino, D. D. Antonis, C. Beels, J. DeGeorge, A. G. De Knaep, D. Ellison, J. A. Fagerland, R. Frank, B. Fritschel, S. Galloway, E. Harpur, C. D. Humfrey, A. S. Jacks, N. Jagota, J. Mackinnon, G. Mohan, D. K. Ness, M. R. O'Donovan, M. D. Smith, G. Vudathala, L. Yotti, *Regul. Toxicol. Pharmacol.* **2006**, *44*, 198–211. https://doi.org/10.1016/j.yrtph.2005.12.001
22. Guidance for industry: Genotoxic and Carcinogenic Impurities in Drug Substances and Products: Recommended Approaches (Draft), U.S. Food and Drug Administration (FDA), **2008**.
23. ICH: Guidance for industry, M7 (R1) Addendum: Application of the principles of the ICH M7 guideline to calculation of compound-specific acceptable intake, ICH, **2015**.
24. G. Szekely, M. C. Amores de Sousa, M. Gil, F. C. Ferreira, W. Heggie, *Chem. Rev.* **2015**, *115*, 8182–8229. https://doi.org/10.1021/cr300095f
25. N. V. V. S. S.Raman, A. V. S. S. Prasad, K. Ratnakar Reddy, *J. Pharm. Biomed. Anal*. **2011**, *55*, 662–667. https://doi.org/10.1016/j.jpba.2010.11.039
26. Z. Cimarosti, F. Bravo, P. Stonestreet, F. Tinazzi, O. Vecchi, G. Camurri, *Org. Process Res. Dev.* **2010**, *14*, 993–998. https://doi.org/10.1021/op900242x
27. D. A. Pierson, B. A. Olsen, D. K. Robinson, K. M. DeVries, D. L. Varie, *Org. Process Res. Dev.* **2009**, *13*, 285–291. https://doi.org/10.1021/op8002129
28. A. Teasdale, S. Fenner, A. Ray, A. Ford, A. Phillips, *Org. Process Res. Dev.* **2010**, *14*, 943–945. https://doi.org/10.1021/op100071n
29. N. Lapanja, B. Zupančič, R. Toplak časar, D. Orkič, M. Uštar, A. Satler, S. Jurca, B. Doljak, *Org. Process Res. Dev.* **2015**, *19*, 1524–1530. https://doi.org/10.1021/acs.oprd.5b00061
30. A. Teasdale, D. Elder, S. J. Chang, S. Wang, R. Thompson, N. Benz, I. H. Sanchez Flores, *Org. Process Res. Dev.* **2013**, *17*, 221–230. https://doi.org/10.1021/op300268u
31. D. P. Elder, G. Okafo, M. McGuire, *Org. Process Res. Dev.* **2013,** *17*, 1036–1041. https://doi.org/10.1021/op400139z
32. D. Q. Liu, T. Q. Chen, M. A. McGuire, A. S. J. Kord, *J. Pharm. Biomed. Anal.* **2009**, *50*, 144-150. https://doi.org/10.1016/j.jpba.2009.04.002
33. M. McLaughlin, R. K. Dermenjian, Y. Jin, A. Klapars, M. V. Reddy, M. J. Williams, *Org. Process Res. Dev.* **2015**, *19*, 1531–1535. https://doi.org/10.1021/acs.oprd.5b00263

Povzetek

Mutagene nečistote predstavljajo velik problem za farmacevtsko industrijo, regulatorne oblasti in javno zdravje. Prva regulatorna smernica, ki je obravnavala nadzor genotoksičnih nečistot je bila izdana leta 2006, sledile pa so številne dopolnitve in izboljšave. Junija 2014 je bila s strani mednarodne konference o harmonizaciji zahtev izdana smernica ICH M7, ki v primerjavi s prvotnimi smernicami ponuja bolj pragmatične možnosti za nadzor genotoksičnih nečistot v zdravilnih učinkovinah. Poleg analitskega spremljanja genotoksičnih nečistot ima sedaj farmacevtska industrija preko smernice ICH M7 možnost kontrolne strategije, ki sloni na razumevanju procesa sinteze in na oceni vpliva procesnih parametrov na nivo pridobljenih in nastalih nečistot. Ta pristop je predlagal in prvi opisal A. Teasdale s sodelavci. Predlagani pristop izračuna teoretičnih faktorjev očiščenja je bil v zadnjih letih uporabljen na številnih praktičnih primerih. Objavljeni rezultati kažejo na to, da lahko s tem pristopom precej dobro napovemo sposobnost očiščenja nečistot skozi proces. Upati velja, da bo omenjeni pristop kmalu na voljo v obliki računalniškega orodja, ki bo splošno sprejemljiv s strani regulatornih oblasti.

Review

The Lock is the Key: Development of Novel Drugs through Receptor Based Combinatorial Chemistry

Nikola Maraković and Goran Šinko*

Institute for Medical Research and Occupational Health, Ksaverska cesta 2, p.p. 291, HR-10001 Zagreb, Croatia

** Corresponding author: E-mail: gsinko@imi.hr*

Received: 16-12-2016

Abstract

Modern drug discovery is mainly based on the *de novo* synthesis of a large number of compounds with a diversity of chemical functionalities. Though the introduction of combinatorial chemistry enabled the preparation of large libraries of compounds from so-called building blocks, the problem of successfully identifying leads remains. The introduction of a dynamic combinatorial chemistry method served as a step forward due to the involvement of biological macromolecular targets (receptors) in the synthesis of high affinity products. The major breakthrough was a synthetic method in which building blocks are irreversibly combined due to the presence of a receptor. Here we present various receptor-based combinatorial chemistry approaches. Huisgen's cycloaddition (1,3-dipolar cycloaddition of azides and alkynes) forms stabile 1,2,3-triazoles with very high receptor affinity that can reach femtomolar levels, as the case with acetylcholinesterase inhibitors shows. Huisgen's cycloaddition can be applied to various receptors including acetylcholinesterase, acetylcholine binding protein, carbonic anhydrase-II, serine/threonine-protein kinase and minor groove of DNA.

Keywords: Drug design; Dynamic combinatorial chemistry; Huisgen's cycloaddition; *in situ* click-chemistry; Receptor-accelerated synthesis; Receptor-assisted combinatorial chemistry

1. Introduction

The main focus of drug discovery is the identification of compounds that can modify molecular targets associated with certain diseases inducing a positive response. While natural products have inspired the design of most drugs in the past, the processes of lead discovery and optimization today rely on the preparation of large collections of new compounds, referred to as "libraries". Choosing large numbers of structurally diverse compounds is primarily governed by the complexity of natural products, which increases the difficulty, time, and cost of the preparation of such compounds. Also, as suggested by a computational study by Bohacek *et al*., the total number of "drug-like" compounds (< 30 non-hydrogen atoms, < 500 Daltons; only H, C, N, O, P, S, F, Cl and Br; stable in the presence of water and oxygen) is as large as 10^{63} indicating that the vast majority of "drug-like" compounds are yet to be discovered.[1] The introduction of combinatorial chemistry seemed to resolve the problem of preparing large libraries by focusing on building libraries of more complex compounds from simple building blocks. Building blocks are combined in a maximum number of possible combinations through independent synthesis. In the final step, each compound is independently tested for activity.

Independent testing of a large number of newly synthesized compounds significantly reduces the potential of conventional combinatorial methods. However, by the early 2000s, it became clear that conventional combinatorial chemistry turned out to be much less efficient than expected with only a few developed drugs reported and most industrial combinatorial chemistry libraries were disbanded.[2]

In 1894, the German chemist Emil Fischer suggested a model of enzyme specificity by which an enzyme and its substrate possess specific complementary geometric shapes that fit exactly one into another like a lock and key. Although this model is more than 100 years old, E. Fischer's idea is still valid. Dixon and Villar showed that a protein can bind a set of structurally diverse molecules with similar affinities in the nanomolar range, whereas analogues closely related to one of the good binders show only weak affinities (> 2.5 mM).[3] Chemists created an approach where novel potentially bioactive compounds are not synthesized by pure statistical reorganization of joi-

ning building blocks but forcing them in the right direction by including a macromolecular target (receptor) itself in this process. This was done through the introduction of a receptor-assisted combinatorial chemistry (RACC), sometimes also referred to as target-guided synthesis (TGS).[4] In contrast to conventional combinatorial methods, in RACC the macromolecular target (protein or DNA) is directly involved in the choice of joining building blocks.

The concept of RACC can be divided into dynamic combinatorial chemistry (DCC) and receptor-accelerated synthesis (RAS), also called kinetically controlled TGS. In DCC, the reaction that joins the building blocks is reversible, whereas RAS uses only reactive building blocks joined irreversibly. The subset of RAS called *in situ* click chemistry, which uses the Huisgen's 1,3-dipolar cycloaddition of azides and alkynes (Huisgen's cycloaddition) to irreversibly join the building blocks, will be covered with special interest.[5,6]

2. Dynamic Combinatorial Chemistry Method

Dynamic combinatorial chemistry is a subset of RACC in which building blocks are joined through a reversible covalent reactions, generating a large equilibrium-controlled library of compounds referred to as a dynamic combinatorial library (DCL).[7,8] The addition of biological targets during the generation of DCL stabilizes the library members with the highest affinity toward the biological target, moving the equilibrium toward high-affinity members. A comparison of the composition of the library with and without the biological target leads to the identification of a hit compound. Therefore, the synthesis and screening of library members are combined in one step, which speeds-up the process of hit identification.

Moreover, hit identification is possible without any specific receptor assays used. Instead, increased amounts of the highest affinity library members are detected with established analytical methods like HPLC, mass spectrometry (MS), NMR spectroscopy or even X-ray crystallography.[9,10] It may be more advantageous for the library to amplify many members with moderate affinities than just a few with high affinities. This behaviour reflects the complex nature of DCLs consisted of members interconnected through a set of equilibrium reactions.[11] To address these problems numerous theoretical studies of DCLs have been done.[12–16] The studies suggested that, unless excessive amounts of molecular target are used, good binders have a high probability of being significantly amplified. However, a major limitation for application of DCC in drug discovery is the limited number of reversible covalent reactions appropriate to be used to synthesize DCLs. Drug discovery applications of DCC require the following reaction conditions: (i) reaction at a biologically relevant temperature, (ii) compatibility with aqueous media, (iii) reaction at (close to) physiological pH and (iv) compatibility with the target functional groups.[17,18] Compatibility with aqueous media is the most challenging condition as there are more reactions that have been developed in organic solvents than under aqueous conditions, thus preventing the use of a wider range of equilibration reactions. Additionally, the use of organic solvents in DCC is limited by the strong tendency of solvents to denature the target (enzyme, receptor, etc.). Examples of DCC applications for the discovery of high affinity ligands for biological receptors have been reported, including formation of DCLs of imines,[19,20] hydrazones,[21,22] oxime ethers,[23] sulfides,[24] disulfides[25–28] and alkenes.[29]

2. 1. Reversible Imine Formation

Huc and Lehn were the first to demonstrate the concept of DCC application in drug discovery by identifying inhibitors of carbonic anhydrase (CA) using a DCL of imines formed from amines and aldehydes.[19] In addition to the fast and reversible nature of condensation between amines and aldehydes to imines, reversible imine formation is very convenient for drug discovery because it yields a Schiff base, a very common motive in metabolites and biologically active compounds.[30,31] To detect products by HPLC, they "locked-in" the equilibrium by irreversible reduction of imines to corresponding amines using $NaBH_3CN$ to fix the composition of the library prior to detection.

Hochgürtel *et al*. created an imine library by condensing a diamine with more than fifty different ketones in the presence of neuraminidase from an influenza virus (Fig. 1).[20] After reduction of imines, LC/MS analysis identified several hits (**1**–**4**). The negative control experiment included library synthesis in the presence of the bovine serum albumin (BSA). The second control experiment was carried out in the presence of the neuraminidase and Zanamivir, a potent competitive inhibitor of the neuraminidase. On both occasions, initial hit **4** was identified. The most abundant compound **3** lacked inhibitory potency, whereas the strongest inhibitor **2** was amplified three-fold less than **3**. The authors suggested that this result could be explained by the lock-in reaction. Actual molecular species undergoing equilibration are imines and hemiaminals. The receptor amplifies the amount of these intermediates that are then reduced to fix the library composition. Reduced products have different structural and electronic properties and their interaction with the biological target may be worse, or better, than originating intermediates. This represents a major drawback for the application of reversible imine formation to the construction of DCLs in the presence of a biological target.

Recent progress in analytical methods used for identification of binders from DCL had enabled access to larger libraries. For example, Guo *et al.* introduced a

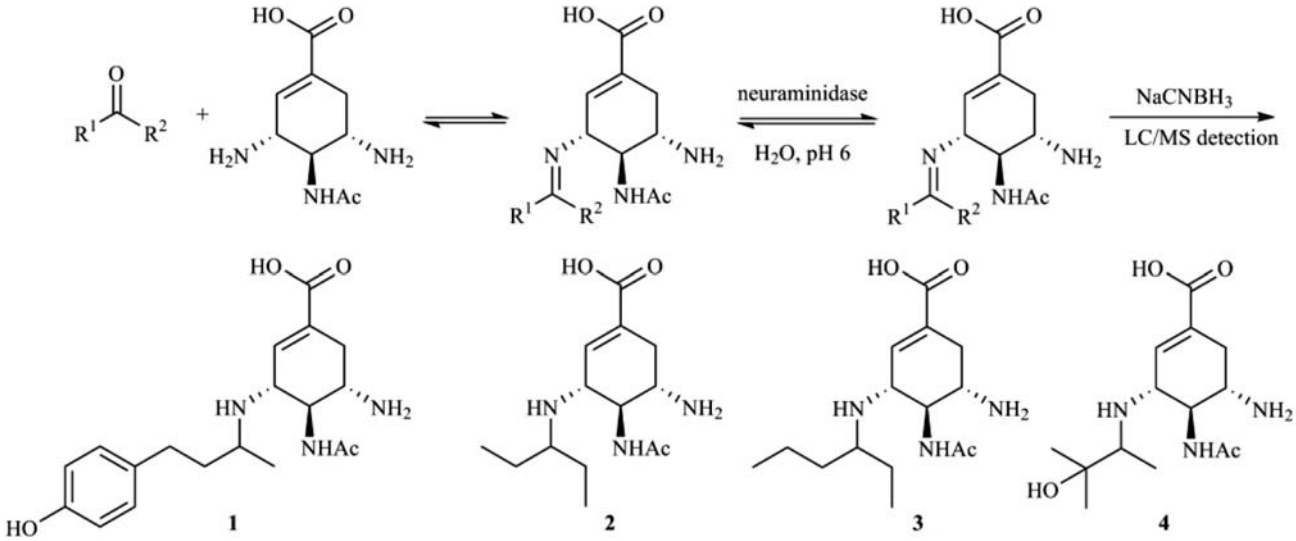

Figure 1. Formation of a library of potential neuraminidase inhibitors by condensing a diamine with several ketones.[20]

protocol for analysis of imine-based DCL using a suitable size-exclusion chromatography (SEC) column to retain all non-binders from DCL followed by denaturation of eluted protein-ligand complexes and MS analysis of binders.[32]

2. 2. Disulfide Interchange

To demonstrate utility of a disulfide interchange for DCC approach, Ramström and Lehn designed a DCL of disulfides capable of binding to concavalin A (Con A), a member of lectins.[25,33] DCL of disulfide carbohydrate dimers (Table 1) was generated by incubating disulfide dimers with an initiating reagent dithiothreitol (DTT) capable of reducing some disulfides to thiols. DTT is oxidized to a stable 6-membered cyclic disulfide that should not take part in the interconversion of the library disulfides. Upon initiation, interconversion between disulfides occurred with the rate dependent on pH. At pH 7.4, a reasonable rate of interconversion was obtained and receptor binding was not affected. Disulfide interchange could be stopped by lowering the pH (< 5) and final equilibrium distribution of DCL analyzed by HPLC. In the absence of any receptor, all expected ditopic combinations were generated in approximately equal amounts. When a receptor Con A was present during the interconversion, a significant amount of the bis-mannoside (Man/Man) and the mannose-containing heterodimers (Man/Gal, Man/Ara, Man/Xyl) was found to be bound to the receptor.[25] Moreover, receptor-induced shifts in equilibrium resulted in the amplification of mannose-containing dimers, which is in accordance with concepts of the DCC approach.

One of the major drawbacks of using DCL of disulfides to identify potent inhibitors of protein targets is the labile nature of disulfide bond. However, once identified disulfide compounds can be replaced with their carbon

Table 1. Structures of the disulfide-linked carbohydrate dimers.[25]

Compound[a]		α/β	R^{2a}	R^{2e}	R^{4a}	R^{4e}	R^5	n
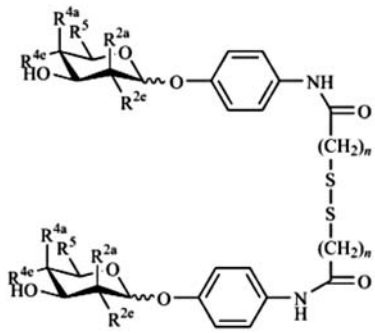	(Man/Man)	α	OH	H	H	OH	CH_2OH	3
	(Gal C_2/Gal C_2)	β	H	OH	OH	H	CH_2OH	2
	(Gal C_3/Gal C_3)	β	H	OH	OH	H	CH_2OH	3
	(Glc/Glc)	β	H	OH	H	OH	CH_2OH	2
	(Ara/Ara)	β	H	OH	OH	H	H	2
	(Xyl/Xyl)	β	H	OH	H	OH	H	2

[a] Man = D-mannose; Gal C_2 = D-galactose, n = 2; Gal C_3 = D-galactose, n = 3; Glc = D-glucose; Ara = L-arabinose; Xyl = D-xylose

analogues, with bioisosteric thioether or amide linker instead of the disulfide bond. Using modified MS analysis that enables analysis of DCLs of thiols/disulfides under non-denaturing conditions, Schofield *et al.* have identified inhibitors to various protein targets by preparing carbon analogues of identified disulfide compounds.[27,34]

2. 3. Reversible Acylhydrazone Formation

Ramström *et al.* developed DCLs of constituents potentially capable of binding to plant Con A using reversible hydrazidecarbonyl/acylhydrazone inter-conversion.[21] Acylhydrazone libraries were generated from a series of oligohydrazide core building blocks **A**–**I** and a set of aldehyde counterparts **5**–**10** based on six common, naturally occurring carbohydrates, potentially capable of interacting with the binding site of Con A (Fig. 2). A set of initial 15 building blocks could give rise to a library containing at least 474 different species. Also, 15 sub-libraries were formed by mixing all building blocks except one specific hydrazide or aldehyde building block under the same conditions.[21] Following equilibration libraries were subsequently subjected to the lectin assay in which the inhibitory potency of library constituents was monitored.

The resulting inhibitory effects of the sub-libraries have been matched to the activity of the complete library. The largest effect was noticed on the removal of the mannose unit from complete DCL indicating that the mannose unit is necessary for inhibition. Similarly, trivalent core building block **G** was the most active. The effect of the compound assembled from these two fragments was estimated in a binding assay, resulting in an IC_{50} value in the micromolar range (22 μM), indicating that the DCC approach using reversible hydrazidecarbonyl/acylhydrazone interconversion enabled the identification of a novel tritopic mannoside showing potent binding to Con A (Fig. 3).

However, the full potential of acylhydrazone-based DCLs in drug discovery is somewhat limited because of the requirement for acidic pH which is incompatible with most protein targets. Greaney *et al.* have managed to circumvent this obstacle by introducing nucleophilic catalysis of reversible acylhydrazone formation by using aniline as a nucleophilic catalyst at less acidic pH and thus identify acylhydrazone inhibitors of GST isozymes.[35,36]

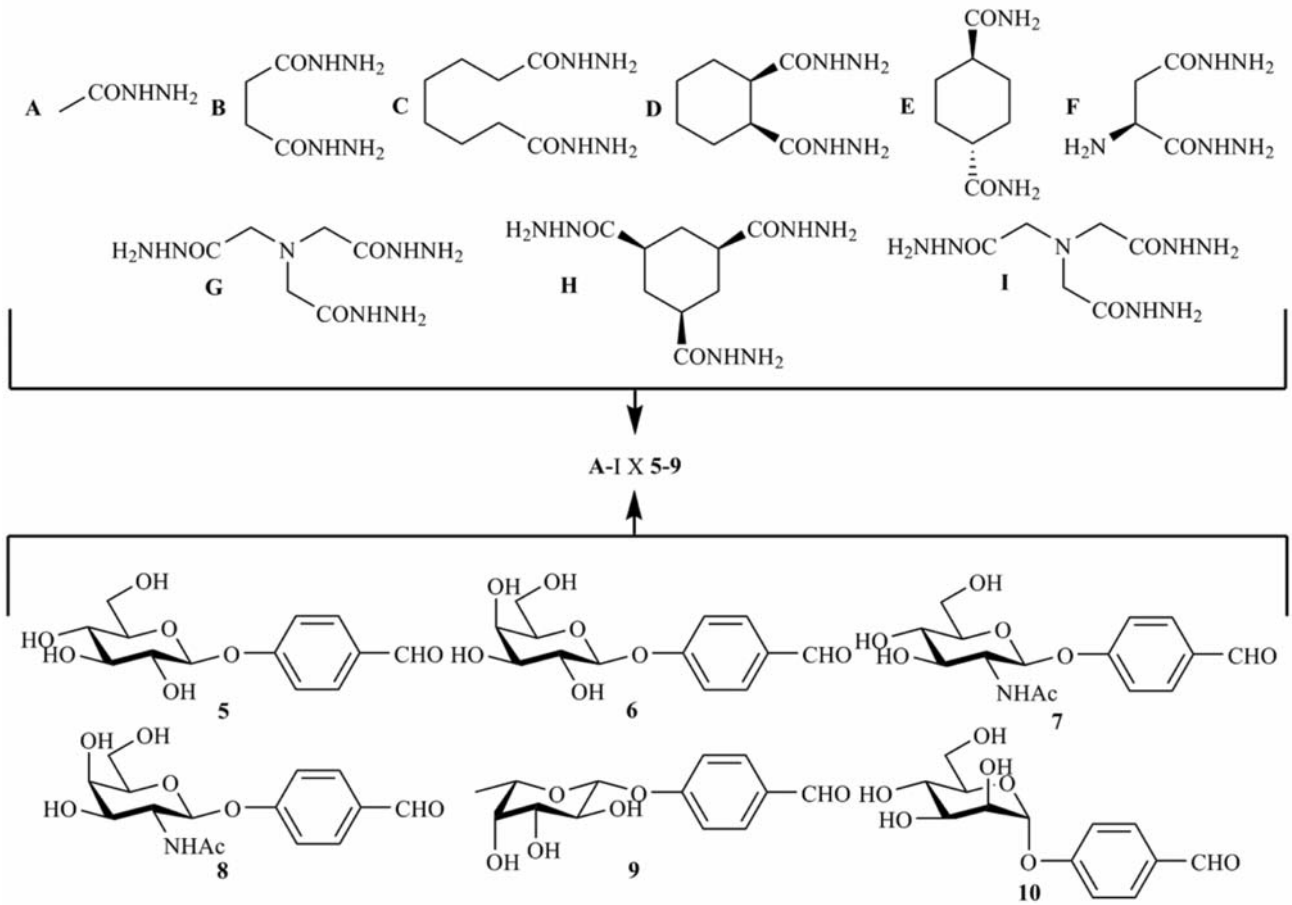

Figure 2. A series of oligohydrazide **A**–**I** and aldehyde building blocks **5**–**10** generating an acylhydrazone dynamic combinatorial library of potential plant lectin Con A inhibitors.[21]

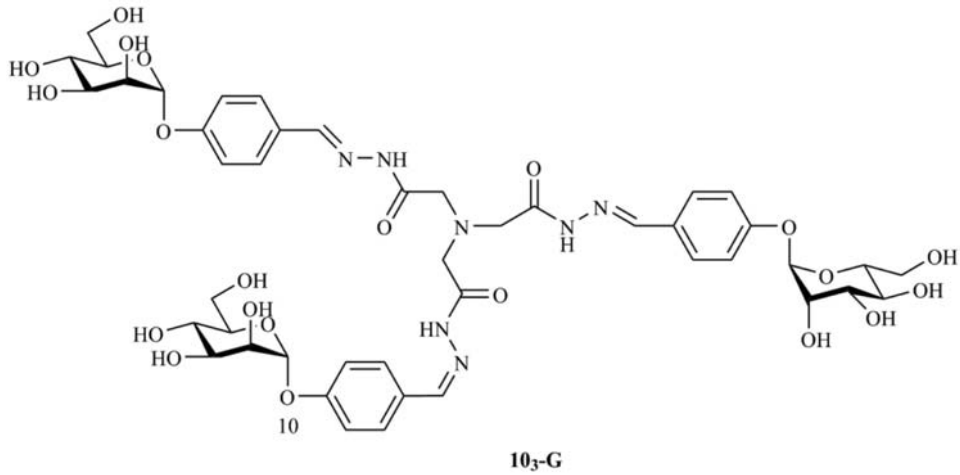

Figure 3. Compound **10_3-G** identified as the best binder to Con A (IC_{50} = 22 μM) from the acylhydrazone dynamic combinatorial library generated from a series of oligohydrazide and aldehyde building blocks.[21]

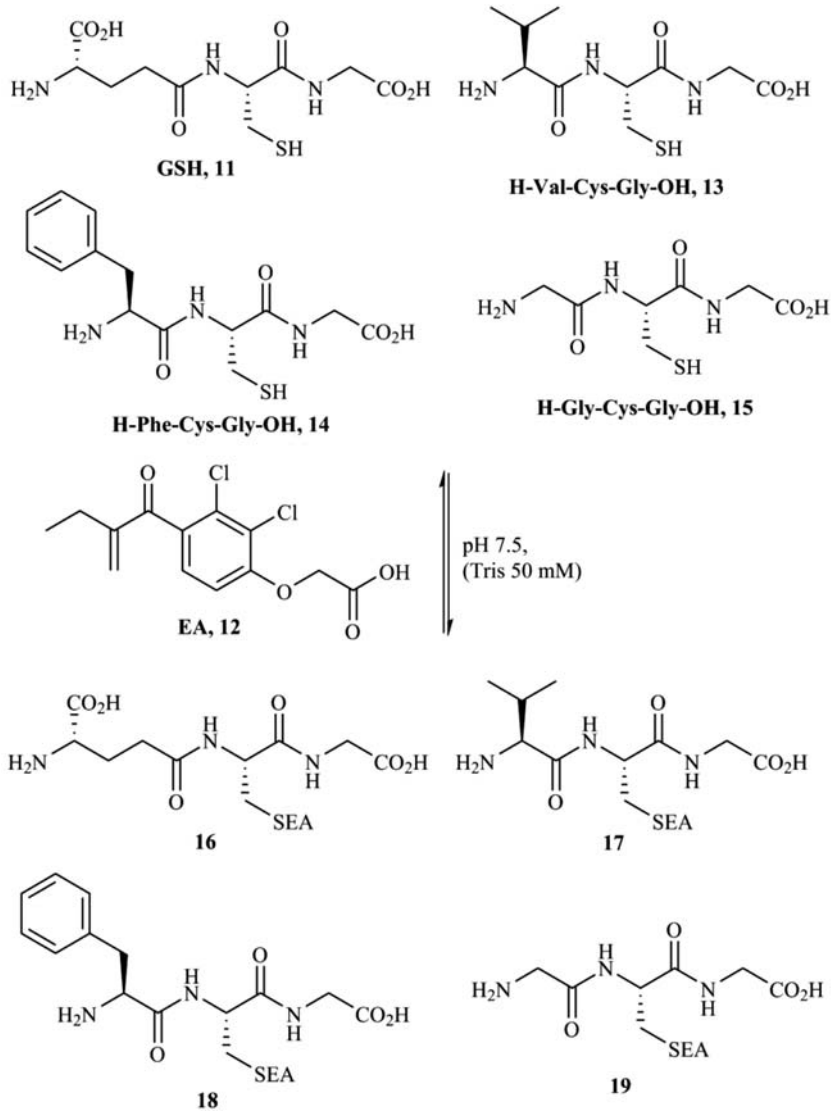

Figure 4. Dynamic combinatorial library composed of glutathione (GSH) conjugates potentially capable of binding to glutathione S-transferase (GST) generated from GSH, GSH analogues, and ethacrynic acid (EA).[37]

2. 4. Conjugate Addition of Thiols to Enones

Shi and Greaney extended the number of reversible chemical reactions suitable for DCL generation by using conjugated addition of thiols to enones.[24] Shi and Greaney designed a biased DCL generated using glutathione (GSH; **11**), three GSH analogues **13–15**, and the enone ethacrynic acid (EA; **12**) (Fig. 4).[37] Three analogues were expected to be misfits for the G site of glutathione S-transferase (GST) since the γ-glutamyl residue is critical for binding,[38] thus biasing the DCL equilibrium composition in the presence of GST toward the GSH adduct **16**. EA is an inhibitor of GST and has provided a structural scaffold for development of GST inhibitors. Blank DCL, assembled in the absence of GST resulted in the distribution of four conjugates **16–19**. Upon incubation with GST from *Schistosoma japonica* (*Sj*GST), DCL reduced to the expected GS-EA adduct **16**. Adduct **16** was increased from 35% of total conjugate concentration to 92% at equilibrium, due to large differences in binding affinity between **16** and peptides lacking the γ-glutamyl residue. Control experiments with BSA instead of *Sj*GST produced no changes to the blank DCL composition, confirming that the active site of *Sj*GST is responsible in amplification of **16**.

Shi *et al*. used the thiol addition methodology to create new GST inhibitors from nonbiased DCLs. Since

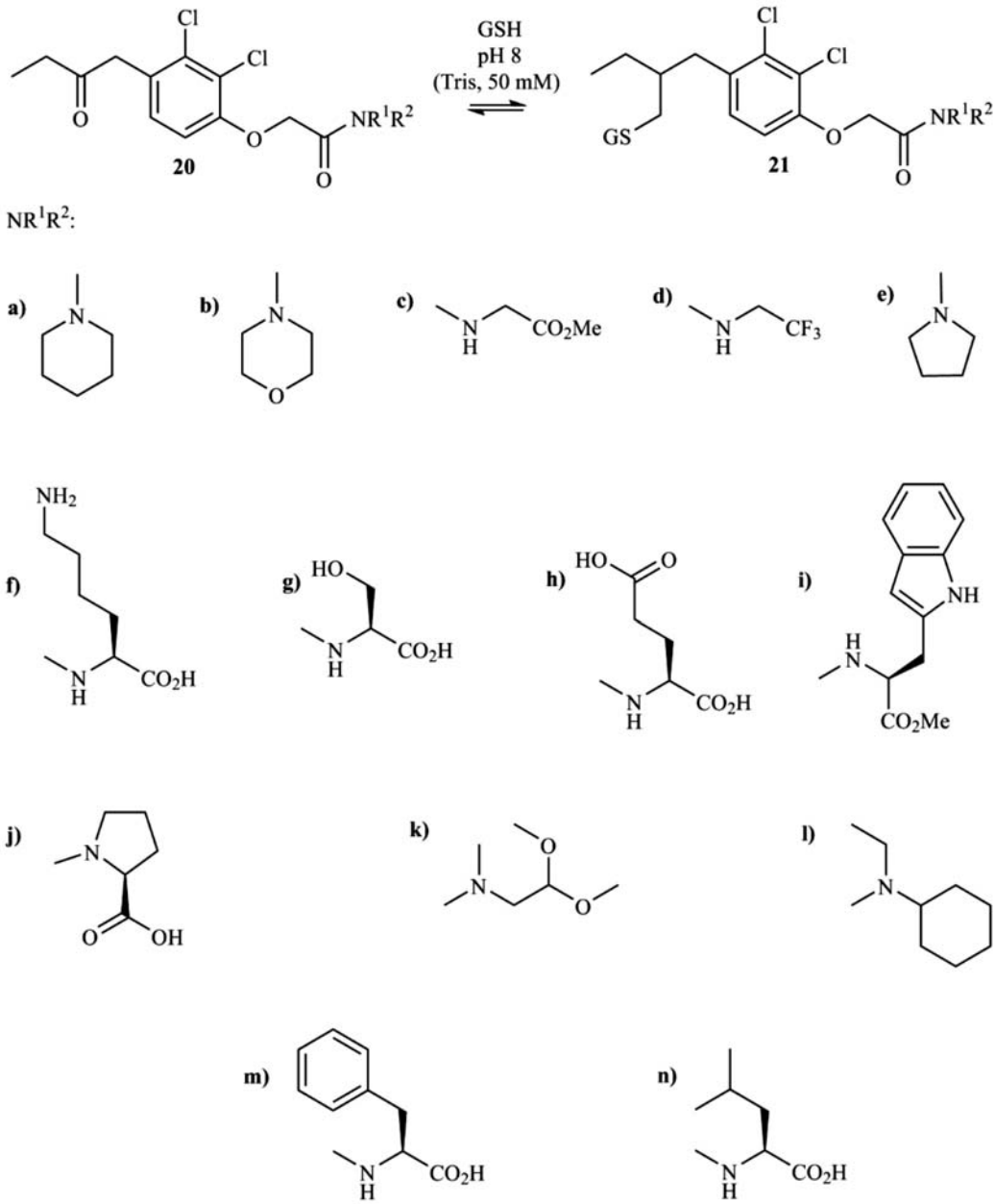

Figure 5. A nonbiased DCL of potential GST inhibitors generated from glutathione (GSH) and 14 enone ethacrynic acid analogues.[37]

structural features of the H site change across different GST isozymes, the authors explored the H site of *Sj*GST by constructing a DCL with reversed stoichiometry from that in biased DCL, whereby 14 EA analogues reacted with GSH to afford 14 GS-EA adducts (Fig. 5). MS analysis and deconvolution studies revealed that adducts **21a**,**m** and **n** were amplified in the presence of *Sj*GST, while adduct **21f** was suppressed. To examine the inhibition potency of *Sj*GST, **21a**, **21n**, non-amplified adduct **21b**, and the suppressed adduct **21f** were synthesized and their IC_{50} values measured. Results indicated that the extent of DCL amplification reflected the relative binding affinities of DCL components for the *Sj*GST. Piperidine and leucine amides **21a** (IC_{50} = 0.61 μM) and **21n** (IC_{50} = 1.40 μM) were amplified from the library at the expense of the weaker binder lysine amide **21f** (IC_{50} = 8.2 μM). Moreover, contrary to the proposed model structure of the *Sj*GST/GS-EA Michaelis complex which identified a series of residues that could interact with the EA carboxylic acid group,[39] amplified adducts **21a** and **21n** indicated that the carboxylic acid group of EA is not essential for binding in the H site and may be extended without change of inhibitory activity.

3. Receptor-Accelerated Synthesis

Receptor-accelerated synthesis (RAS), also called kinetically controlled TGS, is a subset of RACC, which uses kinetic control to increase the relative amounts of the highest-affinity library members during library generation.[4,40] While the library members in the DCC approach are generated *via* reversible reactions, RAS uses building blocks which irreversibly combine into larger molecules. Process of hit identification and optimization takes advantage of combining synthesis and screening into one step (Fig. 6). Step 1 includes synthesis of reactive building blocks, while in step 2 these building blocks irreversibly combine due to the presence of a receptor. The hit identification consists of determining whether a formation of a product is significantly accelerated in the presence of a target molecule (receptor).

The selectivity for one or more products over others arises from two factors, one related to the binding of building blocks to the receptor, and the other to the ability of a receptor to accelerate their irreversible joining. With regard to the binding of the starting building blocks to the receptor, simultaneous binding of highest-affinity building blocks in close proximity leads to rate acceleration. However, upon joining the starting building blocks to the product, the binding interactions of building blocks to the receptor may strengthen or weaken in accordance with the Fischer's lock and key model. Thus, highest-affinity building blocks might not form a product with the highest affinity for the receptor. As far as the ability of a given receptor to promote the coupling of reactive building blocks is concerned, it is important to note that receptors do not normally act as coupling catalysts. The demands for a reaction suitable for RAS are different from the DCC approach or from a conventional organic reaction. Ideally, complementary reactive groups should combine very slowly in solution generating a stable product with no or only minor side products. Kolb *et al.* identified Huisgen's cycloaddition as the one having the ideal reactivity profile for RAS.[41,42] This methodology has been successfully applied in numerous examples known as *in situ* click chemistry.[43] So far, RAC approaches have included C–N bond formation,[44–46] C–S bond formation,[47–49] C–C bond formation,[50] and ami-

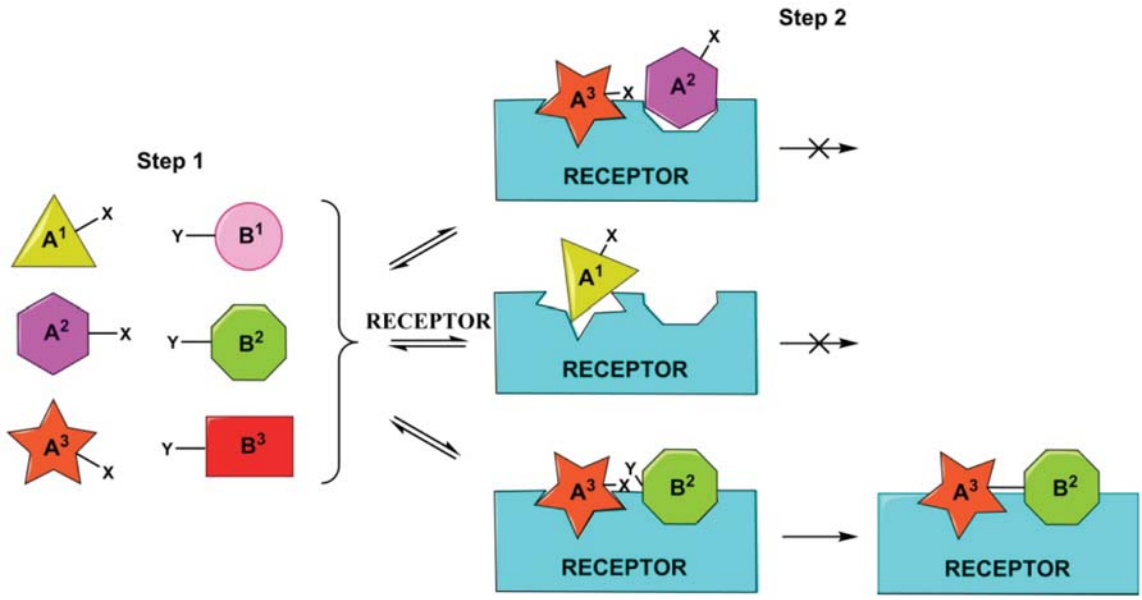

Figure 6. Receptor-accelerated synthesis for hit discovery and optimization. Products are created from blocks properly stabilized within the receptor.

de formation from thio acids and sulfonyl azides, also referred to as "sulfo-click reaction".[51,52] Some of these approaches are described in more detail below.

3. 1. Substitution Reaction Using a Thiol as the Nucleophile

Huc and Nguyen were the first to demonstrate the utility of a substitution reaction using a thiol as a nucleophile for the identification of an inhibitor *via* RAS approach.[47] This reaction is widely used in organic chemistry since thiols are more reactive than alcohols. In initial study, they chose to target a zinc-containing metalloenzyme, bovine CA-II (EC 4.2.1.1).[53] CA-II isozymes play a role in many important biological processes, including respiration, bone respiration, calcification, acid secretion, and pH control. The CA-II active site is a conical cleft with the Zn(II) ion located at its bottom with two secondary hydrophobic binding sites located in close proximity of this cleft. They tested the ability of CA-II to accelerate the formation of *para*-substituted aromatic sulfonamide inhibitors **24a**–**e** using competition assays optimized to limit side reactions, such as disulfide formation, alkyl chloride hydrolysis, and trialkyl sulfonium formation (Fig. 7).[47]

Thiol **22** was treated with two competing alkyl chlorides in buffered water at pH 6 for 48 h, first in the absence of CA-II, then in the presence of CA-II. HPLC analysis of the final thioether products confirmed that CA-II strongly favours formation of more potent inhibitors. For example, when chloride **23a** competes with **23d**, the yield of more potent inhibitor **24d** changes from 50% in the absence of CA-II to 92% in its presence. On the contrary, when products have similar affinities for CA-II, their final yields are negligibly affected by the presence of CA-II. To confirm that CA-II serves as the reaction vessel, Huc and Nguyen conducted several control experiments, including varying CA-II concentration, replacing CA-II by BSA, replacing thiol **22** by a thiol that has no affinity for CA-II, and adding an inhibitor of CA-II, methazolamide.[54] All of these experiments confirmed that the active site of CA-II templates product formation.

Besides alkyl halides, thiols can also react with epoxide rings in protein-templated irreversible formation of biologically active ligands. Okhanda *et al.* have utilized such epoxide ring opening to identify inhibitors of recombinant human 14-3-3 protein, involved in immunoglobulin class switching, *via* RAS approach.[48]

3. 2. Amide Formation Between Thio Acids and Sulfonyl Azides

The choice of biological target for the RAS or the RACC is not limited to enzymes only. It has been shown that RAS can be utilized to discover small molecules that modulate or disrupt protein-protein interactions (PPIs) called protein-protein interaction modulators (PPIMs). PPIs are crucial for a large number of vital biological processes and interesting in the development of novel therapies for a variety of diseases.[55] Among PPI targets for cancer treatment are also proteins of the Bcl-2 family. Some of the Bcl-2 proteins act as anti-apoptotic proteins (Bcl-2,

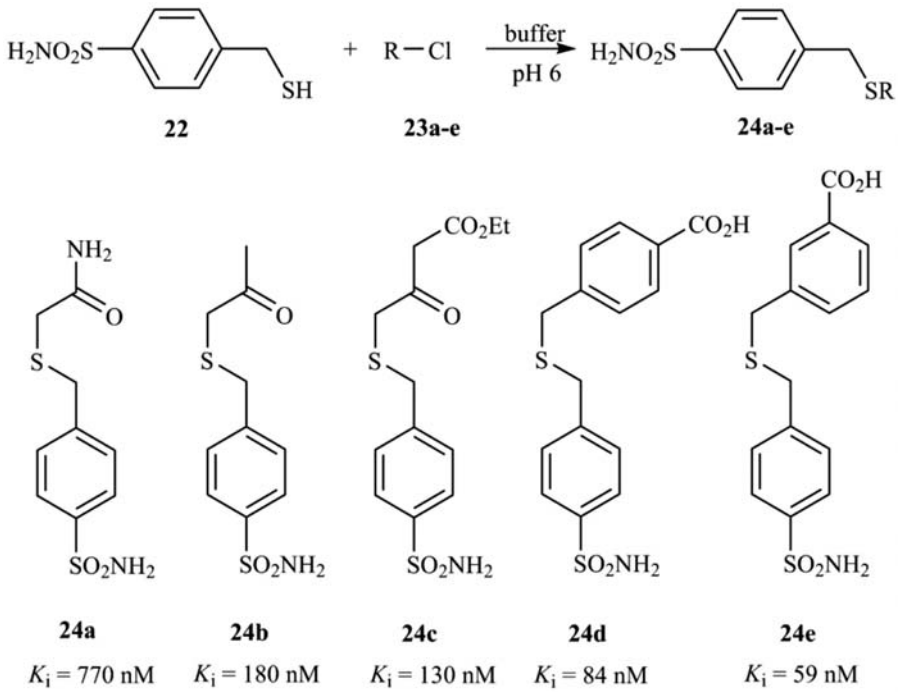

Figure 7. The formation of *para*-substituted aromatic sulfonamide inhibitors **24a**–**e** of CA-II.[47]

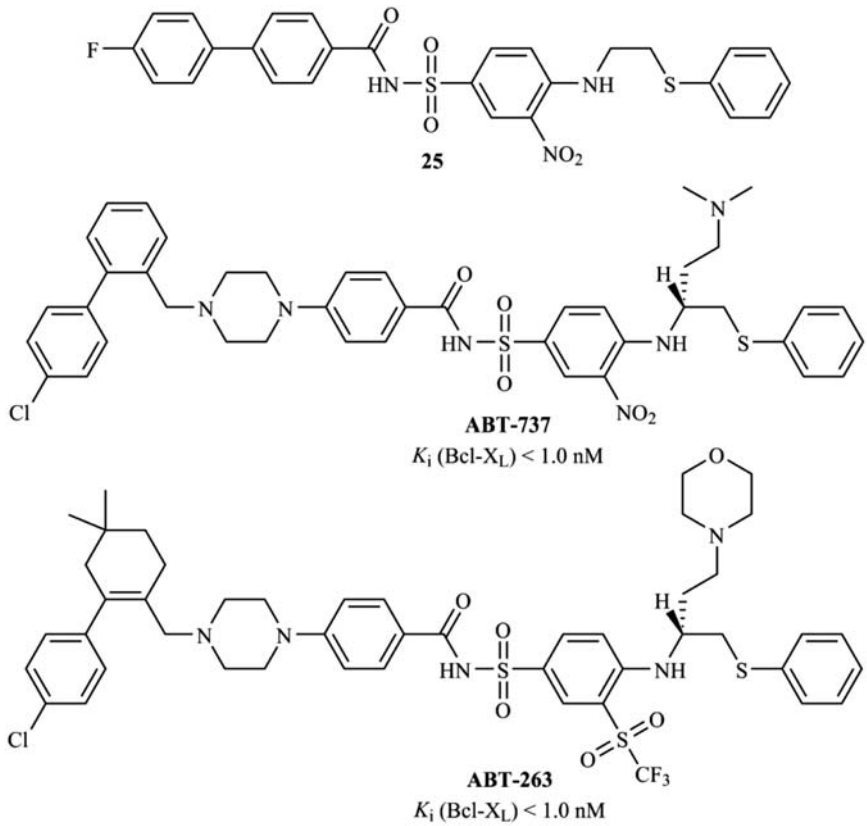

Figure 8. *N*-Acylsulfonamide compounds targeting Bcl-X_L.[57–59]

Bcl-X_L, and Mcl-1) and others as pro-apoptotic proteins. Pro-apoptotic proteins can be further classified into multi-domain BH1-3 proteins (Bax and Bak) and BH3-only proteins (Bad, Bim, and Noxa).[56] Bcl-2 proteins play an important role in the apoptosis. Most likely, apoptosis is initiated by binding the BH3 domain of BH3-only proteins

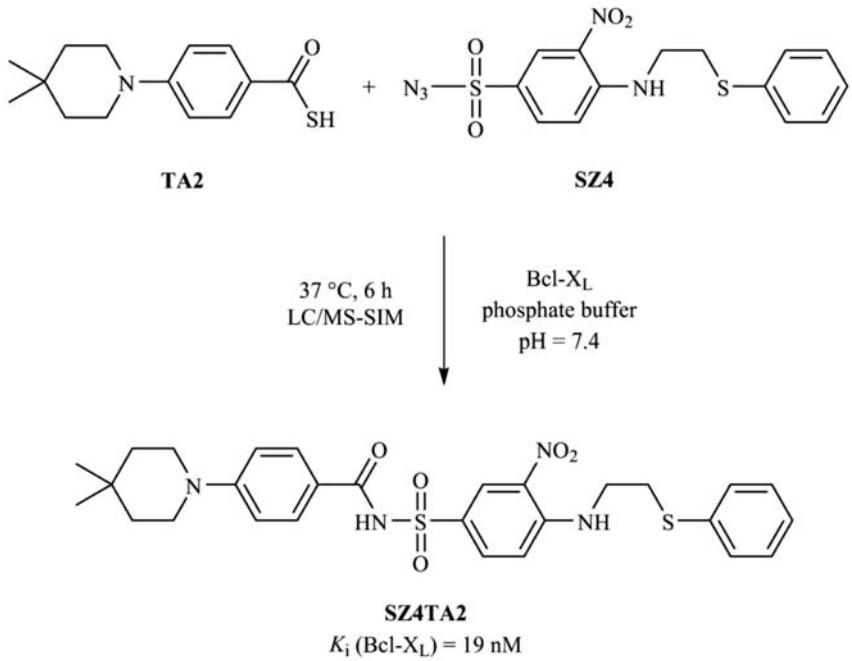

Figure 9. PPIM identification *via* sulfo-click RAS approach.[60]

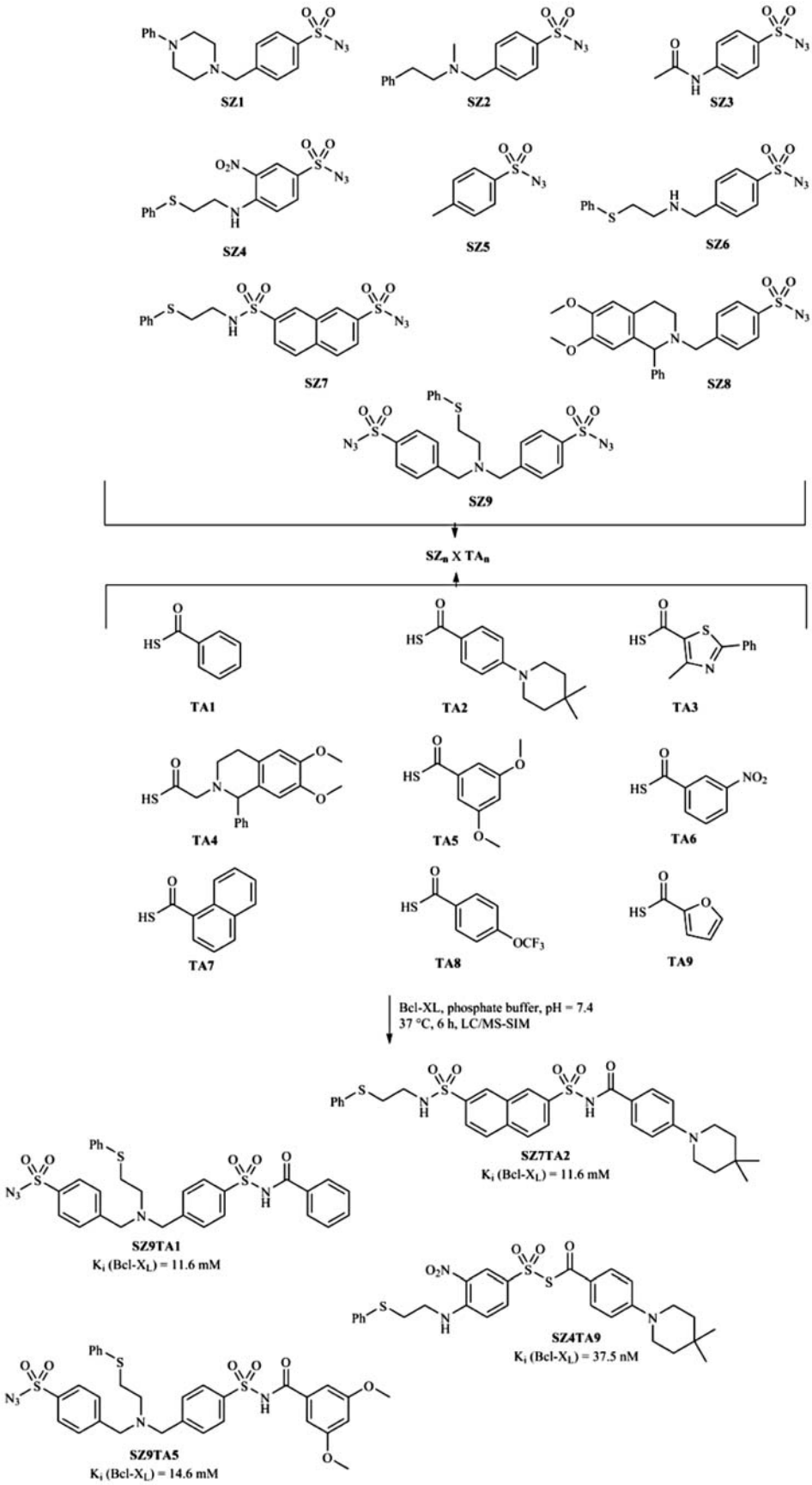

Figure 10. Screening of anti-apoptotic Bcl-X_L *via* sulfo-click RAS approach for PPIM discovery.[51]

into a hydrophobic groove on the surface of anti-apoptotic proteins. Therefore, designing a molecule capable of mimicking the BH3 domain is a promising strategy for novel anticancer treatments. Thus, *N*-acylsulfonamides **25**, **ABT-737**, and **ABT-263**, capable of disrupting Bcl-X_L-Bad interaction, were prepared (Fig. 8).[57–59]

Hu *et al.* applied the RAS approach for the discovery of *N*-acylsulfonamide PPIMs.[60] They designed building blocks structurally similar to **ABT-737** and **ABT-263**, having a sulfonyl azide or a thio acid functional groups, and incubated these as binary mixture together with Bcl-XL for 6 h. LC/MS analysis revealed that, of all the 18 possible products, only *N*-acylsulfonamide **SZ4TA2** was detected (Fig. 9).

Control experiments involving incubation of reactive building blocks in the absence of Bcl-X_L or in the presence of Bcl-X_L and various BH3-containing peptides, confirmed that the surface of Bcl-X_L protein acts as a template for the sulfo-click reaction. To generate new hit compounds, Kulkarni *et al.* designed two sublibraries, one with thio acids and the other with sulfonyl azides, among which were those with a structural resemblance to **ABT-737** or **ABT-263** and those that were randomly chosen.[51] Eighty-one binary mixtures containing one thio acid (**TA1**–**TA9**) and one sulfonyl azide (**SZ1**–**SZ9**) were incubated with the protein Bcl-X_L for 6 h at 37 °C (Fig. 10).

LC/MS analysis of binary mixtures with or without Bcl-X_L present during reaction resulted in elevated amounts of **SZ4TA2**, and three new products **SZ7TA2**, **SZ9TA1**, and **SZ9TA6** in the presence of Bcl-X_L. Control experiments with native and mutated pro-apoptotic Bim BH3 peptides and Bcl-X_L proteins indicated that protein-templated *N*-acylsulfonamide formation happened solely at the binding sites of Bcl-X_L. In order to evaluate the IC_{50}, all four hit compounds were subjected to dose-response studies and binding studies.[60] All of the hit compounds show high to modest affinity for Bcl-X_L protein and can modulate the interaction between Bcl-X_L and BH3 peptide ligand.

Nature of sulfo-click reaction and substrate scope challenge its applicability in the RAS approach. As thioacids are nucleophilic, readily dimerize, and present storage and stability issues, their preparation and handling is therefore very demanding.[61] Namelikonda *et al.* optimized the one-pot deprotection/amidation variant of sulfo-click reaction in the presence and absence of Bcl-X_L starting from the 9-fluorenylmethyl (Fm)-protected thioesters and sulfonylazides.[52] Optimal deprotection of Fm thioesters **TA1'**–**TA3'** prepared from thioacid building blocks **TA1**–**TA3** was achieved in one minute at room temperature with 3.5% 1,8-diazabicycloundec-7-ene (DBU)/DMF. Resulting thioacids **TA1**–**TA3** were immediately diluted with methanol and incubated with sulfonylazides **SZ1**–**SZ6** as binary mixtures in the presence and absence of Bcl-X_L. Product analysis failed to detect an increased amount of the previously reported hit compound **SZ4TA2** in the presence of Bcl-X_L, presumably due to the change in pH of the incubation sample probably due to the strong basicity of DBU. Experiments were repeated with a weaker base (5% piperidine/DMF), and the amount of **SZ4TA2** was increased to the same level as before containing purified thioacid **TA2**. However, a side reaction producing piperidine amide was observed, but this unwanted byproduct did not interfere with Bcl-X_L templated reaction.

4. *In situ* Click Chemistry

So far, only a RAS approach using a combination of strong nucleophilic (basic) and electrophilic (acidic) building blocks has been discussed. However, a subset of receptor-accelerated synthesis, termed *in situ* click chemistry, has been developed utilizing the Huisgen's cycloaddition,[5,6] a reaction independent to the acid-base reactivity paradigm, as shown in literature.[62–67]

4. 1. The Huisgen's 1,3-Dipolar Cycloaddition

The Huisgen's 1,3-dipolar cycloaddition of azides and alkynes to form 1,2,3-triazoles is a model example among the reactions that meet the criteria of click chemistry (Fig. 11).[41] Originally introduced by Barry Sharpless in 1999, click chemistry refers to a group of reactions that generate carbon-heteroatom bonds.

Click chemistry has been successfully applied in many areas, including organic synthesis,[68–72] bioconjugation,[73–75] drug discovery,[4,24,76,77] and polymer and material sciences.[78–81] Huisgen's cycloaddition is preferred since azides and alkynes are easy to implement and are inert in the acidic/basic environments and under physiological conditions. However, spontaneous cycloaddition is very slow, since reaction proceeds only if azide and alkyne in-

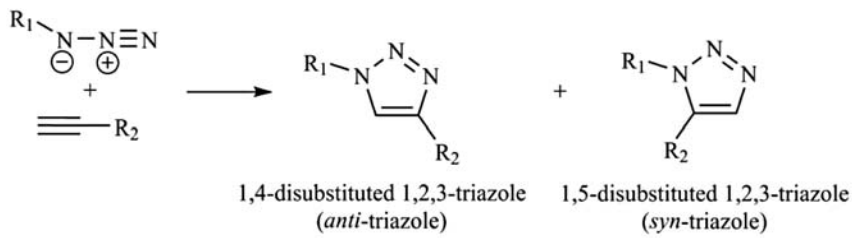

Figure 11. Huisgen's 1,3-dipolar cycloaddition of azides and alkynes.[41]

teract properly oriented. It was only after the discovery of dramatic rate acceleration of the azide-alkyne cycloaddition under copper(I) catalysis that it gained its popularity.[82,83] This reaction exclusively forms 1,4-disubstituted 1,2,3-triazoles (*anti*-triazoles). The 1,5-disubstituted 1,2,3-triazoles (*syn*-triazoles) are prepared by using magnesium acetylides or ruthenium catalysis.[84,85] Recently, efficient recyclable nanocatalysts have been developed for regioselective synthesis of 1,2,3-triazoles in water.[86] Thermal reaction is extremely slow and gives a mixture of isomers which are chromatographically separable. In addition, 1,2,3-triazole moieties have some favourable physicochemical properties attractive for application to the drug discovery and biomedicine. They are very stable to both metabolic and chemical degradation, being inert to hydrolytic, oxidizing, and reducing conditions, even at higher temperatures.[25] Due to resemblance with amide moiety in size, dipolar moment, and H-bond acceptor capacity, the 1,2,3-triazole ring can serve as its non-classic bioisostere.[44,45,87,88] Since 1,2,3-triazoles are basic aromatic heterocyclic compounds, they are bioisosteres of aromatic rings and double bonds.[65,66] Additionally, the aforementioned physicochemical properties of 1,2,3-triazole moiety together with similarity to amide bond, make it a useful linker to generate "twin drugs",[42,67,83] bidentate inhibitors,[83–85,89] linkers to immobilized fluorescent tags or small molecules,[71] and anion receptors.[90]

4. 2. *In situ* Click Chemistry Using Acetylcholinesterase as a Template

Inspired by a report by Mock *et al.* on dramatic rate acceleration of azide and alkyne cycloaddition by sequestering azide and alkyne moieties inside the cavity of cu-

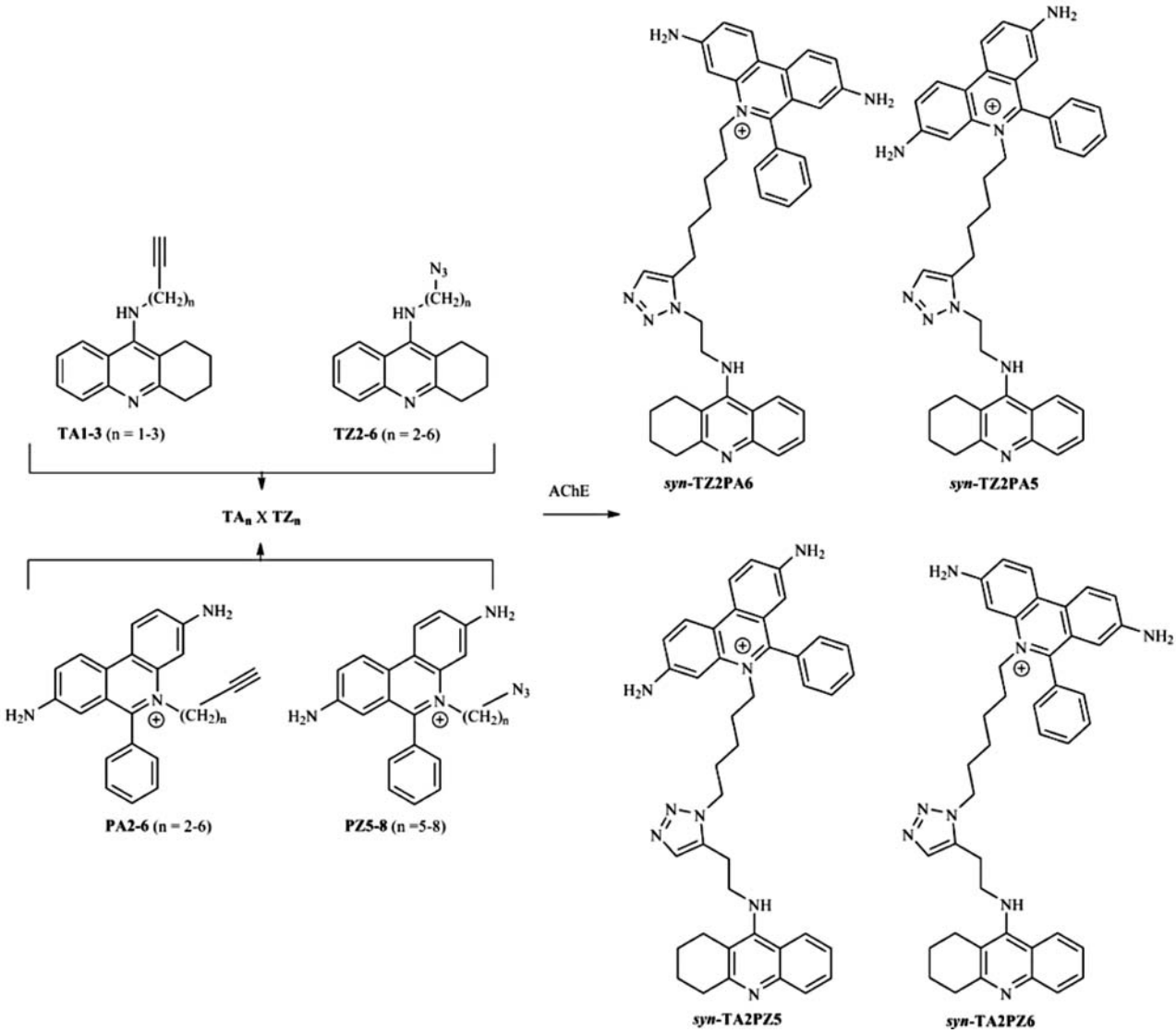

Figure 12. *In situ* click chemistry screening of binary mixtures of tacrine/phenylphenanthridinium-based building blocks for the discovery of bivalent inhibitors to AChE.[91,98]

curbituril, a macrocycle made of glycouril,[89] Lewis *et al*. were the first to investigate the potential of Huisgen's cycloaddition for application to target-guided synthesis.[91] In their proof-of-concept study, they selected enzyme acetylcholinesterase (AChE; EC 3.1.1.7) which plays a vital role in neuro-transmission in central and peripheral nervous system.[92,93] The active site of AChE is a narrow gorge with the catalytic binding site located at its bottom. The second binding site, known as peripheral site, is at the rim of the active site.[94,95] Since reversible AChE inhi-

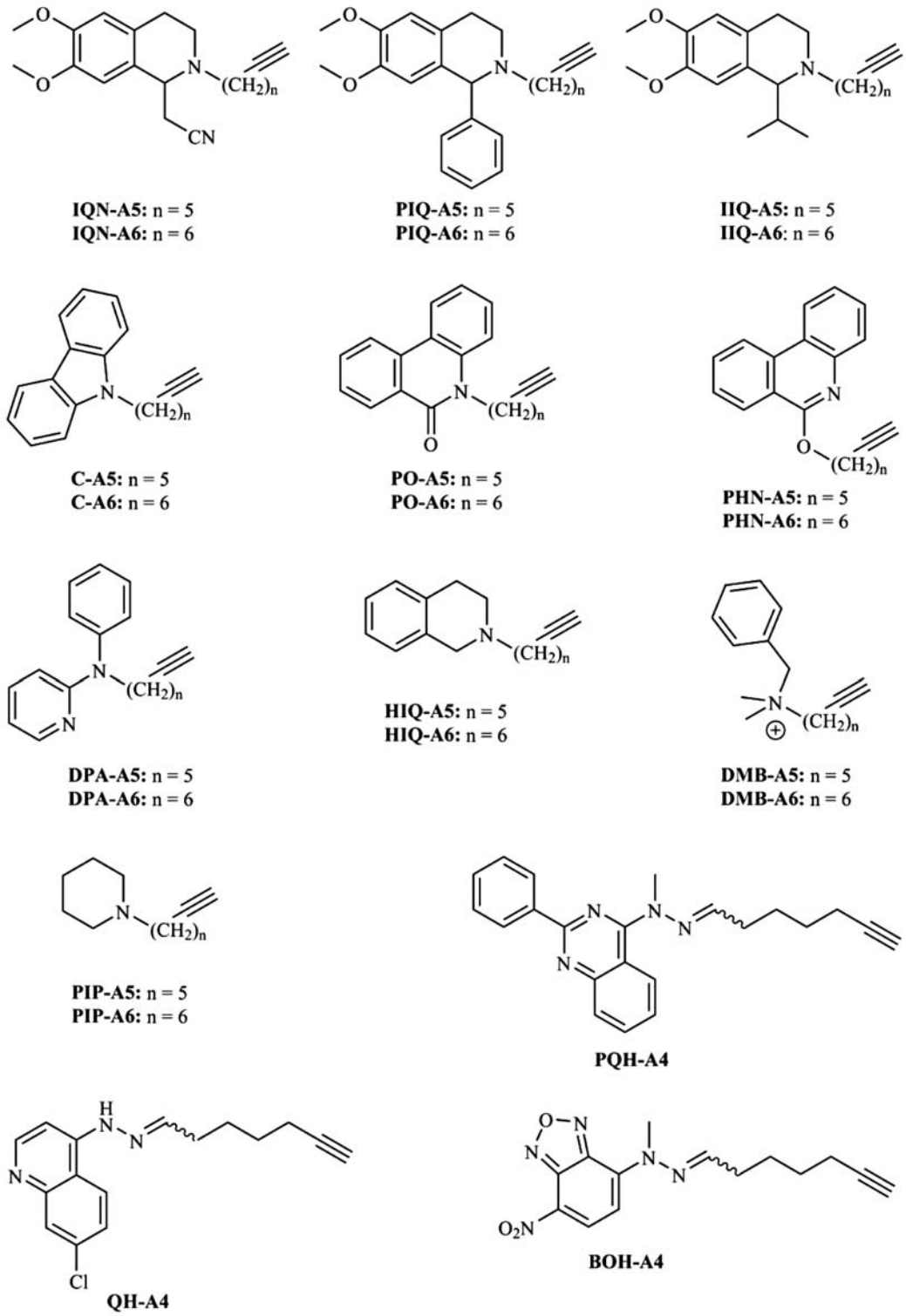

Figure 13. A library of acetylene building blocks for *in situ* click chemistry screening of AChE.[106]

bitors are used clinically to treat neurodegenerative disorders, such as Alzheimer's disease,[96] various small-molecule ligands specific for each binding site have been developed, together with such which simultaneously bind to both sites and therefore possess higher affinity for AChE.[97–99] Moreover, dimerization of an inactive fragment of a selective and potent reversible AChE inhibitor Huperzine A has shown that an inactive ligand can be transformed into highly potent inhibitors.[100] To address the possibility of self-assembly of bivalent AChE inhibitors *via* Huisgen's cycloaddition, Lewis *et al.* used a library of known site-specific inhibitors based on tacrine (a catalytic site binder with K_d of 18 nM) and phenylphenanthridinium (a peripheral site binder with K_d of 1.1 μM) derivatized with alkyl chains bearing terminal azide and alkyne moieties (Fig. 12).[99,100]

Each of the binary mixtures was incubated with AChE at room temperature for 6 days. Upon examination of binary mixtures, it was established that only **TZ2 + PA6** combination gave a detectable amount of the triazole product.[101] Blocking the active site with reversible (tacrine) or irreversible (diisopropyl fluorophosphate) inhibitor blocked formation of the triazole product, confirming that the active site is a template for reaction. HPLC analysis revealed that the enzyme-templated product is exclusively a *syn*-izomer. A comparison of the dissociation constant of *syn*-**TZ2PA6** (K_d is 77 fM) and *anti*-**TZ2PA6** (K_d is 720 fM) showed that AChE templated the formation of a more potent inhibitor. Comparison of kinetic parameters and literature data for related non-covalent inhibitors of AChE, revealed that *in situ* generated *syn*-**TZ2PA6** was the most potent non-covalent AChE inhibitor known at the time.[99,102–104]

Manetsch *et al.* revisited the AChE system to screen for additional *in situ* hits.[105] LC/MS analysis revealed three new hit compounds – **TZ2PA5**, **TA2PZ6**, and **TA2PZ5** – in addition to the **TZ2PA6**. All of the products were identified as *syn*-isomers with dissociation constants in femtomolar and picomolar range. Krasiński *et al.* substituted phenylphenanthridinium moeity with aromatic heterocycles that were not previously known to interact with AChE while tacrine building block **TZ2** was chosen as an "anchor molecule" (Fig. 13).[106]

Analysis of binary **TZ2**/acetylene mixtures with AChE revealed that only phenyltetrahydro-isoquinolines **PIQ-A5** and **PIQ-A6** formed significant amounts of triazole products identified as *syn*-isomers. Incubation of a mixture of 10 acetylene building blocks with **TZ2** and AChE gave only expected triazole products **TZ2PIQ-A5** and **TZ2PIQ-A6** demonstrating the feasibility of multicomponent screening. With the equilibrium dissociation constant of only 33 fM, **TZ2PIQ-A5** surpasses the inhibition potency of *syn*-**TZ2PA6**.

Beside the development of potent reversible AChE inhibitors for treating Alzheimer's disease, another kind of medical treatment has preoccupied the attention of researchers in the field. Organophosphorus (OP) nerve agents acting as irreversible AChE inhibitors represent a constant threat to the general population because of their use as warfare agents in armed conflicts and terrorist attacks or as pest control agents.[107,108] Thus, the current therapy in case of OP nerve agent poisonings includes an AChE reactivator of the quaternary pyridinium oxime family.[109,110] However, due to their permanent positive charge, these compounds do not readily cross the blood-brain barrier and thus cannot reactivate AChE in the central nervous system.[111] Therefore, attempts have been made to develop centrally acting reactivators using click-chemistry approach.[112,113] The AChE related enzyme butyrylcholinesterase (BChE) is present in the plasma in high concentrations and differs in the amino acid composition.[114,115] BChE is capable of hydrolyzing a variety of esters and plays an important role in the bioconversion of carbamates and other ester-based prodrugs.[116–118] Both AChE and BChE display selectivity and stereoselectivity in interaction with reversible or irreversible inhibitors, various esters and carbamates.[119–123] The *in situ* click-chemistry approach may help in the development of novel chiral reactivators tailored by cholinesterase itself thus avoiding cumbersome synthetic procedures and/or enantiomer separation.

4. 3. *In situ* Click Chemistry Experiments with Acetylcholine Binding Protein

Recently, Grimster *et al.* reported the preparation of ligands for nicotinic acetylcholine receptors (nAChRs) *via in situ* click chemistry thus expanding the templation potential of this approach to more flexible intersubunit binding sites.[124] As a member of a superfamily of neurotransmitter ligand-gated ion channels, nAChRs have been investigated as therapeutic targets for medical treatment of central nervous system (CNS) disorders such as schizophrenia, nicotine addiction, and Alzheimer's disease.[125–127] However, the development of novel and potent ligands for specific receptor subtypes using classical drug discovery approaches has been difficult because of the nAChR membrane disposition, receptor subtypes diversity, and the dynamic nature of the binding site. Grimster *et al.* turned their attention to the *in situ* click chemistry approach with the acetylcholine binding protein (AChBP) as a structural surrogate for nAChRs.[124] AChBPs are homologous to the *N*-terminal 210 amino acids in the extracellular receptor domain with flexible subunit interface, thus imitating recognition properties of nAChRs. Initially, screening the triazole library synthesized under standard Cu-catalyzed azide alkyne cycloaddition reaction conditions against AChBPs from *Lymnaea stagnalis* (*Ls*), *Aplysia californica* (*Ac*), and the Y55W *Aplysia californica* mutant (*Ac*Y55W) revealed compound **26** as the strongest binder to all three nAChR surrogates, with the dissociation constant in the nanomolar range for *Ls* AChBP (Fig. 14).

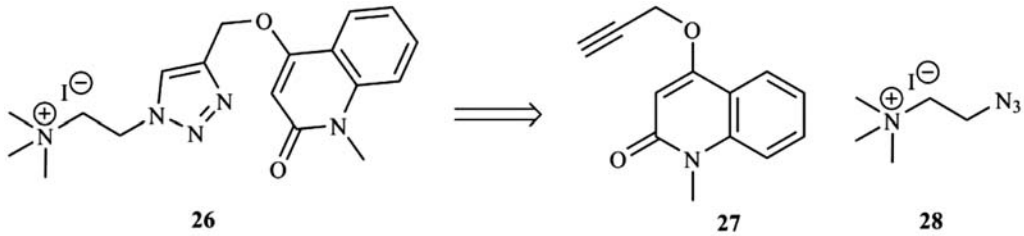

Figure 14. Compound **26** with high affinity to *Lymnaea stagnalis*, *Aplysia californica*, and the Y55W *Aplysia californica* mutant AChBPs and constituent alkyne **27** and azide **28** shown in retrosynthetic representation.[124]

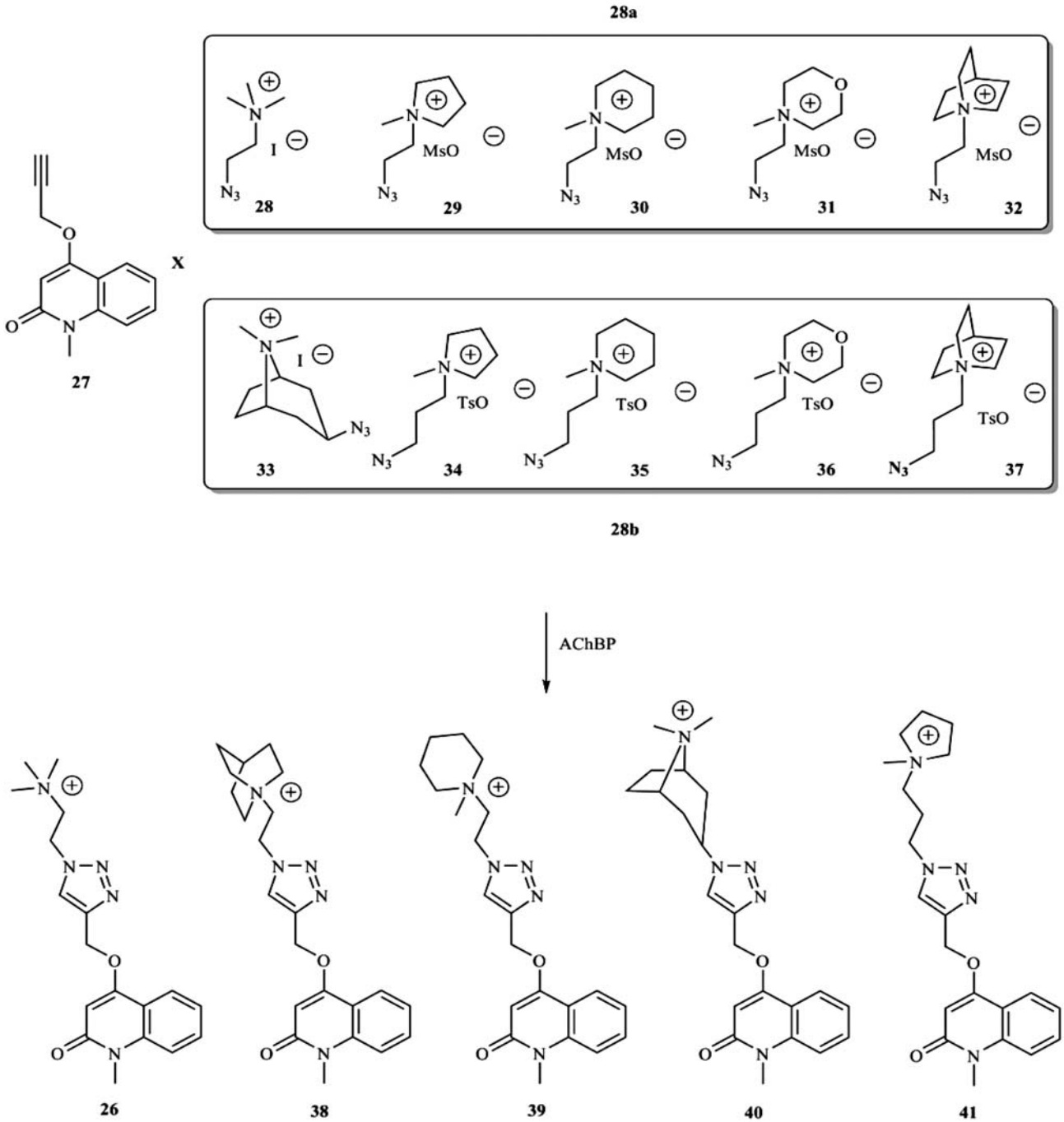

Figure 15. *In situ* click chemistry screening of azide libraries **28a** and **28b** against alkyne **27**.[124]

To confirm that flexible subunit interfaces in the AChBPs are capable to template the formation of **26**, the constituent alkyne **27** and azide **28** were incubated in the presence of *Ls*, *As*, and *Ac*Y55W AChBPs in sodium phosphate buffer at room temperature for 3 days. Analysis of the reaction mixture by LC/MS–SIM method confirmed that *Ls* AChBP successfully catalyzed the formation of compound **26**, while both *Ac* and *Ac*Y55W AChBPs gave the product but in much lower amount. Control reaction with *Ls* AChBP inhibited with a known competing ligand methyllycaconitine (MLA) gave a relatively low amount of product, thus confirming that the ACh binding site at flexible subunit interface indeed served as the template for the cycloaddition reaction. The search for new compounds with improved affinity and selectivity for closely related AChBPs continued using triazole **26** as a lead. Azide libraries **28a** and **28b** comprising building blocks with quaternary nitrogen centers, were incubated with alkyne **27** in the presence of *Ls*, *As*, and *Ac*Y55W AChBPs at room temperature for 3 days (Fig. 15).

LC/MS–SIM analysis revealed that *Ls* AChBP catalyzed the formation of triazole products **26**, **38**, **39**, **40**, and **41** more efficiently than *Ac* or *Ac*Y55W AChBPs. It was also shown that the amount of *in situ* generated product is related to its affinity to the specific AChBP. For instance, the most amplified triazole **40** was shown to possess the highest affinity (K_d = 0.96 nM) to *Ls* AChBP. Next, the alkyne library with the previously tested quinolone derivative **27** and diversely substituted aryl propargyl ethers was incubated with azide **33** in the presence of *Ls*, *Ac*, and *Ac*Y55W AChBPs. LC/MS–SIM analysis revealed that all of the tested alkynes underwent AChBP-templated cycloaddition reactions with azide **33**. However, the previously described triazole **40** was again formed in the highest amount with the highest affinity for all AChBPs. Finally, azides **28**–**37** were mixed with alkynes in the presence of *Ls* AChBP for 10 days. Analysis revealed that **40** was formed in the greatest amount, thus demonstrating that *Ls* AChBP can catalyze the formation of the highest affinity product from a bulk of various azides and alkynes present in the reaction mixture, analogously to the AChE system. All *in situ* click chemistry experiments with AChBPs included BSA control reaction which exhibited no product formation. Crystal structure of triazole **40** in complex with *Ac* AChBP confirmed a bound conformation, and a pose predicted from previously seen conformations of quaternary amines that bind to nAChRs through cation-quadrupole interactions involving π-electron-rich aromatic side chains (*e.g.*, tryptophan).[128] Triazole moiety forms a hydrogen bond with a neighbouring water molecule which again suggests that precursors in *in situ* click chemistry drive a conformation preferred by the triazole product rather than accommodating a conformation of the free protein, a fact previously reported for the AChE system.

4. 4. DNA Minor Groove Templation Role

The templation potential of *in situ* click chemistry can be expanded to the minor groove of double-helical DNA, as shown by Poulien-Kerstien and Dervan[129] and more recently by Imoto *et al.*[130] In their pioneer work, Poulien-Kerstien and Dervan explored the Huisgen's cycloaddition to link two aromatic-substituted hairpin polyamides capable of sequence-specific binding to DNA in the DNA-templated reaction. Polyamides composed of three aromatic amino acids, *N*-metylpyrrole (Py), *N*-methylimidazole (Im), and *N*-methyl-3-hydroxypyrrole, distinguish four Watson–Crick base pairs by a set of pairing rules and represent a potential way to modulate transcription.[131] Longer binding-site size is considered to be crucial for application in gene regulation since longer sequences should occur less frequently in genome leading to the development of various polyamide motifs for selective targeting.[132,133] The most promising strategy came from chemical ligation of two hairpin polyamides to form dimers.[134,135] However, though having an excellent affinity and specificity to 10 base pair (bp) DNA sequences, hairpin dimers lack the cell and nuclear uptake properties of smaller hairpins, apparently due to size and shape.[136] Six-ring hairpin polyamides with alkyne **42a** and **42b** or azide **43a** and **43b** moieties with different linker lengths were designed so that their matching sites are adjacent on the DNA, which allows the formation of hairpin dimers *in situ* (Fig. 16).[137–140]

Experiments were carried out at 37 °C at pH 7.0 with equimolar concentrations of one azide, one alkyne and DNA duplex A (1 μM). When any pair of hairpin polyamides (**42a** + **43a**, **42a** + **43b**, **42b** + **43a**, **42b** + **43b**) was combined in solution, HPLC analysis of the reaction mixtures (verified using matrix-assisted laser desorption/ionization-time of flight mass spectrometry) revealed significant acceleration of formation of hairpin dimers in the presence of DNA template with respect to the nontemplated reaction between **42a** and **43a**. The rate of dimer formation from **42a** and **43b** was slower than the rate of formation from **42a** and **43a**, presumably due to the additional flexibility in the linker of **43b**, which allows the reactants to more freely adopt nonproductive conformation. Also, the rate of product formation from pairings of **42b** with **43a** and **43b** is decreased due to the differences in the reactivity between **42a**, activated with an electron withdrawing group (EWG), and EWG-free alkyne **42b**. Moreover, when the alkynyl reactant is substituted with an EWG, stereoelectronics of the reaction pathway favoured formation of 1,4-regioisomer.[141] Thermal reaction between **42a** and **43a** or **43b** afforded predominantly the 1,4-regioisomeric products, while DNA-templated reactions afforded them exclusively. When the EWG-free alkyne **42b** was paired with either **43a** or **43b**, each thermal reaction produced two corresponding regioisomers in a ratio of 1:1, while DNA-templated reaction produced only a single isomer (**42b** + **43a**) or a ratio of 3:1 (**42b** + **43b**).

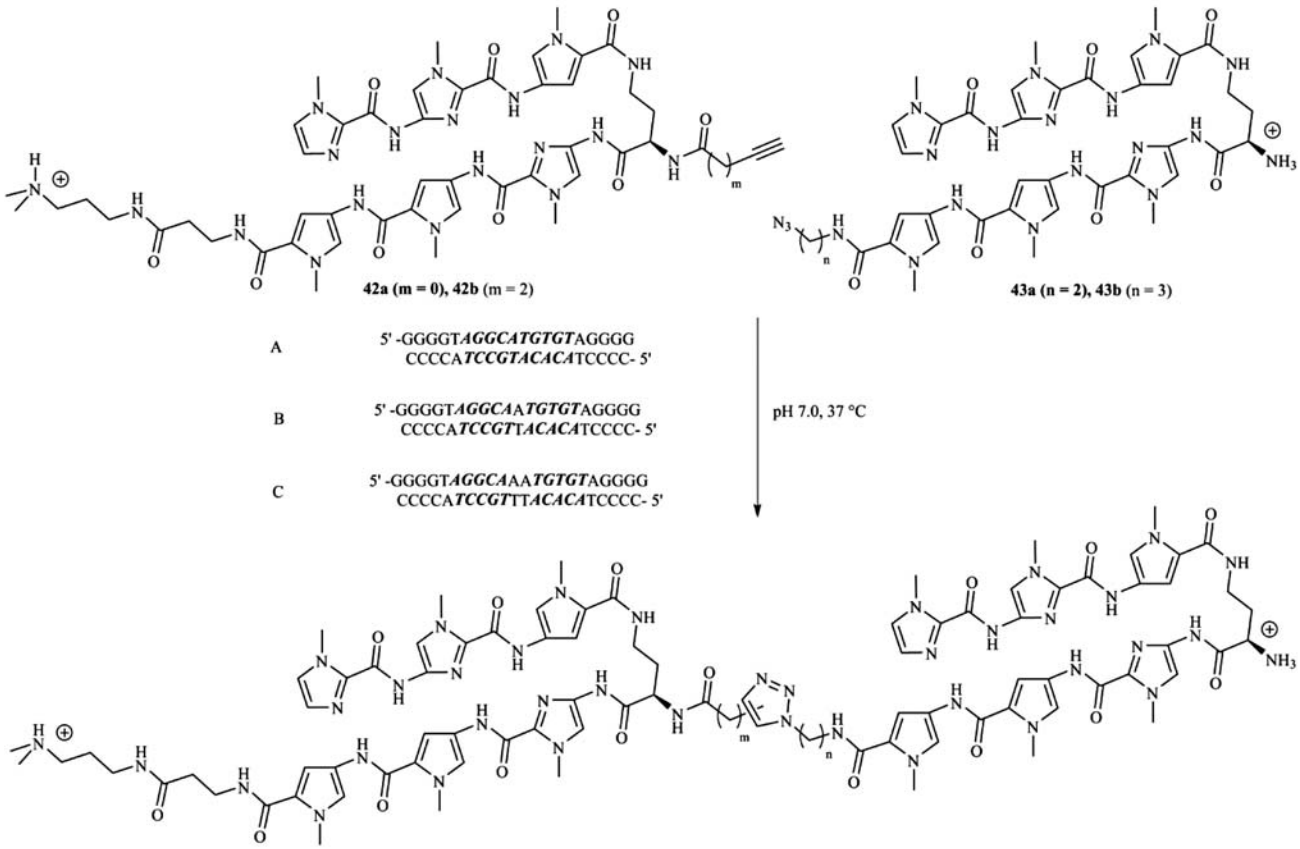

Figure 16. DNA-templated dimerization of hairpin polyamides on DNA duplexes with hairpin binding sites separated with zero (A), one (B), or two (C) base pairs.[130]

DNA-templated cycloadditions were found to be sensitive upon separation of the hairpin-binding sites with additional bp. Thus, upon insertion of one bp between two adjacent five bp hairpin-binding sites for the hairpin polyamides **42a**,**b** and **43a**,**b** (DNA duplex B), the only product formed from **42b** and **43b** was detected with about 50% yield. When two intervening bp were inserted (DNA duplex C), no product was detected using various pairs of hairpin polyamides. DNA-templated cycloadditions were also found to be sensitive upon DNA sequence of the two hairpin-binding sites, as illustrated by the mismatch tolerance study of optimal pair **42a** and **43a**. When a single bp mismatch is present under azide hairpin polyamide-binding or under each of the two harpin-binding sites, the rate of the hairpin dimer-forming cycloaddition is nearly halved or lowered over 2.5 fold, respectively. However, when the concentration of reacting hairpins **42a** and **43a** was varied from 1 μM to 0.5 μM, a threshold concentration that defined the ability of hairpins to distinguish between match site and double bp mismatch site was detected somewhere between 1 μM and 0.75 μM. The authors suggested that, at some lower concentration, an additional threshold exists that allows hairpins to distinguish the match site from a single bp mismatch site, rendering the possibility to increase the ratio of hairpin dimer formation on match over mismatch DNA and the overall hairpin dimer yield.

Recently, Di Antonio *et al.* have demonstrated the ability of the *in situ* click chemistry multicomponent approach to identify potent and selective small molecules binding a region of chromosomes formed by guanine-rich sequences of DNA called G-quadruplex (G4).[142] In their study, they selected G4 formed by the human telomeric DNA (H-Telo).[143] No adduct was formed when the reaction mixture was incubated in the absence of DNA, in the presence of double-stranded DNA, or in the presence of telomeric oligonucleotides pre-annealed to prevent G4 formation, thus confirming that H-Telo serves as a reaction pot. Moreover, adducts obtained from a reaction conducted in the presence of RNA G4-structure demonstrated selective RNA versus DNA G4 structure binding. More recently, Glassford *et al.* have expanded the templation potential of the *in situ* click chemistry to *E. coli* 70S ribosomes or their 50S subunits and thus synthesized potent macrolide antibiotics that target bacterial ribosome.[144] Also, the *in situ* click chemistry approach has been applied to explore the conformational space of the ligand binding site of a *M. tuberculoisis* transcriptional repressor EthR which regulates the transcription of monooxygenase EthA and thus controls the sensitivity of *M. tuberculoisis* to an-

tibiotic ethionamide. The *in situ* formed inhibitor, displayed 10-fold higher activity than the starting azide, and induced a significant conformational change of the ligand-binding domain of EthR.[145]

5. Iterative *in situ* Click Chemistry

In addition to the development of coupled bivalent enzyme inhibitors targeting the active site, *in situ* click chemistry can produce multivalent ligands active on protein surface, such as allosteric, interfacial, or non-functional surface sites. Once a bivalent ligand has been formed *via in situ* approach from the corresponding azide and alkyne building blocks, that biligand can serve as an anchor ligand for the identification of a triligand, and so forth, in a so-called iterative *in situ* click chemistry approach. This approach has been successfully introduced by Agnew *et al.* to identify a triligand antibody-like capture agent against human or bovine CA-II (h(b)CA-II) (Fig. 17).[146]

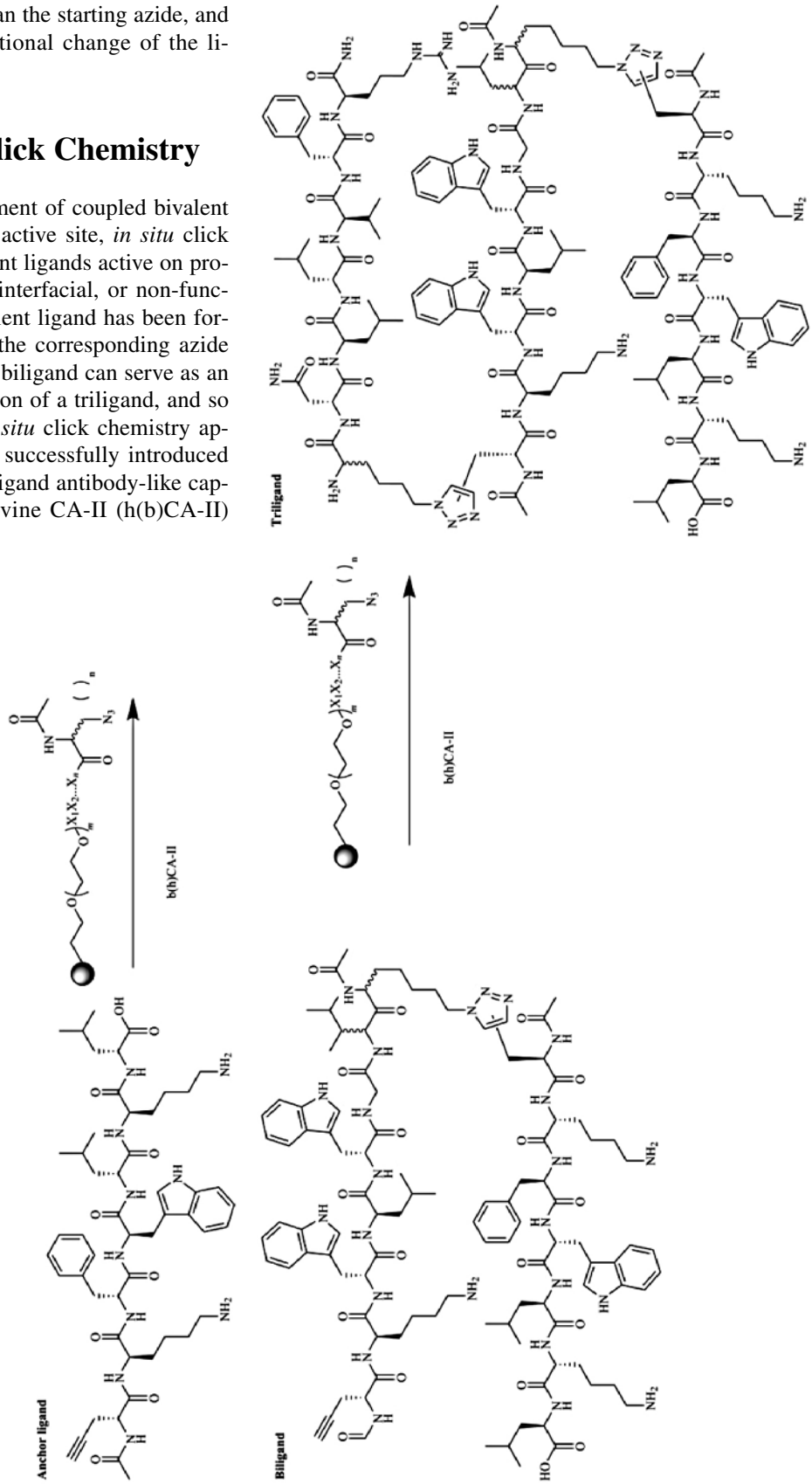

Figure 17. Iterative *in situ* click chemistry approach for developing triligand capture agent for human or bovine carbonic anhydrase II (b(h)CA-II).[146]

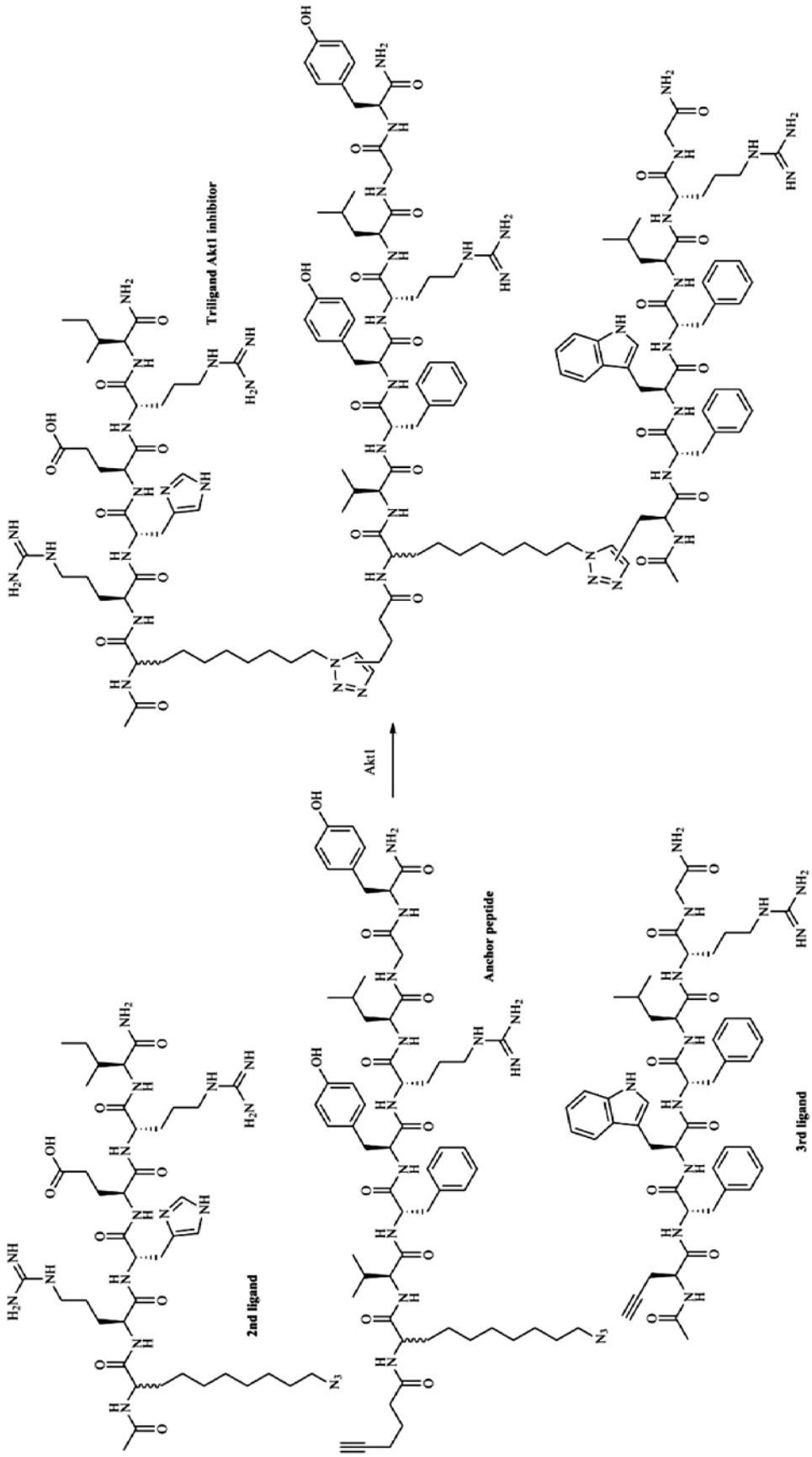

Figure 18. *In situ* click chemistry approach for developing triligand capture agent/inhibitor for Akt1 kinase.[150]

The first anchor ligand was identified by screening a comprehensive one-bead-one-compound (OBOC) peptide library consisting of short chain peptides, against fluorescently labelled bCA-II.[147,148] Analysis of the position-dependent frequency of amino acids identified the anchor ligand, a short heptapeptide comprised of non-natural D-amino acids and a terminal, acetylene-containing amino acid D-propargylglycine (D-Pra), showing an approximately 500 μM affinity for bCA-II. This anchor ligand was used in the second screen against the OBOC peptide library, in which peptides were modified with an azide linker, in the presence of bCA-II to identify the triazole product showing a 3 μM binding affinity for bCA-II. The screen was repeated with this terminal D-Pra-containing biligand as the new anchor unit to identify a triligand, which exhibited strong binding affinities against bCA-II (64 nM) and hCA-II (45 nM). However, no regioselectivity was observed for the two triazoles in the triazole capture agent. On-bead, protein-templated triligand formation was confirmed by an enzyme-linked colorimetric assay containing a biotin conjugate of the biligand anchor.[149] The triligand was only formed in the presence of b(h)CA-II, and not when b(h)CA-II was absent or other proteins (transferrin, BSA) used instead. Similarly, on-bead, protein-templated formation was not observed when the incorrect biligand anchor was used. The triligand did not interfere with bCA-II intrinsic esterase activity, which indicated that it binds away from the active site.

The strategy described was also applied to identify a high-specificity, triligand capture agent/inhibitor for Akt1 kinase.[150] Akt1 kinase is responsible for signal transduction from the plasma membrane to downstream effector molecules that control cell growth, apoptosis, and translation.[151] To ensure the development of an allosteric site inhibitor, Millward *et al.* carried out an initial screen against a large OBOC peptide library on a kinase preinhibited with an ATP-competitive inhibitor, **Ac7**.[150] One of the *N*-terminal azido-amino acid-containing peptides generated in the initial screen showed almost 95% inhibition of the Akt1 kinase in the absence and presence of the conjugated small molecule inhibitor and was therefore employed as an anchor for biligand development (Fig. 18).

The most promising candidate from biligand screens was modified with 5-hexynoic acid at the *N*-terminus and used as an anchor ligand for triligand development which finally resulted in the tertiary peptide containing two triazole moieties. An analytical assay based on immune-PCR[152] revealed that the click reaction between the on-bead secondary peptide and the soluble anchor peptide was approximately 10-fold more efficient in the presence of Akt1 than in its absence, confirming the requirement for the target protein to template the click reaction. The biligand showed 100-fold improvement in its affinity for Akt relative to the anchor peptide, while the triligand showed 2–3 fold affinity gain for Akt1 (K_d = 200 nM). The specificity characterization of the anchor, biligand, and triligand for a panel of His-tagged protein kinases revealed that the anchor was very specific for the Akt1 protein, with only modest cross-reactivity to GSK3β protein kinase. The biligand showed reduced specificity, with significant binding to GSK3β. For the triligand, binding to GSK3β was reduced to the level observed for the anchor peptide. These observations indicate that large improvements in affinity may come at the expense of reduced specificity, whereas increased specificity is not necessarily accompanied by increased affinity. This inverse correlation between affinity and selectivity is in accordance with previous studies on small molecule protein kinase inhibitors,[153] antibody–small molecule interactions,[154] DNA–protein interactions,[155] and protein–protein interactions.[156] Measuring Akt1 kinase activity under varying substrate and triligand concentrations eliminated the possibility of a competitive mode of Akt1 inhibition by the triligand with respect to ATP and peptide substrates.[150] This confirmed that the triligand binds to a location away from the active site of the kinase and that inhibition occurs *via* an allosteric mechanism. Finally, the anchor, biligand, and triligand were tested for the ability to recognize Akt from the ovarian cancer cell line OVCAR3 in immunoprecipitation (IP) experiments. IP experiments confirmed the increased affinity of the biligand relative to the anchor peptide in OVCAR3 cell lysates from both cells stimulated with a combination of epidermal growth factor (EGF) and insulin and from untreated control cells. The triligand showed somewhat increased IP of Akt relative to the biligand only in lysates from induced cells. However, an analysis of the total IP protein by SDS-PAGE electrophoresis showed low non-selective binding for all ligands. The authors observed IP of the protein that likely corresponds to the GSK3β kinase by the triligand, and to a lesser degree, by the anchor and the biligand.[150] The underlying rationale for GSK3 binding to ligands is yet to be explained. However, IP experiments confirm the increase in capture efficiency of ligands, particularly in stimulated cells, as they are being translated from anchor to triligand with their affinity and selectivity criteria increased.

6. Conclusion

Receptor-based combinatorial chemistry is a promising strategy developed for identifying possible leads in drug discovery whereby the biomolecular target of interest is used to "fish out" building blocks that couple into high affinity compounds. Theoretical studies have shown that, unless excessive amounts of a molecular target are used, high affinity compounds have a high probability of being significantly amplified over other possible combinations of building blocks. Also, any significantly amplified compound is guaranteed to be a high affinity compound.

The examples listed in this review have illustrated the potential of various receptor-based combinatorial che-

mistry approaches to identify high affinity compounds and, in some occasions, their potential to elucidate the binding modes of substrates to their biomolecular target.

The *in situ* click chemistry approach combines building blocks through 1,3-dipolar cycloaddition of azides and alkynes (Huisgen's cycloaddition). This approach is predominantly used for the discovery of enzyme inhibitors targeting enzyme active sites as illustrated with examples from the AChE system, although the templation potential of this approach can be extended to more flexible intersubunit binding sites and even minor groove of double-helical DNA. Examples from AChE and AChBP systems have shown that *in situ* click chemistry allows one to freeze in-frame conformations that associate with high-affinity inhibitors and are normally not detected by conventional structural methods. These findings set out a stage for developing unusual strategies of drug design where the most selective compounds would induce distinctive conformations of the target.

More efficient and synergistic approaches that combine receptor based combinatorial chemistry with *in silico* methods such as *de novo* structure based design (SBD) or molecular docking studies limit the selection of the coupling partners that have to be incubated with protein target to the ones based on retrosynthesis of *in silico* designed hits thus indicating that the full potential of receptor based combinatorial chemistry in drug discovery is yet to be discovered.[157,158]

7. Acknowledgements

This work was supported by the Croatian Science Foundation (Grant HRZZ 4307 PI: Z. Kovarik).

8. References

1. R. S. Bohacek, C. McMartin, W. C. Guida, *Med. Res. Rev.*, **1996**, *16*, 3–50. https://doi.org/10.1002/(SICI)1098-1128(199601)16:1<3::AID-MED1>3.0.CO;2-6
2. H. N. Weller, D. S. Nirschl, E. W. Petrillo, M. A. Poss, C. J. Andres, C. L. Cavallaro, M. M. Echols, K. A. Grant-Young, J. G. Houston, A. V. Miller, R. T. Swann, *J. Comb. Chem.*, **2006**, *8*, 664–669. https://doi.org/10.1021/cc050164h
3. St.L. Dixon, H. O. Villar, *J. Chem. Inf. Comp. Sci.*, **1998**, *38*, 1192–1203. https://doi.org/10.1021/ci980105+
4. J. D. Cheeseman, A. D. Corbett, J. L. Gleason, R. J. Kazlauskas, *Chem. Eur. J.*, **2005**, *11*, 1708–1716. https://doi.org/10.1002/chem.200400371
5. R. Huisgen, G. Szeimies, L. Moebius, *Chem. Ber.*, **1967**, *100*, 2494–2507. https://doi.org/10.1002/cber.19671000806
6. R. Huisgen, In: 1,3-Dipolar cycloaddition – introduction, survey, mechanism., A. Padwa, Ed., Wiley: New York, **1984**, Vol. 1, pp. 1–176.
7. P. T. Corbett, J. Leclaire, L. Vial, K. R. West, J.-L. Wietor, J. K. M. Sanders, S. Otto, *Chem. Rev.*, **2006**, *106*, 3652–3711. https://doi.org/10.1021/cr020452p
8. M. Mondal, A. K. Hirsch, *Chem. Soc. Rev.*, **2015**, *44*, 2455–2488. https://doi.org/10.1039/C4CS00493K
9. Y. Kubota, S. Sakamoto, K. Yamaguchi, M. Fujita, *Proc. Natl. Acad. Sci. USA*, **2002**, *99*, 4854–4856. https://doi.org/10.1073/pnas.082643499
10. M. S. Congreve, D. J. Davis, L. Devine, C. Granata, M. O'Reilly, P. G. Wyatt, H. Jhoti, *Angew. Chem., Int. Ed.*, **2003**, *42*, 4479–4482. https://doi.org/10.1002/anie.200351951
11. S. Otto, *J. Mater. Chem.*, **2005**, *15*, 3357–3361. https://doi.org/10.1039/b500703h
12. A. V. Eliseev, M. I. Nelen, *Chem. Eur. J.*, **1998**, *4*, 825–834. https://doi.org/10.1002/(SICI)1521-3765(19980515)4:5<825::AID-CHEM825>3.0.CO;2-7
13. J. S. Moore, N. W. Zimmerman, *Org. Lett.*, **2000**, *2*, 915–918. https://doi.org/10.1021/ol0055723
14. Z. Grote, R. Scopelliti, K. Severin, *Angew. Chem., Int. Ed.*, **2003**, *42*, 3821–3825. https://doi.org/10.1002/anie.200351623
15. P. T. Corbett, S. Otto, J. K. M. Sanders, *Chem. Eur. J.*, **2004**, *10*, 3139–3143. https://doi.org/10.1002/chem.200400300
16. K. Severin, *Chem. Eur. J.*, **2004**, *10*, 2565–2580. https://doi.org/10.1002/chem.200305660
17. J.-M. Lehn, R. A. Woods, D. H. Bartón, J. E. Corrie, D. A. Widdowson, *Chem. Eur. J.*, **1977**, *5*, 2455–2463. https://doi.org/10.1002/(SICI)1521-3765(19990903)5:9<2455::AID-CHEM2455>3.0.CO;2-H
18. S. J. Rowan, S. J. Cantrill, G. R. L. Cousins, J. K. M. Sanders, J. F. Stoddart, *Angew. Chem., Int. Ed.*, **2002**, *41*, 899– 952. https://doi.org/10.1002/1521-3773(20020503)41:9<1460::AID-ANIE11111460>3.0.CO;2-N
19. I. Huc, J.-M. Lehn, *Proc. Natl. Acad. Sci. USA*, **1997**, *94*, 2106–2110. https://doi.org/10.1073/pnas.94.6.2106
20. M. Hochgürtel, R. Biesinger, H. Kroth, D. Piecha, M. W. Hofmann, S. Krause, O. Schaaf, C. Nicolau, A. V. Eliseev, *J. Med. Chem.*, **2003**, *46*, 356–358. https://doi.org/10.1021/jm025589m
21. O. Ramström, S. Lohmann, T. Bunyapaiboonsri, J.-M. Lehn, *Chem. Eur. J.*, **2004**, *10*, 1711–1715. https://doi.org/10.1002/chem.200305551
22. M. Sindelar, K. T. Wanner, *ChemMedChem*, **2012**, 7, 1678–1690. https://doi.org/10.1002/cmdc.201200201
23. N. Nazarpack-Kandlousy, J. Zweigenbaum, J. Henion, A.V. Eliseev, *J. Comb. Chem.*, **1999**, *1*, 199–206. https://doi.org/10.1021/cc980036b
24. B. Shi, R. Stevenson, D. J. Campopiano, M. F. Greaney, *J. Am. Chem. Soc.*, **2006**, *128*, 8459–8467. https://doi.org/10.1021/ja058049y
25. O. Ramström, J.-M. Lehn, *Chem. Bio. Chem.*, **2000**, *1*, 41– 48. https://doi.org/10.1002/1439-7633(20000703)1:1<41::AID-CBIC41>3.0.CO;2-L
26. L. Milanesi, C.A. Hunter, S.E. Sedelnikova, J.P. Waltho, D. A. Widdowson, *Chem. Eur. J.*, **2006**, *12*, 1081–1087. https://doi.org/10.1002/chem.200500357

27. E. C. Y. Woon, M. Demetriades, E. A. L. Bagg, W. Aik, S. M. Krylova, J. H. Y. Ma, M. Chan, L. J. Walport, D. W. Wegman, K. N. Dack, M. A. McDonough, S. N. Krylov, C. J. Schofield, *J. Med. Chem.*, **2012**, *55*, 2173–2184. https://doi.org/10.1021/jm201417e
28. C. Saiz, V. Castillo, P. Fontán, M. Bonilla, G. Salinas, A. Rodríguez-Haralambides, S. G. Mahler, *Mol. Diversity*, **2014**, *18*, 1–12. https://doi.org/10.1007/s11030-013-9485-3
29. S.-A. Poulsen, L.F. Bornaghi, *Bioorg. Med. Chem.*, **2006**, *14*, 3275–3284. https://doi.org/10.1016/j.bmc.2005.12.054
30. P. K. Mehta, P. Christen, *Adv. Enzymol. Relat. Areas Mol.*, **2000**, *74*, 129–184.
31. K. M. El-Mahdy, A. M. El-Kazak, M. Abdel-Megid, M. Seada1, O. Farouk, *Acta Chim. Slov.* **2016**, *63*, 18–25. https://doi.org/10.17344/acsi.2015.1555
32. Z. Fang, W. He, X. Li, Z. Li, B. Chen, P. Ouyang, K. Guo, Bioorg. *Med. Chem. Lett.*, **2013**, *23*, 5174–5177. https://doi.org/10.1016/j.bmcl.2013.07.011
33. H. Lis, N. Sharon, *Chem. Rev.*, **1998**, *98*, 637–674. https://doi.org/10.1021/cr940413g
34. N. R. Rose, E. C. Y. Woon, G. L. Kingham, O. N. F. King, J. Mecinović, I. J. Clifton, S. S. Ng, J. Talib-Hardy, U. Oppermann, M. A. McDonough, C. J. Schofield, *J. Med. Chem.*, **2010**, *53*, 1810–1818. https://doi.org/10.1021/jm901680b
35. A. J. Clipson, V. T. Bhat, I. McNae, A. M. Caniard, D. J. Campopiano, M. F. Greaney, *Chem. – Eur. J.*, **2012**, *18*, 10562–10570. https://doi.org/10.1002/chem.201201507
36. V. T. Bhat, A. M. Caniard, T. Luksch, R. Brenk, D. J. Campopiano, M. F. Greaney, *Nat. Chem.*, **2010**, *2*, 490–497. https://doi.org/10.1038/nchem.658
37. B. Shi, M. F. Greaney, *Chem. Commun.*, **2005**, *7*, 886–888. https://doi.org/10.1039/b414300k
38. C. Andersson, E. Mosialou, A. E. Adang, G. J. Mulder, A. van Der Gen, R. Morgenstern, *J. Biol. Chem.*, **1991**, *266*, 2076–2079.
39. R. M. F. Cardoso, D. S. Daniels, C. M. Bruns, J. A. Tainer, *Proteins*, **2003**, *51*, 137–146. https://doi.org/10.1002/prot.10345
40. H. Xiangdong, R. Manetsch, *Chem. Soc. Rev.*, **2010**, *39*, 1316–1324. https://doi.org/10.1039/b904092g
41. H. C. Kolb, M. G. Finn, K. B. Sharpless, *Angew. Chem., Int. Ed.*, **2001**, *40*, 2004–2021. https://doi.org/10.1002/1521-3773(20010601)40:11<2004::AID-ANIE2004>3.0.CO;2-5
42. H. C. Kolb, K. B. Sharpless, *Drug Discovery Today*, **2003**, *8*, 1128–1137. https://doi.org/10.1016/S1359-6446(03)02933-7
43. K. B. Sharpless, R. Manetsch, *Expert Opin. Drug Discovery*, **2006**, *1*, 525–538. https://doi.org/10.1517/17460441.1.6.525
44. J. Inglese, S. J. Benkovic, *Tetrahedron*, **1991**, *47*, 2351–2364. https://doi.org/10.1016/S0040-4020(01)81773-7
45. S. E. Greasley, T. H. Marsilje, H. Cai, S. Baker, S. J. Benkovic, D. L. Boger, I. A. Wilson, *Biochemistry*, **2001**, *40*, 13538–13547. https://doi.org/10.1021/bi011482+
46. Y. Yu, L. Ye, K. Haupt, K. Mosbach, *Angew. Chem., Int. Ed.*, **2002**, *41*, 4459–4463. https://doi.org/10.1002/1521-3773(20021202)41:23<4459::AID-ANIE4459>3.0.CO;2-2
47. R. Nguyen, I. Huc, *Angew. Chem., Int. Ed.*, **2001**, *40*, 1774–1776. https://doi.org/10.1002/1521-3773(20010504)40:9<1774::AID-ANIE17740>3.0.CO;2-G
48. T. Maki, A. Kawamura, N. Kato, J. Ohkanda, *Mol. Biosyst.*, **2013**, *9*, 940–943. https://doi.org/10.1039/C2MB25388G
49. E. Oueis, F. Nachon, C. Sabot, P.-Y. Renard, *Chem. Commun.*, **2014**, *50*, 2043–2045. https://doi.org/10.1039/c3cc48871c
50. T. Asaba, T. Suzuki, R. Ueda, H. Tsumoto, H. Nakagawa, N. Miyata, *J. Am. Chem. Soc.*, **2009**, *131*, 6989–6996. https://doi.org/10.1021/ja807083y
51. S. S. Kulkarni, X. Hu, K. Doi, H.-G. Wang, R. Manetsch, *ACS Chem. Biol.*, **2011**, *6*, 724–732. https://doi.org/10.1021/cb200085q
52. N. K. Namelikonda, R. Manetsch, *Chem. Commun.*, **2012**, *48*, 1526–1528. https://doi.org/10.1039/C1CC14724B
53. A. M. Cappalonga Bunn, R. S. Alexander, D. W. Christianson, *J. Am. Chem. Soc.*, **1994**, *116*, 5063–5068. https://doi.org/10.1021/ja00091a006
54. G. S. Ponticello, M. B. Freedman, C. N. Habecker, P. A. Lyle, H. Schwam, S. L. Varga, M. E. Christy, W. C. Randall, J. J. Baldwin, *J. Med. Chem.*, **1987**, *30*, 591–597. https://doi.org/10.1021/jm00387a002
55. J. A. Wells, C. L. McClendon, *Nature*, **2007**, *450*, 1001–1009. https://doi.org/10.1038/nature06526
56. N. N. Danial, S. J. Korsmeyer, *Cell*, **2004**, *116*, 205–219. https://doi.org/10.1016/S0092-8674(04)00046-7
57. T. Oltersdorf, S. W. Elmore, A. R. Shoemaker, R. C. Armstrong, D. J. Augeri, B. A. Belli, M. Bruncko, T. L. Deckwerth, J. Dinges, P. J. Hajduk, M. K. Joseph, S. Kitada, S. J. Korsmeyer, A. R. Kunzer, A. Letai, C. Li, M. J. Mitten, D. G. Nettesheim, S. C. Ng, P. M. Nimmer, J. M. O'Connor, A. Oleksijew, A. M. Petros, J. C. Reed, W. Shen, S. K. Tahir, C. B. Thompson, K. J. Tomaselli, B. L. Wang, M. D. Wendt, H. C. Zhang, S. W. Fesik, S. H. Rosenberg, *Nature*, **2005**, *435*, 677–681. https://doi.org/10.1038/nature03579
58. M. D. Wendt, W. Shen, A. Kunzer, W. J. McClellan, M. Bruncko, T. K. Oost, H. Ding, M. K. Joseph, H. C. Zhang, P. M. Nimmer, S. C. Ng, A. R. Shoemaker, A. M. Petros, A. Oleksijew, K. Marsh, J. Bauch, T. Oltersdorf, B. A. Belli, D. Martineau, S. W. Fesik, S. H. Rosenberg, S. W. Elmore, *J. Med. Chem.*, **2006**, *49*, 1165–1181. https://doi.org/10.1021/jm050754u
59. A. M. Petros, J. Dinges, D. J. Augeri, S. A. Baumeister, D. A. Betebenner, M. G. Bures, S. W. Elmore, P. J. Hajduk, M. K. Joseph, S. K. Landis, D. G. Nettesheim, S. H. Rosenberg, W. Shen, S. Thomas, X. L. Wang, I. Zanze, H. C. Zhang, S. W. Fesik, *J. Med. Chem.*, **2006**, *49*, 656–663. https://doi.org/10.1021/jm0507532
60. X. Hu, J. Sun, H.-G. Wang, R. Manetsch, *J. Am. Chem. Soc.*, **2008**, *130*, 13820–13821. https://doi.org/10.1021/ja802683u

61. C. E. Hoyle, A. B. Lowe, C. N. Bowman, *Chem. Soc. Rev.*, **2010**, *39*, 1355–1387. https://doi.org/10.1039/b901979k
62. W. R. Dichtel, O. S. Miljanic, J. M. Spruell, J. R. Heath, J. F. Stoddart, *J. Am. Chem. Soc.*, **2006**, *128*, 10388–10390. https://doi.org/10.1021/ja063127i
63. R. L. Weller, S. R. Rajski, *Org. Lett.*, **2005**, *7*, 2141–2144. https://doi.org/10.1021/ol0504749
64. P. Wu, A. Feldman, A. K. Nugent, C. J. Hawker, A. Scheel, B. Voit, J. Pyun, J. M. J. Fréchet, K. B. Sharpless, V. V. Fokin, *Angew. Chem., Int. Ed.*, **2004**, *43*, 3928–3932. https://doi.org/10.1002/anie.200454078
65. A. J. Link, M. K. S. Wink, D. A. Tirrell, *J. Am. Chem. Soc.*, **2004**, *126*, 10598–10602. https://doi.org/10.1021/ja047629c
66. N. J. Agard, J. A. Prescher, C. R. Bertozzi, *J. Am. Chem. Soc.*, **2004**, *126*, 15046–15047. https://doi.org/10.1021/ja044996f
67. Q. Wang, T. R. Chan, R. Hilgraf, V. V. Fokin, K. B. Sharpless, M. G. Finn, *J. Am. Chem. Soc.*, **2003**, *125*, 3192–3193. https://doi.org/10.1021/ja021381e
68. D. C. Rees, M. Congreve, C. V. Murray, R. Carr, *Nat. Rev. Drug Discov.*, **2004**, *3*, 660–672. https://doi.org/10.1038/nrd1467
69. D. A. Erlanson, R. S. McDowell, T. O'Brien, *J. Med. Chem.*, **2004**, *47*, 3463–3482. https://doi.org/10.1021/jm040031v
70. D. A. Erlanson, S. K. Hansen, *Curr. Opin. Chem. Biol.*, **2004**, *8*, 399–406. https://doi.org/10.1016/j.cbpa.2004.06.010
71. R. Carr, M. Congreve, C. V. Murray, D. C. Rees, *Drug Discov. Today*, **2005**, *10*, 987–992. https://doi.org/10.1016/S1359-6446(05)03511-7
72. D. Das, T. Chanda, L. Rokhum, *Acta Chim. Slov.*, **2015**, *62*, 775–783.
73. S. B. Shuker, P. J. Hajduk, R. P. Meadows, S. V. Fesik, *Science*, **1996**, *274*, 1531–1534. https://doi.org/10.1126/science.274.5292.1531
74. A. Schuffenhauer, S. Ruedisser, A. Marzinzik, W. Jahnke, P. Selzer, E. Jacoby, *Curr. Top. Med. Chem.*, **2005**, *5*, 751–762. https://doi.org/10.2174/1568026054637700
75. 63M. J. Hartshorn, C. V. Murray, A. Cleasby, M. Frederickson, I. J. Tickle, H. Jhoti, *J. Med. Chem.*, **2005**, *48*, 403–413.
76. J. R. Huth, C. Sun, *Comb. Chem. High Throughput Screening*, **2002**, *5*, 631–643. https://doi.org/10.2174/1386207023329941
77. M. Mammen, S. K. Chio, G. M. Whitesides, *Angew. Chem., Int. Ed.*, **1998**, *37*, 2755–2794. https://doi.org/10.1002/(SICI)1521-3773(19981102)37:20<2754::AID-ANIE2754>3.0.CO;2-3
78. O. Ramström, J.-M. Lehn, *Nat. Rev. Drug Discov.*, **2002**, *1*, 26–36. https://doi.org/10.1038/nrd704
79. S. Otto, R. L. E. Furlan, J. K. M. Snaders, *Drug Discov. Today*, **2002**, *7*, 117–125. https://doi.org/10.1016/S1359-6446(02)00006-5
80. B. Debruin, P. Hauwert, J. N. H. Reek, *Angew. Chem., Int. Ed.*, **2006**, *45*, 2660–2663. https://doi.org/10.1002/anie.200504480
81. A. Valade, D. Urban, J. M. Beau, *ChemBioChem*, **2006**, *7*, 1023–1027. https://doi.org/10.1002/cbic.200600022
82. V. V. Rostovtsev, L. G. Green, V. V. Fokin, K. B. Sharpless, *Angew. Chem., Int. Ed.*, **2002**, *41*, 2596–2599. https://doi.org/10.1002/1521-3773(20020715)41:14<2596::AID-ANIE2596>3.0.CO;2-4
83. C. W. Tornøe, C. Christensen, M. Meldal, *J. Org. Chem.*, **2002**, *67*, 3057–3064. https://doi.org/10.1021/jo011148j
84. A. Krasinski, V. V. Fokin, K. B. Sharpless, *Org. Lett.*, **2004**, *6*, 1237–1240. https://doi.org/10.1021/ol0499203
85. L. Zhang, X. Chen, P. Xue, H. H. Y. Sun, I. D. Williams, K. B. Sharpless, V. V. Fokin, G. Jia, *J. Am. Chem. Soc.*, **2005**, *127*, 15998–15999. https://doi.org/10.1021/ja054114s
86. J. Albadi, A. Alihosseinzadeh, A. Mansournezhad, *Acta Chim. Slov.*, **2015**, *62*, 617–624. https://doi.org/10.17344/acsi.2014.1211
87. D. L. Boger, N. E. Haynes, P. A. Kitos, M. S. Warren, J. Ramcharan, A. E. Marolewski, S. J. Benkovic, *Bioorg. Med. Chem.*, **1997**, *5*, 1817–1830. https://doi.org/10.1016/S0968-0896(97)00120-X
88. D. Rideout, *Science*, **1986**, *233*, 561–563. https://doi.org/10.1126/science.3523757
89. W. L. Mock, T. A. Irra, J. P. Wepsoec, M. Adhya, *J. Org. Chem.*, **1989**, *54*, 5302–5308. https://doi.org/10.1021/jo00283a024
90. D. Makuc, T. Merckx, W. Dehaen, J. Plavec, *Acta Chim. Slov.*, **2016**, *63*, 484–488. https://doi.org/10.17344/acsi.2016.2251
91. W. G. Lewis, L. G. Green, F. Grynszpan, Z. Radić, P. R. Carlier, P. Taylor, M. G. Finn, K. B. Sharpless, *Angew. Chem., Int. Ed.*, **2002**, *41*, 1053–1057. https://doi.org/10.1002/1521-3773(20020315)41:6<1053::AID-ANIE1053>3.0.CO;2-4
92. D. M. Quinn, *Chem. Rev.*, **1987**, *87*, 955–979. https://doi.org/10.1021/cr00081a005
93. P. Taylor, Z. Radić, *Annu. Rev. Pharmacol. Toxicol.*, **1994**, *34*, 281–320. https://doi.org/10.1146/annurev.pa.34.040194.001433
94. J. L. Sussman, M. Harel, F. Frolow, C. Oefner, A. Goldman, L. Toker, I. Silman, *Science*, **1991**, *253*, 872–879. https://doi.org/10.1126/science.1678899
95. M. Harel, I. Schalk, L. Ehret-Sabatier, F. Bouet, M. Goeldner, C. Hirth, P. H. Axelsen, I. Silman, J. L. Sussman, *Proc. Natl. Acad. Sci. USA*, **1993**, *90*, 9031–9035. https://doi.org/10.1073/pnas.90.19.9031
96. E. Albert, F. Phillip, In: Alzheimer Disease: From Molecular Biology to Therapy., R. Berker, E. Giacobini, Eds., Birkhauser: Boston, **1996**, pp. 211–215.
97. Y.-P. Pang, P. Quiram, T. Jelacic, F. Hong, S. Brimijoin, *J. Biol. Chem.*, **1996**, *271*, 23646–23649. https://doi.org/10.1074/jbc.271.39.23646
98. P. R. Carlier, D.-M. Du, Y.-F. Han, J. Liu, E. Perola, I. D. Williams, Y.-P. Pang, *Angew. Chem., Int. Ed.*, **2000**, *39*, 1775–1777.

https://doi.org/10.1002/(SICI)1521-3773(20000515)39:10<1775::AID-ANIE1775>3.0.CO;2-Q
99. Z. Radić, P. Taylor, *J. Biol. Chem.*, **2001**, *276*, 4622–4633. https://doi.org/10.1074/jbc.M006855200
100. P. R. Carlier, Y.-F. Han, E. S.-H. Chow, C. P.-L. Li, H.-S. Wang, T. X. Lieu, H. S. Wong, Y.-P. Pang, *Bioorg. Med. Chem.*, **1999**, *7*, 351–357. https://doi.org/10.1016/S0968-0896(98)00213-2
101. Z. Shen, J. J. Thomas, C. Averbuj, K. M. Broo, M. Engelhard, J. E. Crowell, M. G. Finn, G. Siuzdak, *Anal. Chem.*, **2001**, *73*, 612–619. https://doi.org/10.1021/ac000746f
102. Z. Radić, R. Duran, D. C. Vellom, Y. Li, C. Cervenansky, P. Taylor, *J. Biol. Chem.*, **1994**, *269*, 11233–11239.
103. M. Harel, D. M. Quinn, H. K. Nair, I. Silman, J. L. Sussman, *J. Am. Chem. Soc.*, **1996**, *118*, 2340–2346. https://doi.org/10.1021/ja952232h
104. P. Camps, B. Cusack, W. D. Mallender, R. El Achab, J. Morral, D. Muñoz-Torrero, T. L. Rosenberry, *Mol. Pharmacol.*, **2000**, *57*, 409–417.
105. R. Manetsch, A. Krasiñski, Z. Radić, J. Raushel, P. Taylor, K. B. Sharpless, H. C. Kolb, *J. Am. Chem. Soc.*, **2004**, *126*, 12809–12818. https://doi.org/10.1021/ja046382g
106. A. Krasiñski, Z. Radić, R. Manetsch, J. Raushel, P. Taylor, K. B. Sharpless, H.C. Kolb, *J. Am. Chem. Soc.*, **2005**, *127*, 6686–6692. https://doi.org/10.1021/ja043031t
107. T. C. Marrs, *Pharmacol. Ther.*, **1993**, *58*, 51–66. https://doi.org/10.1016/0163-7258(93)90066-M
108. N. Yanagisawa, H. Morita, T. Nakajima, *J. Neurol. Sci.*, **2006**, *249*, 76–85. https://doi.org/10.1016/j.jns.2006.06.007
109. M. Jokanović, M.P. Stojiljković, *Eur. J. Pharmacol.*, **2006**, *553*, 10–17. https://doi.org/10.1016/j.ejphar.2006.09.054
110. F. Worek, P. Eyer, N. Aurbek, L. Szinicz, H. Thiermann, *Toxicol. Appl. Pharmacol.*, **2007**, *219*, 226–234. https://doi.org/10.1016/j.taap.2006.10.001
111. P. Taylor, In: Goodman and Gilman's the Pharmacological Basis of Therapeutics, 13th ed., L.L. Brunton, B.A. Chabner, B.C. Knollman, Eds., McGraw-Hill: New York, **2011**, pp. 239-254.
112. R. K. Sit, Z. Radić, V. Gerardi, L. Zhang, E. Garcia, M. Katalinić, G. Amitai, Z. Kovarik, V. V. Fokin, K. B. Sharpless, P. Taylor, *J. Biol. Chem.*, **2011**, *286*, 19422–19430. https://doi.org/10.1074/jbc.M111.230656
113. Z. Kovarik, N. Maček, R.K. Sit, Z. Radić, V. V. Fokin, K. B. Sharpless, P. Taylor, *Chem. Biol. Interact.*, **2013**, *203*, 77–80. https://doi.org/10.1016/j.cbi.2012.08.019
114. O. Lockridge, C. F. Bartels, T. A. Vaughan, C. K. Wong, S. E. Norton, L. L. Johnson, *J. Biol. Chem.*, **1987**, *262*, 549– 557.
115. M.-M. Mesulam, A. Guillozet, P. Shaw, A. Levey, E.G. Duysen, O. Lockridge, *Neuroscience*, **2002**, *110*, 627–639. https://doi.org/10.1016/S0306-4522(01)00613-3
116. A. Tunek, L. A. Svensson, *Drug Metab. Dispos.*, **1988**, *16*, 759–764.
117. E. Reiner, Z. Radić, In: Cholinesterases and Cholinesterase Inhibitors, 1st ed., E. Giacobini, Ed., Martin Dunitz Ltd.: London, **2000**, pp. 103–121.
118. B. M. Liederer, R. T. Borchardt, *J. Pharm. Sci.*, **2006**, *95*, 1177–1195. https://doi.org/10.1002/jps.20542
119. Z. Kovarik, Z. Radić, H.A. Berman, V. Simeon-Rudolf, E. Reiner, P. Taylor, *Biochem. J.*, **2003**, *373*, 33–40. https://doi.org/10.1042/bj20021862
120. A. Bosak, I. Gazić, V. Vinković, Z. Kovarik, *Arch. Biochem. Biophys.*, **2008**, *471*, 72–76. https://doi.org/10.1016/j.abb.2007.12.007
121. M. Katalinić, G. Rusak, J. Domaćinović Barović, G. Šinko, D. Jelić, R. Antolović, Z. Kovarik, *Eur. J. Med. Chem.*, **2010**, *45*, 186–192. https://doi.org/10.1016/j.ejmech.2009.09.041
122. G. Šinko, Z. Kovarik, E. Reiner, V. Simeon-Rudolf, J. Stojan, *Biochemie*, **2011**, *93*, 1797–1807. https://doi.org/10.1016/j.biochi.2011.06.023
123. A. Bosak, I. Gazić Smilović, G. Šinko, V. Vinković, Z. Kovarik, *J. Med. Chem.*, **2012**, *55*, 6716–6723. https://doi.org/10.1021/jm300289k
124. N. P. Grimster, B. Stump, J. R. Fotsing, T. Weide, T. T. Talley, J. G. Yamauchi, Á. Nemecz, C. Kim, K.-Y. Ho, K. B. Sharpless, P. Taylor, V. V. Fokin, *J. Am. Chem. Soc.*, **2012**, *134*, 6732–6740. https://doi.org/10.1021/ja3001858
125. J. P. Changeux, S. J. Edelstein, Nicotinic Acetylcholine Receptors: From Molecular Biology to Cognition, 1st ed., Johns Hopkins University Press: New York, **2005**.
126. J. P. Changeux, A. Taly, *Trends Mol. Med.*, **2008**, *14*, 93–102. https://doi.org/10.1016/j.molmed.2008.01.001
127. J. P. Changeux, *Nat. Rev. Neurosci.*, **2010**, *11*, 389–401. https://doi.org/10.1038/nrn2849
128. X. Xiu, N. L. Puskar, J. A. P. Shanata, H. A. Lester, D. A. Dougherty, *Nature*, **2009**, *458*, 534–537. https://doi.org/10.1038/nature07768
129. A. T. Poulin-Kerstien, P. B. Dervan, *J. Am. Chem. Soc.*, **2003**, *125*, 15811–15821. https://doi.org/10.1021/ja030494a
130. S. Imoto, T. Hirohama, F. Nagatsugi, *Bioorg. Med. Chem. Lett.*, **2008**, *18*, 5660–5663. https://doi.org/10.1016/j.bmcl.2008.08.074
131. B. E. Edelson, P. B. Dervan, *Curr. Opin. Struct. Biol.*, **2003**, *13*, 284–299. https://doi.org/10.1016/S0959-440X(03)00081-2
132. J. W. Trauger, E. E. Baird, P. B. Dervan, *J. Am. Chem. Soc.*, **1998**, *120*, 3534–3535. https://doi.org/10.1021/ja9800378
133. M. Faria, C. Giovannangeli, *J. Gene Med.*, **2001**, *3*, 299–310. https://doi.org/10.1002/jgm.192
134. I. Kers, P. B. Dervan, *Bioorg. Med. Chem.*, **2002**, *10*, 3339–3349. https://doi.org/10.1016/S0968-0896(02)00221-3
135. P. Weyermann, P. B. Dervan, *J. Am. Chem. Soc.*, **2002**, *124*, 6872–6878. https://doi.org/10.1021/ja020258k
136. J. M. Belitsky, S. J. Leslie, P. S. Arora, T. A. Beerman, P. B. Dervan, *Bioorg. Med. Chem.*, **2002**, *10*, 3313–3318. https://doi.org/10.1016/S0968-0896(02)00204-3
137. R. K. Bruick, P. E. Dawson, S. B. H. Kent, N. Usman, G. F. Joyce, *Chem. Biol.*, **1996**, *3*, 49–56. https://doi.org/10.1016/S1074-5521(96)90084-8

138. J. L. Czlapinski, T. L. Sheppard, *J. Am. Chem. Soc.*, **2001**, *123*, 8618–8619. https://doi.org/10.1021/ja0162212
139. D. Summerer, A. Marx, *Angew. Chem., Int. Ed.*, **2002**, *41*, 89–90. https://doi.org/10.1002/1521-3773(20020104)41:1<89::AID-ANIE89>3.0.CO;2-G
140. Z. J. Gartner, R. Grubina, C. T. Calderone, D. R. Liu, *Angew. Chem., Int. Ed.*, **2003**, *42*, 1370–1375. https://doi.org/10.1002/anie.200390351
141. R. N. Warrener, D. N. Butler, D. Margetić, F. M. Pfeffer, R. A. Russell, *Tetrahedron Lett.*, **2001**, *41*, 4671–4675. https://doi.org/10.1016/S0040-4039(00)00685-7
142. M. Di Antonio, G. Biffi, A. Mariani, E.-A. Raiber, R. Rodriguez, S. Balasubramanian, *Angew. Chem., Int. Ed.*, **2012**, *51*, 11073–11078. https://doi.org/10.1002/anie.201206281
143. A. Ambrus, D. Chen, J. Dai, T. Bialis, R. A. Jones, D. Yang, *Nucleic Acids Res.*, **2006**, *34*, 2723–2735. https://doi.org/10.1093/nar/gkl348
144. I. Glassford, C. N. Teijaro, S. S. Daher, A. Weil, M. C. Small, S. K. Redhu, D. J. Colussi, M. A. Jacobson, W. E. Childers, B. Buttaro, A. W. Nicholson, A. D. MacKerell, B. S. Cooperman, R. B. Andrade, *J. Am. Chem. Soc.*, **2016**, *138*, 3136–3144. https://doi.org/10.1021/jacs.5b13008
145. N. Willand, M. Desroses, P. Toto, B. Dirié, Z. Lens, V. Villeret, P. Rucktooa, C. Locht, A. Baulard, B. Deprez, *ACS Chem. Biol.*, **2010**, *5*, 1007–1013. https://doi.org/10.1021/cb100177g
146. H. D. Agnew, R. D. Rohde, S. V. Millward, A. Nag, W.-S. Yeo, J. H. Hein, S. M. Pitram, A. T. Ahad, A. M. Burns, J. R. Krom, V. V. Fokin, K. B. Sharpless, J. R. Heath, *Angew. Chem., Int. Ed.*, **2009**, *48*, 4944–4948. https://doi.org/10.1002/anie.200900488
147. K. S. Lam, S. E. Salmon, E. M. Hersh, V. J. Hruby, W. M. Kazmierski, R. J. Knappt, *Nature*, **1991**, *354*, 82–84. https://doi.org/10.1038/354082a0
148. D. G. Udugamasooriya, S. P. Dineen, R. A. Brekken, T. Kodadek, *J. Am. Chem. Soc.*, **2008**, *130*, 5744–5752. https://doi.org/10.1021/ja711193x
149. G. Liu, K. S. Lam, In: Combinatorial Chemistry-A Practical Approach Series., H. Fenniri, Ed., Oxford University Press: New York, **2000**, pp. 43–44.
150. S. W. Millward, R. K. Henning, G. A. Kwong, S. Pitram, H. D. Agnew, K. M. Deyle, A. Nag, J. Hein, S. S. Lee, J. Lim, J. A. Pfeilsticker, K. B. Sharpless, J. R. Heath, *J. Am. Chem. Soc.*, **2011**, *133*, 18280–18288. https://doi.org/10.1021/ja2064389
151. I. Vivanco, C. L. Sawyers, *Nat. Rev. Cancer*, **2002**, *2*, 489–501. https://doi.org/10.1038/nrc839
152. C. M. Niemeyer, M. Adler, R. Wacker, *Trends Biotechnol.*, **2005**, *23*, 208–216. https://doi.org/10.1016/j.tibtech.2005.02.006
153. S. L. Posy, M. A. Hermsmeier, W. Vaccaro, K.-H. Ott, G. Todderud, J. S. Lippy, G. L. Trainor, D. A. Loughney, S. R. Johnson, *J. Med. Chem.*, **2011**, *54*, 54–66. https://doi.org/10.1021/jm101195a
154. J. F. Schildbach, D. J. Panka, D. R. Parks, G. C. Jager, J. Novotny, L. A. Herzenberg, M. Mudgett-Hunter, R. E. Bruccoleri, E. Haber, M. N. Margolies, *J. Biol. Chem.*, **1991**, *266*, 4640–4647.
155. L. Jen-Jacobson, *Biopolymers*, **1997**, *44*, 153–180. https://doi.org/10.1002/(SICI)1097-0282(1997)44:2<153::AID-BIP4>3.0.CO;2-U
156. J. T. Nguyen, M. Porter, M. Amoui, W. T. Miller, R. N. Zuckermann, W. A. Lim, *Chem. Biol.*, **2000**, *7*, 463–473. https://doi.org/10.1016/S1074-5521(00)00130-7
157. C. Peruzzotti, S. Borrelli, M. Ventura, R. Pantano, G. Fumagalli, M. S. Christodoulou, D. Monticelli, M. Luzzani, A. C. Fallacara, C. Tintori, M. Botta, D. Passarella, *ACS Med. Chem. Lett.*, **2013**, *4*, 274–277. https://doi.org/10.1021/ml300394w
158. M. Mondal, N. Radeva, H. Köster, A. Park, C. Potamitis, M. Zervou, G. Klebe, A. K. H. Hirsch, *Angew. Chem., Int. Ed.*, **2014**, *53*, 3259–3263. https://doi.org/10.1002/anie.201309682

Povzetek

Sodobno odkrivanje zdravil v glavnem temelji na *de novo* sintezah velikega števila spojin z različnimi kemijskimi funkcionalnimi skupinami. Čeprav je kombinatorialna kemija omogočila pripravo velikih knjižnic spojin iz različnih gradnikov, še vedno ostaja težava identifikacije spojin vodnic. Odkritje dinamičnih metod kombinatorialne kemije predstavlja korak naprej, saj pri sami sintezi visoko afinitetnih produktov vključuje biološke makromolekularne tarče (receptorje). Glavni preboj predstavlja sintezna metoda pri kateri se gradniki ireverzibilno povežejo le ob prisotnosti receptorja. Predstavljamo različne pristope v kombinatorialni kemiji, ki temeljijo na prisotnosti receptorjev. Pri Huisgenovi cikloadiciji (1,3-dipolarna cikloadicija azidov z alkini) nastanejo stabilni 1,2,3-triazoli; pogosto z zelo visokimi afinitetami do receptorja, ki lahko dosežejo celo femtomolarno območje, kot prikazuje primer z inhibitorji acetilholinesteraze. Huisgenovo cikloadicijo lahko uporabimo tudi pri različnih drugih receptorjih: acetilholinesterazi; proteinih, ki vežejo acetilholin; karboanhidrazi-II, serin/treonin-proteinski kinazi in pri vezavi na mali žleb DNA.

Scientific paper

Computational Investigation of the Dissociative Adsorption of Dichloroacetylene (C_2Cl_2) on N Functionalized Carbon and Carbon Germanium (CGe) Nanocone Sheets in the Gas Phase and Dimethyl Sulfoxide

Meysam Najafi*

Young Researchers and Elite Club, Kermanshah Branch, Islamic Azad University, Kermanshah, Iran

** Corresponding author: E-mail: meysamnajafi2016@gmail.com*
Phone: +98-8337243181 Fax: +98-8337243181

Received: 25-06-2016

Abstract

The possibility of dichloroacetylene-sensing on carbon nanocone sheet and carbon germanium nanocone sheet surfaces has been investigated. The effects of nitrogen functionalization and dimethyl sulfoxide on the adsorption of dichloroacetylene gas on carbon nanocone sheet and carbon germanium nanocone sheet surfaces were investigated. Results reveal that adsorption of dichloroacetylene on studied nanocone sheets were exothermic. Results show that, adsorption energy value of dichloroacetylene on carbon germanium nanocone sheet surface were more negative than corresponding values of carbon nanocone sheet. Results reveal that, N functionalization and dimethyl sulfoxide, increase and decrease the absolute adsorption energy value of dichloroacetylene on studied nanocone sheets, respectively. These results show that, there were good linearity dependencies between adsorption energy and orbital energy values of studied nanocone sheets.

Keywords: COSMO, DMSO, nanocone sheet, C_2Cl_2, sensor

1. Introduction

Dichloroacetylene is an oily pyrophoric chemical compound with the chemical formula C_2Cl_2. The compound is volatile at standard temperature and pressure and explodes on contact with air. It is a toxic compound.[1–3] It displays nephrotoxic effects to rats, but not to humans. It can be made from the compound trichloroethylene.[1–3] The most common effect that the compound has on humans is the development of disorders.[1–3]

These disorders can persist for any amount of time between a number of days and a number of years. Exposure to the chemical can also cause a large range of other symptoms, including a headache, vomiting and nausea, jaw pain, cranial nerve palsy, appetite loss and acute lung edema. C_2Cl_2 level of carcinogenetic in humans is not classifiable, although there are small amounts of evidence that suggest that the chemical is carcinogenic in animals.[4,5]

Studies on male rats and rabbits have shown that inhalation of C_2Cl_2 can cause tubular necrosis, focal necrosis, and other nephrotoxic effects.[6,7] Additionally, the rabbits that were given C_2Cl_2 experienced hepatotoxic and neuropath logical effects. Inhalation of C_2Cl_2 also causes benign tumors of the livers and kidneys of rats. The chemical increase the incidences of lymphomas.[9–10]

In recent years, Carbon nanocone sheet (C-NCS) and their functionalized derivatives as gas toxic sensors have been used, widely. In addition to C-NCS, there are other nanocone sheets which are found experimentally such as carbon germanium nanocone sheets (CGe-NCS).[11–19] In the current study, the interactions of C_2Cl_2 gas with C-NCS and CGe-NCS with disclination angles of 240° exploring its potential application as C_2Cl_2 gas sensor will be theoretically investigated. The N functionalization of nanostructures is very important and it can effectively change the electronic structures of nanostructures.[19,20]

Ibrahim and et al.[21] in previous study, polymerization of aniline by Cu (II) montmorillonite studied using attenuated total reflection Fourier-transform infrared

(ATR-FTIR) spectroscopy. Also experimental spectra were compared with that calculated by AM1, PM3, PM5, MINDO, Hartree-Fock, HF/6-31G(d), as well as Density Functional Theory, BLYP/DZVP and B3LYP/6-31g(d,p). Ibrahim and et al.[22] used Density functional theory (DFT) to investigate both the structure and vibrational frequencies of acetate group. A model of B3LYP with four basis set was used to optimize and locate the energy minimum of the acetic acid molecule. Ibrahim and et al.[23] studied molecular structure of gelatin by using Fourier transform infrared spectroscopy FTIR. The spectrum was subjected to deconvolution in order to elucidate the constituents of the molecular structure. Ibrahim and et al.[24] promised nanomaterials in the field of optical sensors due to their unique properties. Emeraldine base of polyaniline (Nano EB-PANI) was prepared, characterized and applied as an optical formaldehyde sensor.

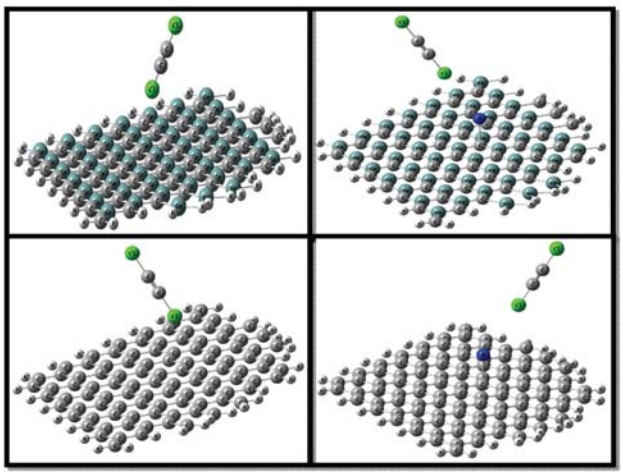

Figure 1. Complexes of C_2Cl_2 with C-NCS, CGe-NCS, N-C-NCS and N-CGe-NCS.

In previous study, Warshel and et al.[25] utilized computer simulations to elucidate the true molecular basis for the experimentally observed effect. They start by reproducing the trend in the measured change in catalysis upon mutations. They discuss the role of flexibility and conformational dynamics in catalysis, once again demonstrating that their role is negligible and that the largest contribution to catalysis arises from electrostatic preorganization.

In previous studies, Warshel and et al.[26,27] described a general approach for exploring the energetics of different feasible models of the action of CcO, using the observed protein structure, established simulation methods and a modified Marcus' formulation. They start by reviewing our methods for evaluation of the energy diagrams for different proton translocation paths and then present a systematic analysis of various constraints that should be imposed on any energy diagram for the pumping process.

In previous study, Warshel and et al.[28] considered the current state of simulations of electrostatic energies in macromolecules as well as the early developments of this field. They focused on the relationship between microscopic and macroscopic models, considering the convergence problems of the microscopic models and the fact that the dielectric 'constants' in semimacroscopic models depend on the definition and the specific treatment.

In previous study, Warshel and et al.[29] described application of the calculated geometry and vibrations to the analysis of vibronic structure. A preliminary account of the use of observed vibronic structure for determination of the geometry of excited electronic states was given.

In previous study,[30] it be observed that the predominant initiation reaction for oxidation of methane, propene, and o-xylene under fuel lean conditions involved hydrogen abstraction of the methyl hydrogen by molecular oxygen forming hydroperoxyl and hydrocarbon radical species.

The study of adsorption of toxic gas on the solid surface of nanostructures in order to identify the suitable sensor to remove or reduce the toxic gas are important in environmental issue. C_2Cl_2 has a toxic effect on humans who are exposed to it.

Therefore adsorption C_2Cl_2 by nano structures is important and fundamental objects of present paper are: (1) to investigate the C_2Cl_2 adsorption on C-NCS and CGe-NCS surfaces; (2) to compare the C_2Cl_2 adsorption ability of C-NCS and CGe-NCS; (3) to identify the effect of N functionalization of studied C-NCSs and CGe-NCSs on adsorption of C_2Cl_2; (4) to explore how the solvent alter the C_2Cl_2 adsorption on studied C-NCS and CGe-NCS surfaces; (5) To find the C-NCS and CGe-NCS with highly effective detection of C_2Cl_2.

2. Computational Details

In this paper, structure of C-NCS (constructed of 108 C atoms) and CGe-NCS (constructed of 54 C and 54 Ge atoms) with disclination angles of 240° and their N functionalized derivatives were geometry optimized in the gas phase and solvent. Also the structure of complexes of studied C-NCSs and CGe-NCSs with C_2Cl_2 molecule were geometry optimized in gas phase and solvent (structures were shown in figure 1). In order to avoid boundary effects, atoms at the open ends of the studied C-NCSs and CGe-NCSs were saturated with hydrogen atoms.[19] All the calculations were performed using the DFT/B3LYP method and 6-31G(d,p) basis set within the GAMESS package.[19,31,32]

Also, harmonic vibrational frequencies have been calculated, enabling us to confirm the real minima. Solvation effects were included through the use of the polarized continuum model (PCM).[19,33] The B3LYP is a reliable and common used level of theory in the study of different na-

nostructures.[19,34–36] A dielectric constant of 46.7 was used corresponding to that for dimethyl sulfoxide (DMSO) as the solvent.

The adsorption energy (E_{ad}) of C_2Cl_2 molecule on the C-NCS and CGe-NCS is obtained using the following equation:

$$E_{ad} = E\,(\text{nanocone sheet}/C_2Cl_2) - E\,(\text{nanocone sheet}) - E\,(C_2Cl_2) + E_{BSSE} \quad (1)$$

where E(nanocone sheet/C_2Cl_2) is the energy of C-NCS or CGe-NCS–C_2Cl_2 complex, and E(nanocone sheet) and E(C_2Cl_2) are referred to the energies of C-NCS or CGe-NCS and C_2Cl_2 molecule, respectively. The negative value of E_{ad} indicates the exothermic specificity of the adsorption. The basis set superposition error (BSSE) has been corrected for all of the interactions.[37]

3. Results and Discussion

3. 1. The Ead values of C_2Cl_2 Gas on Studied Nanocone Sheet Surfaces in Gas Phase and DMSO

The calculated E_{ad} values of C_2Cl_2 gas on C-NCS and CGe-NCS and their N functionalized derivatives (N-C-NCS and N-CGe-NCS) in gas phase and DMSO were reported in the table 1. Results in table 1 show that, the E_{ad} values of C_2Cl_2 on C-NCS and CGe-NCS in gas phase were –3.13 and –3.48 eV, respectively. Also the E_{ad} values of C_2Cl_2 on C-NCS and CGe-NCS in DMSO are –2.94 and –3.25 eV, respectively.

Results in table 1 show that, the E_{ad} values of C_2Cl_2 on N-C-NCS in gas phase and DMSO were –3.66 and –3.48 eV, respectively. Also the E_{ad} values of C_2Cl_2 on N-CGe-NCS in gas phase and DMSO were –4.06 and –3.87 eV, respectively.

Results reveal that, N functionalization of C-NCS increase the absolute E_{ad} values of C_2Cl_2 in comparison to C-NCS ca 0.53 and 0.54 eV in gas phase and DMSO, respectively. Results indicated that, DMSO decrease the absolute E_{ad} values of C_2Cl_2 on N-C-NCS and N-CGe-NCS in comparison to gas phase ca 0.18 and 0.19 eV, respectively.

Results indicate that the absolute E_{ad} values of the C_2Cl_2 on studied nanocone sheets decreased in the following order in gas phase and DMSO: C-NCS < N-C-NCS < CGe-NCS < N-CGe-NCS. In according to obtained E_{ad} values of C_2Cl_2 on studied nanocone sheet surfaces in gas phase and DMSO, it can be concluded that N-CGe-NCS and C-NCS have higher and lower ability to adsorption of C_2Cl_2, respectively.

Table 1. Calculated E_{ad} (in eV) of C_2Cl_2 on C-NCS, CGe-NCS, N-C-NCS and N-CGe-NCS surfaces in gas phase and DMSO.

DMSO	Gas phase	Nanostructure
–2.94	–3.13	C-NCS
–3.25	–3.48	CGe-NCS
–3.48	–3.66	N-C-NCS
–3.87	–4.06	N-CGe-NCS

These results in this section can be interpreted with a known fact that Ge atoms in studied CGe-NCS stabilize the CGe-NCS and their C_2Cl_2-CGe-NCS complexes; hence, these results in increased absolute E_{ad} in comparison to studied C-NCS in gas phase, DMSO.[19]

Also results show that in compare to gas phase, DMSO attenuate the absolute E_{ad} values of C_2Cl_2 on studied nanocone sheet surfaces ca 0.197 eV. Fundamental reason for decrease in absolute E_{ad} values in DMSO, could be an unequal stabilization/destabilization of the studied nanocone sheets and their complexes with C_2Cl_2 in DMSO.[19]

Therefore results in this study show that, the N-CGe-NCS and C-NCS have the most and less absolute E_{ad} values of C_2Cl_2 on studied nanocone sheet surfaces.

3. 2. The E_{HOMO} and E_{LUMO} of Studied Nanocone Sheets

In this work the E_{HOMO}, E_{LUMO} and E_{HLG} values of C-NCS and CGe-NCS and their N functionalized derivatives were calculated and reported in table 2. In this section the dependencies of between E_{ad} corresponding E_{HOMO}, E_{LUMO} and E_{HLG} values of studied nanocone sheets were investigated.

Results show that, calculated E_{HOMO} values of studied nanocone sheets range from –5.58 to –6.12 eV. Therefore obtained absolute E_{HOMO} values of studied nanocone sheets show that the N-CGe-NCS and C-NCS have higher and lower tendency to lose electron, respectively.[19]

Results reveal that, calculated E_{LUMO} values of studied nanocone sheets range from –3.57 to –3.94 eV. Therefore obtained E_{LUMO} values of studied nanocone sheets show that the N-CGe-NCS and C-NCS have higher and lower capacity to accept electrons, respectively. [19]

Results indicated that, calculated E_{HLG} values of studied nanocone sheets range from 1.64 to 2.55 eV. Therefore E_{HLG} values of studied nanocone sheets show that the N-CGe-NCS have lower stability and higher reactivity and C-NCS have lower reactivity.[19]

In according to obtained results in table 2, it can be concluded that N functionalization of C-NCS and CGe-NCS increase the absolute E_{LUMO} values and decrease the absolute E_{HOMO} and E_{HLG} values in comparison to C-NCS and CGe-NCS. The computed E_{ad} values of C_2Cl_2 on studied nanocone sheet surfaces are corrected against corresponding calculated E_{HOMO}, E_{LUMO} and E_{HLG} values of studied nanocone sheets. Equations obtained from the linear regression are as follows:

$$E_{ad} = -1.71 \times (E_{HOMO}) - 13.54 \quad (2)$$

$$E_{ad} = 2.49 \times (E_{HOMO}) + 5.72 \quad (3)$$

$$E_{ad} = 1.03 \times (E_{HLG}) - 5.74 \quad (4)$$

The correlation coefficients of equations 2, 3 and 4 reached ca 0.985, 0.992 and 0.990, respectively. These results show that, there are good linearity dependencies between E_{ad} and orbital energy (E_{HOMO}, E_{LUMO} and E_{HLG}) values of studied nanocone sheets. This can be useful in the selection of suitable nanocone sheets with enhanced C_2Cl_2 adsorption potential.[19]

As mentioned in tables 1 and 2, this can be concluded the calculated E_{ad} and orbital energy scales have same trends for averment C_2Cl_2 adsorption potential of studied nanocone sheets. Therefore results in this study, reveal that N-CGe-NCS has highest and C-NCS has lowest C_2Cl_2 adsorption potential among studied nanocone sheets.[19]

Table 2. Calculated E_{HOMO} (in eV), E_{LUMO} (in eV) and E_{HLG} (in eV) of C-NCS, CGe-NCS, N-C-NCS and N-CGe-NCS.

E_{HLG}	E_{LUMO}	E_{HOMO}	Nanostructure
2.55	–3.57	–6.12	C-NCS
2.16	–3.69	–5.85	CGe-NCS
2.03	–3.74	–5.77	N-C-NCS
1.64	–3.94	–5.58	N-CGe-NCS

Finally higher absolute E_{ad} and E_{LUMO} values and lower E_{HOMO} and E_{HLG} values for studied nanocone sheets are appropriate benchmarks to approval the C_2Cl_2 adsorption potential. Therefore it can be concluded the E_{ad}, E_{HOMO}, E_{LUMO} and E_{HLG} values of studied nanocone sheets can consider as important parameters to predicate and propose suitable nanocone sheets with enhanced C_2Cl_2 adsorption potential. [19]

4. Conclusion

In this study the E_{ad} values of C_2Cl_2 gas on C-NCS and CGe-NCS surfaces in gas phase were investigated using density functional theory calculations. The effects of N functionalization and DMSO on the adsorption of C_2Cl_2 gas on C-NCS and CGe-NCS surfaces were investigated. Results reveal that adsorptions of C_2Cl_2 on studied nanocone sheets were exothermic and experimentally possible from the energetic viewpoint. Results show that, E_{ad} value of C_2Cl_2 on CGe-NCS surface are more negative than corresponding values of C-NCS. Results reveal that, N functionalization and DMSO causing an increase and decrease the absolute E_{ad} values of C_2Cl_2 on studied nanocone sheets, respectively. Results show that, there are good linearity dependencies between E_{ad} and orbital energy values of studied nanocone sheets. Therefore it can be concluded the E_{ad} and orbital energy values of studied nanocone sheets can consider as important parameters to propose suitable nanocone sheets with enhanced C_2Cl_2 adsorption potential.

5. Acknowledgment

Thank colleagues for their valuable discussion on the computational affairs.

6. Abbreviations

HOMO (highest occupied molecular orbital), LUMO (lowest unoccupied molecular orbital), HLG (HOMO–LUMO gap), DFT (density functional theory), B3LYP (Becke 3-parameter Lee, Yang and Parr), DMSO (dimethyl sulfoxide), C-NCS (carbon nanocone sheet), CGe-NCS (carbon germanium nanocone sheet) and polarized continuum model (PCM), BSSE (basis set superposition error).

7. References

1. D. Reichert, D. Ewald, D. Henschler, *Food and Cosmetics Toxicology*, **1975**, *13*, 511–515. https://doi.org/10.1016/0015-6264(75)90004-8
2. T. R. Melita, »Dichloroacetylene«, Homopolymers of Dihaloacetylenes (Ph.D. Thesis), **1999**. 57–60.
3. P. P. Richard, Sittig's Handbook of Toxic and Hazardous Chemicals and Carcinogens, **2011**.
4. L. M. Dorozhkin and I. A. Rozanov, *J. Analyt. Chem.* **2001**, *56*, 399–416. https://doi.org/10.1023/A:1016662616648
5. T. Hübert, L. Boon-Brett, G. Black, and U. Banach, *Sens. Actuat. B: Chem.* **2011**, *157*, 329–352. https://doi.org/10.1016/j.snb.2011.04.070
6. J. F. Currie, A. Essalik, and J. C. Marusic, *Sens. Actuat. B: Chem.* **1999**, *59*, 235–241. https://doi.org/10.1016/S0925-4005(99)00227-0
7. G. Valacchi, P. A. Davis, Oxidants in Biology: A Question of Balance, Springer Science Business Media. **2011**.
8. H. Greim, T. Wolff, M. Höfler, E. Lahaniatis, *Archives of toxicology*, **1984**, *56*, 74–7. https://doi.org/10.1007/BF00349074
9. D. L. Purich, , 2009.
10. K. Ho and W. Hung, *Sens. Actuat. B: Chem.* **2001**, *79*, 11–16. https://doi.org/10.1016/S0925-4005(01)00782-1
11. J. C. Yang and P. K. Dutta, *Sens. Actuat. B: Chem.* **2010**, *143*, 459–463. https://doi.org/10.1016/j.snb.2009.09.023
12. Y. Yan, N. Miura, and N. Yamazoe, *Sens. Actuat. B: Chem.* **1995**, *24*, 287–290. https://doi.org/10.1016/0925-4005(95)85062-7
13. A. Khodadadi, S. S. Mohajerzadeh, Y. Mortazavi, A. M. Miri, *Sens. Actuat. B: Chem.* **2001**, *80*, 267–271. https://doi.org/10.1016/S0925-4005(01)00915-7

14. G. Korotcenkov, *Sens. Actuat. B: Chem.* **2007**, *121,* 664–678. https://doi.org/10.1016/j.snb.2006.04.092
15. M. Machado, R. Mota, P. Piquini, *Microelectron. J.* **2003**, *34*, 545–547. https://doi.org/10.1016/S0026-2692(03)00044-2
16. J. B. Halpern, A. Bello, J. Gilcrease, G. L. Harris, M. He, *Microelectron. J.* **2009**, *40,* 316–318. https://doi.org/10.1016/j.mejo.2008.07.022
17. J. Beheshtian, M. Kamfiroozi, Z. Bagheri, A. Ahmadi, *Chin. J. Chem. Phys.* **2012**, *25*, 60–64. https://doi.org/10.1088/1674-0068/25/01/60-64
18. A. Ahmadi, J. Beheshtian, M. Kamfiroozi, *J. Mol. Model.* **2012**, *18*, 1729–1734. https://doi.org/10.1007/s00894-011-1202-5
19. M. Najafi, *Appl. Surf. Sci.* **2016**, *384*, 380–385. https://doi.org/10.1016/j.apsusc.2016.05.050
20. J. Beheshtian, M. Kamfiroozi, Z. Bagheri, A. Ahmadi, *Comp. Mater. Sci.* **2012**, *54*, 115–118. https://doi.org/10.1016/j.commatsci.2011.09.039
21. M. Ibrahima, E. Koglin, *Acta Chim. Slov.* **2005**, *52*, 159–163.
22. M. Ibrahima, E. Koglin, *Acta Chim. Slov.* **2004**, *51*, 453-460.
23. M. Ibrahim, A. A. Mahmoud, O. Osman, M. Abd ElAal, M. Eid, *Spectrochimica Acta Part A* **2011**, *81*, 724–729. https://doi.org/10.1016/j.saa.2011.07.012
24. O. Wessam, A. Rehab, E. Hanan, I. Medhat A. Elfeky, *Recent Patents on Nanotechnology*, **2015**, *9*, 195–203.
25. A. J. Adamczyka, J. Cao, Sh. C. L. Kamerlin, A. Warshel, *Proc. Natl. Acad. Sci. USA*, **2011**, *108*, 14115–14120. https://doi.org/10.1073/pnas.1111252108
26. A. Warshel, Computer Modelling of Chemical Reactions in Enzymes and Solutions, John Wiley and Sons, 1991, New York.
27. M. H. M. Olsson, P. E. M. Siegbahn, M. R. A. Blomberg, A. Warshel, *Biochimica et Biophysica Acta*, **2007**, *1767*, 244–260.
28. A. Warshel, P. K. Sharma, M. Kato, W. W. Parson, *Biochimica et Biophysica Acta*, **2006**, *1764*, 1647–1676.
29. A. Warshel, *Israel J. Chem.* **1973**, *11*, 709–717. https://doi.org/10.1002/ijch.197300067
30. K. Chenoweth, Adri C. T. van Duin, W. A. Goddard, *J. Phys. Chem. A* **2008**, *112*, 1040–1053. https://doi.org/10.1021/jp709896w
31. M. Schmidt, K. Baldridge, J. Boatz, S. Elbert, M. Gordon, J. Jensen, S. Koseki, N. Matsunaga, K. Nguyen, S. Su, T. Windus, M. Dupuis, *J. Comput. Chem.* **1993**, *14*, 1347–1363. https://doi.org/10.1002/jcc.540141112
32. S. Grimme, *J. Comput. Chem.* **2004**, *25*, 1463–1471. https://doi.org/10.1002/jcc.20078
33. J. Andzelm, C. Kolmel, *J. Chem. Phys.* **1995**, *103*, 9312–9320. https://doi.org/10.1063/1.469990
34. L. H. Gan, J. Q. Zhao, *Physica E* **2009**, *41*, 1249–1252. https://doi.org/10.1016/j.physe.2009.02.014
35. J. Beheshtian, A. A. Peyghan, Z. Bagheri, *Appl. Surf. Sci.* **2012**, *258*, 8171–8176. https://doi.org/10.1016/j.apsusc.2012.05.016
36. T. C. Dinadayalane, J. S. Murray, M. C. Conch a, P. Politzer, J. Leszczynski, *J. Chem. Theory Comp.* **2010**, *6*, 1351–1357. https://doi.org/10.1021/ct900669t
37. S. F. Boys, F. Bernardi, *Mol. Phys.* **1970**, *19*, 553–566. https://doi.org/10.1080/00268977000101561

Povzetek

S pomočjo funkcionalno gostotne teorije v plinski fazi smo proučevali možnost zaznavanja C_2Cl_2 na C-NCS in CGe-NCS površinah. Proučevali smo tudi učinke N funkcionalizacije in DMSO na adsorpcijo C_2Cl_2 na teh površinah. Rezultati kažejo, da je adsorpcija C_2Cl_2 na površini nanstožcev eksotermna in z energetskega vidika možna. Energija adsorpcije, E_{ad}, C_2Cl_2 na CGe-NCS površini je bolj negativna od E_{ad} na C-NCS. Izkazalo se je, da N funkcionalizacija povzroči zvišanje in DMSO znižanje absolutne vrednosti E_{ad} C_2Cl_2 na proučevane nanostožce. Dokazali smo tudi linearno zvezo med E_{ad} in orbitalnimi energijami nanostožcev.

Scientific paper

Infrared Spectroscopy for Analysis of Co-processed Ibuprofen and Magnesium Trisilicate at Milling and Freeze Drying

Manoj Acharya, Satyaki Mishra, Rudra N. Sahoo and Subrata Mallick*

Faculty of Pharmaceutical Sciences, Siksha 'O' Anusandhan University, Kalinganagar, Khandagiri Square, Bhubaneswar, OR, India.

** Corresponding author: E-mail: subratamallick@soauniversity.ac.in; s_mallickin@yahoo.com; profsmallick@gmail.com*
Fax: +91-674-2386271; Tel: +91-674-2386209

Received: 28-07-2016

Abstract

Assessment of interactions of ibuprofen and magnesium trisilicate after co-processing has been carried out by infrared spectroscopy. Dry-state ball-milling and, aqueous state kneading and freeze-drying were performed. FTIR spectroscopy of co-processed materials described acid–base reaction between the carboxylic acid containing ibuprofen to a significant extent. Increased absorbance of carboxylate peak accompanied by a consistently reduced absorbance of the carbonyl acid peak was evident. Absorbance of carboxylate peak was more in freeze-dried sample compared to milled product. Intermolecular hydrogen bonding between ibuprofen and magnesium trisilicate in the co-processed material has been suggested. Inhibition of crystal morphology has been noticed in the photomicrographs of both the products. DSC report has shown absence or significantly decreased melting endotherm representing almost complete amorphization of ibuprofen. Release of drug increased greatly after co-processing in comparison to crystalline ibuprofen. Freeze-dried samples have improved drug release more significantly compared to ball-milled samples.

Keywords: Infrared spectroscopy; co-milling; co-freeze drying; scanning electron microscopy; differential scanning calorimetry.

1. Introduction

Infrared spectroscopy is a workhorse technique for pharmaceutical analysis in recent years. Infrared spectrum represents the molecular absorption and transmission, creating a molecular fingerprint of the sample. It corresponds to the frequencies of vibrations between the bonds of the atoms. Material is a unique combination of atoms and no two compounds produce the exactly same infrared spectrum. Changes in the frequency and shape of the bands of a drug could be utilized for the analysis of possible redistribution of electronic density in the structure of the molecule for the assessment of interactions.

Ibuprofen, the most commonly prescribed NSAIDs[1] [chemical formula: $(CH_3)_2CHCH_2C_6H_4CH(CH_3)COOH$] is known to induce injury of the gastrointestinal tract and cause changes in the permeability and structural properties of the membrane.[2,3] Magnesium trisilicate is used therapeutically as an antacid in the treatment of peptic ulcers. Via a neutralization reaction it increases the pH of gastric juice. After precipitation colloidal silica can coat gastrointestinal mucosa which can confer further protection. Indigestion, heartburn, or gastroesophageal reflux can sometimes be symptoms of more serious conditions such as stomach ulcers or stomach cancer. Doctor consultation is necessary before taking magnesium trisilicate when an individual is taking a non-steroidal anti- inflammatory drug. Magnesium trisilicate interacts with a number of drugs and alter their absorption, thereby reducing their effectiveness.[4–8] Enteric coatings designed to prevent the dissolution in the stomach may also be damaged by magnesium trisilicate.[9] Magnesium trisilicate is a compound of magnesium oxide and silicon dioxide with varying proportions of water (2MgO,3SiO2,xH2O) (USP 28). Magne-

sium trisilicate is a solid adsorbent and could also be utilized to improve the dissolution of poorly soluble drugs.[10,11] Solid-dispersion granules of a poorly water-soluble drug containing microporous magnesium aluminosilicate (Neusilin) prepared by hot-melt granulation technique has shown improved dissolution of drug.[12,13] The solid dispersion granules of BAY 12-9566 containing Neusilin were successfully compressed into tablets and increased dissolution. The hydrogen-bonding potential of silanol groups on the surface of Neusilin brought about the increase in the drug release rate.

In the present study assessment of interactions of ibuprofen and magnesium trisilicate has been undertaken by infrared spectroscopy after milling together in the dry-state and freeze-drying after aqueous state kneading. Ball milling is a powerful tool for particle size reduction and processing in the pharmaceutical industries.[14] It is also a device for effecting chemical reactions by mechanical energy in dry-state and at ambient temperatures.[15,16] Ball milling presents a greener route for many processes compared to the use of microwave and ultrasound as energy sources. Impact and attrition during ball milling can bring about changes in the crystal structure of the drug and can induce amorphization[17–22] and improve bioavailability.[23] Freeze drying is a standard process used to stabilize and store the drug products in the pharmaceutical industries.[24] FTIR spectroscopy was monitored to identify the mechanism of interaction[25–27] of the carboxylic acid-containing drug ibuprofen with magnesium trisilicate. The interaction study has also been monitored by scanning electron microscopy and differential scanning calorimetry (DSC). Afterward, in-vitro drug release from the formulated co-processed powder was carried out to assure about the biological availability of the drug.[28] The detailed infrared spectroscopy of this type of interaction after co-processing by dry-state milling, and aqueous state equilibration and freeze drying has rarely been reported earlier. Nokhodchi et al.,[29] crystallized ibuprofen in presence of starch derivatives for improved pharmaceutical performance and found no significant change in FTIR spectroscopy and concluded that there is no change in molecular level of ibuprofen. Ibuprofen solid dispersions prepared using polyethylene glycol 4000 have shown no significant change in FT-IR spectra.[27]

2. Experimental

2. 1. Materials

Ibuprofen was obtained from Tejani Life care, Cuttack, India and magnesium trisilicate (USP 28) was purchased from Burgoyne & Co, India (not less than 20% of magnesium oxide and not less than 45% of silicon dioxide; loss on ignition 17.0–34.0%). All other chemicals used were of analytical reagent grade.

2. 2. Co-processing of Ibuprofen and Magnesium Trisilicate

Crystalline powder of ibuprofen and magnesium trisilicate powder were mixed for approximately 5 minutes by simple blending process using mortar and spatula at laboratory ambient condition in the dry-state (~30 °C; ~60% RH) without trituration. Ibuprofen and magnesium trisilicate (physical mixtures) weight ratios (3: 1, 2: 1, 1: 1 and 1: 2) were maintained as per formulation and left for immediate use in the co-process of dry-state ball-milling and, aqueous state kneading and freeze-drying.

2. 3. Dry-state Ball-milling

The powder mixture of ibuprofen and magnesium trisilicate in the weight ratios was placed into a cylindrical vessel of ball mill (Swastik Electric and Scientific Work, India) and 1 h period of constant milling was performed in the dry-state at lab ambient condition of ~30 °C, ~60% RH. Significant increase in temperature of the milled material has not been detected at the end of the co-process. Ball charged in the vessel allowed smooth cascading motion, and significant attrition and impact during dry-state milling while operating the mill at 100 rpm for 1 h.

2. 4. Aqueous State Kneading and Freeze-drying

Aqueous state kneading was performed by adding small amount of water in the physical powder mixtures of ibuprofen and magnesium trisilicate and left for a period of about 12 h at ambient conditions for equilibration. The kneaded samples were freeze-dried using a laboratory vacuum freeze dryer (4kg, 220 V) with attached vacuum (220V, 2.7A, 370W, 1400r/min, 50Hz) (Lark, Penguin Classic Plus, India) for 10–12 hours for effective drying. The pressure during freeze-drying was adjusted to 15–20 Pa while temperature maintained approximately at –40 °C. The freeze-dried samples were preserved in the desiccator till further analysis.

The ball-milled and freeze-dried samples were left at ambient condition (~60% RH, ~30 °C) for few hours and dried in an incubator (Labotech, India) at 50 °C. The powder materials were passed through mesh 44 (opening ~350 μm) and assayed for drug content determination from the absorbance measured at 222 nm (λ_{max}) in the UV visible Spectrophotometer (Jasco-V630 UV Spectrophotometer Spectrometer, Software: Spectra Manager) using standard calibration curve of ibuprofen.

2. 5. Ibuprofen–magnesium Trisilicate Interaction Study

FTIR spectra of pure crystalline ibuprofen and co-processed powder samples were performed for a compa-

rative study between co-milling and co-freeze drying interaction. All the samples were mixed thoroughly with potassium bromide in the ratio of 1:100. KBr discs were prepared by compressing the powders at a pressure of 6 tonnes for 10 min in a Hydraulic pellet press (Technosearch Instruments, Maharashtra, India). FTIR spectrometer (FTIR-4100 type A, Jasco, Tokyo, Japan) was used for collecting all scans from 4000–400 cm^{-1} of 80 accumulations at a resolution of 4 cm^{-1} and scanning speed of 2 mm/s. Spectral Manager for Windows software (Jasco, Tokyo, Japan) was used for data acquisition and holding.

2. 6. Surface Morphology and Thermal Analysis of the Particle

Surface morphology and crystalline nature of the particulate samples were investigated using Scanning electron microscope (Instrument JSM-6390, Jeol, Tokyo, Japan). The powder samples were dried and sputtered with gold and scanned at room temperature using an accelerated voltage of 10 kV (Wd 19 and Spot_Size 48). Thermal behavior of the powder samples was characterized using a Differential scanning calorimeter (DSC, Universal V4.2E TA Instruments). Samples approximately 5–6 mg were weighed accurately and put into crimped aluminum pans with a pin hole in the lid. All samples were heated at a heating rate of 10 °C/min in an atmosphere of nitrogen gas purge at 50 ml/min from 30 and 300 °C.

2. 7. Drug release Studies

Powdered samples containing 10 mg equivalent of ibuprofen were dispersed in 900 ml of distilled water and drug release was carried out using USP XXIV type II dissolution apparatus (Electrolab, dissolution tester USP TDT 06L, India) at a temperature of 37 ± 0.2 °C and paddle rotation set at 100 rpm. Ibuprofen concentration was determined by UV absorption at 222 nm. Aliquots were withdrawn at appropriate time intervals of 5, 10, 15, 30, 60, 90 and 120 min, and replaced with a fresh dissolution medium. After proper rinsing of the cuvette and filtration of the aliquot through a 0.45 μm membrane filter, absorbance was recorded using the UV-Visible Spectro photometer. Standard calibration curve was used for calculating the respective concentration and the data were utilized to estimate cumulative percent drug release. Cumulative percent drug release was reported as the mean of not less than three determinations.

3. Results and Discussion

The dry-state co-milling and aqueous state co-processing could be analogous to the commonly followed processes in the tablet granulation department of pharmaceutical industries. These processes are effective, simple and scalable for interaction study. Due to presence of varying amount of bound moisture in native magnesium trisilicate the co-milled materials became moisty in nature and needed drying. Instant character of the freeze-dried samples is to absorb moisture like a sponge when left at ambient condition of ~60% RH and 30 °C for few hours and drying in an incubator at 50 °C becomes necessary. The co-processed dried and equilibrated powder materials were passed through mesh of opening ~350 μm and assayed for actual drug content determination. Ibuprofen–magnesium trisilicate interaction study has been characterized by FTIR, and the usefulness of this powerful technique has been supported by scanning electron microscopy and differential scanning calorimetry as described below. Drug release from the formulated dosage form is important and ultimately related to the bioavailability of the drug. Dissolution of ibuprofen from the co-processed material has also been described below. Formulation detail and code of ibuprofen samples co-processed with magnesium trisilicate has been mentioned in Table 1.

3. 1. FTIR Analysis

Spectral data of FTIR band assignments of ibuprofen and co-processed samples are tabulated in Table 2.

Table 1. Formulation code of ibuprofen samples co-processed with magnesium trisilicate (Ibuprofen = IB, Magnesium trisilicate = MTS).

Formulation code	Drug: MTS ratio	Co-processing	Ibuprofen assay (%)
IB	–	–	–
IB1M1pm	1 : 1	Physical mixture without trituration	–
IB3M1B	3 : 1	Dry-state Ball-milling for one hour	71.61 ± 5.1
IB2M1B	2 : 1	Dry-state Ball-milling for one hour	68.65 ± 4.6
IB1M1B	1 : 1	Dry-state Ball-milling for one hour	46.09 ± 3.5
IB1M2B	1 : 2	Dry-state Ball-milling for one hour	37.54 ± 2.8
IB3M1F	3 : 1	Aqueous state equilibration and freeze-drying	74.11 ± 3.2
IB2M1F	2 : 1	Aqueous state equilibration and freeze-drying	68.55 ± 3.8
IB1M1F	1 : 1	Aqueous state equilibration and freeze-drying	48.65 ± 2.4
IB1M2F	1 : 2	Aqueous state equilibration and freeze-drying	30.54 ± 2.1

Table 2. Spectral data of FTIR of ibuprofen and co-processed samples

Band	Tentative assignments	Wavenumber (cm^{-1})									
		Ibuprofen	MTS	IB_3M_1F	IB_2M_1F	IB_1M_1F	IB_1M_2F	IB_3M_1B	IB_2M_1B	IB_1M_1B	IB_1M_2B
1	OH stretching	absent	3200–3550 bb	3200–3550 bb	3200–3550 bb	3200–3550 bb	3200–3550 bb	3200–3550 bb	3200–3550 bb	3200–3550 bb	3200–3550 bb
2	CH2 asym str	3094 m	–	absent	absent	absent	absent	3096 w	3096 w	absent	absent
3	CH3 asym str	2958 vs	–	2955 vs	2955 vs	2954 vs	2954 vs	2955 vs	2955 vs	2954 vs	2953 vs
4	CH2 sym str	2868 m	–	2868 m	2868 m	2868 m	2868 m	2869 m	2869 m	2869 m	2869 m
5	O-H…O valance str combination	2729 m	–	2729 aa	2729 aa	2729 aa	2729 aa	2730 w	2730 w	2730 vw	Absent
6	O-H…O valance str combination	2630 m	–	Absent	Absent	Absent	Absent	2631 vw	2632 vw	Absent	Absent
7	C=O str	1722 vs	–	1720 vw	1720 vw	1720 vw	Absent	1720 m	1720 m	1720 w	Absent
8	carboxylate stretching mode	Absent	–	1600–1650 m	1600–1650 m	1600–1650 m	1600–1650 s	1600–1650 w	1600–1650 w	1600–1650 m	1600–1650 s
9	aromatic C=C str	1507 s	–	1512 vw	1511 vw	1512 vvw	1512 vvw	1509 m	1508 m	1511 vw	1511 vw
10	CH3 asym deformation, CH2 scissoring	1462 s	–	1462 vw	1463 vw	1463 vw	1463 vw	1462 m	1462 m	1463 vw	1464 vw
11	CH-CO deformation	1420 s	–	1421 vw	1421 vw	1421 vw	1415 vw	1420 m	1420 m	1421 vw	1421 vw
12	CH3 sym str	1380 s	–	1383 vvw	1382 vvw	1382 vvw	1384 vvw	1380 w	1381 w	1380 vw	1381 vvw
13	OH in plane deformation	1321 s	–	1322 vw	1321 vw	1322 vw	1322 vvw	1321 m	1321 w	1322 vw	1325 vvw
14	=C-H in plane deformation	1268 s	–	1268 vw	1268 vw	1268 vw	1268 vvw	1263 m	1269 w	1269 vw	1268 vvw
15	C…C str	1230 vs	–	1231 vw	1231 vw	1230 vw	1230 vvw	1231 m	1231 w	1232 vw	1232 vvw
16	C-O str	1183 s	–	1183 vw	1184 vw	1183 vw	1183 vvw	1184 m	1184 w	1185 vw	1185 vvw
17	=C-H in plane deformation	1122 w	–	merger	merger	merger	merger	merger	merger	merger	merger
18	=C-H in plane deformation	1067 m	–	merger	merger	merger	merger	merger	merger	merger	merger
19	Si-O-Si asym str	Absent	1027 bb	~1027 mbb	~1027 mbb	~1027 bb	~1027 bb	~1027 mbb	~1027 mbb	~1027 bb	~1027 bb
20	C-H in plane deformation	1008 m	–	merger	merger	merger	merger	merger	merger	merger	merger
21	C-O-C str	970 m	–	970 w	970 vw	970 vvw	970 vvw	970 w	970 w	970 vw	970 vvw
22	CH3 rocking vibration	935 s	–	948 vw	948 vw	948 vvw	absent	935 w	936 w	936 vw	936 vvw
23	C-H out of plane vibration	866 s	–	866 vw	866 vw	866 vvw	absent	866 w	866 w	866 vw	865 vw
24	CH2 rocking	779 s	–	780 w	780 w	780 vw	780 vvw	779 w	779 w	780 vw	780 vvw
25	C=C ring str, C...C skeletal vibration	746 w	–	746 vw	746 vw	746 vw	746 vvw	746 vw	746 vw	746 vvw	746 vvw
26	C-H out of plane deformation	668 s	–	669 vvw	669 vvw	669 vvw	669 vvw	668 m	668 w	669 vw	669 vvw
27	C-H in plane ring deformation	636 w	–	636 vvw	636 vvw	635 vvw	635 vvw	636 w	636 w	636 vw	636 vvw
28	C...C deformation	588 m	–	588 vvw	588 vvw	588 vvw	588 vvw	588 m	588 w	588 vw	588 vvw
29	CH2 in plane rocking	522 m	–	522 vvw	522 vvw	522 vvw	522 vvw	522 m	522 w	522 vvw	522 vvw
30	CH2/CH3 deformation vibration	479 vw	–	472 vw	462 vw	464 vw	461 vw	461 vw	464 vw	462 vw	462 vw
31	O-Si-O bending	Absent	471 bb	464 m	461 m	463 bb	463 bb	464 m	464 m	464 bb	464 bb
32	C=C-C ring asym bending	421 w	–	420 aa	421 aa	421 aa	421 aa	420 vvw	421 vvw	421 vvw	421 vvw

(s- strong; bb- broad band; mbb- medium broad band; w- weak; sym-symmetrical; asym-asymmetrical; str-stretching; m- medium; vs- very strong; vw – very weak; vvw – very very weak; aa- almost absent.)

The very strong band at 2958 cm^{-1} in the FTIR spectrum of ibuprofen is assigned to CH_3 asymmetric stretching.[30] Ibuprofen has also shown the presence of free acid carbonyl peak at 1722 cm^{-1} with high intensity,[27,31] but became very weak when co-milled in the dry-state as well as co-freeze-dried after aqueous state kneading and equilibration with magnesium trisilicate (Fig. 1*a*,*b*). As the magnesium trisilicate ($2MgO,3SiO_2,xH_2O$) contains magnesium oxide (not less than 20% of magnesium oxide as per USP 28) and the acidic nature of the carboxylic acid group of ibuprofen, the possibility of an acid–base interaction between the drug and MgO of magnesium trisilicate was explored. Also, very high intensity peak of ibuprofen at 1230 cm^{-1} was due to C-C stretching[32] became gradually medium, weak, very weak and absent as the magnesium trisilicate amount increased in both the co-processed materials IB_3M_1F to IB_1M_2F and IB_3M_1B to IB_1M_2B. A strong band noticed at 779 cm^{-1} in ibuprofen was due to CH_2 rocking vibration and the intensity observed to be weaker and weaker after co-processing.[33,34] CH_2 asymmetric stretching vibration (3094 cm^{-1} and 2868 cm^{-1}) and CH_2 inplane rocking vibration (522 cm^{-1}) were also detected in pure ibuprofen and found weaker and absent when co-milled and freeze dried after co-kneading. CH_2 asymmetric stretching vibration (3094 cm^{-1} and 2868 cm^{-1}), CH_3 asymmetric deformation (1462 cm^{-1}), CH_3 rocking of strong intensity (935 cm^{-1}), and CH_2 inplane

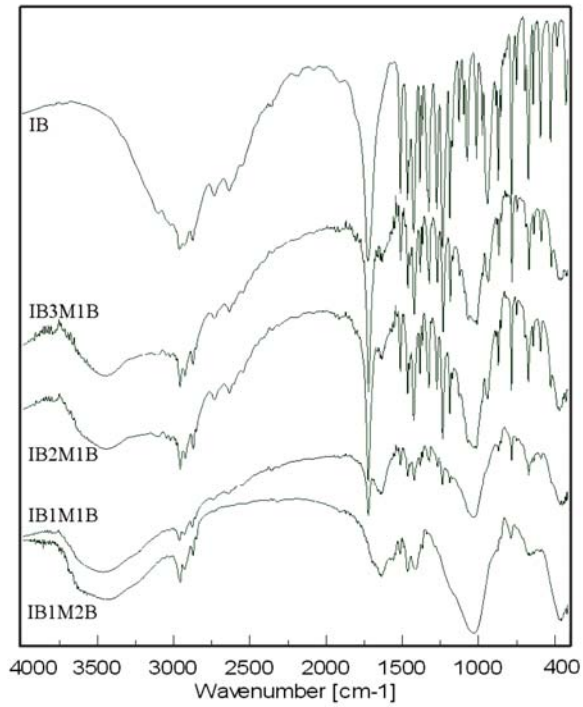

Figure 1. (contd.)**Figure 1.** FTIR spectroscopy of co-processed ibuprofen and magnesium trisilicate after dry-state ball-milling (a) MTS, IB, IB3M1F, IB2M1F, IB1M1F, and IB1M2F; and aqueous state equilibration and freeze-drying (b) IB, IB3M1B, IB2M1B, IB1M1B, and IB1M2B (abbreviations are explained in Table 1).

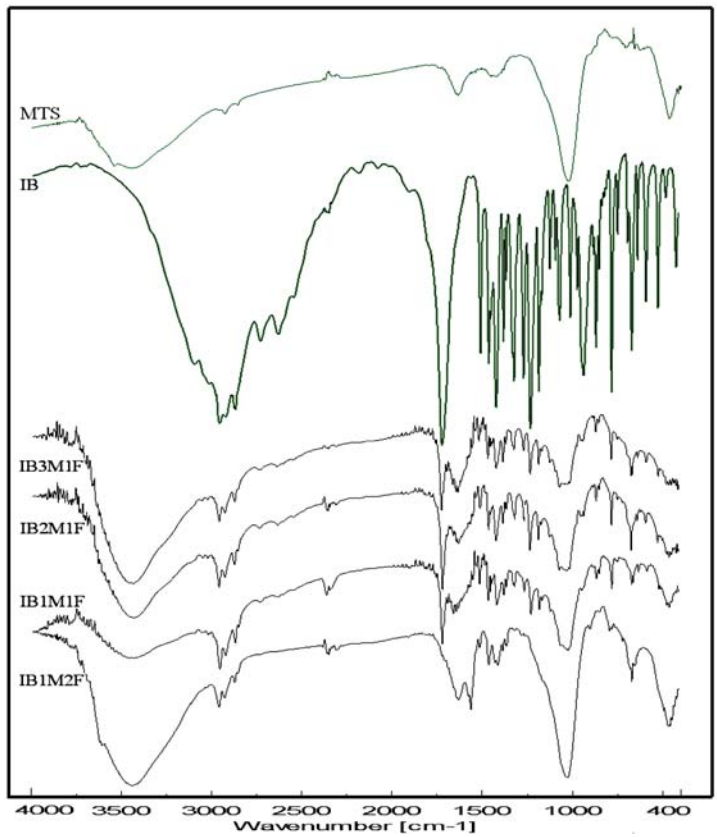

Figure 1. (contd.)

rocking vibration (522 cm^{-1}) were also detected in pure ibuprofen. Poor band performance was perceived in the co-processed formulations. C-O stretching (1183 cm^{-1}), CH_2 scissoring vibration (1462 cm^{-1}) and CH-CO deformation (1420 cm^{-1}) contributed their presence strongly in ibuprofen alone and weakly in the co-processed powder. An acid–base reaction between the carboxylic acid containing ibuprofen and MgO containing MTS in presence of moisture can describe the changes in the FTIR spectra of co-processed formulations. The reaction has been facilitated in presence of water when co-freeze-dried after aqueous state kneading and equilibration with magnesium trisilicate and also co-milled in the dry-state containing varying proportions of water in the MTS compound. Carboxylate ion shows peak in the range of 1600–1650 cm^{-1} in the FTIR spectrum and this change was detected as a function of IB/MTS ratio. A reduction in absorbance of the carbonyl acid peak accompanied by a corresponding increase in the absorbance of carboxylate peak was prominent and the absorbance of carboxylate peak was relatively

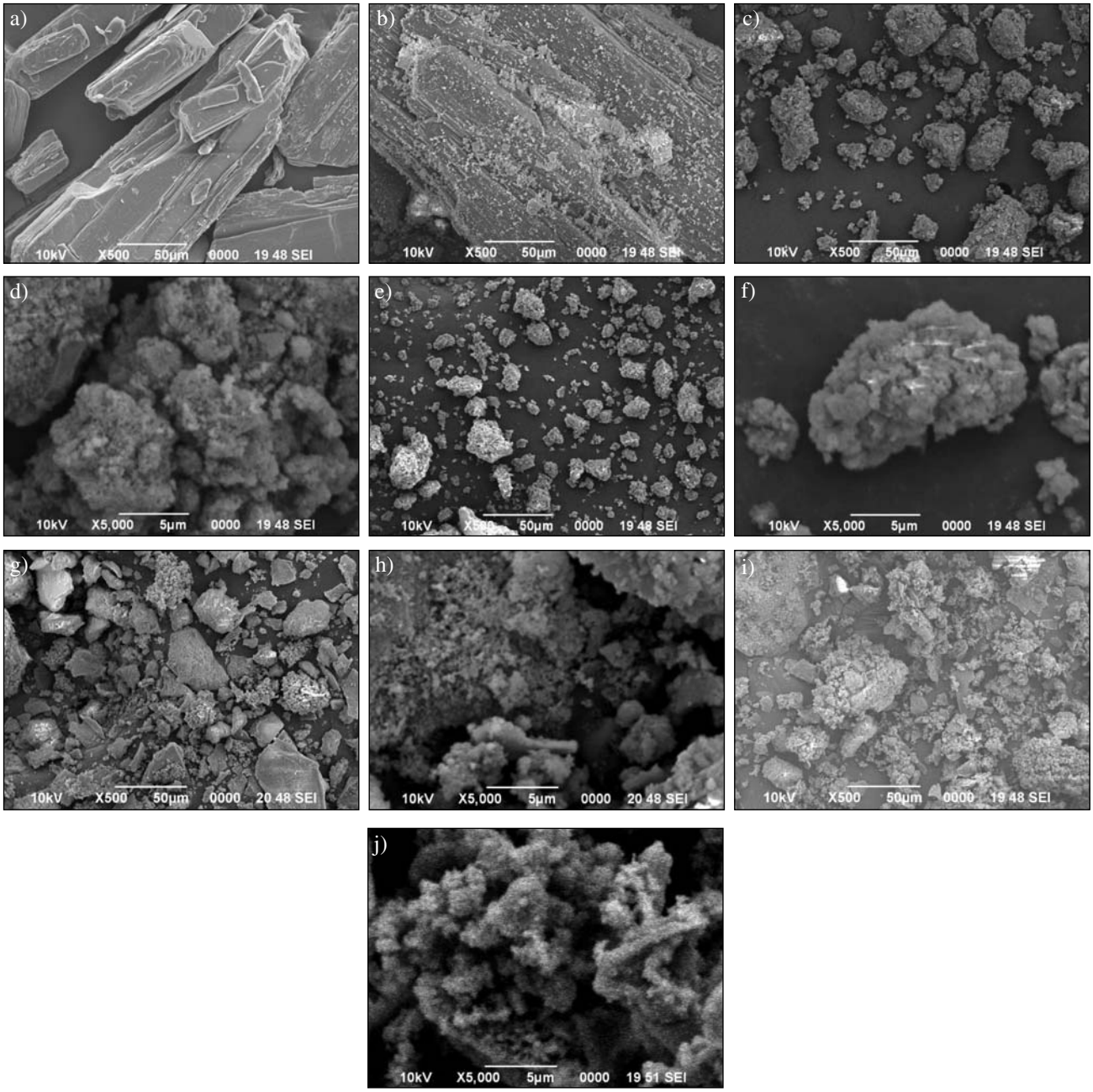

Figure 2. (a) Ibuprofen pure, (b) IB_1M_1pm, (c) IB_1M_1B (X500), (d) IB_1M_1B (X5000), (e) IB_1M_2B (X500), (f) IB_1M_2B (X5000), (g) IB_1M_1F (X500), (h) IB_1M_1F (X5000), (i) IB_1M_2F (1:2)F(X500), and (j) IB_1M_2F (X5000) (abbreviations are explained in Table 1).

more in freeze-dried product compared to milled product. A large broad band between 3550 to 3200 cm^{-1} ascribed to the presence of the O-H stretching frequency of silanol group bonded to the inorganic structure of MTS (containing SiO_2), and also hydrogen bonds between adsorbed water and silanol.[25,35] This large broad band is absent in ibuprofen pure drug but consistently maintained in all the co-processed materials could be due to intermolecular hydrogen bonding. The band related to the silanol (Si-O-Si) asymmetric stretching was found at 1027 cm^{-1} with high intensity in MTS and also in the co-processed formulations. Silanol asymmetric stretching intensity increased with the amount of MTS in the formulation. Another peak at 471 cm^{-1} in MTS due to O-Si-O bending[36] prominently observed in the formulations. The small changes in the band intensity, band orientation and overlapping indicated only van der Waals or dipole-dipole interactions between ibuprofen and magnesium trisilicate molecules.

3. 2. Characterization by Scanning Electron Microscopy and Differential Scanning Calorimetry

Scanning electron microscopy is a powerful tool to study the inhibition of crystal growth morphology. Fig. 2 shows distinctive plate like layers due to the crystalline nature in the initial samples of pure ibuprofen. Physical mixture of drug and magnesium trisilicate in 1:1 ratio (IB_1M_1pm) shows the presence of ibuprofen crystal geometry very clearly with slightly damaged morphology. Markedly reduced particle size has been noticed not only in the co-milled materials but also in the freeze-dried formulations after aqueous state kneading and co-processing. Crystal geometry of ibuprofen has been significantly disappeared in both the co-processed materials.

Sub-micron and nano-crystalline agglomeration were observed particularly in the milled material whereas, freeze-dried materials have shown porous bed of irregular nanoparticles developing grain boundaries in the crystal structure indicating loss of crystal geometry. These grain boundaries supposed to disrupt the motion of dislocations and reduce the crystallite size of ibuprofen in the co-processed powder.[37]

Differential scanning calorimetry is frequently used in pharmaceutical research as an analytical tool for the identification and interaction study of active drug after co-processing with other pharmaceutical compounds.[38–43] It can explain the miscibility/incompatibility with its effects on thermal stability, yielding results promptly and efficiently.[44] Thermograms after differential scanning calorimetry of pure ibuprofen and co-processed powder samples are presented in Fig 3. Ibuprofen has shown the melting endotherm at 76.7 °C which is approximately similar to the literature value.[33] With the increase of MTS amount in the co-processed material melting temperature and enthalpy (data not mentioned) have been decreased markedly signifying the material is made up of a number of smaller crystals or crystallites, and paracrystalline phases. Melting endotherm of IB_1M_2B and IB_1M_2F has been disappeared indicating an almost amorphous structure where the atomic position is limited to short range order only. Amorphous phase of ibuprofen could be possible to pro-

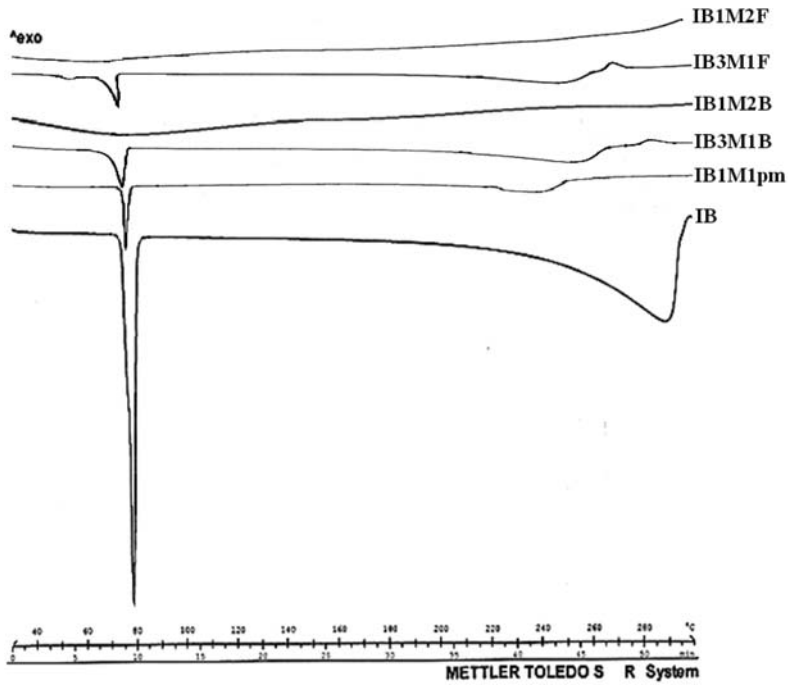

Figure 3. Differential scanning calorimetry of co-processed ibuprofen and magnesium trisilicate after dry-state ball-milling, and aqueous state equilibration and freeze-drying (abbreviations are explained in Table 1).

duce by solid state co-milling with kaolin.[31] The interaction between ibuprofen and the porous silica adsorbents indicated a significant loss of crystallinity of ibuprofen by the DSC studies.[13]

3. 3. In-vitro Release of Ibuprofen

In-vitro drug release profiles of the co-processed material up to 120 min have been depicted in the Fig. 4*a,b*. The powder materials have shown significantly improved dissolution of drug after co-processing. Crystalline ibuprofen exhibited only 52.89% dissolution whereas, dry-state co-milling of ibuprofen and magnesium trisilicate has improved dissolution to a great extent (77.98 to 85.84%). Formulated powder samples of aqueous state co-processing and freeze-drying of ibuprofen and magnesium trisilicate have presented relatively more improved drug release (84.87 to 100.29%). Percentage release of ibuprofen increased gradually with the gradual increase in magnesium trisilicate proportion in the freeze-dried samples. Mixtures of ibuprofen and magnesium trisilicate have presented substantially higher dissolution compared to the pure drug. Magnesium oxide (MgO) in magnesium trisilicate and carboxylic acid containing ibuprofen brought about the acid–base reaction and the hydrogen-bonding potential of silanol groups of SiO_2 in the surface of magnesium trisilicate facilitated collectively the increase in the drug dissolution rate. Dissolution of nimesulide from pharmaceutical formulations exhibited better dissolution when the formulations contain micronized nimesulide crystals and medium become alkaline rather than acidic.[28] Increased proportion of magnesium trisilicate in the mixture might have consumed the carboxylic acid containing ibuprofen and more of hydrogen-bonding potential of silanol groups can describe the increased release of ibuprofen of the co-processed formulations. Otsuka et al. have been able to transform the crystalline polymorphs of indomethacin to amorphous states during milling which had 60% higher dissolution than the crystalline state.[20] The increased dissolution of drug from solid dispersions possibly be related to the decreased drug crystallinity or effective wetting of the reduced drug particles.[45–48] Co-processing of ibuprofen with magnesium trisilicate for enhanced dissolution possibly be a promising approach for improvement of ibuprofen bioavailability.[47]

4. Conclusions

Detailed infrared spectroscopy has been utilized for the assessment of interactions of ibuprofen and magnesium trisilicate after dry-state ball-milling and, aqueous state kneading and freeze-drying. Changes in the frequency and shape of ibuprofen bands after co-processing have been detected for the analysis of redistribution of electronic density in the structure of ibuprofen molecule. Changes in the FTIR spectroscopy of co-processed formulations can describe acid–base reaction between the carboxylic acid containing ibuprofen and MgO of magnesium trisilicate (2MgO,3SiO2,*x*H2O). Varying proportions of water in the magnesium trisilicate facilitated the reaction in the dry-state milling rather gently while, aqueous state equilibration and freeze-drying brought about the reaction considerably. Reduced absorbance of the carbonyl acid peak accompanied by a consistently increase in the absorbance of carboxylate peak was prominently visible and the absorbance of carboxylate peak was rather more in freeze-dried product compared to milled sample.

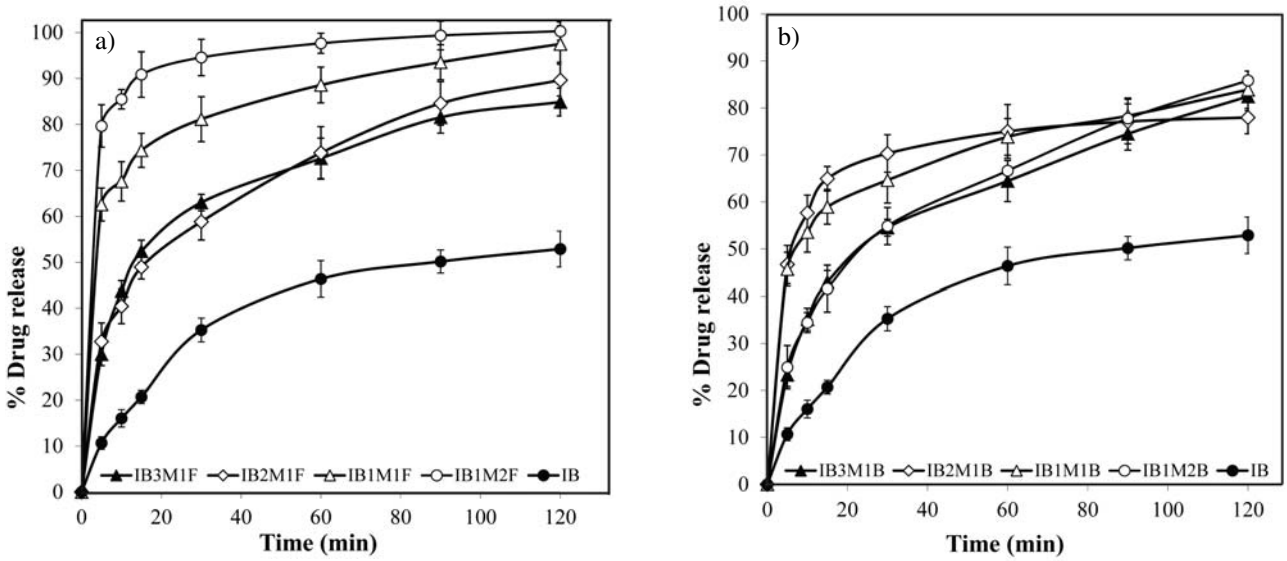

Figure 4. Dissolution profiles of co-processed ibuprofen and magnesium trisilicate: (*a*) dry-state ball-milling samples; (*b*) freeze-dried samples after aqueous state equilibration (abbreviations are explained in Table 1).

O-H stretching frequency of silanol group due to the presence of SiO_2 in the structure of MTS and the hydrogen bonds between adsorbed water and silanol attributed a large broad band between 3550 to 3200 cm^{-1} in all the co-processed materials and not in ibuprofen pure drug spectrum. That is the indication of intermolecular hydrogen bonding between ibuprofen and magnesium trisilicate in the co-processed material. Scanning electron microscopy revealed the inhibition of crystal growth morphology in both the co-processed materials. Milled material has shown sub-micron and nano-crystalline accumulation but, porous bed of irregular nanoparticles with developing grain boundaries was observed in the crystal structure of the freeze-dried samples. Missing of melting endotherm in the DSC report of IB_1M_2B and IB_1M_2F signified almost complete amorphization of ibuprofen. Significantly decreased melting temperature and enthalpy of ibuprofen in the other co-processed materials indicated inhibition of crystal growth to a great extent. Significantly increased dissolution of drug has been noticed after co-processing compared to crystalline ibuprofen alone. Freeze-dried process presented relatively more enhanced drug release compared to ball-milled samples.

5. Acknowledgments

The authors are very much grateful to Prof. Manoj Ranjan Nayak, President, Siksha O Anusandhan University for his inspiration and facilities.

Conflict of Interest

None

6. References

1. R. Jones, *Am. J. Med.* **2001**, *110*, S4–S7. https://doi.org/10.1016/S0002-9343(00)00627-6
2. L. M. Lichtenberger, Y. Zhou, E. J. Dial, R. M. Raphael, *J. Pharm. Pharmacol.* **2006**, *58*, 1421–1428. https://doi.org/10.1211/jpp.58.10.0001
3. C. S. Levin, J. Kundu B. G. Janesko, G. E. Scuseria, R. M. Raphael, N. J. Halas, *J. Phys. Chem. B.* **2008**, *112*, 14168–14175. https://doi.org/10.1021/jp804374e
4. D. M. Moss, M. Siccardi, D. J. Back, A. Owen, *J. Antimicrob. Chemother.* **2013**, *68*, 1627–1634. https://doi.org/10.1093/jac/dkt084
5. V. F. Naggar, S. A. Khalil, M. W. Gouda, *J. Pharm. Sci.* **1978**, *67*, 1029–1030. https://doi.org/10.1002/jps.2600670746
6. V. F. Naggar, S. A. Khalil, *Clin. Pharmacol. Ther.* **1979**, *25*, 857–863. https://doi.org/10.1002/cpt1979256857
7. V. F. Naggar, S. A. Khalil, *Pharmazie.* **1980**, *35*, 412–416.
8. S. A. Babhair, M. Tariq, *Res. Commun. Chem. Pathol. Pharmacol.* **1983**, *40*, 165–168.
9. Magnesium Trisilicate Mixture BP - Summary of Product ... – eMC (Last Updated on eMC 30-Jul-2015) https://www.medicines.org.uk/emc/medicine/25289
10. F. Carli, E. Chiellini, Pharmaceutical composition comprising a water/oil/water double microemulsion incorporated in a solid support. **2004**, Google Patents.
11. X. Pan, The application of porous adsorbents to increase the dissolution rate of low solubility drugs, dissertation. **2002**, University of Maryland.
12. M. K. Gupta, D. Goldman, R. H. Bogner, Y-C. Tseng, *Pharm. Dev. Technol.* **2001**, *6*, 563–572. https://doi.org/10.1081/PDT-120000294
13. M. K. Gupta, R. H. Bogner, D. Goldman, Y-C. Tseng, *Pharm. Dev. Technol.* **2002**, *7*, 103–112. https://doi.org/10.1081/PDT-120002236
14. M. Mihelcic, A. S. Vuk, D. Vrhovsek, F. Svegl, M. Hajzeri, B. Orel, *Acta Chim. Slov.* **2014**, *61*, 517–529.
15. T. Friscic, in: A. Stolle, B. Ranu (Ed.): Ball Milling Towards Green Synthesis: Applications, Projects, Challenges, Royal Society of Chemistry, Thomas Graham House, Cambridge, UK, **2015**, pp. 151–189.
16. Y. Liu, X. Wang, H. Liu, Z. Dong, S. Li, H. Gea, M.Yan, *RSC Adv.* **2015**, *5*, 60460–60466.
17. G. Buckton, A. Choularton, A. E. Beezer, S. M. Chatham, *Int. J. Pharm.* **1988**, *47*, 121–128. https://doi.org/10.1016/0378-5173(88)90222-0
18. S. Kitamura, A. Miyamae, S. Koda, Y. Morimoto, *Int. J. Pharm.* **1989**, *56*, 125–134. https://doi.org/10.1016/0378-5173(89)90005-7
19. M. Otsuka, T. Ofusa, Y. Matsuda, *Colloids Surf. B: Biointerf.* **1999**, *13*, 263–273. https://doi.org/10.1016/S0927-7765(99)00014-4
20. M. Otsuka, T. Matsumoto, N. Kaneniwa, *Chem. Pharm. Bull.* **1986**, *34*, 1784–1793. https://doi.org/10.1248/cpb.34.1784
21. B. Karolewicz, A. Górniak, A. Owczarek, E. ŻurawskaPłaksej, A. Piwowar, J. Pluta, *J. Therm. Anal. Cal.* **2014**, *115*, 2487–2493. https://doi.org/10.1007/s10973-014-3661-2
22. H. Al-Hamidi, K. Asare-Addo, S. Desai, M. Kitson, A. Nokhodchi, *Drug Dev Ind Pharm.* **2015**, *41*, 1682–1692. https://doi.org/10.3109/03639045.2014.991401
23. E. Klosinska-Szmurlo, M. Grudzien, K. Betlejewska-Kielak, F. Plucinski, J. Biernacka, A. P. Mazurek, *Acta Chim. Slov.* **2014**, *61*, 827–834.
24. M. J. Pikal, in: J. C. May, L. Rey, (Ed.): Freeze-Drying/ Lyophilization of Pharmaceutical & Biological Products, **2004**, Marcel Dekker, Inc. New York, U.S.A.
25. A. O. Jorgetto, S. P. Pereira, R. I. V. da Silva, M. J. Saeki, M. A. U. Martines, V. A. Pedrosa1, G. R. de Castro, *Acta Chim. Slov.* **2015**, *62*, 111–121.
26. A. Górniak, B. Karolewicz, H Czapor-Irzabek, O. Gładysz, *Farmacia*, **2016**, *64*, 244–251.
27. M. Newa, K. H. Bhandari, D. X. Li, J. O. Kim, D. S. Yoo, J. A. Kim, B. K. Yoo, J. S. Woo, H. G. Choi, C. S. Yong, *Biol. Pharm. Bull.* **2008**, *31*, 939–945. https://doi.org/10.1248/bpb.31.939

28. B. Tubic, A. Uzunovic, S. Pilipovic, Z. Gagic, *Acta Chim. Slov.* **2016**, *63*, 193–199. https://doi.org/10.17344/acsi.2015.2168
29. A. Nokhodchi, A. Homayouni, R. Araya, W. Kaialy, W. Obeidat, K. Asare-Addo, *RSC Adv.* **2015**, *5*, 46119-46131. https://doi.org/10.1039/C5RA06183K
30. R. M. Silverstein, G. C. Bassler, T. C. Morrill, in: J. Stiefel (Ed.): Infrared spectroscopy: Spectrometric identification of organic compounds, John Wiley and Sons, Singapore, **1991**, pp. 91–164.
31. S. Mallick, S. Pattnaik, K. Swain, P. K. De, A. Saha, G. Ghoshal, A. Mondal, *Eur J Pharm Biopharm*. **2008**, *68*, 346–351. https://doi.org/10.1016/j.ejpb.2007.06.003
32. S. G. Kazarian, G. G. Martirosyan, *Int J Pharm*. **2002**, *232*, 81–90. https://doi.org/10.1016/S0378-5173(01)00905-X
33. A. Nokhodchi, O. Amire, M. Jelvehgari, *Daru* **2010**, *18*, 74–83.
34. S. R. Matkovic, G. M. Valle, L. E. Briand, *Latin Am Appl Res*. **2005**, *35*, 189–195.
35. E. DeOliveira, J. D. Torres, C. C. Silva, A. A. M. Luz, P. Bakuzis, A. G. S. Prado, *J Braz Chem Soc*. **2006**, *17*, 994–999. https://doi.org/10.1590/S0103-50532006000500026
36. A. Carreno, E. Schott, X. Zarate, R. Arratia-Perez, J. C. VegaDe, M. Mardones, J. M. Manriquez, I. Chavez, *J Chil Chem Soc*. 2011, *56*, 692–696.
37. P. R. Cantwell, M. Tang, S. J. Dillon, J. Luo, G. S. Rohrer, M. P. Harmer, *Acta Mater*. 2014, *62*, 1–48. https://doi.org/10.1016/j.actamat.2013.07.037
38. S. Mallick, *Indian J Pharm Sci*. **2004**, *2*, 142–147.
39. S. Pattnaik, K. Swain, S. Mallick, Z. Lin, *Int J Pharm*. **2011**, *406*, 106–110. https://doi.org/10.1016/j.ijpharm.2011.01.009
40. R. Mohapatra, S. Mallick, A. Nanda, R. N. Sahoo, A. Pramanik, A. Bose, D. Das, L. Pattnaik, *RSC Adv*. **2016**, *6*, 31976–31987.
41. B. Tita, T. Jurca, G. Rusu, G. Bandur, D. Tita, *Rev Chim (Bucharest)*. **2013**, *64*, 1089–1095.
42. B. Tita, E. Marian, G. Rusu, G. Bandur, D. Tita, *Rev Chim (Bucharest).* **2013**, *64*, 1390–1394.
43. B. Panda, A. S. Parihar, S. Mallick, *Int J Biol Macromol*. **2014**, *67*, 295–302. https://doi.org/10.1016/j.ijbiomac.2014.03.033
44. K. Klimova, J. Leitner, *Thermochim Acta*., **2012**, *550*, 59–64. https://doi.org/10.1016/j.tca.2012.09.024
45. M. Newa, K. H. Bhandari, D. H. Oh, Y. R. Kim, J. H. Sung, J. O. Kim, J. S. Woo, H. G. Choi, C. S. Yong, *Arch. Pharm. Res*. **2008**, *31*, 1497–1507. https://doi.org/10.1007/s12272-001-2136-8
46. H. H. Baek, D. H. Kim, S. Y. Kwon, S. J. Rho, D. W. Kim, H. G. Choi, Y. R. Kim, C. S. Yong, *Arch. Pharm. Res*. **2012**, *35*, 683–689. https://doi.org/10.1007/s12272-012-0412-4
47. B. Karolewicz, M. Gajda, A. Owczarek, J. Pluta, A. Górniak, *Trop. J. Pharm. Res.* **2014**, *13*, 1225–1232. https://doi.org/10.4314/tjpr.v13i8.5
48. B. Karolewicz, M. Gajda, A. Owczarek, J. Pluta, A. Górniak, *Pharmazie*, **2014**, *69*, 589–594.

Povzetek

Zmes ibuprofena in magnezijevega trisilikata smo pripravili na dva načina: s suhim mletjem in z liofilizacijo vodne raztopine. Nastali zmesi smo preučevali s FTIR spektroskopijo. Opazili smo povečano absorpcijo kaboksilatne skupine povezane z zmanjšanjem absorbance karbonilne kisline, kar kaže na določeno reakcijo karboksilne kisline v ibuprofenu. Absorbanca karboksilne skupine je bila bolj izrazita v liofiliziranem vzorcu, kar kaže na možne intermolekularne vezi med ibuprofenom in magenezijevim trisilikatom v tem primeru priprave zmesi. Razliko smo opazili tudi na fotomikrografskih posnetkih in pri DSC meritvah tališča. Sproščanje ibuprofena iz liofiliziranega vzorca je hitrejše kot pa iz vzorca, pripravljenega s suhim mletjem.

Scientific paper

MnO_2 Submicroparticles from Chinese Brush and Their Application in Treatment of Methylene Blue Contaminated Wastewater

Qi Wang,[1,*] Chunlei Ma,[1] Wanjun Li,[1] Meng Fan,[2] Songdong Li[1] and Lihua Ma[3,*]

[1] *Chemistry & Chemical Engineering Department, Taiyuan Institute of Technology, Taiyuan 030008, China.*

[2] *Research Center for Eco-Environmental Sciences in Shanxi, Taiyuan 030009, China*

[3] *Department of Chemistry, University of Houston at Clear Lake, Houston 77058, USA*

* *Corresponding author: E-mail: wangqitit@163.com; mal@uhcl.edu.*

Received: 30-07-2016

Abstract

Eggshell membrane (ESM) is selected as biotemplate to prepare MnO_2 submicroparticles (SMPs) using Chinese Brush with sodium hydroxide solution. The size with average 710 nm of the obtained materials is in good consistency with the microsructured biotemplate. An efficient and convenient absorbent for methylene blue (MB) is developed. The removal efficiency could reach up to 93% in 35 min under room temperature without pH adjusting owing to the excellent adsorption from ESM itself and hydroxyl group formed on the surface of MnO_2 crystal in the aqueous solution. Materials on the membrane can be separated from the wastewater simply to avoid the secondary pollution caused by the leak of material. This interesting approach to MnO_2 SMPs and facile operation for MB adsorption could open a new path to the submicro-materials based wastewater treatment.

Keywords: MnO_2 particles, biotemplate, eggshell membrane, methylene blue

1. Introduction

Synthesis of inorganic materials by biotemplating as a burgeoning technique has emerged for years in a wide variety of research fields.[1] The use of biotemplate makes the synthetic procedure simple and product controllable taking advantage of the nature of their own. Biotemplates like organisms (butterfly wing,[2] hair,[3] wood fiber[4,5] and pollen[6]), microorganisms (bacteria,[7,8] fungus,[9,10] and viruses[11]) and biological macromolecules (DNA,[12–14] RNA,[15] proteins,[16–19] and polysaccharides[20]) were reported to prepare inorganic materials. Among these templates, proteins have gained more popularity by researchers,[21] ranging from ferritin,[22–25] bovine serum albumin (BSA)[26–31] to collagen[32–34]. However, proteins from natural extracted or artificial synthetic are difficult to obtain and thus cost a lot. This could be a pivotal limitation for the large-scale synthesis and practical application of the biotemplated materials.

Eggshell membrane (ESM) is a kind of biomaterial with great imperative though it is generally considered as a domestic waste.[35] This microscopic biopolymeric fibrous net is composed mainly of proteins (80–85%), 10% of which are collagens and 70–75% are other proteins and glycoproteins.[36] Due to the unique structure and property, ESM has been utilized as a biotemplate for synthesis of inorganic materials. Novel metal materials such as gold nanoparticles, silver nanoparticles, macroporous silver network, Pt-Ag/polymers, have been constructed through ESM templating.[37–40] On the other hand, sulfide,[41] selenide,[42] oxidide[43,44] have been synthesized using ESM as a template. Besides, other kinds of material based on ESM have been studied.[45–47]

As a kind of inorganic nanomaterials, MnO_2 have drawn much attention because of their flexible structures and unique properties and have been applied to catalysis, ion exchange, supercapacitors, molecule adsorption, biosensors and so on.[48] One of the recent applications has fo-

cused on the MnO_2 based micromotors.[49–52] And micromotors containing manganese oxide and noble metal or graphene have also been studied.[53–55]

In this work, by consideration of its special microstructure, abundant component of protein, we choose ESM as the biotemplate to help synthesize MnO_2. Most important of all, ESM could be obtained expediently and free of charge. Furthermore, on the basis of the interaction between protein and metal ions, a novel and interesting procedure with Chinese Brush to grow MnO_2 submicroparticles (MnO_2 SMPs) on ESM is developed. As reported by Furuichi et al, hydroxyl groups could be formed on the surface of MnO_2 in aqueous solutions.[56] Cao et al confirmed that the hydroxyl groups were involved in the adsorption.[48] Therefore, combining the adsorption capacities of both ESM itself[57] and hydroxyl groups formed on the surface of MnO_2 in the aqueous media, these accessible MnO_2 SMPs are applied successfully to the treatment of methylene blue (MB) wastewater.

2. Experimental

2. 1. Reagents and Apparatus

Deionized water with conductivity of 18.2 mΩ cm^{-1} was used in this experiment from a water purification system (ULUPURE, Chengdu, China). Manganese acetate ($MnAc_2$, M_w = 245.09, AR) and methylene blue (MB) were purchased from Kemiou Chemical Co. Ltd. (Tianjin, China). Sodium hydroxide (NaOH, AR) and all the other reagents were at least of analytical grade. Eggshell was obtained from Hongye student mess hall of Taiyuan Institute of Technology, and eggshell membrane was peeled off from the shell carefully. Diluents with different pH values were prepared by titrating with 0.1 mol L^{-1} sodium hydroxide or hydrochloric acid solution to the required pH values.

Scanning electron microscopy (SEM) of ESM and MnO_2 SMPs were carried out on a Quanta 200 FEG scanning electron microscope. The size distribution of as-prepared nanomaterial was performed at a laser particle sizer (Malvern Nano-ZS90). The X-ray photoelectron spectroscopy (XPS) was measured with an AXIS ULTRA DLD electron spectrometer (Kratos) using monochromatic Al Kα radiation for analysis of the surface composition and chemical states of the product. Thermogravimetry (TG) measurement was carried out in air at a heating rate of 10 °C min^{-1} on a Rigaku TG thermal analyzer (Rigaku Co., Japan). The UV-vis absorption spectra were recorded on a TU-1901 UV-vis spectrophotometer (Puxi, China).

2. 2. Synthesis of MnO_2 SMPs

MnO_2 SMPs in this experiment were synthesized through a simple and interesting method. In a typical process, eggshell membrane (ESM) was firstly peeled off carefully from a fresh eggshell and cleaned 10 times with deionized water to remove residual egg white and then dried at room temperature. The clean ESM was cut into small pieces and soaked into 0.1 mol L^{-1} manganese acetate solution with a certain proportion (0.5 g to 100 mL). After 12 hours, the adsorbed ESM pieces were taken out and washed 5 times with deionized water and placed onto a watch glass to dry. At last, a Chinese Brush was dipped in 0.1 mol L^{-1} NaOH solution for 20 seconds. NaOH solution as ink was brushed evenly on the adsorbed ESM. Five minutes later, the color change of the membrane from white to light brown indicated that the MnO_2 SMPs were synthesized successfully. The MnO_2/ESM piece was washed and dried to preserve for characterization and practical use.

2. 3. Treatment of Methylene Blue Wastewater

15 mg MnO_2/ESM materials and equal amounts of ESM, as a control experiment, were placed in the 4 mL MB solution with the concentration of 8 mg L^{-1} under stirring. After 35 min, materials and ESM were taken out to stop the adsorption. The UV-vis spectra of MB solutions after adsorption were recorded immediately at room temperature. All of the absorption intensity of MB measurement was set at wavelength 664 nm. The removal efficiency (R, %) and adsorption capacity (q_e, mg g^{-1}) were calculated using the equations below:

$$R = \frac{C_0 - C_e}{C_0} \times 100\% \quad (1)$$

$$q_e = \frac{(C_0 - C_e) \times V}{W} \quad (2)$$

where C_0 and C_e (mg L^{-1}) stand for the initial and final concentrations of MB in the treatment solutions, respectively, V is the volume of the mixture solution (L), and W is the mass of adsorbent used (g).

3. Results and Discussion

3. 1. Synthesis Mechanism

Scheme 1 displays the schematic diagram of the synthesis process of submicro-structured MnO_2 on ESM using Chinese Brush. As reported, eggshell membrane is composed of fibrous proteins with different kinds of acidic/basic amino acid residues like –OH, –COOH, $–NH_2$, –SH, etc on the surface. When ESM pieces were soaked into the manganese acetate solution, Mn^{2+} showed a trend (from lone electron pair of heteroatom and unoccupied orbital in Mn atom) to adsorb onto the "active site" on the ESM, which resulted in a uniformly dispersive distribution of Mn^{2+} on the fibrous proteins. After washing and drying

at the room temperature, Chinese Brush with NaOH solution was brushed on the adsorbed ESM. This step caused a reaction in situ between Mn^{2+} and OH^- around these "active site" and as a result MnO_2 were obtained after 5 min.[57] Owing to the uniformly dispersion of Mn^{2+} on the membrane, MnO_2 particles were generated and grew along with the fibrous proteins to form a biomimetic material.

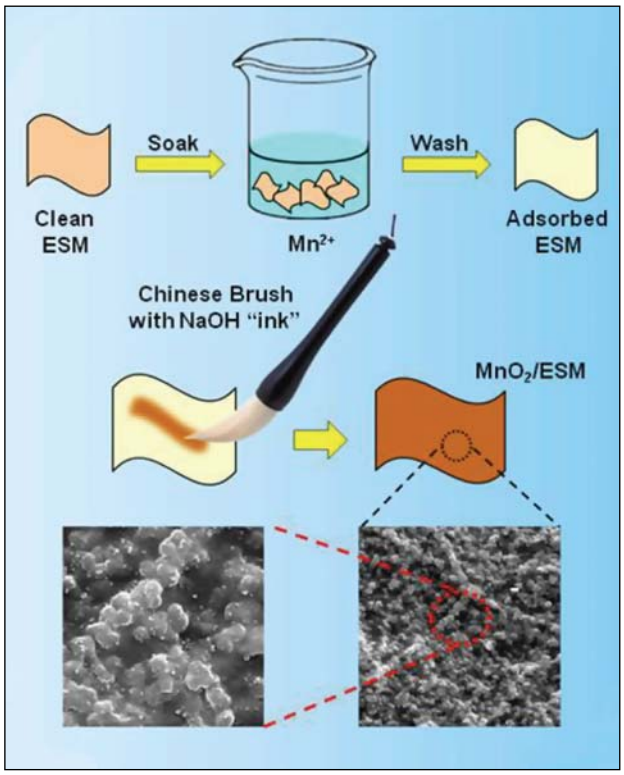

Scheme 1. The schematic diagram of the synthesis process of MnO_2 SMPs on ESM using Chinese Brush.

3. 2. Characterization of MnO_2 SMPs

3. 2. 1. Scanning Electron Microscopy

Morphologies of ESM before and after MnO_2 preparation were investigated for comparison. Figure 1a displays the scanning electron microscopy (SEM) images of ESM, in which multilayer and overlapping fibrous proteins are observed. After the reaction with MnO_2, by contrast, plenty of spherical particles array densely on the adsorbed membrane (Figure 1b and Figure S1a). Interestingly, particles arraying along with the original fiber-like protein is observed, and it is more obvious and straightforward in SEM image with smaller amplification factor (Figure S1a). To measure the particle size of synthesized material, a Nano Particle Analyzer testing was carried out. The results are shown in Figure S1b. And an average diameter of ~710 nm is obtained, which is a good consistency with the microstructured biotemplate.

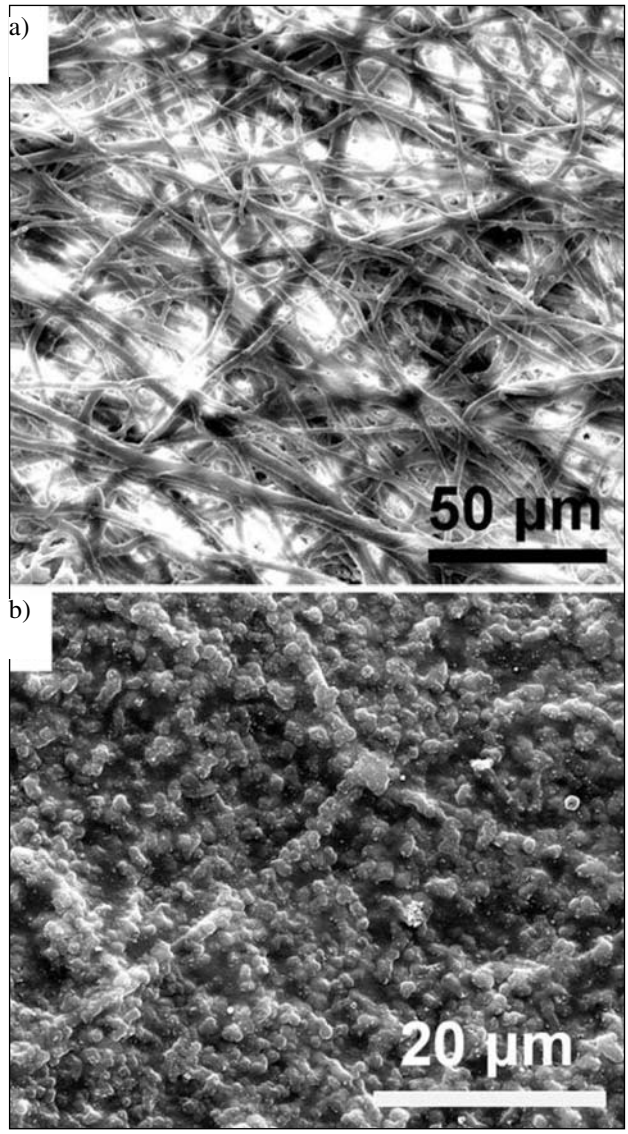

Figure 1. SEM images of (a) ESM and (b) MnO_2 SMPs. Scale bar were 50 μm and 20 μm, respectively.

3. 2. 2. UV-Vis Spectroscopy and X-ray Photoelectron Spectroscopy

The UV-Vis spectrum of as-prepared MnO_2 SMPs is shown in Figure S2. A single absorption peak at 360 nm is found. To investigate the surface composition and elemental analysis for the resultant MnO_2 SMPs, the X-ray photoelectron spectroscopy (XPS) was carried out. In the full scan spectrum (Figure S3), it shows that the synthesized material is composed of elements Mn 2p, O 1s, C 1s and N 1s. The elements C 1s, N 1s and partial O 1s come from proteins in ESM. To examine the details, XPS spectra of Mn 2p and O 1s were measured. As shown in Mn 2p spectrum (Figure 2a), two peaks are observed at 654.2 and 642.4 eV, which can be assigned to Mn $2p_{1/2}$ and Mn $2p_{3/2}$, respectively. Meanwhile, the O 1s spectrum (Figure 2b) can be resolved into three peaks. The strongest peak at

531.4 eV corresponds to the Mn–O–H, the other two small peaks (532.2 eV and 530.0 eV) adjacent reveal the existence of H–O–H and Mn–O–Mn, respectively. As a consequence, the aforementioned findings confirm that the as-prepared submicroparticles are MnO_2.

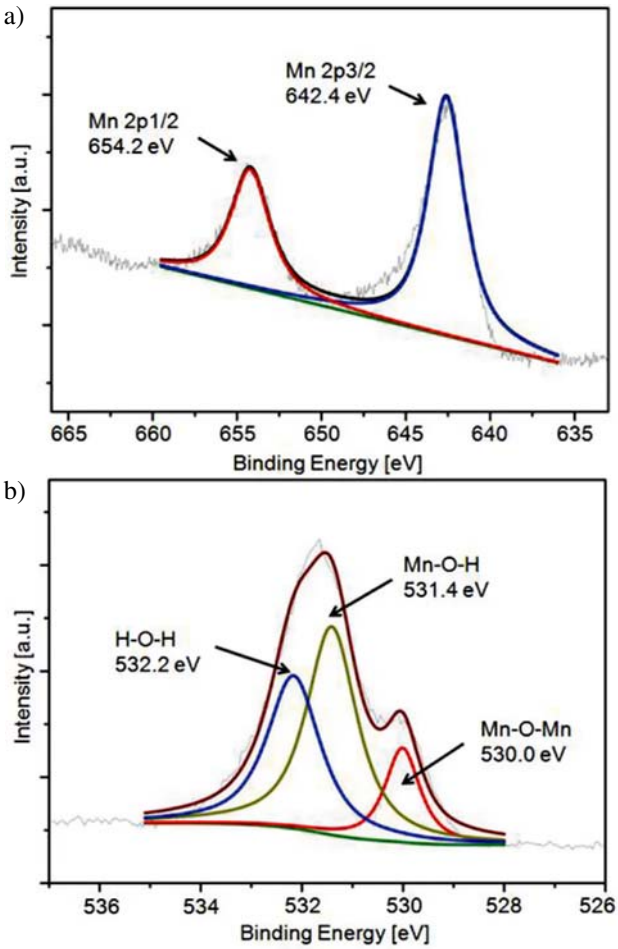

Figure 2. (a) Mn2p and (b) O1s XPS spectra of as-prepared MnO_2 SMPs.

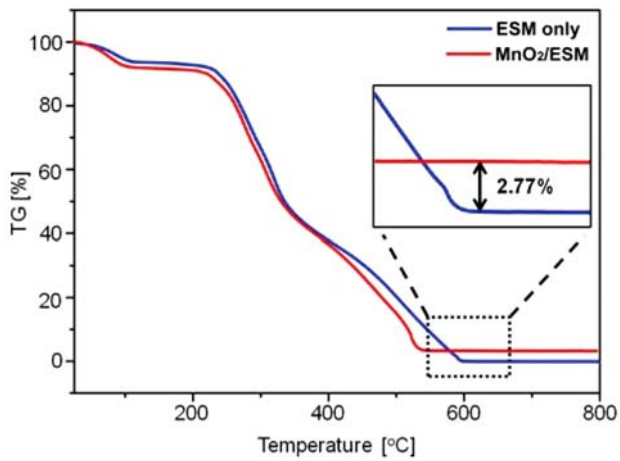

Figure 3. The TG curves of ESM and as-prepared MnO_2 SMPs.

3. 2. 3. Thermogravimetry Analysis

Furthermore, a thermogravimetry (TG) analysis was carried out to illustrate the content of the composite (Figure 3). Blue and red curves indicate the mass changes of ESM only and synthesized MnO_2/ESM material, respectively. It can be seen that ESM, as a kind of protein, is burnt out at about 600 °C and the quality is almost zero (blue curve in Figure 3). To study the relative amount of MnO_2 SMPs coated on ESM, dotted portion in Figure 3 is zoomed in. It is vividly shown that the curves remain unchanged with the temperature rising afterwards. However, the horizontal part of MnO_2/ESM is obviously higher than that of ESM only, which is attributed to the inorganic material existence. The difference of two horizontal curves stands for the relative amount of MnO_2 SMPs in ESM, which is calculated to be 2.77%.

3. 3. Methylene Blue Wastewater Treatment

The detailed characterization and measurement demonstrate that the synthesized material is ESM coated

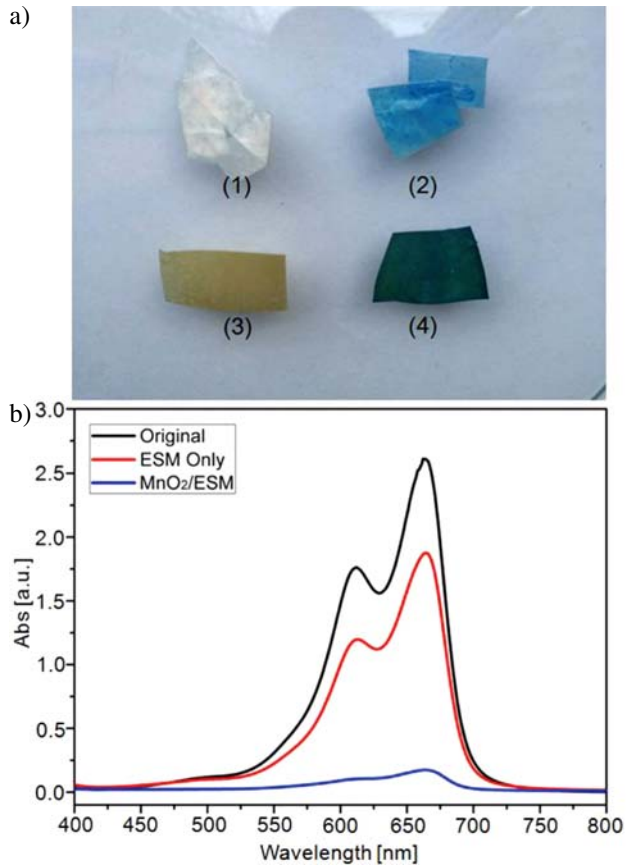

Figure 4. (a) Photographs of ESM and MnO_2/ESM before and after adsorption of MB [(1) ESM only; (2) ESM only after adsorption of MB; (3) MnO_2/ESM SMPs; (4) MnO_2/ESM after adsorption of MB.]. (b) The UV-vis absorption spectra of MB before and after adsorption by ESM only and MnO_2/ESM.

MnO_2 SMPs (MnO_2/ESM). Owing to the handy operation of "put in" and "take out", these materials were further applied to removal of MB. Figure 4a displays the photographs of ESM and MnO_2/ESM before and after adsorption of MB. Two sets of contrastive pictures show that ESM itself is capable of adsorbing for MB. Light pink ESM (1) turns into blue (2) after adsorption of a certain amount of MB. However the color change degree of MnO_2/ESM before and after adsorption is bigger: brown MnO_2/ESM (3) becomes dark green (4). The UV-Vis absorption spectra of MB before and after adsorption by ESM only and MnO_2/ESM are recorded in Figure 4b. It is evidently indicated that the absorption intensity of MB at 664 nm after MnO_2/ESM adsorption is significantly smaller than the one treated with ESM only. Figure S4a exhibits the equation of linear regression of MB solutions, by which the removal efficiencies of ESM and MnO_2/ESM adsorption are calculated in Figure S4b. Inset photographs shows the color change of MB solution before and after adsorption: (5) is original MB solution; (6) and (7) are MB solution after ESM and MnO_2/ESM adsorption, respectively. The color gap between (5) and (7) keeps pace with the removal efficiency of 93% by MnO_2/ESM adsorption.

3. 4. Investigation of Time and pH for Adsorption

Adsorption time for MB by MnO_2/ESM adsorption was investigated by UV-Vis spectroscopy as shown in Figures 5a and S5a. Under different adsorption time the absorption intensity decreases gradually as a function of time and remains the same after 35 min, which represents the whole adsorption process. Figure S5a shows the time dependent removal efficiency curve for MB, it can be seen that the removal efficiency increases rapidly at first 10 min and flats out gradually afterwards. A maximal removal efficiency of 93% is obtained at 35 min. Moreover, Figure S5b demonstrates the effect of pH condition on the adsorption by MnO_2/ESM. It turns out that the removal efficiency is kept in the range of 50%–62% under different pH values. The pH is not a factor to influence within the experimental error. It is worth noting that the removal efficiency under a certain pH condition is not as high as that in the distilled water solution. The additional adsorption for ions, which was used to adjust the acidity of the solution, took charge of this phenomenon. The desorption of MB was performed by placing the adsorbed MnO_2/ESM into deionized water. Figure 5b shows the absorption spectra of MB by adsorption for 35 min and desorption for 24 h. It is seen obviously that the shape and position of absorption peak are the same before and after adsorption, which indicates that the molecule structure of MB keeps unchanged during the removal procedure. Therefore, the removal procedure is an adsorption-desorption equilibrium process.

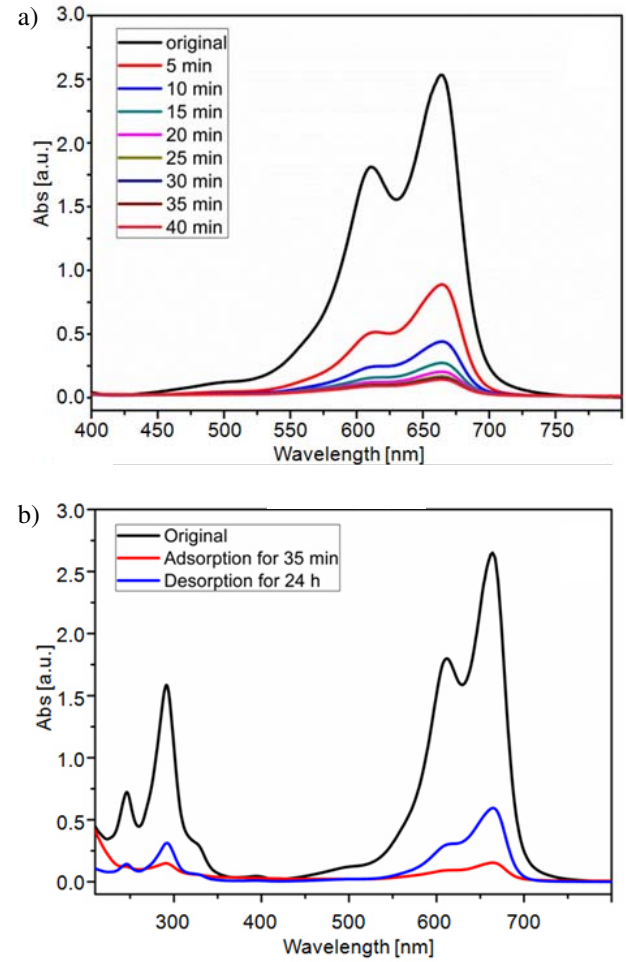

Figure 5. (a) The UV-vis absorption spectra of MB under different time by MnO_2/ESM adsorption. (b) The UV-vis absorption spectra of MB by adsorption for 35 min and desorption for 24 h.

3. 5. Study of Kinetics and Adsorption Isotherm

In order to better understand the adsorption behavior of MB on MnO_2/ESM, the adsorption capacities at different time (q_t) were recorded. As shown in Figure 6a, the adsorption of MB increases gradually with the time prolonged and becomes balanced after 35 min. Based on this, experimental data are calculated and organized in Figure 6b to investigate the adsorption kinetics. Two kinetic models are generally used to evaluate the adsorption,[59] and it can be concluded that the adsorption process of MB on MnO_2/ESM is in accordance with the pseudo-second-order model (correlation coefficient of 0.99508 for pseudo-first-order model and 0.99915 for pseudo-second-order model).

Moreover, the effect of initial MB concentration on equilibrium adsorption capacity (q_e) is shown in Figure 7a, where the adsorption capacity steadily enhances with increasing the initial concentration of MB added. The adsorption behavior of MB on MnO_2/ESM

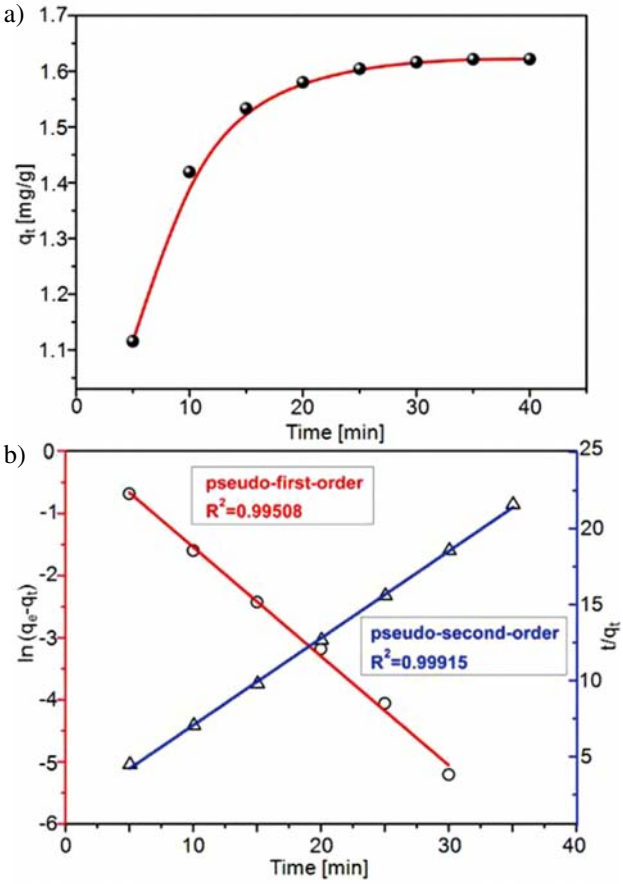

Figure 6. (a) Effect of adsorption time on adsorption capacity of MnO_2/ESM in MB solutions. (b) Pseudo-first-order (red line) and pseudo-second-order (blue line) models for MB adsorption.

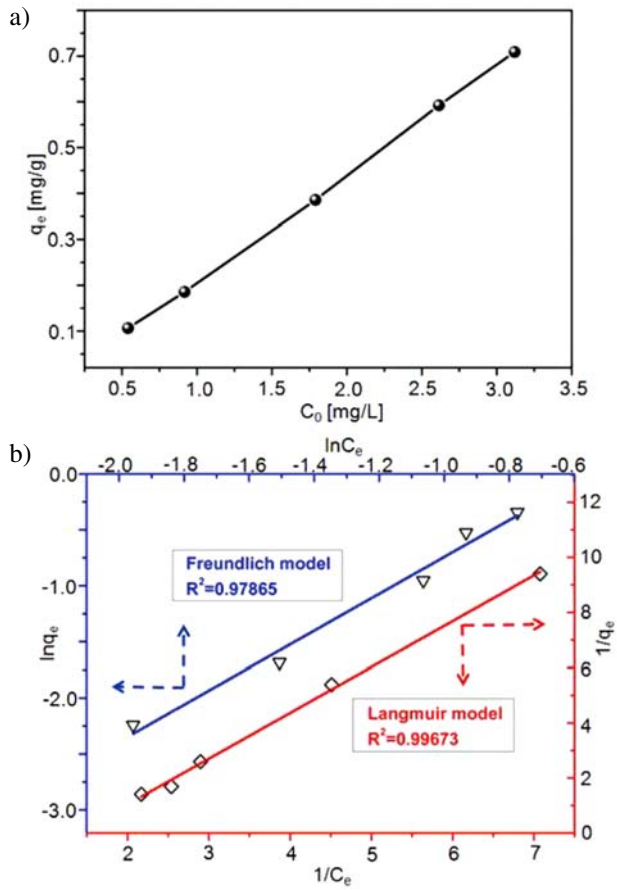

Figure 7. (a) Effect of initial concentrations of MB on equilibrium adsorption capacity of MnO_2/ESM in MB solutions. (b) Langmuir (red line) and Freundlich (blue line) isotherms models for MB adsorption.

was further studied through Langmuir and Freundlich isotherms models (Figure 7b), which were common adsorption isotherms models for evaluating the adsorption process.[59] According to the data calculation and linear fitting, it is concluded that Langmuir model is able to interpret the MB adsorption process better (correlation coefficients are 0.9967 and 0.9787 for Langmuir isotherms and Freundlich isotherms models, respectively).

3. 6. Effect of Hydrogen Peroxide on Removal of MB

The effect of H_2O_2 on the dye MB as a function of time monitored by UV-visible spectra was investigated in Figure S6a. We observed that the presence of H_2O_2 affected the absorbance of dye itself about 5% in 35 min and the shape of the peaks underwent no change. Then the effect of H_2O_2 with various concentrations on the removal efficiency of dye MB decontamination by MnO_2 was examined. The results are showed in Figure S6b. It is straightforward that H_2O_2 decreases the removal efficiency of dye MB by MnO_2.

4. Conclusions

The MnO_2 submicroparticles were prepared through an eggshell membrane based biotemplating method. The size of MnO_2 SMPs kept correspondence with the diameter of the fibrous proteins, which indicated the bio-inspired growth of MnO_2 SMPs. Taking advantages of macro-operability and adsorption performance stemmed from both protein membrane and hydroxyl on the surface of MnO_2 in the aqueous solution, the ESM coated MnO_2 SMPs was applied to the MB wastewater treatment. The adsorption process followed the pseudo-second-order kinetic model and Langmuir isotherms model, and the removal efficiency could reach up to 93% under room temperature without pH adjustment. This simple, green and interesting approach gives a facile concept of metal oxide materials synthesis, which is considered of great potential applications in wastewater treatment area.

5. Acknowledgements

This work was supported by the Key Science Fund Project of Taiyuan Institute of Technology (2015LZ01)

and the Program for the (Reserved) Discipline Leaders of Taiyuan Institute of Technology. We thank Institute of Coal Chemistry, Chinese Academy of Science for the material characterization.

6. References

1. A. Kumar and V. Kumar, *Chem. Rev.* **2014**, *14*, 7044–7078. https://doi.org/10.1021/cr4007285
2. W. Zhang, D. Zhang, T. Fan, J. Ding, J. Gu, Q. Guo and H. Ogawa, *Mater. Sci. Eng. C* **2009**, *29*, 92–96. https://doi.org/10.1016/j.msec.2008.05.013
3. Y. Kim, *Biomacromolecules* **2003**, *4*, 908–913. https://doi.org/10.1021/bm0257558
4. C. R. Rambo and H. Sieber, *Adv. Mater.* **2005**, *17*, 1088–1091. https://doi.org/10.1002/adma.200401049
5. M. L. Chacón-Patiño, C. Blanco-Tirado, J. P. Hinsetroza and M. Y. Combariza, *Green Chem.* **2013**, *15*, 2920–2928. https://doi.org/10.1039/c3gc40911b
6. S. R. Hall, H. Bolger and S. Mann, *Chem. Commun.* **2003**, 2784–2785. https://doi.org/10.1039/b309877j
7. I. W. -S. Lin, C. -N. Lok and C. -M. Che, *Chem. Sci.* **2014**, *5*, 3144–3150. https://doi.org/10.1039/c4sc00138a
8. R. Ramanathan, A. P. O'Mullane, R. Y. Parikh, P. M. Smooker, S. K. Bhargava and V. Bansal, *Langmuir* **2011**, *27*, 714–719. https://doi.org/10.1021/la1036162
9. S. K. Das, J. Liang, M. Schmidt, F. Laffir and E. Marsili, *ACS Nano* **2012**, *6*, 6165–6173. https://doi.org/10.1021/nn301502s
10. L. M. Rösken, S. Körsten, C. B. Fischer, A. Schönleber, S. van Smaalen, S. Geimer and S. Wehner, *J. Nanopart. Res.* **2014**, *16*, 2370. https://doi.org/10.1007/s11051-014-2370-x
11. C. Yang, C. -H. Choi, C.-S. Lee and H. Yi, *ACS Nano* **2013**, *7*, 5032–5044. https://doi.org/10.1021/nn4005582
12. M. G. Warner and J. E. Hutchison, *Nat. Mater.* **2003**, *2*, 272–277. https://doi.org/10.1038/nmat853
13. S. -Y. Pu, A. Zinchenko, L. -L. Qin, C. -W. Ye, M. Xu and S. Murata, *Mater. Lett.* **2014**, *130*, 168–171. https://doi.org/10.1016/j.matlet.2014.05.066
14. W. -Y. Chen, G. -Y, Lan and H. -T. Chang, *Anal. Chem.* **2011**, *83*, 9450–9455. https://doi.org/10.1021/ac202162u
15. L. A. Gugliotti, D. L. Feldheim and B. E. Eaton, *Science* **2004**, *304*, 850. https://doi.org/10.1126/science.1095678
16. J. Xie, Y. Zheng and J. Y. Ying, *J. Am. Chem. Soc.* **2009**, *131*, 888–889. https://doi.org/10.1021/ja806804u
17. J. M. Galloway and S. S. Staniland, *J. Mater. Chem.* **2012**, *22*, 12423–12434. https://doi.org/10.1039/c2jm31620j
18. R. M. Choueiri, A. Klinkova, H. Thérien-Aubin, M. Rubinstein and E, Kumacheva, *J. Am. Chem. Soc.* **2013**, 1*35*, 10262–10265. https://doi.org/10.1021/ja404341r
19. L. Au, B. Lim, P. Colletti, Y. -S. Jun and Y. Xia, *Chem. -Asian J.* **2010**, *5*, 123–129. https://doi.org/10.1002/asia.200900468
20. R. Murugan and S. Ramakrishna, *Biomaterials* **2004**, *25*, 3829. https://doi.org/10.1016/j.biomaterials.2003.10.016
21. M. B. Dickerson, K. H. Sandhage and R. R. Naik, *Chem. Rev.* **2008**, *108*, 4935–3978. https://doi.org/10.1021/cr8002328
22. R. K. Watt, O. D. Petrucci and T. Smith, *Cata. Sci. Technol.* **2013**, *3*, 3103–3110. https://doi.org/10.1039/c3cy00536d
23. C. Sun, H. Yang, Y. Yuan, X. Tian, L. Wang, Y. Guo, L. Xu, J. Lei, N. Gao and G. J. Anderson, *J. Am. Chem. Soc.* **2011**, *133*, 8617–8624. https://doi.org/10.1021/ja200746p
24. J. Fan, J. –J. Yin, B. Ning, X. Wu, Y. Hu, M. Ferrari, G. J. Anderson, J. Wei, Y. Zhao and G. Nie, *Biomaterials* **2011**, *32*, 1611–1618. https://doi.org/10.1016/j.biomaterials.2010.11.004
25. M. Suzuki, M. Abe, T. Ueno, S. Abe, T. Goto, Y. Toda, T. Akita, Y. Yamada and Y. Watanabe, *Chem. Commun.* **2009**, 4871–4873. https://doi.org/10.1039/b908742g
26. M. Li, D. -P. Yang, X. Wang, J. Lu and D. Cui, *Nanoscale Res. Lett.* **2013**, *8*, 1–5. https://doi.org/10.1186/1556-276X-8-1
27. H. Cao, D. -P. Yang, D. Ye, X. Zhang, X. Fang, S. Zhang, B. Liu and J. Kong, *Biosens. Bioelectron.* **2015**, *68*, 329–335. https://doi.org/10.1016/j.bios.2015.01.003
28. C. Hu, D. -P. Yang, Z. Wang, P. Huang, X. Wang, D. Chen, D. Cui, M. Yang and N. Jia, *Biosens. Bioelectron.* **2013**, *41*, 656–662. https://doi.org/10.1016/j.bios.2012.09.035
29. C. Hu, D. -P. Yang, F. Zhu, F. Jiang, S. Shen and J. Zhang, *ACS Appl. Mater. Interfaces* **2014**, *6*, 4170–4178. https://doi.org/10.1021/am405841k
30. C. Hou, D. Yang, B. Liang and A. Liu, *Anal. Chem.* **2014**, *86*, 6057–6063. https://doi.org/10.1021/ac501203n
31. Q. Liu, X. Jiang, S. Gao, H. Xu and L. Sun, *Mater. Lett.* **2014**, *128*, 322–324. https://doi.org/10.1016/j.matlet.2014.04.108
32. E. I. Alarcon, K. Udekwu, M. Skog, N. L. Pacioni, K. G. Stamplecoskie, M. González-Béjar, N. Polisetti, A. Wickham, A. Richter-Dahlfors and M. Griffith, *Biomaterials* **2012**, *33*, 4947–4956. https://doi.org/10.1016/j.biomaterials.2012.03.033
33. X. Huang, H. Wu, S. Pu, W. Zhang, X. Liao and B. Shi, *Green Chem.* **2011**, *13*, 950–957. https://doi.org/10.1039/c0gc00724b
34. P. Zhang, J. Lan, Y. Wang and C. Z. Huang, *Biomaterials* **2015**, *36*, 26–32. https://doi.org/10.1016/j.biomaterials.2014.08.026
35. M. Baláž, *Acta. Biomater.* **2014**, *10*, 3827–3843. https://doi.org/10.1016/j.actbio.2014.03.020
36. N. Li, L. Niu, Y. Qi, C. K. Y. Yiu, H. Ryou, D. D. Arola, J. Chen, D. H. Pashley, F. R. Tay, *Biomaterials* **2011**, *32*, 8743–8752. https://doi.org/10.1016/j.biomaterials.2011.08.007
37. P. S. Devi, S. Banerjee, S. R. Chowdhury and G. S. Kumar, *RSC Adv.* **2012**, *2*, 11578.
38. Q. W. Tang, J. H. Wu, Z. Y. Tang, Y. Li, J. M. Lin and M. L. Huang, *J. Mater. Chem.* **2011**, *21*, 13354–13364. https://doi.org/10.1039/c1jm11857a
39. Q. W. Tang, Z. Y. Tang, J. H. Wu, J. M. Lin and M. L. Huang, *RSC Adv.* **2011**, *1*, 1453–1456.

40. M. Liang, R. Su, W. Qi, Y. Yu, L. Wang and Z. He, *J. Mater. Sci.* **2014**, *49*, 1639–1947. https://doi.org/10.1007/s10853-013-7847-y
41. H. Su, J. Xu, J. J. Chen, W. J. Moon and D. Zhang, *Appl. Phys. A* **2012**, *106*, 93–97. https://doi.org/10.1007/s00339-011-6561-3
42. H. Su, N. Wang, Q. Dong and D. Zhang, *J. Membr. Sci.* **2006**, *283*, 7–12. https://doi.org/10.1016/j.memsci.2006.07.010
43. R. Camaratta, A. N. C. Lima and M. D. Reyes, *Mater. Res. Bull.* **2013**, *48*, 1569–1574. https://doi.org/10.1016/j.materresbull.2012.12.047
44. Z. Wang, X. Shao, X. Hu, G. Parkinson, K. Xie, D. Dong and C. Z. Li, *Catal. Today* **2014**, *228*, 199–205. https://doi.org/10.1016/j.cattod.2014.01.006
45. M. K. Rath, B. H. Choi, M. J. Ji and K. T. Lee, *Ceram. Int.* **2014**, *40*, 3295–3304. https://doi.org/10.1016/j.ceramint.2013.09.105
46. D. H. Dong, Y. Z. Wu, X. Y. Zhang, J. F. Yao, et al, *J. Mater. Chem.* **2011**, *21*, 1028–1032. https://doi.org/10.1039/C0JM03061A
47. S. M. Pourmortazavi, M. Taghdiri, N. Samimi and M. Rahimi-Nasravadi, *Mater. Lett.* **2014**, *121*, 5–7. https://doi.org/10.1016/j.matlet.2014.01.142
48. J. Cao, Q. H. Mao, L. Shi and Y. T. Qian, *J. Mater. Chem.* **2011**, *21*, 16210–16215. https://doi.org/10.1039/c1jm10862j
49. O. M. Wani, M. Safdar, N. Kinnunen and J. Jänis, *Chem. Eur. J.* **2016**, *22*, 1244–1247. https://doi.org/10.1002/chem.201504474
50. M. Safdar, O. M. Wani and J. Jänis, *ACS Appl. Mater. Interfaces* **2015**, *7*, 25580–25585. https://doi.org/10.1021/acsami.5b08789
51. M. Safdar, T, D, Minh, N. Kinnunen and J. Jänis, *ACS Appl. Mater. Interfaces* **2016**, *8*, 32624–42629. https://doi.org/10.1021/acsami.6b12024
52. L. Wang, J. Chen, X. Feng, W. Zeng, R. Liu, X. Lin, Y. Ma and L. Wang, *RSC Adv.* **2016**, *6*, 65624–65630.
53. X. Chen, G. Wu, T. Lan and W. Chen, *Chem. Commun.* **2014**, *50*, 7157–7159. https://doi.org/10.1039/c4cc01533a
54. X. Feng, Y. Zhang, Y. Li, Z. Huang, S. Chen, Y. Ma, L. Zhang, L. Wang and X. Yan, *Chem. Lett.* **2015**, *44*, 399–401. https://doi.org/10.1246/cl.140971
55. H. Wang, G. Zhao and M. Pumera, *J. Am. Chem. Soc.* **2014**, *136*, 2719–2722. https://doi.org/10.1021/ja411705d
56. H. Tamura, T. Oda, M. Nagayama and R. Furuichi, *J. Electrochem. Soc.* **1989**, *136*, 2782–2786. https://doi.org/10.1149/1.2096286
57. T. Yang, M. L. Chen, X. W. Hu, Z. W. Wang, J. H. Wang and P. K. Dasgupta, *Analyst* **2011**, *136*, 83–89. https://doi.org/10.1039/C0AN00480D
58. X. Liu, Q. Wang, H. H. Zhao, L. C. Zhang, Y. Y. Su and Y. Lv, *Analyst* **2012**, *137*, 4552–4558. https://doi.org/10.1039/c2an35700c
59. L. Y. Hao, H. J. Song, L. C. Zhang, X. Y. Wan, Y. R. Tang and Y. Lv, *J. Colliod Interface Sci.* **2012**, *369*, 381–387. https://doi.org/10.1016/j.jcis.2011.12.023

Povzetek

Kot bio-predlogo (biotemplate) za pripravo submikronskih delcev MnO_2 smo izbrali membrano jajčne lupine in uporabili kitajske čopiče pomočene v raztopino natrijevega hidroksida. Povprečna velikost tako pridobljenih delcev je bila 710 nm in je skladna z mikrostrukturo bio-predloge. Tako smo pripravili učinkovit in priročen absorbent za barvilo metilen modro. Učinkovitost odstranjevanja barvila lahko doseže do 93% v 35 minutah pri sobni temperaturi brez uravnavanje pH, tudi zaradi odličnega adsorpcije iz membrane jajčnih lupin in hidroksilnih skupin na površini kristalov MnO_2 v vodni raztopini. Materiale na membrani lahko ločimo od odpadne vode, izogniti pa se moramo sekundarnemu onesnaženju. S tem zanimivim pristopom k sintezi submikronskih delcev MnO_2 in učinkovitostjo odstranjevanja barvila metilen modro bi se lahko odprla nova pot priprave submikronskih materialov, pomembnih za čiščenje odpadnih voda.

Scientific paper

Development of Chemistry Pre-Service Teachers During Practical Pedagogical Training: Self-Evaluation vs. Evaluation by School Mentors

Vesna Ferk Savec* and Katarina S. Wissiak Grm

Faculty of Education, University Ljubljana, Kardeljeva ploščad 16, 1000 Ljubljana, Slovenia

** Corresponding author: E-mail: vesna.ferk@pef.uni-lj.si*

Received: 16-08-2016

Abstract

The research presented in this article deals with the self-evaluation of 4th year pre-service chemistry teachers' progress during their second year practical pedagogical training in chemistry teaching at primary schools (students' age 13–15 years) in comparison to the perception of their progress by their school mentors. The sample consisted of 21 pre-service teachers and 21 school mentors, in-service chemistry teachers, at primary schools. For the purpose of following to pre-service chemistry teachers' development, the pre-service teachers as well as their mentors completed the "Questionnaire for monitoring students' progress", focusing on eight characteristics of professional development during practical pedagogical training. The results reveal that student-teachers were stricter in their self-evaluation in comparison to their school mentors after their first chemistry lecture at school during the practical pedagogical training; however, after their last lecture, the evaluations were similar for most of the characteristics. The development of five randomly selected student-teachers is presented in detail from their own perspectives, as well as from their school mentors' perspectives.

Keywords: Chemistry teacher education, practical pedagogical training, pre-service chemistry teachers, in-service chemistry teachers, school mentors

1. Introduction

Within the framework of the education of pre-service teachers, practical pedagogical training is viewed as a crucial component in their professional development as teachers.[1,2] Hascher and Hagenauer[3] reviewed different terms referring to the various forms of practical training in teacher education, e.g. teaching practicum, student teaching, field experiences, teaching practice, clinical training, clinical teacher education, (guided) teaching experiences, internship, school practicum, school-based teacher education, and school placement. In this article, we use the term *practical pedagogical training* (PPT), which we define as a mandatory module in a pre-service teacher-education programme that takes place at school under the supervision of a school mentor, who is an in-service teacher of a specific school subject. PPT is aimed at providing pre-service teachers with an opportunity to gain experience in the classroom through their own teaching and/or co-teaching facilitated by continuous feedback about their teaching from their school mentor.

PPT and their contribution to the learning of pre-service teachers have been an area of interest to researchers, teacher educators and teachers. Some studies have focused on *pre-service teachers* development, their beliefs, experiences, and expectations, as well as the challenges and their concerns relating to the PPT.[4–8] Another group of studies focused on *mentors* and the mentoring provided by experienced teachers in schools.[9–12] A third group of studies focused on the work of *teacher educators* in finding ways to support pre-service teachers in developing their teaching of specifics subject in school environments.[13–16]

According to the literature review of Lawson et al.,[17] a broad range of factors play roles in the PPT process for pre-service teachers. Among the outcomes in their review, the collaboration between student-teachers and mentors emerged as significant for the professional and individual development of pre-service teachers. It was pointed out that mentors' feedback is also a crucial aspect of the mentor-pre-service teacher relationship, from the viewpoint of prospective teachers.

Another viewpoint highlights pre-service teachers' individual differences and the effects of the characteristics of individual student-teachers on the processes during PPT and their outcomes.[18–20]

Hascher and Kittinger[21] proposed students-teachers' learning and performance model to explain learning in PPT. Their model assumes that the quality of learning processes and learning outcomes during PPT is influenced by *structural aspects* (e.g. single or tandem placement, short- or long-term practicum), *organizational aspects* (e.g. university-school cooperation, school mentor professionalization), and *social aspects* (e.g. school social climate, teacher candidate's integration into the teaching staff). Their model also recognizes the role of individual factors of pre-service teachers such as *cognition* (e.g. pre-knowledge, attitudes, beliefs), *motivation* (e.g. interest, goal orientation), and *emotions* (e.g. enjoyment, anger) to contribute to the learning process. The model as well recognizes that factors at different levels (e.g. the culture of teacher education at the macro-level versus the teacher candidate-mentor interaction at the micro-level) co-determine the outcomes of teacher education.[20,21]

This article focuses on the self-evaluation of pre-service chemistry teachers' progress during their PPT in primary schools in comparison to the perception of their progress by their school mentors, who observed their teaching during PPT and provided feedback after each of the lessons.

2. The Context and the Purpose of the Study

At the Faculty of Education of the University of Ljubljana, Slovenia, the PPT of pre-service chemistry teachers commences in the 3rd year of tertiary education and continues in the 4th year. PPT is organized in collaboration between teacher educators at the university and selected primary school mentors. It is conducted in primary schools in Slovenia. Within the framework of PPT, student-teachers prepare lesson plans and teach chemistry in the 8th and 9th years of Slovenian primary schools (the students are 14 to 15 years old). At selected primary schools, pre-service teachers have a school mentor (experienced in-service chemistry teacher). The role of the school mentor is to give directions prior to the commencement of PPT for successful inclusion in the current teaching plan, within the framework of which the student-teachers conduct and attend lessons during the time of PPT. The school mentor is also present during all of the lessons that the student-teacher conducts and, directly after each lesson, provides the student-teacher with feedback on the positive aspects of the individual performance, as well as on necessary improvements.

In order to improve pre-service teachers' learning possibilities during PPT, we attempted to adjust PPT to pre-service teachers' suggestions based on previous research.[7] Specifically, we have considered the following main proposals given by the pre-service chemistry teachers:[7] (1) longer PPT, (2) independent choice of location and school for PPT, and (3) the possibility of doing PPT in several schools in cooperation with a number of different school mentors. The changes that have been introduced in PPT with regard to student-teachers' suggestions[7] are presented in Table 1.

This article deals with pre-service chemistry teachers', 4th-year student-teachers, development during their second-year experience with teaching during their PPT. The article focuses on the monitoring of pre-service chemistry teachers' first and the last lecture during their PPT based on their own and their school mentors' perceptions of eight characteristics of student-teachers' development measured by the "Questionnaire for monitoring students' progress".[7]

The study addresses the following research question:

How do pre-service chemistry teachers evaluate their development in comparison with their school mentors on their second-year experience with teaching during their PPT?

Table 1. Changes that have been introduced in PPT with regard to student-teachers' suggestions

Student-teachers' suggestions for optimization of PPT based on the evaluation of PPT[7]	State of PPT in the 2008/09 academic year[7] – before optimization	State of PPT in the 2014/15 academic year – after optimization
(1) Student-teachers' suggestion for a longer PPT;	• Five school days per academic year;	• Ten school days per academic year;
(2) Student-teachers' suggestion for an independent choice of location and school for PPT;	• Seven primary schools • Within the Ljubljana Urban Municipality, Slovenia; • Schools chosen by the University; • 2–3 student-teachers conducted PPT simultaneously at the same school at the time;	• Twenty-one primary schools (for 4th year student-teachers); • All Slovenian regions; • Schools chosen independently by each of the student-teachers; • One student conducted PPT at each of the schools;
(3) Student-teachers' suggestion for the possibility of doing PPT in several schools in cooperation with a number of different school mentors;	• Each of the student-teachers had the possibility to collaborate with one school mentor in the same academic year in the framework of PPT;	• Each of the student-teachers had the possibility to collaborate with several school mentors in the same academic year in the framework of PPT;

3. Method

3. 1. Instruments

For the purpose of the investigation, the "Questionnaire for monitoring students' progress"[7] was applied. The questionnaire showed appropriate internal consistency (Cronbach $\alpha = 0.89$).[7]

The questionnaire enables reflection on pre-service teachers' development during PPT, in particular with regards to the following eight student-teacher characteristics:

(1) the pre-service teacher's self–esteem while conducting the lessons
–referred to as *Self-esteem* in this article,
(2) the pre-service teacher's ability to establish discipline in class
–referred to as *Discipline* in this article,
(3) the suitability of the pre-service teacher's explanation of the chemistry topic taught
–referred to as *Explanation* in this article,
(4) the ability of the pre-service teacher to anticipate the appropriate amount of material to present during the lesson
–referred to as *The amount of contents* in this article,
(5) the pre-service teacher's experimental skills
–referred to as *Experimental skills* in this article,
(6) the pre-service teacher's expertise in providing an appropriate response to the students
–referred to as *Response* in this article,
(7) the pre-service teacher's ability to involve students actively
– referred to as *Active student's involvement* in this article, and
(8) the pre-service teacher's self-dependence in preparing for the lesson
–referred to as *Self-dependence* in this article.

Pre-service teachers and their school mentors evaluated pre-service teachers' development regarding each of the above-listed specific characteristics with a mark in the range 1–5, in which "1" represents the lowest student-teachers' competence and "5" the highest student-teachers' competence.

3. 2. Sample

The sample consisted of student-teachers ($N = 21$) enrolled in the 2014/15 academic year in the 4th year of the undergraduate programmes "Chemistry and Biology" or "Chemistry and Physics" or "Chemistry and Home Economics" at the Faculty of Education, University of Ljubljana. The student-teachers involved were predominantly female ($N = 20$), and only one was male ($N = 1$); their average age was 23.91 years. Due to their future profession, they are referred to as *pre-service teachers* or *student-teachers* in this article.

In addition to the pre-service teachers their *school mentors*, experienced in-service chemistry teachers ($N = 21$), from the twenty-one primary schools where PPT took place, were also involved in this study. All participating school mentors were female, and their average age was 46.20 years. In average, they had 20.81 years of experience in the teaching of the subject of chemistry in primary schools.

In this study, the development of five 4th year pre-service chemistry teachers, who were chosen from the sample via random selection, is presented in detail from their own perspectives as well as from their school mentors' perspectives. Each student-teacher in PPT only had one mentor and visited only one school. In order to assure anonymity of student-teachers, their names – presented in the results of the article – are pseudonyms, i.e. Ina (female), Sara (female), Jan (male), Mara (female) and Ula (female).

3. 3. Data Collection

The PPT for 4th year student-teachers was conducted in April 2015 at twenty-one primary schools throughout Slovenia. Every student spent two weeks (10 days) at an independently selected primary school, which was their second year experience of teaching chemistry. Each student-teacher monitored their own progress every day during PPT with the aid of the "Questionnaire for monitoring students' progress"[7]. The school mentors evaluated student-teachers' development by the use of "Questionnaire for monitoring students' progress"[7] twice – after their first and last chemistry lecture during PPT.

3. 4. Data Analysis

3. 4. 1. Analysis of the "Questionnaire for Monitoring Students' Progress "

The results collected from pre-service chemistry teachers and their school mentors in the "Questionnaire for monitoring students' progress"[7] were entered into MS Excel, and appropriate calculations and figures were prepared. Further analysis was conducted using the Statistical Package for the Social Sciences (SPSS), version 21. The nonparametric test Wilcoxon Ranks Test (Z) was used to evaluate significant differences in perceptions of student-teachers' characteristics by pre-service teachers in comparison to their school mentors. Pre-service teachers' comments accompanying the numerical data were transcribed.

4. Results and Discussion

At the pre-service teachers' first teaching of chemistry at school during their second year PPT, their school mentors evaluated the student-teachers' characteristics with higher values in comparison to pre-service teachers self-evaluation as can be seen from the mean values in Table 2. At the pre-service teachers' final teaching of chemistry at school during their second-year PPT, student-teachers' competences were again investigated. From the

Table 2. The mean values for eight characteristics measured by "Questionnaire for monitoring students' progress"[7] from student-teachers' and school mentors' perspectives after their first and final presentation during PPT

Characteristic	First presentation in PPT				Final presentation in PPT			
	Pre-service-teachers		School mentors		Pre-service-teachers		School mentors	
	Mean	SD	Mean	SD	Mean	SD	Mean	SD
Self-esteem	3.39	0.70	4.39	0.61	4.92	0.26	4.72	0.46
Discipline	3.33	1.19	4.17	0.92	4.94	0.24	4.94	0.24
Explanation	3.78	0.73	3.94	0.64	4.83	0.38	4.72	0.46
The amount of contents	3.39	1.24	4.44	0.70	4.72	0.46	5.00	0.00
Experimental skills	3.72	1.13	4.00	0.69	4.72	0.46	4.56	0.51
Response	4.11	0.68	4.22	0.65	4.69	0.46	4.78	0.43
Active student's involvement	3.44	1.10	4.39	0.78	4.72	0.46	4.44	0.70
Self-dependence	3.89	1.23	4.33	0.69	4.83	0.38	4.50	0.62

mean values in Table 2, it can be determined that their perception of their own competence was closer to that of their school mentor's at that time.

For the pre-service teachers' first teaching of chemistry, Wilcoxon Ranks Test showed significant differences in perception between pre-service teachers and their school mentors about the future teachers competence in four characteristics: Self-esteem ($Z = -2.924$, $p = 0.003$), Discipline ($Z = -2.223$, $p = 0.026$), The amount of contents ($Z = -2.799$, $p = 0.005$), Active student's involvement ($Z = -2.315$, $p = 0.021$). In contrast, no significant differences were found in the other four characteristics Explanation ($Z = -0.566$, $p = 0.572$), Experimental skills ($Z = -0.366$, $p = 0.714$), Response ($Z = -0.540$, $p = 0.589$), Self-dependen-

Table 3: Ina's self-evaluation of her skills and knowledge in specific fields at her *first and final presentation* during their PPT in comparison with the evaluation of her school mentor

Ina's self-evaluation of her skills and knowledge [Scale 1 to 5]

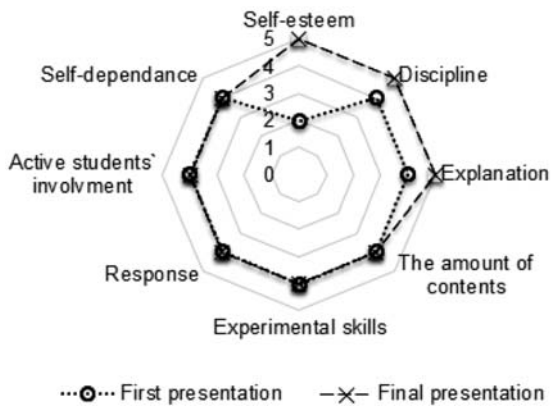

To the question "How did you perceive the course of the lesson in the role of chemistry teacher?" Ina explained:

After her first presentation:
"After a year outside the school climate, I did not feel very self-confident, since I had not met students yet."

After her final presentation:
"During the practical pedagogical training, I had gained self-confidence, had a better feeling regarding explaining teaching topic and was better when came to establishing discipline in the class."

Teacher's evaluation of Ina's skills and knowledge [Scale 1 to 5]

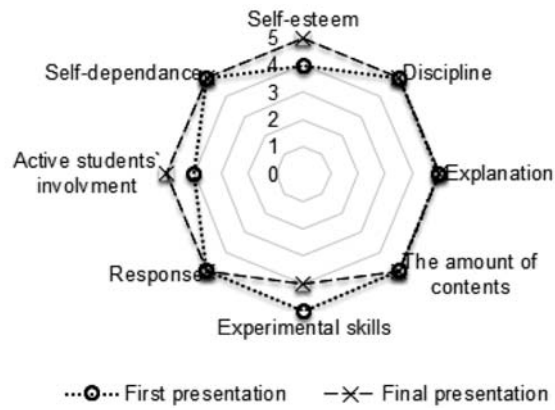

To the question "How did you perceive the course of the lesson with Ina in the role of chemistry teacher?" Ina's school mentor explained:

After her first presentation:
"She presented the new chemistry topic thoroughly through the experimental work. Ina's explanation was clear and she was able to adapt to the students' rhythm of knowledge comprehension."

After her final presentation:
"During the lessons, she succeeded in applying all the teaching goals designed in advanced. Students were able to be actively involved in the process of presenting the new chemistry topic. Experimental work was carried out in a correct and appropriate manner. The content of the chemistry topic was properly introduced."

ce ($Z = -1.310$, $p = 0.190$). Based on these results, it can be summarized that pre-service teachers are more realistic in estimating their competence for explanations of the chemistry topic taught, their experimental skills, their ability for providing an appropriate response to the students in the classrooms and their self-dependence in preparing for the lesson. However, pre-service teachers seem to be stricter in evaluation of their appearance of self-esteem while conducting the lessons and ability to establish discipline in class during lessons, also their ability to anticipate the appropriate amount of contents to present during the lesson and to actively involve students seem to be underestimated with regard to the perception of their school mentors.

For the pre-service teachers' final teaching of chemistry, the Wilcoxon Ranks Test showed significant differences in perception between pre-service teachers and their school mentors about the future teachers' competence in only one of eight characteristics, in the amount of contents ($Z = -2.236$, $p = 0.025$). No significant differences were found in other seven characteristics: Self-esteem ($Z = -1.536$, $p = 0.125$), Discipline ($Z = 0.000$, $p = 1.000$), Explanation ($Z = -0.707$, $p = 0.480$), Experimental skills ($Z = -0.832$, $p = 0.405$), Response ($Z = -1.342$, $p = 0.180$), Active student's involvement ($Z = -1.387$, $p = 0.166$), Self-dependence ($Z = -1.897$, $p = 0.058$). Based on these results, it can be summarized that pre-service teachers gained more realistic estimation of their competences during the time of PPT in comparison to their school mentors' perceptions.

To obtain insight into the situation of individual pre-service teachers', examples of the individual evaluations of eight characteristics are presented for five student-teachers in comparison with their development as seen by their school mentors.

4. 1. Example 1: 4th-year student-teacher Ina

After her first lesson, it is clear from Table 3 that the student Ina had perceived herself as having very little self-confidence, which was in contradiction with her teacher mentor's comprehension of her behavior. In general, the teacher mentor

Table 4. Sara's self-evaluation of her skills and knowledge in specific fields at her *first and final presentation* during their PPT in comparison with the evaluation of her school mentor

Sara's self-evaluation of her skills and knowledge [Scale 1 to 5]	**Teacher's evaluation of Sara's skills and knowledge [Scale 1 to 5]**
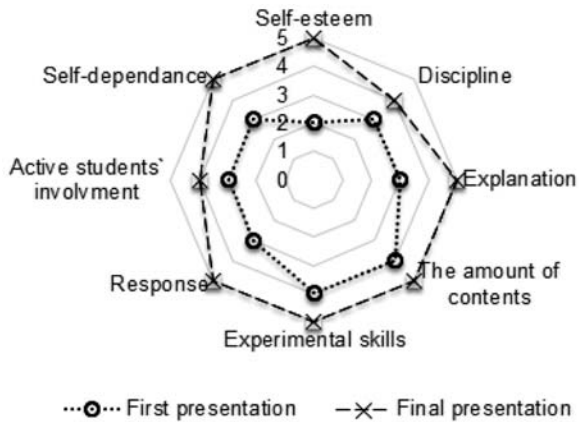	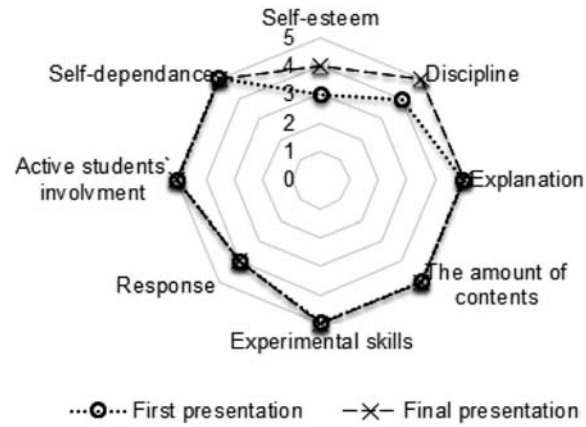
To the question "How did you perceive the course of the lesson in the role of chemistry teacher?" Sara explained:	To the question "How did you perceive the course of the lesson with Ina in the role of chemistry teacher?" Sara's school mentor explained:
After her first presentation: "I was satisfied with the way I was able to carry out the teaching lesson, since I was able to ask students enough different questions. The students were also very active, since they were involved in the teaching and learning process properly."	**After her first presentation:** "Sara was able to perform the lesson very well, involving students in the teaching and learning process. Her explanations were clear, and the lecture was designed appropriately due to the logical structure from the beginning to the end. She only could check the students intensively by reviewing their notes during the lesson."
After her final presentation: "I feel that my ability to establish discipline in the class has improved; students are listening to me and are willing to cooperate. I also feel that I am doing better when performing experiments in the class, I am no longer frightened when demonstrating the chemical experiment in front of the students in the class."	**After her final presentation:** "Sara is more confident and convincing when introducing new chemistry topics. She skillfully reacted when waiting for the experiment to occur, since the safety rules in the lab had been revised."

had seen Ina's presence in the class as being very appropriate regarding all the significant characteristics observed.

At Ina's final presentation (Table 3) in the class during PPT, her self-evaluation opinion had improved; she saw herself in a much better light also with regard to explanation of the topics taught and establishing discipline in the class. Ina's teacher mentor's opinion was consistent with Ina's self-evaluation, however the mentor described her improvement to the highest level in all areas described by influential characteristics.

4. 2. Example 2: 4th-year student-teacher Sara

At her first presentation (Table 4) the student-teacher Sara had seen all of her influential characteristics through self-assessment as being quite low, except regarding the chemical experiment demonstration and the ability to anticipate the appropriate amount of matter to be presented during the lesson which is not coherent with her comment, where she stated that she is quite satisfied with the lesson. Also Sara's school mentor's opinion is very positive; except regarding Sara's self-esteem, she evaluated Sara with quite high marks regarding all other influential characteristics observed.

From Table 4, it can be determined that the situation had changed significantly by Sara's last presentation during PPT. While conducting the final chemistry lesson, Sara had perceived herself to be very appropriate while grading all the influential characteristics; she only marked herself a bit lower regarding the successful involvement of

Table 5: Jan's self-evaluation of her skills and knowledge in specific fields at his *first and final presentation* during their PPT in comparison with the evaluation of her school mentor

Jan's self-evaluation of her skills and knowledge [Scale 1 to 5]	**Teacher's evaluation of Jan's skills and knowledge [Scale 1 to 5]**
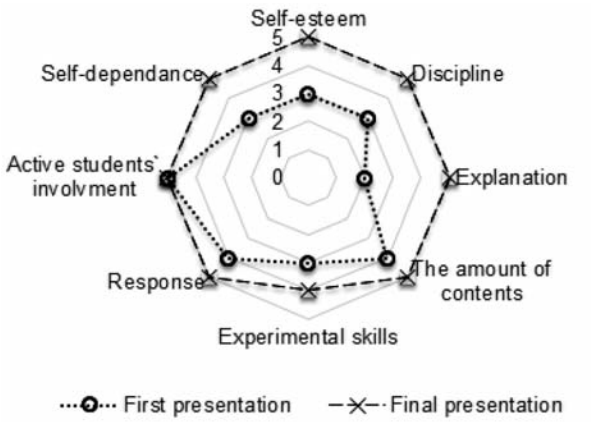	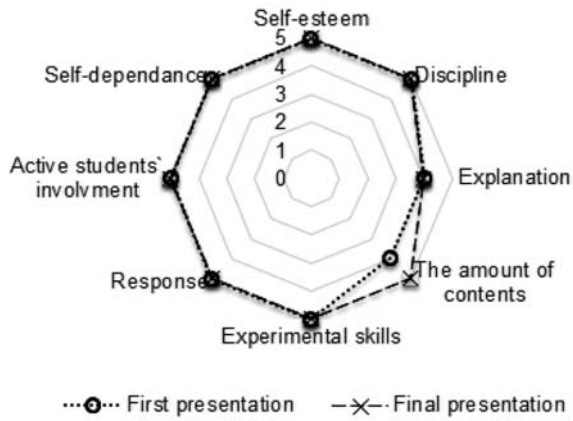
To the question "How did you perceive the course of the lesson in the role of chemistry teacher?" Jan explained: **After his first presentation:** "A bit frightened... it has been a year since I have been in front of the class performing the teaching lecture." **After his final presentation:** "My school mentor complimented me."	To the question "How did you perceive the course of the lesson with Ina in the role of chemistry teacher?" Jan's school mentor explained: **After his first presentation:** "Jan's teacher plan was correctly prepared in advance regarding the content and timetable. He was able to give brief and effective instructions to the students. Worksheets were appropriately prepared in advance; consequently, students were able to complete them independently, and then they were all checked at the end of the lesson. Therefore, students were active throughout the teaching process." **After his final presentation:** "Jan carried out the lesson independently. Prior to his lesson, he attended the observation of my class, and then he repeated the same topic. He carried out experimental group work successfully; the instructions were clearly and briefly delivered in advance. The results of the experiments were analysed with the students and therefore they successfully concluded the teaching lesson together."

students in the lesson, thereby she described her improvement in various areas also in her comment. The opinion of Sara's teacher mentor was very similar; she gave her very good marks regarding almost all important characteristics observed and pointed out her improvement regarding confidence as well as the quality of teaching.

4. 3. Example 3: 4th-year student-teacher Jan

It is clear from Table 5, that at his first presentation, the student-teacher Jan had evaluated all of his influential characteristics much more strictly than his school mentor did. Jan was not satisfied especially with his ability to clearly explain the topics thought; he commented to perceive himself as being frightened in the classroom after one-year pause since last practical pedagogical training in his third year of the study.

It can be seen from Table 5, that the situation had changed during the time of practical pedagogical training, as at Jan's final presentation, he was very satisfied with his lesson. Jan and his mentor's opinions were quite consistent, except regarding Jan's experimental skills and the suitability of Jan's explanation of the topic taught.

4. 4. Example 4: 4th-year student-teacher Mara

It is clear from Table 6 that Mara had seen her suitability of explanation of the topic taught to be extremely

Table 6. Mara's self-evaluation of her skills and knowledge in specific fields at her *first and final presentation* during their PPT in comparison with the evaluation of her school mentor

Mara self-evaluation of her skills and knowledge [Scale 1 to 5]	**Teacher's evaluation of Mara's skills and knowledge [Scale 1 to 5]**
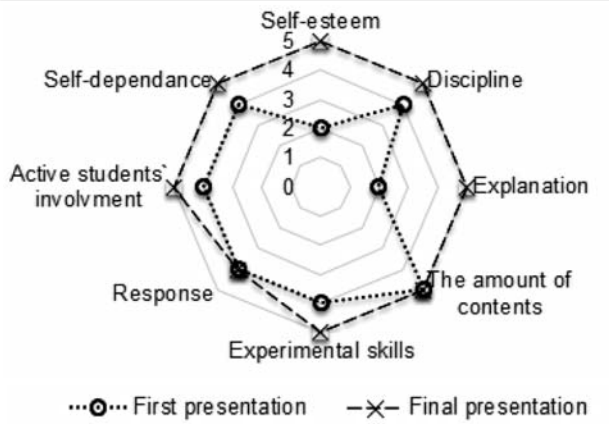	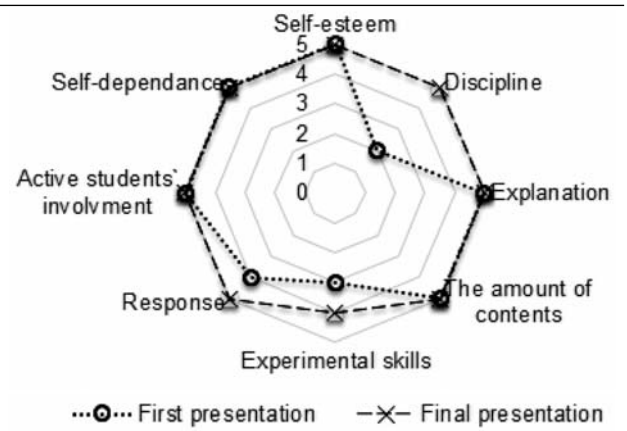
To the question "How did you perceive the course of the lesson in the role of chemistry teacher?" Mara explained: **After her first presentation:** "My first lesson presentation after one year outside the school practice. I feel I am able to carry out the teaching lesson appropriately, but I do need my teacher mentor to supervise me and give me a proper advice where needed." **After her final presentation:** "My last day of practical pedagogical training. I am full of new impressions and experiences. I feel I am no longer so nervous, and I have gained self-confidence."	To the question "How did you perceive the course of the lesson with Ina in the role of chemistry teacher?" Mara's school mentor explained: **After her first presentation:** "In the future, Mara should work on step-by-step explanations of new chemical concepts introduced to the students during her lesson. For the whole image of the teaching lesson, it would be beneficial to add visual elements for better introducing and launching the new chemistry topics. There were some troubles with the time component of the teaching plan, which consequently was not appropriately carried out. She had quite a few problems with correct use of Slovenian language, as she spoke in a dialect." **After her final presentation:** "Mara should try to show a little bit more enthusiasm while teaching in the classroom. Consequently, the atmosphere in the classroom would be improved. The lesson should be more compact. In these terms, she should try to connect the parts of the lesson more tightly. However, she improved her teaching image in comparison to the last year of her PPT in our school. I recommend that she works on developing her natural body language when performing the teaching process."

low at her first presentation, and she consequently also marked her self-esteem extremely low. Her school mentor did not evaluate her very well either, since she detected troubles with introducing and launching the new topics, as well as with the time component of the teaching plan and the discipline in the classroom.

At her last presentation, both Mara and her teacher mentor changed their opinions as can be seen in Table 6. All the important characteristics were marked excellent by her teacher mentor, except in the case of Mara's experimental skills, where she can still improve. In the opinion of her school mentor, it is also important that in the future, she Mara shows more enthusiasm while teaching in the classroom.

4. 5.Example 5: 4th-year student-teacher Ula

At her first presentation, it is clear from Table 7, that Ula was not satisfied with her teaching and that she had perceived all of her influential characteristics more strictly than her teacher mentor had. From her comment it is obvious, that she felt a relieve after her first lesson as she describes, that feels less nervous and to gain more control over the situation in the classroom.

Table 7. Ula's self-evaluation of her skills and knowledge in specific fields at her *first and final presentation* during their PPT in comparison with the evaluation of her school mentor

Ula's self-evaluation of her skills and knowledge [Scale 1 to 5]	**Teacher's evaluation of Ula's skills and knowledge [Scale 1 to 5]**
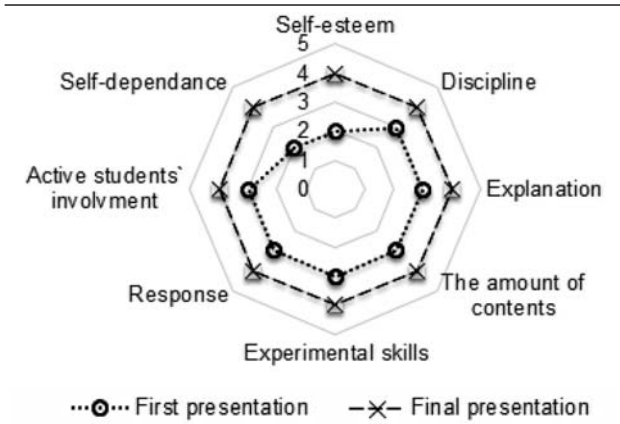	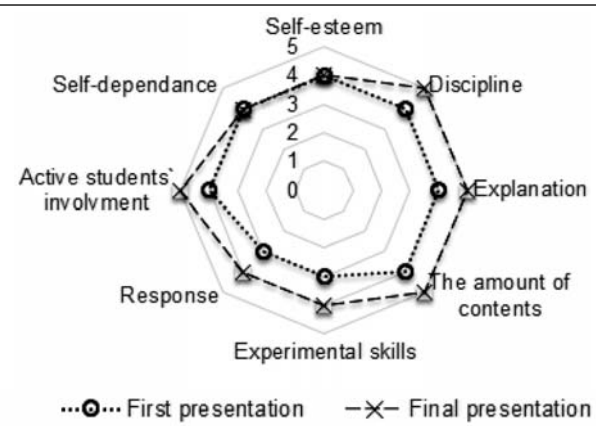
To the question "How did you perceive the course of the lesson in the role of chemistry teacher?" Ula explained: **After her first presentation:** "The first teaching lessons have been successfully applied. I felt less nervous and have had more control over the situation in the classroom." **After her final presentation:** "The last day of my practical pedagogical training. I am full of new impressions; I am feeling much less nervous, and I have gained much self-confidence."	To the question "How did you perceive the course of the lesson with Ina in the role of chemistry teacher?" Ula's school mentor explained: **After her first presentation:** "Ula was able to prepare a compact teaching lesson plan, firstly, suitable for checking student's pre-knowledge and secondly for the introduction of new chemistry concepts, which has to be presented in the teaching lesson. Before this point, she had needed quite a lot of help, but after my careful review, she finally succeeded to prepare a good, complex and systematic teaching lesson plan. During carrying out the teaching lesson in the class, she had to face some problems, regarding the discipline, but it was an expected and understandable situation, since the class is, in general, a bit problematic." **After her final presentation:** "Ula was able to prepare an interesting lesson presenting the chemistry concepts in a way interesting for teaching and learning. Her appropriate teaching plan comprises several teaching methods; the students were actively engaged by discussion and question making; she was able to include context-based teaching goals were students enjoy real self-reflection regarding ecological problems presented during the teaching and learning process."

Ula's teaching improved during the practical pedagogical training, as the situation had changed at Ula's final presentation (Table 7). Ula described, that she gained new ideas and valuable experience during practical pedagogical training. In the case of four evaluated characteristics the teacher mentor saw Ula's ability even better than Ula did. These four characteristics were the following: the pre-service teacher's ability to establish discipline in class, the suitability of the pre-service teacher's explanation of the topic taught, the ability of the pre-service teacher to anticipate the appropriate amount of contents to present during the lesson and the pre-service teacher's ability to involve students actively. The mentor especially pointed out that Ula's teaching plan involved different teaching methods and that the students were actively engaged by discussion and question making.

Regarding the 4th-year student-teachers' PPT, it can be summarized from the overall results (Table 2), as well as from the analysis of individual teacher-students' reflections (Tables 3–7), that the school mentors were far less strict in evaluation of the student-teachers' performances in the class. All the teacher mentor's observations, especially regarding the students' first presentations, were far less demanding and much more indulgent regarding the student's behaviour in the class than the student-teachers' views of their selves were. However, regarding school mentor's and student-teachers' views of the last lesson in the class during their practical pedagogical training, there were far more matching reviews seen in comparison with their evaluations obtained at the first lessons in the class. The mentors' comment in the tables are in most cases also much longer than the comments of the student-teachers. The focus of student-teachers' comments, especially after their first lesson, is mostly about their self-esteem. Student-teachers report about their low confidence after one-year brake after the practical pedagogical training in the third year of their studies, they claim to be nervous, to be frighten during teaching, while in the case of the mentors, they are more specific and report about different skills by student-teachers, e.g. structure of chemistry lesson, students' active involvement, discipline in the classroom, student-teachers' enthusiasm during teaching, etc..

5. Conclusion

This investigation presents 4th-year pre-service chemistry teachers' development during their second-year experience with teaching during their PPT from their own perspective as well as from that of their school mentors. In particular, it focused on the monitoring of pre-service chemistry teachers' first and last chemistry lesson during their PPT based on their own and their school mentors' perceptions of eight characteristics of pre-service teachers' development measured by the "Questionnaire for monitoring students' progress". [7]

The results revealed that after their first chemistry lecture pre-service teachers and their school mentors estimated similar values of four of eight student-teacher characteristics, e.g. no statistically significant differences found for the explanation of the chemistry topic taught, their experimental skills, their ability for providing an appropriate response to the students in the classrooms and their self-dependence in preparing for the lesson. However, pre-service teachers seem to be stricter than their school mentors are; statistically significant differences found in the evaluation of their appearance of self-esteem while conducting the lessons and ability to establish discipline in class during lesson, as well as their ability to anticipate the appropriate amount of contents to present during the lesson and to involve students actively. According to the results following the last chemistry lecture during PPT, it can be concluded that pre-service teachers gained more realistic estimations of their knowledge and skills with regard to the eight observed characteristics, when compared to their school mentors' perception, as the statistically significant difference was observed only in their evaluation of their ability to anticipate the appropriate amount of contents to present during the lesson. From the content point of comments, it can be concluded, that mentors' comments in the tables are in most cases longer than the comments of the student-teachers. Student-teachers' comments, especially after their first lesson, are mostly about their self-esteem, while in the case of the mentors, they are more specific and report about different skills by student-teachers, e.g. structure of chemistry lesson, teaching methods, students' active involvement, discipline in the classroom, student-teachers' enthusiasm during teaching, etc. When focusing on specific characteristics, the results are in line with previous research findings,[7] in which the lowest value by pre-service teacher was also ascribed to their ability to establish discipline in the classroom and higher grades were ascribed to their ability to involve students actively in the lesson, followed by their self-dependence in preparing for the lesson.

Similarly, to previous studies,[17] it can be concluded that school mentors' feedback to student-teachers is a very important part of PPT, especially because they observe student-teachers' progress from a broader, more holistic perspective of their future profession – chemistry teacher. Therefore, sustained efforts should be focused on productive school-university collaboration, but also to raising of the awareness for the need of in-service chemistry teachers' sustainable education in their subject area in relation to recent findings from chemical education research, e.g. studying the impact of different experimental methods in chemistry teaching on school practice,[24,25] studying the impact of the online knowledge assessment system on students' knowledge,[26] the development of concept maps as learning materials to foster students' meaningful learning of organic reactions.[27]

6. References

1. M. S. Trevisan, *Am. J. Eval.* **2004**, *25*, 255–272. https://doi.org/10.1177/109821400402500212
2. T. Lawson, M. Çakmak, M. Gündüz, H. Busher, *Eur. J. Teach. Educ.* **2015**, *38*, 392–407. https://doi.org/10.1080/02619768.2014.994060
3. T. Hascher, G. Hagenauer, *Int. J. Educ. Res.* **2016**, *77*, 15–25. https://doi.org/10.1016/j.ijer.2016.02.003
4. M. Beeth, E. Adadan, *J. Sci. Teacher Educ.* **2006**, *17*, 103–120. https://doi.org/10.1007/s10972-006-9013-8
5. M. Poulou, *Eur. J. Teach. Educ.* **2007**, *30*, 91–110. https://doi.org/10.1080/02619760600944993
6. A. Maskan1, R. Efe, *J. Turk. Sci. Educ.* **2011**, *8*, 64–77.
7. K. S. Wissiak Grm, V. Ferk Savec, *Acta Chim. Slov.* **2014**, *61*, 729–739.
8. V. Ferk Savec, K.S.Wissiak Grm, in: I. Devetak, S. A. Glažar (Eds.): Learning with understanding in the chemistry classroom, Springer, Dordrecht, **2014**, pp. 375–395. https://doi.org/10.1007/978-94-007-4366-3_18
9. T. Kwan, F. Lopez-Real, *Asia-Pac. J. Teach. Educ.* **2005**, *33*, 275–287. https://doi.org/10.1080/13598660500286267
10. T. Kwan, F. Lopez-Real, *Teach. Teach. Educ.* **2010**, *26*, 722–731. https://doi.org/10.1016/j.tate.2009.10.008
11. R. N. Stanulis, K. T. Ames, *Prof. Educ.* **2009**, *33*, 28–38.
12. A. Ambrosetti, J. Dekkers, *Aust. J. Teach. Educ.* **2010**, *35*, 42–55.
13. J. Worthy, *Int. J. Qual. Stud. Educ.* **2005**, *18*, 379–398. https://doi.org/10.1080/09518390500082699
14. G. T. M. Ten Dam, S. Blom, *Teach. Teach. Educ.* **2006**, *22*, 647–660. https://doi.org/10.1016/j.tate.2006.03.003
15. D. J. Trumbull, K. Fluet, *Teach. Teach. Educ.* **2008**, *24*, 1672–1685. https://doi.org/10.1016/j.tate.2007.12.001
16. T. H. Levine, *Teach. Teach. Educ.* **2011**, *27*, 930–941. https://doi.org/10.1016/j.tate.2011.03.004
17. T. Lawson, M. Çakmak, M. Gündüz, H. Busher, *Eur. J. Teach. Educ.* **2015**, *38*, 392–407. https://doi.org/10.1080/02619768.2014.994060
18. F. Frost, M. Prenzel, T. Seidel, in: L. Ostern, K. Smith, R. Ryghaug, T. Krüger, M. B. Postholm (Eds.): Teacher education research between national identity and global trends, Akademika, Trondheim, **2013**, pp. 139–162.
19. T. Hascher, F. Hofmann, in: K.-H. Arnold, A. Gröschner, T. Hascher (Eds.): Pedagogical field experiences in teacher education, Waxmann, Münster, **2014**, pp. 257–276.
20. T. Hascher, G. Hagenauer, *Int. J. Educ. Res.* **2016**, *77*, 15–25. https://doi.org/10.1016/j.ijer.2016.02.003
21. T. Hascher, C. Kittinger, in: K.-H. Arnold, A. Gröschner, T. Hascher (Eds.): Pedagogical field experiences in teacher education, Waxmann, Münster, **2014**, pp. 221–235.
22. Z. Shechtman, M. Levy, J. Leichtentritt, *J. Educ. Res.* **2005**, *98*, 144–155. https://doi.org/10.3200/JOER.98.3.144-155
23. I. Timoštšuk, A. Ugaste, *Teach. Teach. Educ.* **2010**, *26*, 1563–1570. https://doi.org/10.1016/j.tate.2010.06.008
24. M. Vrtačnik, N. Gros, *Acta Chim. Slov.* **2013**, *60*, 209–220.
25. A. Logar, V. Ferk Savec, *Acta Chim. Slov.* **2011**, *58,* 866–875
26. B. Kralj, S. A. Glažar, *Acta Chim. Slov.* **2013**, *60*, 433–441.
27. B. Šket, S. A. Glažar, J. Vogrinc, *Acta Chim. Slov.* **2015**, *62*, 462–472. https://doi.org/10.17344/acsi.2014.1148.

Povzetek

V članku predstavljena raziskava se ukvarja s samo-evalvacijo napredka med praktičnim pedagoških usposabljanjem bodočih učiteljev kemije, študentov četrtega letnika, v primerjavi z mnenjem njihovih mentorjev na šoli. Vzorec sestavlja 21 bodočih učiteljev kemije in 21 njihovih mentorjev, izkušenih učiteljev kemije na osnovnih šolah. Za namen spremljanja razvoja bodočih učiteljev kemije med praktičnim pedagoških usposabljanjem so bodoči učitelji in njihovi mentorji izpolnjevali »Vprašalnik za spremljanje razvoja bodočih učiteljev kemije«, ki temelji na evalvaciji osmih karakteristik strokovnega razvoja učiteljev kemije. Rezultati kažejo, da so bili bodoči učitelji kemije v samo-evalvaciji bolj strogi od svojih mentorjev, še posebno po prvi izvedeni uri pouka kemije, medtem ko so bile ocene po zadnji izvedeni uri podobne z ocenami mentorjev glede večine ocenjevanih karakteristik. Podrobneje je predstavljen razvoj petih naključno izbranih bodočih učiteljev kemije iz njihovega osebnega vidika, kakor tudi iz perspektive njihovih mentorjev.

Scientific paper

Preparation and Catalytic Study on a Novel Amino-functionalized Silica-coated Cobalt Oxide Nanocomposite for the Synthesis of Some Indazoles

Mohammad Ali Ghasemzadeh,*[,1] Bahar Molaei,[2] Mohammad Hossein Abdollahi-Basir[1] and Farzad Zamani[3]

[1] *Department of Chemistry, Qom Branch, Islamic Azad University, Qom, I. R. Iran*

[2] *Young Researchers and Elite Club, Shahr-e-Qods Branch, Islamic Azad University, Tehran, Iran*

[3] *School of Chemistry, University of Wollongong, New South Wales, 2522, Australia*

* *Corresponding author: E-mail: Ghasemzadeh@qom-iau.ac.ir*

Received: 18-08-2016

Abstract

In this research an efficient synthesis of a novel nanocomposite including SiO_2@(3-aminopropyl)triethoxysilane-coated cobalt oxide (Co_3O_4) nanocomposite has been reported by three step method. The structure and magnetic characterization of Co_3O_4@SiO_2@NH_2 have been done by using various spectroscopic analyses which include FT-IR, X-ray powder diffraction, scanning electron microscopy, transmission electron microscopy, energy dispersive X-ray spectroscopy and vibrating sample magnetometry. Amino-functionalized SiO_2 coated Co_3O_4 nanocomposite exhibited superparamagnetic behavior and strong magnetization at room temperature. The average crystallite sizes of the Co_3O_4 are 23.7 nm. The obtained magnetic nanocomposite showed excellent catalytic activity as a new heterogeneous magnetic catalyst for the synthesis of some indazole derivatives under mild reaction conditions along with high level of reusability.

Keywords: Co_3O_4@SiO_2@NH_2, heterogeneous catalyst, spectroscopic analysis, indazole derivatives, nanocomposite

1. Introduction

Over the last decade, organic–inorganic magnetic nanocomposites have become interesting as magnetic catalysts in both academic and industrial fields.[1–3] The spinel cobalt oxide Co_3O_4 is a magnetic semiconductor and widely used catalyst for a variety of reactions.[4–5] The use of this magnetic nanoparticle catalyst can address the isolation and recycling problem encountered in many heterogeneous and homogenous catalytic reactions. Most importantly, the magnetic-supported catalysts show not only high catalytic activity but also high degree of chemical stability. The Co_3O_4 surface has a strong affinity for silica, and the cobalt-oxide NPs were easily coated with silica via the sol–gel process.[6] It has been exhibited that the formation of silica coating on the surface of Co_3O_4 NPs can hinder their aggregation and keep their chemical stability.[7] In addition, the silanol (Si–OH) groups, which have often located in the terminal of silica coating surface, SiO_2 is stable under acidic conditions and inert to redox reactions, as compared with the organic coating materials, and hence functions like an ideal shell composite to protect the inner Co_3O_4 partciles. Silica-coated Co_3O_4 nanocomposite, i.e., Co_3O_4@SiO_2, has recently been investigated for potential biomedical applications.[8–10] Additionally, the SiO_2 coating shell has an abundance of surface hydroxyl groups which can be easily coupled with organosilanes by formation of Si–O–Si covalent bonds. The importance of this field is highlighted by the use of bio molecules which control the self-assembly of nanodevices.[11–13] This led to the idea of preparing an active catalyst, Co_3O_4@SiO_2@NH_2, through morphology-controlled synthesis which ensure that faces which are active specifically are exposed predominantly at the surface. As well as, to the best of our knowledge, no attempt has been made to synthesis of Co_3O_4@SiO_2@NH_2 nanostructures. In this study, a novel Co_3O_4 magnetic nanocomposite was developed by grafting amino groups covalently onto the surfaces of Co_3O_4@SiO_2 nanocomposite.

The resulted nanocomposite was characterized by Fourier transform infrared (FTIR), transmission electron microscopy (TEM), X-ray powder diffraction (XRD), scanning electron microscopy (SEM) and vibrating sample magnetometer (VSM). This study on the synthesis of Co_3O_4@SiO_2@NH_2 nanocomposite may open up new routes in the research for highly active catalysts.

In continuing our efforts towards the development of efficient and environmentally benign heterogeneous catalysts,[14–18] herein, Co_3O_4@SiO_2@NH_2 nanocomposite was prepared as a highly efficient magnetic catalyst by a simple method. The main goal of this catalytic synthesis was to introduce a novel and effective magnetic nanocomposite to expand the use of these types of composites for organic reactions. In order to investigate the catalytic activity of this magnetic catalyst, synthesis of some indazole derivatives have been done via two-component reactions.

2. Experimental

2. 1. Chemicals and Apparatus

Chemicals were purchased from the Sigma-Aldrich and Merck in high purity. All of the materials were of commercial reagent grade and have been used without further purification. The α,ά-bis (substituted-arylidene) cycloalkanones were synthesized via aldol condensation as described previously.[19,20] All melting points are uncorrected and were determined in capillary tube on Boetius melting point microscope. The ultrasonic irradiation was used in reactions by a multi-wave ultrasonic generator (Sonicator 3200; Bandelin, MS 73, Germany), equipped with a converter/transducer and titanium oscillator (horn), 12.5 mm in diameter, operating at 20 kHz with a maximum power output of 200 W. The ultrasonic generator automatically adjusted the power level. ^{1}H NMR and ^{13}C NMR spectra were obtained on Bruker 400 MHz spectrometer with $CDCl_3$ as solvent using TMS as an internal standard. FT–IR spectrum was recorded on Magna-IR, spectrometer 550. The elemental analyses (C, H, N) were obtained from a Carlo ERBA Model EA 1108 analyzer. Powder X-ray diffraction (XRD) was carried out on a Philips diffractometer of X'pert Company with mono chromatized Cu Kα radiation (λ = 1.5406 Å). Microscopic morphology of products was visualized by SEM (LEO 1455VP). The mass spectra were recorded on a Joel D-30 instrument at an ionization potential of 70 eV. Transmission electron microscopy (TEM) was performed with a Jeol JEM-2100UHR, operated at 200 kV. Magnetic properties were obtained on a BHV-55 vibrating sample magnetometer (VSM) made by MDK-I.R.Iran. The compositional analysis was done by energy dispersive analysis of X-ray (EDX, Kevex, Delta Class I).

2. 2. Preparation of Co_3O_4 Nanoparticles

Co_3O_4 MNPs were prepared according to previously reported procedure by Vela et. al with some modifications.[21] Firstly, cobalt nitrate hexahydrate (8.60 g) was dissolved in 100 ml of ethanol and the resulting mixture was stirred vigorously. Then, the mixture was heated up to 50 °C and kept for 30 min. Finally oxalic acid (2.14 g) was added quickly to the solution and the reaction mixture was stirred for 2 h at 50 °C. The formed precipitate which includes cobalt (II) oxalate was collected by centrifuges and then the prepared cobalt (II) oxalate powder was calcined at 400 °C for 2 h to produce Co_3O_4 nanoparticles.

2. 3. Preparation of Co_3O_4@SiO_2 Nanoparticles

Co_3O_4@SiO_2 MNPs were prepared according to the slightly modified previously reported method by Vela et. al.[21] Briefly, CTAB (2.2 g) was added to a solution of 0.5 g of Co_3O_4 nanoparticles in EtOH (350 mL), and then concentrated ammonia aqueous solution (40 mL, 28 wt %) was added dropwise to the reaction mixture under sonication. After the treatment for 20 min which followed by the addition of tetraethylorthosilicate (TEOS) (0.4 mL in 10 mL of EtOH) to the mixture under ultrasound irradiation, then solution was stirred for 20 h at room temperature. Co_3O_4 nanoparticles coated with porous SiO_2 shell were collected by centrifugation and washed three times with deionised water and then were calcined at 600 °C for 6 h.

2. 4. Preparation of Co_3O_4@SiO_4@NH_2 Nanocomposite

Co_3O_4@SiO_2 nanoparticles (0.5 g) were added to the three-necked flask and ultrasonically dispersed for 15 min in dry toluene (25 mL). Afterwards, 1 mililiter (4.27 mmol) of 3-aminopropyltriethoxysilane (APTES) was added into the flask, and the reaction mixture was refluxed at 110 °C with continuous stirring for 10 h under nitrogen atmosphere. After completion of the reaction, the resulting amine-functionalized Co_3O_4@SiO_2 was gathered by centrifugation and washedwith water and ethanol for several times. Finally, it was dried at 50 °C under vacuum conditions for 10 h (Scheme1).

Nitrogen content of the amine-grafted sample was estimated by back titration using NaOH (0.1 mol/L).[22–24] First, the known amount of the catalyst was stirred in HCl (0.5 mol/L) for 30 min. Then, the mixture was filtrated and titrated with NaOH (0.1 mol/L). Nitrogen content of the catalyst was 5.86 mmol/g using 8.54 mmol/g trimethoxysilylpropylamine.

2. 5 .General Procedure for Synthesis of Some Indazole Derivatives

In a typical procedure, a mixture of α,ά-bis (substituted-arylidene) cycloalkanone (1 mmol), phenyl hydra-

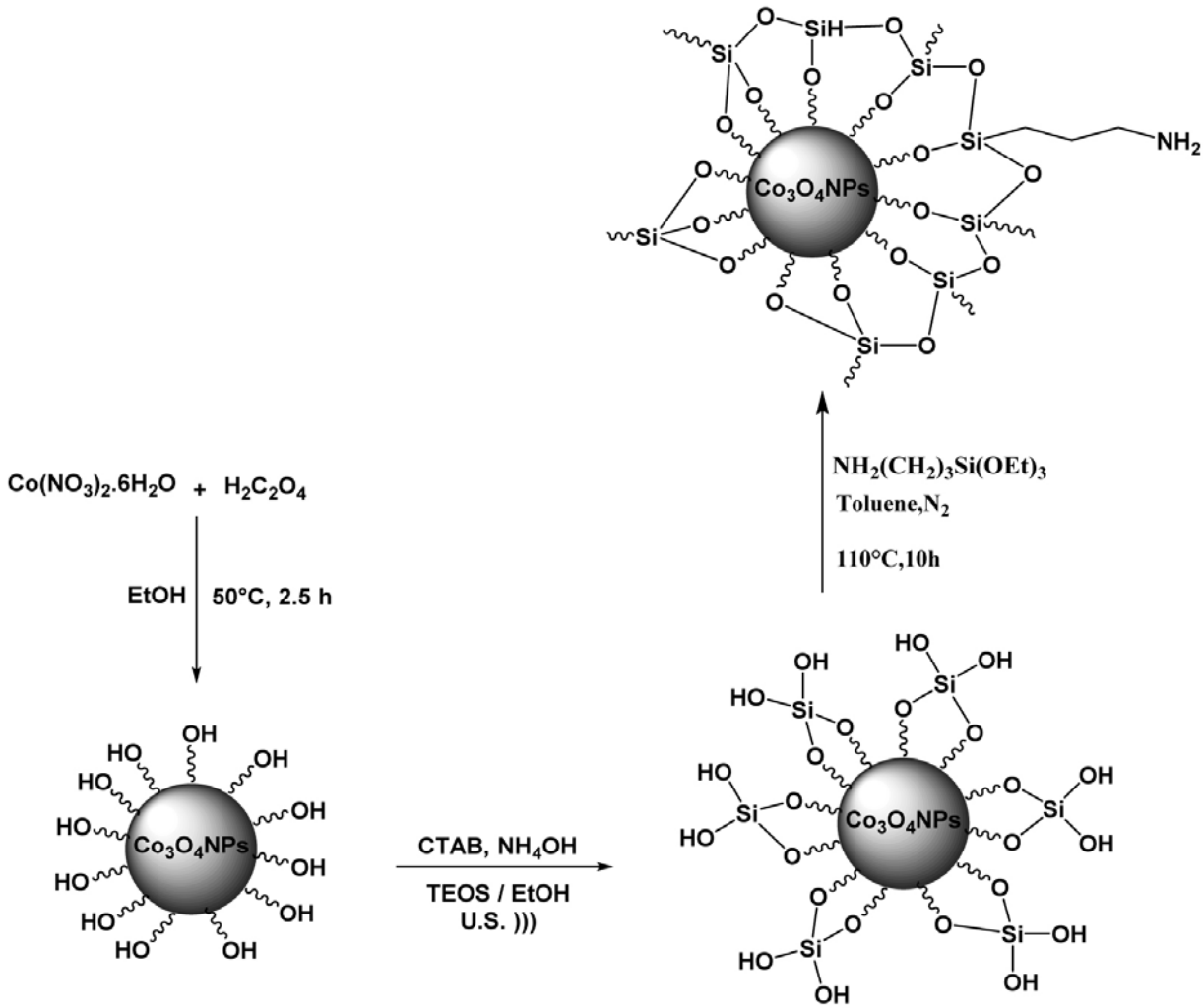

Scheme 1. Preparation steps for fabricating Co_3O_4@SiO_2@NH_2 nanocomposite

zine (2 mmol), and Co_3O_4@SiO_2@NH_2 (0.003 g) were placed in a round-bottom flask. The suspension was stirred under solvent-free conditions at 80 °C. Completion of the reaction was monitored by Thin Layer Chromatography (TLC). After termination of the reaction, the catalyst was separated from the solid crude product by using an external magnet. The precipitated solid was then collected and recrystallized from ethanol to afford the pure product.

The products were identified with ^{1}HNMR, ^{13}CNMR and FT–IR spectroscopic techniques.

3. Results and Discussion

3. 1. Catalyst Characterization

The synthesis strategy of $Co_3O_4/SiO_2/NH_2$ MNPs involves three steps. Figure 1 shows the XRD patterns of prepared Co_3O_4, Co_3O_4@SiO_2 and Co_3O_4@SiO_2@NH_2. All the XRD patterns show raising background which is attributed to X-ray fluorescence since Cu–K_α has been used as the X-ray source during the measurements.[25]

The reflections of XRD pattern of Co_3O_4 in Fig. 1a confirm the synthesis of cubic normal spinel Co_3O_4 (JCPDS file no. 42–1467). Fig. 1b shows the SiO_2 coating of Co_3O_4 by the presence of the new broad peak at 2è approximately 22–25°. As shown in Figure 1, the characteristic peaks of Co_3O_4 are also observed for Co_3O_4@SiO_2 and Co_3O_4@SiO_2@NH_2, which represent the stability of the crystalline phase of Co_3O_4 nanoparticles during silica coating and surface amino-functionalization. Although these characteristic diffraction peaks are weakened in Co_3O_4@SiO_2 and Co_3O_4@SiO_2@NH_2, because of the silica coating and surface amino-functionalization. The average crystallite sizes of the Co_3O_4 in Figure 1 (a, b and c) which have been estimated by using the Scherrer equation were 23.5, 24.2 and 26.0 nm respectively.

Further information about the chemical structure of Co_3O_4, Co_3O_4@SiO_2 and Co_3O_4@SiO_2@NH_2 nanocomposites have been obtained from FT–IR spectroscopy

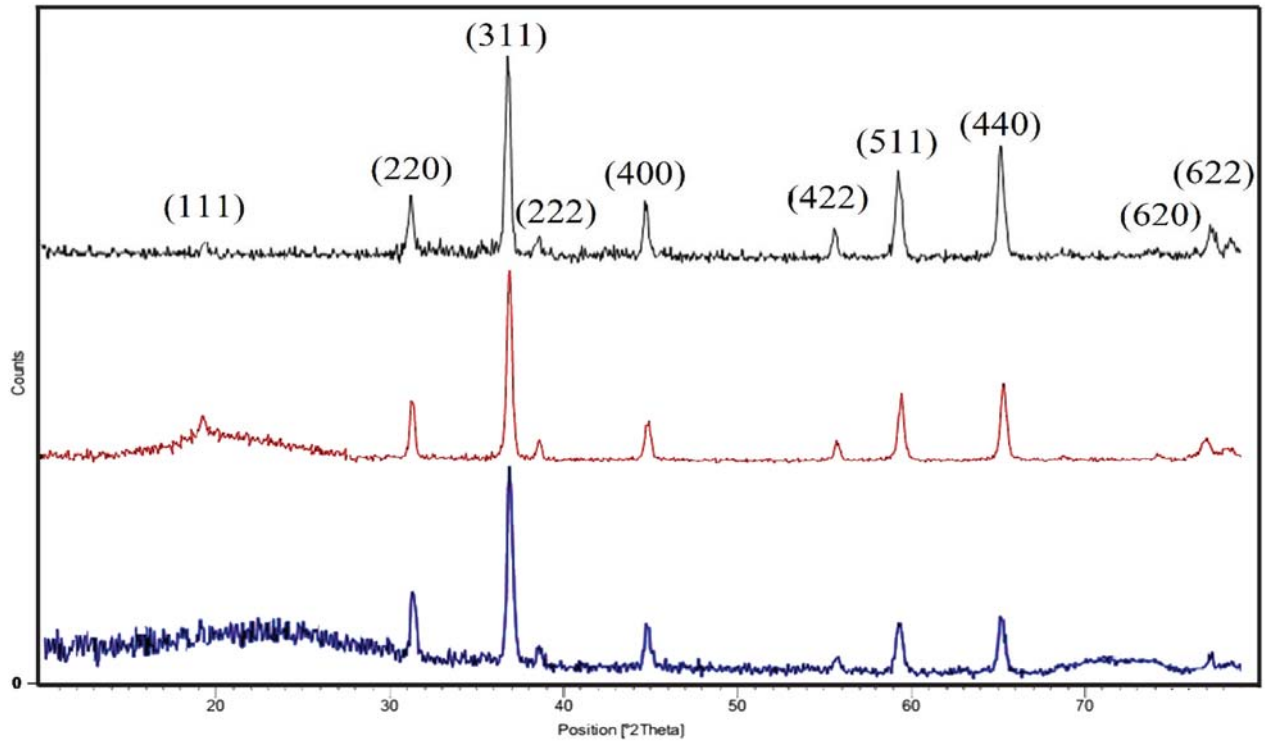

Figure 1. X-ray diffraction of Co_3O_4 (a), Co_3O_4@SiO_2 (b) and Co_3O_4@SiO_2–NH_2 (c) MNPs.

shown in Figure 2. For all three nanoparticles, the analyses indicated two strong absorption bands at 565 and 662 cm^{-1} which correspond to the vibrations of Co–O in Co_3O_4.

The peaks at 460 and 1070 cm^{-1} are attributed to the Si–O–Si bond stretching of Co_3O_4@SiO_2 and Co_3O_4@SiO_2@NH_2. The weak intensity band at 830 cm^{-1} can be

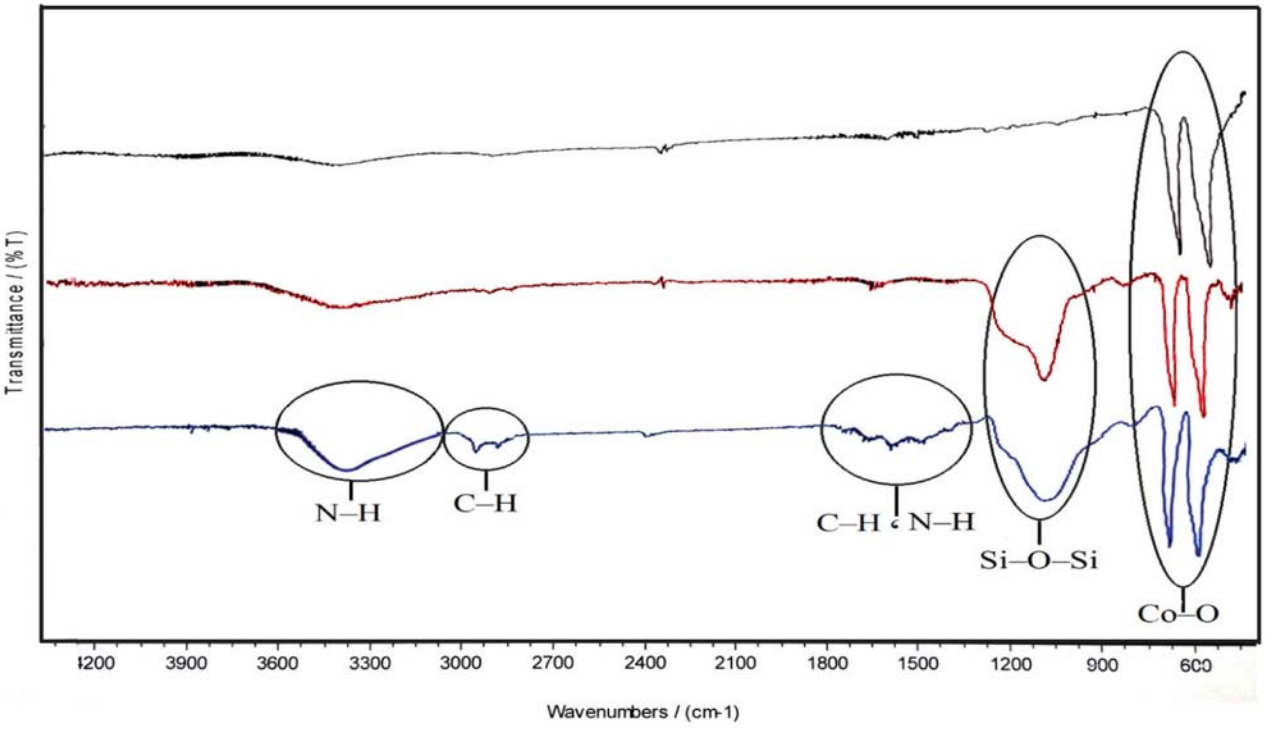

Figure 2. Comparative FT–IR spectra of Co_3O_4 (a), Co_3O_4@SiO_2 (b) and Co_3O_4@SiO_2–NH_2 (c) MNPs.

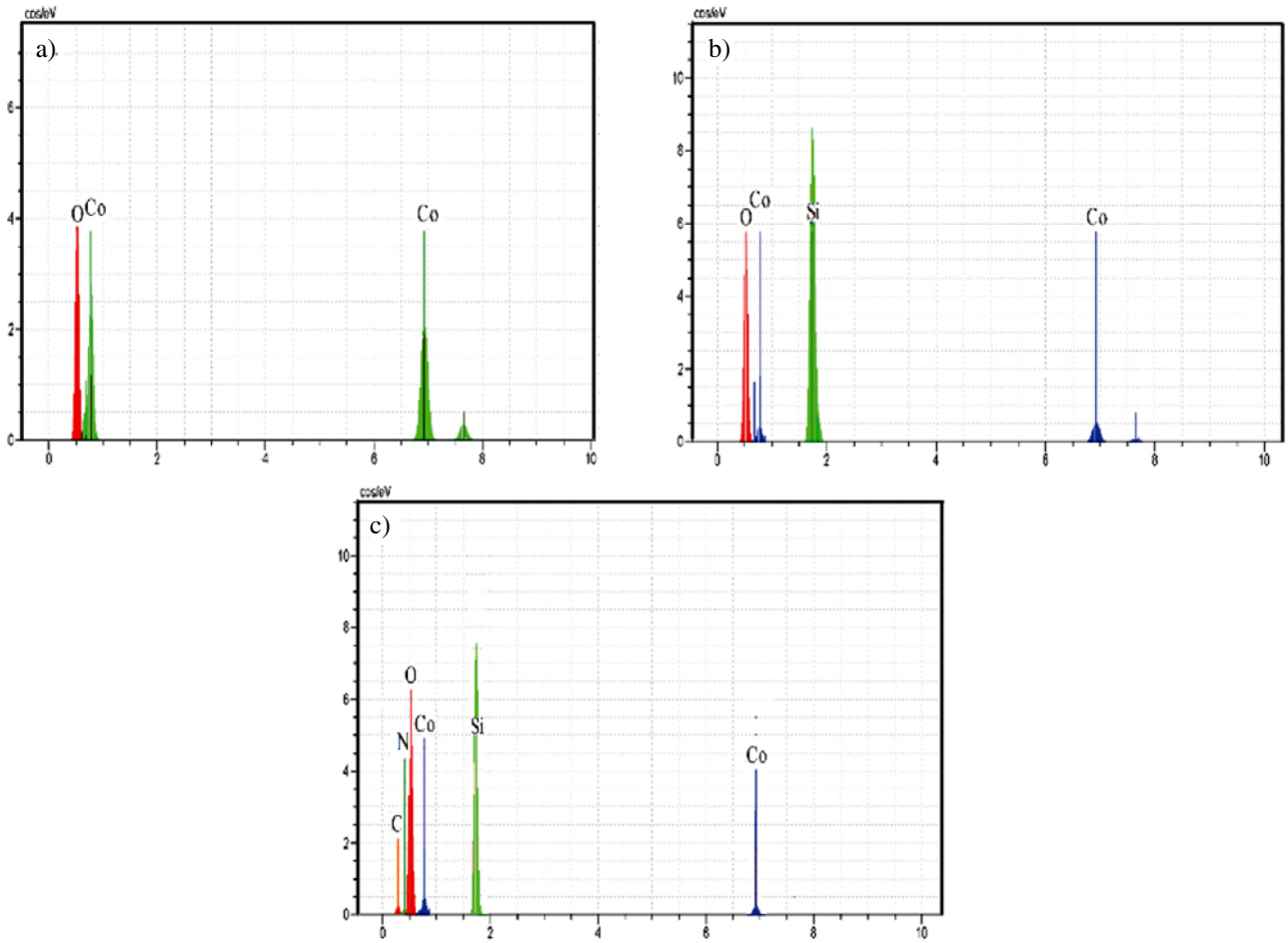

Figure 3. EDX spectra of Co_3O_4 (a), $Co_3O_4@SiO_2$ (b) and $Co_3O_4@SiO_2–NH_2$ (c) MNPs.

ascribed to the stretching of non-bridging oxygen atom in Si–OH bond. Therefore the silica coating on the surface of Co_3O_4 nanoparticles were confirmed by these absorption bands (Figure 2b and 2c). As indicated in Figure 2c, the peaks of $Co_3O_4@SiO_2@NH_2$ are located at 1480 cm^{-1} (C–H bending), 2880 cm^{-1} (C–H stretching), 1645 cm^{-1} (N–H bending), and 3360 cm^{-1} (N–H stretching). These peaks indicated that APTES has been bonded with the surface of $Co_3O_4@SiO_2$. The characteristic peaks of C–H stretching and N–H bending for the synthesized $Co_3O_4@SiO_2@NH_2$ are too weak to be observed clearly. Therefore, another analytical method, EDX, was employed to prove that the amine group has been bonded on the surface of $Co_3O_4@SiO_2$.[26–28]

Figure 3 shows the EDX data for Co_3O_4, $Co_3O_4@SiO_2$, $Co_3O_4@SiO_2@NH_2$ MNPs. In Figure 3 c, the weight ratio for C: N: O: Si: Co was calculated to be 12: 3.5: 36: 6.5: 42. These data demonstrate formation of $Co_3O_4@SiO_2@NH_2$ nanocomposite.

Figure 4 represents the room-temperature magnetization curves of the Co_3O_4, $Co_3O_4@SiO_2$ and $Co_3O_4@SiO_2–NH_2$ MNPs which have been obtained using a VSM. As it can be observed, there are no hysteresis, coercivity and remanence in the three synthesized nanoparticles which indicate their typical superparamagnetic property. The plots which have been shown in Figure 4 exhibited a change in saturation magnetization (Ms) of the particles

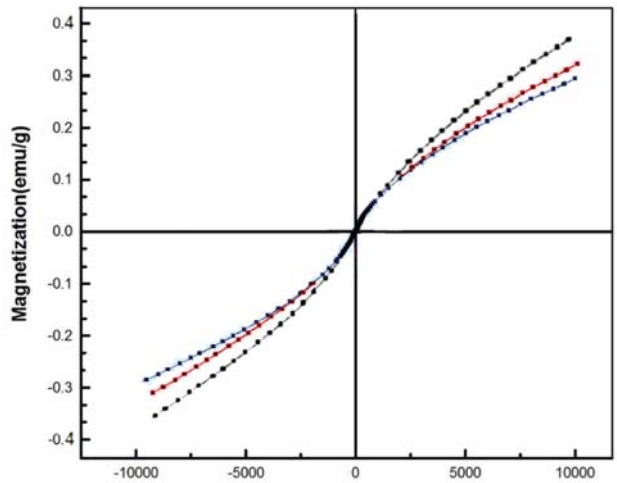

Figure 4. VSM magnetization curves of the Co_3O_4 (a), $Co_3O_4@SiO_2$ (b) and $Co_3O_4@SiO_2–NH_2$ (c) MNPs.

after incorporation of a NH_2/SiO_2 shell. The Ms values were measured to be 47.1, 36.9 and 33.8 emu/g respectively. It is clear that saturation magnetization of silica-coated Co_3O_4 nanoparticles is lower than that of pristine Co_3O_4 nanoparticles, and saturation magnetization of $Co_3O_4@SiO_2–NH_2$ is lower than $Co_3O_4@SiO_2$. This reduction in saturation magnetization can be attributed to the surface effects such as magnetically inactive layer which contains spins that are not collinear with the magnetic field.[29] Because the silica coating is a nonmagnetic mass, and this decrease was ascribed to the contribution of the nonmagnetic NH_2/SiO_2 shell to the total mass of the particles.

Figure 5 shows TEM image of amino-functionalized SiO_2 coated Co_3O_4 nanoparticles. Typical size of the structure has been measured about 50 nm, and the aggregation of the nanoparticles can be observed clearly. Therefore, the TEM observation confirmed the formation of an amino-functionalized SiO_2 around the Co_3O_4 nanoparticles with typical nanostructure.

The scanning electron microscopy (FE–SEM) of the $Co_3O_4@SiO_2@NH_2$ MNPs shows the morphology and structure of the as-prepared samples (Figure 6). The Co_3O_4 nanoparticles are irregular sheets (non-spherical) in shape and hard aggregated powders with diameters ranging from 35 to 80 nm as seen in Figure 6a. The irregular Bullet-shaped $Co_3O_4@SiO_2$ nanoparticles with diameters ranging from 95 to 220 nm are shown in Figure 6b. This illustrated that SiO_2 has been successfully coated on the Co_3O_4 nanoparticles. The micrograph of

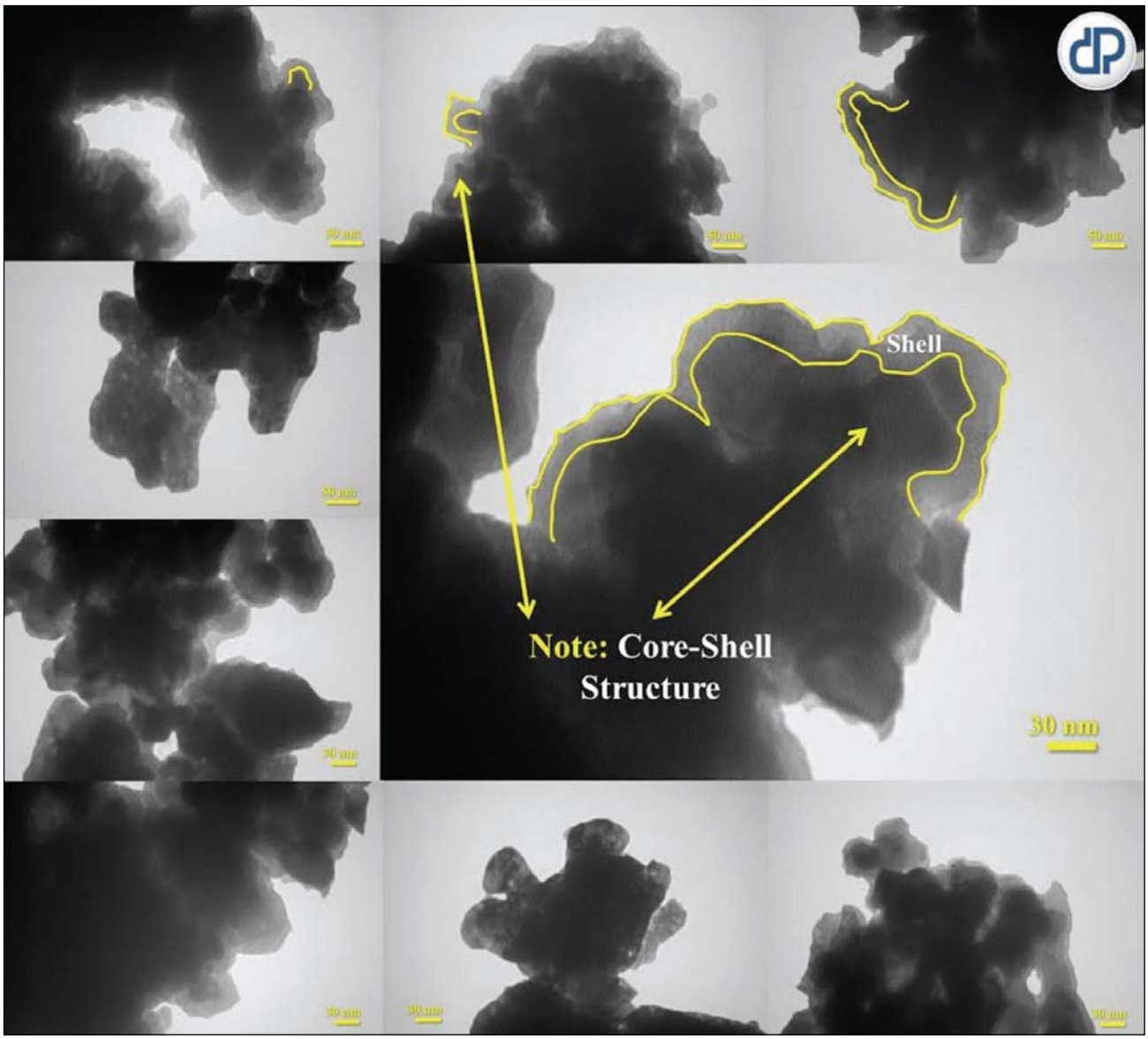

Figure 5. TEM images of $Co_3O_4@SiO_2@NH_2$ MNPs

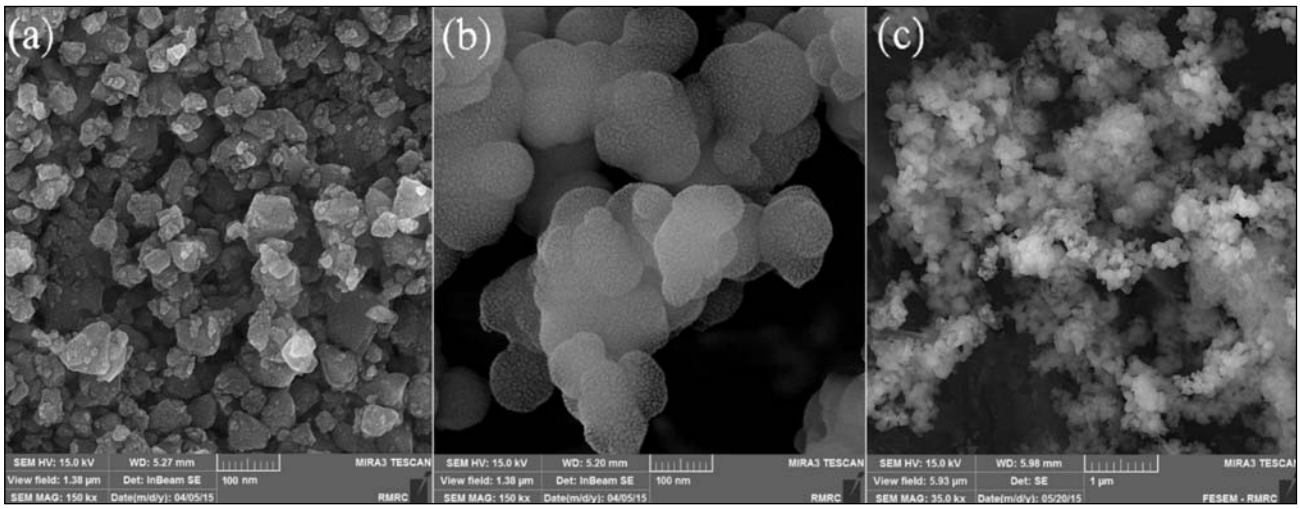

Figure 6. SEM images of Co_3O_4 (a), $Co_3O_4@SiO_2$ (b) and $Co_3O_4@SiO_2–NH_2$ (c) MNPs.

$Co_3O_4@SiO_2@NH_2$ MNPs represents a cloudy network of particles with spherical shape, as indicated in TEM image. This network is the result of self-poly condensation of aminopropylsilane groups.

3. 2. Catalyst Testing for the Synthesis of Some 7-benzylidene-2,3-diphenyl-3,3a,4,5,6,7-hexahydro-2H-indazole Derivatives

In order to optimize the reaction conditions and to obtain the best catalytic activity, the synthesis of 7-benzylidene-2,3-diphenyl-3,3a,4,5,6,7-hexahydro-2H-indazole derivatives was chosen as a model reaction. The reactions were conducted under solvent-free conditions at 80 °C (Scheme 2).

The synthesis of 7-benzylidene-2,3-diphenyl-3,3a,4,5,6,7-hexahydro-2H-indazoles with different amounts of the $Co_3O_4@SiO_2@NH_2$ MNPs has been considered. It was observed that while the amount of catalyst increased from 0 to 0.003 g, the product yield raised from 0% to 98% significantly. No reaction yield without using the catalyst corroborates that the $Co_3O_4@SiO_2@NH_2$ MNP catalyst plays a pivotal role in the synthesis of 7-benzylidene-2,3-diphenyl-3,3a,4,5,6,7-hexahydro-2H-indazole derivatives.

In the respect of industrial aims, reusability of the catalyst was examined by repeating the model reaction under the optimizedreaction conditions (Table 1). In order to reuse the catalyst after each cycle, it was separated by a magnet, washed several times with deionized water and chloroform. Then, it was dried in oven at 60 °C and reused in the next run. According to the results, the $Co_3O_4@SiO_2@NH_2$ MNPs can be reused six times without any significant loss of activity in this organic reaction. Moreover, nitrogen content of the catalyst was estimated by back titrationafter sixth cycle (5.72 mmol/g), which indicates low NH_2 leaching during the reaction.

Table 1. Reusability of the $Co_3O_4@SiO_2–NH_2$ nanocomposite

Yield (%)					
First	**Second**	**Third**	**Fourth**	**Fifth**	**Sixth**
98	96	95	92	91	87

In order to evaluate scope of this research, we tried to prepare a range of 7-benzylidene-2, 3-diphenyl-3,3a,4,5,6,7-hexahydro-2H-indazole derivatives under the same reaction conditions. The results are presented in (Table 2).[30]

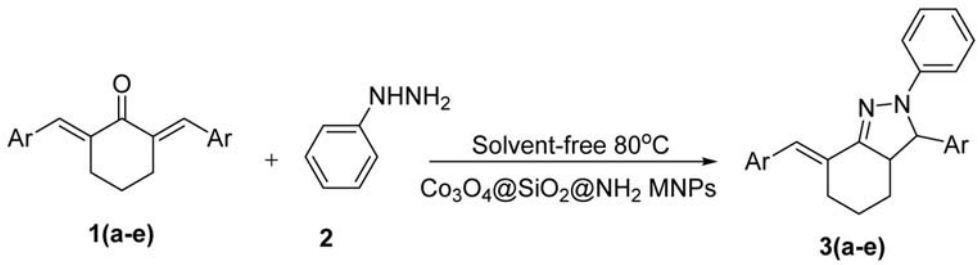

Scheme 2. The model reaction for the synthesis of 7-benzylidene-2,3-diphenyl-3,3a,4,5,6,7-hexahydro-2H-indazole

Table 2. Co_3O_4@SiO_2–NH_2 catalyzed synthesis of some indazoles [a]

Entry	Product [b]	Time (min)	Yield (%) [c]	Lit. M.p.°C	M.p.°C
1	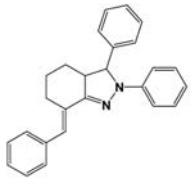 3a	17	94	136–138[30]	136–136
2	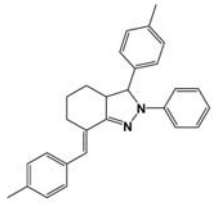 3b	20	91	141–143[30]	142–144
3	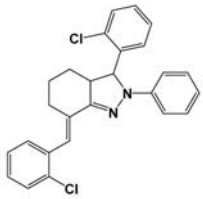 3c	15	93	156–158[30]	155–157
4	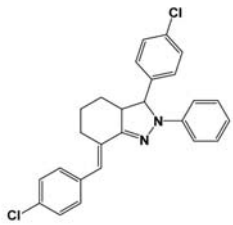 3d	12	96	174–176[30]	174–176
5	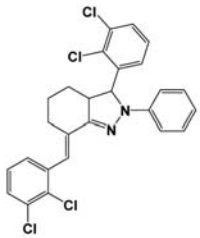 3e	10	98	202–204[30]	200–202

[a] Reaction conditions: phenyl hydrazine (1 mmol), α,ά-bis (substituted-arylidene) cycloalkanone (1 mmol), catalyst (0.003 g, Co_3O_4@SiO_2–NH_2), under solvent-free conditions at 80 °C [b] Products were characterized by FT–IR, ^{1}H NMR and ^{13}C NMR analysis [c] Isolated yield.

4. Conclusions

In this research, Co_3O_4 nanoparticles were coated with amino-functionalized SiO_2 as organic shell via three step method. The average crystallite size of the Co_3O_4 was calculated 23.7 nm, by using the Scherrer equation. The synthesized nanocomposite exhibited super paramagnetic behaviour at room temperature because of the magnetically inactive layer of SiO_2@NH_2. The saturation magnetization of Co_3O_4@SiO_2@NH_2 MNPs is less than that of pure Co_3O_4 nanoparticles. This new magnetic nanocomposite showed the following advantages: (a) simple preparation; (b) recoverability and easy separation by an external magnet, c) highly effective for chemical transformations as a heterogeneous catalyst. These unique results open new perspectives for application of these types of

magnetic nanocomposites in many reactions. Moreover, we have developed a facile, convenient and environmentally benign synthesis of some 7-benzylidene-2,3-diphenyl-3,3a,4,5,6,7-hexahydro-2H-indazole derivatives by utilizing novel nano-scale materials including Co_3O_4@ SiO_2@NH_2 nanocomposite.

5. Acknowledgements

This work is funded by the Research Affairs Office of the Islamic Azad University, Qom Branch, Qom, I. R. Iran [grant number 2014-13929].

6. References

1. K. K. Senapati, S. Roy, C. Borgohain, P. Phukan, *J. Mol. Catal. A Chem.*, **2012**, *352*, 128–134. https://doi.org/10.1016/j.molcata.2011.10.022
2. D. Lee, J. Lee, H. Lee, S. Jin, T. Hyeon, B. M. Kim, *Adv. Synth. Catal.*, **2006**, *348*, 41–46. https://doi.org/10.1002/adsc.200505354
3. R. Abu-Rezig, H. Alper, D. Wang, M. L. Post, *J. Am. Chem. Soc.*, **2006**, *128*, 5279–5282. https://doi.org/10.1021/ja060140u
4. S. Zafeiratos, T. Dintzer, D. Teschner, R. Blume, M. Hävecker, A. Knop-Gericke, and R Schlogl, *J. Catal.*, **2010**, *269*, 309–317. https://doi.org/10.1016/j.jcat.2009.11.013
5. A. Yu. Khodakov, J. Lynch, D. Bazin, B. Rebours, N. Zanier, B. Moisson, P. Chaumette, *J. Catal.*, **1997**, *168*, 16–25. https://doi.org/10.1006/jcat.1997.1573
6. D. Yang, J. Hu, S. Fu, *J. Phys. Chem. C.*, **2009**, *113*, 7646–7651. https://doi.org/10.1021/jp900868d
7. Z. Bo, X. JianMin, L. Yu Qi, L. HuiZhou, *Sci China Ser B-Chem.*, **2008**, *51*, 145–151.
8. C. W. Lu, Y. Hung, J. K. Hsiao, M. Yao, T. H. Chung, Y. S. Lin, S. H. Wu, S. C. Hsu, H. M. Liu, C. Y. Mou, C. S. Yang, D. M. Huang, Y. C. Chen, *Nano Lett.*, **2007**, *7*, 149–154. https://doi.org/10.1021/nl0624263
9. P. Ashtari, X. X. He, K. Wang, P. Gong, *Talanta.*, **2005**, *67*, 548–554. https://doi.org/10.1016/j.talanta.2005.06.043
10. X. Zhao, Y. Shi, T. Wang, Y. Cai, G. Jiang, *J. Chromatogr. A.*, **2008**, *1188*, 140–147. https://doi.org/10.1016/j.chroma.2008.02.069
11. C. A. Mirkin, *MRS Bull.*, **2000**, *25*, 43–54. https://doi.org/10.1557/mrs2000.123
12. M. Bagheri, M. Masteri-Farahani, M. Ghorbani, *J. Magn. Magn. Mater.*, **2013**, *327*, 58–63. https://doi.org/10.1016/j.jmmm.2012.09.038
13. T. Z. Yang, C. M. Shen, H. J. Gao, *J. Phys. Chem. B.*, **2005**, *109*, 23233–23236. https://doi.org/10.1021/jp054291f
14. M. A. Ghasemzadeh, M. H. Abdollahi-Basir, *Acta. Chim. Slov.* **2016**, *63*, 627–637. https://doi.org/10.17344/acsi.2016.2386
15. M. A. Ghasemzadeh, *Acta. Chim. Slov.*, **2015**, *62*, 977–985. https://doi.org/10.17344/acsi.2015.1501
16. J. Safaei-Ghomi, M. A. Ghasemzadeh, *J. Serb. Chem. Soc.*, **2011**, *75*, 679–684.
17. F. Zamani, S. Kiapour, *Catal. Commun.*, **2014**, *45*, 1–6. https://doi.org/10.1016/j.catcom.2013.10.027
18. F. Zamani, S. M. Hosseini, *Catal. Commun.*, **2014**, *43*, 164–168. https://doi.org/10.1016/j.catcom.2013.09.029
19. G. H. Mahdavinia, S. Rostamizadeh, A. M. Amani, M. Mirzazadeh, *Green Chem. Lett. Rev.*, **2012**, *5*, 255–281. https://doi.org/10.1080/17518253.2011.617317
20. G. H. Mahdavinia, M. Mirzazadeh, *E. J. Chem.*, **2012**, *9*, 49–54. https://doi.org/10.1155/2012/390528
21. C. C. Lin, Y. Guo, J. Vela, *ACS Catal.*, **2015**, *5*, 1037-1044. https://doi.org/10.1021/cs501650j
22. J. Alauzun, A. Mehdi, C. Reyé, R. J. P. Corriu, *J. Am. Chem. Soc.*, **2006**, *128*, 8718–8719. https://doi.org/10.1021/ja0622960
23. Y. Shao, J. Guan, S. Wu, H.Liu, B. Liu, Q. Kan, *Microporous Mesoporous Mater.*, **2010**, *128*, 120–125. https://doi.org/10.1016/j.micromeso.2009.08.013
24. F. Zamani, E. Izadi, *Chin. J. Catal.*, **2014**, *35*, 21–27 https://doi.org/10.1016/S1872-2067(12)60685-8
25. C. Suryanarayana, M. G. Norton, X-Ray Diffraction: A Practical Approach, Plenum Press, **1998**. https://doi.org/10.1007/978-1-4899-0148-4
26. J. Wang, S. Zheng, Y. Shao, J. Liu, Z. Xu, D. Zhu, *J. Colloid Interface Sci.*, **2010**, *349*, 293–299. https://doi.org/10.1016/j.jcis.2010.05.010
27. A. A. M. Gomaa, F. A. Osama, M. A. Salah, Y. M. Mashitah, C. F. Feng, *J. Solid State Electro. chem.*, **2014**, *18*, 2505–2512. https://doi.org/10.1007/s10008-014-2510-3
28. S. Esposito, M. Turco, G. Ramis, G. Bagnasco, P. Pernice, C. Pagliuca, M. Bevilacqua, *J Solid State Chem.*, **2007**, *180*, 3341–3350. https://doi.org/10.1016/j.jssc.2007.09.032
29. M. Yamaura, R. L. Camilo, L. C. Sampaiob, M. A. Macedoc, M. Nakamurad, H. E. Tomad, *J. Magn. Magn. Mater.*, **2004**, *279*, 210–217. https://doi.org/10.1016/j.jmmm.2004.01.094
30. G. H. Mahdavinia, M, Mirzazadeh, Z. Karimi-Jaber, *Green Chem Lett. Rev.*, **2015**, *8*, 13–15. https://doi.org/10.1080/17518253.2014.976280

Povzetek

V tej raziskavi poročamo o učinkoviti sintezni poti v treh stopnjah s katero smo pripravili nov nanokompozit kobaltovega oksida (Co_3O_4) prevlečen s SiO_2 @ (3-aminopropil)-trietoksisilanom. Strukturne in magnetne lastnosti kompozita Co_3O_4 @ SiO_2 @ NH_2 smo določili s pomočjo različnih metod: infrardečo spektroskopijo (FT–IR), rentgensko praškovno difrakcijo, vrstično elektronsko mikroskopijo (SEM), presevno elektronsko mikroskopijo (TEM), energijsko disperzijsko spektroskopijo (EDX) in magnetometrijo z vibrirajočim vzorcem (VSM). V nanokompozitu Co_3O_4, ki je prevlečen z amino funkcionaliziranim SiO_2 je opaziti superparamagnetne lastnosti in močno magnetizacijo pri sobni temperaturi. Povprečne velikosti kristalitov Co_3O_4 so 23,7 nm. Dobljeni magnetni nanokompozit je pokazal odlično katalitsko aktivnost kot novi heterogeni magnetni katalizator za sintezo nekaterih derivatov indazola pri blagih reakcijskih pogojih in visoko stopnjo ponovne uporabe.

Scientific paper

Forward Osmosis in Wastewater Treatment Processes

Jasmina Korenak,[1] Subhankar Basu,[2] Malini Balakrishnan,[2] Claus Hélix-Nielsen[1,3] and Irena Petrinic[1]

[1] *University of Maribor, Faculty of Chemistry and Chemical Engineering, Smetanova ulica 17, SI-2000 Maribor, Slovenia*

[2] *The Energy and Resources Institute (TERI), Darbari Seth Block, IHC Complex, Lodhi Road, New Delhi 110003, India*

[3] *Technical University of Denmark, Department of Environmental Engineering, Bygningstorvet 115, DK2800 Kgs. Lyngby, Denmark.*

** Corresponding author: E-mail: jasmina.korenak@um.si*
Tel: +386 2 2294 474 Fax: +386 2 2527 774

Received: 30-08-2016

Abstract

In recent years, membrane technology has been widely used in wastewater treatment and water purification. Membrane technology is simple to operate and produces very high quality water for human consumption and industrial purposes. One of the promising technologies for water and wastewater treatment is the application of forward osmosis. Essentially, forward osmosis is a process in which water is driven through a semipermeable membrane from a feed solution to a draw solution due to the osmotic pressure gradient across the membrane. The immediate advantage over existing pressure driven membrane technologies is that the forward osmosis process *per se* eliminates the need for operation with high hydraulic pressure and forward osmosis has low fouling tendency. Hence, it provides an opportunity for saving energy and membrane replacement cost. However, there are many limitations that still need to be addressed. Here we briefly review some of the applications within water purification and new developments in forward osmosis membrane fabrication.

Keywords: Biomimetic membranes, Desalination, Draw solutions, Forward osmosis, Wastewater treatment

1. Introduction

The last decade has witnessed extensive research and technological achievements in water production and wastewater treatment processes. Also, it is being realized that water, energy and food are inter-connected – often expressed as the *water-energy-food nexus.* This necessitates further developments to establish more energy efficient solutions. Therefore, a growing number of academic and industrial research groups around the world are conducting work on water treatment and reuse – in particular, within membrane-based water treatment.

Forward Osmosis (FO) is one example of a promising membrane process and potentially a sustainable alternative/supplement to reverse osmosis (RO) process for wastewater reclamation and sea/brackish water desalination. FO has shown good performance in a variety of applications, such as desalination, concentration of wastewater and resource recovery, wastewater treatment and it is also attracting attention as a potential technology to augment water supplies using seawater and wastewater.[1–3] However, Van der Bruggen et al (2015) stated that FO as stand-alone process is usually not viable for water treatment purposes.[4]

Nevertheless, membrane fouling limits its large-scale applications. To reduce the membrane fouling in FO, many improvements has been attempted, e.g. synthesis of different membrane materials, fabrication of membrane modules, membrane coatings etc. Further, there have been improvements in the productivity and decrease in the cost of synthetic membranes used for water and wastewater applications.

One of the novelties in membrane development research field is application of biomimetic membranes in separation processes including FO.[5] Biomimetics is defined as the study of the structure and function of biological systems and processes as models or inspiration for the sustainable design and engineering of materials and machines. In particular the use of aquaporins (AQPs) – biological water channel proteins[6] which are highly selective and effective has prompted considerable interest in recent years.[7]

In this paper, we review, (i) the membrane process based on osmotic pressure, principles and transport of water molecules, (ii) applications of FO in water purification, and (iii) recent developments in FO membrane fabrication.

2. Osmotically Driven Membrane Processes

FO is a membrane process in which no hydrostatic pressure is applied. The transport of water molecules across a semi-permeable membrane occurs due to the osmotic pressure difference of solutions on either side of the membrane. The natural flow of water is from the low solute concentration side to the high solute concentration side across a semi-permeable membrane to equilibrate the osmotic pressure difference.

PRO is an osmosis process in which there is a hydraulic pressure applied to the high concentration solution, but the osmotic pressure difference is higher, so the water flux is still opposite to the flux in RO process. PRO possesses characteristics intermediate between FO and RO, where water from a low osmotic pressure feed solution (FS) diffuses through a membrane into a pressurized high osmotic pressure draw solution (DS). In order for water transport to occur, the osmotic pressure difference between the FS and DS should exceed the hydrostatic pressure on the DS side. The classical PRO application is electrical power generation which can be achieved by de-

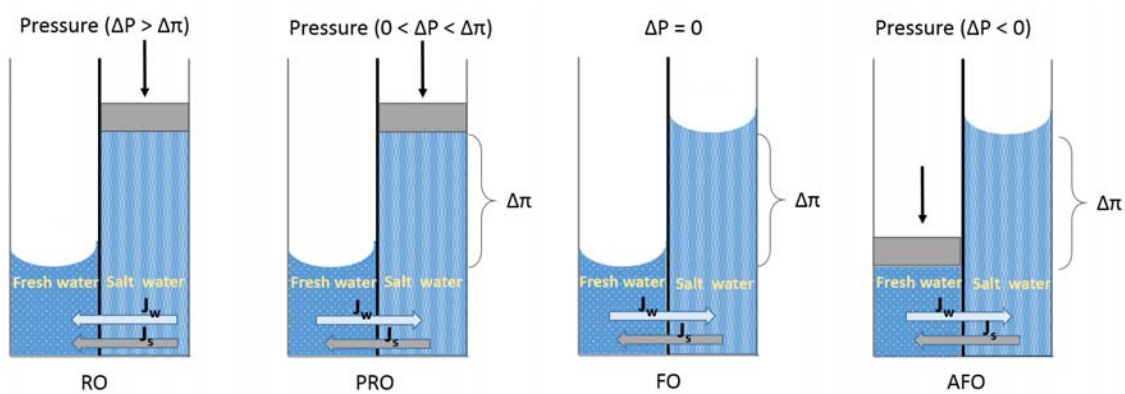

Figure 1. Osmotic processes in membrane filtration. ΔP is applied hydraulic pressure; Δπ is osmotic pressure difference between the two solutions; J_w is water flux; J_s is salt reverse flux

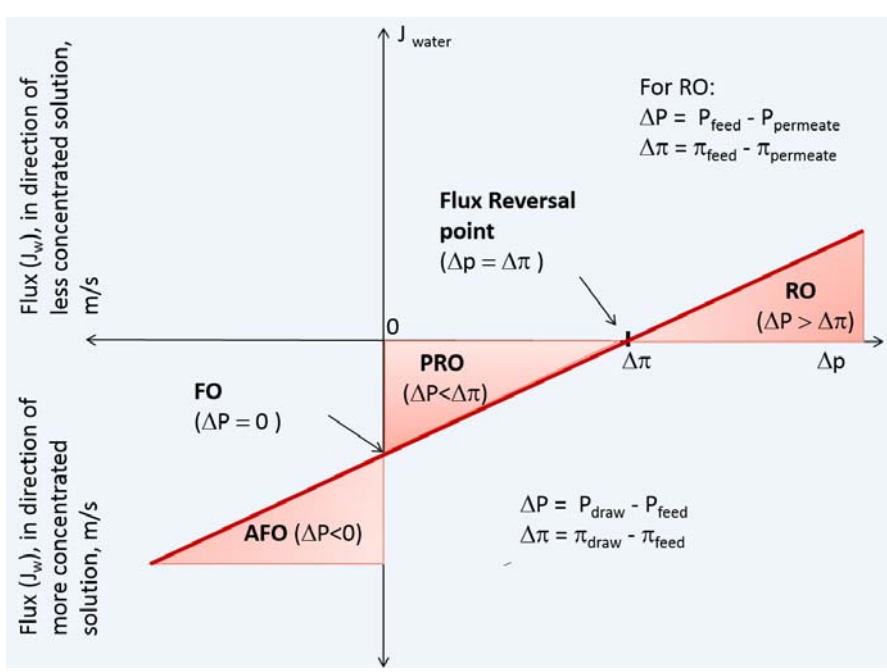

Figure 2. Relationship between water flux and applied pressure in RO, PRO, FO, and AFO.

pressurizing the diluted seawater through a hydro-turbine or generator set.[8]

Pressure-assisted forward osmosis (AFO) has been proposed that applies the pressure at the feed side to further enhance the performance of the FO process to increase water flux. AFO adds a medium pressure pump to a conventional FO system. The system takes advantage of additional hydraulic pressure that results in water transport in both mechanisms: flux driven by hydraulic pressure (RO mechanism) and that by osmotic pressure (FO mechanism).

Figure 1 describes the flux directions of the permeating water in the RO, PRO, FO and AFO processes respectively. The theoretical water flux across the membrane (J_w) is calculated using a variation of Darcy's law:

$$(J_w) = A_w \times (\sigma\Delta\pi - \Delta P) \quad (1)$$

where, A_w is the pure water permeability coefficient of the membrane, ΔP is the applied hydrostatic pressure, $\Delta\pi$ is the differential osmotic pressure, and σ is the reflection coefficient which represents the rejection capability of a membrane. A perfect semipermeable membrane has $\sigma = 1$. Fig. 2 presents the relation between water flux and applied pressure.

In RO, solutes diffuse from the feed into permeate. However, in FO, solutes diffuse in two directions: from the feed into the DS (i.e., forward diffusion) and simultaneously from the DS into the feed (i.e., reverse diffusion). Reverse permeation of solutes from the DS into the FS decreases the osmotic driving force and consequently this reduces the water transport. In a FO system, this could dramatically increase the costs of the process.

The flux of a solute (J_s) through semipermeable membranes is governed by chemical potential gradients and is commonly described by Fick's law:

$$J_s = B(C_i - C_{Fm}) \quad (2)$$

where B is the solute permeability coefficient and C_i and C_{Fm} represent the solute concentration at the membrane-solution interface on the DS side and FS side, respectively.

3. The Forward Osmosis Process

In FO process, the water molecules are drawn from the FS through a semi-permeable membrane to the DS side (from a lower osmotic pressure to a higher osmotic pressure side). The driving force of the process is an osmotic pressure generated by the concentrated DS. The process ends when the hydraulic difference between the two solutions equals the osmotic pressure difference.

The semi-permeable membranes used in FO has comparable rejection range in size of pollutants (1nm and below) as RO membranes. Purified water is produced during the process and the DS is diluted. Thus, FO offers several advantages; (i) high rejection of a wide range of contaminants, (ii) reduction in energy consumption, (iii) lower brine discharge, and (iv) lower membrane fouling propensity compared to pressure-driven membrane processes.[2, 9]

The main challenges in the FO process are related to:

– Development of high performance, such as higher water flux and lower salt reverse flux of FO membranes.
– Reduction in concentration polarisation of membranes.
– Ensuring low DS reverse solute flux across the membrane.
– Economical reuse and regeneration of the DS.

4. Types of DS

In the FO process, the concentrated solution is commonly known as the DS although different terms can be found in the open literature. The DS plays an important role in the efficiency and performance of the process, and the selection of appropriate DS is crucial.

The driving force involved in FO is shown in Fig. 3; where C_s, C_d, a_s, a_d and μ_s, μ_d are the solute concentrations, water activities and water chemical potentials in the feed (s) and draw (d) solution, respectively.

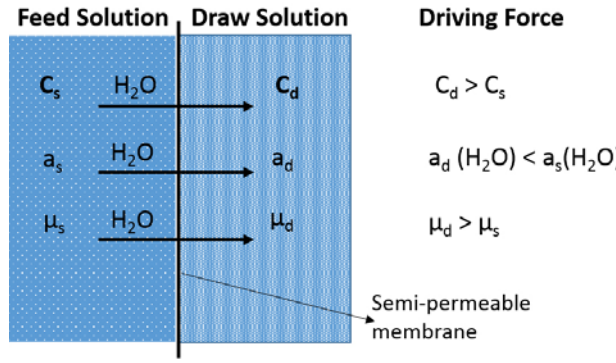

Figure 3. Schematic representation of the driving force involved in FO in an ideal system where only water (H_2O) is transported across the membrane (i.e. 100% solute rejection by the membrane).[10]

In this process it is the ability of the draw solution to generate the relevant osmotic pressure level that is paramount.[11] The osmotic pressure of solution is affected by adding a second solute that can influence the solute–solvent interaction. Solutes disturb the solvent structure. In the case of water as the solvent, the presence of solute affects the structure of liquid water. In pure liquid water, the molecules are heavily hydrogen bonded in an ordered structure. The presence of ions disturb such structures by creating strong electric fields, the water dipoles are then arranged in an orderly manner and strongly bound, thus

affecting the freedom of water molecules and influencing their hydrogen bond system.[12]

Osmotic pressure of a solution π can be expressed by the Morse equation (applies to solutions with dilute concentrations, i.e. <0.5M), as follows:

$$\pi = iMRT = i\left(\frac{n}{V}\right)RT = -\frac{RT}{V_w}ln(a_w) \quad (3)$$

where i is the van't Hoff factor, M is the molarity of the solute which is equal to the ratio of the number of solute moles (n) to the volume of the solution (V), R is the gas constant of 8.3145 J K^{-1} mol^{-1}, and T is the absolute temperature. The right side of the equation includes the chemical potential of water which allows for calculating the activity of water a_w where V_w is the molar volume of water.

Hence, to achieve a high osmotic pressure, a good solubility of the draw solute in water is required to get a high n or M value. In addition, an ionic compound which is able to fully dissociate to produce more ionic species is preferred because it may result in a high i value. This indicates that multivalent ionic solutes are the most favourable. Therefore, compounds with high water solubility and a high degree of dissociation are potential candidates as draw solutes.

Different DS and their physio-chemical properties are presented in Table 1.

Since FO is an osmotic-driven process, a higher osmotic potential of DS than the feed solution is essential to induce a water flux. In addition, it must exhibit minimum reverse transport from the DS side to the feed side, be easily separated and re-used upon water extraction or be readily available if regeneration is not required.

Further to these characteristics, a desirable DS should be non-toxic, highly soluble, of neutral pH, inert and causing a minimum chemical or physical impact on the membrane, low molecular weight and low viscosity to reduce the concentration polarisation, be relatively low cost, and stable.

Many studies have been performed to identify appropriate draw solutes over the past few decades.[22] Based on the available literature, NaCl appears to be the most promising DS (approximately 40% of experiments), due to its high solubility, low cost and relatively high osmotic potential. It has been used as a DS in concentrations from 0.3 M to 6 M, but is often used at 0.5 M simulating the osmotic pressure of seawater and prompting the use of real seawater or RO brine as a DS.[3] Nevertheless, the type of wastewater (feed solution) and the required product purity have influence on the DS selection also. Some studies have used magnetic and/or hydrophilic nanoparticles as a DS.[23,24] However, it seems that there are only few that can be selected as a perfect draw solute, since the regeneration step has to be included for draw solution. As such, the benefits of the process have to be larger than the costs of DS and the additional regeneration step. [4]

4. 1. Fouling in Osmotically Driven Membrane Processes

Fouling is due to the deposition of retained matter (particles, colloids, macromolecules, salts, etc.) on the membrane surface or inside the membrane pores. The interaction (chemical and hydrodynamic) between the foulants and the membrane surface reduces the membrane water flux either temporarily or permanently.[25] There are

Table 1. Overview of draw solutes used in FO processes.

Draw solute(s)	Conc.	Osmotic pressure (bar)	Feed solution	J_s (g/m²h)	J_w (L/m²h)	Ref.
EDTA-2Na[a]	0,61 M	60	Raw wastewater	0.1	3.3	13
NaOAc	1,49 M	60		0.4	5.4	
NaCl	1,27 M	60		2.4	5.5	
EDTA-2Na and NP7[b]	0.1M and 15 mM	7.31	DI water	0,067	2.65	14
EDTA-2Na and NP9[c]	0.1M and 15 mM	7.4	DI water	0.092		
PUF[d]/hydrogel composites	50 to 89 wt% of hydrogel		DI water		3.9 to 17.9	15
PSSP[e]	20 wt%	20.85	DI water	0.14	14.50	16
PAspNa[f]	0.3 g/mL	51.5 atm	DI water	4.9	31.8	17
Sucrose	1	26.7	DI water		12.9	18
PAA-Na[g]	0.72 g/mL	44	DI water	0.18	22	19
HCOONa[h]	0.68	28	DI water	2.73	9.4	20
Sodium hexa-carboxylatophenoxy phosphazene	0.067	None	DI water		7	21

[a] Ethylenediaminetetraacetic acid disodium salt [b] Nonylphenol ethoxylate surfactants, Tergitol NP7 [c] Nonylphenol ethoxylate surfactants, Tergitol NP9 [d] Polyurethane foam [e] Oligomeric poly(tetrabutylphosphonium styrenesulfonate)s [f] Poly (aspartic acid sodium salt) [g] Polyacrylic acid sodium salts [h] Sodium formate

four major types of fouling: (1) organic fouling, which is caused by macromolecular organic compounds such as alginate, protein, and natural organic matters; (2) inorganic fouling, which is due to crystallization of sparingly soluble mineral salts when the salt concentration exceeds saturation; (3) biofouling, which involves bacteria deposition, attachment, and subsequent growth to form biofilm; and (4) colloidal fouling, which results from the deposition of colloidal particles.[26] Depending on its severity, fouling can have varied degree of adverse impact on membrane performance, such as decreasing water flux, deteriorating product water quality, and increasing maintenance burden.[27] Furthermore, the foulants might also chemically degrade the membrane material.[28] Fouling is a considerable problem that occurs in most liquid membrane processes and consequently influences the economics of the operation. Hence, a lot of research has been done to reduce the impacts of fouling in pressure driven membrane processes. The problem can be addressed by changing operational conditions, cleaning, membrane surface modification, and membrane material choices.

However, fouling in osmotically driven membrane processes is different from fouling in pressure driven membrane processes (Figure 4). Depending on the membrane orientation, the deposition of foulants occurs on different membrane surfaces. In FO process, foulant deposition occurs on the relatively smooth active layer. In PRO and other pressure driven processes, the foulant deposition takes place on the rough support layer side, or even within the support layer.[25]

Recent studies have demonstrated that membrane fouling in FO process is relatively low compared to the pressure driven processes. The reversible fouling can be minimized by optimizing the hydrodynamics, and a variety of contaminants can be effectively removed by physical cleaning.[2,30–33] In FO process, fouling due to organic materials is more severe than inorganic material.[34] Alginate as a model foulant was studied in FO and RO.[30] NaCl was used as draw solute in FO and feed solute in RO, severe flux decline in FO was observed than in RO. However, when dextrose was used as draw solute in FO, the flux decline was almost identical to RO. This indicates a cake formation from reverse salt flux. Humic acid filtration shows higher flux decline in FO than in RO. This also occurs in colloidal fouling with silica particles.[35] The flux decline is attributed to intermolecular bridging of humic acid molecules by the salt ions.

A strong correlation between intermolecular adhesion and fouling in FO was observed. Strong foulant-foulant interactions, such as adhesion, causes faster accumulation of foulant on the membrane surface.[36] It was further concluded that Ca binding, permeation and hydrodynamic shear force are some of the major factors that influences the rate of membrane fouling. The combined effect of organic and inorganic fouling using alginate and gypsum ($CaSO_4$) as model foulants was found to have a synergistic effect between the two foulants; the coexistence of the two foulants displayed a severe flux decline than the individual foulants.[37]

Alginate fouling and gypsum scaling on the membrane surface could be removed by physical cleaning. However, this observation is true when cellulose acetate membrane is used in FO process. The water flux recovery after physical cleaning of gypsum was less than with a polyamide thin film composite membrane.[32] These findings demonstrate that membrane surface modification and material choices should be an effective strategy to mitigate FO membrane fouling.

Motsa et al (2014) reported that membrane orientation had an impact on fouling behaviour since the membrane fouled more easy when operated in PRO mode than in FO mode. There was severe permeate flux decline in PRO mode mainly due to the calcium–alginate complexes blocking the pores in the support layer.[38] Yong Ng and Parid, focused on the impact of lower organic loads (10, 30, 50 ppm) in secondary effluents with calcium inclusion on

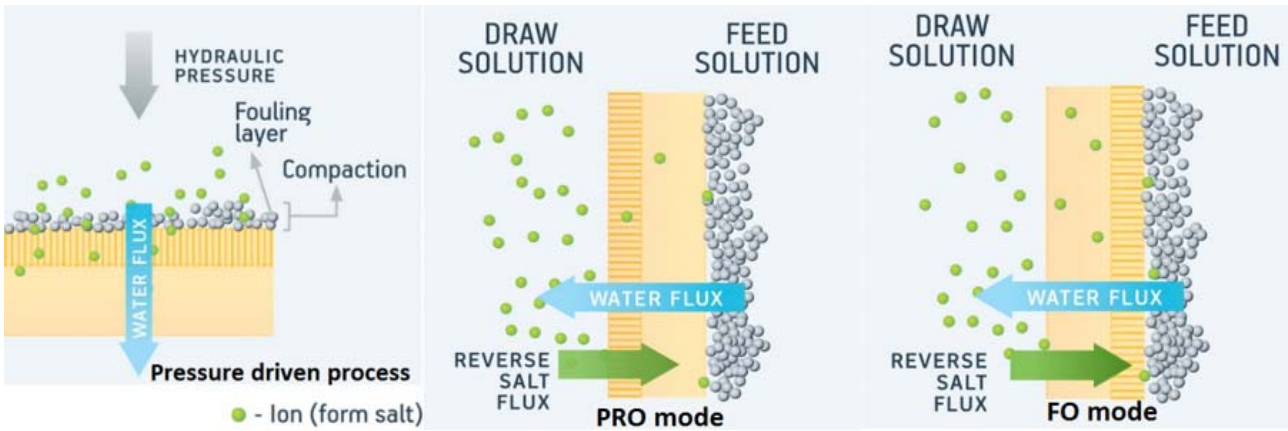

Figure 4. Illustration of the fouling mechanisms in membrane processes a) fouling in RO and osmotically driven membrane processes (b) fouling in PRO mode; (c) fouling in FO mode.[29]

the fouling characteristics of FO membranes both in the FO and PRO modes.[39] In their work, they demonstrated that the FO mode had lower fouling compared to the PRO mode, which was also seen by other authors.[31,40] This was attributed to the denser, smoother and tighter structure of the membrane active layer which prevented the adhesion and accumulation of foulants on the membrane surface, while the porous support layer, being a looser structure, allowed the accumulation and deposition of the foulants on its surface and inside the membrane, by the mechanisms of direct interception and subsequent pore plugging.

Thus it is clear that the nature of fouling in osmotically driven membrane process is different from fouling in pressure driven membrane processes. Further investigations of the mechanism of FO fouling are required to fully understand the differences. The mechanism of fouling is complex and depends on many factors such as water quality, temperature, system design, membrane cleaning, water flow, membrane surface etc. To mitigate fouling, these factors need to be considered in the process design and development.

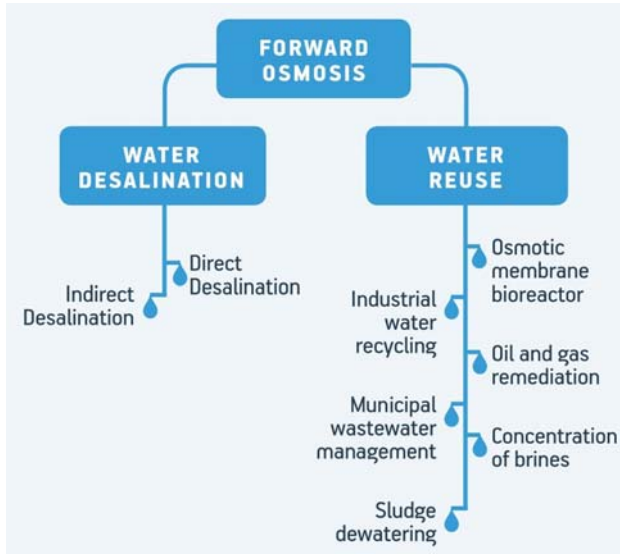

Figure 5. Applications of FO in the water industry, desalination (left) and water reuse (right).[11]

5. Forward Osmosis Applications

FO has a potential benefit as it requires a low hydraulic pressure compared to the pressure-driven process (RO). FO has low energy consumption therefore it involves lower costs, and with appropriate draw solutes and its regeneration methods, the process could be developed to be economically feasible and technically sound.

While FO has been investigated in a wide range of applications, including power generation, seawater/brackish water desalination, wastewater treatment and food processing, this review focuses mainly on wastewater treatment.

In general, there are two clusters of applications concerning FO in the water production and water treatment industry (Figure 5), (i) desalination and (ii) water reuse.[11]

5. 1. Desalination

In early 1970s, the FO process was proposed as pretreatment step to the RO process.[41] However, the advent of commercial FO cellulose triacetate (CTA) membranes prompted applications within seawater/brackish water desalination. With the FO desalination process, fresh water can be obtained *directly* (Figure 6) obtained from saline water (seawater or brackish water) at low (or no) pressure. This can be obtained by using an osmotic reagent based on volatile salts such as NH_4HCO_3 as the DS[3,22]. A DS recovery process is needed to separate the draw solute from the solution.[42] and in this case raising the DS temperature abo-

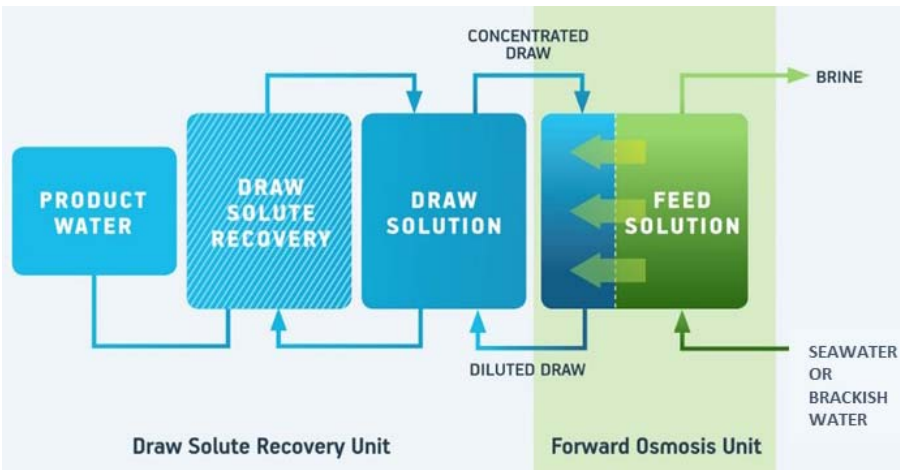

Figure 6. FO process for desalination of seawater/brackish water.

ve 60 °C will produce CO_2 and NH_3 which can then be reused to produce NH_4HCO_3 in the next cycle[43]. Also, polymer hydrogels and modified magnetic particles have been suggested as DS in FO desalination with no pressure required.

Indirect FO desalination uses a high salinity water (e.g. seawater/brackish water) as the DS and a poor-quality water source such as wastewater effluent or urban storm water runoff as FS.[44,45] The diluted seawater/brackish water DS can then be desalinated using low pressure reverse osmosis (LPRO). The FO-LPRO hybrid process reduces the cost of the total desalination process compared to pure RO[33]. This is due to the fact that desalination occurs with a lower salinity and can run at 50% recovery [46]. Nicoll (2013) compared three different desalination systems: i) conventional pre-treatment with a dual media filter (DMF), cartridge filtration and SWRO; ii) UF based pre-treatment with SWRO; and iii) conventional pre-treatment feeding a FO/RO plant. The summary calculations showed that the DMF/FO/RO configuration has the lowest energy consumption.[46]

Many studies were focused on DS and their recovery for FO desalination. Different draw solutes (i.e. NaCl, KCl, $CaCl_2$, $MgCl_2$, $MgSO_4$, Na_2SO_4 and $C_6H_{12}O_6$) were investigated for seawater desalination using a hybrid FO–NF process.[47] Nanoparticles (superparamagnetic) were also tested as a DS in FO desalination, where the nanoparticles could be regenerated by UF.[24]

5. 2. Wastewater Treatment

Most FO approaches for poor quality water treatment and reuse are similar to the direct seawater desalination method, where poor-quality water is used as feed, while a DS is used to reduce the volume of the feed. The DS is further treated by other post-treatment process for the recovery of the salt (e.g. RO, membrane distillation).

In general, wastewater has lower osmotic pressure and higher fouling propensity. FO integrated with membrane distillation (MD) process was studied for treatment of municipal wastewater, where stable water flux was attained in a continuous operation at the recovery rate up to 80%.[48] The FO showed a moderate to high rejection of most organic contaminants while MD rejected the residual contaminants to achieve a near complete rejection in the hybrid process. To recover clean water from secondary wastewater effluent, a photovoltaic powered FO – electrodialysis (FO-ED) process was tested. The process resulted in high removal of total organic carbon (TOC) from the feed wastewater and production of fresh water.[49] By using FO and ED through solar energy, this process has been able to supply potable water in isolated and remote areas and islands. In addition, FO process showed several benefits for space missions, including high wastewater recovery, low energy cost and minimized resupply. Further, natural steroid hormones were removed from wastewater by FO membrane contactors. FO has also been used for other wastewater such as oily wastewater, industrial and municipal wastewater, nuclear wastewater, landfill leachate, oil-water separation.[50] Additionally, application of FO for wastewater treatment was performed in membrane bioreactor (Figure 7), called osmotic membrane bioreactor (OsMBR).

Submerged membrane bioreactors (MBRs) involve biodegradation and membrane filtration in a single reactor. It has become one of the most commonly applied

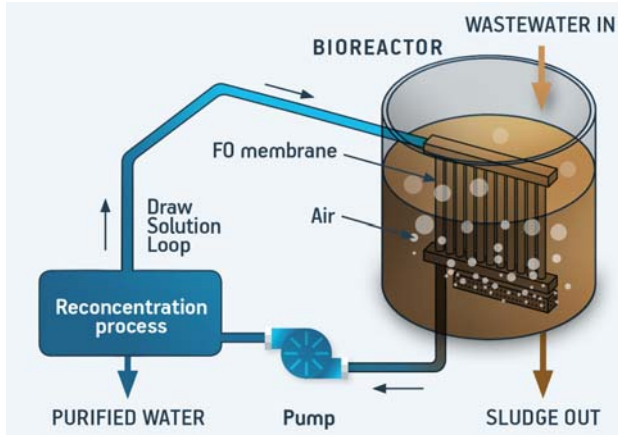

Figure 7. Schematic representation of an OsMBR.[2]

technologies in the treatment of different types of wastewater. FO process replaces the pressure driven membrane process (microfiltration, ultrafiltration) used in MBR. Integration of FO in MBR provides lower fouling propensity, no applied hydraulic pressure, and equally good quality effluent. Unlike the conventional MBR, FO-MBR does not involve high pressure diffused air for reducing the cake layer formation on the membrane surface and pump for collecting the effluent. In addition, FO provides a more sustainable flux and reliable removal of contaminants. The study of novel FO-MBR or osmotic MBR (OsMBR) has been initiated in the last five years.[40,51] A salt accumulation model to investigate FO performance in OsMBR shows that the ratio of the membrane salt permeability (B) to the water permeability (A) (i.e. B/A) and the ratio of hydraulic retention time (HRT) to sludge retention time (SRT) (i.e. HRT/SRT) are two important parameters for the optimization of OsMBR operation.[52] To minimize the flux decline caused by salt accumulation, these two ratios should be low.

6. Recent FO Membrane Developments

The ideal FO membrane exhibits high water permeability and solute rejection, minimal external and internal concentration polarization (ICP) as well as high chemical and mechanical stability. These features are somewhat contradictory. For example, a low ICP requires a low

Table 2. An overview of various FO application in last five years

Feed	Process / FO membrane material / DS / module: Objective	Remarks
Synthetic wastewater with sludge	Submerged OsMBR / CTA / NaCl (aq.) / Flat-sheet: Water reclamation from wastewater	The bioinspired surface modification improved the antifouling ability of the CTA FO membrane.[53]
Polyvinyl chloride (PVC) latex	FO / CTA / NaCl (aq.) / Flat-sheet: Condensation of PVC latex with FO as a pretreatment step	The apparent TOC rejection in the FO process is slightly higher than that in RO.[54]
Boiler feed water (BFW)	FO / PA-TFC / NaCl (aq.) / Flat-sheet: treatment of BFW of steam assisted gravity drainage (SAGD) process	Reducing the temperature (during fabrication) of the organic solution down to –20 °C effectively reduced the thickness of the PA selective layer.[55]
High-nutrient sludge	FO-MD / TFC / Na_3PO_4 (aq.) / Flat-sheet: concentrating high-nutrient sludge in an FO–MD hybrid system	At pH 9, the Na_3PO_4 was providing a high water flux and mitigating salt leakage resulting from the formation of the high charge of phosphate and complexion.[56]
Wastewater with sludge	OsMBR / – / Fertilizer / – /: anaerobic fertilizer-drawn forward osmosis membrane bioreactor (AnFDFOMBR) for biogas production	Mono-ammonium phosphate (MAP) showed the highest biogas production while other fertilizers exhibited an inhibition effect on anaerobic activity with solute accumulation.[57]
Raw sewage	FO-MD / CTA / NaCl (aq.) / Flat-sheet: Direct sewer mining	Trace organic contaminants (TrOC) transport through the FO membrane is governed by "solute-membrane" interaction, whereas that through the MD membrane is strongly correlated to TrOC volatility.[48]
Secondary wastewater effluent	FO-ED / CTA / NaCl (aq.) / Flat-sheet, parallel plate-and-frame module: Potable water production, utilization of natural energy for water treatment and reuse	In the ED unit, the diluted draw solution was desalted and high-quality water was produced; the concentrate was recycled to the FO unit and reused as the draw solution.[49]
Synthetic wastewater	FO / CTA / NaCl (aq.) / Flat-sheet: Tetracycline recoverable separation from antibiotic wastewater	An effective treatment of tetracycline antibiotic wastewater as well as the recovery of antibiotics from the wastewater.[58]
Synthetic surfactant wastewater	FO / CTA / NaCl (aq) / Flat-sheet: Dehydrate and treat Olive Mill Wastewater (OMWW)	Complete decolorization of permeate, and more than 98% rejection to OMWW components, including biophenols and ions.[59]
Synthetic dye wastewater	FO-CF(coagulation/flocculation) / TFC / Poly(acrylic acid) NaCl (aq) / Flat-sheet: treatment and reuse of textile wastewater	Remarkable reverse fouling behaviour has been observed where the Jw of the fouled membrane was fully restored to the initial value by physical flushing without using any chemicals.[60]
Wastewater containing heavy metals	FO / cellulose acetate butyrate (CAB) / NaCl (aq.) / Hollow fiber: Water reclamation from emulsified oily wastewater through FO under the PRO mode	Water flux declines slightly by 10% after a 12 h oil/water test under the PRO mode and water flux of the fouled membrane can be restored to 97% by simple water rinse.[61]

S-value (structural parameter) which in turn requires a low thickness and high porosity. Thus, providing sufficient mechanical stability to a thin highly porous membrane is one of the key outstanding problems in FO membrane development.

The membrane structural parameter S is defined as:

$$S = K \times D = \frac{t_s \times \tau}{\varepsilon}$$

where D is the diffusion coefficient of the draw solute, t_s is the support layer thickness, τ the tortuosity, and ε the porosity.[62]

Several materials have been investigated for FO membrane fabrication. These include materials based on cellulose, polyamide (and other polymers), and polyelectrolytes. Also so-called mixed matrix membranes have been investigated. These membranes typically consist of 'fillers' or inclusions (e.g. zeolites) embedded in a polymeric matrix. A special case is the concept of biomimetic FO membranes where aquaporin proteins are incorporated in the membrane enhancing water flux while preserving high solute rejection.

Cellulose acetate (CA) and cellulose triacetate (CTA) have been used in RO membrane fabrication since the 1960s so it is perhaps not surprising that FO membra-

Table 3. List of commercial producers and developers of FO membranes

Company	Membrane Type	Configuration	Status
Aquaporin A/S	Biomimetic aquaporin	Hollow fiber and flat sheet	Commercial
Oasys Water	Thin film composite	Flat sheet	Commercial
Fluid Technology Solutions, Inc.	Cellulose tri-acetate	Flat sheet	Commercial
Nitto Denko	Composite semipermeable membrane	-	Development
Woongjin Chemical Co., Ltd.	Composite membrane	–	Development
Porifera	Thin film composite	Flat sheet	Commercial

nes based on CTA were amongst the first to be commercially available from Hydration Technologies Incorporated (HTI).[63] In recent years there have been significant developments in CA and CTA based FO membrane both in flat sheet and hollow fibre geometries. Generally, these membranes are fabricated in a phase inversion process where a polymer is transformed in a controlled way from a solution state to a solid state. Thus, when a polymer solution (polymer plus solvent) is cast on a suitable support and immersed in a coagulation bath containing a non-solvent precipitation occurs because of the exchange of solvent and non-solvent. The procedure allows for making membranes with very low S-values (of the order of 50 μm) which makes them potentially good FO membranes. The general trend is that CA membranes have acceptable water fluxes but tend to have lower rejection (and thus higher reverse solute fluxes) whereas the opposite trend is the case for CTA based FO membranes.[64]

The cellulose hydroxyl can be reacted with reagents to generate cellulose esters beyond CA and CTA. These include materials such as cellulose propionate (CP), cellulose acetate butyrate (CAB) or cellulose acetate propionate (CAP). Dual layer FO hollow fibres made from CA and CAP show superior performance compared to CA-based flat sheet or hollow fibre membranes. However, the limited stability to temperature and pH generally restricts the use of cellulose-based materials.[64]

Cellulose-based membranes were dominant throughout the 1960s until the advent of thin film composite (TFC) membranes in the 1970s. Most TFC membranes are made with a porous, highly permeable support such as polysulfone, which is coated with a cross-linked aromatic polyamide thin film.[65] The coating – also sometimes referred to as the active layer – provides the solute rejection properties while the support provides the mechanical stability. The typical coating is made by interfacial polymerization to create a 100–200 nm thick polyamide coating exemplified by the reaction between *m*-phenyl diamine and trimesoyl chloride monomers.

A good polyamide layer requires optimization of the exact monomer composition, reaction time, temperature and ambient humidity. In FO membranes, addition of the detergent sodium dodecyl sulfate (SDS) can enhance solute rejection without major impact on the water flux, and post treatment using SDS/glycerol followed by thermal annealing facilitates removal of unreacted monomers resulting in increased free volume and reduced thickness leading to improved flux without detrimental effects on rejection.[66,67] The presence of cetyltrimethylammonium chloride (CTAC) which can react with the m-Phenylene diamine (MPD) can decrease water flux while increasing the solute rejection. Thus, there are a number of possibilities for fine-tuning FO membrane active layers.

A good support for a TFC membrane shows a low ICP and typically supports are based on polysulfone or polyethersulfone.[62] Also bucky papers made from Carbon Nanotubes (CNTs) and nanofiber mats formed from electrospun fibres have been suggested as good FO membrane support due to high porosity and tensile strength.[68,69] Structurally it has been argued that an open 'finger' like structure of the support is to be favoured over a more dense 'sponge' like structure.[70] However a more open structure is also mechanically weaker and a more dense structure also may have a higher ICP. An obvious compromise would be to have an anisotropic support with a sponge structure interfacing the active layer supported by a finger like structure below.[62,71] But the structural features are not the only determinants for FO membrane performance. A sponge like support structure may in fact give rise to a higher water flux than a finger like structure provided that hydrophilicity and thickness are well controlled.[72–74] This illustrates the complexity behind ICP where many specific physico-chemical factors give rise to a phenomenological effect.

Polyelectrolytes have attracted considerable attention over the last decade as an alternative to the TFC approach. The typical polyelectrolyte membrane consists of a layer-by-layer (LbL) deposition of alternating cationic and anionic electrolyte-films onto a suitable support where hydrolysed (and thus negatively charged) polyacrylonitrile is an exemplary material. Large scale production of LbL assembled membranes has proved to be difficult; nevertheless, the approach offers the potential of fabricating membranes with good rejection combined with good solvent resistance and thermal stability.[75,76]

One of the latest design approaches for FO (and RO) membranes is based on the concept of membrane biomimetics where technological developments take cues from nature.[77,78] The basic concept is based on the fact that biological membranes have excellent water transport characteristics.

They employ natural proteins known as aquaporins (AQPs) to regulate the flow of water, providing increased permeability and near-perfect solute rejection.[79] Thus by using reconstituted AQPs as building blocks one can create membranes with unique flux and rejection properties.[80] AQP membrane design approaches have been recently reviewed.[7] According to membrane structural design, AQPs incorporated biomimetic membranes can be classified into two basic types, (1) AQPs containing vesicle encapsulated membranes (VEMs), where AQPs containing vesicles (proteoliposomes or proteo-polymersomes) are immobilized in a dense polymer layer and (2) AQP containing supported (lipid or polymer) membrane layers (SMLs).

AQP-based membranes are currently being produced and commercialised by the Danish company Aquaporin A/S, its Singaporean affiliate, Aquaporin Asia Pte. Ltd., and its Joint Ventures AquaPoten Limited in China and Aquaporin Space Alliance in Denmark in flat sheet and hollow fibre geometries. The membranes are currently tested in several processes including pesticide removal, CO_2 capture, and water reuse in space and textile wastewater treatment.[81–84]

7. Conclusions

The FO process used in wastewater treatment and water purification shows promising results, and has many advantages in comparison to the conventional water/wastewater treatment processes.

The studies are focused on improving the FO process by developing new membranes, membrane surface modifications, different DSs and their compatibility with various wastewaters. However, there are other issues (e.g. membrane fouling, raw water characteristics) in FO process that needs to be studied. FO processes are highly compatible with other treatment processes therefore, the whole treatment process could become more cost effective by incorporating FO process. As it is seen from the literature, many studies and improvements were done on the membrane materials and their surface, and new technologies were implemented, such as membranes with biological materials (aquaporins).

Higher quality water is in demand due to the imposition of new and ever-changing water quality standards. Therefore, interest in FO technology is growing as a potential, cost- competitive and reliable alternative.

8. Acknowledgements

The authors would like to acknowledge financial support from the Slovenian Research Agency (Javna Agencija za Raziskovalno Dejavnost RS) for their Project No. 1000 - 14 - 0552) and Department of Science and Technology (DST), Government of India for Grant No. INT/Slovenia/P-15/2014. CHN also acknowledges support from the Innovation Fund Denmark via the IBISS and MENENTO projects.

9. References

1. E. M. Garcia-Castello, J. R. Mccutcheon, M. Elimelech, *J. Membr. Sci.*, **2009**, *338*, 61–66. https://doi.org/10.1016/j.memsci.2009.04.011
2. A. Achilli, T. Y. Cath, E. A. Marchand, A. E. Childress, *Desalination*, **2009**, *239*, 10–21. https://doi.org/10.1016/j.desal.2008.02.022
3. L. Chekli, S. Phuntsho, H. K. Shon, S. Vigneswaran, J. Kandasamy, A. Chanan, *Desalin. Water Treat.*, **2012**, *43*, 167–184. https://doi.org/10.1080/19443994.2012.672168
4. B. Van Der Bruggen, P. Luis, *Reviews in Chemical Engineering*, **2015**, *31*, 1–12. https://doi.org/10.1515/revce-2014-0033
5. Y.-X. Shen, P. O. Saboe, I. T. Sines, M. Erbakan, M. Kumar, *J. Membr. Sci.*, **2014**, *454*, 359–381. https://doi.org/10.1016/j.memsci.2013.12.019
6. P. Agre, *Proc. Am. Thorac. Soc.*, **2006**, *3*, 5–13. https://doi.org/10.1513/pats.200510-109JH
7. C. Tang, Z. Wang, I. Petrinić, A. G. Fane, C. Hélix-Nielsen 2015. Biomimetic aquaporin membranes coming of age.
8. F. Wicaksana, A. G. Fane, C. Tang, R. Wang, in: Hélix-Nielsen, C. (ed.) Biomimetic Membranes for Sensor and Separation Applications. **2012**,
9. T. Y. Cath, *Desalin. Water Treat.*, **2010**, *10*, 279–286. https://doi.org/10.5004/dwt.2010.1760
10. M. Hamdan, A. O. Sharif, G. Derwish, S. Al-Aibi, A. Altaee, *J. Food Eng.*, **2015**, *155*, 10–15. https://doi.org/10.1016/j.jfoodeng.2015.01.010
11. S. Zhao, L. Zou, C. Y. Tang, D. Mulcahy, *J. Membr. Sci.*, **2012**, *396*, 1–21. https://doi.org/10.1016/j.memsci.2011.12.023
12. B. Hribar, N. T. Southall, V. Vlachy, K. A. Dill, *J. Am. Chem. Soc.*, **2002**, *124*, 12302–12311. https://doi.org/10.1021/ja026014h
13. A. J. Ansari, F. I. Hai, W. Guo, H. H. Ngo, W. E. Price, L. D. Nghiema, *Sci. Total Environ.*, **2016**, *566–567*, 559–566. https://doi.org/10.1016/j.scitotenv.2016.05.139
14. H. T. Nguyen, N. C. Nguyen, S.-S. Chen, H. H. Ngo, W. Guo, C.-W. Li, *Sci. Total Environ.*, **2015**, *538*.
15. J. Wei, Z.-X. Low, R. Ou , G. P. Simon, H. Wang, *Water Res.*, **2016**, *96*, 292–298. https://doi.org/10.1016/j.watres.2016.03.072
16. J.-J. Kim, H. Kang, Y.-S. Choi, Y. A. Yu, J.-C. Lee, *Desalination*, **2016**, *381*, 84–94. https://doi.org/10.1016/j.desal.2015.11.013
17. G. Gwak, B. Jung, S. Han, S. Hong, *Water Res.*, **2015**, *80*, 294–305. https://doi.org/10.1016/j.watres.2015.04.041
18. J. Su, T.-S. Chung, B. J. Helmer, J. S. De Wit, *J. Membr. Sci.*, **2012**, *396*, 92–100. https://doi.org/10.1016/j.memsci.2012.01.001

19. Q. Ge, J. Su, G. L. Amy, T.-S. Chung, *Water Res.*, **2012**, *46*, 1318–1326. https://doi.org/10.1016/j.watres.2011.12.043
20. K. S. Bowden, A. Achilli, A. E. Childress, *Bioresour. Technol.*, **2012**, *122*, 207–216. https://doi.org/10.1016/j.biortech.2012.06.026
21. M. L. Stone, A. D. Wilson, M. K. Harrup, F. F. Stewart, *Desalination*, **2013**, *312*, 130–136. https://doi.org/10.1016/j.desal.2012.09.030
22. Q. Ge, M. Ling, T.-S. Chung, *J. Membr. Sci.*, **2013**, *442*, 225–237. https://doi.org/10.1016/j.memsci.2013.03.046
23. Q. Ge, J. Su, T.-S. Chung, G. Amy, *Ind. Eng. Chem. Res.*, **2011**, *50*, 382–388. https://doi.org/10.1021/ie101013w
24. M. M. Ling, T.-S. Chung, *Desalination*, **2011**, *278*, 194–202. https://doi.org/10.1016/j.desal.2011.05.019
25. A. Seidel, M. Elimelech, *J. Membr. Sci.*, **2002**, *203*, 245–255. https://doi.org/10.1016/S0376-7388(02)00013-3
26. E. M. Vrijenhoek, S. Hong, M. Elimelech, *J. Membr. Sci.*, **2001**, *188*, 115–128. https://doi.org/10.1016/S0376-7388(01)00376-3
27. Q. Li, E. M., *Environ. Sci. Technol.*, **2004**, *38*, 4683–4693. https://doi.org/10.1021/es0354162
28. D. Rana, T. Matsuura, *Chemical Reviews*, **2010**, *110*, 2448–2471. https://doi.org/10.1021/cr800208y
29. I. L. Alsvik, M.-B. Hägg, *Polymers*, **2013**, *5*, 303–327. https://doi.org/10.3390/polym5010303
30. S. Lee, C. Boo, M. Elimelech, S. Hong, *J. Membr. Sci.*, **2010**, *365*, 34–39. https://doi.org/10.1016/j.memsci.2010.08.036
31. B. Mi, M. Elimelech, *J. Membr. Sci.*, **2010**, *348*, 337–345. https://doi.org/10.1016/j.memsci.2009.11.021
32. B. Mi, M. Elimelech, *Environ. Sci. Technol.*, **2010**, *44*, 2022–2028. https://doi.org/10.1021/es903623r
33. T. Y. Cath, N. T. Hancock, C. D. Lundin, C. Hoppe-Jones, J. E. Drewes, *J. Membr. Sci.*, **2010**, *362*, 417–426. https://doi.org/10.1016/j.memsci.2010.06.056
34. S. Zhao, L. Zou, D. Mulcahy, *J. Membr. Sci.*, **2011**, *382*, 308–315. https://doi.org/10.1016/j.memsci.2011.08.020
35. C. Boo, S. Lee, M. Elimelech, Z. Meng, S. Hong, *J. Membr. Sci.*, **2012**, *390–391*, 277–284. https://doi.org/10.1016/j.memsci.2011.12.001
36. B. Mi, M. Elimelech, *J. Membr. Sci.*, **2008**, *320*, 292–302. https://doi.org/10.1016/j.memsci.2008.04.036
37. Y. Liu, B. Mi, *J. Membr. Sci.*, **2012**, *407–408*, 136–144. https://doi.org/10.1016/j.memsci.2012.03.028
38. M. M. Motsa, B. B. Mamba, A. D'haese, E. M. V. Hoek, A. R. D. Verliefde, *J. Membr. Sci.*, **2014**, *460*, 99–109. https://doi.org/10.1016/j.memsci.2014.02.035
39. V. Parida, H. Y. Ng, *Desalination*, **2013**, *312*, 88–98. https://doi.org/10.1016/j.desal.2012.04.029
40. J. Zhang, W. L. C. Loong, S. Chou, C. Tang, R. Wang, A. G. Fane, *J. Membr. Sci.*, **2012**, *403–404*, 8–14. https://doi.org/10.1016/j.memsci.2012.01.032
41. J. R. Mccutcheon, R. L. Mcginnis, M. Elimelech, *Desalination*, **2005**, *174*, 1–11. https://doi.org/10.1016/j.desal.2004.11.002
42. D. Li, X. Zhang, G. P. Simon, H. Wang, *Water Res.*, **2013**, *47*, 209–215. https://doi.org/10.1016/j.watres.2012.09.049
43. R. L. Mcginnis, M. Elimelech, *Desalination*, **2007**, *207*, 370–382. https://doi.org/10.1016/j.desal.2006.08.012
44. Z. Li, R. Valladares Linares, M. Abu-Ghdaib, T. Zhan, V. Yangali-Quintanilla, G. Amy, *Water Res.*, **2014**, *48*, 200–209. https://doi.org/10.1016/j.watres.2013.09.028
45. R. Valladares Linares, Z. Li, M. Abu-Ghdaib, C.-H. Wei, G. Amy, J. S. Vrouwenvelder, *J. Membr. Sci.*, **2013**, *447*, 50–56. https://doi.org/10.1016/j.memsci.2013.07.018
46. P. Nicoll, Forward Osmosis as a pre-treatment to reverse osmosis, The International Desalination Association World Congress on Desalination and Water Reuse, Tianjin, China, **2013**.
47. C. H. Tan, H. Y. Ng, *Desalin. Water Treat.*, **2010**, *13*, 356. https://doi.org/10.5004/dwt.2010.1733
48. M. Xie, L. D. Nghiem, W. E. Price, M. Elimelech, *Environ. Sci. Technol.*, **2013**, *47*, 13486–13493. https://doi.org/10.1021/es404056e
49. Y. Zhang, L. Pinoy, B. Meesschaert, B. Van Der Bruggen, *Environ. Sci. Technol.*, **2013**, *47*, 10548–10555.
50. P. H. H. Duong, T.-S. Chung, *J. Membr. Sci.*, **2014**, *452*, 117–126. https://doi.org/10.1016/j.memsci.2013.10.030
51. W. J. Yap, J. Zhang, W. C. L. Lay, B. Cao, A. G. Fane, Y. Liu, *Bioresour. Technol.*, **2012**, *122*, 217–222. https://doi.org/10.1016/j.biortech.2012.03.060
52. D. Xiao, C. Y. Tang, J. Zhang, W. C. L. Lay, R. Wang, A. G. Fane, *J. Membr. Sci.*, **2011**, *366*, 314–324. https://doi.org/10.1016/j.memsci.2010.10.023
53. F. Li, Q. Cheng, Q. Tian, B. Yang, Q. Chen, *Bioresour. Technol.*, **2016**, *211*, 751–758. https://doi.org/10.1016/j.biortech.2016.03.169
54. T. Takahashi, M. Yasukawa, H. Matsuyam, *J. Membr. Sci.*, **2016**, *514*, 547–555. https://doi.org/10.1016/j.memsci.2016.04.012
55. B. Khorshidi, A. Bhinder, T. Thundat, D. Pernitsky, M. Sadrzadeh, *J. Membr. Sci.*, **2016**, *511*, 29–39. https://doi.org/10.1016/j.memsci.2016.03.052
56. N. C. Nguyen, H. T. Nguyen, S.-T. Ho, S.-S. Chen, H. H. Ngo, W. Guo, S. S. Ray, H.-T. Hsu, *Sci. Total Environ.*, **2016**, *557–558*, 44–50. https://doi.org/10.1016/j.scitotenv.2016.03.025
57. Y. Kim, L. Chekli, W.-G. Shim, S. Phuntsho, S. Li, N. Ghaffour, T. Leiknes, H. K. Shon, *Bioresour. Technol.*, **2016**, *210*, 26–34. https://doi.org/10.1016/j.biortech.2016.02.019
58. S.-F. Pan, M.-P. Zhu, J. P. Chen, Z.-H. Yuan, L.-B. Zhong, Y.-M. Zheng, *Sep. Purif. Technol.*, **2015**, *153*, 76–83. https://doi.org/10.1016/j.seppur.2015.08.034
59. A. Y. Gebreyohannes, E. Curcio, T. Poerio, R. Mazzei, G. Di Profio, E. Drioli, L. Giorno, *Sep. Purif. Technol.*, **2015**, *147*, 292–302. https://doi.org/10.1016/j.seppur.2015.04.021
60. G. Han, C.-Z. Liang, T.-S. Chung, M. Weber, C. Staudt, C. Maletzko, *Water Research*, **2016**, *91*, 361–370. https://doi.org/10.1016/j.watres.2016.01.031
61. G. Han, J. S. De Wit, T.-S. Chung, *Water Res.*, **2015**, *81*, 54–63. https://doi.org/10.1016/j.watres.2015.05.048
62. N. Yip, A. Tiraferri, W. Phillip, J. Schiffman, M. Elimelech, *Environ Sci Technol*, **2010**, *44*, 3812–3818. https://doi.org/10.1021/es1002555

63. J. Herron.Asymmetric forward osmosis membranes. United States of America patent application 7,445,712B2, **2008**.
64. J. Su, R. Ong, P. Wang, T.-S. Chung, B. Helmer, J. De Wit, *AIChE J.* , **2013**, *59*, 1245–1254. https://doi.org/10.1002/aic.13898
65. W. J. Lau, A. F. Ismail, N. Misdan, M. A. Kassim, *Desalination*, **2012**, *287*, 190–199. https://doi.org/10.1016/j.desal.2011.04.004
66. C. Klaysom, S. Hermans, A. Gahlaut, S. Van Craenenbroeck, V. I. F. J., *J Membr Sci* **2013**, *445*, 25–33. https://doi.org/10.1016/j.memsci.2013.05.037
67. R. Ong, T.-S. Chung, J. De Wit, B. Helmer, *J Membr Sci* **2015**, *473*, 63–71. https://doi.org/10.1016/j.memsci.2014.08.046
68. L. Dumée, J. Lee, K. Sears, B. Tardy, M. Duke, S. Gray, *J Membr Sci* **2013**, *427*, 422–430. https://doi.org/10.1016/j.memsci.2012.09.026
69. N.-N. Bui, J. Mccutcheon, *Envi-ron Sci Technol* **2012**, *47*, 1761–1769. https://doi.org/10.1021/es304215g
70. A. Tiraferri, N. Yip, W. Phillip, J. Schiffman, M. Elimelech, *J Membr Sci*, **2011**, *367*, 340–352. https://doi.org/10.1016/j.memsci.2010.11.014
71. J. Wei, C. Qiu, C. Tang, R. Wang, A. Fane, *J Membr Sci* **2011**, *372*.
72. P. Sukitpaneenit, T.-S. Chung, *Environ Sci Technol* **2012**, *46*, 7358–7365. https://doi.org/10.1021/es301559z
73. G. Han, T.-S. Chung, M. Toriida, S. Tamai, *J Membr Sci* **2012**, *423–424*, 543–555. https://doi.org/10.1016/j.memsci.2012.09.005
74. N. Widjojo, T.-S. Chung, M. Weber, C. Maletzko, V. Warzelhan, *J Membr Sci* **2011**, *383*, 214–223. https://doi.org/10.1016/j.memsci.2011.08.041
75. Q. Saren, C. Q. Qiu, C. Tang, *Environ Sci Technol* **2011**, *45*, 5201–5208. https://doi.org/10.1021/es200115w
76. M. Bruening, D. Dotzauer, P. Jain, L. Ouyang, G. Baker, *Langmuir* **2008**, *24*, 7663–7673. https://doi.org/10.1021/la800179z
77. P. Holme Jensen, D. Keller, C. Hélix Nielsen.Membrane for filtering of water. WO 2006/122566, 2006, **2006**.
78. C. H. Nielsen, *Anal. Bioanal. Chem*, **2009**, *395*, 697–718. https://doi.org/10.1007/s00216-009-2960-0
79. M. A. Knepper, J. B. Wade, J. Terris, C. A. Ecelbarger, D. Marples, B. Mandon, C. L. Chou, B. K. Kishore, S. Nielsen, *Kidney Int*, **1996**, *49*, 1712–1717. https://doi.org/10.1038/ki.1996.253
80. Y. Zhao, C. Qiu, X. Li, A. Vararattanavech, X. Li, W. Shen, J. Torres, C. Hélix-Nielsen, W. Rong, X. Hu, A. G. Fane, C. Y. Tang, *J. Membr. Sci*, **2012**, *423–424*, 422–428. https://doi.org/10.1016/j.memsci.2012.08.039
81. H. T. Madsen, N. Bajraktari, C. Hélix-Nielsen, B. Van Der Bruggen, E. G. Søgaard, *J. Membr. Sci.*, **2015**, *476*, 469–474. https://doi.org/10.1016/j.memsci.2014.11.055
82. W. Ye, J. Ling, H. T. Madsen, E. G. Søgaard, C. Hélix-Nielsen, P. Luis, B. Van Der Bruggen, *J. Membr. Sci*, **2015**, *498*, 75–85. https://doi.org/10.1016/j.memsci.2015.09.010
83. T. Hill, B. W. Taylor, International Conference on Environmental Systems (ICES). San Diego, CA; United States, **2012**
84. I. Petrinic, C. Hélix-Nielsen, *Tekstil*, **2015**, *63*, 252–260.

Povzetek

V zadnjih letih se membranska tehnologija vse pogosteje uporablja v procesih čiščenja odpadne vode in vode za proizvodnjo. Procesi membranske filtracije so enostavni za izvajanje in dajejo kakovostni produkt/filtrat za nadaljnjo uporabo tako v industrijske namene kot tudi za proizvodnjo pitne vode. Ena od obetavnih tehnologij za proizvodnjo vode in obdelavo odpadnih voda je proces osmoze. Princip delovanja osmoze predstavlja metodo čiščenja vode, ki deluje brez hidravličnega tlaka, kar zagotavlja trajnostno (nizkoenergetsko) tehnologijo obdelave vode. Gonilna sila je razlika v kemijskem potencialu med vhodno in gonilno raztopino, ki sta ločeni z membrano, prepustno samo za vodo. Prednost osmoze pred obstoječimi visokotlačnimi membranskimi procesi je ravno delovanje brez dodatnega visokega tlaka, kar vodi tudi k manj pogostemu mašenju membran. Torej, omogoča delovanje z nižjo porabo energije ter podaljša življenjsko dobo membran. Vendar pa še vedno obstajajo nekatere pomembne tehnološke pomanjkljivosti procesa. V prispevku je predstavljena uporabnost tehnologije osmoze pri različnih sistemih čiščenja ter razvoj proizvodnje osmoznih membran.

Scientific paper

A Novel High-performance Electrospun Thermoplastic Polyurethane/Poly(vinylidene fluoride)/Polystyrene Gel Polymer Electrolyte for Lithium Batteries

Yuanyuan Deng, Zeyue He, Qi Cao*, Bo Jing, Xianyou Wang and Xiuxiang Peng

Key Laboratory of Environmentally Friendly Chemistry and Applications of Minister of Education, College of Chemistry, Xiangtan University, Xiangtan 411105, China

** Corresponding author: E-mail: wjcaoqi@163.com*

Received: 06-09-2016

Abstract

A novel high-performance gel polymer electrolyte (GPE) based on poly(vinylidene fluoride) (PVDF), thermoplastic polyurethane (TPU) and polystyrene (PS) has been prepared. Its characteristics are investigated by scanning electron microscopy (SEM), thermal analysis (DSC), universal testing machines (UTM), galvanostatic charge-discharge and electrochemical impedance spectroscopy. The GPE based on TPU/PVDF/PS (10 wt.%) show a high ionic conductivity of 5.28×10^{-3} S cm^{-1} with the electrochemical stability window of 5.0 V. In addition, its first charge-discharge capacity reached to 169.5 mAh g^{-1}, high mechanical strength and stability to allow safe operation in rechargeable lithium ion polymer batteries.

Keywords: Gel polymer electrolytes; Electrospinning; Poly (vinylidene fluoride); Polystyrene; Thermoplastic polyurethane

1. Introduction

Polymer-based nanocomposites have attracted considerable academic and industrial attention over the years.[1,2] Various combinations of polymer matrices and nanofillers have been investigated. It is known to us that superior performance of lithium ion battery is determined by active electrode materials and excellent electrolytes. Among them, gel polymer electrolytes (GPEs) have been reported with high ionic conductivity at room temperature, stable and well compatibility with lithium electrodes,[3–5] and good mechanical stability. There are many ways to produce GPEs such as phase inversion method, γ-ray irradiation method, solvent casting technique, thermally induced phase separation technique, and electrospinning technique.[6–8] In these methods, electrospinning technique which made the solution of polymer into lots of uniform and slender nanofibers under high voltage is a simple, controllable and efficient approach. Thermoplastic polyurethane (TPU) contains two-phase microstructure which are soft segments and hard segments.[9–11] The hard sections are incompatible with the soft section in thermodynamics, while these two phases are interconnected throughout each other. The whole system benefits from these two phases since that the hard parts afford spatial stability and the soft phases are conducive to good ionic conductivity owing to the soft segments don't form ionic cluster after being dissolved alkali metal salt. Many investigations were devoted to copolymerizing TPU with other polymers for processing GPEs. Some articles based on coaggregant like thermoplastic polyurethane (TPU)/linear poly (ethylene oxide) (PEO) (TPU-PEO), thermoplastic polyurethane (TPU)/polyacrylonitrile (PAN) (TPU-PAN) and polyurethane/poly (vinylidene fluoride) (PU-PVDF) as GPEs for rechargeable lithium batteries have been reported lately.[12–14] Different concentrations of thermoplastic polyurethanes/poly(vinylidene fluoride-co- hexafluoro propylene) (TPU/PVDF-HFP) derived from some researchers including our study group member Xiuxiang Peng having done related research.[15] Poly (vinylidene fluoride) (PVDF) is a semi-crystalline polymer.[16] With low water absorption, high mechanical properties and interfacial stability with lithium metal,[17–19] PVDF has been adopted as polymer electrolyte in lithium ion polymer batteries.[20] Polystyrene (PS) polymers possess excellent mechanical properties: high strength, fatigue resistance

and dimension stability. Besides, it also has high glass transition temperature and high dielectric breakdown field. From the properties of the three kinds of materials, each of these three kinds of materies is very appropriate as a gel polymer matrix.

Our group have done some research, which was the first trial of making TPU/PVDF/PS fiber membranes.[21] In comparison to PU/PVDF, TPU/PS and PVDF/PS films, the TPU/PVDF/PS films show more noticeable electrochemical characteristic and mechanical performance. We would like to continue our efforts to develop TPU/PVDF/PS porous fibrous films by electrospinning using different concentration polymer solutions. In order to investigate the influence of various polymer concentration stresses on the TPU/PVDF/PS fiber membranes, membrane morphology, charge and discharge capacity, ionic conductivity, and mechanical properties will be examined systemically. In this study, we expect to provide a deep investigation and insight on the preparation of TPU/PVDF/PS microporous fiber membranes with prominent electrochemical and mechanical performance. Primary results showed that it is very suitable for application in lithium ion batteries.

2. Experimental

2. 1. Materials

Thermoplastic polyurethane (TPU, yantaiwanhua, 1190A), polystyrene (PS,yangzishihua) and poly(vinylidene fluoride) (PVDF, Alfa Aesar) were dried under vacuum at 80 °C for 24 h. $LiClO_4 \cdot 3H_2O$ (AR, Sinopharm Chemical Reagent Co., Ltd.) was dehydrated in vacuum oven at 120 °C for 72 h. 1.0 M Liquid electrolyte was made by dissolving a certain quality of $LiClO_4$ in ethylene carbonate (EC, Shenzhen capchem technology Co., Ltd.)/propylene carbonate (PC, Shenzhen capchem Technology Co. Ltd.) (1/1, v/v). N, N-dimethylforamide (DMF) and acetone were analytical purity and used as received without further treatment.

2. 2. Preparation of TPU/PVDF/PS fibrous Membrane

In the first place, a certain amount of dried PVDF, TPU and PS (6:6:1, wt/wt/wt) were dissolved in the mixture of acetone/N, N-dimethylacetamide (1:3, wt/wt) forming a 9 wt.% solution, then they were stirred by mechanical stirring for 12 h at room temperature. Then 10 wt.%, 11 wt.%, 12 wt.% TPU/PVDF/PS solutions were made by the same way. After being stayed for 10 minutes to remove air bubbles, the viscous blending polymer solution was put into the needle injection pump. The tip of the needle was connected to high voltage source (24.5kV) and electrospined at ambient atmosphere. Porous fibrous films were obtained on the collector plate. The electrospun porous fibrous films were finally dried under vacuum at 80 °C for 12 h.

2. 3. Preparation of Gel Polymer Electrolytes

The thickness of the TPU/PVDF/PS nonwoven films used was about 100 μm. At room temperature, the dried TPU/PVDF/PS nonwoven films were activated by 1 M $LiClO_4$-EC/PC liquid electrolyte solutions for 1 h in a glove box filled with argon. Wipe the surface of swelled membranes by filter paper and then get the gel polymer electrolytes.

2. 4. Membrane Characterization

Scanning electron microscope (SEM, Hitachi S-3500 N, Japan) was used to examine the morphology of the films. The thermal stability of the films was monitored using thermogravimetric analysis (model TQAQ 50, TA Company, USA). DSC measurements were carried out under the temperature range from 20–200 ° at a scan rate of 10 °/min. The mechanical strength of the gel polymer electrolyte films was measured by universal testing machines (UTM, Instron Instruments). There are some difficulties in surveying the "wet" films (with electrolyte), therefore the test was measured the mechanical properties of the "dry" membrane (without electrolyte). The extension rate was kept at 5 mm min^{-1}. The dimensions of the sheet used were 2 cm × 5 cm × 150–250 μm (width × length × thickness). The porosity was investigated by immersing the membranes into n-butanol for 1 h and then calculated by using the following relation:

$$P = \frac{W_W - W_d}{\rho_b V_p} \times 100\ \% \quad (1)$$

W_w and W_d are the mass of the wet and dry membrane, respectively, $\tilde{n}_b$ is the density of n-butanol, and V_p is the volume of the dry membrane.

The electrolyte uptake was determined by measuring the weight increase and calculated according to Eq:

$$Uptake(\%) = \frac{W - W_0}{W_0} \times 100\% \quad (2)$$

W_0 is the weight of dried films and W is the weight of swelled films.

The ionic conductivity of the composite film was measured with SS/PE/SS blocking cell by AC impedance measurement using Zahner Zennium electrochemical analyzer with a frequency range of 0.1–1 MHz. The thin films were prepared about 100μm in thickness and 1.96 cm^2 in area for impedance measurement. Thus, the ionic conductivity could be calculated from the following equation:

$$\sigma = \frac{h}{R_b S} \quad (3)$$

In Eq. (3), σ is the ionic conductivity, R_b is the bulk resistance, h and S are the thickness and area of the films, respectively.

2. 5. Cell Assembly and Performance Characteristics

Electrochemical stability was measured by a linear sweep voltammetry (LSV) of a Li/PE/SS cell using Zahner Zennium electrochemical analyzer at a scan rate of 5 mV s^{-1}, with voltage from 2 V to 6 V. For charge-discharge cycling tests, the Li/PE/$LiFePO_4$ cell was assembled. The cell was subjected to electrochemical performance tests using an automatic charge-discharge unit, Neware battery testing system (model BTS-51, ShenZhen, China), between 2.5 and 4.2 V at 25 °C, at different current densities.

3. Results and Discussion

3. 1. Morphology and Structure

Fig. 1 shows the SEM images of the membranes prepared by electrospinning of different concentrations of 9 to 12 wt.% TPU/PVDF/PS polymer solution. All of these four membranes show a microporous structure, but we can see that the fibers of TPU/PVDF/PS (Fig.1(b)10 wt.%) are relatively uniform and slender, with the diameter distribution about 1μm. While the fibers of TPU/PVDF/PS (Fig.1 (a)9 wt.%) are cross linked unevenly in the middle part of it. Both of the fibers of TPU/PVDF/PS (Fig.1(c)11 wt.%) and (Fig.1(d)12 wt.%) diameter distribution values are thicker than the fibers of TPU/PVDF/PS (Fig.1(b)10 wt.%), so do the fiber smoothness.

From the principle of electrospinning we know there are many factors that can affect fiber membranes' morphology. The parameters influencing the morphology of electrospun fiber membranes contain the distance between the nozzle of the syringe and the collector, the applied voltage, dielectric constant of the solution and the concentration of the polymer solution. In this work, the only difference is the concentration of the polymer solution. Finally, we found that TPU/PVDF/PS polymer solution of 10 wt.% is the best for electrospinning. After blending, there is interface between different materials. The interfacial interation force which has a great influence on the morphology of electrospinning film, the greater the force, the poorer the performance of membrane. The interface force is the minimum when the mass fraction is 10%, which is why the membranes of TPU/PVDF/PS (10 wt.%) is smooth and slender.

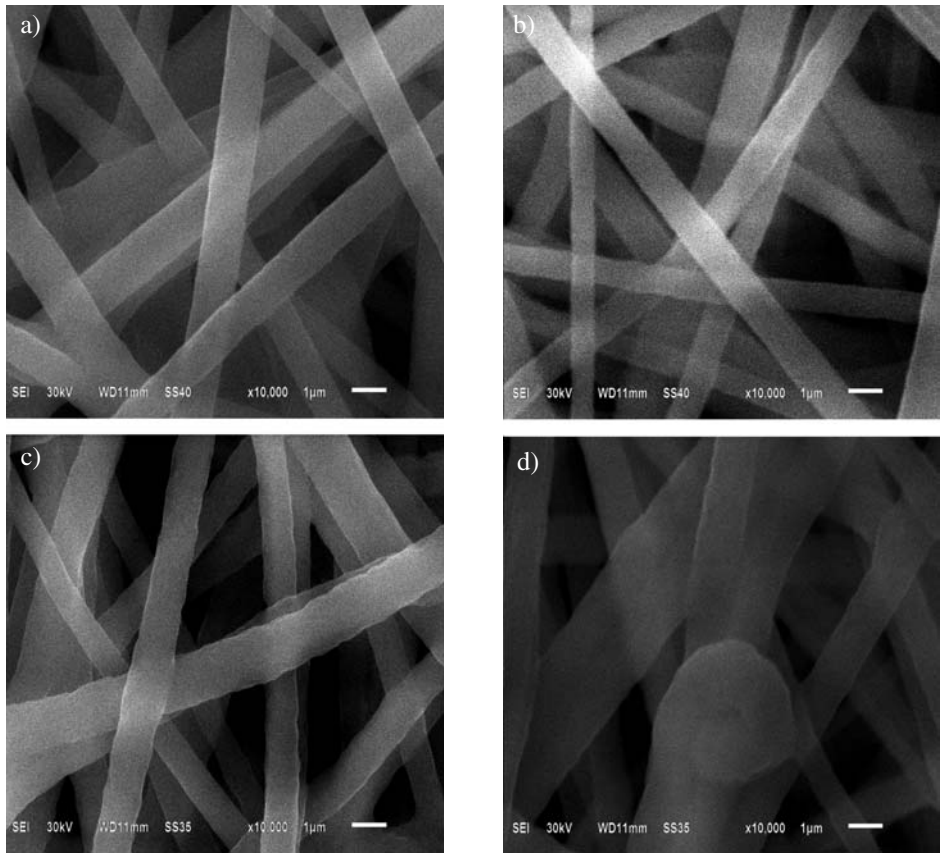

Fig. 1. SEM images of TPU/PVDF/PS electrospun membranes (a) 9 wt.% (b) 10 wt.% (c) 11 wt.% (d) 12 wt.%

3. 2. DSC Analysis

Typical DSC curves of the nanofibrous membranes varied with the relative weight of PVDF/TPU/ PS, which are presented in Fig.2. From the Table 1, the crystallinity of TPU/PVDF/PS (9 wt.%) is 20.43%; the crystallinity of TPU/PVDF/PS (10 wt.%) is 13.64%; the crystallinity of TPU/PVDF/PS (11 wt.%) is 21.37%; the crystallinity of TPU/PVDF/PS (12 wt.%) is 26.65%. We can find that the crystallinity decreased when concentration increased from 9 wt.% to 10 wt.%. However, with the concentration continuing to increase, the crystallinity gets enlargement. So we can get a conclusion that 10 wt.% concentration has the lowest degree of crystallinity.

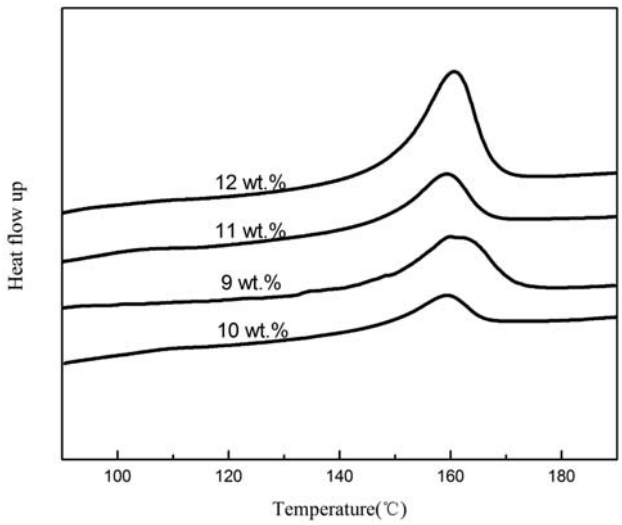

Fig. 2. DSC thermograms of different concentration of TPU/ VDF/PS

Table 1. Thermodynamic properties of different concentration of TPU/PVDF/PS

Sample	ΔH_f (J/g)	Crystallinity χ_c (%)
TPU/PVDF/PS (9 wt.%)	8.91	20.43
TPU/PVDF/PS (10 wt.%)	6.61	13.64
TPU/PVDF/PS (11 wt.%)	11.39	21.37
TPU/PVDF/PS (12 wt.%)	15.5	26.65

3. 3. Electrolyte Uptake and Ionic Conductivity

Fig.3 shows the uptake behaviors of the electrospun fibrous membranes. The percentage of electrolyte uptake can be calculated according to Eq(A). The TPU/PVDF/PS (9 wt.%) fibrous film shows an electrolyte uptake of about 310% within 2 min, The TPU/PVDF/PS(10 wt.%) fibrous film is 331%, The TPU/PVDF/PS (11 wt.%) fibrous film is 296%, The TPU/PVDF/PS (12 wt.%) fibrous film is 274% after 15 min, it is found that the electrolyte uptake of these four membranes become stabile. The uptake of the electrolyte solution reaches up to 320% (9 wt.%), 341% (10 wt.%), 305% (11 wt.%), 298% (12 wt.%), respectively. The absorption of large quantities of liquid electrolyte by the composite membranes results from the high porosity of the membranes and the high amorphous content of the polymer. The fully interconnected pore structure makes fast penetration of the liquid into the membrane possible, and hence the uptake process is stabile within the initial 15 min. TPU/PVDF/PS (10 wt.%) membrane owns the highest porosity, so it also has the highest electrolyte uptake percentage. Furthermore, the TPU/ PVDF/PS (10 wt.%) membrane's average fiber diameter is minimal that leads to the increasing in the absorption ratio of the electrolyte solution. Because the porosity and the surface area of the pore wall of the film will increasing with the average fiber diameter decreasing. The increasing of surface area of the pore wall and more pores result in a higher uptake of the liquid electrolyte, which means more Li^+ in the same volume.[22]

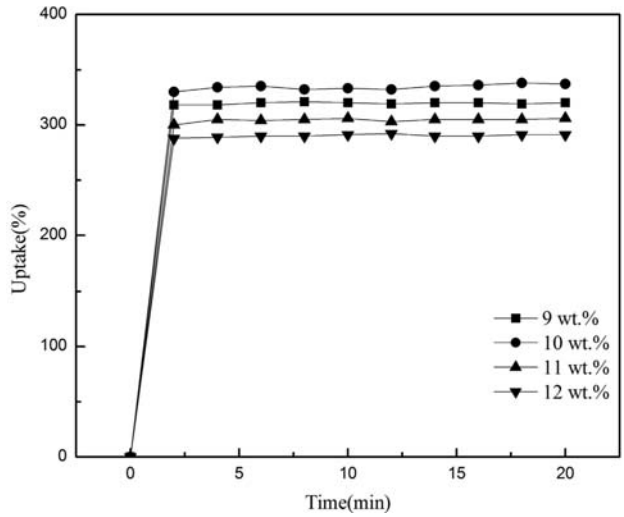

Fig. 3. The uptake behavior of the TPU/PVDF/PS electrospun fibrous films

Fig.4 shows the impedance spectra of TPU/PVDF/ PS based fibrous polymer electrolyte. It is typical AC impedance for gel polymer electrolyte. The self-resistance (R) is the major contribution to the total resistance and ionic conductivity is calculated according to Eq.(3). The ionic conductivity of TPU/PVDF/PS (10 wt.%) membrane was 5.28×10^{-3} mS cm^{-1} at room temperature. From table 2, we know that the ionic conductivity of TPU/PVDF/PS (10 wt.%) membrane is maximal , and the body resistance of TPU/PVDF/PS (10 wt.%) membrane is the smallest. The solution crystallinity, porosity and absorption rate have relationships with the self-resistance, from the previous experimental results we can know why the ionic conductivity of TPU/PVDF/PS (10 wt.%) membrane is the biggest.

Table 2. Different concentration of TPU/PVDF/PS membranes' parameters and ionic conductivity

Materials	Rb(Ω)	H(cm)	S(cm^{-2})	σ(10^{-3}S cm^{-1})
TPU/PVDF/PS (9 wt.%)	2.92	0.0014	2.02	2.37
TPU/PVDF/PS (10 wt.%)	1.12	0.0012	2.03	5.28
TPU/PVDF/PS (11 wt.%)	4.67	0.0014	1.98	1.51
TPU/PVDF/PS (12 wt.%)	5.2	0.0012	2.05	1.13

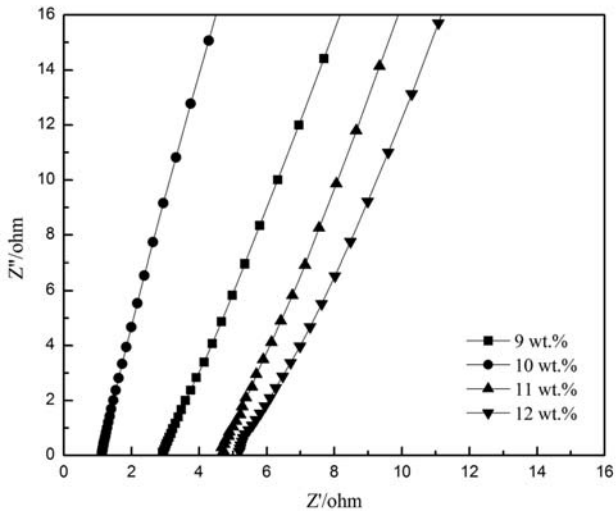

Fig. 4. Impedance spectra of gel polymer electrolytes

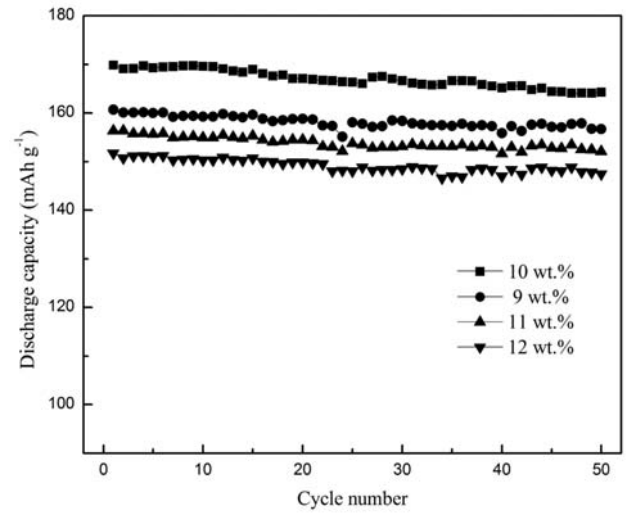

Fig. 6. The cycle performance (discharge capacitie) of different concentrations of GPE based on electrospun TPU/PVDF/PS membranes

3. 4. Evaluation in Li/LiFePO_4 Cell

Fig.5 shows the first charge-discharge capacity curves of the cells with GPEs of TPU/PVDF/PS. The GPEs of TPU/PVDF/PS (10 wt.%) delivers a charge capacity of 169.81 mAh g^{-1} and discharge capacity of 169.5 mAh g^{-1}, which is about 99% of the theoretical capacity. The GPEs of TPU/PVDF/PS (9 wt.%; 11 wt.%; 12 wt.%) deliver a charge capacity of 161.79 mAh g^{-1}; 159.49 mAh g^{-1}; 151.82 mAh $g^{-1}$and discharge capacity of 160.65 mAh g^{-1}; 156.32 mAh g^{-1}; 151.74 mAh g^{-1}. The Li cells with GPEs have been evaluated for cycle ability property under the 0.1 C rate at 25 °C and the results are shown in Fig. 6. The cell with GPE (10 wt.%) has a highest discharge capacities in the whole 50 cycles. From the above data, we can know that the GPEs of TPU/PVDF/PS (10 wt.%) owns the best charge-discharge capacity and cycle ability property.

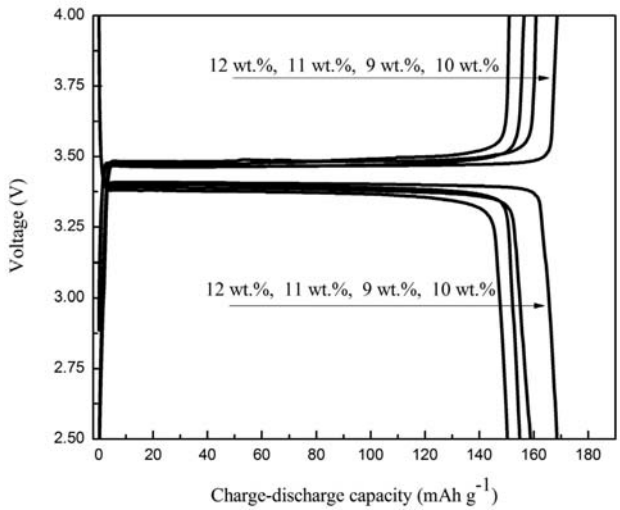

Fig. 5. first Charge-discharge capacity of different concentration of GPEs based on electrospun TPU/PVDF/PS membrane

3. 5. Mechanical Property

The stress-strain curves of different concentrations of electrospun PVDF/TPU/PS membranes are presented in Fig. 7, and their mechanical properties are summarized in Table 3. Because no phase separation of the nanofibrous membranes was observed from SEM, the nanofibrous membranes presented acceptable mechanical properties to be applied into practice.[23] It can be found that PVDF/TPU/PS (10 wt.%) membrane owns the longest elongation of 98.2% and can bear the tensile strength below 12.9 MPa. Both the tensile strength and elongation are better than others. Because electrospun membranes are constituted by three kinds of polymer, all of three kinds of polymer are dissolved in the mixture of acetone/*N*,*N*-dimethylacetamide (1:3, wt/wt) solution, and there is interfacial force between each others. As we know that the PVDF/TPU/PS (10 wt.%) membrane's interfacial

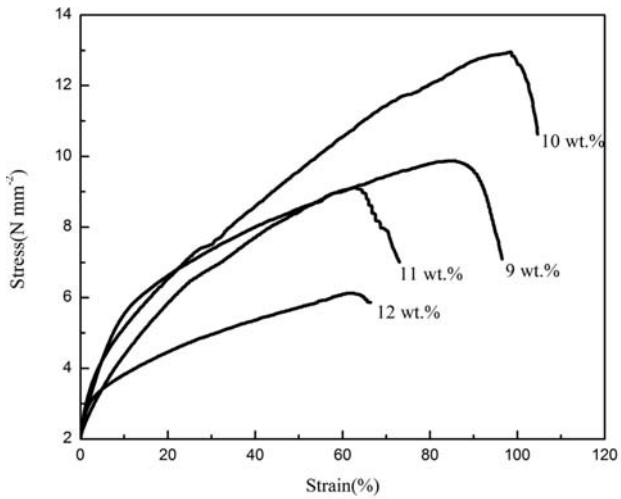

Fig. 7. Stress strain curves of different concentration of electrospun PVDF/TPU /PS membranes

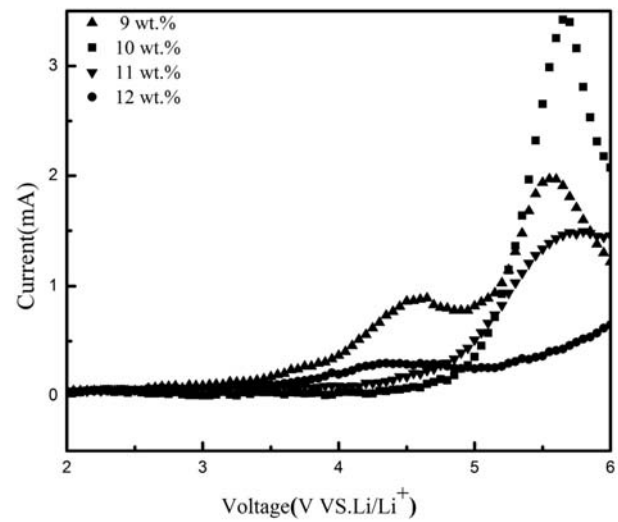

Fig. 8. Linear sweep voltammograms of the gel polymer electrolytes

Table 3. Mechanical properties of different concentration of electrospun PVDF/TPU /PS

Samples	Stress (Mpa)	Strain (%)
TPU/PVDF/PS (9 wt.%)	9.9 ± 0.2	85.4 ± 0.2
TPU/PVDF/PS (10 wt.%)	11.9 ± 0.2	94.2 ± 0.2
TPU/PVDF/PS (11 wt.%)	9.14 ± 0.2	63.2 ± 0.2
TPU/PVDF/PS (12 wt.%)	6.16 ± 0.2	62.8 ± 0.2

force is the smallest, so do the crystallinity of PVDF/TPU/PS (10 wt.%) membrane. The greater the degree of crystallinity, the worse of the toughness. So the PVDF/TPU/PS (10 wt.%) membrane has the best mechanical properties.

3. 6. Electrochemical Stability

The results of electrochemical stability tests of the gel polymer electrolytes by LSV are shown in Fig.8. From Fig.8, the electrochemical stability of the gel polymer electrolyte with PVDF/TPU/PS (10 wt.%) membrane is 4.9 V. And their electrochemical stability follows the order: TPU/PVDF/PS (10 wt.%) 4.9 V> TPU/PVDF/PS (11 wt.%) 4.3 V> TPU/PVDF/PS (9 wt.%) 4.0 V> TPU/PVDF/PS (12 wt.%) 3.6 V. It is clearly that the gel polymer electrolyte of TPU/PVDF/PS (10 wt.%) shows the best electrochemical stability, which may due to better compatibility with liquid electrolyte and nanofibrous membranes with less leakage of liquid electrolytes. In addition, the electrochemical stability was also influenced by the large and fully interconnected pores, high porosity, higher specific surface area, uniform morphology of membranes and the AFD. From the SEM images of TPU/PVDF/PS electrospun membranes you can know that the gel polymer electrolyte of TPU/PVDF/PS (10 wt.%) possesses high porosity and surface area. Therefore the gel polymer electrolyte of TPU/PVDF/PS (10 wt.%) is best for applications in lithium-ion.

4. Conclusions

GPEs based on fibrous TPU/PVDF/PS blend membranes were prepared by electrospinning the polymer solution in DMF/acetone (3:1, w/w) at room temperature. It has been observed that the optimum proportion of a novel high-performance gel polymer electrolyte is TPU/PVDF/PS (10 wt.%). It has a high ionic conductivity of 5.28 × 10^{-3} mS cm^{-1} with electrochemical stability up to 5.0 V versus Li^+/Li at room temperature. The first charge-discharge capacity of gel polymer electrolyte lithium battery based on PVDF/TPU/PS (10 wt.%) is about 169.5 mAh g^{-1} at 25 °. The PDVF/TPU/PS (10 wt.%) mixed film owns the longest elongation of 98.2%, and it can bear the tensile strength below 12.9 MPa. Both the tensile strength and elongation are excellent. The PVDF/TPU/PS (10 wt.%) based gel polymer electrolyte is the optimum proportion of a novel high-performance gel polymer electrolyte for rechargeable lithium batteries.

5. Acknowledgements

The workers gratefully appreciate the financial supports from the Youth Project of National Nature Science Foundation of China (No. 51203131).

6. References

1. Zhu YS, Wang FX, Liu LL, Xiao SY, Chang Z, Wu YP, *Energy Environ.* **2013**, *6*, 618–624.

https://doi.org/10.1039/C2EE23564A
2. Theron SA, Zussman E, Yarin AL, *J. polymer.* **2004**, *45*, 2017–2030.
3. J. J. Xu, H. Ye, *Electrochem. Commun.* **2005**, *7*, 829–835. https://doi.org/10.1016/j.elecom.2005.04.034
4. S.-I. Kim, H.-S. Kim, S.-H. Na, S.-I. Moon, Y.-J. Kim, N.-J. Jo, *Electrochim. Acta.* **2004**, *50*, 317–321. https://doi.org/10.1016/j.electacta.2003.12.068
5. N. Wu, B. Jing, Q. Cao, X. Wang, H. Kuang, Q. Wang, *J. Appl. Polym. Sci.* **2012**, *125*, 2556–2563. https://doi.org/10.1002/app.36523
6. C. R. Yang, Z. D. Jia, Z. C. Guan, L. M. Wang, *J. Power Sources.* **2009**, *189*, 716–720. https://doi.org/10.1016/j.jpowsour.2008.08.060
7. P. Raghavan, J. W. Choi, J. H. Ahn, G. Cheruvally, G. S. Chauhana, H. J. Ahn, C.Nah, *J. Power Sources.* **2008**, *184*, 437–443. https://doi.org/10.1016/j.jpowsour.2008.03.027
8. R. Prasanth, N. Shubha, H. H. Hng, M. Srinivasan, *J. Power Sources.* **2014**, *245*, 283–291. https://doi.org/10.1016/j.jpowsour.2013.05.178
9. M. Digar, S.-L. Hung, H.-L. Wang, T.-C. Wen, A. Gopalan, *Polymer.* **2002**, *43*, 681–691. https://doi.org/10.1016/S0032-3861(01)00655-3
10. J. Van Heumen, J. Stevens, *Macromolecules.* **1995**, *28*, 4268–4277. https://doi.org/10.1021/ma00116a030
11. H.-H. Kuo, W.-C. Chen, T.-C. Wen, A. Gopalan, *J. Power Sources*, **2002**, *110*, 27–33. https://doi.org/10.1016/S0378-7753(02)00214-8
12. Y.-L. Du, T.-C. Wen, Mater, *Chem. Phys.* **2001**, *71*, 62–69. https://doi.org/10.1016/S0254-0584(01)00271-1
13. P. Santhosh, T. Vasudevan, A. Gopalan, K.-P. Lee, *Mater. Sci. Eng. B.* **2006**, *135*, 65–73. https://doi.org/10.1016/j.mseb.2006.08.033
14. Ten-Chin Wen, Han-Hsin Kuo, A. Gopalan, *Solid State Ionics.* **2002**, *147*, 171–180.
15. X. X. Peng, L. Zhou, Q. Cao, *J. Solid State Electrochem.* **2016**, *20*, 255–262 https://doi.org/10.1007/s10008-015-3030-5
16. N. Wu, Q. Cao, X. Wang, Q. *Che*n, *Solide State Ionics.* **2011**, *203*, 42–46. https://doi.org/10.1016/j.ssi.2011.08.020
17. W. W. Cui, D. Y. Tang, Z. L. Gong, *J. Power Sources.* **2013**, *223*, 206–213. https://doi.org/10.1016/j.jpowsour.2012.09.049
18. Y. S. Zhu, S. Y. Xiao, Y. Shi, Y. Q. Yang, Y. P. Wu, *J. Mater. Chem. A.* **2013**, *1*, 7790–7797. https://doi.org/10.1039/c3ta00167a
19. L. Zhou, N. Wu, Q. Cao, B. Jing, X. Y. Wang, Q. Wang, H. Kuang, *Solid State Ionics.* **2013**, *249–250*, 93–97. https://doi.org/10.1016/j.ssi.2013.07.019
20. S. S. Sekhon, H. P. Singh, *Solide State Ionics.* **2002**, *169*, 152–153.
21. X. L. Tang, Q. Cao, X. Y. Wang, X. X. Peng, J Zeng, *RSC Adv.*, **2015**, *5*, 58655– 58662
22. L. Zhou, Q. Cao, B. Jing, X. Y. Wang, X. L. Tang, N. Wu, *J. Power Sources.* **2014**, *263*, 118–124. https://doi.org/10.1016/j.jpowsour.2014.03.140
23. W. L. Li, Y. H. Wu, J. W. Wang, D. Huang, L. Z. Chen, *European Polymer Journal.* **2015**, *67*, 365–372. https://doi.org/10.1016/j.eurpolymj.2015.04.014

Povzetek

Pripravili smo visoko učinkovit gel polimerni elektrolit (GPE), ki temelji na polivinilidenfluoridu (PVDF), termoplastičnem poliuretanu (TPU) in polistirenu (PS). Njegove lastnosti smo preučevali z naslednjimi tehnikami: vrstično elektronsko mikroskopijo (SEM), termično analizo (DSC), meritvami mehanskih lastnosti (UTM) in elektrokemijsko impedančno spektroskopijo. Gel polimerni elektroliti (GPE), ki temeljijo na TPU/PVDS/PS (10 wt.%) imajo visoko ionsko prevodnost 5.28×10^{-3} S cm^{-1} in elektrokemijsko okno stabilnosti 5.0 V. Poleg tega pa prva kapaciteta polnjenja in praznjenja doseže 169.5 mAh g^{-1}. Zaradi dobrih mehanskih lastnosti in stabilnosti bi bili ti materiali lahko uporabni v litij ionskih polimernih baterijah.

Scientific paper

Synthesis, Characterization and Cytotoxicity of Substituted [1]Benzothieno[3,2-*e*][1,2,4]triazolo [4,3-*a*]pyrimidines

Samir Botros,[1] Omneya M. Khalil,[1] Mona M. Kamel[1] and Yara S. El-Dash[1,*]

[1] *Pharmaceutical Organic Chemistry Department, Faculty of Pharmacy, Cairo University, P.O. Box 11562, Cairo, Egypt*

** Corresponding author: E-mail: yara.el-dash@pharma.cu.edu.eg*
Tel: +202 27043364 / Fax: +202 3635140

Received: 10-09-2016

Abstract

A new series of 4-benzyl-6,7,8,9-tetrahydro[1]benzothieno[3,2-*e*][1,2,4]triazolo[4,3-*a*]pyrimidines was synthesized motivated by the widely reported anticancer activity of thieno[2,3-*d*]pyrimidines and triazolothienopyrimidines. The *in vitro* cytotoxic activity of some selected compounds was evaluated against two human cell lines: prostate cancer (PC-3) and colon cancer (HCT-116). A preliminary study of the structure–activity relationship of the target compounds was discussed. Most of the synthesized compounds showed remarkable activity on the tested cell lines, while compound **16c** had the highest potency against the PC-3 cell line with an IC_{50} of 5.48 μM compared to Doxorubicin (IC_{50} = 7.7 μM), the reference standard used in this study. On the other hand, **6c** and **18c** were the most active against HCT-116 (IC_{50} = 6.12 and 6.56 μM, respectively) relative to IC_{50} = 15.82 μM of the standard. Thus, some of the synthesized thienopyrimidine derivatives, specially **6c**, **16c** and **18c**, have the potential to be developed into potent anticancer agents.

Keywords: Thienopyrimidines; 1,2,4-Triazoles; Anticancer activity; PC-3; HCT-116

1. Introduction

Despite decades of research that have resulted in an enormous leap in cancer therapy, cancer remains a major cause of death worldwide thus there is a continuous need for the discovery and development of new anticancer agents.[1,2] It is worth mentioning that 60% of world's total new annual cases occur in Africa, Asia and Central and South America.[3]

Thiophenes have been reported to possess interesting biological activities particularly as anticancer agents.[4,5] Many research groups reported the synthesis of biologically active thiophene derivatives through the well-known Gewald reaction.[6,7] As an example, Mohareb *et al.*[8] synthesized some thiophene derivatives and investigated their antitumor activity. The prepared compounds exhibited GI_{50} ranging from 0.02 to 0.08 μM against MCF-7, NCI-H450 and SF-268 cell lines compared to Doxorubicin.

Meanwhile, thieno[2,3-*d*]pyrimidines represent an important class of bioactive heterocycles attracting much attention due to their wide range of biological and pharmaceutical activities.[9,10]

The presence of pyrimidine ring in the basic building scaffolds of DNA and RNA modules (thymine, cytosine and uracil) is probably the reason of their diverse biological activities.[11] In addition, the tricyclic system, cycloalkylthieno[2,3-*d*]pyrimidine, which is considered to be a bioisostere of quinazoline, has been used as a core for the mechanism-based design and synthesis of a variety of compounds for anticancer therapy.[12–16]

On the other hand, the 1,2,4-triazole heterocycle is of great value as a building block in the structure of several anticancer drug candidates.[11,17,18] Letrozole, Anastrozole and Ribavirin are representative examples of commercially available anticancer drugs containing triazole scaffolds (Fig. 1).[19–21] Among these heterocycles, the mercapto substituted 1,2,4-triazole ring systems have been well studied and so far a variety of biological activities have reported for them.[17,22,23]

Recently, 4-amino-1,2,4-triazol-3-thione was used as an intermediate for the synthesis of several biologically active fused heterocyclic compounds where the amino and mercapto groups are appropriate nucleophile centers for many chemical modifications.[24] Further, many alkylated

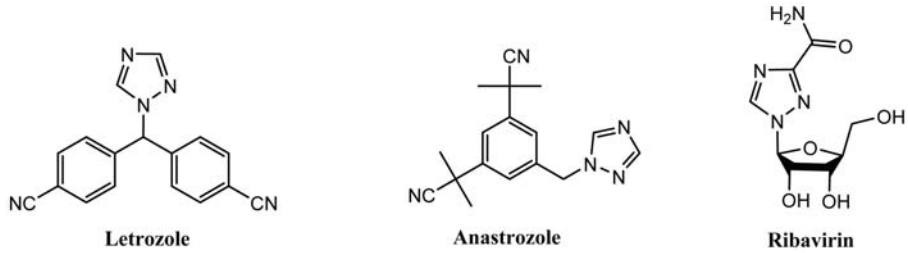

Figure 1. Chemical structures of anticancer drugs containing triazole moiety available on the market.

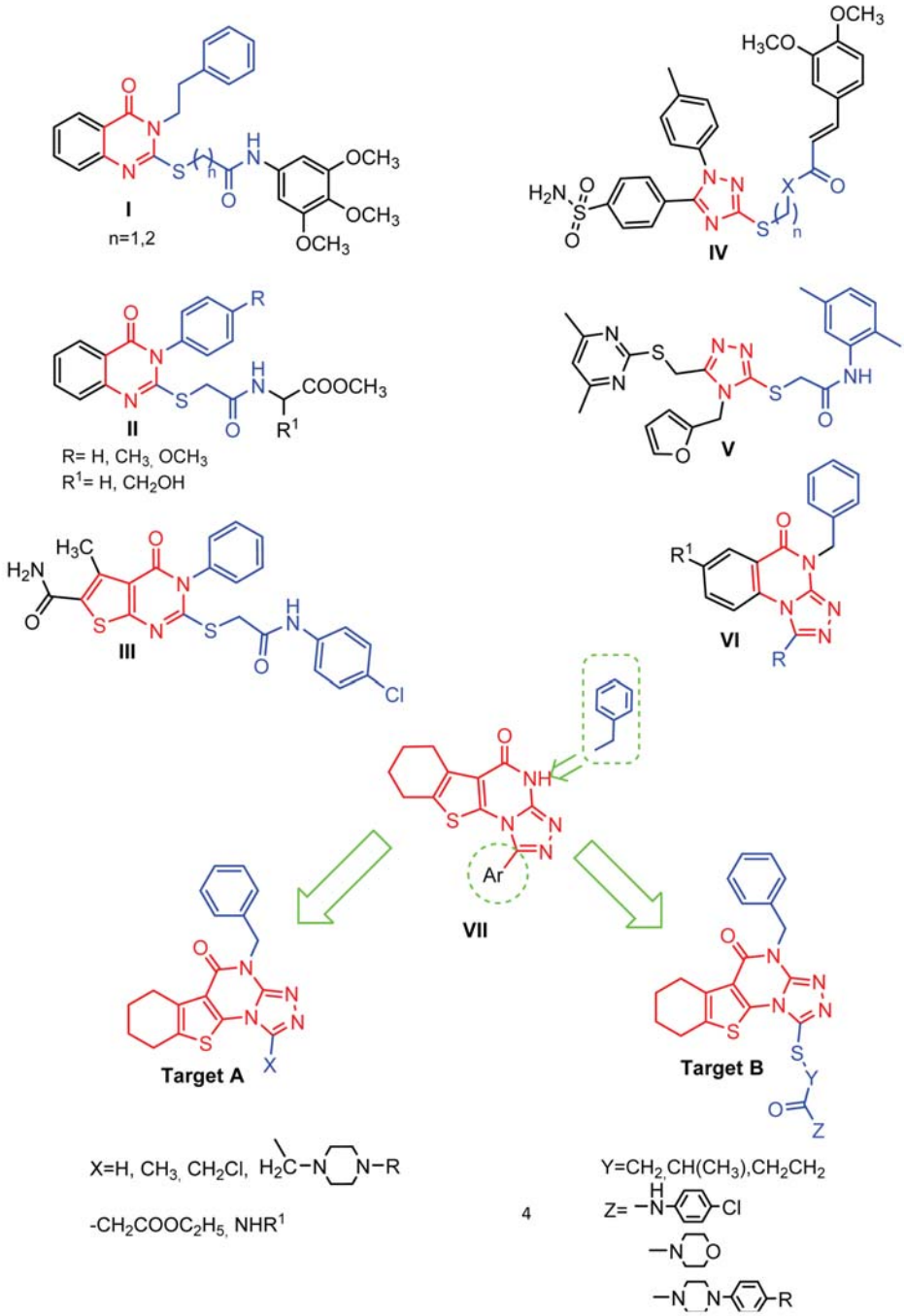

Figure 2. Structures of some reported pyrimidines, thieno[2,3-*d*]pyrimidines and triazole derivatives with cytotoxic activity showing the possible chemical optimization to obtain target compounds A and B

mercapto 1,2,4-triazoles linked to various aromatic ring systems either through amide or ester linkages have been reported to exhibit significant antitumor activities.[25–27]

In the last few years, many research groups investigated thienopyrimidine derivatives fused to 1,2,4-triazole moiety as potential cytotoxic agents.[28–30] For example, the fusion of a triazole ring to cycloalkylthieno[2,3-*d*]pyrimidine (**VII**) showed significant *in vitro* cytotoxic activity against human colorectal cancer cells (HCT-116) (IC_{50} = 2.8 μg/mL) compared to the reference drug Doxorubicin (Fig. 2).[31]

In our search for new classes of potential anticancer agents, the aforementioned findings prompted us to synthesize a series of 4-benzyl[1]benzothieno[3,2-*e*][1,2,4]triazolo[4,3-*a*] pyrimidines with varying the substitution at position 1 (Target compound A) in order to investigate the effect of combining these bioactive moieties on the anticancer activity. Moreover, we aimed in this work to prepare a series of 4-benzyl[1]benzothieno[3,2-*e*][1,2,4]triazolo[4,3-*a*] pyrimidines bearing various *S*-(substituted amino alkyl) moieties at position 1 (Target compound B) to act as cytotoxic agents. In this series, different alkyl linkers and different aliphatic and aromatic amines were used to study the effect of these variations on the cytotoxic activity. Some selected compounds were tested for possible anti-cancer activity against two cell lines (PC-3 and HCT-116).

2. Experimental

2. 1. Chemistry

All melting points were determined with Stuart SMP10 apparatus and the values given are uncorrected. IR spectra (KBr, cm^{-1}) were determined on Shimadzu IR 8400s spectrophotometer (Faculty of Pharmacy, Cairo University, Egypt). ^{1}H-NMR and ^{13}C-NMR spectra were recorded on Mercury 300-BB 300 MHz (Microanalytical Center, Faculty of Science, Cairo University, Egypt) and Bruker 400-BB 400 MHz spectrometers (Microanalytical Unit, Faculty of Pharmacy, Cairo University, Egypt) using TMS as the internal standard. Chemical shift values are given in ppm on δ scale. Mass spectra were recorded on Hewlett Packard 5988 spectrophotometer (Microanalytical Center, Faculty of Science, Cairo University, Egypt). Elemental analyses were carried out at the Regional center for Mycology and Biotechnology, Faculty of Pharmacy, Al Azhar University, Egypt; values found were within ±0.35% of the theoretical ones. Progress of the reactions was monitored by TLC using aluminum sheets precoated with UV fluorescent silica gel (Merck 60F 254) and visualized using UV lamp. The solvent system used was chloroform : benzene : methanol [9:5:2].

The starting compounds, ethyl 2-amino-4,5,6,7-tetrahydro[1]benzothiophene-3-carboxylate (**1**),[32] 3-benzyl-2-sulphanyl-5,6,7,8-tetrahydro[1]benzothieno[2,3-*d*]pyrimidin-4(*3H*)-one (**2**)[33] and the α- and β-chloroamides (**13a–d**, **14a–d**, **15a–d**)[34–40] were prepared according to reported procedures.

2. 1. 1. 3-Benzyl-2-hydrazino-5,6,7,8-tetrahydro[1]benzothieno[2,3-*d*]pyrimidin-4(3*H*)-one (3)

A mixture of 3-benzyl-2-sulphanyl-5,6,7,8-tetrahydro[1]benzothieno[2,3-*d*]pyrimidin-4(*3H*)-one (**2**) (1.64 g, 50 mmol) and hydrazine hydrate 99–100% (7 mL, 140 mmol) in dry pyridine (25 mL) was heated under reflux for 25 h. The mixture was evaporated under reduced pressure and the residue was treated with ethanol. The solid product was collected by filtration, washed with ethanol, dried and crystallized from ethyl acetate.

Yield: 50%; mp: 226–228 °C; IR (KBr, cm^{-1}): 3248–3211 (NH, NH_2), 3061–3035 (CH aromatic), 2916, 2848 (CH aliphatic), 1666 (C=O), 1624, 1568, 1529 (C=C aromatic); ^{1}H-NMR (DMSO-d_6) δ: 1.75–1.78 (m, 4H, 2 × CH_2 at C-6, C-7), 2.62–2.74 (m, 2H, CH_2 at C-5), 2.79–2.81(m, 2H, CH_2 at C-8), 5.21 (s, 2H, N$\underline{CH_2}$$C_6H_5$), 6.98 (s, 1H, NH, D_2O exchangeable), 7.15–7.34 (m, 5H, Ar-H); EI-MS *m/z* 326 (M^+, 26.29%); Anal. Calcd for $C_{17}H_{18}N_4OS$ (326.42): C, 62.55; H, 5.56; N, 17.16. Found: C, 62.74; H, 5.64; N, 17.38.

2. 1. 2. 4-Benzyl-6,7,8,9-tetrahydro[1]benzothieno[3,2-*e*][1,2,4]triazolo[4,3-*a*]pyrimidin-5(4*H*)-one (4a)

A mixture of 3-benzyl-2-hydrazino-5,6,7,8-tetrahydro[1]benzothieno[2,3-*d*]pyrimidin-4(*3H*)-one (**3**) (0.32 g, 1 mmol) and formic acid (5 mL, 130 mmol) was heated under reflux for 4 h. The white precipitate formed upon cooling was collected by filtration, washed with water, dried and crystallized from ethyl acetate.

Yield: 78%; mp: 198–200 °C; IR (KBr, cm^{-1}): 3115 (CH aromatic), 2922, 2850 (CH aliphatic), 1670 (C=O), 1595, 1552, 1517 (C=C aromatic); ^{1}H-NMR ($CDCl_3$-d_6) δ: 1.81–1.92 (m, 4H, 2 × CH_2 at C-7, C-8), 2.76–2.79 (m, 2H, CH_2 at C-6), 3.02–3.06 (m, 2H, CH_2 at C-9), 5.48 (s, 2H, N$\underline{CH_2}$$C_6H_5$), 7.26–7.67 (m, 5H, Ar-H), 8.37 (s, 1H, aromatic CH); EI-MS *m/z* 336 (M^+, 35.04), 91 ($[C_7H_7]^+$, 100%); Anal. Calcd for $C_{18}H_{16}N_4OS$ (336.4): C, 64.26; H, 4.79; N, 16.65. Found: C, 64.42; H, 4.86; N, 16.90.

2. 1. 3. 4-Benzyl-1-methyl-6,7,8,9-tetrahydro[1]benzothieno[3,2-*e*][1,2,4]triazolo[4,3-*a*]pyrimidin-5(4*H*)-one (4b)

A mixture of **3** (0.32 g, 1 mmol) and acetic acid (10 mL, 70 mmol) was heated under reflux for 6 h. The reaction mixture was poured onto ice cold water (25 mL). The white precipitate formed was collected by filtration, washed with water, dried and crystallized from acetonitrile.

Yield: 85%; mp: 242–244 °C; IR (KBr, cm^{-1}): 3061, 3043 (CH aromatic), 2937, 2870 (CH aliphatic), 1664 (C=O), 1593, 1558, 1541 (C=C aromatic); ^{1}H-NMR ($CDCl_3$-d_6) δ: 1.83–1.91 (m, 4H, 2 × CH_2 at C-7, C-8), 2.75 (s, 3H, CH_3), 2.77–2.78 (m, 2H, CH_2 at C-6), 3.04–3.07 (m, 2H, CH_2 at C-9), 5.44 (s, 2H, N$\underline{CH_2}$$C_6H_5$), 7.22–7.66 (m, 5H, Ar-H); ^{13}C-NMR ($CDCl_3$-d_6) δ: 12.07, 22.06, 22.97, 24.92, 25.63, 45.94, 118.29, 128.15, 128.63, 129.73, 130.91, 134.06, 136.12, 138.67, 144.07, 149.09, 156.29; EI-MS *m/z* 350 (M^+, 64.90), 91 ($[C_7H_7]^+$, 100%); Anal. Calcd for $C_{19}H_{18}N_4OS$ (350.42): C, 65.12; H, 5.18; N, 15.99. Found: C, 65.38; H, 5.29; N, 16.31.

2. 1. 4. 1-Chloromethyl-4-benzyl-6,7,8,9-tetrahydro[1]benzothieno[3,2-*e*][1,2,4]triazolo [4,3-*a*] pyrimidin-5(4*H*)-one (5)

To a solution of **3** (1 g, 3 mmol) in dry DMF (10 mL), chloroacetyl chloride (1.5 mL, 20 mmol) was added dropwise with cooling. The solution was then heated under reflux in a boiling water bath for 9 h. After cooling, the reaction mixture was poured onto ice-cold water and the suspension formed was stirred at room temperature for 2 h. The separated solid was collected by filtration, washed with cold water, dried and crystallized from methanol.

Yield: 88%; mp: 188–190 °C; IR (KBr, cm^{-1}): 3080, 3040 (CH aromatic), 2939, 2852 (CH aliphatic), 1681 (C=O), 1622, 1591, 1550 (C=C aromatic); ^{1}H-NMR (DMSO-d_6) δ: 1.74–1.80 (m, 4H, 2 × CH_2 at C-7, C-8), 2.76–2.80 (m, 2H, CH_2 at C-6), 2.82–2.87 (m, 2H, CH_2 at C-9), 5.11 (s, 2H, $\underline{CH_2}$Cl), 5.29 (s, 2H, N$\underline{CH_2}$$C_6H_5$), 7.15–7.34 (m, 5H, Ar-H); EI-MS *m/z* 386 (M+2, 3.9); 384 (M^+, 16.95%); Anal. Calcd for $C_{19}H_{17}ClN_4OS$ (384.87): C, 59.29; H, 4.45; N, 14.56. Found: C, 59.41; H, 4.52; N, 14.71.

2. 1. 5. General procedure for the preparation of compounds 6a–d

A mixture of **5** (0.25 g, 0.6 mmol) and the appropriate *N*-substituted piperazine (4 mmol) in absolute ethanol (30 mL) was heated under reflux for 6 h. The product obtained was collected by filtration, washed with water and crystallized from the suitable solvent.

4-Benzyl-1-[[4-methylpiperazin-1-yl]methyl]-6,7,8,9-tetrahydro[1]benzothieno[3,2-*e*][1,2,4]triazolo[4,3-*a*]pyrimidin-5(4*H*)-one (6a). Crystallized from aqueous ethanol; yield: 36%; mp: 172–174 °C; IR (KBr, cm^{-1}): 3040, 3020 (CH aromatic), 2922, 2850 (CH aliphatic), 1677 (C=O), 1591 (C=C aromatic); ^{1}H-NMR ($CDCl_3$-d_6) δ: 1.86–1.92 (m, 4H, 2 × CH_2 at C-7, C-8), 2.27 (s, 3H, CH_3), 2.43–2.50 (m, 4H, 2 × CH_2 piperazine), 2.63–2.70 (m, 2H, CH_2 at C-6), 2.78–2.81 (m, 2H, CH_2 at C-9), 3.06–3.10 (m, 4H, 2 × CH_2 piperazine), 3.88 (s, 2H, CH_2), 5.46 (s, 2H, N$\underline{CH_2}$$C_6H_5$), 7.28–7.69 (m, 5H, Ar-H); EI-MS *m/z* 448 (M^+, 0.57), 91 ($[C_7H_7]^+$, 100%); Anal. Calcd for $C_{24}H_{28}N_6OS$ (448.56): C, 64.26; H, 6.29; N, 18.73. Found: C, 64.38; H, 6.37; N, 18.56.

4-Benzyl-1-[[4-phenylpiperazin-1-yl]methyl]-6,7,8,9-tetrahydro[1]benzothieno[3,2-*e*][1,2,4]triazolo[4,3-*a*]pyrimidin-5(4*H*)-one (6b). Crystallized from ethyl acetate; yield: 48%; mp: 228–230 °C; IR (KBr, cm^{-1}): 3057, 3032 (CH aromatic), 2941, 2918, 2848, 2821 (CH aliphatic), 1672 (C=O), 1587, 1558, 1539 (C=C aromatic); ^{1}H-NMR ($CDCl_3$-d_6) δ: 1.85–1.87 (m, 4H, 2 × CH_2 at C-7, C-8), 2.77–2.80 (m, 6H, CH_2 at C-6 and 2 × CH_2 piperazine), 3.05–3.10 (m, 2H, CH_2 at C-9), 3.18–3.19 (m, 4H, 2 × CH_2 piperazine), 3.95 (s, 2H, CH_2), 5.47 (s, 2H, N-$\underline{CH_2}$-C_6H_5), 6.83–7.70 (m, 10H, Ar-H); EI-MS *m/z* 511 (M+1, 4.13), 510 (M^+, 6.27%); Anal. Calcd for $C_{29}H_{30}N_6OS$ (510.63): C, 68.21; H, 5.92; N, 16.46. Found: C, 68.44; H, 5.98; N, 16.82.

4-Benzyl-1-[[4-(4-chlorophenyl)piperazin-1-yl]methyl]-6,7,8,9-tetrahydro[1]benzothieno[3,2-*e*][1,2,4]triazolo[4,3-*a*]pyrimidin-5(4*H*)-one (6c). Crystallized from ethyl acetate; yield: 51%; mp: 254–256 °C; IR (KBr, cm^{-1}): 3100, 3040 (CH aromatic), 2929, 2819 (CH aliphatic), 1670 (C=O), 1581, 1550, 1510 (C=C aromatic); ^{1}H-NMR ($CDCl_3$-d_6) δ: 1.86–1.88 (m, 4H, 2 × CH_2 at C-7, C-8), 2.77–2.80 (m, 6H, CH_2 at C-6 and 2 × CH_2 piperazine), 3.05–3.10 (m, 2H, CH_2 at C-9), 3.12–3.13 (m, 4H, 2 × CH_2 piperazine), 3.96 (s, 2H, CH_2) 5.47 (s, 2H, N-$\underline{CH_2}$-C_6H_5), 6.87–7.70 (m, 9H, Ar-H); EI-MS *m/z* 546 (M+2, 32.02), 544 (M^+, 37.08%); Anal. Calcd for $C_{29}H_{29}ClN_6OS$ (545.08): C, 63.90; H, 5.36; N, 15.42. Found: C, 64.07; H, 5.44; N, 15.67.

4-Benzyl-1-[[4-(4-methoxymphenyl)piperazin-1-yl]methyl]-6,7,8,9-tetrahydro[1]benzothieno[3,2-*e*][1,2,4]triazolo[4,3-*a*]pyrimidin-5(4*H*)-one (6d). Crystallized from acetonitrile; yield: 37%; mp: 238–240 °C; IR (KBr, cm^{-1}): 3040, 3000 (CH aromatic), 2926, 2808 (CH aliphatic), 1681 (C=O), 1591, 1556, 1535 (C=C aromatic); ^{1}H-NMR ($CDCl_3$-d_6) δ: 1.85–1.87 (m, 4H, 2 × CH_2 at C-7, C-8), 2.75–2.78 (m, 6H, CH_2 at C-6 and 2 × CH_2 piperazine), 3.05–3.09 (m, 6H, CH_2 at C-9 and 2 × CH_2 piperazine), 3.75 (s, 3H, OCH_3), 3.94 (s, 2H, CH_2) 5.47 (s, 2H, N-$\underline{CH_2}$-C_6H_5), 6.83–7.70 (m, 9H, Ar-H); EI-MS *m/z* 541 (M+1, 5.84), 540 (M^+, 15.74), 91 ($[C_7H_7]^+$, 100%); Anal. Calcd for $C_{30}H_{32}N_6O_2S$ (540.68): C, 66.64; H, 5.97; N, 15.54. Found: C, 66.88; H, 6.05; N, 15.66.

2. 1. 6. 4-Benzyl-6,7,8,9-tetrahydro[1]benzothieno[3,2-*e*][1,2,4]triazolo[4,3-*a*]pyrimidin-1,5(2H,4*H*)-dione (7)

A mixture of **3** (0.64 g, 2 mmol) and *N,N*-carbonyldiimidazole (CDI) (0.7 g, 4.3 mmol) in dry benzene (30 mL) was heated under reflux for 15 h. After cooling,

the solvent was evaporated under reduced pressure and the residue was triturated with cold water. The solid product was collected by filtration, dried and crystallized from acetonitrile.

Yield: 81%; mp: 306–308 °C; IR (KBr, cm^{-1}): 3170 (NH), 3055, 3034 (CH aromatic), 2933, 2852 (CH aliphatic), 1720, 1683 (2 × C=O), 1610, 1560, 1523 (C=C aromatic); ^{1}H-NMR (DMSO-d_6) δ: 1.78–1.80 (m, 4H, 2 × CH_2 at C-7, C-8), 2.73–2.80 (m, 2H, CH_2 at C-6), 2.81–2.84 (m, 2H, CH_2 at C-9), 5.05 (s, 2H, N$\underline{CH_2}C_6H_5$), 7.28–7.35 (m, 5H, Ar-H), 12.0 (s, 1H, NH, D_2O exchangeable); ^{13}C-NMR (DMSO-d_6) δ: 22.03, 22.86, 24.47, 25.22, 43.86, 115.40, 127.84, 128.14, 128.80, 130.05, 131.47, 136.45, 138.97, 141.21, 149.17, 156.63; EI-MS *m/z* 352 (M^+, 32.62), 91 ($[C_7H_7]^+$, 100%); Anal. Calcd for $C_{18}H_{16}N_4O_2S$ (352.41): C, 61.35; H, 4.58; N, 15.90. Found: C, 61.54; H, 4.65; N, 15.88.

2. 1. 7. General procedure for the preparation of compounds 8a–e

A mixture of **3** (0.32 g, 1 mmol) and the appropriate isothiocyanate (2 mmol) in absolute ethanol (30 mL) was heated under reflux for 8 h. The precipitated product was collected by filtration, dried and crystallized from ethanol/$CHCl_3$ (2:1).

4-Benzyl-1-methylamino-6,7,8,9-tetrahydro[1]benzothieno[3,2-*e*][1,2,4]triazolo[4,3-*a*]pyrimidin-5(4*H*)-one (8a). Yield: 43%; mp: 206–208 °C; IR (KBr, cm^{-1}): 3370, 3196 (NH), 2944, 2880 (CH aliphatic), 1681 (C=O), 1575, 1537, 1506 (C=C aromatic); ^{1}H-NMR (DMSO-d_6) δ: 1.74–1.80 (m, 4H, 2 × CH_2 at C-7, C-8), 2.62–2.65 (m, 2H, CH_2 at C-6), 2.78–2.81 (m, 2H, CH_2 at C-9), 2.81 (s, 3H, CH_3), 5.22 (s, 2H, N$\underline{CH_2}C_6H_5$), 7.19–7.38 (m, 5H, Ar-H), 9.29 (s, 1H, NH, D_2O exchangeable); ^{13}C-NMR (DMSO-d_6) δ: 22.34, 23.10, 24.76, 25.67, 31.21, 43.31, 115.03, 127.09, 127.56, 127.66, 128.86, 130.82, 136.52, 138, 151.17, 158.15, 164.13; EI-MS *m/z* 365 (M^+, 68.95), 91 ($[C_7H_7]^+$, 97.00%); Anal. Calcd for $C_{19}H_{19}N_5OS$ (365.45): C, 62.44; H, 5.24; N, 19.16. Found: C, 62.61; H, 5.30; N, 19.34.

4-Benzyl-1-ethylamino-6,7,8,9-tetrahydro[1]benzothieno[3,2-*e*][1,2,4]triazolo[4,3-*a*]pyrimidin-5(4*H*)-one (8b). Yield: 46%; mp: 200–202 °C; IR (KBr, cm^{-1}): 3358, 3257, 3169 (NH), 2972, 2848 (CH aliphatic), 1681 (C=O), 1571, 1535, 1506 (C=C aromatic); ^{1}H-NMR (DMSO-d_6) δ: 0.96 (t, J = 7.2 Hz, 3H, CH_3), 1.76–1.79 (m, 4H, 2 × CH_2 at C-7, C-8), 2.65–2.70 (m, 2H, CH_2 at C-6), 2.80–2.85 (m, 2H, CH_2 at C-9), 3.39 (q, J = 7.2 Hz, 2H, $\underline{CH_2}$-CH_3), 5.26 (s, 2H, N$\underline{CH_2}C_6H_5$), 7.19–7.36 (m, 5H, Ar-H), 9.30 (s, 1H, NH, D_2O exchangeable); ^{13}C-NMR (DMSO-d_6) δ: 14.28, 21.80, 22.57, 24.24, 25.14, 38.20, 42.64, 126.56, 127.03, 128.35, 130, 130.32, 133.61, 136, 150.52, 157.64, 163.8; EI-MS *m/z* 379 (M^+, 100), 91 ($[C_7H_7]^+$, 97.00%).

4-Benzyl-1-butylamino-6,7,8,9-tetrahydro[1]benzothieno[3,2-*e*][1,2,4]triazolo[4,3-*a*]pyrimidin-5(4*H*)-one (8c). Yield: 30%; mp: 172–174 °C; IR (KBr, cm^{-1}): 3360, 3178 (NH), 2924, 2850 (CH aliphatic), 1685 (C=O), 1535, 1454 (C=C aromatic); ^{1}H-NMR (DMSO-d_6) δ: 0.76 (t, J = 14.7 Hz, 3H, CH_3), 1.18–1.23 (m, 2H, $\underline{CH_2}$-CH_3), 1.31–1.36 (m, 2H, CH_2-$\underline{CH_2}$-CH_2), 1.75–1.80 (m, 4H, 2 × CH_2 at C-7, C-8), 2.61–2.65 (m, 2H, CH_2 at C-6), 2.75–2.77 (m, 2H, CH_2 at C-9), 3.36 (t, J = 12.6 Hz, 2H, NH-$\underline{CH_2}$), 5.19 (s, 2H, N$\underline{CH_2}C_6H_5$), 7.18–7.38 (m, 5H, Ar-H), 9.20 (s, 1H, NH, D_2O exchangeable); EI-MS *m/z* 407 (M^+, 1.32), 91 ($[C_7H_7]^+$, 100%); Anal. Calcd for $C_{22}H_{25}N_5OS$ (407.53): C, 64.84; H, 6.18; N, 17.18. Found: C, 65.01; H, 6.22; N, 17.39.

4-Benzyl-1-allylamino-6,7,8,9-tetrahydro[1]benzothieno[3,2-*e*][1,2,4]triazolo[4,3-*a*]pyrimidin-5(4*H*)-one (8d). Yield: 38%; mp: 184–186 °C; IR (KBr, cm^{-1}): 3360, 3167 (NH), 2924, 2850 (CH aliphatic), 1685 (C=O), 1651 (C=N), 1531, 1454 (C=C aromatic); ^{1}H-NMR (DMSO-d_6) δ: 1.75–1.80 (m, 4H, 2 × CH_2 at C-7, C-8), 2.64–2.70 (m, 2H, CH_2 at C-6), 2.79–2.82 (m, 2H, CH_2 at C-9), 4.00–4.08 (m, 2H, CH_2 allylic), 4.98–5.01 (m, 1H, $\underline{CH_2}$=CH), 5.11–5.14 (m, 1H, $\underline{CH_2}$=CH), 5.24 (s, 2H, N$\underline{CH_2}C_6H_5$), 5.69–5.74 (m,1H, CH_2=$\underline{CH}$), 7.18–7.33 (m, 5H, Ar-H), 9.40 (s, 1H, NH, D_2O exchangeable); ^{13}C-NMR (DMSO-d_6) δ: 21.82, 22.59, 24.23, 25.16, 42.73, 45.50, 115, 117, 126.59, 127, 128.31, 130.32, 131, 134.54, 136.4, 138.6, 151, 158.2, 164.1; EI-MS *m/z* 391 (M^+, 2.27), 91 ($[C_7H_7]^+$, 100%); Anal. Calcd for $C_{21}H_{21}N_5OS$ (391.49): C, 64.43; H, 5.41; N, 17.89. Found: C, 64.67; H, 5.48; N, 18.04.

4-Benzyl-1-[(4-methoxyphenyl)amino]-6,7,8,9-tetrahydro[1]benzothieno[3,2-*e*][1,2,4]triazolo[4,3-*a*] pyrim idin-5(4*H*)-one (8e). Yield: 65%; mp: 244–246 °C; IR (KBr, cm^{-1}): 3215 (NH), 3111, 3070 (CH aromatic), 2941, 2835 (CH aliphatic), 1683 (C=O), 1618 (C=N), 1543, 1512, 1487 (C= C aromatic); ^{1}H-NMR (DMSO-d_6) δ: 1.77–1.79 (m, 4H, 2 × CH_2 at C-7, C-8), 2.72–2.79 (m, 2H, CH_2 at C-6), 2.80–2.86 (m, 2H, CH_2 at C-9), 3.74 (s, 3H, OCH_3), 5.14 (s, 2H, N$\underline{CH_2}C_6H_5$), 6.87–7.37 (m, 9H, Ar-H), 9.39 (s, 1H, NH, D_2O exchangeable); EI-MS *m/z* 457 (M^+, 0.75), 91 ($[C_7H_7]^+$, 100%); Anal. Calcd for $C_{25}H_{23}N_5O_2S$ (457.55): C, 65.63; H, 5.07; N, 15.31. Found: C, 65.79; H, 5.12; N, 15.47.

2. 1. 8. Ethyl(4-benzyl-5-oxo-4,5-dihydro-6,7,8,9-tetrahydro[1]benzothieno[3,2-*e*][1,2,4] triazolo[4,3-*a*] pyrimidin-1-yl) acetate (9)

A mixture of **3** (0.32 g, 1 mmol) and diethyl malonate (2 mL, 13 mmol) was refluxed for 9 h. The reaction was allowed to cool, the formed residue was triturated with ethanol, collected by filtration, dried and crystallized from isopropanol to yield the title compound **9**.

Yield: 41%; mp: 220–222 °C; IR (KBr, cm^{-1}): 3035, 3055 (CH aromatic), 2935, 2854 (CH aliphatic), 1732, 1678 (2 × C=O), 1635 (C=N), 1589, 1539, 1504 (C=C aromatic); ^{1}H-NMR (DMSO-d_6) δ: 1.18 (t, J = 7.2 Hz, 3H, CH_3), 1.78–1.82 (m, 4H, 2 × CH_2 at C-7, C-8), 2.63 (s, 2H, $\underline{CH_2}$-CO), 2.77–2.81 (m, 2H, CH_2 at C-6), 2.91–2.98 (m, 2H, CH_2 at C-9), 4.16 (q, J = 7.2 Hz, 2H, $\underline{CH_2}$-CH_3), 5.28 (s, 2H, N$\underline{CH_2}C_6H_5$), 7.28–7.37 (m, 5H, Ar-H); ^{13}C-NMR (DMSO-d_6) δ: 14.45, 21.92, 22.77, 24.55, 25.52, 32.31, 45.51, 62.0, 117.61, 127.99, 128.39, 128.86, 131.32, 132.78, 136.59, 138.98, 142.06, 149.17, 155.17, 168.17; EI-MS *m/z* 422 (M^+, 60.13), 91 ($[C_7H_7]^+$, 100%); Anal. Calcd for $C_{22}H_{22}N_4O_3S$ (422.46): C, 62.54; H, 5.25; N, 13.26. Found: C, 62.71; H, 5.34; N, 13.48.

2. 1. 9. 4-Benzoyl-1-(3-benzyl-5,6,7,8-tetrahydro-4-oxo-3,4-dihydro[1]benzothieno[2,3-*d*]pyrimidin-2-yl)thiosemicarbazide (10)

To an ice cold solution of ammonium thiocyanate (0.17 g, 2 mmol) in dry acetone (5 mL), a solution of benzoyl chloride (0.3 mL, 2 mmol) in acetone (5 mL) was added dropwise. An ice-cold suspension of **3** (0.34 g, 1 mmol) in acetone (15 mL) was added to the previous mixture. The reaction mixture was heated on a water-bath for 15 h. The reaction mixture was cooled and filtered. The filtrate was evaporated and the obtained product was crystallized from ethanol/$CHCl_3$ (2:1).

Yield: 33%; mp: 114–116 °C; IR (KBr, cm^{-1}): 3346, 3159 (NH), 3057, 3030 (CH aromatic), 2927, 2856 (CH aliphatic), 1687, 1674 (2 × C=O), 1622 (C=N), 1598, 1581, 1539 (C=C aromatic); ^{1}H-NMR (DMSO-d_6) δ: 1.76–1.80 (m, 4H, 2 × CH_2 at C-7, C-8), 2.65–2.73 (m, 2H, CH_2 at C-6), 2.81–2.84 (m, 2H, CH_2 at C-9), 5.31 (s, 2H, N$\underline{CH_2}C_6H_5$), 7.27–7.91 (m, 10H, Ar-H), 9.79, 11.71, 12.49 (s, 3H, NH, D_2O exchangeable); EI-MS *m/z* 489 (M^+, 2.60), 91 ($[C_7H_7]^+$, 100%); Anal. Calcd for $C_{25}H_{23}N_5O_2S_2$ (489.61): C, 61.33; H, 4.73; N, 14.30. Found: C, 61.49; H, 4.79; N, 14.51.

2. 1. 10. 4-Benzyl-1-sulphanyl-6,7,8,9-tetrahydro[1]benzothieno[3,2-*e*][1,2,4]triazolo[4,3-*a*]pyrimidin-5(4*H*)-one (11)

A mixture of **3** (1.4 g, 4.3 mmol), KOH (0.42 g, 7.5 mmol) and CS_2 (4.5 mL, 7.5 mmol) in absolute ethanol (70 mL) was heated under reflux for 25 h. The solvent was evaporated under reduced pressure. The obtained residue was dissolved in H_2O (20 mL) followed by acidification with dilute HCl (1 mL). The precipitated product was collected by filtration, dried and crystallized from methanol.

Yield: 50%; mp: 274–276 °C; IR (KBr, cm^{-1}): 3446 (NH), 3182, 3134 (CH aromatic), 2947, 2852 (CH aliphatic), 1662 (C=O), 1618 (C=N), 1585, 1516, 1489 (C=C aromatic), 1159 (C=S); ^{1}H-NMR (DMSO-d_6) δ: 1.77–1.82 (m, 4H, 2 × CH_2 at C-7, C-8), 2.77–2.80 (m, 2H, CH_2 at C-6), 2.89–2.92 (m, 2H, CH_2 at C-9), 5.14 (s, 2H, N$\underline{CH_2}C_6H_5$), 7.26–7.38 (m, 5H, Ar-H), 14.06 (s, 1H, SH, D_2O exchangeable); EI-MS *m/z* 368 (M^+, 30.43), 91 ($[C_7H_7]^+$, 100%); Anal. Calcd for $C_{18}H_{16}N_4OS_2$ (368.48): C, 58.67; H, 4.38; N, 15.21. Found: C, 58.92; H, 4.41; N, 15.42.

2. 1. 11. General procedure for the alkylation of the thienotriazolopyrimidine 11 yielding 12a,b, 16a–d, 17a–d, 18a–d

A mixture of the triazolo derivative **11** (0.36 g, 1 mmol) and the appropriate alkyl iodide or α- and β-chloroamides (**13a–d, 14a–d, 15a–d**) (1.5 mmol) in the presence of anhydrous sodium acetate (5 mmol) in absolute ethanol (70 mL) was heated under reflux till TLC indicated completion of the reaction. The product precipitated was collected by filtration, dried and crystallized from the appropriate solvent.

4-Benzyl-1-methylsulphanyl-6,7,8,9-tetrahydro[1]benzothieno[3,2-*e*][1,2,4]triazolo[4,3-*a*]pyrimidin-5(4*H*)-one (12a). Reaction time: 12 h, crystallized from ethanol, yield: 43%; mp: 246–248 °C; IR (KBr, cm^{-1}): 2916, 2846 (CH aliphatic), 1674 (C=O), 1585, 1546, 1508 (C=C aromatic); ^{1}H-NMR (DMSO-d_6) δ: 1.76–1.83 (m, 4H, 2 × CH_2 at C-7, C-8), 2.62 (s, 3H, CH_3), 2.79–2.80 (m, 2H, CH_2 at C-6), 2.92–2.93 (m, 2H, CH_2 at C-9), 5.31 (s, 2H, N$\underline{CH_2}C_6H_5$), 7.24–7.42 (m, 5H, Ar-H); EI-MS *m/z* 382 (M^+, 24.5), 91 ($[C_7H_7]^+$, 81.15%); Anal. Calcd for $C_{19}H_{18}N_4OS_2$ (382.5): C, 59.66; H, 4.74; N, 14.65. Found: C, 59.89; H, 4.79; N, 14.91.

4-Benzyl-1-ethylsulphanyl-6,7,8,9-tetrahydro[1]benzothieno[3,2-*e*][1,2,4]triazolo[4,3-*a*]pyrimidin-5(4*H*)-one (12b). Reaction time: 15 h, crystallized from ethanol, yield: 46%; mp: 210–212 °C; IR (KBr, cm^{-1}): 2935, 2854 (CH aliphatic), 1670 (C=O), 1585, 1550, 1508 (C=C aromatic); ^{1}H-NMR (DMSO-d_6) δ: 1.27 (t, 3H, CH_3), 1.75–1.82 (m, 4H, 2 × CH_2 at C-7, C-8), 2.77–2.81 (m, 2H, CH_2 at C-6), 2.90–2.94 (m, 2H, CH_2 at C-9), 3.05 (q, 2H, $\underline{CH_2}$-CH_3), 5.31 (s, 2H, N$\underline{CH_2}C_6H_5$), 7.26–7.43 (m, 5H, Ar-H); EI-MS *m/z* 396 (M^+, 39.74), 91 ($[C_7H_7]^+$, 100%); Anal. Calcd for $C_{20}H_{20}N_4OS_2$ (396.53): C, 60.58; H, 5.08; N, 14.13. Found: C, 60.85; H, 5.14; N, 14.28.

***N*-(4-chlorophenyl)-2-[(4-benzyl-6,7,8,9-tetrahydro-5-oxo-4,5-dihydro[1]benzothieno[3,2-*e*][1,2,4]triazolo[4,3-*a*]pyrimidin-1-yl)sulfanyl]acetamide (16a).** Reaction time: 9.30 h, crystallized from ethyl acetate/ethanol, yield: 57%; mp: 238–240 °C; IR (KBr, cm^{-1}): 3259 (NH), 3190, 3064 (CH aromatic), 2941, 2858 (CH aliphatic), 1685 (br. 2 × C=O), 1591, 1548, 1506 (C=C aromatic); ^{1}H-NMR (DMSO-d_6) δ: 1.76–1.80 (m, 4H, 2 × CH_2 at C-7, C-8), 2.65–2.70 (m, 2H, CH_2 at C-6), 2.88–2.90 (m, 2H, CH_2 at C-9), 3.84 (s, 2H, S$\underline{CH_2}$), 5.32 (s, 2H, N$\underline{CH_2}C_6H_5$), 7.28–7.42 (m, 9H, Ar-H), 10.15 (s, 1H, NH,

D_2O exchangeable); EI-MS *m/z* 537 (M+2, 11.44), 535 (M^+, 25.2), 91 ($[C_7H_7]^+$, 100%); Anal. Calcd for $C_{26}H_{22}ClN_5O_2S_2$ (536.07): C, 58.25; H, 4.14; N, 13.06. Found: C, 58.44; H, 4.11; N, 13.21.

4-Benzyl-1-{[2-morpholino-2-oxoethyl]sulphanyl}-6,7,8,9-tetrahydro[1]benzothieno[3,2-*e*][1,2,4]triazolo[4,3-*a*]pyrimidin-5(4*H*)-one (16b). Reaction time: 5.30 h, crystallized from acetonitrile, yield: 73%; mp: 256–258 °C; IR (KBr, cm^{-1}): 3020, 3000 (CH aromatic), 2966, 2870 (CH aliphatic), 1670, 1633 (2 × C=O), 1585, 1550, 1508 (C=C aromatic); ^{1}H-NMR (DMSO-d_6) δ: 1.78–1.80 (m, 4H, 2 × CH_2 at C-7, C-8), 2.79–2.81 (m, 2H, CH_2 at C-6), 2.92–2.98 (m, 2H, CH_2 at C-9), 3.39 (t, *J* = 9.9 Hz, 4H, CH_2-N), 3.53 (t, *J* = 9.9 Hz, 4H, CH_2-O), 4.18 (s, 2H, S$\underline{CH_2}$), 5.32 (s, 2H, N$\underline{CH_2}C_6H_5$), 7.26–7.42 (m, 5H, Ar-H); EI-MS *m/z* 495 (M^+, 5.25), 91 ($[C_7H_7]^+$, 100%); Anal. Calcd for $C_{24}H_{25}N_5O_3S_2$ (495.62): C, 58.16; H, 5.08; N, 14.13. Found: C, 58.42; H, 5.17; N, 14.29.

4-Benzyl-1-{[2-(4-phenylpiperazin-1-yl)-2-oxoethyl]sulphanyl}-6,7,8,9-tetrahydro[1]benzothieno[3,2-*e*][1,2,4]triazolo[4,3-*a*]pyrimidin-5(4*H*)-one (16c). Reaction time: 5.30 h, crystallized from acetonitrile, yield: 65%; mp: 224–226 °C; IR (KBr, cm^{-1}): 3040, 3000 (CH aromatic), 2918, 2812 (CH aliphatic), 1672, 1635 (C=O), 1585, 1550, 1508 (C=C aromatic); ^{1}H-NMR (DMSO-d_6) δ: 1.78–1.81 (m, 4H, 2 × CH_2 at C-7, C-8), 2.76–2.80 (m, 2H, CH_2 at C-6), 2.91–2.98 (m, 2H, CH_2 at C-9), 3.09–3.14 (m, 4H, 2 × CH_2 piperazine), 3.55–3.60 (m, 4H, 2 × CH_2 piperazine), 4.23 (s, 2H, S$\underline{CH_2}$), 5.32 (s, 2H, N$\underline{CH_2}C_6H_5$), 6.80–7.42 (m, 10H, Ar-H); EI-MS *m/z* 570 (M^+, 1.19), 91 ($[C_7H_7]^+$, 100%); Anal. Calcd for $C_{30}H_{30}N_6O_2S_2$ (570.73): C, 63.13; H, 5.30; N, 14.73. Found: C, 63.40; H, 5.36; N, 14.89.

4-Benzyl-1-{[2-[4-(4-methoxyphenyl)piperazin-1-yl]-2-oxoethyl]sulphanyl}-6,7,8,9-tetrahydro[1]benzothieno[3,2-*e*][1,2,4]triazolo[4,3-*a*]pyrimidin-5(4*H*)-one (16d). Reaction time: 6.30 h, crystallized from ethyl acetate, yield: 83%; mp: 230–232 °C; IR (KBr, cm^{-1}): 3040, 3000 (CH aromatic), 2941, 2818 (CH aliphatic), 1672, 1635 (2 × C=O), 1585, 1548, 1510 (C=C aromatic); ^{1}H-NMR (DMSO-d_6) δ: 1.77–1.79 (m, 4H, 2 × CH_2 at C-7, C-8), 2.76–2.80 (m, 2H, CH_2 at C-6), 2.91–2.99 (m, 6H, CH_2 at C-9 and 2 × CH_2 piperazine), 3.53–3.59 (m, 4H, 2 × CH_2 piperazine), 3.68 (s, 3H, OCH_3), 4.22 (s, 2H, S$\underline{CH_2}$), 5.32 (s, 2H, N$\underline{CH_2}C_6H_5$), 6.80–7.42 (m, 9H, Ar-H); EI-MS *m/z* 600 (M^+, 2.79), 232 (M–$C_{18}H_{16}N_4OS_2$, 100%); Anal. Calcd for $C_{31}H_{32}N_6O_3S_2$ (600.76): C, 61.98; H, 5.37; N, 13.99. Found: C, 62.17; H, 5.46; N, 14.12.

***N*-(4-chlorophenyl)-2-methyl-2-[(4-benzyl-6,7,8,9-tetrahydro-5-oxo-4,5-dihydro[1]benzothieno[3,2-*e*][1,2,4]triazolo[4,3-*a*]pyrimidin-1-yl)sulphanyl]acetamide (17a).** Reaction time: 9.30 h, crystallized from chloroform, yield: 60%; mp: 264–266 °C; IR (KBr, cm^{-1}): 3305, 3261, 3194 (NH), 3066 (CH aromatic), 2945, 2858 (CH aliphatic), 1681 (br. 2 × C=O), 1610, 1589, 1548 (C=C aromatic); ^{1}H-NMR (DMSO-d_6) δ: 1.48 (d, *J* = 6.6 Hz, 3H, CH_3), 1.71–1.79 (m, 4H, 2 × CH_2 at C-7, C-8), 2.60–2.62 (m, 2H, CH_2 at C-6), 2.83–2.85 (m, 2H, CH_2 at C-9), 4.16 (q, *J* = 6.6 Hz, 1H, CH), 5.34 (s, 2H, N$\underline{CH_2}C_6H_5$), 7.23–7.42 (m, 9H, Ar-H), 10.03 (s, 1H, NH, D_2O exchangeable); ^{13}C-NMR (DMSO-d_6) δ: 17.09, 21.43, 22.14, 23.8, 24.68, 44.89, 47.15, 117.43, 120.46, 126.83, 127.44, 127.84, 128.23, 128.31, 131.1, 131.97, 135.97, 137.67, 137.98, 138.53, 149.62, 155.47, 168.49; EI-MS *m/z* 551(M+2, 14.86), 549 (M^+, 19.21), 91 ($[C_7H_7]^+$, 100%); Anal. Calcd for $C_{27}H_{24}ClN_5O_2S_2$ (550.10): C, 58.95; H, 4.40; N, 12.73. Found: C, 59.17; H, 4.48; N, 12.85.

4-Benzyl-1-{[2-morpholino-1-methyl-2-oxoethyl]sulphanyl}-6,7,8,9-tetrahydro[1]benzothieno[3,2-*e*][1,2,4]triazolo[4,3-*a*]pyrimidin-5(4*H*)-one (17b). Reaction time: 5 h, crystallized from ethyl acetate, yield: 65%; mp: 260–262 °C; IR (KBr, cm^{-1}): 2943, 2860 (CH aliphatic), 1670, 1635 (2 × C=O), 1587, 1550, 1508 (C=C aromatic); ^{1}H-NMR (DMSO-d_6) δ: 1.45 (d, *J* = 6 Hz, 3H, CH_3), 1.80–1.85 (m, 4H, 2 × CH_2 at C-7, C-8), 2.78–2.79 (m, 2H, CH_2 at C-6), 2.91–2.95 (m, 2H, CH_2 at C-9), 3.46 (t, *J* = 11 Hz, 4H, CH_2-N), 3.52 (t, *J* = 11 Hz, 4H, CH_2-O), 4.56 (q, *J* = 6 Hz, 1H, CH), 5.33 (s, 2H, N$\underline{CH_2}C_6H_5$), 7.26–7.43 (m, 5H, Ar-H); EI-MS *m/z* 509 (M^+, 2.41), 91 ($[C_7H_7]^+$, 100%); Anal. Calcd for $C_{25}H_{27}N_5O_3S_2$ (509.65): C, 58.92; H, 5.34; N, 13.74. Found: C, 59.13; H, 5.41; N, 13.87.

4-Benzyl-1-{[2-(4-phenylpiperazin-1-yl)-1-methyl-2-oxoethyl]sulphanyl}-6,7,8,9-tetrahydro[1]benzothieno[3,2-*e*][1,2,4]triazolo[4,3-*a*]pyrimidin-5(4*H*)-one (17c). Reaction time: 7 h, crystallized from acetonitrile, yield: 63%; mp: 240–242 °C; IR (KBr, cm^{-1}): 3020, 3000 (CH aromatic), 2931, 2820 (CH aliphatic), 1670, 1629 (2 × C=O), 1598, 1583, 1548 (C=C aromatic); ^{1}H-NMR (DMSO-d_6) δ: 1.48 (d, *J* = 6.6 Hz, 3H, CH_3), 1.73–1.78 (m, 4H, 2 × CH_2 at C-7, C-8), 2.89–2.92 (m, 2H, CH_2 at C-6), 3.02–3.08 (m, 2H, CH_2 at C-9), 3.14–3.20 (m, 4H, 2 × CH_2 piperazine), 3.59–3.70 (m, 4H, 2 × CH_2 piperazine), 4.61 (q, *J* = 6.6 Hz, 1H, CH), 5.33 (s, 2H, N$\underline{CH_2}C_6H_5$), 6.78–7.43 (m, 10H, Ar-H); EI-MS *m/z* 584 (M^+, 2.10), 216 (M–$C_{18}H_{16}N_4OS_2$, 100), 91 ($[C_7H_7]^+$, 72.31%); Anal. Calcd for $C_{31}H_{32}N_6O_2S_2$ (584.76): C, 63.67; H, 5.52; N, 14.37. Found: C, 63.81; H, 5.58; N, 14.59.

4-Benzyl-1-{[2-[4-(4-methoxyphenyl)piperazin-1-yl]-1-methyl-2-oxoethyl]sulphanyl}6,7,8,9-tetrahydro[1]benzothieno[3,2-*e*][1,2,4]triazolo[4,3-*a*]pyrimidin-5(4*H*)-one (17d). Reaction time: 7 h, crystallized from acetonitrile, yield: 83%; mp: 236–238 °C; IR (KBr, cm^{-1}):

2933, 2816 (CH aliphatic), 1670, 1629 (2 × C=O), 1585, 1548, 1510 (C=C aromatic); ^{1}H-NMR (DMSO-d_6) δ: 1.47 (d, J = 7.2 Hz, 3H, CH_3), 1.74–1.79 (m, 4H, 2 × CH_2 at C-7, C-8), 2.65–2.67 (m, 4H, 2 × CH_2 piperazine), 2.89–2.91 (m, 2H, CH_2 at C-6), 2.97–3.01 (m, 2H, CH_2 at C-9), 3.49–3.58 (m, 4H, 2 × CH_2 piperazine), 3.68 (s, 3H, OCH_3), 4.60 (q, J = 7.2 Hz, 1H, CH), 5.33 (s, 2H, N$\underline{CH_2}$C$_6$H$_5$), 6.80–7.43 (m, 9H, Ar-H); ^{13}C-NMR (DMSO-d_6) δ: 19.35, 21.45, 22.18, 23.96, 24.78, 38.66, 45.27, 49.60, 50.04, 55.14, 114.22, 117.0, 120.50, 127.45, 127.95, 128.31, 131.50, 131.88, 135.97, 138.0, 144.86, 149.0, 153.28, 155.56, 168.54; EI-MS *m/z* 614 (M^+, 2.22), 246 (M–$C_{18}H_{16}N_4OS_2$, 100), 91 ($[C_7H_7]^+$, 48.71%); Anal. Calcd for $C_{32}H_{34}N_6O_3S_2$ (614.78): C, 62.52; H, 5.57; N, 13.67. Found: C, 62.74; H, 5.66; N, 13.89.

***N*-(4-chlorophenyl)-3-[(4-benzyl-6,7,8,9-tetrahydro-5-oxo-4,5-dihydro[1]benzothieno[3,2-*e*][1,2,4]triazolo[4,3-*a*]pyrimidin-1-yl)sulphanyl]propanamide (18a).** Reaction time: 34 h, crystallized from chloroform, yield: 68%; mp: 228–230 °C; IR (KBr, cm^{-1}): 3309, 3275 (NH), 3100, 3000 (CH aromatic), 2931, 2840 (CH aliphatic), 1681 (br. 2 × C=O), 1589, 1546 (C=C aromatic); ^{1}H-NMR (DMSO-d_6) δ: 1.74–1.79 (m, 4H, 2 × CH_2 at C-7, C-8), 2.62–2.65 (m, 2H, CH_2 at C-6), 2.72 (t, J = 15 Hz, 2H, $\underline{CH_2}$-CH_2S), 2.83–2.85 (m, 2H, CH_2 at C-9), 3.31(t, J = 15 Hz, 2H, CH_2-$\underline{CH_2}$S), 5.30 (s, 2H, N$\underline{CH_2}$C$_6$H$_5$), 7.22–7.45 (m, 9H, Ar-H), 9.99 (s, 1H, NH, D_2O exchangeable); EI-MS *m/z* 551.8 (M+2, 0.65), 549.8 (M^+, 1.27), 91 ($[C_7H_7]^+$, 100%); Anal. Calcd for $C_{27}H_{24}ClN_5O_2S_2$ (550.10): C, 58.95; H, 4.40; N, 12.73. Found: C, 59.12; H, 4.47; N, 12.91.

4-Benzyl-1-{[2-morpholino-3-oxopropyl]sulphanyl}-6,7,8,9-tetrahydro[1]benzothieno[3,2-*e*][1,2,4]triazolo[4,3-*a*]pyrimidin-5(4*H*)-one (18b). Reaction time: 30 h, crystallized from chloroform, yield: 51%; mp: 198–200 °C; IR (KBr, cm^{-1}): 2947, 2862 (CH aliphatic), 1674, 1639 (2 × C=O), 1589, 1554, 1508 (C=C aromatic); ^{1}H-NMR (DMSO-d_6) δ: 1.74–1.80 (m, 4H, 2 × CH_2 at C-7, C-8), 2.75–2.77 (m, 2H, CH_2 at C-6), 2.77 (t, J = 12.6 Hz, 2H, $\underline{CH_2}$-CH_2S), 2.91–2.95 (m, 2H, CH_2 at C-9), 3.22 (t, J = 12.6 Hz, 2H, CH_2-$\underline{CH_2}$S), 3.43–3.44 (t, 4H, CH_2-N), 3.49–3.51 (t, 4H, CH_2-O), 5.30 (s, 2H, N$\underline{CH_2}$C$_6$H$_5$), 7.25–7.41 (m, 5H, Ar-H); EI-MS *m/z* 509 (M^+, 0.30), 91 ($[C_7H_7]^+$, 100%); Anal. Calcd for $C_{25}H_{27}N_5O_3S_2$ (509.65): C, 58.92; H, 5.34; N, 13.74. Found: C, 59.21; H, 5.36; N, 13.89.

4-Benzyl-1-{[3-(4-phenylpiperazin-1-yl)-3-oxopropyl]sulphanyl}-6,7,8,9-tetrahydro[1]benzothieno[3,2-*e*][1,2,4]triazolo[4,3-*a*]pyrimidin-5(4*H*)-one (18c). Reaction time: 26 h, crystallized from acetonitrile, yield: 40%; mp: 214–216 °C; IR (KBr, cm^{-1}): 2937, 2852 (CH aliphatic), 1676, 1643 (2 × C=O), 1585, 1552, 1508 (C=C aromatic); ^{1}H-NMR (DMSO-d_6) δ: 1.70–1.71 (m, 4H, 2 × CH_2 at C-7, C-8), 2.70–2.81 (m, 4H, CH_2 piperazine), 2.84 (t, J = 6 Hz, 2H, $\underline{CH_2}$-CH_2S), 2.97–2.99 (m, 2H, CH_2 at C-6), 3.04–3.12 (m, 2H, CH_2 at C-9), 3.23 (t, J = 6 Hz, 2H, CH_2-$\underline{CH_2}$S), 3.46–3.50 (m, 4H, CH_2 piperazine), 5.30 (s, 2H, N$\underline{CH_2}$C$_6$H$_5$), 6.79–7.42 (m, 10H, Ar-H); ^{13}C-NMR (DMSO-d_6) δ: 21.39, 22.16, 23.98, 24.79, 31.18, 32.72, 44.83, 47.98, 48.35, 115.63, 119.17, 120.50, 127.37, 127.78, 128.26, 128.88, 131.60, 131.71, 136.02, 138.0, 140.66, 148.0, 150.60, 155.58, 168.22; EI-MS *m/z* 584 (M^+, 4.13), 91 ($[C_7H_7]^+$, 100%); Anal. Calcd for $C_{31}H_{32}N_6O_2S_2$ (584.76): C, 63.67; H, 5.52; N, 14.37. Found: C, 63.84; H, 5.63; N, 14.61.

4-Benzyl-1-{[3-[4-(4-methoxyphenyl)piperazin-1-yl]-3-oxopropyl]sulphanyl}-6,7,8,9-tetrahydro[1]benzothieno[3,2-*e*][1,2,4]triazolo[4,3-*a*]pyrimidin-5(4*H*)-one (18d). Reaction time: 29 h, crystallized from chloroform, yield: 42%; mp: 222–224 °C; IR (KBr, cm^{-1}): 3055, 3001 (CH aromatic), 2949, 2833 (CH aliphatic), 1674, 1641 (2 × C=O), 1587, 1554, 1510 (C=C aromatic); ^{1}H-NMR (DMSO-d_6) δ: 1.71–1.73 (m, 4H, 2 × CH_2 at C-7, C-8), 2.71–2.78 (m, 4H, 2 × CH_2 piperazine), 2.80 (t, J = 6.6 Hz, 2H, $\underline{CH_2}$-CH_2S), 2.83–2.92 (m, 4H, 2 × CH_2 at C-6 and C-9), 3.25 (t, J = 6.6 Hz, 2H, CH_2-$\underline{CH_2}$S), 3.45–3.55 (m, 4H, 2 × CH_2 piperazine), 3.68 (s, 3H, OCH_3), 5.31 (s, 2H, N$\underline{CH_2}$C$_6$H$_5$), 6.79–7.42 (m, 9H, Ar-H); EI-MS *m/z* 616 (M+2, 0.95), 614 (M^+, 4.66), 91 ($[C_7H_7]^+$, 100%); Anal. Calcd for $C_{32}H_{34}N_6O_3S_2$ (614.78): C, 62.52; H, 5.57; N, 13.67. Found: C, 62.70; H, 5.54; N, 13.84.

2. 2. In vitro Anticancer Screening

2. 2. 1. Materials and Methods

The prostate tumor cell line (PC-3) and the colon tumor cell line (HCT-116) were obtained frozen in liquid nitrogen (–180 °C) from the American Type Culture Collection (ATCC) and were maintained in the National Cancer Institute, Cairo, Egypt, by serial sub-culturing. All chemicals used in this study were of high analytical grade. They were obtained from either Sigma-Aldrich or Bio-Rad.

2. 2. 2. Measurement of Potential Cytotoxicity

The cytotoxic activity of some selected compounds was measured *in vitro* against human prostate cancer cell line (PC-3) and colon cancer cell line (HCT-116) at five different doses (0, 5.0, 12.5, 25.0 and 50.0 μg/mL). The screening was carried out at the Pharmacology Unit, Cancer Biology Department, National Cancer Institute, Cairo University using Sulforhodamine-B (SRB) assay, applying the method of Skehan *et al.*[41] as follows.

Cells were plated in 96 multi-well plate (104 cells/well) for 24 h before treatment with the tested compound to allow attachment to the wall of the plate. Different concentrations of the compounds (0, 5.0, 12.5, 25.0 and 50.0 μg/mL) were added to the cell monolayer in tri-

plicate and wells were prepared for each individual dose. Monolayer cells were incubated with the compounds for 48 h at 37 °C in atmosphere of 5% CO_2. After 48 h, cells were fixed, washed and stained with Sulforhodamine-B stain. Excess stain was washed with acetic acid and the attached stain was recovered with Tris EDTA buffer. Color intensity was measured in an ELISA reader. The relation between surviving fraction and drug concentration was plotted to get the survival curve of each tumor cell line. IC_{50} values (the concentration required for 50% inhibition of cell viability) were calculated using sigmodial dose response curve-fitting models (GraphPad, Prizm software incorporated), each concentration was repeated three times. The results are given in Table 1 and represented graphically in Fig. 3.

3. Results and Discussion

3. 1. Chemistry

The synthetic strategies adopted for the synthesis of the intermediate and final compounds are illustrated in Schemes 1 and 2. In Scheme 1, the starting compound ethyl 2-amino-4,5,6,7-tetrahydro[1]benzothiophene-3-carboxylate (**1**) was prepared according to the well-known Gewald procedure.[32] Reacting **1** with benzyl isothiocyanate in acetonitrile afforded the corresponding 3-benzyl-2-sulfanylthienopyrimidine derivative **2**. The **2** formed was treated with 99% hydrazine hydrate in dry pyridine to give the 2-hydrazino derivative **3**. Structural elucidation of **3** was based on IR and ^{1}H-NMR spectroscopy. Reacting the key intermediate **3** with formic acid or acetic acid induced cyclization to the corresponding triazolo derivatives **4a** and **4b**. IR and ^{1}H-NMR spectra confirmed the cyclization through the disappearance of NH and NH_2 signals. The presence of a signal at δ 12.07 ppm in ^{13}C-NMR verified the presence of the CH_3 group in **4b**. Compound **5** was obtained upon treatment of **3** with chloroacetyl chloride in dry DMF. The notable feature in the ^{1}H-NMR spectrum was the appearance of a singlet peak at δ 5.18 ppm indicating CH_2Cl group. The successful formation of the intermediate **5** prompted us to investigate the nucleophilic replacement of the active chlorine atom with different amines. Compound **5** underwent nucleophilic substitution with various substituted piperazines to afford **6a–d**. The ^{1}H-NMR spectra of the products **6a–d** showed the appearance of the protons of the piperazine moiety in the range of δ 2.43–3.19 ppm. Moreover, a singlet signal at δ 3.94–3.96 ppm characteristic to the CH_2 linking the triazole ring and the piperazine ring confirmed the successful incorporation of piperazine moieties.

Compound **7** was obtained in good yield by heating the key intermediate **3** with *N,N*-carbonyldiimidazole in dry benzene. IR spectrum of **7** showed absorption bands at ν 1720 and 1632 cm^{-1} indicating the presence of two C=O groups of the triazole ring and the pyrimidinone ring, respectively. Furthermore, the ^{1}H-NMR spectrum displayed an exchangeable singlet signal at δ 12.0 ppm corresponding to the NH proton of the triazole ring. ^{13}C-NMR spectrum of **7** showed two signals at δ 149.17 and 156.63 ppm confirming the presence of two carbonyl moieties. Furthermore, the reaction of **3** with various isothiocyanates yielded the corresponding 1-substituted aminotriazolo derivatives **8a–e**. ^{1}H-NMR spectra of **8a–e** showed D_2O exchangeable signals in the range of δ 9.29–9.39 ppm assignable to the NH.

On the other hand, reacting **3** with diethyl malonate in acetic acid afforded the unexpected product 1-methyltriazolo derivative **4b**. The formation of **4b** may be explained by the hydrolysis and decarboxylation of the ester group in the intermediate compound **9** in acidic medium. However, the direct interaction of **3** with excess diethyl malonate in the absence of solvent at the refluxing temperature afforded the expected product **9**. The IR spectrum showed the presence of two C=O moieties at ν 1740 and 1666 cm^{-1} while the ^{1}H-NMR spectrum confirmed the presence of the ethyl ester group. Further evidence was obtained from the ^{13}C-NMR spectrum of **9** which confirmed the presence of ethyl ester group through signals at δ 14.45 and 62.0 ppm in addition to a signal at δ 32.31 ppm corresponding to the $–CH_2–$ flanked between the thienopyrimidin-2-ylsulphanyl group and carbonyl function. Furthermore, the reaction of **3** with benzoyl chloride and ammonium thiocyanate in dry acetone afforded the benzoyl thiourea derivative **10**. ^{1}H-NMR spectrum of compound **10** showed the presence of three D_2O exchangeable signals assignable to three NH moieties at δ 9.79, 11.71 and 12.49 ppm.

In Scheme 2, the reaction of **3** with carbon disulfide in ethanolic potassium hydroxide followed by acidification with hydrochloric acid yielded the thiol (**11**) / thione (**11a**) tautomers. One of the objectives of this work was to prepare a series of *S*-alkylated triazolopyrimidine derivatives with varying the linker skeleton as well as varying the bioactive amine to test their cytotoxicity.

Herein, a series of alkylated mercapto 1,2,4-triazoles was synthesized via the reaction of the key intermediate **11** with various alkyl halides or α- and β-chloroamides (**13a–d**, **14a–d**, **15a–d)** in absolute ethanol in the presence of anhydrous sodium acetate to afford the corresponding *S*-alkyl derivatives (**12a**,**b**, **16a–d**, **17a–d**, **18a–d**). The success of alkylation was confirmed by the absence of SH or NH signals in ^{1}H-NMR spectra of **12a** and **12b** together with the appearance of peaks characteristic to methyl and ethyl moieties in each compound, respectively. Moreover, the mass spectrum of **12a**,**b** showed their corresponding molecular ion peaks at *m/z* 382 and 396, respectively.

The structure of the mercapto alkylated derivatives **16a–d**, **17a–d** and **18a–d** linked to different secondary amines with different linkages was supported by elemental analyses and spectral data. IR spectra of all target

compounds indicated the appearance of new amide C=O absorption band at ν 1629–1643 cm^{-1}. Moreover, ^{1}H-NMR spectra of compounds **16a–d**, **17a–d** and **18a–d** showed the disappearance of the SH signal at δ 14.06 ppm. Besides, the alkyl protons in the linker between the triazolopyrimidine ring and the amine appeared as follows;

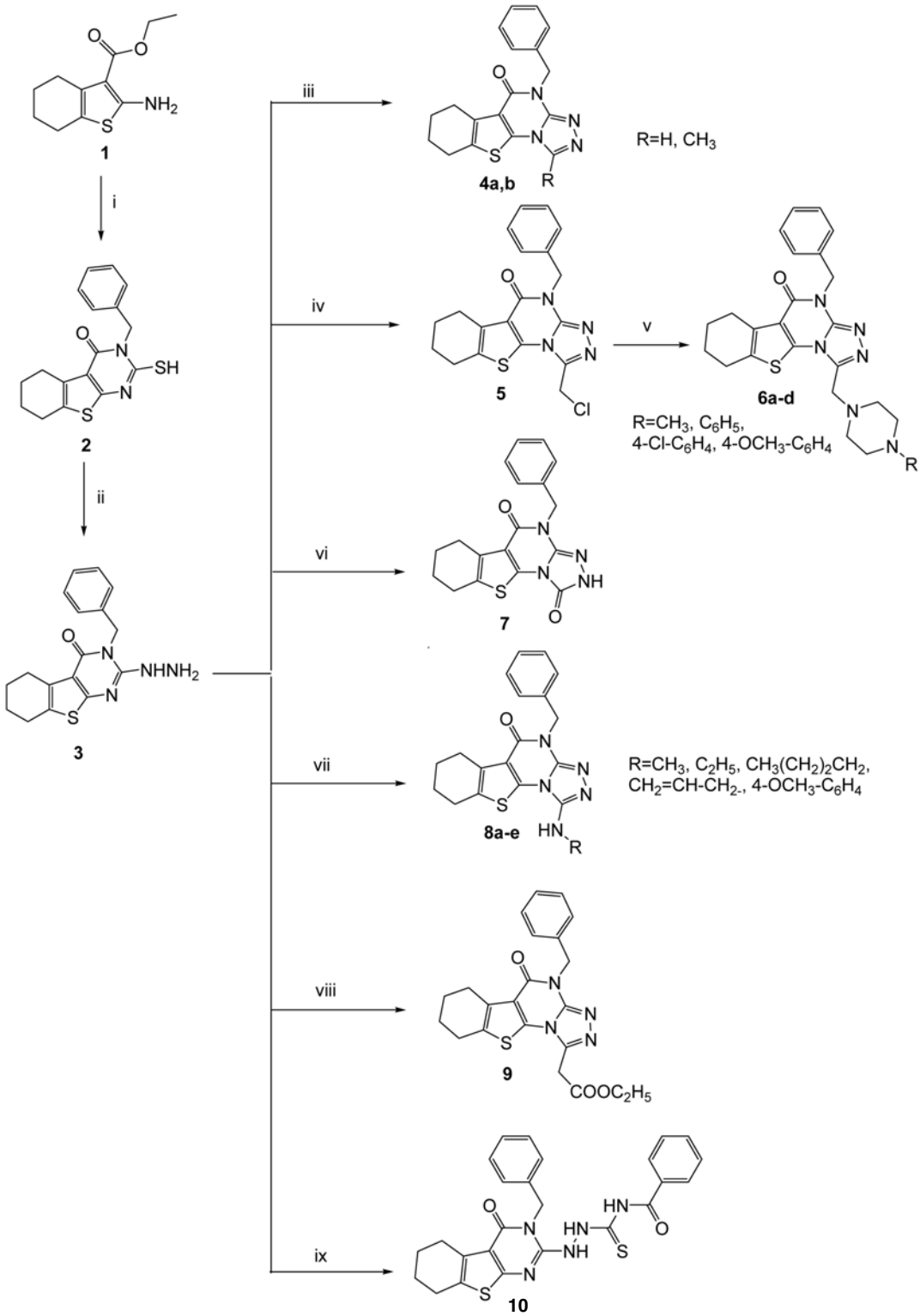

Scheme 1. Synthesis of triazolo derivatives **4a**,**b**, **5**, **6a–d**, **7**, **8a–d**, **9** and **10**: (i) $PhCH_2NCS$ / K_2CO_3 / acetonitrile, followed by acidification; (ii) NH_2–NH_2·H_2O / pyridine, reflux; (iii) RCOOH, reflux; (iv) $ClCH_2COCl$ / DMF, 100 °C; (v) piperazines / EtOH, reflux; (vi) CDI / benzene, reflux; (vii) RNCS / EtOH, reflux; (viii) diethyl malonate, reflux; (ix) benzoyl chloride / NH_4SCN / acetone, reflux.

^{1}H-NMR spectra of **16a–d** showed a characteristic singlet in the range of δ 3.84–4.23 ppm assigned for SCH_2 protons, while the spectra of **17a–d** revealed doublet signals in the range of δ 1.44–1.51 ppm assignable to CH_3 moiety and quartet signals assignable to CH protons in the range of δ 3.93–4.61 ppm. The presence of ethylene fragment (CH_2–CH_2) in compounds **18a–d** was revealed by two triplet signals in the range of δ 2.72–2.87 ppm and δ 3.20–3.40 ppm in ^{1}H-NMR spectra. Further proof for these compounds was obtained using ^{13}C-NMR spectroscopy where the spectrum of compound **18c** showed signals at δ 31.18 and 32.72 ppm assignable to the SCH_2 and

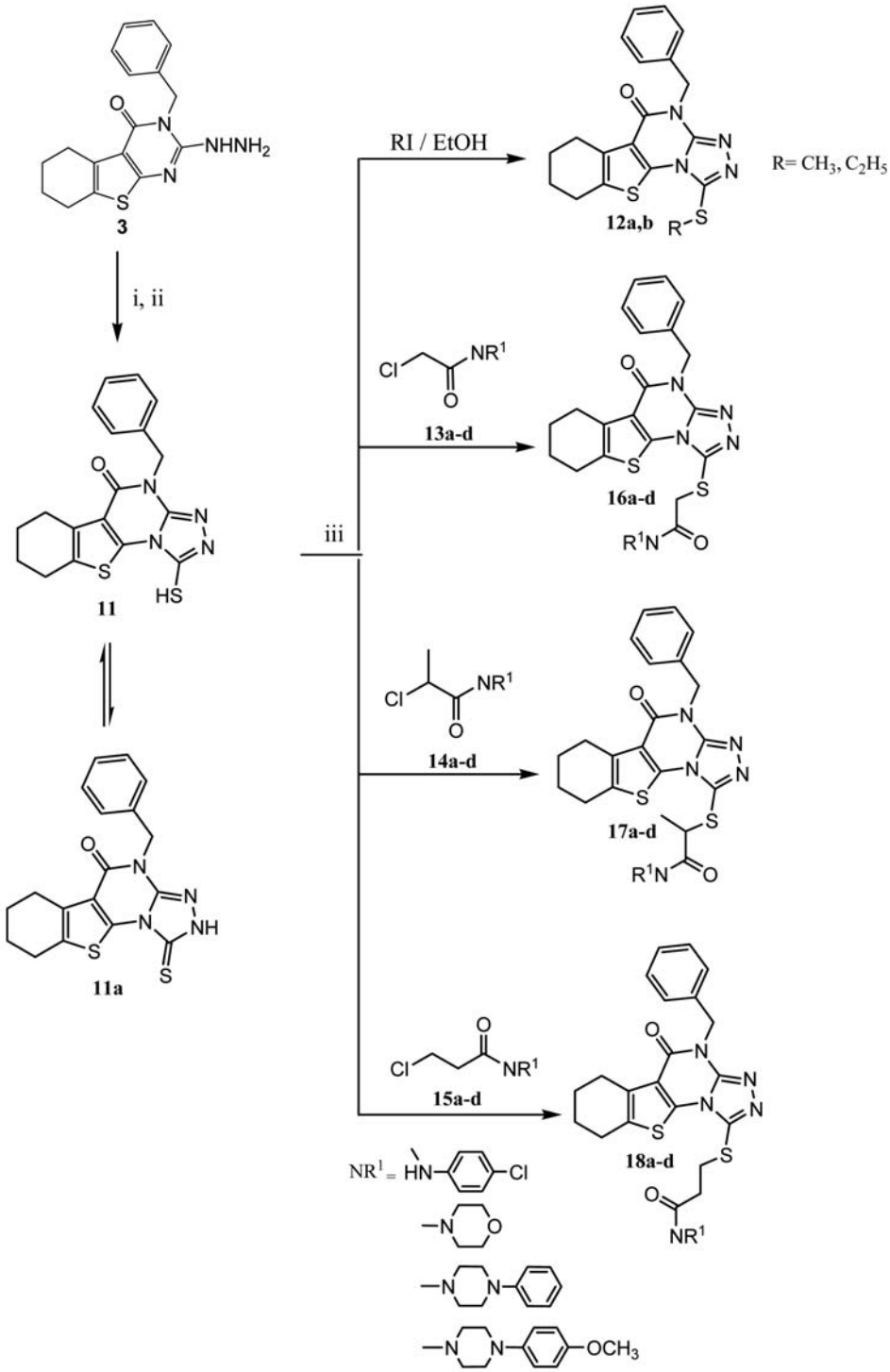

Scheme 2. Synthesis of triazolo derivatives **11**, **12a**,**b**, **16a–d**, **17a–d**, **18a–d**: (i) CS_2 / KOH / EtOH, reflux; (ii) diluted HCl; (iii) anhydrous sodium acetate / EtOH, reflux.

CH_2–CO moieties, respectively. In addition, ^{1}H-NMR spectra of all the target products **16a–d**, **17a–d** and **18a–d** displayed the expected signals of the morpholino, 4-chloroanilino and substituted piperazine moieties.

3. 2. In vitro Cytotoxicity

The *in vitro* cytotoxic activity of 24 selected compounds was evaluated against two human cancer cell lines including cells derived from human prostate cancer (PC-3) and human colon cancer (HCT-116) according to the standard protocol for IC_{50} determination. Doxorubicin (DOX), being one of the most effective anticancer agents, was chosen as the reference standard anticancer drug.[42] The IC_{50} values in μM are listed in Table 1 and the results are represented graphically in Fig. 3.

From the results in Table 1 it is evident that most of the tested compounds displayed moderate to potent cancer cell growth inhibition. Generally, all the tested compounds tended to be more active against HCT-116 than against PC-3. Examining the IC_{50} of the tested compounds against PC-3 cell line revealed that compounds **10**, **12b**, **17b** and **18c** exhibited significant anticancer activities with lower IC_{50} values compared to DOX, with compound **16c** being the most potent with an IC_{50} of 5.48 μM. Meanwhile, compound **12a** showed equipotent activity to DOX, while compounds **6a**, **6c**, **8a**, **17c** and **18a** exhibited IC_{50} values (ranging from 8.25–8.97 μM) very close to DOX (IC_{50} = 7.7 μM) against PC-3. As for the HCT-116 cell line, compounds **6c** and **18c** were the most active (IC_{50} = 6.56 and 6.12 μM, respectively) in contrast to 15.82 μM for the standard on the same cell line. In addition, compounds **4a**, **5**, **6a**, **8a**, **8b**, **8d**, **10**, **12b**, **17b**, **17c**, and **18a** displayed more potent cytotoxic activity compared to the standard with IC_{50} values ranging from 7.4 to 14.77 μM.

Table 1. Results of *in vitro* cytotoxic activity of some selected compounds against human prostate cancer cell line (PC-3) and colon cancer cell line (HCT-116). (Results in bold represent compounds with better activity than DOX.)

Compound no.	IC_{50} in μM*	
	PC-3	HCT-116
4a	13.58	**10.64**
4b	11.41	>100
5	10.13	**12.47**
6a	8.91	**14.77**
6c	8.25	**6.56**
7	11.35	29.51
8a	8.97	**12**
8b	15	**11**
8d	10.7	**12**
8e	10.05	17.15
10	**6.53**	**8.86**
11	>100	>100
12a	**7.8**	20.1
12b	**7**	**7.57**
16a	>100	>100
16c	**5.48**	17.52
17a	>100	60.53
17b	**6.4**	**7.63**
17c	8.5	**7.4**
17d	>100	20.33
18a	8.5	**8.18**
18b	16.01	>100
18c	**7.5**	**6.12**
18d	36	27.32
Doxorubicin	7.7	15.82

* The values given are means of three experiments.

Referring to the IC_{50} values listed in Table 1, the following SAR can be deduced: among the triazolo derivatives **4a** and **4b**, the unsubstituted derivative **4a** showed

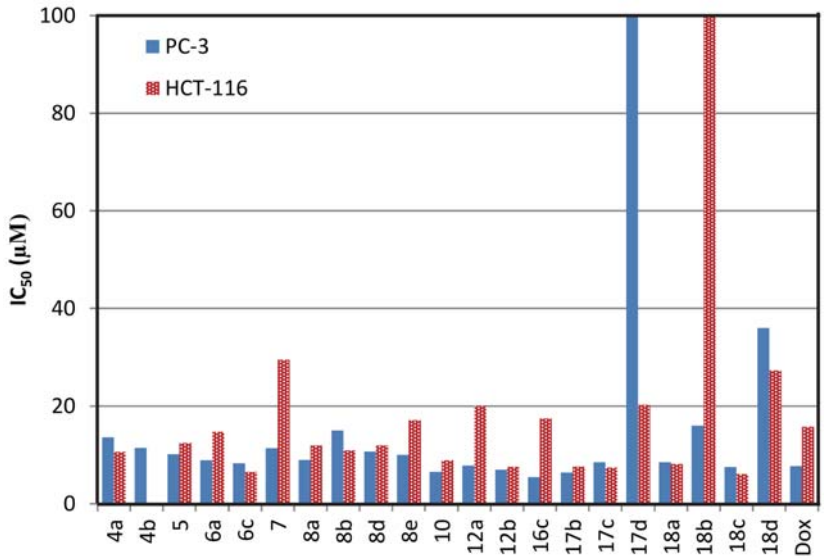

Figure 3. Cytotoxicity of some selected compounds against human prostate cancer cell line (PC-3) and colon cancer cell line (HCT-116)

good activity against HCT-116. Concerning the piperazine derivatives **6a–d**, compounds **6a** and **6c** displayed good activity against both cell lines whereas the 4-chlorophenyl piperazine derivative **6c** showed 2.4 fold higher activity than DOX against HCT-116 cell line in agreement with the reported anticancer activity of derivatives incorporating piperazine scaffolds and halogen atoms.[43,44] Upon analyzing the results of the substituted amino triazoles **8a–e**, compounds **8a**, **8b** and **8d** exhibited higher activity than DOX against HCT-116 but it was difficult to reach conclusions regarding the effect of varying the substituent since the cytotoxicity of **8a–e** was almost the same. The *N*-methyl derivative **8a** was the only potent analogue against PC-3 cell line. Interestingly, compound **10** displayed potent cytotoxic activity against both cell lines in accordance with the reported antitumor activity of thiosemicarbazide derivatives.[45]

Among the 1,2,4-triazole derivatives, the mercapto substituted 1,2,4-triazole ring systems have been studied and so far a variety of antitumor properties have been reported for a large number of these compounds.[25–27] Based on the above findings, we investigated herein in Scheme 2, the structure–activity relationship of *S*-alkylated series of compounds **12a**,**b**, **16a–d**, **17a–d** and **18a–d**, focusing in particular on the effect of the linker skeleton as well as varying the bioactive amine on the cytotoxic activity, the following was observed:

– The incorporation of ethyl substituent in **12b** resulted in a more potent derivative than **12a** against both cell lines.
– Among compounds **16a–d** with CH_2 linker, the 4-phenyl piperazine analogue **16c** showed selective high activity against PC-3.
– The cytotoxic activity of compounds **17a–d** with branched alkyl linker (–$CHCH_3$) showed that the incorporation of morpholine ring (**17b**) and phenyl piperazine moiety (**17c**) resulted in compounds with potent activity against both cell lines.
– The phenyl piperazine derivatives (**16c** and **18c**) afforded better cytotoxic activity compared to other amines against PC-3 and HCT-116, respectively.
–Extending the side chain caused pronounced change in the activity of the 4-chloroaniline derivative **18a** against both cell lines compared to **16a** with acetamide linkage and **17a** with branched linker which were devoid of activity.

4. Conclusion

A series of substituted 4-benzyl[1]benzothieno[3,2-*e*][1,2,4]triazolo[4,3-*a*]pyrimidines was designed, synthesized, and screened for their anticancer activity against PC-3 and HCT-116 cell lines. Many of the newly synthesized compounds showed remarkable activity on the tested cell lines with higher sensitivity towards the HCT-116 cell line. Compounds **10**, **12b**, **17b** and **18c** showed higher cytotoxic activity against both PC-3 and HCT-116 cell lines compared to DOX. Incorporation of a 4-phenylpiperazine moiety resulted in higher activity against both cell lines where compound **16c** was the most active against PC-3 with 1.4 fold higher activity than DOX, while **18c** showed 2.5 fold higher anticancer activity against HCT-116. The obtained results suggest that thienopyrimidines containing 1,2,4-triazole scaffold might be suitable candidates for further chemical modifications in order to obtain more potent and selective anticancer agents.

5. References

1. Global Burden of Disease Cancer Collaboration, *JAMA Oncol*. **2015,** *1*, 505–527. http://dx.doi.org/10.1001/jamaoncol.2015.0735
2. S. Sommerwerk, L. Heller, R. Csuk, *Arch. Pharm. Chem. Life Sci*. **2015**, *348*, 46–54. http://dx.doi.org/10.1002/ardp.201400297
3. K. Kairemo, P. Erba, K. K. Bergstrom, E. K. Pauwels, *J. Curr. Radiopharm*. **2008**, *1*, 30–36. http://dx.doi.org/10.2174/1874471010801010030
4. M. M. Ghorab, M. S. Bashandy, M. S. AlSaid, *Acta Pharm*. **2014**, *64*, 419–431. http://dx.doi.org/ 10.2478/acph-2014-0035
5. R. M. Mohareb, A. E. M. Abdallah, M. H. E. Helal, S. M. H. Shaloof, *Acta Pharm.* **2016**, *66*, 53–68. https://doi.org/10.1515/acph-2016-0005
6. G. Revelant, S. Dunand, S. Hesse, G. Kirsch, *Synthesis*, **2011**, *18*, 2935–2940. http://dx.doi.org/ 10.1055/s-0030-1261032
7. L. Ma, L. Yuan, C. Xu, G. Li, M. Tao, W. Zhang, *Synthesis,* **2013**, *45*, 45–52. http://dx.doi.org/ 10.1055/s-0032-1316821
8. R. M. Mohareb, A. A. Mohamed, A. E. M. Abdallah, *Acta Chim. Slov*. **2016,** *63*, 227–240. http://dx.doi.org/10.17344/acsi.2015.1668
9. V. P. Litvinov, *Russ. Chem. Bull. Int. Ed*., **2004**, *53*, 487–516. http://dx.doi.org/10.1023/B:RUCB.0000035630.75564.2b
10. K. Bozorov, J. Zhao, B. Elmuradov, A. Pataer, *Eur. J. Med. Chem*. **2015**, *102*, 552–573. http://dx.doi.org/10.1016/j.ejmech.2015.08.018
11. A. Ts. Mavrova, D. Wesselinova, J. A. Tsenov, L. A. Lubenov, *Eur. J. Med. Chem*. **2014**, *86*, 676–683. http://dx.doi.org/10.1016/j.ejmech.2014.09.032
12. A. E. Kassab, E. M. Gedawy, *Eur. J. Med. Chem*. **2013**, *63*, 224–230. http://dx.doi.org/10.1016/j.ejmech.2013.02.011
13. M. M. Kandeel, A. A. Mounir, H. M. Refaat, A. E. Kassab, *Int. J. Pharm. Pharm. Sci*. **2012**, *4*, 438–448.
14. H. Li, C. Chen, S. Xu, X. Cao, *J. Chem*. **2013**, *2013*, 1–6. http://dx.doi.org/10.1155/2013/692074
15. H. G. Häcker, A. Haye, K. Sterz, G. Schnakenburg, M. Wiese, M. Gütschow, *Bioorg. Med. Chem. Lett*. **2009**, *19*,

6102–6105. http://dx.doi.org/10.1016/j.bmcl.2009.09.023
16. G. Pochetti, R. Montanari, C. Gege, C. Chevrier, A. G. Taveras, F. Mazza, *J. Med. Chem*. **2009**, *52*, 1040–1049. http://dx.doi.org/10.1021/jm801166j
17. Y. A. Al-Soud, N. A. Al-Masoudi, A. El-Rahman, S. Ferwanah, *Bioorg. Med. Chem*. **2003**, *11*, 1701–1708. http://dx.doi.org/10.1016/S0968-0896(03)00043-9
18. M. M. Kamel, N. Y. M. Abdo, *Eur. J. Med. Chem*. **2014**, *86*, 75–80. http://dx.doi.org/10.1016/j.ejmech.2014.08.047
19. P. Conte, A. Frassoldati, **2007**, *13*, 28–35. http://dx.doi.org/10.1111/j.1524-4741.2006.00359.x
20. K. L. B. Borden, B. Culjkovic-Kraljacic, *Leuk. Lymphoma*. **2010**, *51*, 1805–1815. http://dx.doi.org/10.3109/10428194.2010.496506
21. F. Pettersson, C. Yau, M. C. Dobocan, B. Culjkovic-Kraljacic, H. Retrouvay, R. Puckett, L. M. Flores, I. E. Krop, C. Rousseau, E. Cocolakis, K. L. B. Borden, C. C. Benz, W. H. Miller Jr., *Breast Cancer. Clin. Cancer Res*. **2011**, *17*, 2874–2884. http://dx.doi.org/10.1158/1078-0432.CCR-10-2334
22. B. S. Holla, B. Veerendra, M. K. Shivananda, B. Poojary, *Eur. J. Med. Chem*. **2003**, *38*, 759–767. http://dx.doi.org/10.1016/S0223-5234(03)00128-4
23. A. Duran, H. N. Dogan, S. Rollas, *II Farmaco*. **2002**, *57*, 559–564. http://dx.doi.org/10.1016/S0014-827X(02)01248-X
24. A. Srinivas, *Acta Chim. Slov*. **2016**, *63*, 173–179. https://doi.org/10.17344/acsi.2015.2124
25. T. R. K. Reddy, C. Li, X. Guo, P. M. Fischer, L. V. Dekker, *Bioorg. Med. Chem*. **2014**, *22*, 5378–5391. http://dx.doi.org/10.1016/j.bmc.2014.07.043
26. H. Cai, X. Huang, S. Xu, H. Shen, P. Zhang, Y. Huang, J. Jiang, Y. Sun, B. Jiang, X. Wu, H. Yao, J. Xu, *Eur. J. Med. Chem*. **2016**, *108*, 89–103. http://dx.doi.org/10.1016/j.ejmech.2015.11.013
27. Gel-D. Abuo-Rahma. M. Abdel-Aziz, E. A. Beshr, T. F. Ali, *Eur. J. Med. Chem*. **2014**, *71*, 185–198. http://dx.doi.org/10.1016/j.ejmech.2013.11.006
28. M. M. Kandeel, H. M. Refaat, A. E. Kassab, I. G. Shahin, T. M. Abdelghany, *Eur. J. Med. Chem.* **2015**, *90*, 620–632. http://dx.doi.org/10.1016/j.ejmech.2014.12.009
29. M. A. Shaaban, M. M. Ghorab, H. I. Heiba, M. M. Kamel, N. H. Zaher, M. I. Mostafa, *Arch. Pharm. Chem. Life Sci*. **2010**, *343*, 404–410. http://dx.doi.org/10.1002/ardp.200900150
30. H. I. Heiba, F. A. Ragab, E. Noaman, M. M. Ghorab, M. Galal, *Arzneim-Forsch/Drug Res*. **2006**, *56*, 593–599. http://dx.doi.org/10.1055/s-0031-1296757
31. K. M. Al-Taisan, H. M. A. Al-Hazimi, S. S. Al-Shihry, *Molecules* **2010**, *15*, 3932–3957. http://dx.doi.org/10.3390/molecules15063932
32. K. Gewald, *Chem. Ber*. **1965**, *98(11)*, 3571–3577. http://dx.doi.org/10.1002/cber.19650981120
33. M. B. Devani, C. J. Shishoo, U. S. Pathak, S. H. Parikh, G. F. Shah, A. C. Padhya, *J. Pharm. Sci.* **1976**, *65*, 660–664. http://dx.doi.org/10.1002/jps.2600650507
34. H. Rajak, P. Kumar, P. Parmar, B. S. Thakur, R. Veerasamy, P. C. Sharma, A. K. Sharma, A. K. Gupta, J. S. Dangi, *Eur. J. Med. Chem*. **2012**, *53*, 390–397. http://dx.doi.org/10.1016/j.ejmech.2012.03.058
35. X. Li, X. Zhou, J. Zhang, L. Wang, L. Long, Z. Zheng, S. Li, W. Zhong, *Molecules* **2014**, *19*, 2004–2028. http://dx.doi.org/10.3390/molecules19022004
36. H. P. Dalalian, N. J. Rutherford, S. Kushner, Acylpiperazines and methods of preparing the same, US Patent Number, 2,807,617, date of patent September 24, **1957**. http://www.freepatentsonline.com/2807617.html
37. H. Steinhagen, M. Gerisch, J. Mittendorf, K. -H. Schlemmer, B. Albrecht, *Bioorg. Med. Chem. Lett*. **2012**, *12*, 3187–3190. http://dx.doi.org/10.1016/S0960-894X(02)00602-9
38. E. K. Harvill, R. M. Herbst, and E. G Schreiner, *J. Org. Chem.* **1952**, *17*, 1597–1616. http://dx.doi.org/10.1021/jo50012a006
39. S. Hayao, H. J. Havera, W. G. Strycker, T. J. Leipzig, and R. Rodriguez, *J. Med. Chem.* **1967**, *10*, 400–402. http://dx.doi.org/10.1021/jm00315a025
40. V. N. Devegowda, S. H. Seo, A. N. Pae, G. Nam, K. I. Choi, *Bull. Korean Chem. Soc*. **2012**, *33*, 647–650. http://dx.doi.org/10.5012/bkcs.2012.33.2.647
41. P. Skehan, R. Storeng, *J. Natl. Cancer Inst*. **1990**, *82*, 1107–1112. http://dx.doi.org/10.1093/jnci/82.13.1107
42. Tacar. P. Sriamornsak. C. R. Dass, *J. Pharm. Pharmacol*. **2013**, *65(2)*, 157–170. http://dx.doi.org/10.1111/j.2042-7158.2012.01567.x
43. M. Shaquiquzzaman, G. Verma, A. Marella, M. Akhter, W. Akhtar, M. F. Khan, S. Tasneem, M. M. Alam, *Eur. J. Med. Chem.* **2015**, *102*, 487–529. http://dx.doi.org/10.1016/j.ejmech.2015.07.026
44. Z. Hernandes, S. M. T. Cavalcanti, D. R. M. Moreira, W. Filgueira de Azevedo. A. C. Lima Leite, *Curr. Drug Targets* **2010**, *11*, 303–314. http://dx.doi.org/10.2174/138945010790711996
45. J. He, X. Wang, X. Zhao, Y. J. Liang, H. He, L. Fu, *Eur. J. Med. Chem*. **2012**, *54*, 925–930. http://dx.doi.org/10.1016/j.ejmech.2012.06.003

Povzetek

Številna poročila o proti rakastem delovanju različnih tieno[2,3-*d*]pirimidinov in triazolotienopirimidinov so nas spodbudila k pripravi nove serije 4-benzil-6,7,8,9-tetrahidro[1]benzotieno[3,2-*e*][1,2,4]triazolo[4,3-*a*]pirimidinov. Raziskali smo *in vitro* citotoksično aktivnost izbranih spojin proti dvema človeškima celičnima linijama: raka prostate (PC-3) ter raka debelega črevesa in danke (HCT-116). Izvedli smo tudi začetno študijo odvisnosti med aktivnostjo tarčnih spojin in njihovo strukturo. Večina pripravljenih spojin je izkazala precejšnjo aktivnost proti testiranima celičnima linijama, zlasti obetavna je bila aktivnost spojine **16c** proti celični liniji PC-3 z IC_{50} vrednostjo 5.48 μM, kar je zelo ugodno v primerjavi z vrednostjo za doksorubicin (IC_{50} = 7.7 μM), referenčnim standardom uporabljenim v tej raziskavi. Po drugi strani pa sta se spojini **6c** in **18c** izkazali kot najbolj aktivni proti celični liniji HCT-116 (IC_{50} = 6.12 in 6.56 μM), kar je tudi ugodno v primerjavi z vrednostjo za standard (IC_{50} = 15.82 μM). Zato lahko zaključimo, da bi nekateri izmed sintetiziranih tienopirimidinskih derivatov, zlasti **6c**, **16c** in **18c**, lahko predstavljali potencialno zanimive spojine za nadaljnji razvoj v učinkovita zdravila proti raku.

Scientific paper

Synthesis, Cytotoxic and Anti-proliferative Activity of Novel Thiophene, Thieno[2,3-*b*]pyridine and Pyran Derivatives Derived from 4,5,6,7-tetrahydrobenzo[*b*]thiophene Derivative

Rafat Milad Mohareb,[1,*] Nadia Youssef Megally Abdo[2] and Fatma Omar Al-farouk[3]

[1] *Department of Chemistry, Faculty of Science, Cairo University, Giza, A. R. Egypt*

[2] *Chemistry Department, Faculty of Education, Alexandria University, 21526 Alexandria, Egypt*

[3] *Department of Chemistry, Faculty of Science, American University in Cairo, 5th Settlement, A.R., Egypt*

* *Corresponding author: E-mail: raafat_mohareb@yahoo.com*

Received: 15-09-2016

Abstract

Novel tetrahydrobenzo[*b*]thienopyrole derivatives are synthesized from 2-amino-3-cyano-4,5,6,7-tetrahydrobenzo[*b*]thiophene (**1**) through its reaction with α-chloroacetone to give the corresponding *N*-alkyl derivative **3**. Compound **3** undergoes ready cyclization in sodium ethoxide solution to give the tetrahydrobenzo[*b*]thienopyrrole **4**. The latter compound 4 is used as the key starting material for the synthesis of thiophene, thieno[2,3-*b*]pyridine and pyran derivatives. The cytotoxicity of the synthesized products towards the human cancer cell lines namely gastric cancer (NUGC), colon cancer (DLD-1), liver cancer (HA22T and HEPG-2), breast cancer (MCF-7), nasopharyngeal carcinoma (HONE-1) and normal fibroblast (WI-38) cell lines are measured. Compounds **4**, **7a**, **7b**, **8a**, **8b**, **10c, 10d**, **10f**, **12a**, **12b, 14b** and **15b** exhibit the optimal cytotoxic effect against cancer cell lines. Compounds **7b** and **14b** show the maximum inhibitory effect and these are much higher than the reference CHS-828 (pyridyl cyanoguanidine). On the other hand, the anti-proliferative evaluations of these compounds with high potency against the cancer cell lines L1210, Molt4/C8, CEM, K562, K562/4 and HCT116 show that compounds **7b** and **8b** give IC_{50}'s against Molt4/C8 and CEM cell lines higher than that of the reference, doxorubicin.

Keywords: Tetrahydrobenzo[*b*]thiophene, pyran, thiophene, cytotoxicity, anti-proliferative activity

1. Introduction

Sulfur containing heterocycles paved way for the active research in the pharmaceutical Chemistry. Nowadays benzothiophene derivatives in combination with other ring systems have been used extensively in pharmaceutical applications.[1–3] A large number of compounds containing thiophene system have been investigated because of their broad spectrum of biological activities which include analgesic,[4] antibacterial,[5] antifungal,[6] antiparasitic,[7] antiviral,[8] anti-inflammatory,[9] anticonvulsant,[10] anti-nociceptive,[11] DNA cleavage,[12] herbicidal,[13] antitubercular,[14] protein kinase inhibition,[15] respiratory syndrome protease inactivation,[16] an active ester in the peptide synthesis and agonists of peroxisome proliferator activated receptors.[17] In addition to these considerable biological applications, tetrahydrobenzo[*b*]thiophenes are important intermediates, protecting groups and final products in organic synthesis. Recently, our research group was involved through comprehensive program aiming for the synthesis of 4,5,6,7-tetrahydrobenzo[*b*]thiophene derivatives followed by their antitumor evaluations.[18,19] Moreover, we reported the multi-component reactions with 3-(α-bromoacetyl)coumarin to give pyan and pyrididine derivatives.[20] In continuation of this program we are demonstrating the use of 2-amino-3-cyano-4,5,6,7-tetrahydrobenzo[*b*]thiophene for the synthesis of tetrahydrobenzo[*b*]thienopyrrole derivatives followed by their cytotoxic and the anti-proliferative evaluations.[21,22]

2. Results and Discussion

The reaction of the 2-amino-3-cyano-4,5,6,7-tetrahydrobenzo[*b*]thiophene (**1**) with α-chloroacetone in the presence potassium carbonate afforded the 2-((2-oxopropyl)amino)-4,5,6,7-tetrahydrobenzo[*b*]thiophene-3-carbonitrile (**3**). Compound **3** was characterized by ^{1}H-NMR and ^{13}C-NMR. Thus, the ^{1}H-NMR spectrum display the presence of beside the expected tetrahydrobenzene moiety, a singlet at δ 5.20 ppm indicating the presence of the *N*-CH_2 group, a singlet at δ 2.88 ppm assigned to the CH_3 group and a broad singlet at δ 8.30 ppm due to the NH group. Moreover, the ^{13}C-NMR spectrum showed δ: 19.6 (CH_3), 20.3, 22.0, 25.7 and 34.6 (4 CH_2), 55.6 (CH_2), 116.8 (CN), 124.1, 124.9, 128.7 and 139.5 (thiophene C), 164.8 (C=O). Compound **3** under-

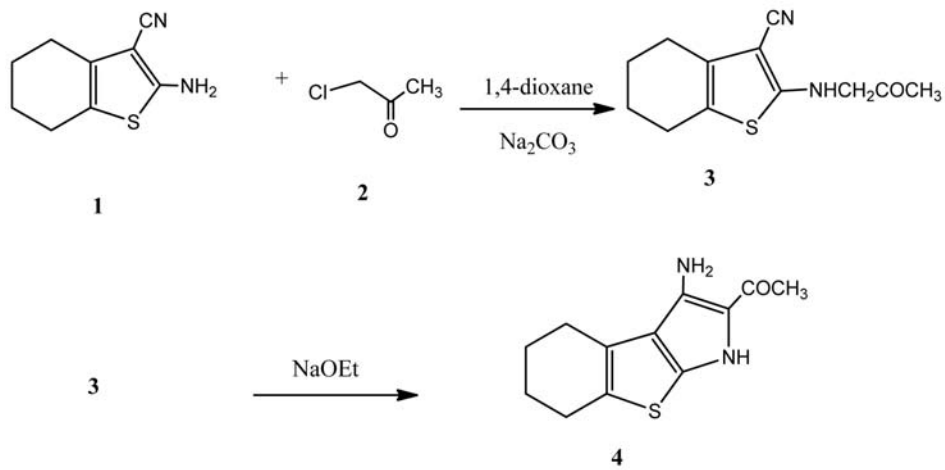

Shema 1. Synthesis of compounds **3** and **4.**

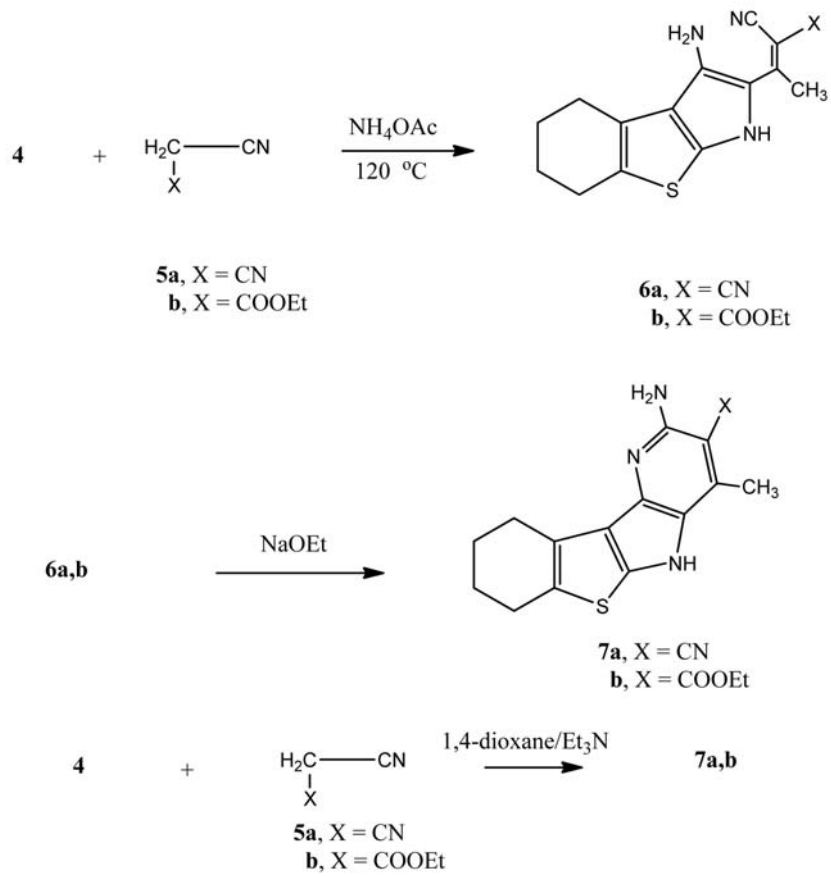

Shema 2. Synthesis of compounds **6a,b** and **7a,b.**

went ready cyclization when heated in sodium ethoxide solution in a boiling water bath to yield the 1-(3-amino-4,5,6,7-tetrahydro-1*H*-benzo[4,5]thieno[2,3-*b*]pyrrol-2-yl)ethanone (**4**) (Scheme 1).

Compound **4** showed interesting reactivity towards different reagents, thus, it reacted with either malononitrile (**5a**) or ethyl cyanoacetate (**5b**) in the presence of ammonium acetate in an oil bath at 120 °C afforded the Knoevenagel condensated products **6a** and **6b**, respectively. The latter products underwent ready cyclization in sodium ethoxide solution to give the annulated products **7a** and **7b**, respectively (Scheme 2). The structures of the latter products were established on the basis of the analytical and spectral data. Thus, the ^{1}H-NMR spectrum of **7a** showed the presence of δ 2.89 ppm assigned to the CH_3 group, a singlet at δ 4.89 ppm indicating the NH_2 group and a singlet at δ 8.33 ppm confirming the presence of the NH group. Moreover, the ^{13}C-NMR spectrum showed δ 19.8 (CH_3), 20.1, 22.7, 25.2 and 34.6 (4 CH_2), 116.8 (CN), 120.1, 122.6, 123.8, 124.2, 125.3, 127.2, 135.6, 142.3 (thiophene, pyrrole, pyridine C) and 168.2 (C=N).

Compound **4** was studied to produce thiophene derivatives through the Gewald's reaction[23–26] as many thiophenes were used as anticancer drugs. Thus, the reaction of compound **4** with either of malononitrile or ethyl cyanoacetate and elemental sulphur gave the thiophene derivatives **8a** and **8b**, respectively. On the other hand, the one pot reaction of compound **4** with either malononitrile or ethyl cyanoacetate and any of benzaldehyde, 4-chlorobenzaldehyde or 4-methoxybenzaldehyde gave the pyran derivatives **10a-f**, respectively. The ^{1}H-NMR and ^{13}C-NMR spectra **10a-f** were consistent with their respective structures. Further confirmations for the structure of compounds **10a-f** were obtained through their synthesis via another synthetic root. Thus, the reaction of compound **4** with the cinnamonitrile derivatives **11a-f** in the presence of a catalytic amount of

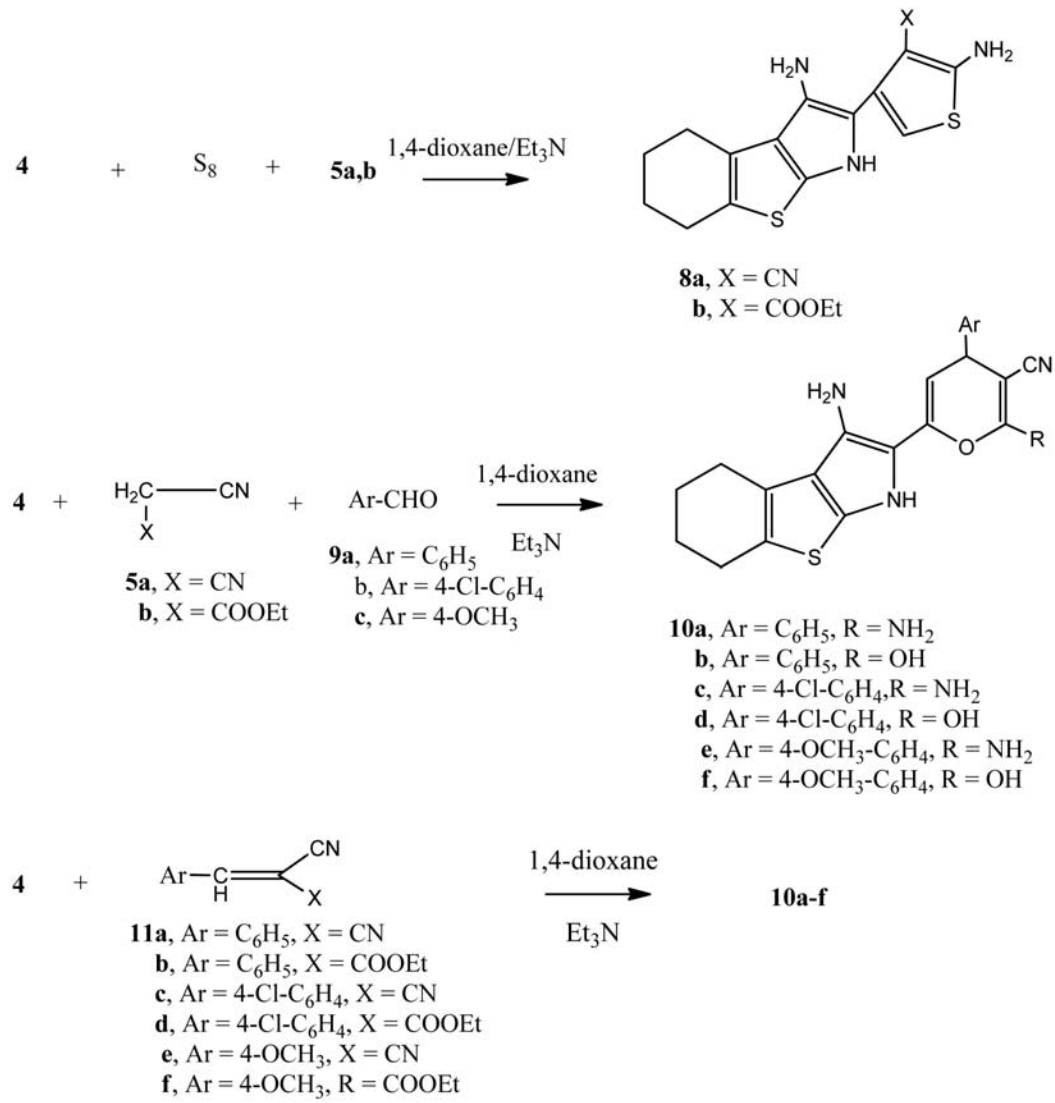

Shema 3. Synthesis of compounds **8a,b** and **10a-f.**

triethylamine gave the same products **10a-f**, respectively (m.p., mixed m.p. and fingerprint IR) (Scheme 3).

Moreover, the reaction of either of compound **8a** or **8b** with ethyl cyanoacetate in refluxing dimethylformamide afforded the 2-amido derivatives **12a** and **12b**, respectively. Formation of the latter products was explained on the condensation of ethyl cyanoacetate with the 2-aminothiophene moiety not to the 3-aminopyrrol moiety on the basis of the ^{1}H-NMR spectra of such products. Thus, the ^{1}H-NMR spectrum of either **12a** or **12b** displayed the missing of the NH_2 group that attached to thiophene ring which is expected to appear within the range δ 5.10-5.24 ppm while that of the 3-aminopyrrole moiety existing at δ 4.81–4.83 ppm. Similar acylation of the 2-aminothiophene was reported before in literature.[27] The high yield of compound **12a**, encouraged us to make further work. Thus, the reaction of **12a** with either of the aryl diazonium salts **13a-d** gave the aryl hydrazo derivatives **14a-d**, respectively. Moreover, compounds **12a,b** underwent ready cyclization in sodium ethoxide to produce the thieno[2,3-*b*]pyridine derivatives **15a** and **15b**, respectively (Scheme 4).

2. 2. Anti-tumor Cell Activity

2. 2. 1. Chemicals and Cell cultures

Fetal bovine serum (FBS) and L-glutamine, were purchased from Gibco Invitrogen Co. (Scotland, UK). RPMI-1640 medium was purchased from Cambrex (New Jersey, USA). Dimethyl sulfoxide (DMSO), doxorubicin, CHS-828, penicillin, streptomycin and sulforhodamine B (SRB) were purchased from Sigma Chemical Co. (Saint

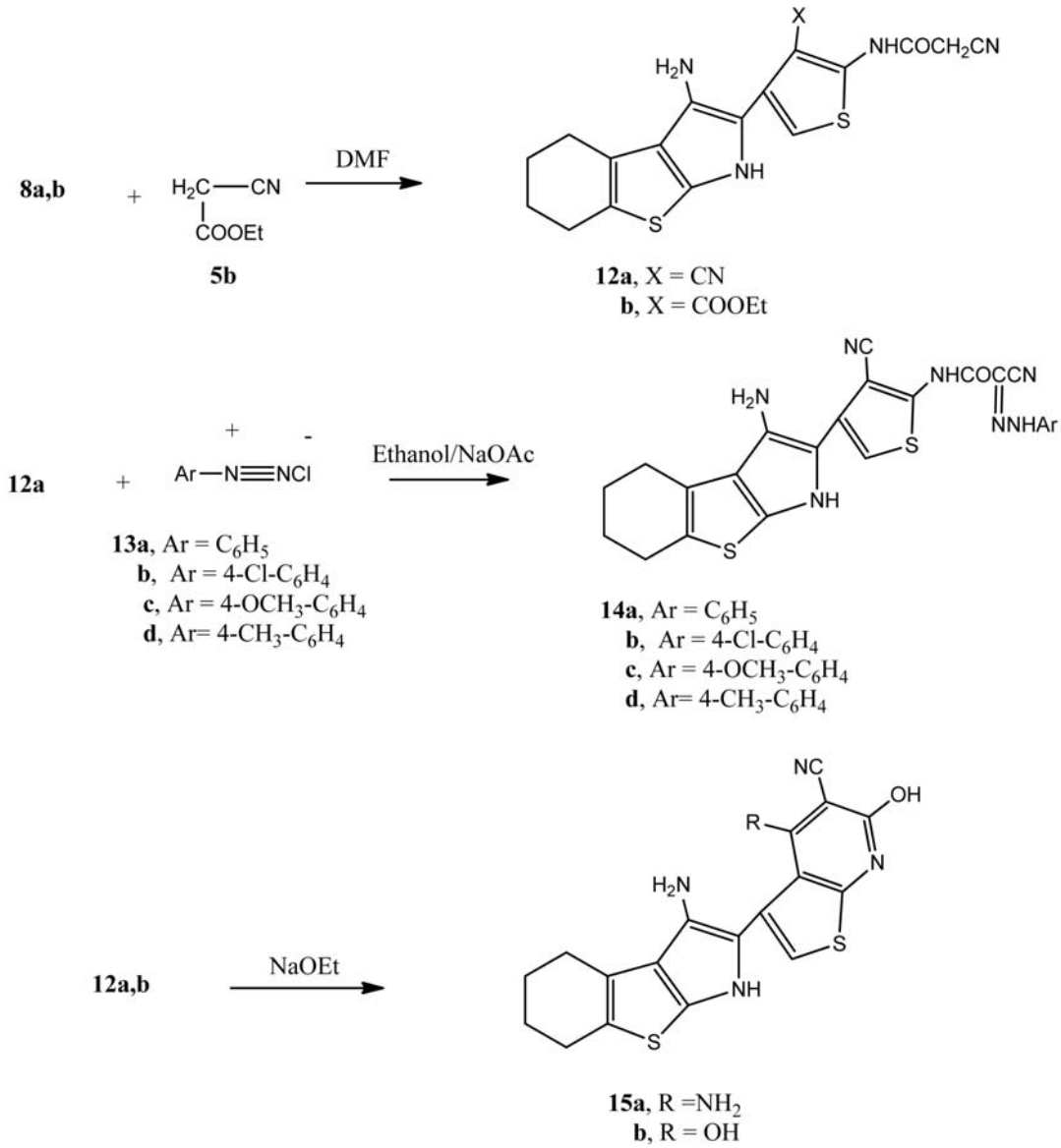

Shema 4. Synthesis of compounds **12a,b-15a,b.**

Louis, USA). The cell cultures was obtained from the European Collection of cell Cultures (ECACC, Salisbury, UK) and human gastric cancer (NUGC), human colon cancer (DLD-1), human liver cancer (HA22T and HEPG-2), human breast cancer (MCF-7), nasopharyngeal carcinoma (HONE-1) and normal fibroblast cells (WI-38) were kindly provided by the National Cancer Institute (NCI, Cairo, Egypt). They grow as monolayer and routinely maintained in RPMI-1640 medium supplemented with 5% heat inactivated FBS, 2 mM glutamine and antibiotics (penicillin 100 U/mL, streptomycin 100 lg/mL), at 37 °C in a humidified atmosphere containing 5% CO_2. Exponentially growing cells were obtained by plating 1.5×10^5 cells/mL for the six human cancer cell lines including cells derived from 0.75×10^4 cells/mL followed by 24 h of incubation. The effect of the vehicle solvent (DMSO) on the growth of these cell lines was evaluated in all the experiments by exposing untreated control cells to the maximum concentration (0.5%) of DMSO used in each assay.

2. 2. 2. In vitro Cytotoxicity Assay

The heterocyclic compounds, prepared in this study, were evaluated according to standard protocols[28,29] for their *in vitro* cytotoxicity against the six human cancer cell lines including cells derived from human gastric cancer (NUGC), human colon cancer (DLD-1), human liver cancer (HA22T and HEPG-2), human breast cancer (MCF-7), nasopharyngeal carcinoma (HONE-1) and a normal fibroblast cells (WI-38). All of IC_{50} values were listed in Table 1. Some heterocyclic compounds were observed with significant cytotoxicity against most of the cancer cell lines tested (IC_{50}=10–1000 nM). Normal fibroblasts cells (WI-38) were affected to a much lesser extent (IC_{50}>10,000 nM). The reference compound used was the CHS-828 which is the pyridyl cyanoguanidine anti-tumor agent.[30] It is a new chemotherapeutic drug in addition it has low toxicity and lacks known patterns of multidrug resistance.[31]

2. 2. 3. Structure-activity Relationship

From Table 1 it is clear that the thiophene moiety was found to be crucial for the cytotoxic effect of the cyclic compounds **3 -15a,b**. Compounds **4**, **7a**, **7b**, **8a**, **8b**, **10c, 10d**, **10f**, **12a**, **12b, 14b** and **15b** exhibited optimal cytotoxic effect against cancer cell lines, with IC_{50}'s in the nM range. Comparing the cytotoxicity of the tetrahydrobenzothiophene **3** and the cyclized product **4**, it is obvious that the cytotoxicity of compound **4** is higher than that of compound **3**. The presence of the pyrrol ring through the tetrahydrobenzo[*b*]thiophene in compound **4** is responsible for its high potency. The condensation reac-

Table 1. Cytotoxicity of the newly synthesized products against a variety of cancer cell lines [IC_{50}[a] (nM)]

Compound No.	Cytotoxicity (IC_{50} in nM)						
	UGC[b]	DLD-1[b]	HA22T[b]	HEPG-2[b]	HONE-1[b]	MCF-7[b]	WI-38[b]
3	2142	1222	1340	1028	1828	2246	NA
4	86	45	313	128	212	310	NA
6a	2101	2380	3258	2266	2380	3330	NA
6b	1335	1140	1072	1154	1064	1258	NA
7a	218	146	220	337	241	380	NA
7b	48	92	260	46	74	32	NA
8a	320	240	230	165	1281	265	NA
8b	48	35	53	170	49	78	NA
10a	1220	1033	2250	1275	2126	2372	NA
10b	1165	1322	2350	2221	2152	1322	NA
10c	330	532	822	442	1529	1224	NA
10d	30	62	74	39	1330	88	NA
10e	1135	2160	2160	814	780	296	NA
10f	149	2220	3210	550	2451	1286	120
12a	69	74	190	448	2871	2690	NA
12b	26	65	38	220	440	57	NA
14a	1350	1160	2290	2120	1126	2230	NA
14b	83	59	80	64	87	48	1330
14c	1480	1156	1346	1226	1275	1240	NA
14d	1245	2160	2180	2220	1869	1765	NA
15a	1845	1210	1218	1076	1270	436	NA
15b	1220	2063	377	740	253	2210	NA
CHS-828	25	2315	2067	1245	15	18	NA

[a] Drug concentration required to inhibit tumor cell proliferation by 50% after continuous exposure of 48 h.
[b] NUGC, gastric cancer; DLD-1, colon cancer; HA22T, liver cancer; HEPG-2, liver cancer; HONE-1, nasopharyngeal carcinoma; MCF-7, breast cancer; WI-38, normal fibroblast cells. NA: Not Active.

tion of compound **4** with either malononitrile or ethyl cyanoacetate to produce compounds **5a** and **5b**, respectively showed a decrease of cytotoxicity. On the other hand, the cyclization of compounds **6a** and **6b** to the benzo[4',5']thieno[3',2':4,5]pyrrolo[3,2-*b*]pyridine derivatives **7a** and **7b** showed remarkable increase of the cytotoxicity. Moreover, it is clear that compound **7b** showed more cytotoxicity than **7a**, this is attributed to the presence of the oxygen rich COOE-t group. The introduction of the second thiophene moiety to compound **4** that gives both of compounds **8a** and **8b** showed high potency-especially-in case of compounds **8b** which was attributed due to the presence of the COOEt. Considering the pyran derivatives **10a-f**, the cytotoxicity of compounds **10c** and **10d** showed the highest values among the six compounds. However, compound **10c** showed high cytotoxicity against the four cancer cell lines HUGC, DLD-1, HA22T and HEPG-2, but it is of great value to notice that compound **10d** showed high cytotoxicity against five cancer cell lines and such cytotoxicity is higher than that of compound **10c**. The high cytotoxicity of compound **10d** is attributed to the presence of the OH and the Cl group as well.

The thiophene derivatives **12a** and **12b** showed high cytotoxicity similarl to that of compounds **8a,b**. Moreover, compound **12b** with the COOE-t showed high potency than that of compound **12a**. The coupling of the diazonium salts **13a-d** with compound **12a** afforded the arylhydrazone derivatives **14a-d**. Compound **14b** with the Cl group showed the maximum cytotoxicity among the arylhydrazone derivatives **14a-d**. Finally, considering the thieno[2,3-*b*]pyridine derivatives **15a,b** where the presence of the OH in compound **15b** conserved an interesting cytotoxicity against the cancer cell lines HA22T, HEPG-2 and HONE-1 with the IC_{50}'s 377, 740, 253 nM, respectively. It is of great value to notice that compounds **7b**, **8b** and **12b** showed the maximum cytotoxicity among the tested compounds.

2. 2. 4. Anti-proliferative Cell Activity Against Cancer Cell Lines

We used a panel of tumor cell lines to test the cytotoxicity of the new compounds, especially those showed high potency against the six cancer cell lines through Table 2. Importantly, this panel included the cell lines and their isogenic sub-lines with the determinants of drug resistance: murine leukemia L1210, T-lymphocyte cell lines Molt4/C8 and CEM, human leukemia R562 and its MDR subline K562/4 that over expressed P-glycoprotein, and the colon carcinoma HCT116. The above determinants alter the response of cells to many anticancer drugs including doxorubicin. Data on cytotoxic (anti-proliferative) activity are presented in Table 2 in which IC_{50} values represent the concentrations that inhibit cell proliferation by 50%. It is clear from Table 2 that tested compounds **4**, **7a**, **7b**, **8a**, **8b**, **10c**, **10d**, **10f**, **12a**, **12b, 14b** and **15b** showed high potency against the cell lines. The benzo[4',5']thieno[3',2':4,5]pyrrolo[3,2-*b*]pyridine derivative **7b** and the benzo[4,5]thieno-[2,3-*b*]pyrrol-2-yl)-thiophene derivative **8b** showed high potency against Molt4/C8 and CEM cell lines and their IC_{50}'s are higher than that of the reference doxorubicin. It is clear from Table 2 that the twelve tested compounds showed high IC_{50} against K562/4 cell line than doxorubicin.

3. Experimental

3. 1. General

All melting points were determined on an electrothermal apparatus (Büchi 535, Switzerland) in an open capillary tube and are uncorrected. ^{13}C-NMR and ^{1}H-NMR spectra were recorded on Bruker DPX200 instrument in DMSO with TMS as internal standard for protons and solvent signals as internal standard for carbon spectra. Chemical shift values are mentioned in ä (ppm). Mass spectra

Table 2. Anti-proliferative activity (IC_{50}) of selected compounds against variety of cell lines

Compound	Cytotoxicity (IC_{50} in nM)					
No.	L1210	Molt4/C8	CEM	K562	K562/4	HCT116
4	1.5 ± 0.5	1.1 ± 0.03	0.3 ± 0.01	0.4 ± 0.08	0.9 ± 0.02	0.8 ± 0.05
7a	0.4 ± 0.1	0.8 ± 0.04	2.0 ± 0.4	1.8 ± 0.03	0.9 ± 0.06	1.3 ± 0.02
7b	0.3 ± 0.08	0.4 ± 0.04	0.9 ± 0.05	1.30 ± 0.08	1.1 ± 0.07	2.4 ± 0.09
8a	1.2 ± 0.09	0.8 ± 0.02	0.6 ± 0.01	0.2 ± 0.01	0.9 ± 0.08	1.4 ± 0.2
8b	1.1 ± 0.06	0.02 ± 0.002	0.7 ± 0.03	0.9 ± 0.06	1.6 ± 0.07	0.8 ± 0.02
10c	0.8 ± 0.05	0.4 ± 0.02	1.3 ± 0.05	0.6 ± 0.02	0.02 ± 0.01	1.2 ± 0.08
10d	0.6 ± 0.02	1.5 ± 0.07	2.5 ± 0.05	1.7 ± 0.02	2.5 ± 0.02	2.8 ± 0.07
10f	1.4 ± 0.05	0.8 ± 0.03	2.6 ± 0.09	0.02 ± 0.01	2.8 ± 0.06	0.4 ± 0.08
12a	2.1 ± 0.05	0.6 ± 0.02	0.5 ± 0.01	0.3 ± 0.01	0.4 ± 0.06	2.4 ± 0.07
12b	1.8 ± 0.09	0.9 ± 0.04	1.8 ± 0.6	0.7 ± 0.06	0.8 ± 0.06	0.9 ± 0.08
14b	0.5 ± 0.03	0.3 ± 0.05	2.6 ± 0.06	0.5 ± 0.07	0.6 ± 0.02	0.1 ± 0.01
15b	0.9 ± 0.02	0.3 ± 0.01	0.6 ± 0.05	2.1 ± 0.07	2.7 ± 1.03	0.3 ± 0.04
Dox.	0.37 ± 0.07	0.20 ± 0.02	0.06 ± 0.02	0.14 ± 0.03	7.2 ± 0.9	1.4 ± 0.1

Doxorubicin (Dox.) was used as the reference drug

were recorded on EIMS (Shimadzu) and ESI-esquire 3000 Bruker Daltonics instrument. Elemental analyses were carried out by the Microanalytical Data Unit Ludwig-Maximilians-Universitat-Munchen, Germany. The progress of all reactions was monitored by TLC on 2 × 5 cm pre-coated silica gel 60 F254 plates of thickness of 0.25 mm (Merck).

3. 1. 1. Synthesis of 2-((2-Oxopropyl)amino)-4,5,6,7-tetrahydrobenzo[*b*]thiophene-3-carbonitrile (3)

To a solution of compound **1** (1.78 g, 0.01 mol) in 1,4-dioxane (40 mL) containing sodium carbonate (1.00 g) α-chloroacetone (0.94 g, 0.01 mol) was added. The reaction mixture was heated under reflux for 2 h then poured onto ice/water and the formed solid product was collected by filtration and crystallized from ethanol.

White crystals; yield: 2.01 g (86%); mp: 182–183 °C; IR (KBr, cm^{-1}): 3465–3328 (NH), 2220 (CN), 1705 (C=O), 1615 (C=C); ^{1}H-NMR (dimethyl sulfoxide (DMSO)-d_6) δ :1.80–1.85 (m, 4H, $2CH_2$), 2.22–2.26 (m, 4H, $2CH_2$), 2.88 (s, 3H, CH_3), 5.20 (s, 2H, CH_2), 8.30 (s, 1H, NH, D_2O exchangeable); ^{13}C-NMR (DMSO-d_6) δ : 19.6, 20.3, 22.0, 25.7, 34.6, 55.6, 116.8, 124.1, 124.9, 128.7, 139.5, 164.8; MS electron impact (EI): *m/z* (%) 234 (M^+). *Anal*. Calcd for $C_{12}H_{14}N_2OS$: C, 61.51; H, 6.02; N, 11.96; S, 13.68. Found: C, 61.82; H, 6.22; N, 11.77; S, 13.73.

Synthesis of 1-(3-Amino-4,5,6,7-tetrahydro-1*H*-benzo[4,5]thieno[2,3-*b*]pyrrol-2-yl)ethanone (4)

A suspension of compound **3** (2.34 g, 0.01 mol) in sodium ethoxide (0.02 mol) [prepared by dissolving metallic sodium (0.46 g, 0.02 g) in absolute ethanol (20 mL] was heated in a boiling water bath for 6 h then poured onto ice/water containing few drops of hydrochloric acid. The formed solid product was collected by filtration and crystallized from 1,4-dioxane.

White crystals; yield: 1.80 g (77%); mp: >300 °C; IR (KBr, cm^{-1}): 3479–3348 (NH, NH_2), 1715 (C=O), 1618 (C=C); ^{1}H-NMR (DMSO-d_6) δ : 1.78–1.83 (m, 4H, $2CH_2$), 2.20–2.27 (m, 4H, $2CH_2$), 2.91 (s, 3H, CH_3), 4.83 (s, 2H, NH_2, D_2O exchangeable), 8.27 (s, 1H, NH, D_2O exchangeable); ^{13}C-NMR (DMSO-d_6) δ: 19.8, 20.2, 22.0, 25.6, 34.8, 124.0, 124.9, 128.5, 139.6, 165.6; MS (EI): *m/z* (%) 234 (M^+). *Anal*. Calcd for $C_{12}H_{14}N_2OS$: C, 61.51; H, 6.02; N, 11.96; S, 13.68. Found: C, 61.68; H, 5.89; N, 12.20; S, 13.83.

3. 1. 2. General Procedure for the Synthesis of Thieno[2,3-*b*]pyrrol Derivatives 6a and 6b

To the dry solid of compound **4** (2.34 g, 0.01 mol) either malononitrile (0.66 g, 0.01mol) or ethyl cyanoacetate (1.13 g, 0.01 mol) was added followed by ammonium acetate (0.50 g, 0.01 mol).The whole reaction mixture was heated in an oil bath at 120 °C for 1h then left to cool. The solidified product was boiled with ethanol then left to cool. The formed solid product was collected by filtration and crystallized from acetic acid.

2-(1-(3-Amino-4,5,6,7-tetrahydro-1*H*-benzo[4,5]thieno[2,3-*b*]pyrrol-2-yl)ethylidene)-malononitrile (6a)

Yellow crystals; yield: 1.92 g (68%); mp: 167–168 °C; IR (KBr, cm^{-1}): 3488–3334 (NH, NH_2), 3054 (CH aromatic), 2227, 2222 (2CN), 1620 (C=C); ^{1}H-NMR (DMSO-d_6) δ: 1.79–1.86 (m, 4H, $2CH_2$), (m, 4H, $2CH_2$), 2.69 (s, 3H, CH_3), 4.86 (s, 2H, NH_2, D_2O exchangeable), 8.29 (s, 1H, NH, D_2O exchangeable); ^{13}C-NMR (DMSO-d_6) δ: 19.4, 20.3, 22.2, 25.6, 34.5, 116.3, 116.9, 122.3, 123.8, 124.0, 124.9, 127.2, 135.2; MS (EI): *m/z* (%) 282 (M^+). *Anal*. Calcd for $C_{15}H_{14}N_4S$: C, 63.80; H, 5.00; N, 19.84; S, 11.36. Found: C, 63.72; H, 4.93; N, 20.05; S, 11.59.

Ethyl 3-(3-amino-4,5,6,7-tetrahydro-1*H*-benzo[4,5]thieno[2,3-*b*]pyrrol-2-yl)-2-cyanobut-2-enoate (6b)

Yellow crystals; yield: 2.46 g (75%); mp: 121–122°C; IR (KBr, cm^{-1}): 3473–3330 (NH, NH_2), 3054 (CH aromatic), 2222 (CN), 1640 (C=C); ^{1}H-NMR (DMSO-d_6) δ: 1.13 (t, 3H, J = 7.26 Hz, CH_3), 1.80–1.86 (m, 4H, $2CH_2$), 2.22–2.27 (m, 4H, $2CH_2$), 2.66 (s, 3H, CH_3), 4.22 (q, 2H, J = 7.26 Hz, CH_2), 4.88 (s, 2H, NH_2, D_2O exchangeable), 8.27 (s, 1H, NH, D_2O exchangeable); ^{13}C-NMR (DMSO-d_6) δ: 16.3, 19.6, 20.2, 22.5, 25.6, 34.8, 116.6, 122.0, 123.5, 124.6, 124.7, 127.2, 134.8, 166.1; MS (EI): *m/z* (%) 329 (M^+). *Anal.* Calcd for $C_{17}H_{19}N_3O_2S$: C, 61.98; H, 5.81; N, 12.76; S, 9.73. Found: C, 62.08; H, 6.07; N, 12.59; S, 9.88.

3. 1. 3. General Procedure for the Synthesis of the Benzo[4',5']thieno[3',2':4,5]-pyrrolo [3,2-*b*]pyridine Derivatives 7a and 7b

Method (A): A suspension of either compound **6a** (2.28 g, 0.01 mol) or **6b** (3.29 g, 0.01 mol) in sodium ethoxide (0.02 mol) [prepared by dissolving metallic sodium (0.46 g, 0.02 mol) in absolute ethanol (20 mL) was heated in a boiling water bath for 8 h then poured onto ice/water containing few drops of hydrochloric acid. The formed solid product was collected by filtration and crystallized from acetic acid.

Method (B): To a solution of compound **4** (2.34 g, 0.01 mol) in 1,4-dioxane (40 mL) containing triethylamine (0.50 mL) either malononitrile (0.66 g, 0.01 mol) or ethyl cyanoacetate (1.13 g, 0.01 mol) was added. The whole reaction mixture, in each case, was heated under reflux for 4 h then poured onto ice/water containing few drops of hydrochloric acid. The formed solid product was collected by filtration and crystallized from acetic acid.

2-Amino-4-methyl-7,8,9,10-tetrahydro-5*H*-benzo [4',5']thieno[3',2':4,5]pyrrolo[3,2-*b*]pyridine-3-carbonitrile (7a)

Yellow crystals; yield: 2.27 g (80%); mp: 232–233 °C; IR (KBr, cm^{-1}): 3474–3314 (NH, NH_2), 3056 (CH aromatic), 2220 (CN), 1626 (C=C); ^{1}H-NMR (DMSO-d_6) δ: 1.76–1.84 (m, 4H, $2CH_2$), 2.21–2.26 (m, 4H, $2CH_2$), 2.89 (s, 3H, CH_3), 4.89 (s, 2H, NH_2, D_2O exchangeable), 8.33 (s, 1H, NH, D_2O exchangeable); ^{13}C-NMR (DMSO-d_6) δ: 19.8, 20.1, 22.7, 25.2, 34.6, 116.8, 120.1, 122.6, 123.8, 124.2, 125.3, 127.2, 135.6, 142.3, 168.2; MS (EI): *m/z* (%) 282 (M^+). *Anal.* Calcd for $C_{15}H_{14}N_4S$: C, 63.80; H, 5.00; N, 19.84; S, 11.36. Found: C, 63.66; H, 4.83; N, 20.25; S, 11.37.

Ethyl 2-amino-4-methyl-7,8,9,10-tetrahydro-5*H*-benzo [4',5']thieno[3',2':4,5]pyrrolo[3,2-*b*]pyridine-3-carboxylate (7b)

Yellow crystals; yield: 2.24 g (68%), mp: 195–196 °C; IR (KBr, cm^{-1}): 3466–3327 (NH, NH_2), 3056 (CH aromatic), 1640 (C=C); ^{1}H-NMR (DMSO-d_6) δ: 1.14 (t, 3H, J = 7.07 Hz, CH_3), 1.82–1.86 (m, 4H, $2CH_2$), 2.20–2.27 (m, 4H, $2CH_2$), 2.88 (s, 3H, CH_3), 4.24 (q, 2H, J = 7.07 Hz, CH_2), 4.84 (s, 2H, NH_2, D_2O exchangeable), 8.32 (s, 1H, NH, D_2O exchangeable); ^{13}C-NMR (DMSO-d_6) δ: 16.2, 19.8, 20.3, 22.5, 25.6, 34.5, 55.6, 120.3, 122.4, 123.8, 124.6, 124.7, 127.6, 133.9, 143.2, 164.4, 168.9; MS (EI): *m/z* (%) 329 (M^+). *Anal.* Calcd for $C_{17}H_{19}N_3O_2S$: C, 61.98; H, 5.81; N, 12.76; S, 9.73. Found: C, 61.68; H, 5.94; N, 12.63; S, 9.90.

3. 1. 4. General Procedure for the Synthesis of [4,5]thieno[2,3-*b*]pyrrol-2-yl)thiophene Derivatives 8a and 8b

To a solution of compound **4** (2.34 g, 0.01 mol) in 1,4-dioxane (40 mL) containing triethylamine (0.50 mL) and elemental sulfur (0.32 g,0.01 mol) either malononitrile (0.66 g, 0.01 mol) or ethyl cyanoacetate (1.13 g, 0.01 mol) was added. The reaction mixture, in each case was heated under reflux for 2 h then was left to cool and the formed solid product, in each case, was collected by filtration and crystallized from ethanol.

2-Amino-4-(3-amino-4,5,6,7-tetrahydro-1*H*-benzo [4,5]thieno[2,3-*b*]pyrrol-2-yl)thiophene-3-carbonitrile (8a)

Orange crystals; yield: 2.42 g (77%), mp: 141–142 °C; IR (KBr, cm^{-1}): 3462–3354 (NH, NH_2), 3053 (CH aromatic), 2221 (CN), 1628 (C=C); ^{1}H-NMR (DMSO-d_6) δ: 1.78–1.84 (m, 4H, $2CH_2$), 2.23–2.28 (m, 4H, $2CH_2$), 4.80, 5.25 (2s, 4H, $2NH_2$, D_2O exchangeable), 6.11 (s, 1H, thiophene H-5), 8.26 (s, 1H, NH, D_2O exchangeable); ^{13}C-NMR (DMSO—d_6) δ: 20.4, 22.9, 25.0, 34.6, 116.6, 120.3, 123.1, 123.8, 124.2, 125.3, 127.2, 139.3, 140.6, 142.3; MS (EI): *m/z* (%) 314 (M^+). *Anal.* Calcd for $C_{15}H_{14}N_4S_2$: C, 57.30; H, 4.49; N, 17.82; S, 20.40. Found: C, 57.44; H, 4.39; N, 18.04; S, 20.28.

Ethyl 2-amino-4-(3-amino-4,5,6,7-tetrahydro-1*H*-benzo[4,5]thieno[2,3-*b*]pyrrol-2-yl)-thiophene-3-carboxylate (8b)

Orange crystals; yield: 2.60 g (74%), mp: 131–132 °C. IR (KBr, cm^{-1}): 3479–3331 (NH_2), 3053 (CH aromatic), 1690 (C=O), 1632 (C=C); ^{1}H-NMR (DMSO-d_6) δ: 1.13 (t, 3H, J = 6.83 Hz, CH_3), 1.81–1.87 (m, 4H, $2CH_2$), 2.22–2.25 (m, 4H, $2CH_2$), 4.23 (q, 2H, J = 6.83 Hz, CH_2), 4.81, 5.03 (2s, 4H, $2NH_2$, D_2O exchangeable), 6.13 (s, 1H, thiophene H-5), 8.30 (s, 1H, D_2O exchangeable); ^{13}C-NMR (DMSO-d_6) δ: 16.0, 20.0, 22.7, 25.6, 34.5, 55.6, 120.8, 122.7, 123.8, 124.6, 124.9, 127.6, 133.9, 143.5, 164.2; MS (EI): *m/z* (%) 361 (M^+). *Anal.* Calcd for $C_{17}H_{19}N_3O_2S_2$: C, 56.48; H, 5.30; N, 11.62; S, 17.74. Found: C, 56.71; H, 5.55; N, 11.42; S, 17.49.

3. 1. 5. General Procedure for the Synthesis of Pyran Derivatives 10a-f

Method (A): General procedure: To a solution of compound **4** (2.34 g, 0.01 mol) in 1,4-dioxane (40 mL) containing triethylamine (0.5 mL), either of malononitrile (0.66 g, 0.01 mol) or ethyl cyanoacetate (1.13 g, 0.01 mol) and either of benzaldehyde (1.06 g, 0.1 mol), 4-chlorobenzaldehyde (1.40 g, 0.01 mol) or 4-methoxybenzaldehyde (1.36 g, 0.01 mol) were added. The reaction mixture was heated under reflux for 1 h and the formed solid product produced from the hot solution was collected by filtration and crystallized from ethanol. Thin layer chromatography revealed just a single spot which proved the presence of a single product.

Method (B): To a solution of compound **4** (2.34 g, 0.01 mol) in 1,4-dioxane (40 mL) containing triethylamine (0.5 mL), either of the cinnamonitrile derivatives **11a-f** (0.01 mol) were added. The reaction mixture was heated under reflux for 2 h and the formed solid product produced from the hot solution was collected by filtration and crystallized from ethanol. Thin layer chromatography revealed just a single spot which proved the presence of a single product.

2-Amino-6-(3-amino-4,5,6,7-tetrahydro-1*H*-benzo [4,5]thieno[2,3-*b*]pyrrol-2-yl)-4- phenyl-4*H*-pyran-3-carbonitrile (10a)

Pale yellow crystals; yield: 3.10 g (80%); mp: 167–168°C; IR (KBr, cm^{-1}): 3489–3321 (NH, NH_2), 3056 (CH aromatic), 2220 (CN), 1630 (C=C); ^{1}H-NMR (DMSO-d_6) δ: 1.76–1.85 (m, 4H, $2CH_2$), 2.21–2.27 (m, 4H, $2CH_2$), 4.83, 5.41 (2s, 4H, $2NH_2$, D_2O exchangeable), 5.66–5.90 (2d, 2H, pyran H-4, H-5), 7.28–7.38 (m, 5H, C_6H_5), 8.24 (s, 1H, NH, D_2O exchangeable); ^{13}C-NMR (DMSO-d_6) δ: 20.6, 22.9, 25.3, 34.8, 39.3, 116.9, 120.6, 122.8, 123.8, 123.9, 125.3, 126.9, 127.2, 129.4, 130.8,

139.3, 140.6, 141.8, 142.3; MS (EI): *m/z* (%) 388 (M^+). *Anal*. Calcd for $C_{22}H_{20}N_4OS$: C, 68.02; H, 5.19; N, 14.42; S, 8.25. Found: C, 67.93; H, 5.32; N, 14.60; S, 8.44.

6-(3-Amino-4,5,6,7-tetrahydro-1*H*-benzo[4,5]thieno [2,3-*b*]pyrrol-2-yl)-2-hydroxy-4-phenyl-4*H*-pyran-3-carbonitrile (10b)

Pale yellow crystals; yield: 2.57 g (66%), mp: 264–265 °C; IR (KBr, cm^{-1}): 3520–3341 (NH, NH_2, OH), 3055 (CH aromatic), 2222 (CN), 1632 (C=C); ^{1}H-NMR (DMSO-d_6) δ: 1.77–1.86 (m, 4H, $2CH_2$), 2.20–2.27 (m, 4H, $2CH_2$), 4.86 (s, 2H, NH_2, D_2O exchangeable), 5.68–5.87 (2d, 2H, pyran H-4, H-5), 7.30–7.41 (m, 5H, C_6H_5), 8.22 (s, 1H, NH, D_2O exchangeable), 10.30 (s, 1H, OH, D_2O exchangeable); ^{13}C-NMR (DMSO-d_6) δ: 20.4, 22.7, 25.4, 34.8, 39.9, 116.7, 120.8, 122.8, 123.3, 123.9, 125.7, 126.9, 127.0, 130.4, 133.6, 139.3, 140.8, 142.0, 142.7; MS (EI): *m/z* (%) 389 (M^+). *Anal*. Calcd for $C_{22}H_{19}N_3O_2S$: C, 67.84; H, 4.92; N, 10.79; S, 8.23. Found: C, 67.60; H, 4.69; N, 10.99; S, 8.40.

2-Amino-6-(3-amino-4,5,6,7-tetrahydro-1*H*-benzo [4,5]thieno[2,3-*b*]pyrrol-2-yl)-4-(4-chlorophenyl-4*H*-pyran-3-carbonitrile (10c)

Pale yellow crystals; yield: 2.87 g (68%); mp: 274–275 °C; IR (KBr, cm^{-1}): 3474–3330 (NH, NH_2), 3055 (CH aromatic), 2220 (CN), 1633 (C=C); ^{1}H-NMR (DMSO-d_6) δ: 1.78–1.85 (m, 4H, $2CH_2$), 2.18–2.25 (m, 4H, $2CH_2$), 4.86, 5.40 (2s, 4H, $2NH_2$, D_2O exchangeable), 5.68–5.73 (2d, 2H, pyran H-4, H-5), 7.30–7.38 (m, 4H, C_6H_4), 8.26 (s, 1H, NH, D_2O exchangeable); ^{13}C-NMR (DMSO-d_6) δ: 20.3, 22.8, 25.5, 34.8, 39.7, 116.7, 120.4, 122.6, 123.9, 124.3, 125.3, 126.9, 128.8, 130.6, 139.0, 140.9, 142.8, 144.3; MS (EI): *m/z* (%) 423 (M^+). *Anal*. Calcd for $C_{22}H_{19}ClN_4OS$: C, 62.48; H, 4.53; N, 13.25; S, 7.58. Found: C, 62.22; H, 4.72; N, 13.51; S, 7.28.

6-(3-Amino-4,5,6,7-tetrahydro-1*H*-benzo[4,5]thieno [2,3-*b*]pyrrol-2-yl)-4-(4-chlorophenyl)-2-hydroxy-4*H*-pyran-3-carbonitrile (10d)

Yellow crystals; yield: 3.21 g (76%), mp: 222–223 °C; IR (KBr, cm^{-1}): 3541–3333 (NH, NH_2), 3055 (CH aromatic), 2220 (CN), 1626 (C=C); ^{1}H-NMR (DMSO-d_6) δ: 1.78–1.87 (m, 4H, $2CH_2$), 2.21–2.28 (m, 4H, $2CH_2$), 4.83 (s, 2H, NH_2, D_2O exchangeable), 5.65–5.72 (2d, 2H, pyran H-4, H-5), 7.30–7.41 (m, 4H, C_6H_4), 8.24 (s, 1H, NH, D_2O exchangeable), 10.28 (s, 1H, OH, D_2O exchangeable); ^{13}C-NMR (DMSO-d_6) δ: 20.2, 22.6, 25.8, 34.3, 39.8, 116.5, 120.2, 122.6, 123.7, 123.9, 125.7, 126.9, 127.4, 130.2, 139.3, 141.3, 142.0, 142.8; MS (EI): *m/z* (%) 424 (M^+). *Anal*. Calcd for $C_{22}H_{18}ClN_3O_2S$: C, 62.33; H, 4.28; N, 9.91; S, 7.56. Found: C, 62.09; H, 4.46; N, 9.75; S, 7.39.

2-Amino-6-(3-amino-4,5,6,7-tetrahydro-1*H*-benzo [4,5]thieno[2,3-*b*]pyrrol-2-yl)-4-(4-methoxyphenyl-4*H*-pyran-3-carbonitrile (10e)

Orange crystals; yield: 3.01 g (72%), mp: 167–168 °C; IR (KBr, cm^{-1}): 3531–3312 (NH, NH_2), 3058 (CH aromatic), 2223 (CN), 1628 (C=C); ^{1}H-NMR (DMSO-d_6) δ: 1.74–1.86 (m, 4H, $2CH_2$), 2.20–2.28 (m, 4H, $2CH_2$), 3.01 (s, 3H, OCH_3), 4.86, 5.22 (2s, 4H, $2NH_2$, D_2O exchangeable), 5.67–5,74 (2d, 2H, pyran H-4, H-5), 7.32–7.38 (m, 4H, C_6H_4), 8.25 (s, 1H, NH, D_2O exchangeable); ^{13}C-NMR (DMSO-d_6) δ: 20.0, 22.8, 25.8, 34.8, 30.8, 39.6, 116.9, 120.6, 122.6, 123.4, 123.9, 125.7, 126.9, 127.6, 130.4, 139.4, 141.7, 142.3, 143.6; MS (EI): *m/z* (%) 418 (M^+). *Anal*. Calcd for $C_{23}H_{22}N_4O_2S$: C, 66.01; H, 5.30; N, 13.39; S, 7.66. Found: C, 66.24; H, 5.48; N, 13.19; S, 7.80.

6-(3-Amino-4,5,6,7-tetrahydro-1*H*-benzo[4,5]thieno [2,3-*b*]pyrrol-2-yl)-2-hydroxy-4-(4-methoxyphenyl)-4*H*-pyran-3-carbonitrile (10f)

Orange crystals; yield: 3.01 g (70%), mp: 229–230 °C; IR (KBr, cm^{-1}): 3566–3332 (NH, NH_2, OH), 3056 (CH aromatic), 2220 (CN), 1626 (C=C); ^{1}H-NMR (DMSO-d_6) δ: 1.74–1.86 (m, 4H, $2CH_2$), 2.22–2.29 (m, 4H, $2CH_2$), 3.08 (s, 3H, OCH_3), 4.83 (s, 2H, NH_2, D_2O exchangeable), 5.64, 5.71 (2d, 2H, pyran H-4, H-5), 7.30–7.44 (m, 4H, C_6H_4), 8.23 (s, 1H, NH, D_2O exchangeable), 10.32 (s, 1H, D_2O exchangeable, OH); ^{13}C-NMR (DMSO-d_6) δ: 20.5, 22.8, 25.3, 34.5, 30.8, 39.1, 116.9, 120.6, 122.6, 123.4, 123.9, 125.7, 126.9, 127.6, 130.6, 139.4, 141.7, 142.3, 143.9; MS (EI): *m/z* (%) 419 (M^+). *Anal*. Calcd for $C_{23}H_{21}N_3O_3S$: C, 65.85; H, 5.05; N, 10.02; S, 7.64. Found: C, 66.19; H, 5.17; N, 10.22; S, 7.59.

3. 1. 7. General Procedure for the Synthesis of Benzo[4,5]thieno-[2,3-*b*]pyrrol-2-yl)-2-(2-Cyanoacetamido)thiophene Derivatives 12a and 12b

To a solution of either compound **8a** (3.14 g, 0.01 mol) or **8b** (3.61 g, 0.01 mol) in dimethylformamide (40 mL) ethyl cyanoacetate was added. The reaction mixture was heated under reflux for 2 h then poured onto ice/water. The formed solid product was collected by filtration and crystallized from ethanol.

***N*-(4-(3-Amino-4,5,6,7-tetrahydro-1*H*-benzo[4,5]thieno [2,3-*b*]pyrrol-2-yl)-3-cyano-thiophen-2-yl)-1-cyanoacetamide (12a)**

Yellow crystals; yield: 3.43 g (90%), mp: 184–185 °C; IR (KBr, cm^{-1}): 3482–3323 (NH, NH_2), 3055 (CH aromatic), 2225, 2220 (2CN), 1705 (C=O), 1630 (C=C); ^{1}H-NMR (DMSO-d_6) δ: 1.79–1.83 (m, 4H, $2CH_2$), 2.25–2.26 (m, 4H, $2CH_2$), 4.83 (s, 2H, NH_2, D_2O exchangeable), 5.20 (s, 2H, CH_2), 6.20 (s, 1H, thiophene H-5), 8.28, 8.32 (2s, 2H, NH, D_2O exchangeable); ^{13}C-NMR (DMSO-d_6) δ: 20.3, 22.9, 25.4, 34.7, 52.7, 116.9, 117.2, 120.3, 123.1, 124.1, 124.6, 125.3, 127.2, 138.8, 141.2,

142.6, 168.2; MS (EI): *m/z* (%) 381 (M^+). *Anal*. Calcd for $C_{18}H_{15}N_5OS_2$: C, 56.67; H, 3.96; N, 18.36; S, 16.81. Found: C, 56.88; H, 3.58; N, 18.56; S, 16.93.

Ethyl 4-(3-amino-4,5,6,7-tetrahydro-1*H*-benzo[4,5] thieno-[2,3-*b*]pyrrol-2-yl)-2-(2-cyano-acetamido) thiophene-3-carboxylate (12b)

Orange crystals; yield: 2.99 g (70%); mp: 194–195 °C; IR (KBr, cm^{-1}): 3453–3320 (NH, NH_2), 3056 (CH aromatic), 2223, 1702, 1688 (2C=O), 1632 (C=C); ^{1}H-NMR (DMSO-d_6) δ: 1.13 (t, 3H, J = 6.83 Hz, CH_3), 1.81–1.87 (m, 4H, $2CH_2$), 2.22–2.25 (m, 4H, $2CH_2$), 4.23 (q, 2H, J = 6.83 Hz, CH_2), 4.81 (s, 2H, NH_2, D_2O exchangeable), 5.23 (s, 2H, CH_2), 6.23 (s, 1H, thiophene H-5), 8.30, 8.34 (s, 2H, 2NH, D_2O exchangeable); ^{13}C-NMR (DMSO-d_6) δ: 16.0, 20.3, 22.2, 25.6, 34.8, 47.1, 51.4, 116.5, 120.4, 122.7, 123.8, 124.3, 124.9, 127.6, 133.9, 143.8, 164.3, 170.2; MS (EI): *m/z* (%) 428 (M^+). *Anal*. Calcd for $C_{20}H_{20}N_4O_3S_2$: C, 56.06; H, 4.70; N, 13.07; S, 14.97. Found: C, 56.22; H, 4.53; N, 13.31; S, 15.07.

3. 1. 8. General Procedure for the Synthesis of Hydrazoacetamide Derivatives 14a-d

To a cold solution (0–5 °C) of compound **12a** (3.81 g, 0.01 mol) in ethanol (50 mL) containing sodium acetate (3.50 g, 0.50 mol) either benzenediazonium chloride (0.01 mol), 4-chlorobenzene-diazonium chloride (0.01 mol), 4-methoxybenzenediazonium chloride (0.01 mol) or 4-methylaniline (0.01 mol) [prepared by adding a cold solution of sodium nitrite (0.70 g, in water (10 mL)) to a cold solution (0–5 °C) of either aniline oil (0.93 g, 0.01 mol), 4-chloroaniline (1.27 g, 0.01 mol) 4-methoxybenzenediazonium chloride (1.24 g, 0.01 mol) or 4-methylaniline (1.07 g, 0.01 mol) in concentrated hydrochloric acid (12 mL) with continuous stirring] was added with continuous stirring. The whole reaction mixture was left at room temperature for 1 h then the formed solid product was collected by filtration and crystallized from acetic acid.

2-((4-(3-amino-4,5,6,7-tetrahydro-1*H*-benzo[4,5]thieno[2,3-*b*]pyrrol-2-yl)-3-cyanothiophen-2-yl)amino)-2-oxo-*N*'-phenylacetohydrazonoyl cyanide (14a)

Red crystals; yield: 3.78 g (78%), mp: 223–224 °C; IR (KBr, cm^{-1}): 3475–3320 (NH), 3053 (CH aromatic), 2223, 2220 (2CN), 1708 (C=O), 1630 (C=C); ^{1}H-NMR (DMSO-d_6) δ: 1.77–1.85 (m, 4H, $2CH_2$), 2.25–2.28 (m, 4H, $2CH_2$), 4.80 (s, 2H, NH_2, D_2O exchangeable), 6.15 (s, 1H, thiophene H-5), 7.25–7.41 (m, 5H, C_6H_5), 8.25, 8.30, 8.56 (3s, 3H, 3NH, D_2O exchangeable); ^{13}C-NMR (DMSO-d_6) δ: 20.5, 22.9, 25.8, 34.7, 116.7, 117.0, 120.2, 121.7, 123.1, 124.0, 124.1, 124.6, 125.3, 126.9, 127.2, 129.3, 133.1, 138.8, 141.2, 142.8, 164.2, 168.7; MS (EI): *m/z* (%) 485 (M^+). *Anal*. Calcd for $C_{24}H_{19}N_7OS_2$: C, 59.36; H, 3.94; N, 20.19; S, 13.21. Found: C, 59.42; H, 3.72; N, 20.53; S, 13.08.

2-((4-(3-Amino-4,5,6,7-tetrahydro-1*H*-benzo[4,5]thieno[2,3-*b*]pyrrol-2-yl)-3-cyanothiophen-2-yl)amino)-*N*'-(4-chlorophenyl)-2-oxoacetohydrazonoyl cyanide (14b)

Red crystals; yield: 4.41 g (85%), mp: 194–195 °C; IR (KBr, cm^{-1}): 3488–3315 (NH, NH_2), 3056 (CH aromatic), 2225, 2220 (2CN), 1710 (C=O), 1628 (C=C); ^{1}H-NMR (DMSO-d_6) δ: 1.79–1.85 (m, 4H, $2CH_2$), 2.23–2.27 (m, 4H, $2CH_2$), 4.83 (s, 2H, NH_2, D_2O exchangeable), 6.12 (s, 1H, thiophene H-5), 7.28–7.39 (m, 4H, C_6H_4), 8.23, 8.32, 8.42 (3s, 3H, 3NH, D_2O exchangeable); ^{13}C-NMR (DMSO-d_6) δ: 20.6, 22.4, 25.8, 34.9, 116.8, 117.3, 120.0, 121.4, 123.1, 124.0, 124.1, 124.8, 125.3, 127.2, 138.8, 140.4, 141.2, 143.4, 164.8, 168.6; MS (EI): *m/z* (%) 520 (M^+). *Anal*. Calcd for $C_{24}H_{18}ClN_7OS_2$: C, 55.43; H, 3.49; N, 18.85; S, 12.33. Found: C, 55.70; H, 3.62; N, 18.59; S, 12.48.

2-((4-(3-Amino-4,5,6,7-tetrahydro-1*H*-benzo[4,5]thieno[2,3-*b*]pyrrol-2-yl)-3-cyanothiophen-2-yl)amino)-*N*'-(4-methoxyphenyl)-2-oxoacetohydrazonoyl cyanide (14c)

Reddish brown crystals; yield: 4.63 g (90%); mp: 168–169 °C; IR (KBr, cm^{-1}): 3462–3335 (NH, NH_2), 3053 (CH aromatic), 2227, 2221 (2CN), 1720 (C=O), 1638 (C=C); ^{1}H-NMR (DMSO-d_6) δ: 1.74–1.82 (m, 4H, $2CH_2$), 2.21–2.28 (m, 4H, $2CH_2$), 3.38 (s, 3H, OCH_3), 4.88 (s, 2H, NH_2, D_2O exchangeable), 6.13 (s, 1H, thiophene H-5), 7.31–7.42 (m, 4H, C_6H_4), 8.21, 8.32, 8.45 (3s, 3H, 3NH, D_2O exchangeable); ^{13}C-NMR (DMSO-d_6) δ: 20.8, 22.7, 25.8, 34.3, 55.3, 116.3, 117.0, 120.3, 121.4, 123.8, 124.0, 124.0, 124.8, 125.9, 127.0, 133.2, 138.2, 140.8, 141.9, 164.9, 168.6; MS (EI): *m/z* (%) 516 (M^+). *Anal.* Calcd for $C_{25}H_{21}N_7O_2S_2$: C, 58.24; H, 4.11; N, 19.02; S, 12.44. Found: C, 58.40; H, 4.26; N, 19.11; S, 12.29.

2-((4-(3-Amino-4,5,6,7-tetrahydro-1*H*-benzo[4,5]thieno[2,3-*b*]pyrrol-2-yl)-3-cyanothiophen-2-yl)amino)-2-oxo-*N*'-(p-tolyl)acetohydrazonoyl cyanide (14d)

Reddish brown crystals; yield: 3.44 g (69%); mp: 129–130 °C; IR (KBr, cm^{-1}): 3482–3318 (NH, NH_2), 3057 (CH aromatic), 2227, 2220 (2CN), 1712 (C=O), 1630 (C=C); ^{1}H-NMR (DMSO-d_6) δ: 1.76–1.83 (m, 4H, $2CH_2$), 2.23–2.28 (m, 4H, $2CH_2$), 2.65 (s, 3H, CH_3), 4.86 (s, 2H, NH_2, D_2O exchangeable), 6.11 (s, 1H, thiophene H-5), 7.30–7.39 (m, 4H, C_6H_4), 8.23, 8.30, 8.48 (3s, 3H, 3NH, D_2O exchangeable); ^{13}C-NMR (DMSO-d_6) δ: 20.4, 22.9, 23.3, 25.8, 34.6, 116.4, 117.3, 120.6, 122.8, 123.8, 124.0, 124.3, 124.8, 125.2, 126.4, 138.8, 140.6, 141.7, 143.9, 164.6, 168.7; MS (EI): *m/z* (%) 500 (M^+). *Anal*. Calcd for $C_{25}H_{21}N_7OS_2$: C, 60.10; H, 4.24; N, 19.62; S, 12.84. Found: C, 60.32; H, 4.52; N, 19.48; S, 12.64.

3. 1. 9. General Procedure for the Synthesis of Thieno[2,3-*b*]pyridine Derivatives 15a and 15b

A suspension of either compound **12a** (3.81 g, 0.01 mol) or **12b** (4.28 g,0.01 mol) in sodium ethoxide (0.02

mol) [prepared by dissolving metallic sodium (0.46 g, 0.02 mol) in absolute ethanol (20 mL] was heated in a boiling water bath for 12 h then poured onto ice/water containing few drops of hydrochloric acid. The formed solid product was collected by filtration and crystallized from 1,4-dioxane.

4-Amino-3-(3-amino-4,5,6,7-tetrahydro-1*H*-benzo[4,5]thieno[2,3-*b*]pyrrol-2-yl)-6-hydroxy-thieno[2,3-*b*]pyridine-5-carbonitrile (15a)

Yellow crystals; yield: 2.29 g (60%); mp: > 300 °C; IR (KBr, cm^{-1}): 3593–3355 (NH, NH_2, OH), 3056 (CH aromatic), 2224 (CN), 1635 (C=C); ^{1}H-NMR (DMSO-d_6) δ: 1.75–1.85 (m, 4H, $2CH_2$), 2.23–2.27 (m, 4H, $2CH_2$), 4.68, 5.09 (2s, 4H, $2NH_2$, D_2O exchangeable), 6.16 (s, 1H, thiophene H-5), 8.28 (s, 1H, NH, D_2O exchangeable), 9.90 (s, 1H, OH, D_2O exchangeable); ^{13}C-NMR (DMSO-d_6) δ: 20.8, 22.9, 25.8, 34.7, 116.7, 120.2, 121.7, 123.1, 124.1, 124.6, 125.3, 126.5, 127.0, 129.6, 138.8, 142.8, 144.5, 162.8; MS (EI): *m/z* (%) 381 (M^+). *Anal.* Calcd for $C_{18}H_{15}N_5OS_2$: C, 56.67; H, 3.96; N, 18.36; S, 16.81. Found: C, 56.93; H, 3.65; N, 18.48; S, 17.09.

3-(3-Amino-4,5,6,7-tetrahydro-1*H*-benzo-4,5]thieno[2,3-*b*]pyrrol-2-yl)-4,6-dihydroxy-thieno[2,3-*b*]pyridine-5-carbonitrile (15b)

Yellow crystals; yield: 2.79 g (73%) g); mp: 289–290 °C; IR (KBr, cm^{-1}): 3578–3345 (NH, NH_2, OH), 3056 (CH aromatic), 2222 (CN), 1628 (C=C); ^{1}H-NMR (DMSO-d_6) δ: 1.79–1.85 (m, 4H, $2CH_2$), 2.23–2.27 (m, 4H, $2CH_2$), 4.86 (s, 2H, NH_2, D_2O exchangeable), 6.17 (s, 1H, thiophene H-5), 8.26 (s, 1H, NH, D_2O exchangeable), 10.29, 10.34 (2s, 2H, D_2O exchangeable, 2OH); ^{13}C-NMR (DMSO-d_6) δ: 20.3, 22.8, 25.8, 34.7, 116.6, 120.2, 121.6, 123.1, 124.7, 124.1, 124.8, 125.3, 126.8, 127.5, 133.2, 140.8, 143.8, 144.2, 162.9; MS (EI): *m/z* (%) 382 (M^+). *Anal*. Calcd for $C_{18}H_{14}N_4O_2S_2$: C, 56.53; H, 3.69; N, 14.65; S, 16.77. Found: C, 56.72; H, 3.46; N, 14.80; S, 16.37.

4. Conclusions

Novel 4,5,6,7-tetrahydro-1*H*-benzo[4,5]thieno[2,3-*b*]pyrrol-derivatives were synthesized in good yields. Some compounds were used to produce annulated products. The cytotoxicity of the newly synthesized compounds indicate that compounds **4**, **7a**, **7b**, **8a**, **8b**, **10c, 10d**, **10f**, **12a**, **12b, 14b** and **15b** showed the highest potency among the tested compounds. In addition, the anti- proliferative evaluations of these twelve compounds indicated that the benzo[4',5']thieno[3',2':4,5]pyrrolo[3,2-*b*]pyridine derivative **7b** and the benzo[4,5]thieno-[2,3-*b*]pyrrol-2-yl)-thiophene derivative **8b** showed high potency against Molt4/C8 and CEM cell lines and their IC_{50}'s are higher than the reference drug "doxorubicin".

5. Acknowledgments

R. M. Mohareb would like to thank the Alexander von Humboldt for affording him regular fellowships in Germany for doing research and completing this work.

6. References

1. S. Xue, H. Guo, M. Liu, J. Jin, D. Ju, Z. Liu, Z. Li, Eur. *J. Med. Chem.* **2015**, *26*, 151–161. http://dx.doi.org/10.1016/j.ejmech.2015.04.016
2. L. Ye, J. He, Z. Hu, Q. Dong, H. Wang, F. Fu, J. Tian, *Food Chem. Toxicol.* **2013**, *52*, 200–206. http://dx.doi.org/10.1016/j.fct.2012.11.004
3. S. Hama, S. Utsumi, Y. Fukuda, K. Nakayama, Y. Okamura, H. Tsuchiya, K. Fukuzawa, H. Harashima, K. Kogure, *J. Controlled Release*. **2012**, *161*, 843–851. http:// 10.1016/j.jconrel.2012.05.031
4. I. M. Fakhr, M. A. Radwan, S. El-Batran, O. M. Abd El-Salam, S. M. El-Shenawy, *Eur. J. Med. Chem.* **2009**, *44*, 1718–1725. http:// 10.1016/j.ejmech.2008.02.034
5. S. Bondock, W. Fadaly, M. A. Metwally, *Eur. J. Med. Chem.* **2010**, *45*, 3692–3701. http://dx.doi.org/10.1016/j.ejmech.2010.05.018
6. C. K. Ryu, S. K. Lee, J. Y. Han, O. J. Jung, J. Y. Lee, S. H. Jeong, *Bioorg. Med. Chem. Lett.* **2005**, *15*, 2617–2620. http://doi.org/10.1016/j.bmcl.2005.03.042
7. L. J. Gonzalez, C. E. Stephens, T. Wenzler, R. Brun, F. A. Tanious, W. D. Wilson, T. Barszcz, K. A. Werbovetz, D. W. Boykin, *Eur. J. Med. Chem.* **2007**, *42*, 552–557. http://dx.doi.org/10.1016/j.ejmech.2006.11.006
8. J. B. Hudson, E. A. Graham, N. Miki, G. H. N. Towers, L. L. Hudson, R. Rossi, A. Carpita, D. Neri, *Chemosphere.* **1989**, *19*, 1329–1343. http://dx.doi.10.1016/0045-6535(89)90080-5
9. K. I. Molvi, K. K. Vasu, S. G. Yerande, V. Sudarsanam, N. Haque, *Eur. J. Med. Chem*. **2007**, *42*, 1049–1058. http://dx.doi.10.1016/j.ejmech.2007.01.007
10. R. Kulandasamy, A. V. Adhikari, J. P. Stables, *Eur. J. Med. Chem.* **2009**, *44*, 4376–4384. http://dx.doi.10.1016/j.ejmech. 2009.05.026
11. H. J. Jung, Y. S. Song, C. J. Lim, E. H. Park, *J. Ethanopharmacol.* **2009**, *126*, 355–360. http://dx.doi.10.1016/j.jep.2009.08.031
12. W. O. Chi, L. H. Chang, *Inorg. Chim. Acta.* **1986**, *125*, 203–206. http://dx.doi. 10.1016/S0020-1693(00)81212-8.
13. D. C. S. Friedman, P. Friedman, *J. Mol. Struct. Theochem*, **1995**, *333*, 71–78. http://dx.doi. 10.1016/0166-1280(94)03930-J
14. M. K. Parai, G. Panda, V. Chaturvedi, Y. K. Manju, S. Sinha, *Bioorg. Med. Chem. Lett.* **2008**, *18*, 289–292. http://dx.doi. 10.1016/j.bmcl.2007.10.083
15. D. Caridha, A. K. Kathcart, D. Jirage, N. C. Waters, *Bioorg. Med. Chem. Lett.* **2010**, *20*, 3863–3867. http://dx.doi.org/10.1016/j.bmcl.2010.05.039

16. G. Fear, S. Komarnytsky, I. Raskin, *Pharm. Therap.* **2007**, *113*, 354–368. http://dx.doi. 10.1016/j.pharmthera.2006.09.001
17. B. O. Al-Najjar, H. A. Wahab, T. S. T. Muhammad, A. C. Shu-Chien, N. A. A. Noruddin, M. O. Taha, *Eur. J. Med. Chem.* **2011**, *46*, 2513–2529. http://dx.doi.org/10.1016/j.bmcl.2010.05.039
18. R. M Mohareb, N. S. Abbas, A. R. Ibrahim, *Acta Chim. Solv.* **2013**, *60*, 583–594. http://dx.doi.org/ 0.17344/acsi.2013.1418
19. R. M. Mohareb, E. Z. El-Arab, K. A. El-Sharkawy, *Sci. Pharm*. **2009**, ***77***, 355–366. http://dx.doi.org/10.3797/scipharm.0901-20
20. R. M. Mohareb, N. Y. Megally Abdo, *Molecules.* **2015**, *20*, 11535–11553. doi:10.3390/molecules200611535
21. R. M. Mohareb, N. Y. Megally Abdo, *Chem. Pharm. Bull.* **2015**, *63*, 678–687. http://dx.doi.org/10.1248/cpb.c15-00115
22. R. M. Mohareb, M. Y. Zaki, N. S. Abbas, *Steroids.* **2015**, *98*, 80–91. http://dx.doi. 10.1016/j.steroids.2015.03.001
23. R. M. Mohareb, F. Al-Omran, *Steroids.* **2012**, *77*, 1551–1559. http://dx.doi.org/10.1016/j.steroids.2012.09.007
24. B. P. McKibben, C. H. Cartwright, A. L. Castelhano, *Tetrahedron Lett*. **1999**, *40*, 5471–5474. http://dx.doi.org/10.1016/S0040-4039(99)01108-9
25. K. Balamurugan, S. Perumal, S. K. Reddy, P. Yogeeswari, D. Sriram, *Tetrahedron Lett.* **2009**, *50*, 6191–6195. http://dx.doi.org/10.1016/j.tetlet.2009.08.085
26. R. M. Mohareb, A. E. Mahmoud, M. A. Abdelaziz, *Med. Chem. Res.* **2014**, *23*, 564–579. http://dx.doi.org/10.1007/s00044-013-0664
27. D. Briel, A. Rybak, C. Kronbach, K. Unverferth, *Eur. J. Med. Chem.* **2010**, *45*, 69–77. http://dx.doi.org/10.1016/j.ejmech.2009.09.025
28. A. Monks, D. Scudiero, P. Skehan, R. Shoemaker, K. Paull, D. Vistica, C. Hose, J. Langley, P. Cronise, A. Waigro-Wolff, M. Gray-Goodrich, H. Campbell, J. Mayo, M. Boyd, *J. Natl. Cancer Inst*. **1991**, *83*, 757–766. http://dx.doi.org/10.1093/jnci/83.11.757
29. K. D. Paull, H. Shoemaker, L. Hodes, A. Monks, D. A. Scudiero, L. Rubinstein, J. Plowman, M. R. Boyd, *J. Natl. Cancer Inst.* **1989**, *81*, 1088–1092. http://dx.doi.org/10.1093/jnci/81.14.1088
30. L. S. Olsen, P. J. Hjarnaa, S. Latini, P. K. Holm, R. Larsson, E. Bramm, L.Binderup, M. W. Madsen, *Int. J. Cancer*. **2004**, *111*, 198–205. http://dx.doi.org/10.1002/ijc.20255
31. A. Svensson, U. Bäckman, E. Jonsson, R. Larsson, R. Christofferson, *Pediatr Res.* **2002**, *51*, 607–611. http://dx.doi.org/10.1203/00006450-200205000

Povzetek

Iz 2-amino-3-ciano-4,5,6,7-tetrahidrobenzo[*b*]tiofena (**1**) smo z reakcijo z with α-kloroacetonom sintetizrali *N*-alkil derivat (**3**), tetrahidrobenzo[*b*]tienopirol. Spojino **3** smo v raztopini natrijevega etoksida s ciklizacijo pretvorili v tetrahidrobenzo[*b*]tienopirol (**4**), ki smo ga uporabili naprej za sinteze derivatov tiofena, tieno[2,3-*b*]piridina in pirana. Citotoksičnost sintetiziranih spojin smo preverili na rakavih celicah želodčnega (NUGC), črevesnega (DLD-1), jetrnega (HA22T in HEPG-2) ter nazofaringealnega karcinoma (HONE-1), raka dojk (MCF-7) in na normalnih fibroblastnih celicah (WI-38). Izkazalo se je, da imajo spojine **4**, **7a**, **7b**, **8a**, **8b**, **10c, 10d**, **10f**, **12a**, **12b, 14b** in **15b** optimalni citotoksični učinek na rakave celice. Spojini **7b** in **14b** kažeta maksimalni inhibicijski efekt, ki je precej večji od efekta referenčne spojine CHS-828 (piridil cianogvanidina).

Scientific paper

Green Biosynthesis of Spherical Silver Nanoparticles by Using Date Palm (*Phoenix Dactylifera*) Fruit Extract and Study of Their Antibacterial and Catalytic Activities

Saeed Farhadi,[1,]* Bahram Ajerloo[1] and Abdelnassar Mohammadi[2]

[1] *Department of Chemistry, Lorestan University, Khoramabad 68151-44316, Iran*

[2] *Department of Biology, Lorestan University, Khoramabad 68151-44316, Iran*

** Corresponding author: E-mail: sfarhadi1348@yahoo.com*
Tel.: +98-6633120618, fax: +98-6633120611

Received: 30-09-2016

Abstract

In this work, we have synthesized spherical silver nanoparticles (Ag NPs) by a low-cost, rapid, simple and ecofriendly approach using Date palm fruit extract as a novel natural reducing and stabilizing agent. The product was characterized by UV-visible spectroscopy, X-ray diffraction (XRD), Fourier transform infrared spectroscopy (FTIR), field emission scanning electron microscopy (FESEM), transmission electron microscopy (TEM), atomic force microscopy (AFM), energy-dispersive X-ray (EDX) spectroscopy and Zeta potential measurements. The reaction conditions including time, content of reducing agent and silver nitrate, temperature and pH were investigated. The optimum yield of Ag NPs was obtained when 10 mM of silver nitrate was reacted with Date fruit extract at pH 11 and heated it to 55 °C within 10 minutes. The elemental and crystalline nature of Ag NPs were confirmed from EDX and XRD analysis. SEM and TEM images showed that the Ag NPs were spherical and with sizes in the range of 25–60 nm. On the base of FT-IR analysis, it can be stated that the functional groups present in bio-molecules of Date fruits are responsible for the reduction and stabilization of Ag NPs, respectively. The Ag NPs showed good antibacterial activity against a few human pathogenic bacteria. The catalytic activity of the Ag NPs for rapid and efficient reduction of toxic nitro compounds into less toxic corresponding amines by using $NaBH_4$ was also investigated.

Keywords: Biosynthesis, Silver nanoparticles, Date palm fruit extract, Antibacterial activity, Nitro reduction, Catalyst

1. Introduction

Among various transition metal nanoparticles, silver nanoparticles (Ag NPs) have attracted considerable attention in nanoscience and nanotechnology due to their excellent optical and electronic properties as well as their wide applications in various fields such as catalysis,[1] surface enhanced Raman scattering,[2] degradation of environmental pollutants,[3] biosensors[4] cancer therapy5 and antibacterial effects.[6] Several synthetic strategies have been developed for the synthesis of Ag NPs including photochemical,[7] sonochemical,[8] sovothermal[9] and spin coating methods.[10] Among these, chemical reduction of a silver ions (Ag^+) in presence of a stabilizer is the most frequently applied method for the preparation of Ag NPs as stable colloidal dispersions in water or organic solvents.[11] The major drawback of chemical method is that the highly reactive chemical reductants as well as the stabilizers such as synthetic polymers, surfactants and dendrimers used in this method cause chemical toxicity and serious environmental problems, thus limiting their utility.

In recent years, biosynthesis of metal nanoparticles has received considerable attention due to the growing need to develop clean and nontoxic chemicals, environmentally friendly solvents and renewable materials.[12] The selection of a non-toxic reducing agent, a cost-effective and easily renewable stabilizing agent and an environmentally benign solvent system are the three main criteria for a greener metal nanoparticles synthesis. In this regard, a great deal of effort has been devoted toward the biosynthesis of silver nanoparticles using bacteria,[13–17] fungi,[18-20] actinomycetes,[21–23] yeast[24] and viruses[25–27] but the rate of nanoparticle synthesis is faster using fruits and plants extracts than microbes, and the pro-

duced nanoparticles are more stable.[28] In recent regards, the synthesis of Ag NPs has been reported by using the natural extract of leaves, seeds and or roots of plants such as *Nelumbo nucifera*,[29] *Anisochilus carnosus,* [30] *Mimusops elengi*,[31] *marine macroalga Chaetomorpha linum,*[32] *Bunium persicum*,[33] *Olea europaea,*[34] *Hamamelis virginiana,*[35] *Justicia adhatoda*,[36] *Suaeda acuminata*,[37] *Mentha piperita*,[38] *Phlomis*,[39] *Pennyroyal,*[40] *Murraya keenigii*,[41] *Mangifera indica*,[42] *Nicotiana tobaccum*,[43] *Bunium persicum,*[44] *Hamamelis virginiana*.[45] However, the reaction time of Ag^+ ions for complete reduction in these works was very long. To enable the biosynthesis methods of Ag NPs to compete with the chemical methods, there is a need to achieve faster synthesis rates with high monodispersion. The use of fruit extracts of plants is an appropriate candidate for this purposes. Several papers on the synthesis of Ag NPs using the extract of fruits such as *Terminalia chebula,*[46] *Solanum trilobatum*,[47] *Dillenia indica,*[48] *Solanum lycopersicums,*[49] *Tanacetum vulgare,*[50] *Crataegus douglasii,*[51] *Emblica Officinalis,*[52] and *Kiwifruit* [53] have been reported in the literatures.

The Date palm tree *(Phoenix dactylifera),* a tropical and subtropical tree, is one of mankind's oldest cultivated plants, and it has played an important role in the day-to-day life of the people for the last 7000 years.[54] Dates are produced in 35 countries worldwide and cultivated on about 2.9 million acres of land. The world production of date fruit estimate to be more than 7000000 metric tons, and Iran (14% of world production) is the second major producer after Egypt (17% of world production). Figure 1 shows the photographs of Date palm trees ant their fruits. The Date fruit is considered to be an inexpensive and easily available important fruit in Iran.[55] The Date palm fruits are an important source of nutrition, especially in the arid regions where due to the extreme conditions, very few plants can grow. Date fruit also shows some functional properties in the food industry, such as water-holding, oil-holding, emulsifying and gel formation. Indeed, Date fruit can be incorporated in food products to modify textural properties, avoid synthesis and stabilize high fat food and emulsions.[56] The study by Abdelhak has shown that different varieties of ripe Date fruits contained mainly p-coumaric, ferulic and sinapic acids and some cinnamic acid derivatives.[57] The in vitro study by Vayalil reported that the aqueous extract of Date fruits has antioxidative and antimutagenic properties.[58] On the other hand, the study by Bilgari had shown

Figure 1(a)-(d) Photographs of Date palm trees and their fruits.

a strong correlation between the antioxidant activity and the total phenolic and total flavonoids of palm dates.[59] The Date fruit is rich in phytochemicals like carbohydrates and sugars, phenolics, sterols, carotenoids, anthocyanins, procyanidins, and flavonoids.[60] Most of the biomolecules can act as reducing and capping agent in the reactions. Then, the Date fruits extract that are inherently rich in these phytochemicals could be used as a novel reducing agent for synthesizing Ag NPs in large-scale production.

In this paper, we report on rapid, simple and low-cost synthesis of Ag NPs by the reduction of aqueous Ag^+ solution using Date fruit extract. To our knowledge, this is the first report on the use of Date fruit for the rapid synthesis of Ag NPs. The nearly monodisperse Ag were formed under mild conditions, without any additive protecting nanoparticles. The formation of Ag NPs was recorded by the UV-visible spectra. Additionally, the obtained Ag NPs were analyzed by Fourier transform infrared (FT-IR) spectra, and X-ray diffraction (XRD), scanning electron microscopy (SEM), transmission electron microscopy (TEM), and energy-dispersive X-ray (EDX) spectroscopy. The rapid approach using Date fruit extract would be suitable for developing a biological process for large-scale production. Various parameters (e.g. concentration of the reactants, reaction temperature, pH and time) were optimized that would increase the yield of nanoparticle synthesis. The antibacterial and catalytic activities of the biologically synthesized Ag NPs were also investigated.

2. Experimental

2. 1. Materials

Silver nitrate ($AgNO_3$), $NaBH_4$, 4-nitrophenol, and 4-nitroanilin were obtained from Merck and were of analytical grade. Double distilled de-ionized water was used for the experiments. All glass wares were properly washed with distilled water and dried in oven.

2. 2. Preparation of Date Palm Fruit Extract

Date Palm fruit extract was used as a reducing and stabilizing agent for the synthesis of Ag NPs. Date palm fruits were purchased from local supermarket in Iran and used for the synthesis of silver nanoparticles. The fresh fruits of Date washed repeatedly with distilled water to remove the dust and organic impurities present in it. About 15 g of fruit were crushed into fine pieces with sterilized knife. The fruit of Date Palm were taken into the 250 ml beaker containing 100 mL double distilled de-ionized water and then the solution was stirred for 30 min and filtered through Whatman No.1 filter paper twice. The obtained light yellow extract was stored in refrigerator at 4 °C. The extract is used as reducing agent as well as stabilizing agent.

2. 3. Synthesis of Ag Nanoparticles

In a typical experiment, Ag NPs were prepared by using Date fruit extract as follows: in a 50 mL round-bottom flask equipped with a magnet bar, 3 ml of aqueous solution of Date fruit extract was mixed with 20 ml of 10 mM aqueous silver nitrate solution. The mixture was then heated at 55 °C under constant stirring for an appropriate time (e.g. 10 min) in an oil bath. The formation process and the optical properties of the silver nanoparticles were identified from both the color change and UV-Vis spectra of the solution**.** In order to remove the Ag NPs product, the solution was centrifuged at 5500 rpm for 20 min. The supernatant was decanted and the precipitate was re-dispersed in double distilled water for another round of centrifugation. The precipitate was then washed with deionized water for three times to remove any impurities if any. Finally, the washed precipitate was dried in an oven maintained at 60 °C for 2 h and finally ground into powder for characterization.

In a similar manner described above, a series of experiments were conducted to investigate the effect of various parameters including reaction time, Ag^+ ion concentration, the Date fruit extract amount, pH and temperature on the reaction. The reaction mixtures were monitored by a UV-Vis spectrophotometer at different time intervals and the Ag NPs were characterized further. The effect of pH on the Ag NPs synthesis was determined by adjusting the pH of the reaction mixtures (10 mM silver nitrate, 3 mL date extract) to 3, 5, 7, 9, 11 or 13 by using 0.1 M HCl or NaOH aqueous solutions. The effect of the silver salt was determined by varying the concentration of silver nitrate (0.1, 1, 10 and 100 mM). The Date fruit extract content was varied to 1, 3, 5, 7, 9 mL, while keeping the silver nitrate concentration at a level of 10 mM. To study the effect of temperature on nanoparticle synthesis, reaction mixtures containing 3 mL Date extract, and 10 mM $AgNO_3$ at pH 11 were incubated at 25, 40, 55 or 70 °C.

2. 4. Methods of Characterization

The UV-visible absorption spectra of Ag NPs colloidal solutions were recorded on a double beam UV-visible spectrometer (Cary 100, VARIAN) operated at a resolution of 2 nm with quartz cells with path length of 1 cm in 300–800 nm range. Blanks were prepared with deionized (DI) water. Infrared spectra were obtained using a FT-IR 160 Schimadzu Fourier transform infrared spectrophotometer using KBr pellets. The XRD pattern of the silver nanoparticles was obtained on an X-ray diffractomer (PANalytical/X'Pert Pro MPD) using Cu Kα (1.54059 Å) radiation. The particle size and shape was confirmed using a scanning electron microscope (MIRA3 TESCAN) equipped with EDX attachment. Transmission electron microscopy (TEM) observations were conducted on a Philips CM120 microscope at the accelerating voltage of 200 kV. AFM images were recorded on a multi-mode ato-

mic force microscopy (ARA-AFM, model Full Plus, ARA Research Co., Iran). The surface charge of samples was measured with Zeta potential measurements in water (NICOMP 380ZLS Zeta potential/Particle sizer). Magnetic measurements were carried out at room temperature using a vibrating sample magnetometer (VSM, Magnetic Daneshpajoh Kashan Co., Iran) with a maximum magnetic field of 10 kOe.

2. 5. Antibacterial Tests

Antibacterial activity of the biosynthesized Ag NPs was evaluated against strains of Gram-positive bacteria: Bacillus cereus (PTCC 1015), Staphylococcus aureus (1431) and Staphylococcus epidermidis (PTCC 1114), Gram–negative bacteria: Escherichia coli (PTCC 1330) and Klebsiella pneumonia (PTCC 1290) by modified Kirby-Bauer disk diffusion method [66]. Bacteria were cultured for 18 h at 37 °C in Nutrient agar medium and then adjusted with sterile saline to a concentration of 2×10^6 cfu/mL. Bacterial suspension in Petri dishes (8 cm) containing sterile Mueller-Hinton agar (MA) were cultured using a sterile cotton swab. The compounds were dissolved in water and sterile paper discs of 6 mm thickness were saturated with 30 µl of silver nanoparticles and then placed onto agar plates which had previously been inoculated with the tested microorganisms. Amikacin (30 µg/disk) for gram negative and penicillin for gram positive (10 µg/disk) was used as positive controls. After incubation at 37 °C for 24 h, the diameter of inhibition zone was measured. The diameter of such zones of inhibition was measured using a meter ruler, and the mean value for each organism was recorded and expressed in millimetres.

2. 6. Catalytic Tests

In order to study the catalytic performance of the biosynthesized Ag NPs, the reduction of 4-nitrophenol (4-NP) to 4-amiophenol (4-AP) by excess sodium borohydride ($NaBH_4$) in aqueous solution was used as the model reaction. In a typical catalytic reaction, 3 mL of aqueous solution of 4-NP (0.1 mM) and 0.5 mL of aqueous $NaBH_4$ (10 mM) solution were mixed together in a standard quartz cell, having 1 cm path length and then 1 mL of aqueous Ag suspensions (0.5 mg mL^{-1}) was added to the reaction mixture under constant magnetic stirring. Immediately after that, the solution was transferred to a standard quartz cell, and the concentration of p-nitrophenol in the reaction mixture was monitored by the UV-visible absorption spectra recorded with a time interval of 2 min in a scanning range of 200–800 nm at ambient temperature. For recycling experiment, after completion of the reaction the catalyst was recovered by centrifugation. The precipitate was washed repeatedly with deionized water in consecutive washing cycles. Ultrasonic treatment was used in every cycle in order to re-disperse the catalyst and remove adsorbed impurities. After washing, the catalyst was used directly for recycling test. After each recycle, the centrifuge supernatant was collected and detected by Atomic absorption spectroscopy to determine the content of Ag metal. The reduction 4-nitroaniline was also investigated under the same conditions.

3. Results and Discussion

3. 1. Phytoreduction of Silver Ions

A study on phytosynthesis of Ag NPs by the aqueous fruit extract of date was carried out in this work. During the visual observation, silver nitrate treated with date fruit extract showed a color change from yellow to brown within 20 min whereas no color change could be observed in silver nitrate solution without date extract (Figure 2). The appearance of yellowish brown color in fruit extract treated flask is a clear indication for the formation of Ag NPs. This color arises due to excitation of surface plasmon resonance (SPR) vibrations in Ag nanoparticles.

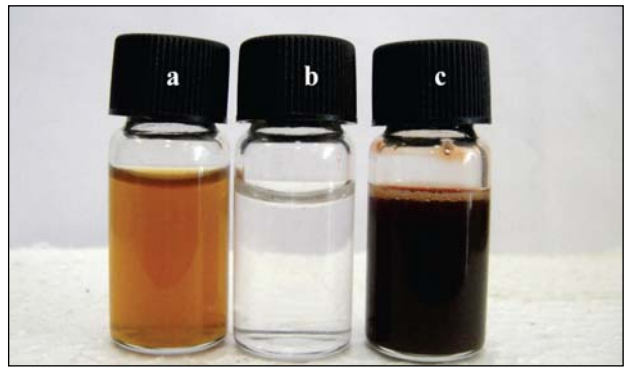

Figure 2. Photographs of: (a) aqueous extract of date fruits, (b) 10 mM of aqueous $AgNO_3$ solutions, and (c) Colloidal aqueous Ag NPs solution formed by reduction of $AgNO_3$ with Date fruit extract.

3. 2. UV–Visible Absorption Studies

UV–Vis spectroscopy is a powerful tool to study the formation of Ag NPs. The reaction mixtures containing silver salt and Date fruit extract were, therefore characterized by UV–Visible spectroscopy. Based on UV–Vis spectroscopy various chemical and physico-parameters (concentration of the fruit extract and silver salt, pH, temperature and reaction time) were optimized for the reduction Ag+ ions to Ag NPs using Date fruit extract.

To optimize the reaction time, a time variation study was carried out using the concentration of $AgNO_3$ (10 mM) and aqueous date extract (3 mL). Figure 3(a) shows the UV–Vis absorption spectra of Ag NPs synthesized at

different time durations. It is observed that the intensity of SPR bands increases as the reaction time progresses and within 10 min a considerable intensity of the SPR bands is achieved. However, these values were hardly changed after 10 min. It suggested that the reduction time of Ag^+ was almost completed within 10 min in the presence of date extract. Therefore, the optimal reaction time for the reduction Ag^+ ions to Ag NPs using Date fruit extract is 10 min. As shown in the inset of Fig. 3(a), after the reaction between Ag^+ and date extract, the color was changed from clear yellow to dark brown and it shows the formation of Ag NPs.

Next, various concentrations of silver nitrate solution (0.1–100 mM) were reacted with 3 mL fruit extract. Figure 3(b), shows the UV–Vis absorption spectra of Ag NPs obtained at different concentrations of $AgNO_3$ (0.1, 1, 10 and 100 mM). At 0.1 mM concentration, an observable SPR band was not appeared, indicating very low yield of Ag NPs formed (Figure 3(b), curve i), but with increasing concentration of $AgNO_3$ to 1 mM, the SPR of Ag NPs appears at 395 nm and remarkably increases with the increase of $AgNO_3$ concentration to 10 mM with increasing in the peak wavelength to 410 nm (Figure 3(b), curves i and ii, respectively). High intensity of the 410 nm SPR band indicates increasing concentration of nanoparticle. However, further increasing the concentration of $AgNO_3$ from 10 to 100 mM did not increase the SPR band further–in contrast, it give a broad SPR band with decreased intensity and shifted to longer wavelength region (~425 nm). This phenomenon may be due to the fast growth of the particles at high concentration. The appearance of red shifted band at higher concentration of $AgNO_3$ suggests the formation of larger particles. The yield of Ag NPs increased with the increase in silver nitrate concentration (0.1–10 mM) and maximum yield was obtained with 10 mM, and this concentration was selected for further studies.

Additionally, the effect of the date extract amount on the synthesis of Ag NPs was investigated under the provided reaction conditions, and the results are shown in Figure 3(c). As observed, with increasing the date extract quantity from 1 to 3 mL in 20 mL of 10 mM Ag^+ ion solution, the intensity of characteristic SPR absorption bands for Ag NPs increases (Figure 3(c), curves i and ii) and then decreases when the date extract increases further (Figure 3(c), curves iii-v). The maximum absorption was found at a concentration of 3 mL fruit extract. From the UV-Vis absorption spectrum in Figure 3(c), it was observed that there is a shift in wavelength from 400 to 412 nm indicating a redshift with increase in date extract concentration from 1 to 3 mL. Accordingly, it can be concluded that with the increase in Date extract amount, the size of Ag nanoparticles increases.

The temperature also affected the process of silver reduction. The effect of reaction temperature was also evaluated with varying reaction temperatures from 25 to 75 °C (Figure 3(d)). As shown in Figure 3(d) (curves i and ii), the reaction mixtures incubated at room temperature (25 °C) and 40 °C showed less pronounced SPR peaks during a long time of 50 min while by heating the reaction mixtures at 55 and 70 °C the reduction process was faster and the intense peaks were developed within a short time of 10 min (Figure 3(d), curves iii and iv). This indicates that higher temperature facilitates the formation of Ag NPs due to the increase in the reaction rate. The maximum SPR peak intensity was detected at 70 °C. However, a slight increase in SPR band intensity occurs at 75 °C when compared with the temperature of 55 °C. Then, the temperature of 55 °C is preferred for further study. It is noteworthy to mention that with the increase in reaction temperature, UV-Vis spectra show sharp narrow peaks at lower wavelength regions (~412 nm at 55 and 70 °C), which indicate the formation of smaller nanoparticles, whereas, at lower reaction temperature, the peaks observed at higher wavelength region (425 nm at 25 °C) which clearly indicates increase in silver nanoparticles size. It is a well-known fact that when the temperature is increased, the reactants are consumed rapidly leading to the formation of smaller nanoparticles [61, 62].

Among the various parameters, the initial pH of solution plays a significant role in the synthesis of metal nanoparticle. Thus, in the present study, the effect of pH on the synthesis of Ag NPs was studied at acidic, natural and basic values using 3 ml Date fruit extract and 10 mM $AgNO_3$. As can be seen in Figure 3(e) (curves i and ii) the formation of Ag nanoparticles was not observed at all at acidic pHs 3 and 5. Under the acidic conditions, biomolecules are likely to be inactivated. This suggests that acidic pH is not favorable for the Ag NPs synthesis. At pH 7, the Ag NPs formation was observed at relatively low concentration, as confirmed by the appearance of a weak absorbance band at about 425 nm (Figure 3(e), curve iii). However, Ag NPs were readily obtained at pH higher than 7, as evidenced through progressive evolution of the characteristic SPR band in the spectral region from 400 to 415 nm. As can be seen in Figure 3(e) (curves iv-vi), the intensity of the SPR band of these Ag NPs increased significantly upon increasing the pH to 9, 11 and then 13, indicating that correspondingly higher yields of Ag NPs were obtained, probably due to the presence of a considerable number of reactive functional groups to bind with silver ions. In addition, a slight red shift of the SPR band of the Ag NPs (from 400 to 415 nm) occurred upon increasing the pH. These results suggest that larger-diameter Ag NPs were obtained at higher pHs. The optimal pH for nanoparticle synthesis was chosen to be pH 11, which is in good agreement with the reported literature.[63] The differences in the amount of Ag NPs obtained over the range of pH could be ascribed to a variation in the dissociation constants (pKa) of functional groups (OH and COOH) on the biomolecules that are involved.[64]

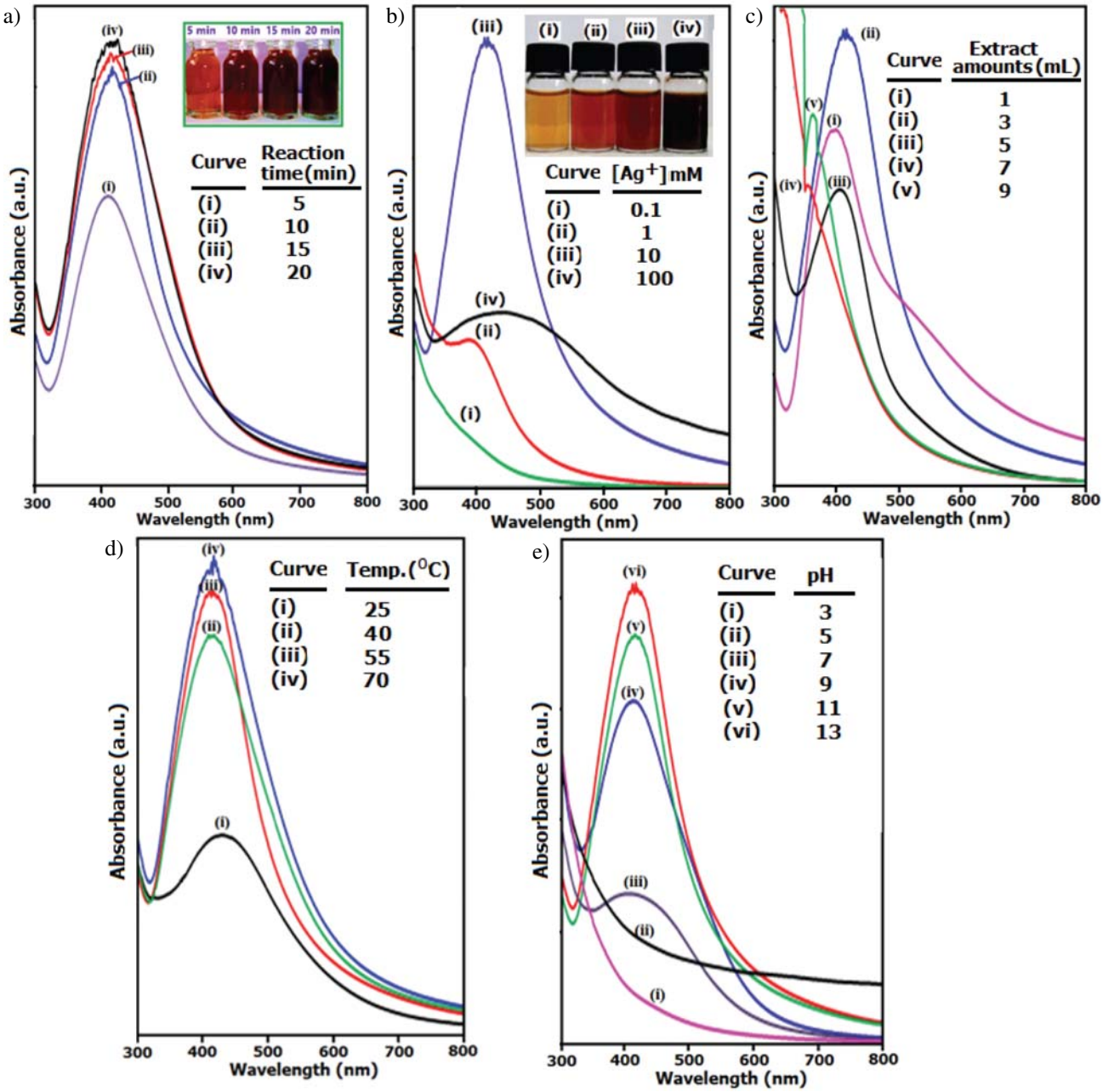

Figure 3. Effect of various parameters on the synthesis of Ag NPs: (a) The effect of reaction time; The inset photo shows the color change of solution with time of reaction, (b) The effect of Ag+ Concentration; The inset photo shows the color change of solution at different concentrations of $AgNO_3$, (c) The effect of different amounts of Date fruit extract, (d) the effect of different temperatures and (e) the effect of pH.

3. 3. XRD Analysis

Figure 4 shows the XRD pattern of Ag NPs synthesized using Date fruit extract after the complete reduction of Ag^+ to Ag under the optimized conditions (10 mM $AgNO_3$, 3 mL Date extract, pH 11 at 55 °C for 10 min). As observed in the XRD pattern, the four characteristic diffraction peaks at 2θ values of 38.10°, 44.15°, 64.67°, and 77.54° can be indexed to the (111), (200), (220), and (311) reflection planes of faced center cubic (fcc) structure of silver (JCPDS card no 04.0784). The considerable broadening of the diffraction peaks demonstrates the nanometer nature of the Ag particles. The average crystallite size of the Ag product is approximately 39.5 nm as estimated by the Debye–Scherrer equation: $D_{XRD} = 0.9\lambda/(\beta\cos\theta)$, where D_{XRD} is the average crystallite size, λ is the wavelength of Cu Kα radiation, β is the corrected full-width at half-maximum of the main diffraction peak of (111), and θ is the Bragg angle. The XRD pattern obtained is consistent with earlier reports.[65,66]

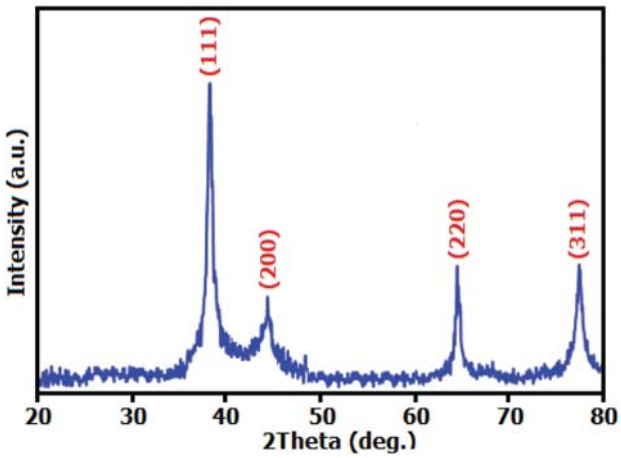

Figure 4. XRD pattern of Ag NPs synthesized by Date fruit extract.

3. 4. SEM, TEM and EDX Analysis

The size and morphology of the Ag NPs were determined via SEM, TEM and AFM images. Figure 5 shows the SEM images of the as-prepared Ag NPs. From the SEM images in different magnifications (Figure 5(a)–(c)), it is clearly evident that the product consists of extremely fine particles with sphere-like morphologies that appreciably aggregated as clusters due to the extremely small dimensions and high surface energy of the obtained nanoparticles. We also can find from the images that the morphology of the particles is almost homogeneous. The resulting images show the presence of large number of spherical nanoparticles with an average particle size of 42.5 nm. The EDX was used to further characterize the composition of the sample. Figure 5(d) shows the EDX spectrum of the Ag NPs prepared by using Date

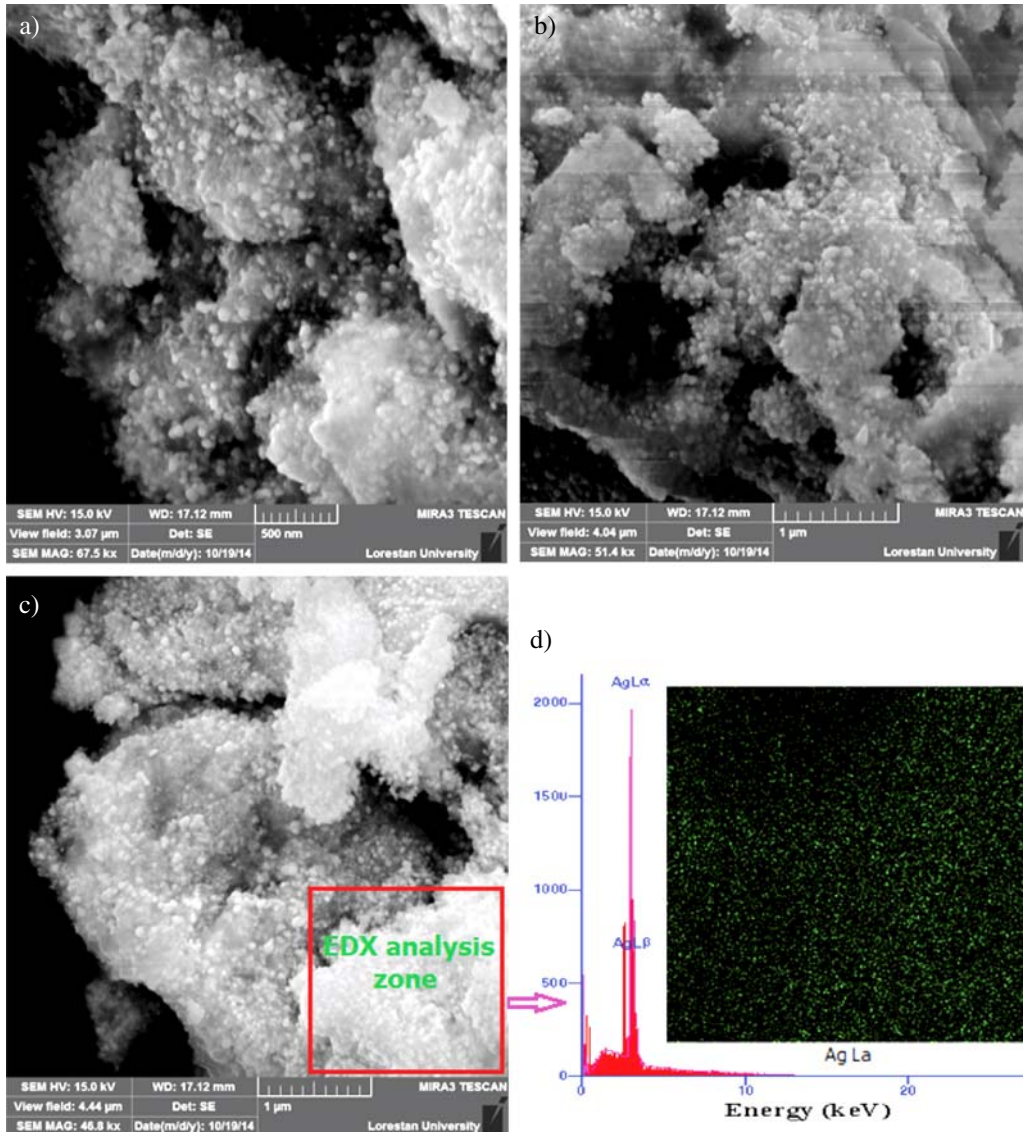

Figure 5. (a–c) SEM images of the as-prepared Ag NPs, (d) EDX elemental spectrum of the Ag NPs. The inset of Figure 5(d) shows EDX elemental mapping for Ag NPs.

fruit extract as reducing agent. The intense peaks around 3.40 keV and 3.45 keV are correspond to the binding energies of Ag $K_{L\alpha}$ and Ag $K_{L\beta}$, respectively, while the peaks situated blow 0.5 keV corresponding of N, C and O from Date fruit extract. Further, the EDX elemental mapping of the product in the inset of Figure 5(d) displays the uniform distribution of the Ag element. The results further indicate that the Ag NPs have been successfully prepared in this work.

The TEM image and size distribution of the Ag NPs are shown in Figure 6. The TEM sample was prepared by dispersing the powder in ethanol by ultrasonic vibration. It can be seen from Figure 6 that the nanoparticles show approximately sphere-like morphologies with a uniform size. Because of the small dimensions and high surface energy of the particles, it is easy for them to aggregate. We also can find from this figure that the morphology of the particles is almost homogeneous. To investigate the size distribution of the Ag NPs, the particle size histogram was also determined from the TEM image. The inset of Figure 6 shows the size distribution of the Ag particles. It is clear that the diameter sizes of the Ag NPs are in the range of 25 to 60 nm with a narrow size distribution. The average particle size is approximately 40 nm, which is in agreement with the result calculated for the half-width of diffraction peaks using the Scherrer's formula, allowing for experimental error.

AFM is a beneficial tool for studying various morphological features and parameters. Since, it has the advantage of probing in deep insights of surface topography qualitatively due to its both lateral and vertical nanometer scale spatial resolution. The AFM images in Figure 7 display the surface morphology of the Ag-NPs formed by Date fruit extract. As observed in Figure 7(a), AFM image reveals the appearance of spherical nanoparticles and their respective particle size and morphology clearly were close to those determined by the SEM and TEM images. As can be seen from Figure 7(b), the surface of Ag NPs sho-

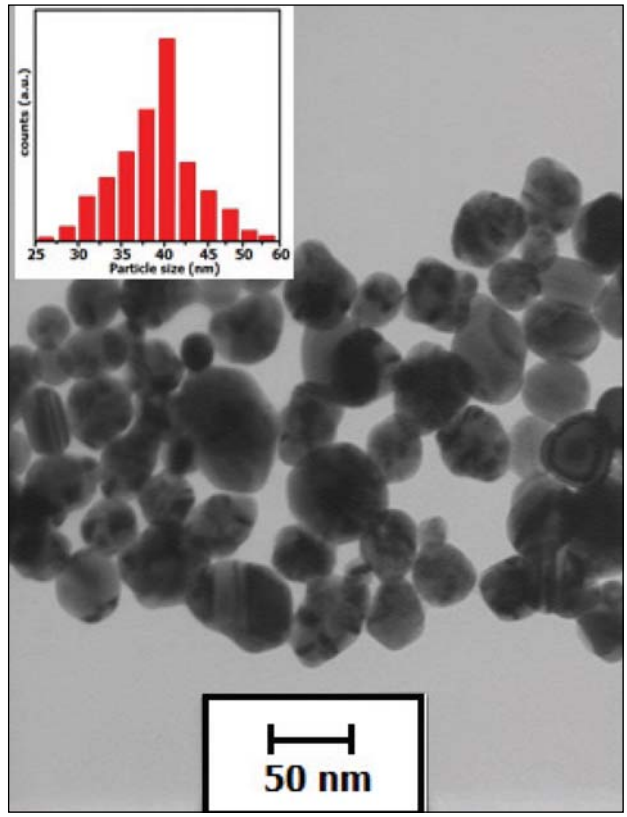

Figure 6. TEM image of the Ag NPs. The inset shows the size distribution of the Ag NPs.

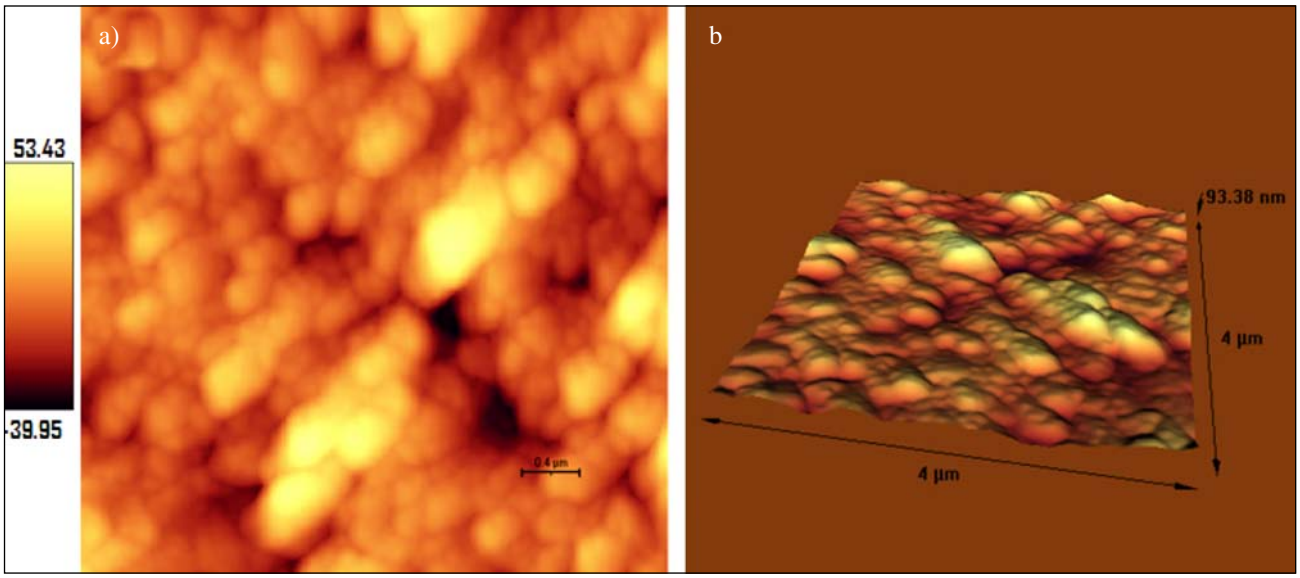

Figure 7. (a) and (b) AFM images of the Ag NPs.

wed a dense and uniform packed structure. Thus, the Ag NPs could provide a biocompatible and rough surface for biological uses, e.g., cell immobilization.

3. 5. Zeta Potential Measurements

Zeta potential provides the information about the stability of nanoparticles and surface charge. Zeta potential is an essential parameter for characterization of stability in aqueous colloidal Ag-NPs suspensions. Zeta potential of the synthesized Ag NPs is pictured in Figure 8. The zeta potential value was measured to be about –35 mV which confirms the good stability of the colloidal Ag NPs aqueous suspension formed by reduction of $AgNO_3$ with Date fruit extract.[67] The high negative values illustrate the repulsion between the particles and thereby attainment of better stability of Ag NPs formation avoiding agglomeration in aqueous solutions.

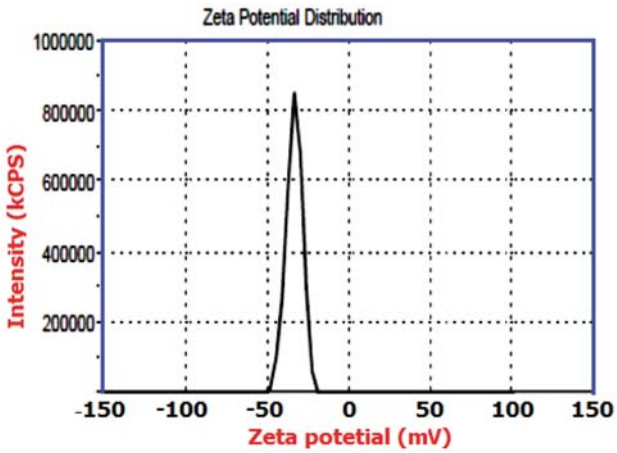

Figure 8. Zeta potential analysis of colloidal Ag NPs solution prepared with Date fruit extract.

3. 6. FT-IR Chemical Analysis

The identification of the possible biomolecules responsible for the reduction and the stabilization of biosynthesized Ag NPs can be achieved by the FTIR studies. It has been reported that the Date palm fruit is rich in phytochemicals like carbohydrates (mainly glucose, sucrose and fructose), phenolic acids, sterols, carotenoids, anthocyanins, procyanidins and flavonoids.[60] Figure 9(A) shows the structures of some phytochemicals present in Date fruits As can be seen, these components are containing carboxyl (–COOH), phenolic –OH and carbonyl (C=O) functional groups. Figure 9(B) shows FT-IR spectra recorded for the Date fruit extract and the Ag NPs synthesized with the Date extract before and after washing. The FT-IR spectrum of Date extract in Figure 9(B) (spectrum a) shows phenolic O–H, C=O, and

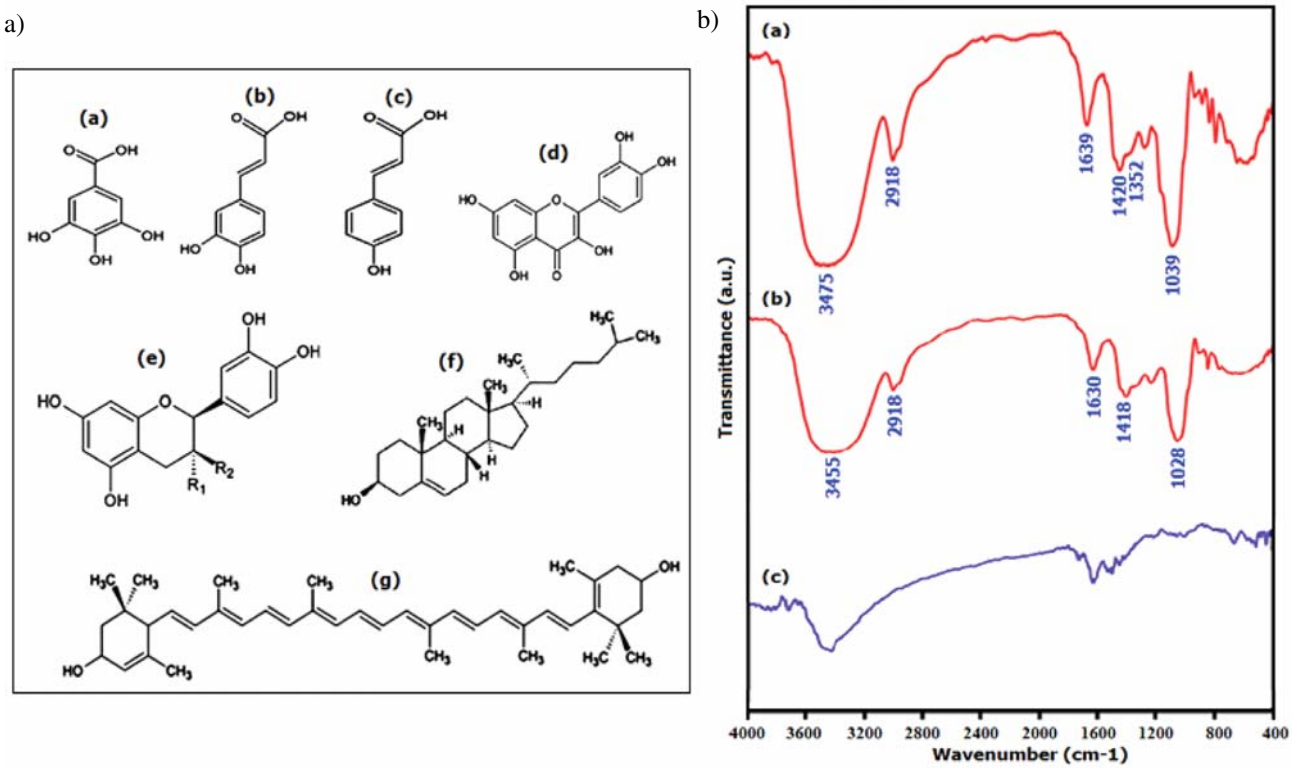

Figure 9. (A) The structure of some of phytochemicals present in Date fruits: (a)-(c) Phenolic acids, (d) a Flavonoid, (e) a Procyanidin, (f) a Sterol, (g) a Carotenoid. (B) FT-IR spectra of: (a) Date palm fruit extract, (b) Ag NPs capped with Date fruit extract solution and (c) Ag NPs after washing with deionized water

C–OH stretching bands, corresponding to a number of bands at 3475, 1639, and 1039 cm^{-1}, respectively. The absorption bands at 2918, 1420, and 1352 cm^{-1} are related to the C–H stretching bands in Date fruit. As shown in Figure 9(B), (spectrum b), after the reduction of $AgNO_3$ the decreases in intensity of bands at 3450 and 1039 cm^{-1} and redshift of these bands signify the involvement of the OH groups in the reduction process. On the hand the shift of the band from 1639 cm^{-1} to 1630 cm^{-1} is attributed to the binding of C=O groups with Ag NPs. On the base of FT-IR analysis, it can be stated that the hydroxyl, carboxyl and carbonyl functional groups present in carbohydrates, flavonoids, tannins and phenolic acids of Date fruit extract may be accountable for the reduction of the Ag^+ ions and stabilization of Ag NPs. In an experiment, the Ag NPs capped with Date extract were washed with deionized water for three times and the FT-IR spectrum of the dried precipitate was again taken for the purity of the sample. As can be clearly seen in Figure 9(B), (spectrum c), the intensity of the characteristic bands of biomolecules markedly decreases after washing the product, confirming the removal of biomolecules on the surface of Ag NPs.

From the FTIR analysis and previously reported mechanisms,[68–70] it can be stated that the hydroxyl and carbonyl groups present in carbohydrates, flavonoids, procyanidin and phenolic compounds are powerful reducing agents and they may be accountable for the bioreduction of Ag^+ ions leading to Ag^0 nanoparticle synthesis. FTIR study confirms that the carbonyl groups of biomolecules have a strong ability to bind metal ions and they may be encapsulated around the Ag NPs forming a protective coat-like membrane to avoid the agglomeration and thus results in nanoparticle stabilization in the medium. Thus, the Date fruit extract components act as bioreductants and surfactants too. The plausible mechanism of the formation of Ag NPs by using a Flavonoid biomolecule as a typical reducing agent is shown in Figure 10. In this pursuit, proteins and all secondary metabolites of extract play a critical role in both reducing and capping mechanism for nanoparticle formation.

3. 7. Antibacterial Activity of Ag Nanoparticles

The antibacterial activity of Ag NPs were analyzed against five bacteria: Bacillus cereus, Staphylococcus aureus, Staphylococcus epidermidis, Klebsiella pneumonia, and Escherichia coli by disk diffusion method. The results of the antibacterial activity of silver nanoparticles were showed in Figure 11. The Figure shows that Ag NPs have good antibacterial activity; bacteria cells have been killed at the concentration of 30 μg/ml. Table 1 represented the inhibition zone of these bacteria. Highest activity of Ag NPs was obtained against epidermidis, while lowest activity were observed against B. cereus and E. coli. Biosynthesized Ag NPs exhibit more antimicrobial activity on

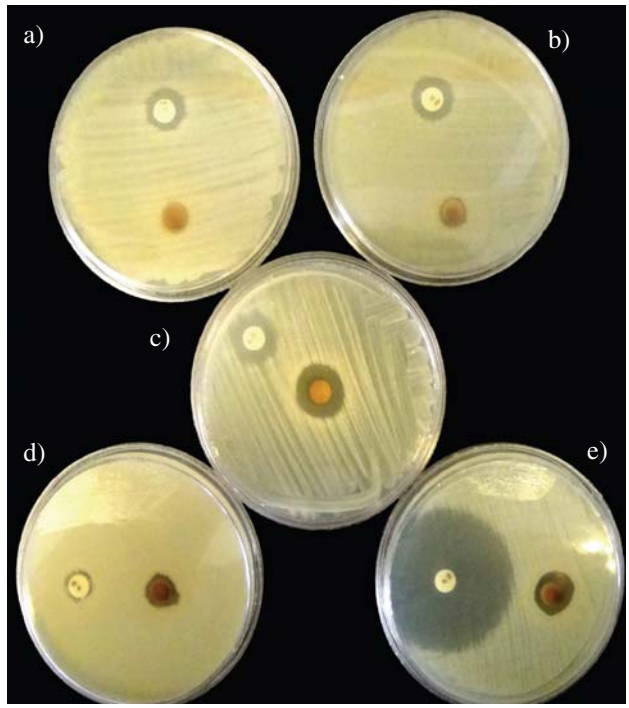

Figure 11. Images of antibacterial activities of Discs 30 μg/mL Ag NPs on (a) E. Coli, (b) K. Pneumonia, (c) S. Epidermidis, (d) B. Cereus. (e) S. Aureus.

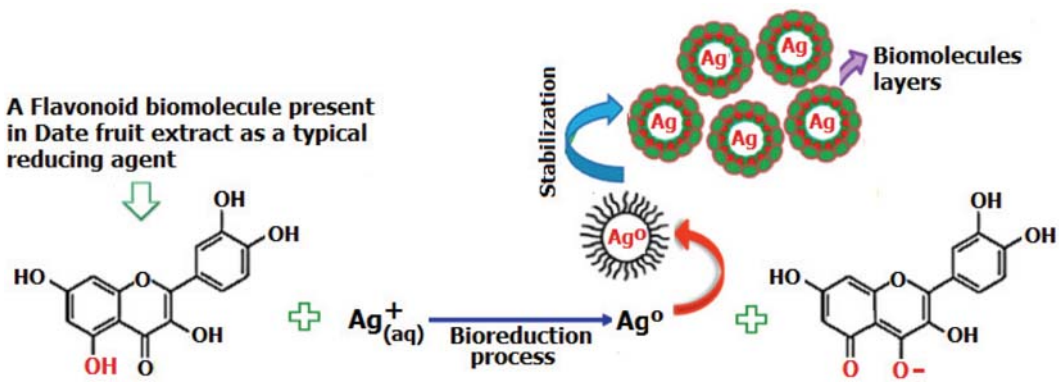

Figure 10. The plausible mechanism of the formation of Ag NPs using Date fruit extract

Table 1. Average of inhibition zones synthesized silver nanoparticles with Date fruit extract.

Entry	Bacteria	Type	Inhibition zone diameter (mm)	
			Silver nanoparticle	Disc standard
1	E. Coli	Gram-negative	11	13
2	K. Pneumonia	Gram-negative	11	13
3	S. Epidermidis	Gram-positive	17	14
4	B. Cereus	Gram-positive	12	11
5	S. Aureus	Gram-positive	13	41

gram-positive microorganism than gram-negative. The potential antimicrobial activities showed by Ag NPs have made them encouraging candidates as novel generation antimicrobials.

3. 8. Catalytic Activity of Ag Nanoparticles

To evaluate the catalytic activity of the Ag NPs prepared in this work by using Date fruit extract, the reduction of 4-nitrophenol (4-NP) and 4-nitroaniline (4-NA) in aqueous solution by excess $NaBH_4$ was used as the model systems. The catalytic process was monitored by UV–Vis spectroscopy as shown in Figure 12. From Figure 12(a), it was seen that an absorption peak of 4-NP undergoes a red shift from 317 to 400 nm immediately upon the addition of aqueous solution of $NaBH_4$, corresponding to a significant change in solution color from light yellow to yellow-green due to formation of 4-nitrophenolate ion. In the absence of Ag NPs catalyst (0.5 mg), the absorption peak at 400 nm remained unaltered for a long duration, indicating that the $NaBH_4$ itself cannot reduce 4-nitrophenolate ion without a catalyst. In the presence of Ag NPs catalyst and $NaBH_4$ the 4-NP was reduced, and the intensity of the absorption peak at 400 nm decreased gradually with time and after about 24 min it fully disappeared (Figure 12(a)). In the meantime, a new absorption peak appeared at about 295 nm and increased progressively in intensity. This new peak is attributed to the typical absorption of 4-aminophenol (4-AP). This result suggests that the catalytic reduction of 4-NP exclusively yielded 4-AP, without any other side products. In the reduction process, the overall concentration of $NaBH_4$ was 10 mM and 4-NP was 0.1 mM. Considering the much higher concentration of $NaBH_4$ compared to that of 4-NP, it is reasonable to assume that the concentration of BH_4^- remains constant during the reaction. In this context, pseudo-first-order kinetics could be used to evaluate the kinetic reaction rate of the current catalytic reaction, together with the UV–Vis absorption data in Figure 12(a). The absorbance of 4-NP is proportional to its concentration in solution; the absorbance at time t (A_t) and time t = 0 (A_0) are equivalent to the concentration at time t (C_t) and time t = 0 (C_0). The rate constant (k) could be determined from the linear plot of $\ln(C_t/C_0)$ versus reduction time in minutes. As expected, a good linear correlation of $\ln(C_t/C_0)$ versus time was obtained as shown in the inset of Figure 12(a), whereby a kinetic reaction rate constant k is estimated to be 1.34×10^{-1} min^{-1}. Figure 12(b) shows the UV-Vis absorption spectra of the reduction of 4-nitroaniline by $NaBH_4$ at various reaction times in the presence of Ag NPs. The observed peak at 385 nm for the 4-nitroaniline shows a gradual decrease in intensity with time and a new peak appeared at 295 nm indicating the formation of p-phenylenediamine (1,4-PD). As shown in Figure 12(b), it took 24 min for the complete reduction of 4-NA in the presence of Ag NPs (0.5 mg).

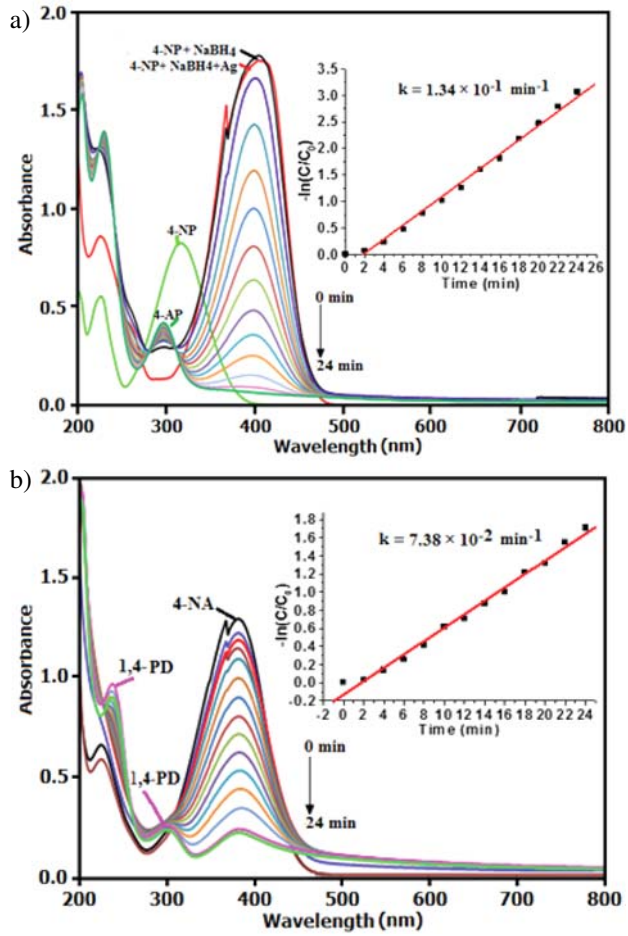

Figure 12. UV–Vis spectra of (a) 0.1 mM 4-nitrophenol (4-NP) with 10 mM NaBH4 and (b) 0.1 mM 4-nitroaniline (4-NA) with 10 mM NaBH4 in the presence of Ag NPs as catalyst. The insets show the plots of $\ln(C_t/C_0)$ against the reaction time for pseudo-first-order reduction kinetics of 4-NP and 4-NA in the presence of excess $NaBH_4$ (10 mM) in aqueous solutions.

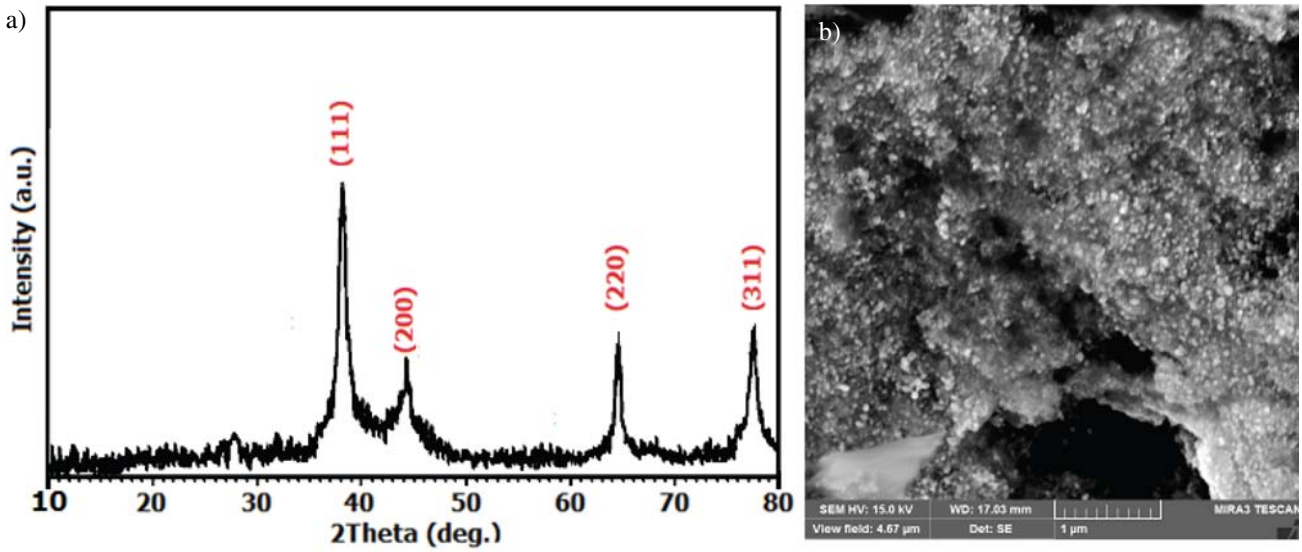

Fig. 13. (a) XRD pattern and (b) SEM image of the recovered Ag NPs after the fourth cycle.

The corresponding k value was 7.38×10^{-2} min^{-1} (see the inset in Figure 12(b)). The results indicated that Ag NPs exhibited considerably high activity for the reduction of nitroarenes with $NaBH_4$ as the hydrogen donor.

The reusability of catalysts is a very important parameter to assess the catalyst practicability. Therefore, the recovery and reusability of the Ag catalyst was investigated for the reduction of 4-NP under the present reaction conditions. After the completion of reaction, Ag NPs were separated from the reaction mixture by centrifugation. The catalyst was washed with water and ethanol several times, dried and employed for the next reaction. The activity of the four consecutive runs (98, 98, 97 and 95%) revealed the practical recyclability of the applied catalyst. No significant loss in activity was observed for up to four catalytic cycles, thereby indicating that the as-prepared catalyst is stable and efficient in the reduction of nitro-compounds. As shown in Fig. 13(a) and (b), XRD and SEM image of the recycled catalyst did not show significant change after the fourth run in comparison with the fresh catalyst (see Figures 4 and 5). This observation confirmed that the Ag NPs are stable under the reaction conditions and are not affected by the reactants.

Moreover, we have compared the obtained results in the reduction of 4-NP with $NaBH_4$ catalyzed by Ag NPs prepared in this work with some reported catalysts in the literature (Table 2). It is clear that with respect to the reaction conditions and/or reaction times, the present method

Table 2. Comparison of the result obtained for the reduction of 4-NP in the present work with those obtained by some reported catalysts.

Entry	Catalyst	Conditions	Time	Ref.
1	Ni-PVA/SBA-15	H_2O, $NaBH_4$, r.t.	85 min	[71]
2	Hierarchical Au/CuO NPs	H_2O, $NaBH_4$, r.t	80 min	[72]
3	Cu NPs	THF/H_2O, $NaBH_4$, 50 °C	2 h	[73]
4	PdCu/graphene	EtOH/H_2O, $NaBH_4$, 50 °C	1.5 h	[74]
5	Au-GO	H_2O, $NaBH_4$, r.t.	30 min	[75]
6	$CoFe_2O_4$ NPs	H_2O, $NaBH_4$, r.t.	50 min	[76]
7	$FeNi_2$ nano-alloy	H_2O, $NaBH_4$, r.t	60 min	[77]
8	$NiCo_2$ nano-alloy	H_2O, $NaBH_4$, r.t.	30 min	[78]
9	CdS/GO	H_2O, $NaBH_4$, r.t.	30 min	[79]
10	dumbbell-like CuO NPs	H_2O, $NaBH_4$, r.t.	32 min	[80]
11	Ni NPs	H_2O, $NaBH_4$, r.t.	16 min	[81]
12	$CuFe_2O_4$ NPs	H_2O, $NaBH_4$, r.t.	14 min	[82]
13	Au NPs	H_2O, $NaBH_4$, r.t.	4 min	[83]
14	Pd/RGO/Fe_3O_4 NPs	H_2O, $NaBH_4$, r.t.	1 min	[84]
15	Cu/Fe_3O_4 NPs	H_2O, $NaBH_4$, r.t.	55 sec	[85]
16	Cu NPs/perlite	H_2O, $NaBH_4$, r.t.	**2.5 min**	[86]
17	**Ag NPs**	**H_2O, $NaBH_4$, r.t.**	**24 min**	**This work**

is more suitable and/or superior (Table 2, entries 1–10). It is clear that reaction in the presence of most reported catalysts required longer reaction times. However, compared with some these reports, the present catalyst also presented close or lower catalytic activity for the reduction of 4-NP (Table 2, entries 11–16). Furthermore, compared with the other catalysts, the Ag NPs can be easily prepared using Date fruit extract without the use of harsh, toxic and expensive chemicals which is very important in practical applications.

4. Conclusions

In the present work, Date fruit extract was used as an effective reducing as well as capping agent for the biosynthesis Ag NPs in aqueous solution. The synthesis of Ag NPs was affected by the variation in reaction conditions such as time, temperature, concentration of extract and silver solution and pH. The synthesized Ag NPs were spherical, 25–60 nm in size, crystal in nature and showed absorption spectrum at ~400–420 nm. The formed Ag NPs were quite stable, showed good antimicrobial activity and were utilized as a catalyst for the reduction of several aromatic nitro-compounds into their corresponding amino derivatives. Thus Date extract can be effectively used for the synthesis of Ag NPs. Further experiments for the synthesis other metal nanoparticles such as Au, Pd, and Cu, using Date fruit extract are in progress in our laboratory. Synthesis of metallic nanoparticles using green resources like Date fruit extract is a challenging alternative to chemical synthesis, since this novel green synthesis is cost effective, pollutant free and eco-friendly synthetic route.

5. Acknowledgements

The authors gratefully acknowledge the Lorestan University Research Council and Iran Nanotechnology Initiative Council (INIC) for their financial supports.

6. References

1. K. Nishioka, T. Sueto, N. Saito, *Appl. Surf. Sci*. **2009**, *255*, 9504–9507. https://doi.org/10.1016/j.apsusc.2009.07.079
2. Y. W. C. Cao, R. C. Jin, C. A. Mirkin, *Sci.* **2002**, *297*, 1536–1540. https://doi.org/10.1126/science.297.5586.1536
3. V. K. Vidhu, D. Philip, *Micron* **2014**, *56*, 54–62. https://doi.org/10.1016/j.micron.2013.10.006
4. C. J. Kirubaharan, D. Kalpana, Y. S. Lee, A. R. Kim, D. J. Yoo, K. S. Nahm, G. G. Kumar, *Ind. Eng. Chem. Res*., **2012**, *51*, 7441–7446. https://doi.org/10.1021/ie3003232
5. M. Rahban, A. Divsalar, A. A. Saboury, A. Golestani, *J. Am. Phys. Chem*. C **2010**, *114*, 5798–5803.
6. M. Miranzadeh, M. Z. Kassaee, L. Sadeghi, M, Sadroddini, M. Razzaghi-Kashani, N. Khoramabadi, *Nanochem. Res.* **2016**, *1*, 1–8.
7. M. Ohtaki, N. Toshima, *Chem. Lett*. **1990**, *4*, 489–492. https://doi.org/10.1246/cl.1990.489
8. Y. Mizukoshi, K. Okisu, Y. Maeda, T. A. Yamamoto, R. Oshima, Y. Nagata, *J. Am. Phys. Chem. B* **1997**, *101*, 7033–7037. https://doi.org/10.1021/jp9638090
9. M. Khademalrasool, M. Farbod, *J. Nanostruct.* **2015,** *5*, 415–422
10. S. Darvishi, S. M. Borghei, S. A. Hashemizadeh, *J. Nanostruct.* **2012,** *2*, 501–504.
11. B. J. Wiley, Y. Sun, Y. Xia, *Acc. Chem. Res.* **2007**, *40*, 1067–1076. https://doi.org/10.1021/ar7000974
12. H. Ahmad, K. Rajagopal, A.H. Shah, *Int. J. Nano Dimens.* **2016**, *7*, 97–108.
13. T. Klaus, R. Joerger, E. Olsson, C. G. Granqvist, *Proc. Natl. Acad. Sci.* **1999***, 96*, 13611–13614. https://doi.org/10.1073/pnas.96.24.13611
14. Y. Roh, R. J. Lauf, A. D. McMillan, C. Zhang, C. J. Rawn, J. Bai, T. J. Phelps, *Solid State Commun.* **2001**, *118*, 529–534. https://doi.org/10.1016/S0038-1098(01)00146-6
15. B. Nair, T. Pradeep, *Cryst. Growth. Des.* **2002**, *2*, 293–298. https://doi.org/10.1021/cg0255164
16. P. Yong, N. A. Rowson, J. P. G. Farr, I. R. Harris, L. E. Macaskie, *Biotechnol. Bioeng.* **2002***, 80*, 369–379. https://doi.org/10.1002/bit.10369
17. M. I. Husseiny, M. A. El-Aziz, Y. Badr, M. A. Mahmoud, *Spectrochim. Acta A* **2007***, 67*, 1003–1006. https://doi.org/10.1016/j.saa.2006.09.028
18. P. Mukherjee, A. Ahmad, D. Mandal, S. Senapati, S. R. Sainkar, M. I. Khan, R. Parishcha, P. V. Ajaykumar, M. Alam, R. Kumar, M. Sastry, *Nano. Lett.* **2001**, *1*, 515–519. https://doi.org/10.1021/nl0155274
19. P. Mukherjee, A. Ahmad, D. Mandal, S. Senapati, S. R. Sainkar, M. I. Khan, R. Ramani, R. Parischa, P. A. Ajaykumar, M. Alam, M. Sastry, R. Kumar, *Angew. Chem. Int. Ed.* **2001***, 40*, 3585–3588. https://doi.org/10.1002/1521-3773(20011001)40:19<3585::AID-ANIE3585>3.0.CO;2-K
20. A. Ahmad, S. Senapati, M. I. Khan, R. Kumar, *J. Biomed. Nanotechnol.* **2005**, *1*, 47–53. https://doi.org/10.1166/jbn.2005.012
21. A. Ahmad, S. Senapati, M. I. Khan, R. Kumar, R. Ramani, V. Srinivas, M. Sastry, *Nanotechnology* **2003**, *14*, 824–828. https://doi.org/10.1088/0957-4484/14/7/323
22. A. Ahmad, S. Senapati, M. I. Khan, R. Kumar, M. Sastry, *Langmuir* **2003**, *19*, 3550–3553. https://doi.org/10.1021/la026772l
23. M. Sastry, A. Ahmad, M. I. Khan, R. Kumar, *Curr. Sci*. **2003**, *85*, 162–170.
24. M. Kowshik, S. Arhtaputre, S. Kharrazi, W. Vogel, J. Urban, S. K. Kulkarni, K. M. Paknikar, *Nanotechnology* **2003**, *14*, 95–100. https://doi.org/10.1088/0957-4484/14/1/321
25. W. Shenton, T. Douglas, M. Young, G. Stubbs, S. Mann, *Adv. Mater.* **1999**, *11*, 253–256.

https://doi.org/10.1002/(SICI)1521-4095(199903)11:3<253::AID-ADMA253>3.0.CO;2-7
26. S. W. Lee, C. Mao, C. Flynn, A. M. Belcher, *Sci.* **2002**, *296*, 892–895. https://doi.org/10.1126/science.1068054
27. A. Merzlyak, S. W. Lee, *Curr. Opin. Chem. Biol.* **2006**, *10*, 246–252. https://doi.org/10.1016/j.cbpa.2006.04.008
28. S. M. Ali, V. Anuradha, N. Yogananth, R. Rajathilagam, A. Chanthuru, S. M. Marzook, *Int. J. Nano Dimens.* **2015**, *6*, 197–204.
29. N. T. M. Tho, T. N. M. An, M. D. Tri, T. V. M. Sreekanth, J.-S. Lee, P. C. Nagajyothi, K. D. Lee, *Acta Chim. Slov.* **2013,** *60,* 673–678.
30. P. P. Vijaya., M. S. Ali, R. S. Saranya, N. Yogananth, V. Anuratha, P. K. Parveen, *Int. J. Nano Dimens.* **2013**, *3*, 255–262.
31. P. Prakash, P. Gnanaprakasam, R. Emmanuel, S. Arokiyaraj, M. Saravanan, *Colloids Surf. B* **2013**, *108*, 255–259. https://doi.org/10.1016/j.colsurfb.2013.03.017
32. R. R. R. Kannan, R. Arumugam, D. Ramya, K. Manivannan, P. Anantharaman, *Appl. Nanosci.* **2013**, *3*, 229–233. https://doi.org/10.1007/s13204-012-0125-5
33. A. Rostami-Vartooni, M. Nasrollahzadeh, M. Alizadeh, *J. Colloid Interface Sci.* **2016**, *470*, 268–275. https://doi.org/10.1016/j.jcis.2016.02.060
34. B. Sadeghi, *Int. J. Nano Dimens.* **2014**, *5*, 575–581.
35. A. Rostami-Vartooni, M. Nasrollahzadeh, M. Alizadeh, J. Alloys Compd. **2016,** *680,* 309–314. https://doi.org/10.1016/j.jallcom.2016.04.008
36. K. M. Ponvel, T. Narayanaraja, J. Prabakaran, *Int. J. Nano Dimens.* **2015**, *6*, 339–349.
37. H. R. Rajabi, H. Deris, H. S. Faraji, *Nanochem. Res.* **2016**, *1*, 177–182.
38. D. M. Ali, N. Thajuddin, K. Jeganathan, M. Gunasekhran, *Colloids Surf. B* **2011**, *85*, 360–365. https://doi.org/10.1016/j.colsurfb.2011.03.009
39. A. R. Allafchian, S. Z. Mirahmadi-Zare, S. A. H. Jalali, S. S. Hashemi, M. R. Vahabi, *J. Nanostruct Chem.* **2016**, *6*, 129–135.
40. S. Sedaghat, A. Esmaeili-Agbolag, S. bagheriyan, *J. Nanostruct Chem.* **2016**, *6*, 25–27. https://doi.org/10.1007/s40097-015-0176-8
41. D. Philip, C. Unni, S. A. Aromal, V. K. Vidhu, *Spectrochim. Acta A* **2011**, *78*, 899–904. https://doi.org/10.1016/j.saa.2010.12.060
42. D. Phillip, *Spectrochim. Acta A* **2011**, *78*, 327–331. https://doi.org/10.1016/j.saa.2010.10.015
43. K. S. Prasad, D. Pathak, A. Patel, P. Dalwadi, R. Prasad, P. Patel, K. Selvaraj, *J. Afr. Biotechnol.* **2011**, *10*, 8122–8130. https://doi.org/10.5897/AJB11.394
44. M. L. Rao, N. Savithramma, *J. Pharm. Sci. Res.* **2011**, *3*, 1117–1121.
45. K. Satyavani, T. Ramanathan, S. Gurudeekan, *Dig. J. Nanomater. Biostruct*. **2011**, *6*, 1019–1024.
46. T. J. I. Edison, M. G. Sethuraman, *Process. Biochem.* **2012**, *47*, 1351–1357. https://doi.org/10.1016/j.procbio.2012.04.025
47. M. Ramar, B. Manikandan, P. N. Marimuthu, T. Raman, A. Mahalingam, P. Subramanian, S. Karthick, A. Munusamy, *Spectrochim. Acta A* **2015**, *140*, 223–228. https://doi.org/10.1016/j.saa.2014.12.060
48. S. Singha, J. P. Saikia, A. K. Buragohain, *Colloids Surf. B* **2013**, *102*, 83–85. https://doi.org/10.1016/j.colsurfb.2012.08.012
49. M. Umadevi, M. R. Bindhu, V. Sathe, *J. Mater. Sci. Technol.* **2013**, *29*, 317–322. https://doi.org/10.1016/j.jmst.2013.02.002
50. R. S. R. Isaac, G. Sakthivel, C. Murthy, *J. Nanotech.* **2013**, *13*, 1–6.
51. M. Ghaffari-Moghaddam, R. Hadi-Dabanlou, *J. Ind. Eng. Chem.* **2014**, *20*, 739–744. https://doi.org/10.1016/j.jiec.2013.09.005
52. P. S. Ramesh, T. Kokila, D. Geetha, *Spectrochim. Acta A* **2015**, *142*, 339–343. https://doi.org/10.1016/j.saa.2015.01.062
53. Y. Gao, Q. Huang, Q. Su, R. Liu, *Spect. Lett*. **2014**, *47*, 790–795. https://doi.org/10.1080/00387010.2013.848898
54. M. Chandrasekaran, A. H. Bahkali, *Saudi J. Biol. Sci.* **2013**, *20*, 105–120. https://doi.org/10.1016/j.sjbs.2012.12.004
55. J. Wang, C. M. Rosell, C. B. Barber, *Food Chem.* **2002**, *79*, 221–226. https://doi.org/10.1016/S0308-8146(02)00135-8
56. A. Paraskevopoulou, D. Boskou, V. Kiosseoglou, *Food Chem.* **2005**, *90*, 627–634. https://doi.org/10.1016/j.foodchem.2004.04.023
57. M. Abdelhak, E. Guendez, K. Eugene, K. Panagiotis, *Food Chem.* **2005**, *89*, 411–420. https://doi.org/10.1016/j.foodchem.2004.02.051
58. P. K. Vayalil, *J. Agric. Food. Chem.* **2002**, *50*, 610–617. https://doi.org/10.1021/jf010716t
59. F. Bilgari, A. F. M. Alkarkhi, A. M. Easa, *Food Chem.* **2008**, *107*, 1636–1641. https://doi.org/10.1016/j.foodchem.2007.10.033
60. M. S. Baliga, B. R. V. Baliga, S. M. Kandathil, H. P. Bhat, P. K. Vayalil, *Food. Res. Int.* **2011**, *44*, 1812–1822. https://doi.org/10.1016/j.foodres.2010.07.004
61. A. M. Fayaz, K. Balaji, P. T. Kalaichelvan, R. Venkatesan, *Colloids Surf. B* **2009**, *74*, 123–126. https://doi.org/10.1016/j.colsurfb.2009.07.002
62. J. Park, J. Joo, S. G. Kwon, Y. Jang, T. Hyeon, *Angew. Chem. Inter. Ed.* **2007**, *46*, 4630–4660.
63. S. M. Roopan, G. Madhumitha, A. A. Rahuman, C. Kamaraj, A. Bharathi, T. V. Surendra, *Ind. Crop. Prod.* **2013**, *43*, 631–635. https://doi.org/10.1016/j.indcrop.2012.08.013
64. H. M. M. Ibrahim, *J. Rad. Res. Appl. Sci.* **2015**, *8*, 265–275.
65. D. A. Kumar, V. Palanichamy, S. M. Roopan, *Spectrochim. Acta A* **2014**, *127*, 168–171. https://doi.org/10.1016/j.saa.2014.02.058
66. R. Kumar, S. M. Roopan, A. Prabhakarn, V. G. Khanna, S. Chakroborty, *Spectrochim. Acta A* **2012**, *90*, 173–176. https://doi.org/10.1016/j.saa.2012.01.029
67. S. Naraginti, A. Sivakumar, *Spectrochim. Acta A* **2014**, *128*, 357–362. https://doi.org/10.1016/j.saa.2014.02.083
68. M. Nasrollahzadeh, S. M. Sajadi, A. Rostami-Vartooni, M. Khalaj, *J. Mol. Catal. A: Chem.* **2015**, *396,* 31–39.

https://doi.org/10.1016/j.molcata.2014.09.029
69. M. Nasrollahzadeh, S. M. Sajadi, A. Rostami-Vartooni, M. Alizadeh, M. Bagherzadeh *J. Colloid Interface Sci.* **2016**, *466*, 360–368. https://doi.org/10.1016/j.jcis.2015.12.036
70. A. Rostami-Vartooni, M. Nasrollahzadeh, M. Salavati-Niasari, M. Atarod, *J. Alloys Compd.* **2016**, *689*, 15–20. https://doi.org/10.1016/j.jallcom.2016.07.253
71. R. J. Kalbasi, A. A. Nourbakhsh, F. Babaknezhad, *Catal. Commun.* **2011**, *12*, 955–960. https://doi.org/10.1016/j.catcom.2011.02.019
72. S. Y. Gao, X. X. Jia, Z. D. Li, Y. L. Chen, *J. Nanopart. Res.* **2012**, *14*, 1–11.
73. Z. Duan, G. Ma, W. Zhang, *Bull. Korean Chem. Soc.* **2012**, *33*, 4003–4006. https://doi.org/10.5012/bkcs.2012.33.12.4003
74. A. K. Shil, D. Sharma, N. R. Guha, P. Das, *Tetrahedron Lett.* **2012**, *53*, 4858–4861. https://doi.org/10.1016/j.tetlet.2012.06.132
75. Y. Choi, H. S. Bae, E. Seo, S. Jang, K. H. Park, B. S. Kim, *J. Mater. Chem.* **2011**, *21*, 15431–15436. https://doi.org/10.1039/c1jm12477c
76. M. Nasrollahzadeh, M. Bagherzadeh, H. Karimi, *J. Colloid Interface Sci.* **2016**, 465, 271–278. https://doi.org/10.1016/j.jcis.2015.11.074
77. K. L. Wu, R. Yu, X. W. Wei, *Cryst. Eng. Commun.* **2012**, *14*, 7626–7632. https://doi.org/10.1039/c2ce25457c
78. K. L. Wu, X. W. Wei, X. M. Zhou, D. H. Wu, X. W. Liu, Y. Ye, Q. Wang, *J. Phys. Chem. C* **201**1, *115*, 16268–16274. https://doi.org/10.1021/jp201660w
79. S. Liu, Z. Chen, N. Zhang, Z. R. Tang, Y. J. Xu, *J. Phys. Chem. C*, **2013**, *117*, 8251–8261. https://doi.org/10.1021/jp400550t
80. W. Che, Y. Ni, Y. Zhang, Y. Ma, *J. Phys. Chem. Solids* **2015**, *77*, 1–7. https://doi.org/10.1016/j.jpcs.2014.09.006
81. D. Z. Jiang, J. Xie, D. Jiang, X. Wei, M. Chen, *Cryst. Eng. Comm.* **2013**, *15*, 560–569. https://doi.org/10.1039/C2CE26398J
82. J. Feng, L. Su, Y. Ma, C. Ren, Q. Guo, X. Chen, *Chem. Eng. J.* **2013**, *221*,16–24. https://doi.org/10.1016/j.cej.2013.02.009
83. Q. Cui, B. Xia, S. Mitzscherling, A. Masic, L. Li, M. Bargheer, H. Möhwald, *Colloids Surf. A: Physicochem. Eng. Aspects* **2015**, *465*, 20–25. https://doi.org/10.1016/j.colsurfa.2014.10.028
84. M. Atarod, M. Nasrollahzadeh, S. M. Sajadi, *J. Colloid Interface Sci.* **2016,** *465,* 249–258 https://doi.org/10.1016/j.jcis.2015.11.060
85. M. Nasrollahzadeh, M. Atarod, S. M. Sajadi, *Appl. Surf. Sci.* **2016**, *364*, 636–644. https://doi.org/10.1016/j.apsusc.2015.12.209
86. M. Nasrollahzadeh, S. M. Sajadi, *Ceram. Int.* **2015**, *41*, 14435–14439. https://doi.org/10.1016/j.ceramint.2015.07.079

Povzetek

V tem članku poročamo o sintezi sferičnih nanodelcev srebra (Ag NPs), ki smo jih sintetizirali s poceni, hitrim, enostavnim in okolju prijaznim pristopom. Za sintezo smo uporabili sadni izvleček datljeve palme kot naraven reducent in stabilizator. Produkte smo karakterizirali z UV-Vis spektroskopijo, rentgensko praškovno difrakcijo (XRD), infrardečo spektroskopijo (FT-IR), vrstično elektronsko mikroskopijo (FE-SEM), presevno elektronsko mikroskopijo (TEM), mikroskopijo na atomsko silo (AFM), energijsko disperzivno rentgensko spektroskopija (EDX) in meritvami zeta potenciala. Preučevali smo različne parametre reakcijskih pogojev kot so čas, množine reducenta in srebrovega nitrata, temperatura, pH. Optimalni reakcijski pogoji sinteze srebrovih nanodelcev (Ag NPs) so bili doseženi v primeru reakcije 10 mM raztopine srebrovega nitrata s sadnim izvlečkom datljeve palme pri pH 11 in temperaturi do 55 ° C v 10 minutah. Elementarno in kristalinično naravo nanodelcev srebra (Ag NPS) smo potrdili z EDX in XRD analizama. SEM in TEM slike so pokazale, da so nanodelci srebra (Ag NPs) sferični, z velikostjo v območju od 25-60 nm. Na osnovi FT-IR analize, lahko rečemo, da so funkcionalne skupine prisotne v bioloških molekulah sadnega izvlečka datljevih palm odgovorne za redukcijo in stabilizacijo nanodelcev srebra (Ag NPs). Dokazali smo njihovo učinkovito antibakterijsko delovanje proti nekaterim patogenim bakterijam. Preučevali smo tudi katalitsko aktivnost nanodelcev srebra (Ag NPs) za hitro in učinkovito zmanjšanje strupenih nitro spojin v manj strupene amine z uporabo $NaBH_4$

Scientific paper

Utilization of Corn Cob and TiO_2 Photocatalyst Thin Films for Dyes Removal

Hui-Yee Gan,[1] Li-Eau Leow[1] and Siew-Teng Ong[1,2,*]

[1,2] *Faculty of Science, Centre for Biodiversity Research, Universiti Tunku Abdul Rahman, Jalan Universiti, Bandar Barat, 31900 Kampar, Perak, Malaysia*

** Corresponding author: E-mail: ongst@utar.edu.my; ongst_utar@yahoo.com*
Tel: 605-4688888; Fax: 605-4661676

Received: 11-10-2016

Abstract

The effectiveness of using TiO_2 and corn cob films to remove Malachite Green oxalate (MG) and Acid Yellow 17 (AY 17) from binary dye solution was studied. The immobilization method in this study can avoid the filtration step which is not suited for practical applications. Batch studies were performed under different experimental conditions and the parameters studied involved initial pH of dye solution, initial dye concentration and contact time and reusability. The equilibrium data of MG and AY 17 conform to Freundlich and Langmuir isotherm model, respectively. The percentage removal of MG remained high after four sorption cycles, however for AY 17, a greater reduction was observed. The removal of both dyes were optimized and modeled via Plackett- Burman design (PB) and Response Surface Methodology (RSM). IR spectrum and surface conditions analyses were carried out using fourier-transform infrared spectrophotometer (FTIR), scanning electron microscope (SEM) and atomic force microscope (AFM), respectively.

Keywords: Malachite Green; Acid Yellow 17; Immoblization; Plackett Burman; Response Surface Methodology

1.Introduction

Dye is a common coloring agent used in textile, paper, ink, food and leather industries. The usage of these dyes has continuously increased and it has been reported that there are more than 100,000 commercial dyes with a rough estimated production of 7×10^5 to 1×10^6 tons per year.[1,2] Although this colored pollutant imparts only a small fraction of the total organic load in wastewater, it is easily recognizable and damages the aesthetic nature of the environment. Many dyes used in these industries are difficult to degrade, as they are generally stable to light and oxidizing agents, as well as resistant to aerobic digestion. Therefore, conventional effluent treatment methods based on oxidation and/or aerobic digestion may not be effective.

Malachite Green (MG) is a water soluble cationic dye that is widely used in aquaculture as an effective fungicide. However, scientific evidence indicated that MG and its metabolites, leucomalachite green (LMG) is environmentally persistent. This dye causes a serious public health hazards as both clinical and experimental observations reveal that MG is a multi-organ toxin.[3–5] As MG belongs to the same group of triphenylmethane dyes as crystal violet, in which carcinogenic effects have been demonstrated, therefore based on this group classification, a carcinogenic effect can be assumed.[4] Acid Yellow 17 (AY 17) is a mono-azo acid dye, widely used in the textile, leather, cosmetic and paper industry. It is also a common additive in household products such as shampoo, detergent, soap and shower gel.[6] This dye synergizes dermatitis to sensitive skin and causes irritation to eyes. Besides, its thermal decomposition emits toxic fumes of CO, CO_2 and NO.[7] Due to these severe problems, water contamination originated from the dyeing and finishing in textile industry has become a major concern.

The most common physical method utilized by textile industry for waste water treatment is adsorption. Amongst all, activated carbon is one of the most popular adsorbents and it has also demonstrated its efficiency in the removal of various pollutants. However, this type of adsorbent remains as a costly material and it is difficult to regenerate. Thus, there is a need to continue exploring other economical feasible treatment method for dyes removal. Maize also known as corn, is one of the major feed grains in the world. However, after the removal of corns, the abundant agriculture residues such as corn cob, corn husk,

corn leaf and corn stalk are often burnt without utilization.[8,9] But corn cob can actually serves as an attractive low cost adsorbent as it possesses some fairly amazing properties. It contains approximately 39.1% cellulose, 42.1% hemicellulose, 9.1% lignin, 1.7% protein and 1.2% ash.[10]

Apart from adsorption technique, photocatalytic oxidation is also one of the emerging technologies for the elimination of organic pollutants. From the literature, photocatalysis have demonstrated different degrees of applicability for the removal of organic pollutants from aqueous solutions and often, this is viewed as a promising method because it requires no addition of chemicals.[11–15] The basic principle involve can be depicted as follows: once excited by light with energy higher than the band gap energy of photocatalyst, pairs of holes (h^+) and electrons (e^-) generate and migrate to the surface to react with adsorbed reactants. The holes, together with other oxidizing species such as hydroxyl radicals resulting from certain photochemical reactions, oxidize the organic pollutants to carbon dioxide, water and some simple mineral acids.[16]

The main drawback for these two wastewater treatment processes was low economical feasible. Often, extra energy or equipment is required for the post-filtration, centrifugation and sedimentation process. Therefore, in this current work, attempt has been made to immobilize both corn cob and TiO_2 onto a thin film to overcome the problem associated with separation of fine particles mentioned earlier. In order to further enhance the usefulness and efficiency of the proposed treatment method, the percentage uptake for both MG and AY 17 were optimized and modeled via Plackett- Burman design (PB) and Response Surface Methodology (RSM).

2. Materials and Methods

2. 1. Adsorbent

Corn cob was collected from Kampar night market and cut into small pieces, approximately 2 cm/ piece. It was then washed several times with distilled water and consequently boiled for 3 hours to remove the adhering dirt and residues. The clean corn cob was then dried in oven at 60 °C for 24 hours. Dried sorbent was subsequently grinded into powder form and passed through 1 mm sieve before stored into the air tight container for further experimental use.

2. 2. Immobilization of TiO_2 and Corn Cob

Chitosan solution was prepared by dissolving 5.05 g of chitosan powder (coarse ground flakes and powder, Sigma-Aldrich Pte. Ltd) in 500 mL of 1% (v/v) acetic acid solution under continuous stirring for a night at room temperature to ensure all the chitosan powder was well dissolved and the solution was bubble free.

TiO_2 Degussa P25 (mainly in anatase form, mean particle size of 30 nm, BET surface area of 50 m^2/g) was dispersed well and free from agglomeration into chitosan solution via the combination of mechanical stirring and sonication methods with slight modicfication.[17] Both corn cob film (1.0 g of corn cob / 63 g chitosan solution) and TiO_2 film (0.25 g of TiO_2 / 63 g chitosan solution) were prepared with evaporative casting method onto a 10.16 × 10.16 cm of polymer plate and dried in oven at 45 °C for 24 hours to evaporate all the moisture. The dried films were then neutralized by soaking it in 0.5 M of NaOH solution for 4 hours. Thereafter, the films were washed till neutral pH and subjected for further drying in oven at 35 °C for 24 hours.

2. 3. Adsorbates

Binary dye solution was selected for this study and it involved the mixing of Acid Yellow 17, AY 17 (C.I.= 18965) and Malachite Green crystal, MG (C.I. = 40000). Both dyes were purchased from Sigma-Aldrich Pte. Ltd and were used as received without further purification. The prepared binary dye solution was kept in dark for prevent degradation from light.

2. 4. Instrumental and Characterization Analysis

The functional groups that present on corn cob film before and after dye removal process were determined using Perkin Elmer FTIR, Spectrum RX1 at the wavenumber range of 400–4000 cm^{-1} with the number of 4 scans *per* sample and resolution of 4.0 cm^{-1}. The surface morphology of corn cob and TiO_2 film was studied by using field emission scanning electron microscope (JEOL FESEM JSM 6701F), operated at emission current of 3.0 kV with working distance of 4.6 mm. Besides, atomic force microscope was also employed (AFM, Park System, XE-70) to observe the surface topography of film before and after the dye removal process by using the contact mode on a 15 × 15 μm^2 area.

2. 5. Batch Study

Batch study was performed under the exposure of sunlight continuously for 4 hours. Light intensity was recorded at every 1 hour interval with UVA/B light meter. Based on the results from our previous studies in the laboratory, the amount of dyes adsorbed by TiO_2 in dark was negligible. Both TiO_2 thin film and corn cob film were immersed in 500 mL of binary dye solution (10.0 mg/L of MG and 40.0 mg/L of AY 17) in the aquarium tank. Aeration was provided by an air pump. At predetermined time intervals, a known volume of dye solution was withdrawn from the tank and analyzed for its dye content using UV-visible spectrophotometer to determine the % of dye removal. The same experimental conditions were employed

throughout the study unless otherwise stated. The percentage uptake of dye was calculated based on Equation 1.

$$\text{Percentage removal (\%)} = \frac{C_o - C_e}{C_o} \times 100\ \% \qquad (1)$$

where,
C_o = Initial concentration of dye, mg/L
C_e = Concentration of dye in equilibrium, mg/L

2. 5. 1. Effect of pH

The removal of dyes at different initial pH was investigated in range of pH 4.45 ± 0.50 (natural pH of the binary dye solution) to 7. Dilute sodium hydroxide (NaOH) solution was added dropwise to adjust the pH to the desire pH, prior to the experiment.

2. 5. 2. Effect of Initial Dye Concentrations and Contact Time

The effect of initial dye concentrations and contact time on the percentage uptake of MG and AY 17 was studied by using the dye concentrations of 20, 40 and 80 mg/L. Dye solution was collected at various time intervals, 5, 10, 15, 30, 60, 120, 180, 240 and 300 minutes and the concentration was determined.

2. 5. 3. Sorption Isotherm

Sorption isotherms were obtained by varying the initial dye concentrations of MG from 10.0 mg/L to 50.0 mg/L and 40.0 mg/L to 80.0 mg/L for AY 17. The experiment was carried out by adding 0.1 g of corn cob film into 20 mL of binary dye solutions. This sorption mixture was then shaken at 150 rpm in a centrifuge tube at room temperature for 4 hours.

2. 5. 4. Reusability of TiO_2 Film and Corn Cob Film

The possibility of repetitive usage of films was studied in this parameter. The same TiO_2 and corn cob films were reused for multiple sorption cycles (up to 4 cycles). Before the films were subjected for the next cycle of sorption process, the previously sorbed dyes were removed from the films by soaking it in 0.5 M NaOH solution for desorption process. This was followed by several washings until neutral and the films were air-dry.

2. 6. Statistical Approach

2. 6. 1. Evaluation of Factors Affecting the Percentage Uptake of Dyes

The effect of various factors that influence the percentage uptake of MG and AY 17 were investigated with Plackett-Burman design. The validity of 3 factors including initial dye concentrations, contact time and initial pH of binary dye solution were screened by Design Expert Version 7.1.3 software to generate 12 experimental designs.

2. 6. 2. Optimization Study

The factors resulted from Plackett-Burman study was continued with central composite design (CCD) model in Response Surface Methodology (RSM) by using Design Expert Version 7.1.3 software. The correlation of factors and percentage uptake for binary dye was described with modified cubic model.

3. Results and Discussion

3. 1. Instrumental Analysis

3. 1. 1. Fourier Transform Infrared Spectroscopy (FTIR)

Figure 1 shows the FTIR spectra of native chitosan film and corn cob film before and after adsorption in the wavenumber range from 4000 to 400 cm^{-1}. From the spectrum, the peak observed at 3436 and 3437 cm^{-1} corresponded to the amine stretching N-H and confirmed the presence of amine group in the chitosan structure. The peaks appeared at 2920 cm^{-1} indicated that the stretching vibration of C–H bond of methylene and methane group, whereas 2844 cm^{-1} shows C–H stretching for sp^3 carbon atom. As for peak observed at 1632, 1638 and 1642 cm^{-1}, this would suggest the presence of N–H bending amine groups. A weak intensity of C=C stretching bands for aromatic rings were assigned at 1425cm^{-1}. It was noticed that the FTIR spectra of corn cob film (before and after adsorption) are very similar to each other. Apart from the limitations in the sensitivity of the instrument, this could also be due to the nature of the process. As it has been postulated that the dye removal process mainly involved adsorption, which is a surface chemistry process, therefore the FTIR spectra before and after the process would shown not much difference. Similar results were reported in the removal of Methylene Blue by using nitrilotriacetic acid modified banana pith.[2]

3. 1. 2. Surface Characterization

The surface morphology involving shape and porosity of the films was studied using SEM. The SEM micrographs that showed the surface texture of TiO_2 film and corn cob film before and after the dyes removal process was presented in Figures 2 and 4. The analysis was performed under the magnification of 10,000×.

From these SEM micrographs, it is apparent that before the dyes removal process, TiO_2 powders has been

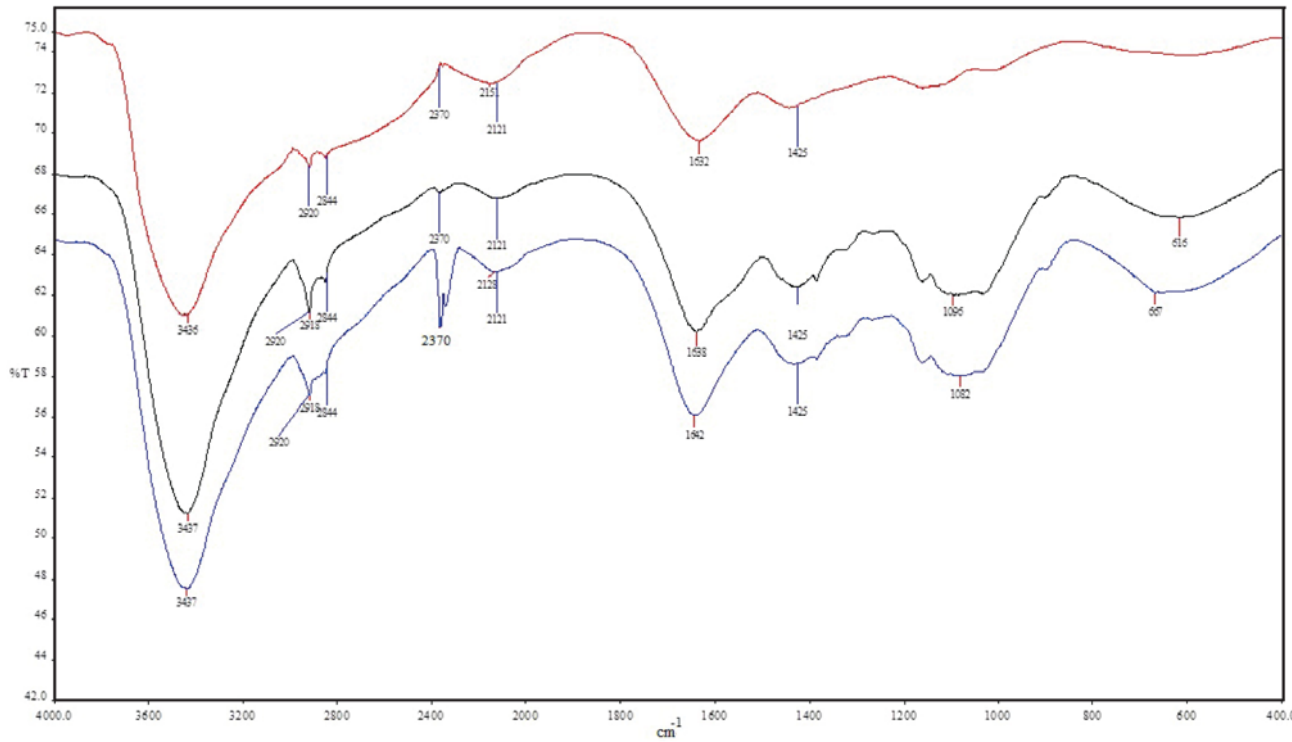

Figure 1. FTIR spectrum of native chitosan film (red) and corn cob film before adsorption (black) and after adsorption (blue)

evenly disperse onto the chitosan matrix. This can be observed from the homogeneity shown by the film (Figure 2a). The energy dispersive X-ray (EDX) analysis was performed on the white spots shown in Figure 2a. The Ti peaks in the spectrum (Figure 3) confirm the presence of TiO_2 in the film. As for corn cob film, it is clear that it is a non-porous type of materials (Figure 4a). Significant difference was observed on film morphology after it undergoes dye removal process. Both of the film's surfaces displayed less uniformity than before dyes removal. It is suggested that the rough and uneven surfaces shown in these films is due to the adhesion of dye molecules.

Besides SEM, color mapping using contact mode, atomic force microscope (AFM) was also employed to

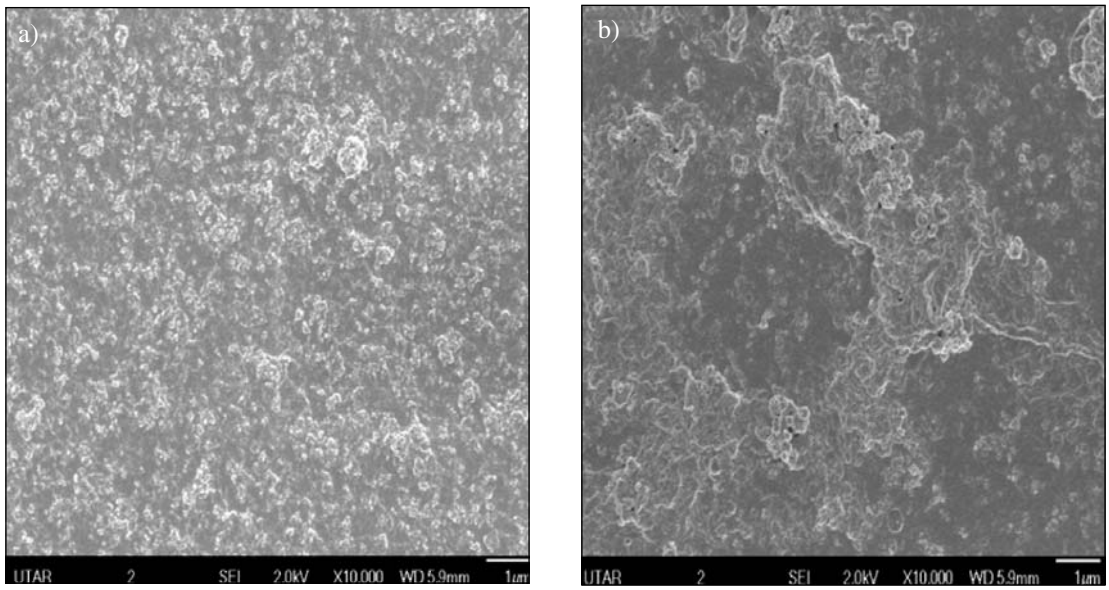

Figure 2. SEM micrographs of TiO_2 film before (a) and after (b) dyes removal process

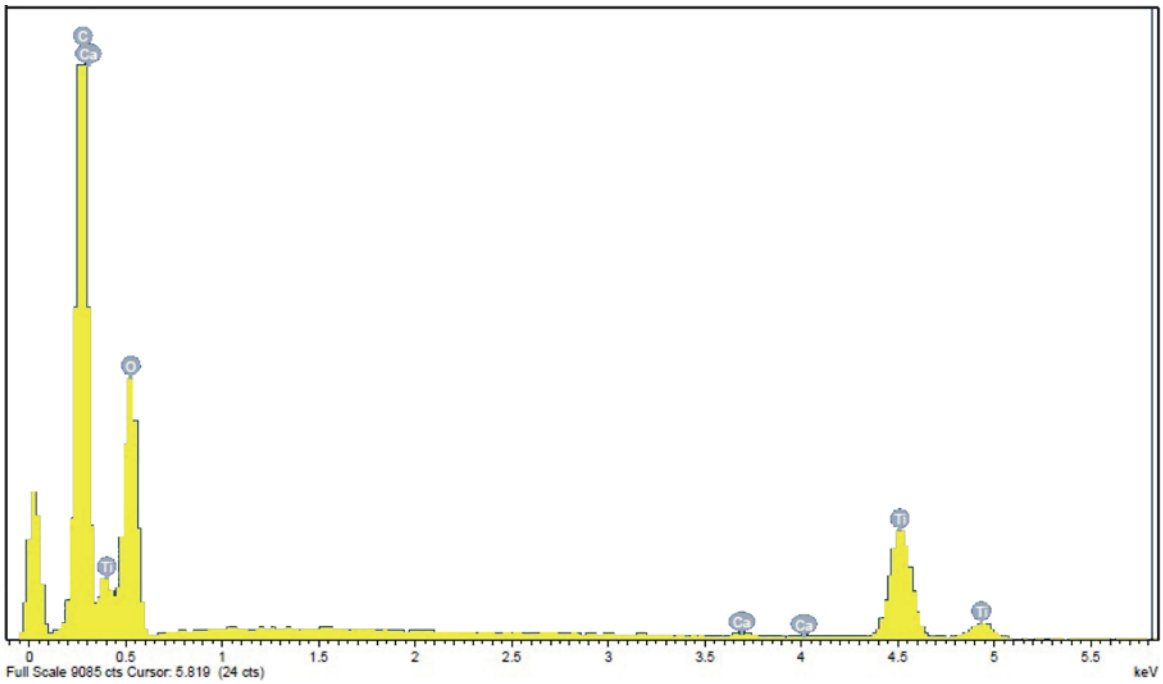

Figure 3. EDX analysis spectrum of the white spot in TiO_2 film

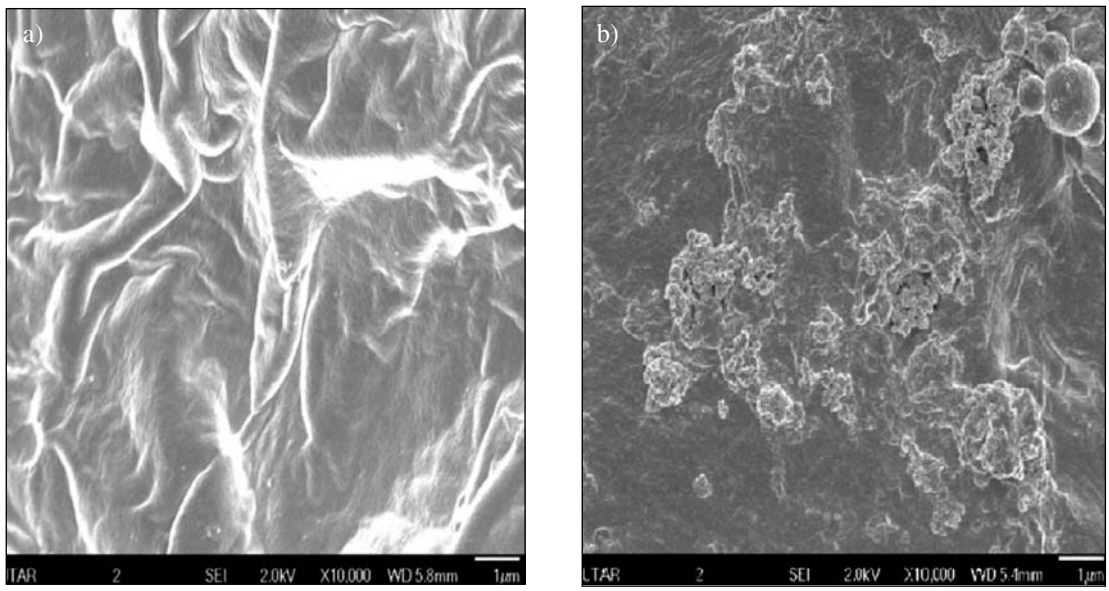

Figure 4. SEM micrographs of corn cob film before (a) and after (b) dyes removal process

define the saturation of film's surface. This is one of the usual methods used for displaying data whereby high features or high topography is illustrated by lighter color and vice versa. From the images obtained (Figures 5–6), films after the dyes removal process exhibited lighter color and rougher surface. This is most probably caused by the agglomeration of dyes. During the removal process, with the introduction of dye molecules on the surface of the films, these films become more intense and this explains the higher topography shown after the removal process.

3. 2. Effect of Initial pH of Dye Solution

Figure 7 shows the percentage uptake of MG and AY 17 from natural pH of binary dye solution (4.54) to 7 after 4 hours of contact time. The pH of dye solution is a crucial controlling parameter as it is going to influence the

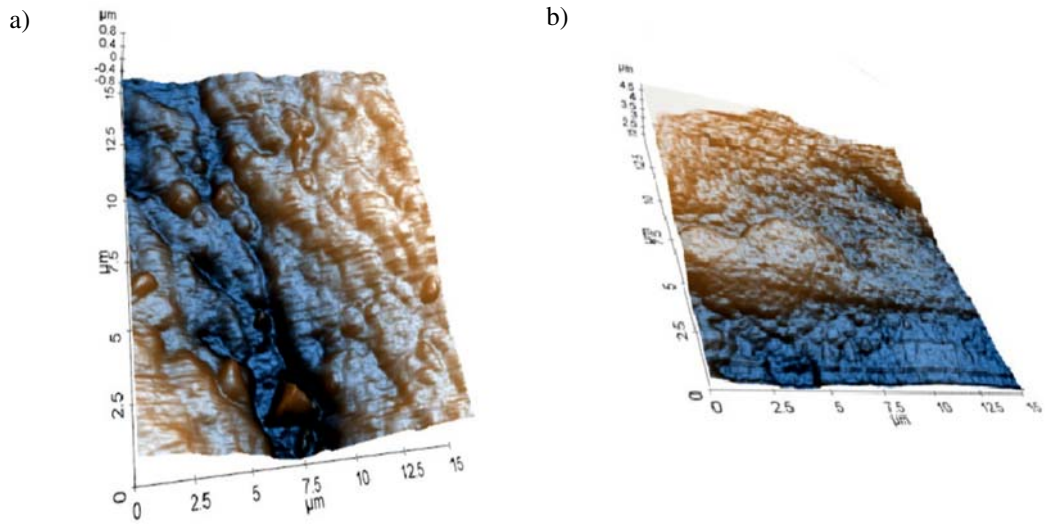

Figure 5. AFM image of TiO_2 film before (a) and after (b) dyes removal process

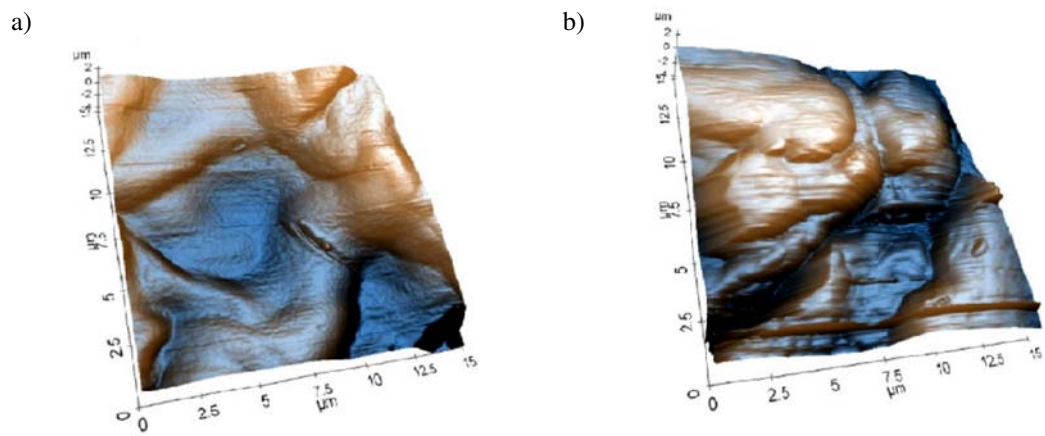

Figure 6. AFM image of corn cob film before (a) and after (b) dyes removal process

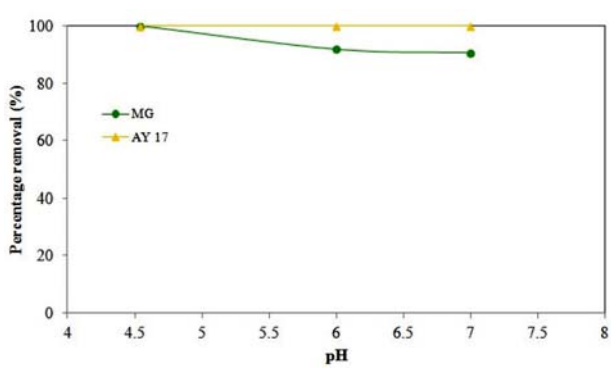

Figure 7. Effect of pH in the removal of MG and AY 17

aqueous chemistry as well as the surface binding sites of adsorbent.[18] Generally, the removal of MG should be increased as the pH of the solution increased whereas for AY 17, higher removal will be facilitated at low pH. However, the current results obtained indicated that the removal of both dyes was more favorable in acidic condition and this agreed well with some of the previously reported works.[19–21]

The high affinity shown by the films in acidic pH can be attributed to the usage of chitosan as the supporting matrix in this study. At lower pH, amino groups of chitosan can be easily protonated to form $–NH_3^+$. With decreasing pH, there will be more protons available to protonate amino groups of chitosan and this enhance the attraction of negatively charged dye (AY 17) towards the cationic amines.[22,23] However, as chitosan is a type of pH sensitive cellulose biopolymer which will dissolve and formed hydrogel under extreme acidic condition, therefore the effect of pH was not carried out beyond pH 4. And since by using the natural pH of the binary dye solution, an appreciate amount of both dyes could be removed simultane-

ously, therefore no pH adjustment was carried out in subsequent experiments.

3. 3. Effect of Initial Dye Concentration and Contact Time

The influence of the contact time was studied in order to identify the equilibrium time for maximum adsorption. Figure 8 indicates the rates of adsorption of MG and AY 17 at various concentrations. The uptake for three different concentrations which were 20, 40 and 80 mg/L for both MG and AY 17 showed the similar adsorption trend. From the results, it can be noticed that the adsorption of dyes was rapid at beginning, followed by a gradual process. This fast uptake at the beginning may be attributed to the large amount of available vacant binding sites of sorbent whereas a subsequent slower adsorption could be related to intraparticle diffusion. The current uptake pattern followed essentially the same trend in most of the reported works dealing with the adsorption studies whereby it can be customarily classified into rapid formation of an equilibrium interfacial concentration, followed by slow diffusion into the adsorbent.[24] With increasing contact time, the percentage uptake of dye removal rate decreased due to limited vacant adsorption sites as the binding sites of sorbent become saturated with dye molecules.[23] Hence, this has turned into a limiting factor for dye uptake. Similar observations were reported in the removal of colored textile wastewater using chitosan and the authors explained that these were due to the competition for active adsorption sites. [20,25] At higher dye concentration, the number of available adsorption sites becomes fewer and many dye molecules competed strongly to the limited adsorption sites. Consequently, large number of dye molecules was not being adsorbed successfully onto the sorbent.

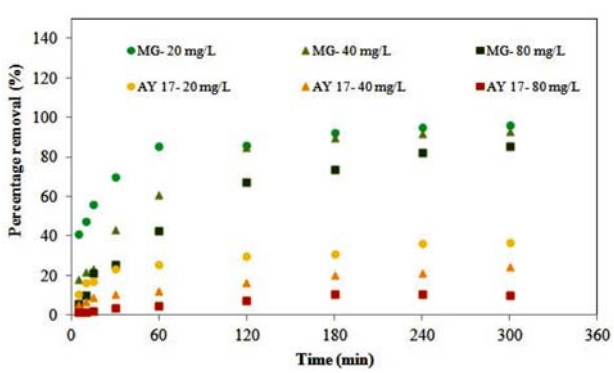

Figure 8. Effect of initial dye concentration and contact time in the removal of MG and AY 17

3. 4. Kinetics Studies

Sorption kinetic studies were explored as it can provide some important insight about the mechanism of adsorption processes as well as describe the reaction pathways. The modeling of the kinetic studies of MG and AY 17 onto the sorbent was examined individually by applying two different kinetic models, namely pseudo-first-order[26] and pseudo-second-order.[27] The applicability of the model was chosen based on their respective linear regression correlation coefficient, R^2 values.

3. 4. 1. Pseudo-first Order Kinetic Model

For pseudo-first order kinetic model, it assumes that the rate of the solute change is directly proportional to the amount of solid uptake with time. The linear equation of pseudo-first order equation is expressed as follows:

$$\log (q_e - q_t) = \log q_e - \frac{K_1}{2.303} t \quad (2)$$

where,
q_e = amount of dyes adsorbed at equilibrium, mg/g
q_t = amount of dyes adsorbed at time t, mg/g
K_1 = rate constant of pseudo–first order, 1/min
t = time, min

A linear graph of log (q_e–q_t) versus time for the adsorption of MG and AY 17 onto the corn cob films at the concentration of 20, 40 and 80 mg/L was plotted (Figure not shown). The experimental, $q_{e(expt)}$ and theoretical, $q_{e(cal)}$ adsorption capacities of dye at equilibrium and the first-order rate constant, K_1 with the correlation coefficient, R^2 for each dye concentration of was tabulated in Table 1. The $q_{e(expt)}$ and K_1 were determined from the intercept and gradient of the kinetic plot, respectively. Based on the re-

Table 1. Adsorption capacities, kinetic model parameters and correlation coefficients based on pseudo-first and pseudo-second order kinetic models

Dye	Initial dye concentration	$q_{e\ (expt)}$ (mg/L)	Pseudo-first order kinetic model			Pseudo-second order kinetic model			
			$q_{e\ (cal)}$ (mg/g)	K_1 (1/min)	R^2 mg/g)	$q_{e,\ cal}$ (mg g^{-1})	K_2 (1/min)	h (mg/g.min)	R^2
MG	20	5.4106	1.4983	0.00253	0.2583	5.0556	0.0286	0.7301	0.9837
	40	9.8819	5.4425	0.01474	0.5810	11.0375	0.0031	0.3831	0.9960
	80	14.8624	10.6856	0.01036	0.8083	18.6220	0.0009	0.2971	0.9830
AY 17	20	2.2865	1.7939	0.006909	0.5023	3.0544	0.0040	0.0370	0.9926
	40	3.3817	2.1857	0.005297	0.6686	3.5727	0.0074	0.0947	0.9758
	80	3.2961	1.6749	0.005758	0.4756	3.3852	0.0137	0.1570	0.9887

sults, for both MG and AY 17, the R^2 values were relatively low and the $q_{e(cal)}$ values gave unreasonable values compared to those determined experimentally. Besides, it was found that the pseudo-first order kinetic equation does not fit well for the whole range of the adsorption process. This clearly indicates the non-applicability of pseudo-first order kinetic model for the studied dyes and implies more than one parameter could be involved in the adsorption process. From the literature, the reviews of experimental works also reveal that (in most cases) the pseudo-first order equation is unable to correlate the measured kinetics well. [28–30]

3. 4. 2. Pseudo-second Order Kinetic Model

The adsorption kinetic data was further studied by using pseudo-second order model. Pseudo-second order model assume that rate limiting step may be chemisorption involving the valence forces transferring through electron sharing or exchanging between sorbent and sorbate as covalent forces, and ion exchange.[29,31] The linear equation of the model was shown:

$$\frac{t}{q_t} = \frac{1}{h} + \frac{1}{q_e}t \quad (3)$$

where $h = K_2 q_e^2$
h = initial rate of adsorption, mg/g.min
K_2 = rate constant of pseudo-second order, g/mg.min

This model is considered more appropriate to represent the kinetic data in biosorption systems and has the following advantages: it does not have the problem of assigning an effective adsorption capacity, the rate constant of pseudo-second-order, and the initial adsorption rate all can be determined from the equation without knowing any parameter beforehand.[29] A linear plot of t/q_t versus t for MG and AY 17 at various concentrations was plotted (Figure 9). The h values were calculated from y-intercept, whereas $q_{e\,(cal)}$ and K_2 values were obtained from the gradient of the linear plot. The R^2 values for both MG and AY 17 were found to be higher and closer to unity. Additionally, based on the tabulated data in Table 1, the theoretical $q_{e\,(cal)}$ shown closer values with the experimental equilibrium adsorption capacities. Therefore, it implies that adsorption of MG and AY 17 were better described by pseudo-second order kinetic model. The pseudo-second order rate constant, K_2 was found to be decrease with increasing dye concentrations (Table 1). This could be related to lower competition among the dyes molecules at lower concentration for the limited available surface adsorption sites.[23]

The values of q_e, K_2 and h against C_o in the corresponding linear plots of the pseudo-second order kinetic model were regressed in order to obtain the expression for theoretical MG and AY 17 concentration. These parameters could be expressed as a function of C_o for MG and AY 17 as follows:

$$q_e = \frac{C_o}{A_q C_o + B_q} \quad (4)$$

$$K_2 = \frac{C_o}{A_k C_o + B_k} \quad (5)$$

$$h = \frac{C_o}{A_h C_o + B_h} \quad (6)$$

where A_q, B_q, A_k, B_k, A_h and B_h are constant for the respective equations and obtained through regression from the linear plots. The generalized predictive models for MG and AY 17 adsorbed at any contact time and initial dye concentrations within the given range with relationship of q_t, C_o and t can be expressed as follow:

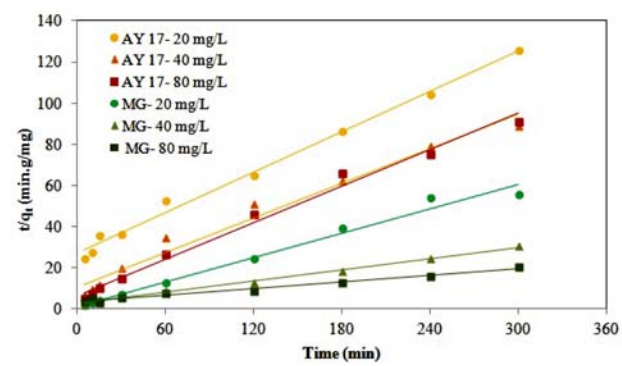

Figure 9. Pseudo second-order kinetics of MG and AY 17

$$q_t = \frac{C_o t}{(A_h)(C_o) + B_h + (A_q C_0 + B_q)t} \quad (7)$$

By substituting the calculated constant values, the theoretical model for MG and AY 17 could be represented as equation below:

$$(MG)q_t = \frac{C_o t}{(4.2273)(C_o) - 48.686 + (-0.0184C_0 + 3.6252)t} \quad (8)$$

$$(AY\ 17)q_t = \frac{C_o t}{(35.714)(C_o) - 847.28 + (0.3298C_0 - 1.1656)t} \quad (9)$$

Theoretical model derived for MG and AY 17 was applied to obtain the adsorption capacity, q_t at any given C_o and t. A comparison between the experimental values and theoretical values was shown in Figure 10.

It is clear that the theoretically generated curves showed good agreement with experimental data for 20 mg/L of MG, but deviations occurred at higher concentrations. This deviation could be related with the formation of multilayers on the sorbent as the dye concentrations in-

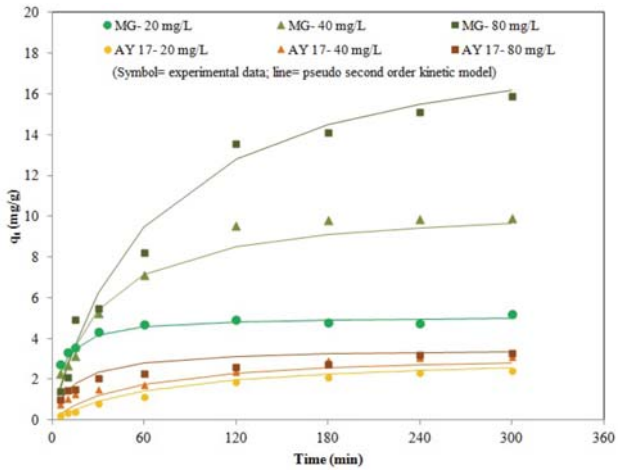

Figure 10. Typical plots of comparison between the measured and pseudo second order modeled time profiles for MG and AY 17 removal

creased.[32] Additionally, deviations were more pronounced in the case of AY 17 and this might be due to the poor R^2 values of the linear graph of q_e, K_2 and h against C_o. Several studies have also reported the suitability of pseudo-second order kinetic model in describing the adsorption process.[33–35]

3. 5. Sorption Isotherm

The sorption isotherm is important as it can be used to describe the interaction between sorbent surface and the dyes molecules. Two different isotherm models were applied, namely Langmuir [36] and Freundlich[37] models which are capable to give some insight into the sorption mechanism and the distribution between sorbate molecules and affinities of the sorbent. The most appropriate correlation equilibrium model was determined based on their respective isotherm constant and correlation coefficient, R^2 value.

The equation of Langmuir isotherm was shown below:

$$\frac{C_e}{q_e} = \frac{C_e}{q_m} + \frac{1}{K_a\, q_m} \tag{10}$$

where,

C_e = Equilibrium liquid phase dye concentration (mg/L)
q_e = Amount of dye absorbed at equilibrium (mg/g)
q_m = Maximum adsorption capacity (mg/g)
K_a = Adsorption equilibrium constant (L/mg)

A linear graph of C_e/q_e against C_e for the adsorption of MG and AY 17 onto corn cob films was plotted and shown in Figures 11 and 12, respectively. The correlation coefficient, R^2 value was 0.9406 for the linear plot of MG, whereas R^2 for AY 17 was 0.9684. This result indicates that monolayer adsorption of AY 17 on the surface of corn cob films system fitted better in Langmuir isotherm, but not for MG. The plot gave a linear regression line provided with gradient of $1/q_m$ and y-intercept of $1/q_mK_a$. The maximum adsorption capacity, q_m for MG and AY 17 were calculated as 35.336 mg/g and 0.241 mg/g, respectively. Meanwhile, Langmuir isotherm constant for the adsorption of MG was 0.882 L/mg and AY 17 was 0.039 L/mg.

In Langmuir isotherm, another important characteristic is that be related to the dimensionless equilibrium parameter, R_L[38] and the values could be calculated by using the equation shown as follow:

$$R_L = \frac{1}{1 + K_a C_o} \tag{11}$$

where,

R_L = Dimensionless equilibrium parameter
K_a = Adsorption equilibrium constant (L/mg)
C_o = Initial concentration of dye solution (mg/L)

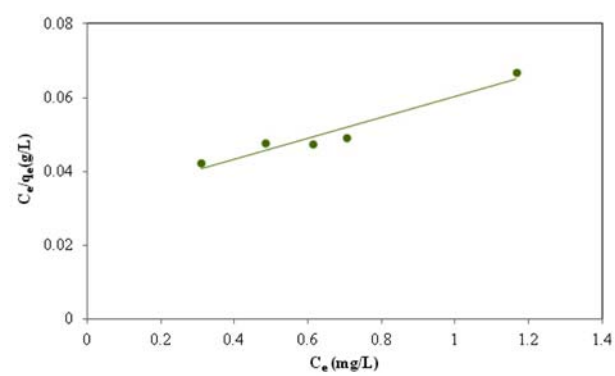

Figure 11. Langmuir isotherm of MG

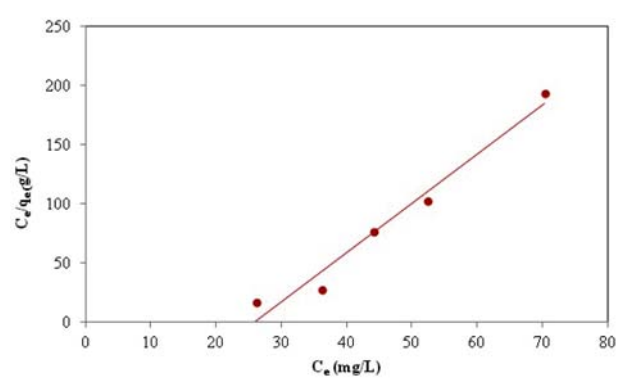

Figure 12. Langmuir isotherm of AY 17

The favorability of MG and AY 17 adsorption system could be predicted based on R_L value (If $R_L > 1$, unfavorable; R_L = , linear; $0 < R_L < 1$, favorable; $R_L = 0$, irreversible). The calculated R_L value lies between 0.0207 to 0.4534 and this indicates that the adsorption process

is favorable and corn cob thin films is a potential adsorbent for the removal of MG and AY 17 from aqueous solution.

The Freundlich isotherm assumes a physiochemical multilayer adsorption process on heterogeneous surfaces energy system. This isotherm is more towards a non-ideal adsorption that is more flexible and does not assume adsorption limit. The exponential Freundlich isotherm model equation is expressed as:

$$q_e = K_F C_e^{1/n} \tag{12}$$

where K_F = Freundlich isotherm constant for adsorption and n = Freundlich constant for intensity of adsorption. By taking the logarithm, the equation will therefore be in a linearized form and appeared as below:

$$\log q_e = \log K_F + \frac{1}{n} \log C_e \tag{13}$$

The graphs of log q_e against log C_e for MG and AY 17 were plotted and shown in Figures 13 and 14, respectively. The linear regression line on the plot could be used to determine the value of 1/n and K_F from gradient and y-intercept, respectively. The coefficients for the linearized forms of the isotherm models for the adsorption of both dyes are listed in Table 2. The results implied that adsorption of MG on the corn cob films was more towards the heterogeneous surface and belong to multilayer adsorption system. The values of n for MG and AY 17 were 1.484 and –0.618 whereas the intensities of Freundlich constant were 16.881 and 333.657, respectively. Adsorption system will be termed as favorable process when the n value is in the range of 1 < n < 10. Based on the n value obtained, the adsorption of MG was termed as favorable. As for AY 17, Langmuir model appears to provide a more reasonable fitting and therefore this explains why a lower n value was obtained.

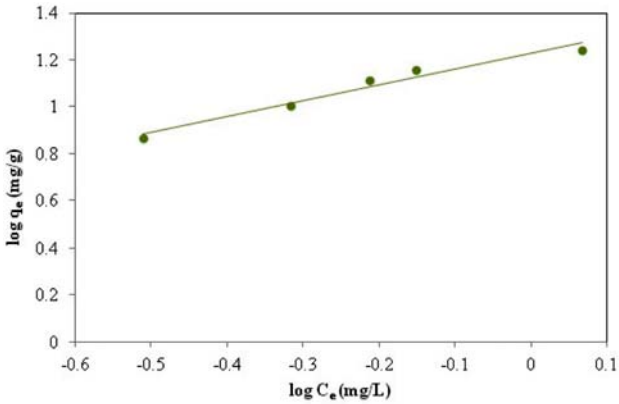

Figure 13. Freundlich isotherm of MG

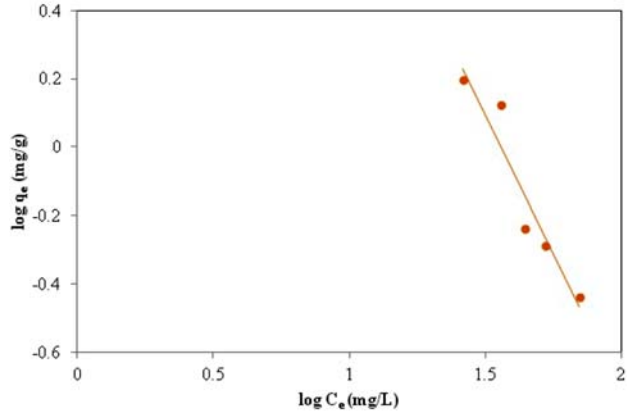

Figure 14. Freundlich isotherm of AY 17

3. 6. Reusability of TiO_2 Film and Corn Cob Film

Reusability is a major concern as this is one of key steps to make this type of economical dyes removal method applicable for practical usage. Therefore, a study on the repetitive usage and recycle of the thin films was performed. Figure 15 shows the effect of repetitive usage of TiO_2 and corn cob films on the percentage removal of MG and AY 17. The percentage removal of MG was maintained around 90 % whereas percentage removal of AY 17 decreased from cycle 1 to 4. This can be attributed by the non-negligible adsorbed dye molecules on the films. Although the film was subjected to regeneration process by using NaOH before the next cycle of usage, some of the AY 17 dye molecules might still be strongly bind to the films and this condition hinders other AY 17 dye molecules from reaching to the active site and subsequently, a lower uptake was observed. As for MG, the recycling method adopted shown that this is a suitable method to desorb the previously attached MG dye and as a result, a high removal efficiency was maintained throughout the process.

Table 2. Langmuir and Freundlich isotherm parameters

Dye	Langmuir			Freundlich		
	q_m, mg/g	K_a, L/mg	R^2	K_F	n	R^2
MG	35.336	0.882	0.9406	16.881	1.484	0.9633
AY 17	0.241	0.039	0.9684	333.657	–0.618	0.9081

3. 7. Statistical Experimental Design-Plackett-Burman (PB) and Response Surface Methodology (RSM)

Statistical approach was employed to determine the important factors and to optimize the experimental condition for the removal of MG and AY 17 in binary dye solution. Design-Expert version 7.1.3 was used to validate the model through function of desirability. Significant factors that affect the dyes removal through combination of photodegradation and adsorption were screened through Plackett- Burman (PB) design.

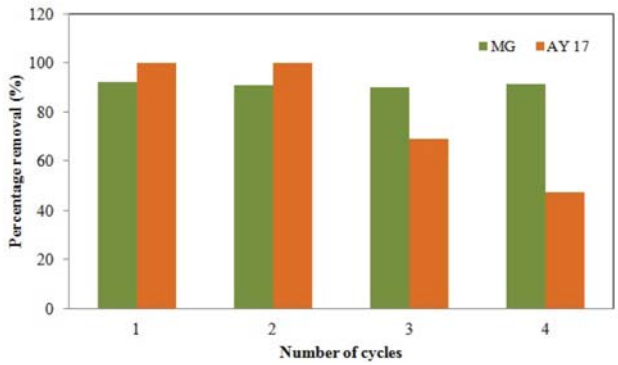

Figure 15. Effect of reusability in the removal of MG and AY 17

A total of three assigned parameters which were initial dye concentrations, contact time and pH were screened in total 12 experimental runs. For both MG and AY 17, the generated experimental condition and the differences of % removal between observed and predicted values were calculated and shown in Tables 3 and 4, respectively. It was observed that the largest and smallest differences between the observed and predicted removal for MG were 1.97% and 13.57%, respectively. As for AY 17, the percentage of differences was recorded in the range of 0.21% to 18.61%. The differences shown between the experimental and predicted percentage of removal is most probably due to the involvement of insignificant variables in the analysis. In some of the previously reported works, the researchers also noticed that there'll some differences in terms of the observed and predicted response and they attributed this kind of deviation to the non-negligible effect of insignificant variables in the design.[2,32]

Table 5 shows the analysis of variance (ANOVA) of both MG and AY 17 in binary dye solution. The studied variables were identified as significant Prob > F was less than 0.05. Based on the value, the studied model was found to be significant. For both MG and AY 17, the significant factors in affecting the removal process were contact time and initial pH of binary dye solution. The effect of contact time was termed as significant and this is closely related to the involvement of various stages in the process of adsorption. As for the effect of pH, this suggests that the degree of ionization of the adsorbate and the surface properties of the adsorbent play an important role in determining the efficiency of the process.

The influential factors identified through PB were further studied and optimized using response surface methodology (RSM). A total of 13 experimental runs were conducted and Table 6 shows the combination of the generated contact time and initial pH. Besides, the observed and predicted response was also presented in the same table. The modified cubic model was employed to describe the correlation between these two important factors and the percentage removal was shown as follows in terms of coded form:

MG in binary dye solution:

$$\% \text{ uptake of MG} = +94.16 + 16.95\,A - 10.04\,B - 9.18\,AB - 15.96\,A^2 - 11.36\,B^2 \quad (14)$$

AY 17 in binary dye solution:

$$\% \text{ uptake of AY 17} = +101.87 + 35.05\,A - 10.06B - 12.41\,AB - 50.89\,A^2 - 6.53\,B^2 \quad (15)$$

Where A = contact time and B = initial pH

Table 3. Plackett-Burman design and results for the percentage removal of MG in binary dye solution

Experiment	Variable Contact time, mins	Initial concentration, mg/L	pH	Observed response, %	Predicted response, %	Differences, %
1	240.00	10.00	7.00	54.05	59.51	–5.46
2	240.00	10.00	7.00	54.05	59.51	–5.46
3	240.00	10.00	4.54	96.74	83.17	13.57
4	240.00	20.00	4.54	93.22	88.43	4.79
5	5.00	20.00	7.00	42.54	44.52	1.97
6	240.00	20.00	7.00	52.54	64.77	–12.23
7	5.00	20.00	4.54	47.08	58.94	–11.86
8	5.00	20.00	7.00	42.54	44.52	1.97
9	5.00	10.00	7.00	38.68	44.52	1.97
10	5.00	10.00	4.54	48.04	53.69	–5.65
11	5.00	10.00	4.54	48.04	53.69	–5.65
12	240.00	20.00	4.54	93.22	88.43	4.79

Tables 7 and 8 were the ANOVA results and from these tables, both models were found to be significant ($P < 0.0001$) with model F-value of 102.21 and 36.37 for MG and AY 17, respectively. The relatively high R^2 values in MG and AY 17 models indicated that there were good agreements between the experimental and predicted va-

Table 4. Plackett-Burman design and results for the percentage removal of AY17 in binary dye solution

Experiment	Variable Contact time, mins	Initial concentration, mg/L	pH	Observed response, %	Predicted response, %	Differences, %
1	5.00	40.00	4.54	11.90	20.60	–8.70
2	5.00	40.00	4.54	11.90	20.60	–8.70
3	240.00	60.00	4.54	100.00	91.89	8.11
4	240.00	40.00	7.00	47.26	53.98	–6.72
5	5.00	60.00	4.54	13.68	28.33	–14.65
6	240.00	60.00	7.00	43.10	61.71	–18.61
7	240.00	60.00	4.54	100.00	91.89	8.11
8	240.00	40.00	7.00	47.28	53.98	–6.70
9	5.00	60.00	7.00	6.67	7.31	–0.64
10	5.00	60.00	7.00	6.67	7.31	–0.64
11	5.00	40.00	7.00	5.43	5.22	0.21
12	240.00	40.00	4.54	100.00	84.16	15.84

Table 5. Regression analysis (ANOVA) of Placktt-Burman of MG and AY 17 in binary dye solution

Dye	Source	Degree of freedom	Sum of squares	Mean square	F-value	Prob > F	Description
MG	Model	3	4369.61	1456.54	14.14	0.0015	Significant
	Contact time	1	2607.80	2607.80	25.32	0.0010	Significant
	Initial MG concentration	1	82.90	82.90	0.80	0.3958	Not significant
	Initial pH	1	1678.91	1678.91	16.30	0.0037	Significant
	Residual	8	823.92	102.99	–	–	–
AY 17	Model	3	15032.24	5010.75	25.77	0.0002	Significant
	Contact time	1	12120.26	12120.26	62.33	0.0001	Significant
	Initial AY 17 concentration	1	179.18	179.18	0.92	0.3652	Not significant
	Initial pH	1	2732.80	2732.80	14.05	0.0056	Significant
	Residual	8	1555.58	194.45	–	–	–
	Total	11	16587.82		–	–	–

Table 6. Central composite design (CCD) matrix for two independent variables and the observed respond on MG and AY 17 in binary dye solution

Experiment	variable Contact time	Initial pH	Respond Experimental % uptake of MG	Predicted % uptake of MG	Differences, %	Experimental % uptake of AY 17	Predicted % uptake of AY 17	Differences, %
1	122.50	5.77	93.1	93.28	–0.18	100	100	0.00
2	240.00	7.00	62.75	64.58	–1.83	45.02	57.03	–12.01
3	122.50	4.54	96.7	93.28	3.42	100	100	0.00
4	5.00	7.00	49.39	49.03	0.36	9.05	11.75	–2.70
5	122.50	5.77	93.1	93.28	–0.18	100	100	0.00
6	122.50	5.77	93.1	93.28	–0.18	100	100	0.00
7	240.00	5.77	100	95.16	4.84	100	86.03	13.97
8	122.50	5.77	93.1	93.28	–0.18	100	100	0.00
9	122.50	5.77	93.1	93.28	–0.18	100	100	0.00
10	240.00	4.54	100	93.28	6.72	100	100	0.00
11	5.00	4.54	49.93	50.76	–0.83	14.4	7.05	7.35
12	5.00	5.77	61.73	61.26	0.47	11.28	15.93	–4.65
13	122.50	7.00	74.23	72.76	1.47	100	85.28	14.72

Table 7. Regression analysis (ANOVA) of RSM of MG

Source	Degree of freedom	Sum of squares	Mean square	F-value	p-value (Prob>F)	Description
Model	5	4351.68	870.34	102.21	<0.0001	Significant
A	1	1723.81	1723.81	202.44	<0.0001	Significant
B	1	605.21	605.21	71.08	<0.0001	Significant
AB	1	336.91	336.91	39.57	0.0004	Significant
A^2	1	703.36	703.36	82.60	<0.0001	Significant
B^2	1	356.31	356.31	41.85	0.0003	Significant
Residual	7	59.61	8.52	–	–	–

R^2: 0.9865, Adjusted R^2: 0.9768, Predicted R^2: 0.8937, Adequate precision: 27.233 and C.V.: 3.58 %

Table 8. Regression analysis (ANOVA) of RSM of AY 17

Source	Degree of freedom	Sum of squares	Mean square	F-value	p-value (Prob>F)	Description
Model	5	17914.53	3582.91	36.37	<0.0001	Significant
A	1	7370.31	7370.31	74.82	<0.0001	Significant
B	1	606.62	606.62	6.16	0.0421	Significant
AB	1	615.78	615.78	6.25	0.0410	Significant
A^2	1	7152.23	7152.23	72.61	<0.0001	Significant
B^2	1	117.70	117.70	1.19	0.3105	Not significant
Residual	7	689.54	98.51	–	–	–

R^2: 0.9629, Adjusted R^2: 0.9365, Predicted R^2: 0.6454, Adequate precision: 14.585 and C.V.: 13.17 %

lues. The R^2 that is close to unity signified a stronger model and it would be able to provide a better response.[39] The signal to noise ratio is represented by adequate precision and a ratio that is greater than 4 is desirable.[40, 41] From this study, the adequate precision for MG and AY 17 models were 27.233 and 14.585, respectively and this shown an adequate signal. The coefficient of variance (C.V.) of MG model was recorded as 3.58% wheraeas for AY 17 model was 13.17%. A low value of C.V. is preferred as this represents a greater precision and reliability of the experiments carried out.[40] As both models have shown an adequate signal, therefore they were used to navigate the design space.

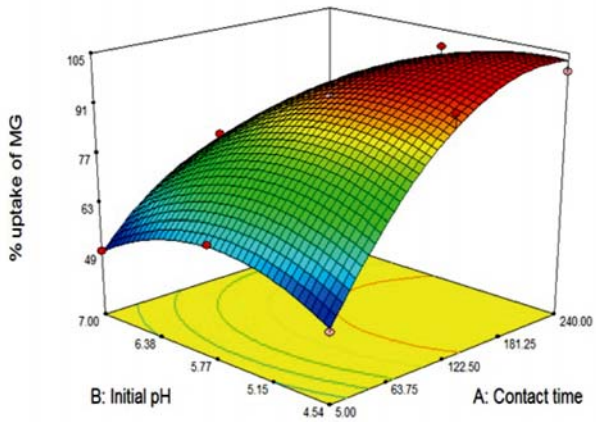

Figure 16. 3D surface plot of MG as a function of initial pH and contact time

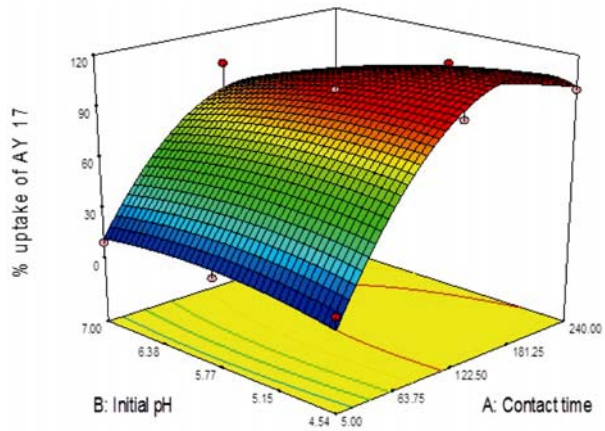

Figure 17. 3D surface plot of AY 17 as a function of initial pH and contact time

Figures 16 and 17 showed the 3D surface plot of MG and AY 17, respectively for the interaction between contact time and initial pH. For the removal of both dyes, a more favourable condition was observed when the contact time was at the maximum point while initial pH was at the minimum point within the studied range. This is because by prolonging the contact time, it leads to more diffusion time and therefore a greater amount of dye molecules can be adsorbed onto the sorbent sites. As for the effect of initial pH, again, this is related to the surface charge and the usage of chitosan as the immobilizing agent.

4. Conclusion

The results from this study have shown the effectiveness of TiO_2 and corn cob films in the removal of MG and AY 17 from aqueous solution. The kinetics of dyes adsorption revealed that dye adsorption was more appropriately described by pseudo-second order model which is a kind of chemisorption process, involving valency forces through the sharing or exchange of electrons between the adsorbent and adsorbate as covalent forces, and ion exchange. The equilibrium data obtained was best conformed to Freundlich isotherm for MG and Langmuir isotherm for AY 17. This indicated that the adsorption of both dyes followed their respective heterogeneous and homogeneous adsorption pattern. The maximum adsorption capacity of MG and AY 17 was 35.336 and 0.241 mg/g, respectively. It is interesting to note that the efficiency of the films remained high after being repeated used for 2 cycles. From the statistical experimental design, it was shown that both models were highly significant with relatively high R^2 values. Within the studied range, the crucial factors in affecting the percentage of removal for both dyes were identified to be contact time and initial pH.

5. Acknowledgements

The authors are thankful for the financial support provided by the Malaysia-Toray Science Foundation through the research grant: 4417/O02. The research facilities provided by Universiti Tunku Abdul Rahman (UTAR) are acknowledged.

6. References

1. V. K. Gupta and Suhas, J. Environ. *Manage.,* **2009**, *90*, 2313–2342. https://doi.org/10.1016/j.jenvman.2008.11.017
2. S. L. Lee, S. W. Liew and S. T. Ong, *Acta Chim. Slov.,* **2016**, *63*, 144–153. https://doi.org/10.17344/acsi.2015.2068
3. S. Srivastava, R. Sinha and D. Roy, *Aquat. Toxicol.,* **2004**, *66*, 319–329. https://doi.org/10.1016/j.aquatox.2003.09.008
4. E. Sudova, J. Machova, Z. Svobodova and T. Vesely, *Veterinarni Medicina,* **2007**, *52*, 527–539.
5. S. T. Ong, S. T. Ong, Y. T. Hung and Y. P. Phung, *Desalin. Water Treat., **2015**, 55,* 1359–1371. https://doi.org/10.1080/19443994.2014.925830
6. J. F. Gao, Q. Zhang, K. Su, R. N. Chen and Y. Z. Peng, *J. Hazard. Mater.,* **2010**, *174*, 215–225. https://doi.org/10.1016/j.jhazmat.2009.09.039
7. M. A. Ashraf, M. Hussain, K. Mahmood, A. Wajid, M. Yusof, Y. Alias and I. Yusoff, Desalin. *Water Treat.,* **2013**, *51*, 4530–4545. https://doi.org/10.1080/19443994.2012.747187
8. L. Zheng, Z. Dang, X. Yi and H. Zhang, J. Hazard. *Mater.,* **2010**, *176*, 650–656. https://doi.org/10.1016/j.jhazmat.2009.11.081
9. A. Buasri, N. Chaiyut, K. Tapang, S. Jaroensin and S. Panphrom, *APCBEE Procedia,* **2012**, *3*, 60 – 64. https://doi.org/10.1016/j.apcbee.2012.06.046
10. B. Barl, C. Biliaderis, E. Murray and A. Macgregor, J. Sci. *Food Agric.,* **1991**, *56*, 195–214. https://doi.org/10.1002/jsfa.2740560209
11. L. Suhadolnik, A. Pohar, B. Likozar and M. Čeh, *Chem. Eng. J.,* **2016**, *303*, 292–301. https://doi.org/10.1016/j.cej.2016.06.027
12. M. Krivec, A. Pohar, B. Likozar and G. Dražić, *AIChE J.,* **2015**, *61*, 572–581. https://doi.org/10.1002/aic.14648
13. M. Bitenc, B. Horvat, B. Likozar, G. Dražić and Z.C. *Orel, Appl. Catal.,* B., **2013**, *136– 137*, 202– 209. https://doi.org/10.1016/j.apcatb.2013.02.016
14. F. Han, V. S. R. Kambala, M. Srinivasan, D. Rajarathnam and R. Naidu, *Appl. Catal., A.,* **2009**, *359*, 25–40. https://doi.org/10.1016/j.apcata.2009.02.043
15. M. A. Rauf and S. Salman Ashraf, *Chem. Eng.* J., **2009**, *151,* 10–18. https://doi.org/10.1016/j.cej.2009.02.026
16. J. M. Herrmann, *Catal. Today,* **1999**, *53*, 115–129. https://doi.org/10.1016/S0920-5861(99)00107-8
17. K. A. M. Amin and M. Panhuis, *Polymers,* **2012**, *4*, 590–599. https://doi.org/10.3390/polym4010590
18. S. L. Chan, Y. P. Tan, A. H. Abdullah and S. T. Ong, J. Taiwan *Inst. Chem. Eng.,* **2016**, *61*, 306–315. https://doi.org/10.1016/j.jtice.2016.01.010
19. M. S. M. Hassan, Radiat. *Phys. Chem.,* **2015**, *115*, 55–61. https://doi.org/10.1016/j.radphyschem.2015.05.038
20. N. M. Mahmoodi, R. Salehi, M. Aramin and H. Bahrami, *Desalination*, **2010**, *267*, 64–72. https://doi.org/10.1016/j.desal.2010.09.007
21. Y. P. Phung, S. T. Ong and P. S. Keng, *J. Chem.,* **2013**, *Article ID 3887865*, 1–7. https://doi.org/10.1155/2013/387865
22. H. Momenzadeh, B. A. R. Tehrano, A. Khosravi, K. Gharanjig and K. Holmberg, *Desalination,* **2011**, *271*, 225–230. https://doi.org/10.1016/j.desal.2010.12.036
23. M. Li, S. Wang, W. Luo, H. Xia, Q. Gao and C. Zhou, J. Chem. *Technol. Biotechnol.,* **2014**, *90*, 1124–1134. https://doi.org/10.1002/jctb.4433
24. S. T. Ong, S. T. Ha, P. S. Keng, C. K. Lee and Y. T. Hung. In *Handbook of Environmental and Waste Management*; Yung-Tse Hung, Lawrence K. Wang, Nazih Shammas (Eds); World Scientific Publishing Co.: Singapore, 2012; 929–978. https://doi.org/10.1142/9789814327701_0021
25. R. D. C. Soltani, A. R. Khataee, M. Safari and S. W. Joo, Int. *Biodeterior. Biodegradation,* **2013**, *85*, 383–391. https://doi.org/10.1016/j.ibiod.2013.09.004
26. S. Lagergren and B. K. Svenska, *Veternskapsakad Handlingar,* **1898**, *24*, 1–39.
27. Y. S. Ho and G. McKay, *Process Biochem.,* **1999**, *34*, 451–465. https://doi.org/10.1016/S0032-9592(98)00112-5
28. W. Plazinski, Adv. Colloid *Interface Sci.,* **2013**, *197–198*, 58–67. https://doi.org/10.1016/j.cis.2013.04.002

29. Y.S. Ho, J Hazard Mater, **2006**, *B136*, 681–689. https://doi.org/10.1016/j.jhazmat.2005.12.043
30. J. Febrianto, A.N. Kosasih, J. Sunarso, Y. H. Ju, N. Indraswati, N. and S. Ismadji, *J Hazard Mater,* **2009**, *162*, 616–645. https://doi.org/10.1016/j.jhazmat.2008.06.042
31. Ho, Y. S. and G. McKay, *Water Res.,* **2000**, *34*, 735–742. https://doi.org/10.1016/S0043-1354(99)00232-8
32. S. T. Ong and C. K. Seou, Desalin. *Water Treat.,* **2014**, 52, 7673–7684. https://doi.org/10.1080/19443994.2013.830684
33. P. Saha, S. Chowdhury, S. Gupta, I. Kumar and R. Kumar, *Clean Soil, Air and Water*, **2000**, *38*, 437–445. https://doi.org/10.1002/clen.200900234
34. T. Santi and S. Manonmani, Malachite Green Removal from aqueous solution by the peel of *Cucumis Sativa* fruit. *Clean Soil, Air and Water*, **2011**, *39*, 162–170. https://doi.org/10.1002/clen.201000077
35. K. T. Karthikeyan and Jothivenkatachalam, J. Environ. *Nanotechnol.,* **2014**, *3*, 69–80. https://doi.org/10.13074/jent.2014.03.142070
36. I. Langmuir, J. Am. *Chem. Soc.,* **1918**, *40*, 1361–1403. https://doi.org/10.1021/ja02242a004
37. H. Freundlich, Phys. *Chem. Soc.,* **1906**, *40*, 1361–1368
38. T. W. Weber and R. K. Chakkravorti, Am. Ins. Chem. Eng. J., **1974**, *20*, 228–238. https://doi.org/10.1002/aic.690200204
39. K. Chauhan, U. Trivedi, and K. C. Patel, *J. Microbial Biotechnol.,* **2006**, *16*, 1410–1415.
40. J. K. Kim, B. R. Oh, H. Shin, C. Eom and S. W. Kim, *Process Biochem.,* **2008**, *43*, 1308–1312. https://doi.org/10.1016/j.procbio.2008.07.007
41. E. C. Khoo, S. T. Ong, Y. T. Hung and S. T. Ha, Desalin. *Water Treat.,* **2013**, *51*, 7109–7119. https://doi.org/10.1080/19443994.2013.791774

Povzetek

Proučevana je bila učinkovitost uporabe filmov z vsebnostjo TiO_2 oziroma mikrodelcev koruznih storžev za odstranjevanje barvil malahitno-zeleno (MG) in kislo-rumeno 17 (AY 17) iz raztopine. Uporabljena metoda imobilizacije se lahko izogne filtraciji, ki v praksi ni primerna. V šaržnih eksperimentih so bili pročevani začetni pH raztopine, začetna koncentracija barvila, kontaktni čas in ponovna uporaba adsorbenta. Ravnotežni podatki za MG in AY 17 sledijo Freundlichovi in Langmuirjevi izotermi. Odstotek odstranjenega MG je ostal visok po štirih sorpcijskih ciklih, vendar je bila za AY 17 dosežena višja redukcija. Odstranjevanje obeh barvil je bilo modelirano in optimirano s pomočjo metode po Plackett-Burmanu (PB) in metode odzivne površine (RSM). Pogoji na površini so bili analizirani s pomočjo infrardeče spektroskopije (IR), fourierjeve transformacijske infrardeče spektroskopije (FTIR), elektronske vrstične mikroskopije (SEM) in mikroskopije na atomsko silo (AFM).

Scientific paper

Synthesis of Some Unique Carbamate Derivatives bearing 2-Furoyl-1-piperazine as a Valuable Therapeutic Agents

Muhammad Athar Abbasi,[1,*] Ghulam Hussain,[1] Aziz-ur-Rehman,[1] Sabahat Zahra Siddiqui,[1] Syed Adnan Ali Shah,[2,3] Muhammad Arif Lodhi,[4] Farman Ali Khan,[4] Muhammad Ashraf,[5] Qurat-ul-Ain,[5] Irshad Ahmad,[6] Rabia Malik,[6] Muhammad Shahid[7] and Zahid Mushtaq[7]

[1] *Department of Chemistry, Government College University, Lahore-54000, Pakistan*

[2] *Faculty of Pharmacy, Universiti Teknologi MARA, Puncak Alam Campus, 42300 Bandar Puncak Alam, Selangor Darul Ehsan, Malaysia*

[3] *Atta-ur-Rahman Institute for Natural Products Discovery (AuRIns), Level 9, FF3, Universiti Teknologi MARA, Puncak Alam Campus, 42300 Bandar Puncak Alam, Selangor Darul Ehsan, Malaysia*

[4] *Department of Biochemistry, Abdul Wali Khan University, Mardan-23200, Pakistan*

[5] *Department of Chemistry, The Islamia University of Bahawalpur, Bahawalpur-63100, Pakistan*

[6] *Department of Pharmacy, The Islamia University of Bahawalpur, Bahawalpur-63100, Pakistan*

[7] *Department of Biochemistry, University of Agriculture, Faisalabad-38040, Pakistan*

* *Corresponding author: E-mail: atrabbasi@yahoo.com; abbasi@gcu.edu.pk*
tel: (+92)-42-111000010, ext. 266.

Received: 12-10-2016

Abstract

The aim of the research work was to synthesize different biologically active carbamate derivatives bearing 2-furoyl-1-piperazine and having modest toxicity. The synthesis was completed as a multiple sequence. The structural confirmation of all the synthesized compounds was obtained by EI-MS, IR and ^{1}H-NMR spectral data. The enzyme inhibition and antibacterial potential of the synthesized compounds was evaluated. To find the utility of the prepared compounds as possible therapeutic agents their cytotoxicity was also checked. All the compounds were active against acetylcholinesterase enzyme, especially **12** and **14** showed very good inhibitory potential relative to Eserine, a reference standard. Almost all the compounds showed good activities against both Gram-positive and Gram-negative bacterial strains.

Keywords: 2-Furoyl-1-piperazine; ^{1}H-NMR; Acetylcholinesterase; Antimicrobial activity; Hemolytic activity

1. Introduction

Heterocyclic compounds are cyclic compounds having hetero atoms e.g, N, O or S, having diverse medicinal importance.[1] Piperazine is a medicinally important heterocyclic nucleus which consists of a six membered ring containing two nitrogen atoms at the positions 1 and 4 in the ring. The piperazine has been classified as a privileged structure and is frequently found in biologically active compounds across a number of different therapeutic areas[2] which encompass anti-microbial, anti-tubercular, anti-psychotic, anti-convulsant, anti-depressant, anti-inflammatory, cytotoxic, anti-malarial, anti-arrhythmic, anti-oxidant and anti-viral activities.[3,4]

Carbamates are derivatives of carbamic acid (NH_2COOH). A carbamate group, carbamate group, carbamate ester and carbamic acids functional groups are unified structurally and often are interconverted chemically. Carbamate esters are also called urethanes. Although most of the literature is concerned with organic carbamates, yet, the inorganic salt ammonium carbamate is produced on a large scale from ammonia and carbon dioxide. The amino groups of the lysine residues in urease and phosphotriesterase also attribute carbamate. The carbamate resulting from aminoimidazole is an intermediate in the biosynthesis of . Carbamoyl phosphate is generated from carboxyphosphate rather than CO_2.[5] The carbamate insecticides featuring the carbamate ester functional group, e.g, Aldicarb, Carbofuran, Carbaryl (Fig. 1) etc., encompass this group.

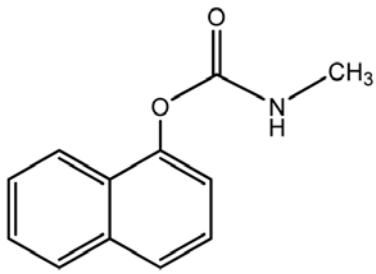

Fig. 1. Carbaryl (insecticide carbamate)

The organophosphate pesticides also hinder this enzyme, although irreversibly, and originate a more severe form of cholinergic poisoning.[6] Iodopropynyl butylcarbamate is a wood and paint preservative and used in the cosmetics[7]. Urethane (ethylcarbamate) was once produced commercially in the United States as an anti-neoplastic agent and for other medicinal purposes. It was found toxic and largely ineffective and is now seldom used as a veterinary medicine.[8]

α-Glucosidase comprises class of hydrolase enzymes, located in the brush border surface membrane of small intestinal cells.[9] The vital function of α-glucosidase is to hydrolyze the 1,4 glycosidic linkage from the non reducing end of the α-glucosides, substrates to produce α-D-glucose and other monosaccharide which are operated as carbon and energy source.[10] For oral anti-diabetic drugs for patients with type-2 *Diabetes mellitus* α-glucosidase inhibitors compounds are used. Postprandial hyperglycemia has a role in the growth of type-2 diabetes and problems associated with disease such as nephropathy and macroangipathy etc.[11] The inhibitors of enzyme can hinder the release of D-glucose of oligosaccharides and disaccharides beginning dietary complex carbohydrates and holdup glucose absorption, resulting in compact postprandial hyperglycemia.[12]

Acetyl and butyrylcholinesterases (AChE/BChE) comprise a family of serine hydrolases. The different specificities for substrates and inhibitors for these enzymes are caused by the differences in amino acid residues of the active sites of AChE and BChE. The enzyme scheme is liable for the termination of acetylcholine at cholinergic synapses. These are main components of cholinergic brain synapses and neuromuscular junctions. The chief function of AChE and BChE is to catalyze the hydrolysis of the neurotransmitter acetylcholine.[13,14] It has been found that BChE is present in appreciably higher quantities in Alzheimer's plaques in the normal age related to non dementia of brains. Cholinesterase inhibitors increase the amount of acetylcholine offered for neuromuscular and neuronal transmission through their reversible or irreversible inhibitory activity.[15] Hence, the search for new cholinesterase inhibitors is consider an important strategy to introduce new drug candidates for the treatment of Alzheimer's disease and other related diseases.[16] Different microbes have been found to be involved in many diseases[17–22] and some of them are included in the current study. So, in continuation of our previous work on carbamates,[23–25] hereby we report the synthesis of some unique carbamates having amalgamation with 2-furoylpiperazine moiety, which might find their utility as potential and safe thereapeutic agents.

2. Results and Discussion

The aim of the present research work was to synthesize new biologically active compounds with low toxicity. Indeed, the current need is to introduce pharmacologically active drugs to help in pharmacy against the increasing resistance of microorganisms.

2. 1. Chemistry

In the present research work, different carbamate derivatives bearing 2-furoyl-1-piperazine were synthesized in a series of steps by a reported method[26] as shown in Scheme 1 and then all the derivatives were screened for enzyme inhibition, antimicrobial and hemolytic activities. The structural analysis of one of the compounds is discussed here in detail for the benefit of the reader. The molecule **16** was synthesized as an off-white amorphous solid having melting point 80–92 °C and molecular formula $C_{19}H_{20}Br_3N_3O_4$, which was confirmed by EI-MS having $[M]^+$ peak at *m/z* 591 and by the number of protons in its ^{1}H-NMR spectrum. The CHN analysis data of this molecule also supported the assignement of its molecular formula. Its structure was corroborated by the distinct ion peak at *m/z* 93 related to *N*-furoyl group and another at *m/z* 332 for *O*-(2,6-dibromophenyl)-*N*-(allyl)carbamate part. The suggested mass fragmentation pattern is given in Fig. 2. In IR spectrum of **16**, characteristic peaks appeared at υ 3406 (N–H), 3086 (Ar C–H), 2882 (R C–H), 1657 (C=O), 1582 (Ar C=C), 1497 (N=O), 1197 (C–O–C), 1110 (C–N–C), 847 (C–N) and 548 cm^{-1} (C–Br) which al-

together confirmed the presence of the carbamate group and 2-furoyl-1-piperazine ring. In the aromatic region of ^{1}H-NMR spectrum, a two-proton singlet appeared at δ 7.67 (s, 2H, H-3 and H-5) which is typical for a 2,4,6-tribromophenyl moiety attached via an oxygen atom. The other three peaks in the aromatic region at δ 7.49 (brs, 1H, H-5'''), 7.04 (d, J = 4.1 Hz, 1H, H-3''') and 6.49 (dd, J = 4.0, 2.0 Hz, 1H, H-4''') are characteristic for a 2-furyl ring. Moreover, a singlet δ 5.19 represents NH of the carbamate group, while the 1,4-disubstituted piperazine ring was deduced through two broad singlets in aliphatic region, and each broad singlet representing two symmetrical methylene groups. These two singlets resonated at δ 3.94 (4H) and δ 3.47 (4H). The former was assigned to symmetrical CH_2-3'' and CH_2-5'' while latter was assigned to symmetrical CH_2-2'' and CH_2-6'' in the piperazine entity. Similary, the presence of a central 1,3-disubstitued propyl group was ascertained by the signals resonating at δ 4.12 (t, J = 6.6 Hz, 2H, CH_2-1'), 3.61–3.57 (m, 2H, CH_2-3') and 2.10 (quintet, J = 6.8 Hz, 2H, CH_2-2'). The ^{1}H-NMR spectrum of this molecule is shown in Fig. 3. So, on the basis of aforementioned spectral evidences, the structure of **16** was confirmed as 2,4,6-tribromophenyl 3-[4-(2-furoyl)-1-piperazinyl]propylcarbamate. All the synthesized carbamate derivatives bearing 2-furoyl-1-piperazine were characterized by IR, ^{1}H-NMR and EI-MS spectral analysis in a similar way.

2. 2. Biological Activities (*in vitro*)

2. 2. 1. Enzyme Inhibition Activity

The synthesized compounds exhibited variable inhibitory potentials against α-glucosidase, acetylcholinesterase and butyrylcholinesterase as evident from their IC_{50} values presented in Table 1. Only two compounds, 2,4,6-tribromophenyl 2-[4-(2-furoyl)-1-piperazinyl]ethylcarbamate (**9**) and 2,4,6-tribromophenyl 3-[4-(2-furoyl)-1-piperazinyl]propylcarbamate (**16**) showed weak inhibitory po-

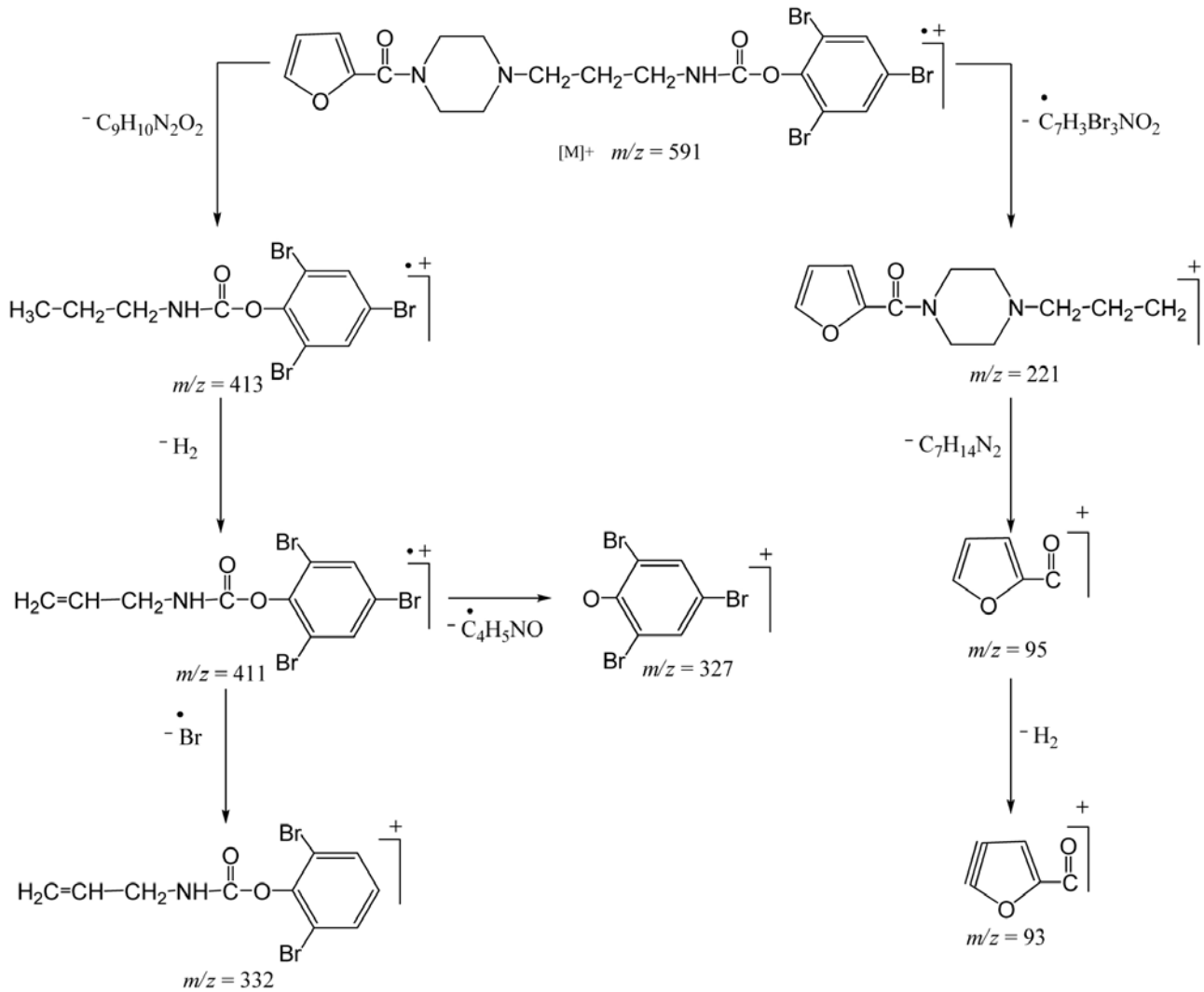

Fig. 2. Suggested mass fragmentation pattern of 2,4,6-tribromophenyl 3-[4-(2-furoyl)-1-piperazinyl]propylcarbamate (**16**).

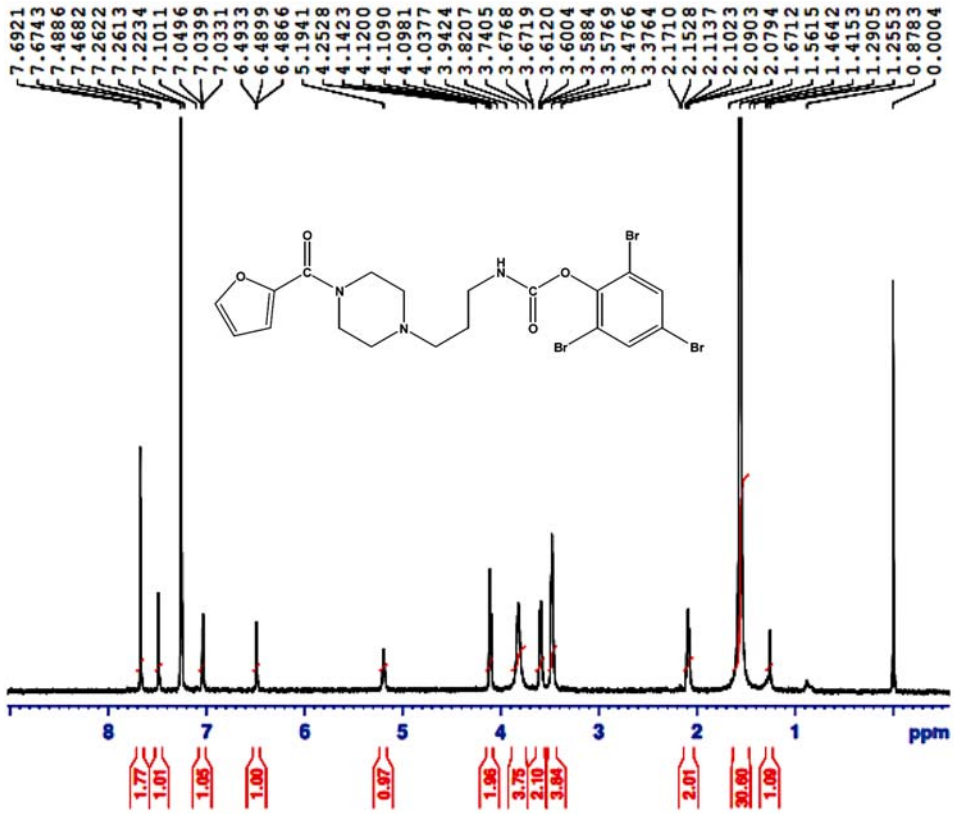

Fig. 3. ^{1}H-NMR spectrum of 2,4,6-tribromophenyl-3-[4-(2-furoyl)-1-piperazinyl]propylcarbamate (**16**)

Table 1. Bioactivity studies of different carbamate derivatives bearing 2-furoyl-1-piperazine

Compound	α-Glucosidase		AchE		BChE	
	% Inhibition	IC_{50} (μM)	% Inhibition	IC_{50} (μM)	% Inhibition	IC_{50} (μM)
5	25.45 ± 0.31	–	78.59 ± 0.23	34.62 ± 0.19	28.35 ± 0.16	–
7	–	–	81.35 ± 0.96	456.45 ± 0.29	–	–
9	94.32 ± 0.28	345.16 ± 0.60	77.15 ± 0.18	32.51 ± 0.03	48.16 ± 0.27	–
12	32.34 ± 0.26	–	81.63 ± 0.15	18.91 ± 0.04	55.71 ± 0.24	361.27 ± 0.13
14	27.67 ± 0.45	–	82.45 ± 0.11	23.22 ± 0.05	33.26 ± 0.25	–
16	85.54 ± 0.32	422.61 ± 0.30	81.76 ± 0.12	24.71 ± 0.07	43.45 ± 0.21	–
Control	**92.23 ± 0.14**[a]	**38.25 ± 0.12**[a]	**91.27 ± 1.17**[b]	**0.04 ± 0.0001**[b]	**82.82 ± 1.09**[b]	**0.85 ± 0.0001**[b]

NOTE: All compounds were dissolved in methanol and experiments were performed in triplicate (mean±SEM, n = 3).
a = Acarbose, b = Eserine, AChE = Acetylcholinesterase, BChE = Butyrylcholinesterase

tential against α-glucosidase, having IC_{50} value of 345.16 ± 0.16 μM and 422.61 ± 0.13 μM, respectively, relative to Acarbose, used as a reference standard having IC_{50} value of 38.25 ± 0.12 μM. This inhibitory potential might be attributed to the presence of 2,4,6-tribromophenyl group in both molecules. All the molecules were active against acetylcholinesterase enzyme but among all molecules phenyl 3-[4-(2-furoyl)-1-piperazinyl]propylcarbamate (**12**) exhibited the best inhibitory potential against this enzyme with IC_{50} value of 18.91 ± 0.04 μM, relative to Eserine, a reference standard having IC_{50} value of 0.04 ± 0.0001 μM. This enhanced inhibitory potential of **12** can be a result of its unique skeleton as a whole. Moreover, this was the only molecule which showed some inhibitory tendency against butyrylcholinesterase enzyme with IC_{50} value of 361.27 ± 0.13 μM. In the future some modified derivatives of this molecule are suggested to show much closer IC_{50} value to the standard Eserine.

2. 2. 2. Antibacterial Activity

All the synthesized molecules were screened against Gram-positive and Gram-negative bacteria, and were found to be excellent-to-good antibacterial agents. The re-

sults are shown as MIC values in Table 2. Among the synthesized carbamates, **16** showed the lowest MIC value (8.96 ± 0.49 μM) against *S. typhi* credibly because of the presence of 2,4,6-tribromophenyl group. In the case of *E. coli*, carbamate **14** showed the lowest MIC value (9.95 ± 0.48 μM) probably due to the presence of 2,4,6-trinitrophenyl group. Against *P. aeruginosa* and *B. subtilis*, **16** and **9** exhibited excellent antibacterial potential with MIC values 9.27 ± 0.16 μM and 9.43 ± 0.85 μM, respectively, predominantly because of the presence of 2,4,6-trinitrophenyl group and 2,4,6-tribromophenyl group, respectively, in these molecules. Similarly, the carbamate **16** also rendered a great antibacterial activity against *S. aureus* with MIC value 16.87 ± 0.41 μM. Amongst the synthesized compounds, **5** and **16** showed MIC values against all the bacterial strains while compound **16** showed the excellent MIC value in the following order towards all bacterial strains: *S. typhi* > *P. aeroginosa* > *B. subtilis* > *E. coli* > *S. aureus*, probably due to the presence of 2,4,6-tribromophenyl moiety. In general, we can say that most of the carbamates possessed very good antibacterial activities against both Gram-positive and Gram-negative bacterial strains and hence these molecules might lead to the discovery of very potent antibacterial agents in future.

2. 2. 3. Hemolytic Activity

Most of the molecules exhibited very modest cytotoxicity values, except **14** (72.38%), yet it was lower than the positive control (Triton-X-100). The lowest activity was shown by the molecule **16** (9.20%), although it was a little higher than the negative controls (PBS). So it can be concluded that these molecules might be further tested for their therapeutic applications in the drug designing program because of their moderate toxicity, as shown in Table 2.

2. 2. 4. Computational Docking

In order to get an insight about the validity of accuracy, the co-crystallized ligands of the following enzymes

Table 2. Antibacterial activity (MIC) and hemolytic activity of different carbamate derivatives bearing 2-furoyl-1-piperazine

Compound	MIC (μM)					Hemolytic activity
	S. typhi (–)	*E. coli (–)*	*P.aeroginosa (–)*	*B. subtilis (+)*	*S. aureus (+)*	%
5	9.08 ± 0.50	17.43 ± 0.61	19.87 ± 0.51	10.85 ± 0.14	19.98 ± 0.58	24.26
7	9.14 ± 0.15	16.98 ± 0.75	18.34 ± 0.92	10.78 ± 0.93	-	15.94
9	9.89 ± 0.17	14.43 ± 0.05	9.87 ± 0.43	9.43 ± 0.85	-	12.10
12	9.88 ± 0.75	15.64 ± 0.32	17.67 ± 0.34	11.76 ± 0.54	-	53.13
14	9.78 ± 0.90	9.95 ± 0.48	17.78 ± 0.33	16.49 ± 0.27	-	72.38
16	8.96 ± 0.49	10.64 ± 0.58	9.27 ± 0.16	9.78 ± 0.62	16.87 ± 0.41	9.20
Ciprofloxacin	**7.45 ± 0.58**	**7.16 ± 0.58**	**7.14 ± 0.18**	**7.29 ± 0.90**	**7.80 ± 0.19**	
PBS						**0.09**
Triton						**100**

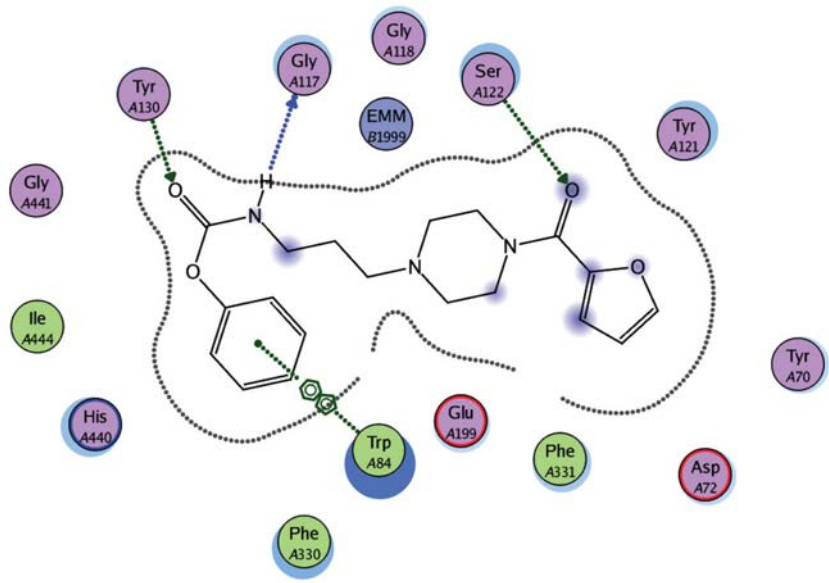

Fig. 4. 2D interacted image of phenyl 3-[4-(2-furoyl)-1-piperazinyl]propylcarbamate (**12**) against acetylcholinestrase.

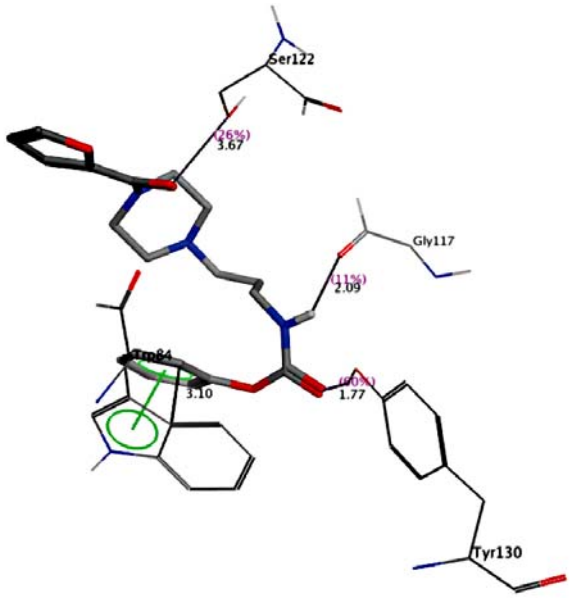

Fig. 5. 3D interacted image of phenyl 3-[4-(2-furoyl)-1-piperazinyl]propylcarbamate (**12**) against acetylcholinestrase.

were extracted and then re-docked into the binding pockets of the receptors. In all these cases, RMSD values between docked and co-crystallized ligands were less than 2 Å which indicates the reliability of docking method and thus showing that our protocol can be used for further studies. Almost all the synthesized derivatives were computationally docked against α-glucosidase, AChE and BChE to explore the binding modes of all the ligands. The carbamate **12** was docked against acetylcholinesterase. There were observed four prominent interactions between **12** and active residues of the protein. First strongest side chain donor interaction was found between TyrA130 and carbonyl oxygen giving a distance of 1.77 Å, second between SerA122 and another carbonyl oxygen with the distance of 3.67 Å. Third strong back bone donor interaction was established between GlyA117 and amide proton of the ligand with a distance of 2.09 Å. Similarly the last hydrophobic interaction of a distance of 3.10 Å was found between TrpA81 and phenyl ring of the ligand as shown in Fig. 4 and 5. From the same compound **12** protein docked complex of butyrylcholinesterase, this interacted weakly

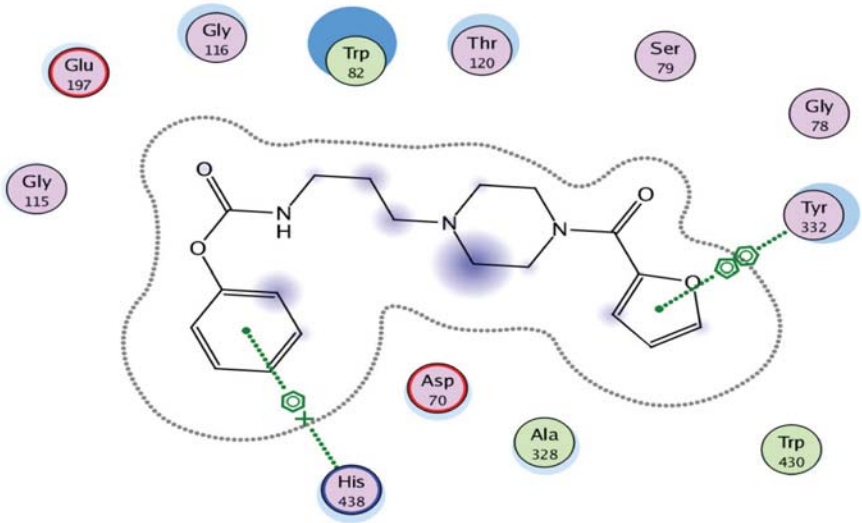

Fig. 6. 2D interacted image of phenyl 3-[4-(2-furoyl)-1-piperazinyl]propylcarbamate (**12**) against butyrylcholinesterase.

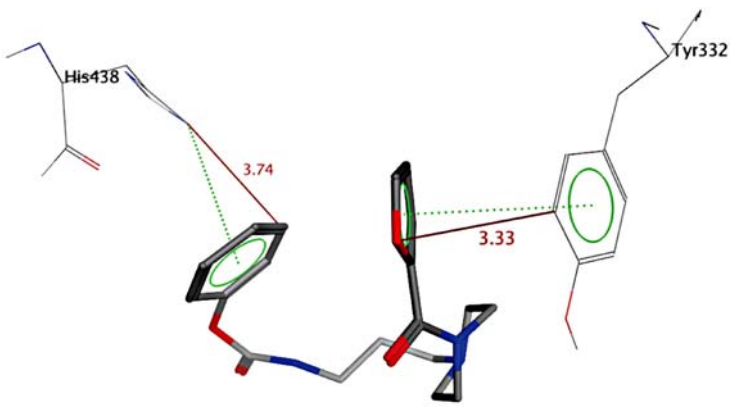

Fig. 7. 3D interacted image of phenyl 3-[4-(2-furoyl)-1-piperazinyl]propylcarbamate (**12**) against butyrylcholinesterase.

with Tyr332 and His438 amino acid residues. Tyr332 displayed arene–arene interaction with furoyl ring with the distance of 3.36 Å, while His438 displayed arene cation interaction with phenyl ring with a distance of 3.74 Å as it is shown in Fig. 6 and 7.

3. Experimental

3. 1. General

Chemicals and solvents of analytical grade were purchased from Sigma Aldrich and Alfa Aesar (Germany). By using an open capillary tube method, melting points were determined on Griffin and George apparatus and are uncorrected. By using thin layer chromatography (TLC) in various percentages of ethyl acetate and *n*-hexane as mobile phase, initial purity of compounds was detected at 254 nm. IR peaks were recorded on a Jasco-320-A spectrometer by using a KBr pellet method. ^{1}H-NMR signals were recorded at 500 MHz in $CDCl_3$ using Bruker spectrometers. EI-MS signals were recorded by utilizing a JMS-HX-110 spectrometer.

3. 2. Synthesis of Phenyl (N-substituted) carbamates 3 and 11

2-Chloroethylamine (2-chloro-1-ethanamine; **2**; 0.1 mol) and 3-bromopropylamine (**10**; 0.1 mol) were taken separately in two iodine flasks, each containing 10 mL distilled water. The pH of the solution was maintained at 9–10 by 10% aqueous Na_2CO_3 followed by the addition of phenyl carbonochloridic acid (phenylchloroformate; **1**; 0.1 mol,) in equimolar ratios in each flask along with vigorous shaking. The reaction mixture in each case was stirred at room temperature for 3–4 h. Progress of the reaction was confirmed by TLC (*n*-hexane : EtOAc; 70:30), visualized by UV lamp. Phenyl 2-chloroethylcarbamate (**3**) and phenyl 3-bromopropylcarbamate (**11**) were collected as white precipitates by filtration. These were washed with distilled water and dried to acquire pure compounds.

3. 3. Nitration of Phenyl (*N*-substituted) carbamates Yielding 6 and 13

Phenyl 2-chloroethylcarbamate (**3**; 0.1 mol) and phenyl 3-bromopropylcarbamate (**11**; 0.1 mol) were taken separately in two 50 mL round bottom flasks. 5–10 mL concentrated H_2SO_4 was added in each flask to dissolve the respective compound. Each mixture was stirred for 15–20 min at room temperature and then equimolar amount of nitric acid was added to each mixture dropwise at 10 °C. Then each reaction mixture was stirred for 4 h and monitored by TLC. On reaction completion, ice cold water was added to the reaction flasks to produce the precipitates which were collected by filtration, washed with distilled water and dried to afford the nitrated compounds **6** and **13**, separately.

3. 4. Bromination of Phenyl (*N*-substituted) carbamates Yielding 8 and 15

Phenyl 2-chloroethylcarbamate (**3**; 0.1 mol) and phenyl 3-bromopropylcarbamate (**11**; 0.1 mol) were taken separately in two 50 ml round bottomed flasks and were dissolved in glacial acetic acid (5–10 mL). Liquid bromine was added slowly in equimolar amount to eack flask. The reaction mixture in each case was stirred at room temperature and monitored with TLC for the completion of the reaction. Distilled water was added to each reaction flask to quench the reaction. Precipitated products were filtered, washed with distilled water and dried to obtain pure brominated compounds **8** and **15**, separately.

3. 5. Synthesis of Different Carbamate Derivatives Bearing 2-Furoyl-1 -piperazine Moiety

2-Furoyl-1-piperazine (**4**; 4.5 mmol) dissolved in 20–30 mL acetonitrile was taken in a 100 mL round bottom flask, solid K_2CO_3 (13.5 mmol) was added and the reaction mixture was refluxed for half an hour followed by the addition of respective carbamates (**3**, **6**, **8**, **11**, **13** or **15**; one in each case) in equimolar ratio. The mixture was refluxed for 4–5 h. TLC was carried out to check the reaction completion (20% ethyl acetate: 80% *n*-hexane). Distilled water was added to the reaction mixture to acquire the respective precipitates. On completion, 1–2 drops of aqueous NaOH were added to the reaction mixture. Precipitates were filtered, washed and dried to obtain the respective carbamates **5**, **7**, **9**, **12**, **14** or **16** (one in each case) bearing 2-furoyl-1-piperazine.

3. 5. 1. Phenyl 2-[4-(2-furoyl)-1-piperazinyl] ethylcarbamate (5)

Sticky brown liquid; Yield: 90%; Mol. F.: $C_{18}H_{21}N_3O_4$; Mol. Mass.: 343 g/mol; IR (KBr, cm^{-1}) ν_{max}: 3406 (N–H), 3086 (Ar C–H), 2882 (R C–H), 1657 (C=O), 1582 (Ar C=C), 1498 (N=O), 1197 (C–O–C), 1110 (C–N–C), 853 (C–N); ^{1}H-NMR (500 MHz, $CDCl_3$, ppm): δ 7.49 (brs, 1H, H-5'''), 7.45 (brt, J = 7.2 Hz, 2H, H-3 and H-5), 7.15 (brt, J = 7.3 Hz, 1H, H-4), 7.07 (brd, J = 7.7 Hz, 2H, H-2 and H-6), 7.01 (d, J = 4.1 Hz, 1H, H-3'''), 6.50 (dd, J = 1.9, 3.2 Hz, 1H, H-4'''), 5.19 (s, 1H, NH), 3.84 (brs, 4H, CH_2-3'' and CH_2-5''), 3.39 (t, J = 6.2 Hz, 2H, CH_2-1'), 2.56 (brt, J = 6.0 Hz, 4H, CH_2-2'' and CH_2-6''), 2.42 (t, J = 6.8 Hz, 2H, CH_2-2'); EI-MS *m/z* 343 $[M]^+$, 207 $[C_{11}H_{15}N_2O_2]^+$, 165 $[C_9H_{11}NO_2]^{\bullet+}$, 163 $[C_9H_9NO_2]^{\bullet+}$, 95 $[C_5H_3O_2]^+$, 94 $[C_6H_5O]^+$, 93 $[C_5HO_2]^+$. Anal. Calc. for $C_{18}H_{21}N_3O_4$ (343.15): C, 62.96; H, 6.16; N, 12.24. Found: C, 62.84; H, 6.25; N, 12.37.

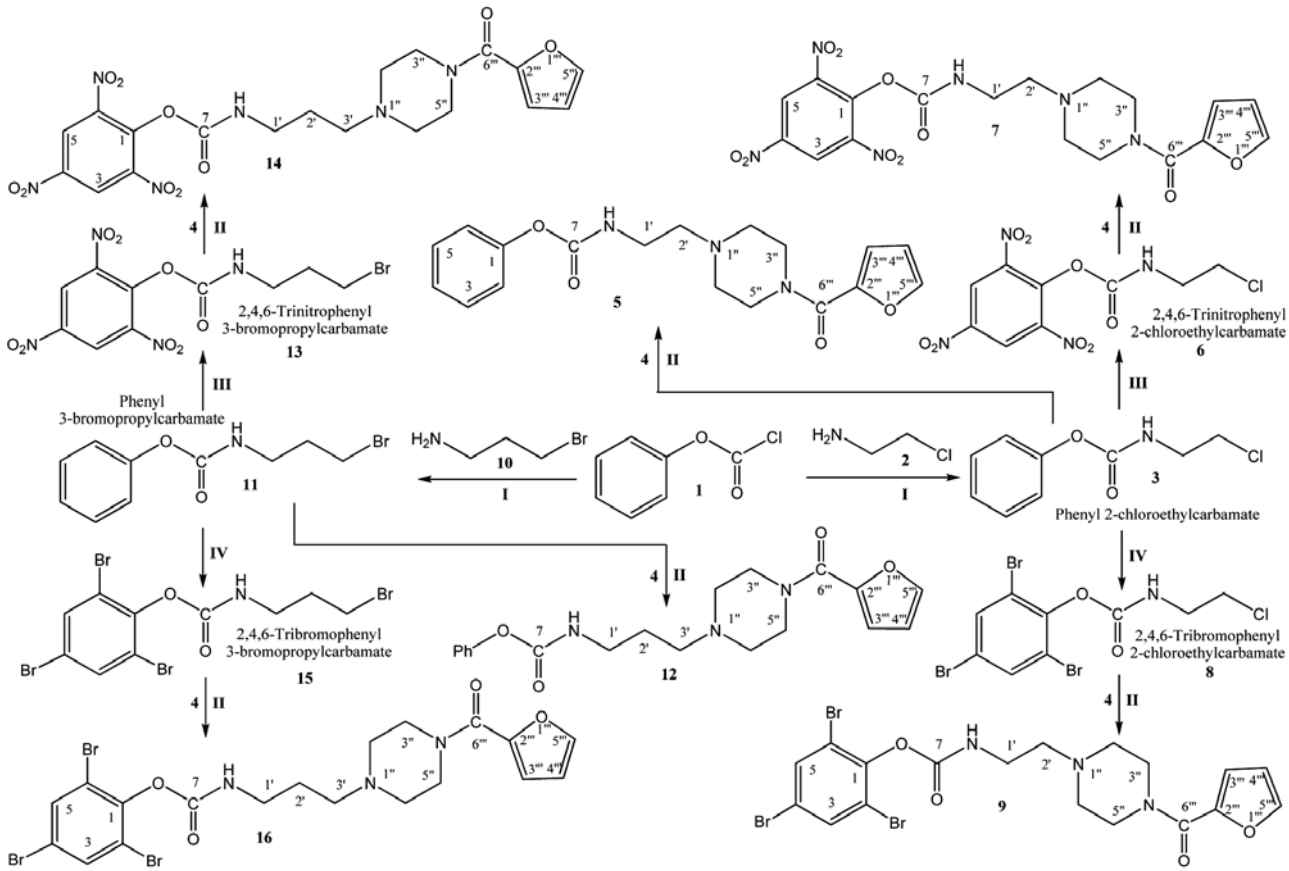

Scheme 1. Outline for the synthesis of different carbamate derivatives bearing 2-furoyl-1-piperazine. Reagents and conditions: (I) 10% aq. Na_2CO_3 soln./pH 9–10/stirring at RT for 3–4 h. (II) 2-Furoyl-1-piperazine (**4**)/CH_3CN/K_2CO_3/reflux for 4–5 h. (III) Conc. HNO_3/conc. H_2SO_4/stirring at RT for 3–4 h. (IV) Br_2/CH_3COOH/stirring at RT for 3–4 h.

3. 5. 2. 2,4,6-Trinitrophenyl 2-[4-(2-furoyl)-1-piperazinyl]ethylcarbamate (7)

Sticky brown liquid: 82%; Mol. F.: $C_{18}H_{18}N_6O_{10}$; Mol. Mass.: 478 g/mol; IR (KBr, cm^{-1}) ν_{max}: 3406 (N–H), 3086 (Ar C–H), 2882 (R C–H), 1657 (C=O), 1582 (Ar C=C), 1490 (N=O), 1197 (C–O–C), 1110 (C–N–C), 848 (C–N); ^{1}H-NMR (500 MHz, $CDCl_3$, ppm): δ 8.15 (s, 2H, H-3 and H-5), 7.49 (brs, 1H, H-5'''), 6.99 (d, J = 4.1 Hz, 1H, H-3'''), 6.49 (dd, J = 1.9, 3.2 Hz, 1H, H-4'''), 5.19 (s, 1H, NH), 3.84 (brs, 4H, CH_2-3'' and CH_2-5''), 3.39 (t, J = 6.2 Hz, 2H, CH_2-1'), 2.56 (brt, J = 6.0 Hz, 4H, CH_2-2'' and CH_2-6''), 2.42 (t, J = 6.8 Hz, 2H, CH_2-2'); EI-MS *m/z* 478 $[M]^+$, 300 $[C_9H_8N_4O_8]^{\bullet+}$, 298 $[C_9H_6N_4O_8]^{\bullet+}$, 254 $[C_9H_6N_3O_6]^+$, 229 $[C_6H_2N_3O_7]^+$, 207 $[C_{11}H_{15}N_2O_2]^+$, 95 $[C_5H_3O_2]^+$, 93 $[C_5HO_2]^+$. Anal. Calc. for $C_{18}H_{18}N_6O_{10}$ (478.11): C, 45.19; H, 3.79; N, 17.57. Found: C, 45.26; H, 3.85; N, 17.66.

3. 5. 3. 2,4,6-Tribromophenyl 2-[4-(2-furoyl)-1 -piperazinyl]ethylcarbamate (9)

Sticky brown liquid; Yield: 85%; Mol. F.: $C_{18}H_{18}Br_3N_3O_4$; Mol. Mass.: 577 g/mol; IR (KBr, cm^{-1}) ν_{max}: 3406 (N–H), 3086 (Ar C–H), 2882 (R C–H), 1657 (C=O), 1582 (Ar C=C), 1491 (N=O), 1197 (C–O–C), 1110 (C–N–C), 853 (C–N), 545 (C–Br); ^{1}H-NMR (500 MHz, $CDCl_3$, ppm): δ 7.75 (s, 2H, H-3 and H-5), 7.47 (brs, 1H, H-5'''), 7.02 (d, J = 4.1 Hz, 1H, H-3'''), 6.47 (dd, J = 1.9, 3.3 Hz, 1H, H-4'''), 5.18 (s, 1H, NH), 3.83 (brs, 4H, CH_2-3'' and CH_2-5''), 3.36 (t, J = 6.1 Hz, 2H, CH_2-1'), 2.58 (brt, J = 6.1 Hz, 4H, CH_2-2'' and CH_2-6''), 2.45 (t, J = 6.8 Hz, 2H, CH_2-2'); EI-MS *m/z* 577 $[M]^+$, 399 $[C_9H_8Br_3NO_2]^{\bullet+}$, 397 $[C_8H_6Br_3NO_2]^{\bullet+}$, 318 $[C_9H_8Br_2NO_2]^+$, 327 $[C_6H_2Br_3O]^+$, 207 $[C_{11}H_{15}N_2O_2]^+$, 95 $[C_5H_3O_2]^+$, 93 $[C_5HO_2]^+$. Anal. Calc. for $C_{18}H_{18}Br_3N_3O_4$ (576.88): C, 37.27; H, 3.13; N, 7.24. Found: C, 37.34; H, 3.21; N, 7.33.

3. 5. 4. Phenyl 3-[4-(2-furoyl)-1-piperazinyl] propylcarbamate (12)

Sticky brown liquid; Yield: 87%; Mol. F.: $C_{19}H_{23}N_3O_4$; Mol. Mass.: 357 g/mol; IR (KBr, cm^{-1}) ν_{max}: 3406 (N–H), 3086 (Ar C–H), 2882 (R C–H), 1657 (C=O), 1582 (Ar C=C), 1496 (N=O), 1197 (C–O–C), 1110 (C–N–C), 850 (C–N); ^{1}H-NMR (500 MHz, $CDCl_3$, ppm): δ 7.49 (brs, 1H, H-5'''), 7.42 (brt, J = 7.1 Hz, 2H, H-3 and

H-5), 7.16 (brt, J = 7.4 Hz, 1H, H-4), 7.09 (brd, J = 7.8 Hz, 2H, H-2 and H-6), 7.05 (d, J = 4.0 Hz, 1H, H-3'''), 6.48 (dd, J = 1.9, 4.0 Hz, 1H, H-4'''), 5.15 (s, 1H, NH), 4.10 (t, J = 6.7 Hz, 2H, CH_2-1'), 3.90 (brs, 4H, CH_2-3'' and CH_2-5''), 3.64–3.56 (m, 2H, CH_2-3'), 3.46 (brs, 4H, CH_2-2'' and CH_2-6''), 2.19 (quintet, J = 6.7 Hz, 2H, CH_2-2'); EI-MS *m/z* 357 $[M]^+$, 221 $[C_{12}H_{17}N_2O_2]^+$, 179 $[C_{10}H_{13}NO_2]^{\bullet+}$, 177 $[C_{10}H_{11}NO_2]^{\bullet+}$, 95 $[C_5H_3O_2]^+$, 93 $[C_6H_5O]^+$, 93 $[C_5HO_2]^+$. Anal. Calc. for $C_{19}H_{23}N_3O_4$ (357.17): C, 63.85; H, 6.49; N, 11.76. Found: C, 63.92; H, 6.56; N, 11.82.

3. 5. 5. 2,4,6-Trinitrophenyl 3-[4-(2-furoyl)-1-piperazinyl]propylcarbamate (14)

Sticky brown liquid; Yield: 86%; Mol. F.: $C_{19}H_{20}N_6O_{10}$; Mol. Mass.: 492 g/mol; IR (KBr, cm^{-1}) ν_{max}: 3406 (N–H), 3086 (Ar C–H), 2882 (R C–H), 1657 (C=O), 1582 (Ar C=C), 1492 (N=O), 1197 (C–O–C), 1110 (C–N–C), 855 (C–N); ^{1}H-NMR (500 MHz, $CDCl_3$, ppm): δ 7.96 (s, 2H, H-3 and H-5), 7.48 (brs, 1H, H-5'''), 7.02 (d, J = 4.0 Hz, 1H, H-3'''), 6.46 (dd, J = 2.0, 4.0 Hz, 1H, H-4'''), 5.16 (s, 1H, NH), 4.10 (t, J = 6.7 Hz, 2H, CH_2-1'), 3.95 (brs, 4H, CH_2-3'' and CH_2-5''), 3.60–3.57 (m, 2H, CH_2-3'), 3.48 (brs, 4H, CH_2-2'' and CH_2-6''), 2.14 (quintet, J = 6.8 Hz, 2H, CH_2-2'); EI-MS *m/z* 492 $[M]^+$, 314 $[C_{10}H_{10}N_4O_8]^{\bullet+}$, 312 $[C_{10}H_8N_4O_8]^{\bullet+}$, 266 $[C_{10}H_8N_3O_6]^+$, 228 $[C_6H_2N_3O_7]^+$, 221 $[C_{12}H_{17}N_2O_2]^+$, 95 $[C_5H_3O_2]^+$, 93 $[C_5HO_2]^+$. Anal. Calc. for $C_{19}H_{20}N_6O_{10}$ (492.12): C, 46.35; H, 4.09; N, 17.07. Found: C, 46.44; H, 4.17; N, 17.19.

3. 5. 6. 2,4,6-Tribromophenyl 3-[4-(2-furoyl)-1-piperazinyl]propylcarbamate (16)

Off-white amorphous solid; Yield: 90%; m.p.: 80–92 °C; Mol. F.: $C_{19}H_{20}Br_3N_3O_4$; Mol. Mass.: 591 g/mol; IR (KBr, cm^{-1}) ν_{max}: 3406 (N–H), 3086 (Ar C–H), 2882 (R C–H), 1657 (C=O), 1582 (Ar C=C), 1497 (N=O), 1197 (C–O–C), 1110 (C–N–C), 847 (C–N), 548 (C–Br); ^{1}H-NMR (500 MHz, $CDCl_3$, ppm): δ 7.67 (s, 2H, H-3 and H-5), 7.49 (brs, 1H, H-5'''), 7.04 (d, J = 4.1 Hz, 1H, H-3'''), 6.49 (dd, J = 2.0, 4.0 Hz, 1H, H-4'''), 5.19 (brs, 1H, NH), 4.12 (t, J = 6.6 Hz, 2H, CH_2-1'), 3.94 (brs, 4H, CH_2-3'' and CH_2-5''), 3.61–3.57 (m, 2H, CH_2-3'), 3.47 (brs, 4H, CH_2-2'' and CH_2-6''), 2.10 (quintet, J = 6.8 Hz, 2H, CH_2-2'); EI-MS *m/z* 591 $[M]^+$, 413 $[C_{10}H_{10}Br_3NO_2]^{\bullet+}$, 411 $[C_{10}H_8Br_3NO_2]^{\bullet+}$, 332 $[C_{10}H_{10}Br_2NO_2]^+$, 328 $[C_6H_3Br_3O]^{\bullet+}$, 221 $[C_{12}H_{17}N_2O_2]^+$, 95 $[C_5H_3O_2]^+$, 93 $[C_5HO_2]^+$. Anal. Calc. for $C_{19}H_{20}Br_3N_3O_4$ (590.90): C, 38.41; H, 3.39; N, 7.07. Found: C, 38.49; H, 3.44; N, 7.18.

3. 6. Biological Activity Assays (*in vitro*)

3. 6. 1. α-Glucosidase Assay

The α-glucosidase inhibition activity was performed in accordance with the slightly modified method of Pierre *et al.*[27] Total volume of the reaction mixture of 100 µL contained 70 µL 50 mM phosphate buffer saline, pH 6.8, 10 µL (0.5 mM) test compound, subsequently the addition of 10 µL (0.057 units) enzyme. The contents were mixed, preincubated for 10 min at 37 °C and pre-read at 400 nm. The reaction was initiated by the addition of 10 µL of 0.5 mM substrate (*p*-nitrophenylglucopyranoside). Acarbose was used as positive control. After 30 min of incubation at 37 °C, absorbance was measured at 400 nm using Synergy HT microplate reader. All experiments were carried out in duplicates. The percent inhibition was calculated by the following equation:

$$\text{Inhibition (\%)} = \frac{Control - Test}{Control} \times 100 \quad (1)$$

IC_{50} values (concentration at which there is 50% in enzyme catalyzed reaction) compounds were calculated using EZ-Fit Enzyme Kinetics Software (Perrella Scientific Inc. Amherst, USA).

3. 6. 2. Cholinesterase Inhibition Assay

The AChE and BChE inhibition activities were performed according to the method of Ellman *et al.*, with minor modifications.[28] Total volume of the reaction mixture was 100 µL. It contained 60 µL Na_2HPO_4 buffer with concentration of 50 mM and pH 7.7. Ten µL test compound (0.5 mM per well) was added, followed by the addition of 10 µL (0.005 unit per well) enzyme. The contents were mixed and pre read at 405 nm. Then contents were pre incubated for 10 mins at 37 °C. The reaction was initiated by the addition of 10 µL of 0.5 mM per well substrate (acetylthiocholine iodide / butyrylthiocholine iodide), after that the addition of 10 µL DTNB (0.5 mM per well). After 15 mins of incubation at 37 °C absorbance was measured at 405 nm. All experiments were carried out with their individual controls in triplicate. Eserine (0.5 mM per well) was used as a positive control. The inhibition (%) and IC_{50} were calculated by the same method as described in α-glucosidase assay.

3. 6. 3. Antibacterial Activity

The antibacterial activity was evaluated in sterile 96-wells microplates under aseptic conditions. The method is rooted in the principle that microbial cell number increases as the microbial growth proceeds in a log phase of growth which results in increased absorbance of broth medium.[29,30] Three gram-negative (*Salmonella typhi*, *Escherichia coli* and *Pseudomonas aeruginosa*) and two gram-positive bacteria (*Bacillus subtilis*, *Staphylococcus aureus*) were included in the study. The organisms were maintained on stock culture agar medium. The test samples with suitable solvents and dilutions were pipette into wells (20 µg per well). Overnight maintained fresh bacte-

rial culture after suitable dilution with fresh nutrient broth was poured into wells (180 µL). The initial absorbance of the culture was strictly maintained between 0.12–0.19 at 540 nm. The total volume in each well was kept to 200 µL. The incubation was done at 37 °C for 16–24 hours with lid on the microplate. The absorbance was measured, before and after incubation and the difference was noted as an index of bacterial growth at 540 nm by using microplate reader. The percent inhibition was calculated by using the formula:

$$\text{Inhibition (\%)} = \frac{X - Y}{X} \times 100 \quad (2)$$

where X is absorbance in the control with bacterial culture and Y is absorbance in the test sample. Results are mean of triplicate ($n = 3$, ± SEM). Ciprofloxacin was used as the standard. Minimum inhibitory concentration (MIC) was measured with suitable dilutions (5–30 µg per well) and results were calculated using EZ-Fit 5 Perrella Scientific Inc. Amherst USA software, and data expressed as MIC.

3. 6. 4. Statistical Analysis

The results are written as mean ± SEM after performance in three-folds and statistical analysis by Microsoft Excel 2010. Minimum inhibitory concentration (MIC) was calculated by using different dilutions (ranging 5–30 µg per well) and EZFit Perrella Scientific Inc. Amherst USA software.

3. 6. 5. Hemolytic Activity

Hemolytic activity was done by a reported method.[31,32] Bovine blood was obtained from the Department of Clinical Medicine and Surgery, University of Agriculture, Faisalabad, Pakistan. After centrifugation, separation and washing, the % RBCs lysis was computed by noting the absorbance.

3. 6. 6. Molecular Docking Methodology

For the prediction of bioactive conformations, various synthesized compounds were docked into the active pockets of the following chosen proteins/enzymes by using the default parameters of MOE-Dock program. Earlier to dock the ligands into enzyme molecules, Builder of MOE 2009-10 was implemented to sketch the structures of synthesized compounds. Energy minimization was carried out up to 0.05 gradients by using MMFF94x force field through the default parameter of the MOE energy minimization algorithm. Then the energy minimized molecules were saved in the mdb file format as an input database for molecular docking in the subsequent step.

The enzyme molecules of α-glucosidase (PDB ID code: 3NO4), acetylcholinesterase (PDB ID code: 1GQR) and butyrylcholinesterase (PDB ID code: 1POP) were retrieved from Protein Data Bank having the possible resolutions of 2.02 Å, 1.69 Å and 2.30 Å respectively. Then all the water molecules were extracted from the receptor enzymes and 3D protonation was carried out through Protonate 3D Option. Energies of protein molecules were minimized by using the default parameters of MOE 2009-10 energy minimization algorithm (gradient: 0.05, Force Field: MMFF94X). Then all the ligands were docked into the binding pockets (selective residues/amino acids) of the above enzymes using default parameters of MOE-Dock Program. To increase the validity of docking protocol, redocking was also applied.[33] LigPlot which is implemented in MOE (Molecular Operating Environment) was used to determine the interactions between enzymes and ligands.

4. Conclusion

The structures of synthesized unique carbamate derivatives bearing 2-furoyl-1-piperazine moieties were elucidated by spectral techniques. All the derivatives showed decent inhibitory potential against acetylcholinestrase enzyme and almost all the derivatives were active against the studied strains of Gram-positive and Gram-negative bacteria. The results of cytotoxicity studies were used to evaluate their cytotoxicity profile as these molecules exhibited modest toxicity. Hence, these molecules may be considered as suitable therapeutic entrants for the drug designing programs leading to some life saving medication.

5. Acknowledgement

The authors are highly thankful to Higher Education Commission (HEC) of Pakistan for providing financial support in this study.

6. References

1. R. Kharb, P. C. Sharma, A. Bhandari, M. Shaharyar, *Der. Pharmacia. Lett.* **2012**, *4*, 652–657.
2. J. Faist, W. Seebacher, R. Saf, R. Brun, M. Kaiser, R. Weis, Eur. J. Med. Chem. **2012**, 47, 510–519. https://doi.org/10.1016/j.ejmech.2011.11.022
3. K. Kulig, J. Sapa, D. Maciag, B. Filipek, B. Malawska, Arch. Pharm. **2007**, 340, 466–475. https://doi.org/10.1002/ardp.200700039
4. A. Pietrzycka, M. Stepniewski, A. M. Waszkielewicz, H. Marona, Acta Pol. Pharm. **2006**, 63, 19–24.
5. S. Bartoschek, J. A. Vorholt, R. K. Thauer, B. H. Geierstanger, C. Griesinger, Eur. J. Biochem. **2001**, 267, 3130–3138. https://doi.org/10.1046/j.1432-1327.2000.01331.x
6. R. L. Metcalf: "Insect Control" in Ullmann's Encyclopedia of Industrial Chemistry, Wiley-VCH, Weinheim, **2002**.

7. S. Badreshia, Am. J. Contact. Dermat. **2002**, 13, 77–79.
8. J. F. Holland, H. Hosley, C. Scharlau, Blood **1966**, 27, 328–342.
9. A. J. Hirsh, S. Y. Yao, J. D. Young, C. I. Cheeseman, Gastroenterology **1997**, 113, 205–211. https://doi.org/10.1016/S0016-5085(97)70096-9
10. S. Chiba, Biosci., Biotechnol. Biochem. **1997**, 61, 1233–1239. https://doi.org/10.1271/bbb.61.1233
11. A. D., Baron, Diabetes Res. Clin. Pract. **1998**, 40, 51–55.
12. H. E. Lebovitz, Clin. North Am. **1997**, 26, 539–551.
13. M. Cygler, J. D. Schrag, J. Sussman, L. M. Harel, I. Silman, M. K. Gentry, Protein Sci. **1993**, 2, 366–382. https://doi.org/10.1002/pro.5560020309
14. V. Tougu, Curr. Med. Chem. **2001**, 1, 155–170.
15. P. Substance In: Handbook of experimental pharmacology. Ed. G. Bertaccini, Berlin, Springer Verlag, **1982**, *59/II*, 85–105.
16. S. Gauthier, *Drug & Aging* **2001**, *18*, 853–862. https://doi.org/10.2165/00002512-200118110-00006
17. World Health Organization. Typhoid vaccines: WHO position paper. Wkly. Epidemiol. Rec. **2000**, 75, 257–264.
18. J. A. Crump, S. P. Luby, E. D. Minta, Bull. WHO. **2004**, 82, 346–353.
19. A. A. Bahiru, S. A. Emire, A. K. Ayele, Acad. J. Microbiol. Res. **2013**, 1, 1–10.
20. M. Rosenfeld, J. Emerson, F. Accurso, D. Armstrong, R. Castile, K. Grimwood, P. Hiatt, Pediatr. Pulmonol. **1999**, 28, 321–328. https://doi.org/10.1002/(SICI)1099-0496(199911)28:5<321::AID-PPUL3>3.0.CO;2-V
21. V. R. Barbe, S. P. Cruveiller, F. Kunst, P. Lenoble, G. Meurice, A. Sekowska, D. Vallenet, T. Wang, I. Moszer, C. M. digue, A. Danchin, Microbiology **2009**, 155, 1758–1775. https://doi.org/10.1099/mic.0.027839-0
22. F. D. Lowy, *Trends Microbiol*. **1998**, *8*, 341–344. https://doi.org/10.1016/S0966-842X(00)01803-5
23. M. A. Abbasi, A. Hafeez, Aziz-ur-Rehman, K. M. Khan, M. Ashraf, S. A. Ejaz, Asian J. Pharma. Hea. Sci. **2012**, 2, 461–466.
24. M. A. Abbasi, A. Sonia, Aziz-ur-Rehman, K. M. Khan, M. Ashraf, I. Afzal, N. Ambreen, M. Shahid, M. Abbas, J. Chem. Soc. Pak. **2013**, 35, 385–390.
25. Aziz-ur-Rehman, S. Naeem, M. A. Abbasi, S. Rasool, K. Nafeesa, I. Ahmad, S. Afzal, Sci. Iran. **2015**, 22, 2241–2248. https://doi.org/10.12966/jsmr.06.02.2014
26. P. S. Nayak, B. Narayana, B. K. Sarojini, J. Fernandes, Akshatha, *J. Single Mol. Res.* **2014**, 2, 20–26.
27. P. Chapdelaine, R. R. Tremblay, J. Y. Dube, *Clin. Chem*. **1978**, *24*, 208–211.
28. G. L. Ellman, K. D. Courtney, V. Andres, R. M. Featherstone, Bio. Pharm. **1961**, 7, 88–95. https://doi.org/10.1016/0006-2952(61)90145-9
29. M. Kaspady, V. K. Narayanaswamy, M. Raju, G. K. Rao, Lett. Drug Des. Discov. **2009**, 6, 21–28. https://doi.org/10.2174/157018009787158481
30. C.-R. Yang, Y. Zang, M. R. Jacob, S. I. Khan, Y.-J. Zhang, X.-C. Li, Antimicrob. Agents. Chemother. **2006**, 50, 1710–1714. https://doi.org/10.1128/AAC.50.5.1710-1714.2006
31. P. Sharma, J. D. Sharma, J. Ethnopharmacol. **2001**, 74, 239–243. https://doi.org/10.1016/S0378-8741(00)00370-6
32. W. A. Powell, C. M. Catranis, C. A. Maynard, *Lett. Appl. Microbiol.* **2000**, *31*, 163–168. https://doi.org/10.1046/j.1365-2672.2000.00782.x
33. M. J. Bostro, J. R. Greenwood, J. Gottfries, Mol. Graph. Model. **2003**, 21, 449–462. https://doi.org/10.1016/S1093-3263(02)00204-8

Povzetek

Namen predstavljenega raziskovalnega dela je bila sinteza različnih biološko aktivnih karbamatnih derivatov, ki bi vsebovali 2-furoil-1-piperazinski fragment in bi bili le malo strupeni. Sintezo smo izvedli kot večstopenjsko sekvenco. Strukturno potrditev pripravljenih spojin smo izvedli s pomočjo EI-MS, IR in ^{1}H-NMR spektroskopskih metod. Za pripravljene spojine smo določili tudi sposobnost inhibicije encimov in njihovo antibakterijsko delovanje. Da bi ugotovili potencialno uporabnost dobljenih spojin kot terapevtskih učinkovin, smo določili tudi njihovo citotoksičnost. Vse spojine so se izkazale kot aktivne proti acetilholinesterazi; spojini **12** in **14** sta izkazovali še posebej dobro inhibitorno aktivnost v primerjavi z referenčnim standardom ezerinom. Skoraj vse spojine so se pokazale kot učinkovite tudi proti Gram-pozitivnim in Gram-negativnim bakterijskim sevom.

Scientific paper

Nitrogen Doped Graphene Nickel Ferrite Magnetic Photocatalyst for the Visible Light Degradation of Methylene Blue

Rajinder Singh, Jigmet Ladol, Heena Khajuria and Haq Nawaz Sheikh*

Department of Chemistry, University of Jammu, Jammu Tawi,180 006 India

** Corresponding author: E-mail: hnsheikh@rediffmail.com*

Received: 14-10-2016

Abstract

A facile approach has been devised for the preparation of magnetic $NiFe_2O_4$ photocatalyst ($NiFe_2O_4$-NG) supported on nitrogen doped graphene (NG). The $NiFe_2O_4$-NG composite was synthesized by one step hydrothermal method. The nanocomposite catalyst was characterized by Powder X-ray diffraction (PXRD), Scanning electron microscopy (SEM), Transmission electron microscopy (TEM), Fourier transform infrared spectroscopy (FTIR), Ultraviolet–visible spectroscopy (UV-Vis) and Vibrating sample magnetometry (VSM). It is found that the combination of $NiFe_2O_4$ nanoparticles with nitrogen-doped graphene sheets converts $NiFe_2O_4$ into a good catalyst for methylene blue (MB) dye degradation by irradiation of visible light. The catalytic activity under visible light irradiation is assigned to extensive movement of photogenerated electron from $NiFe_2O_4$ to the conduction band of the reduced NG, effectively blocking direct recombination of electrons and holes. The $NiFe_2O_4$ nanoparticles alone have efficient magnetic property, so can be used for magnetic separation in the solution without additional magnetic support.

Keywords: Nanostructures, photodegradation, nickel ferrite, catalysts, absorption, UV/Vis spectroscopy.

1. Introduction

Photocatalysis especially by TiO_2 has been widely used for the purification of waste water. The energy band gap of 3.2 eV is required for the excitation of electron by light in TiO_2 catalyst so UV light can only be used in the process of photodegradation. The development of visible light sensitive photocatalysts by band gap modifications and external surface changing for waste water treatment and degradation of organic dye is an active area in photocatalysis.[1–7] Graphene has attracted the attention due to various applications.[8–11] Graphene has sp^2 hybridized carbon and one atom thick (2-D) sheet of conjugated system and extraordinary physical and chemical properties.[12–16] There has been so much focus to develop graphene-metal oxide photocatalysts such as TiO_2-graphene and ZnO-graphene for the photodegradation of organic dye by the irradiation of visible light.[17–22] The heterogeneous systems are mostly used to perform the photodegradation reactions. The repeated use of photocatalysts after degradation is of great importance for sustainable use of the catalyst. The magnetic nanoparticles anchored on solid support serve as heterogenous catalyst allowing facile separation of catalyst from reaction products.[23] Superparamagnetic copper ferrite-graphene nanocomposite prepared via hydrothermal method acts as excellent catalyst for the reduction of nitroarenes. The big advantage of the catalyst is that it can be easily recovered and retains the catalytic activity even after five catalytic cycles.[24] Copper–cobalt ferrites prepared by hydrothermal method from co-precipated precursor serve as efficient catalyst in the decomposition of methanol to CO and H_2.[25] The various metal ferrites have been used as catalysts in phenols decomposition, detoxification of CO gas from automobile exhaust, anodic material for lithium ion batteries.[26–29] Nickel ferrite ($NiFe_2O_4$) has the inverse spinel structure. The ferrimagnetism arises due to antiparallel spin of Fe^{3+} ions present at tetrahedral sites and Ni^{2+} occupying octahedral sites.[30] The Nickel ferrite is considered as the efficient magnetic material which has good electrical resistivity, high-Curie temperature and chemical stability. Magnetic nanoparticles of nickel ferrite have been used to manufacture titania-coated nickel ferrite, which can act as magnetically separable photocatalyst.[31] The TiO_2 doped $NiFe_2O_4$ nanopar-

ticles possess band gap of 2.19 eV and have displayed enhanced photocatalytic activity as compared to TiO_2 for degradation of Rhodamine B dye in aqueous solution under visible light irradiation.[32] Pure nickel ferrite is photo-catalytically inactive but its composite with another semiconductor (e.g., graphene sheets) can find an effective mechanism for separation of charges leading to increased photocatalytic performance. One such example is Zn-Fe_2O_4-graphene photocatalyst and its great performance in the photocatalytic degradation of MB under visible light irradiation.[33] Carbon material doped with a heteroatom, such as B, N or S, can increase the pseudo capacitance by manipulating its electronic properties and chemical reactivity leading to increased performance of doped grapheme.[34–37] Nitrogen-doped graphene (NG) has great utility because of its higher specific capacitance matched to the pristine graphene and good durability, therefore, enabling its use as electrode materials for supercapacitors and applications in photocatalysis.[38]

In this paper, we report the development of one step method to design magnetically separable nitrogen doped graphene-based photocatalyst having excellent catalytic activity. The approach is designed to deposit $NiFe_2O_4$ nanocrystals on nitrogen doped graphene sheets via a one-step hydrothermal method. Interestingly, in the presence of nitrogen doped graphene, the inert nanocrystals of $NiFe_2O_4$ have been converted into a highly efficient catalyst for the methylene blue (MB) degradation under visible light irradiation. In addition, $NiFe_2O_4$ nanoparticles themselves have a magnetic property, which makes the $NiFe_2O_4$–NG composite magnetically separable in liquid medium.

2. Experimental

2. 1. Materials

Iron(III) nitrate nonahydrate $Fe(NO_3)_3 \cdot 9H_2O$, Nickel(II) nitrate hexahydrate $Ni(NO_3)_2 \cdot 6H_2O$, graphite powder flakes, phosphoric acid and hydrogen peroxide were purchased from Alfa Aesar. All chemicals were used as received without further purification. Ethanol, urea, sodium hydroxide and sulphuric acid were purchased from Sigma Aldrich. Deionized water was used throughout.

2 .2. Synthesis of Magnetic $NiFe_2O_4$-Nitrogen Doped Graphene Composite Photocatalyst

Purified natural graphite was used for the synthesis of graphene oxide (GO) by the well known method given by Hummers and Offeman.[39] The graphene oxide (GO) (0.08 g) was dispersed in 20 ml of absolute ethanol and sonicated for 45 min. In a separate beaker 0.28 g of $Ni(NO_3)_2 \cdot 6H_2O$ and 0.78g of $Fe(NO_3)_3 \cdot 9H_2O$ mixture was added to 10 ml absolute ethanol with constant stirring for 30 min forming homogenous solution. The two solutions were mixed and pH of the mixture solution was kept 10.0 using 6 M NaOH solution and then 1 g urea was added into it. The resulting mixture was put into a 50 mL Teflon-lined stainless steel autoclave and heated to 180 °C for 18 h in an oven. After cooling the reaction mixture to room temperature and the precipitates were filtered, washed with distilled water and dried in oven at 70 °C for 12 h. The product was named as $NiFe_2O_4$–NG. Same method was applied to synthesize pure $NiFe_2O_4$ with the modification that GO and urea were excluded. Sulfur was estimated as $BaSO_4$ by gravimetric method and Chloride was estimated as AgCl by Volhard's method.[40]

2. 3. Spectroscopic and Microscopic Measurements

The phase and size of the as-prepared samples were determined from powder X-ray diffraction (PXRD) using D8 X-ray diffractometer (Bruker) at a scanning rate of 12° min^{-1} in the 2θ range from 10° to 70°, with Cu Kα radiation (λ = 0.15405 nm). Scanning electron microscopy (SEM) micrographs of the samples were recorded on FEI Nova Nano SEM 450. High Resolution Transmission Electron Microscopy (HRTEM) was recorded on Tecnai G2 20 S-TWIN Transmission Electron Microscope with a field emission gun operating at 200 kV. The samples for TEM measurements were prepared by evaporating a drop of the colloid onto a carbon coated copper grid. The infrared spectra were recorded on Shimadzu Fourier Transform Infrared Spectrometer (FT-IR) over the range of wave number 4000–400 cm^{-1} and the standard KBr pellet technique was employed. The magnetic moment as a function of applied field was recorded using Vibrating Sample Magnetometer (VSM), Lakeshore 7410. All the measurements were performed at room temperature.

2. 4. Photocatalytic Activity Measurement

The catalytic activity of the as synthesized sample was performed by degradation of organic dye MB under the irradiation of visible light. For the Photo irradiation 500 W xenon lamp was used fitted with UV cut-off filters (JB450) in order to completely remove any radiation below 420 nm ensuring the exposure to only visible light. The whole procedure was performed at 25 °C. A 100 mL of MB dye solution was prepared (20 mg/L concentration) and 0.025 g of photocatalyst was mixed with dye solution. The resulting mixture was stirred for 60 min before illumination in order to establish the adsorption – desorption equilibrium between MB and catalyst surface. At same instant of time 5 mL of dye-catalyst mixture was taken out and concentration of the residual dye was determined with the help of UV-vis spectroscopy by measuring the absorption at 664 nm. The absorbance of dye at 664 nm was monitored with time after fixed intervals of time. The absor-

bance of dye with time without catalyst was also recorded for reference.

3. Results and Discussion

3. 1. PXRD Measurements

The structural characterization of the nanoparticles has been carried out by Powder X-ray diffraction technique using Cu*K*α radiation. Figure 1(a–b) show the differences of phase composition between GO and NG. The doping of nitrogen in GO can be clarified easily by PXRD spectrum. The PXRD pattern of GO exhibits a characteristic (002) peak of graphite emerging at 24.2°. Compared with GO, it is found that the (002) peak of NG appears at 26.3` which indicates that nitrogen atoms have entered into the crystal lattice of graphite and caused the increased distance between the graphite layers. This confirms the formation of nitrogen-doped graphene by urea assisted hydrothermal reaction. Figures 1c, d show the PXRD diffraction patterns of the pure $NiFe_2O_4$ and as prepared $NiFe_2O_4$–NG. The diffraction peaks at 30.9°, 35.7°, 43.4°, 53.7°, 57.2° and 63.2° corresponding to the planes (220), (311), (400), (422), (511) and (440) are allocated to spinel-type $NiFe_2O_4$ (JCPDS No. 54–0964).[41] Similar diffraction patterns are observed for $NiFe_2O_4$–NG. The nitrogen doped graphene oxide can be reduced by the alcohol under hydrothermal conditions and no peak at (002) is observed in the composite. It can also be related to well exfoliation of the NG sheets in the resulting composite material. So the diffraction pattern of NG disappears in the XRD pattern of $NiFe_2O_4$–NG.

The average crystallite size of these nanoparticles was calculated according to the Scherrer's equation.

$$\beta = \frac{k\lambda}{LCos\theta} \quad (1)$$

where, L (nm) is the crystallite size, λ (nm) is the wavelength of the Cu Kα radiant, λ = 0.15405 nm, β(°) is the full-width at half-maximum (FWHM) of the diffraction peak, θ is the diffraction angle and *K* is the Scherrer constant equal to 0.89. All the major peaks were used to calculate the average crystallite size of the $NiFe_2O_4$ and $NiFe_2O_4$–NG nanoparticles. The estimated average crystallite sizes of nanoparticles are in the range of 80–120 nm.

3. 2. SEM and TEM Analysis

Figure 2a shows representative scanning electron microscopy and transmission electron microscopy images of the prepared GO. From the SEM image, morphology and structure of as-prepared graphene oxide sample was investigated. GO sheets were cast on a gold coated (100 nm) Si/SiO_2 substrate. It has been found that the graphene flakes have wrinkled surfaces. Furthermore, in the TEM image (Figure 3a) GO shows layer-by-layer stacked structure and has wrinkled paper like morphology. Such morphological changes can be attributed to the increased formation of phenolic and epoxy functional groups on the basal plane of GO. The curled and overlapped nanosheets can be clearly observed. The SEM image (Figure 2b) and TEM image (Figure 3b) reveal that nitrogen-doped grapene nanosheets exhibit a typical wrinkled structure, which results from stable bending thermodynamically.[42,43]

Figures 2(c–d) show SEM images of the $NiFe_2O_4$ and $NiFe_2O_4$–NG samples where as Figures 3(c–d) show TEM images of the $NiFe_2O_4$ and $NiFe_2O_4$–NG samples. In Figure 2c and Figure 3c, $NiFe_2O_4$ nanoparticles are clear-

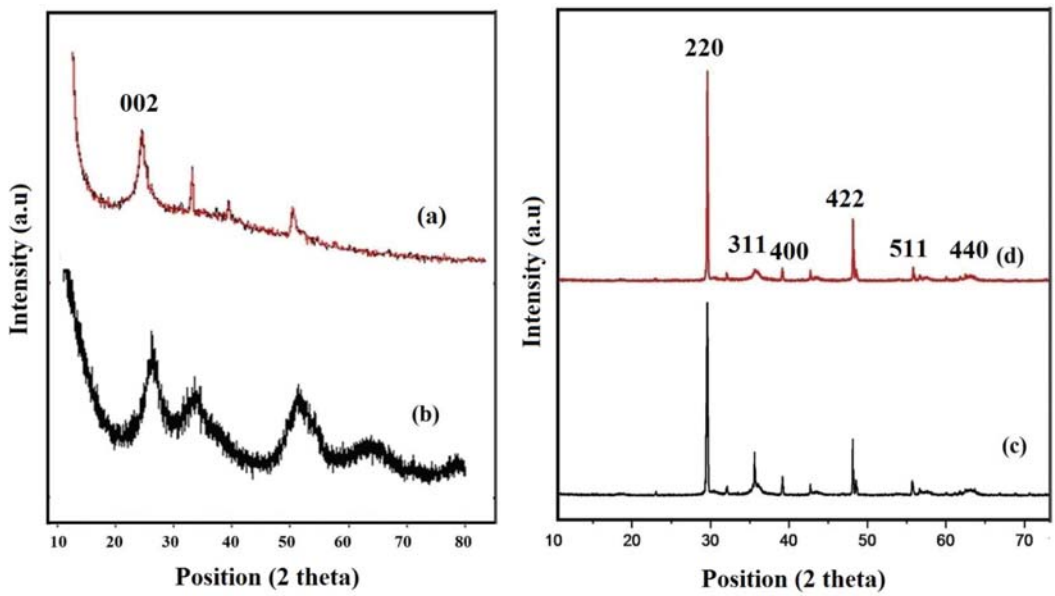

Figure 1. PXRD patterns of (a) GO, (b) NG, (c) $NiFe_2O_4$ and (d) $NiFe_2O_4$–NG.

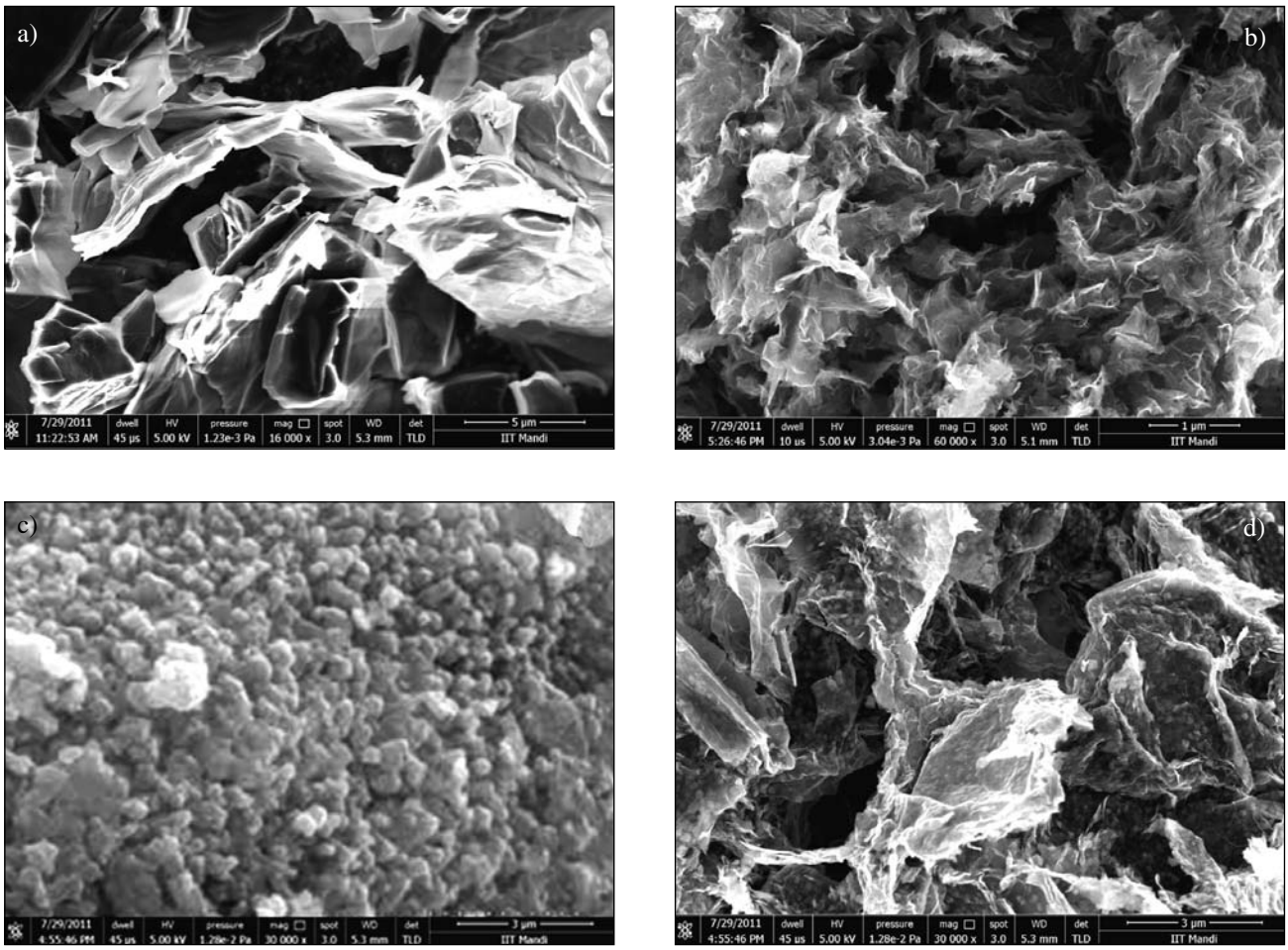

Figure 2. SEM images of (a) GO (b) NG (c) $NiFe_2O_4$ and (d) $NiFe_2O_4$–NG.

ly visible in the SEM and TEM images. The $NiFe_2O_4$ nanoparticles distributed on NG to form nanoparticles bound on the surface of NG sheets is seen in the Figure 2d and Figure 3d. Measurements showed that the average diameter of $NiFe_2O_4$–NG particles is approximately 80 nm. The particle size data obtained from TEM data are in very close agreement to the size calculated from the Debye–Scherrer method.

3. 3. FT-IR Characterization

Figure 4(a–d) shows the FTIR spectra of GO, NG, $NiFe_2O_4$ and $NiFe_2O_4$–NG. There are many O-containing groups that exist on GO sheets, such as hydroxyl, epoxy, and carboxyl groups. Majority of the O-containing groups will disappear after reduction. FTIR bands at 1050, 1220, 1405 and 1730 cm^{-1} were observed for GO. These bands correspond to C–O stretching, C–O–C stretching, O–H deformation vibration and C=O carbonyl stretching.[44] FTIR bands at 1400 cm^{-1} due to C=C stretching is observed in NG and the νC=O band at 1730 cm^{-1} completely disappeared due to reduction. The bands located at 1180 and 1565 cm^{-1} in Figure 4b are assigned to the ν C-N and ν C=C respectively. The FTIR spectra suggest N doping of GO. Figure 4 (c–d) shows the FT-IR bands of $NiFe_2O_4$ and $NiFe_2O_4$–NG. The bands observed in the range of 620–650 cm^{-1} corresponds to the intrinsic stretching vibrations of the M–O in the tetrahedral site. The second band around 3400–3500 cm^{-1} corresponds to O–H stretching vibrations.[45] Furthermore, it is observed that almost all the characteristic bands of oxygen containing functional groups (C=O, O–H, C–OH and C–O–C) disappeared in the FT-IR spectrum of $NiFe_2O_4$–NG depicting the change in the surface morpholgy of NG–$NiFe_2O_4$ composite. These findings show that $NiFe_2O_4$ nanoparticles are bonded to the NG. The results above show the heteroatom N was entered in the graphene structure and the $NiFe_2O_4$–NG composites was prepared favourably.

3. 4. Photocatalytic Measurements

The adsorption of light by the photocatalysts is the key feature of photocatalysis method. Figure 5a show the

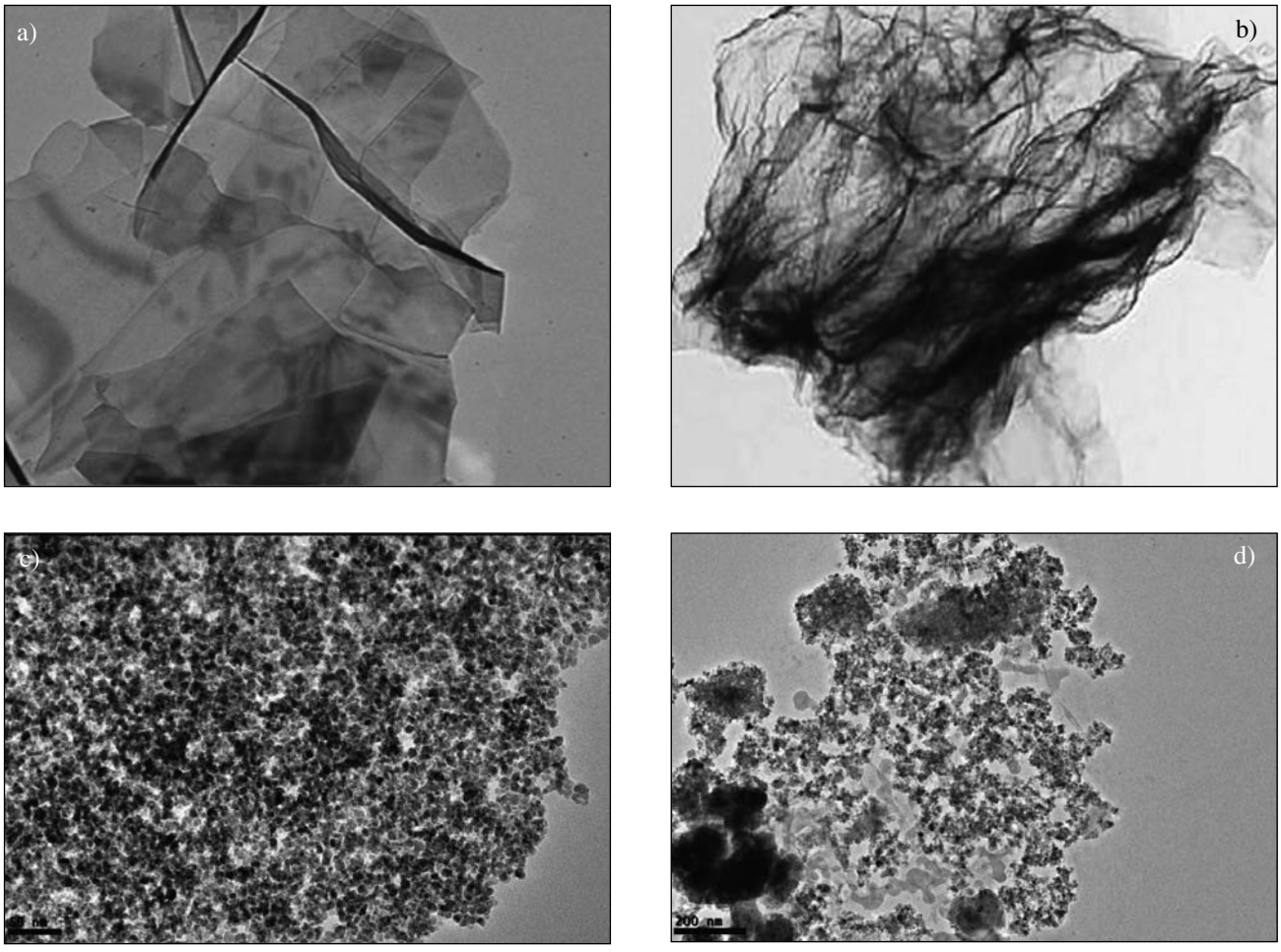

Figure 3. TEM images of (a) GO, (b) NG, (c) $NiFe_2O_4$ and (d) $NiFe_2O_4$–NG

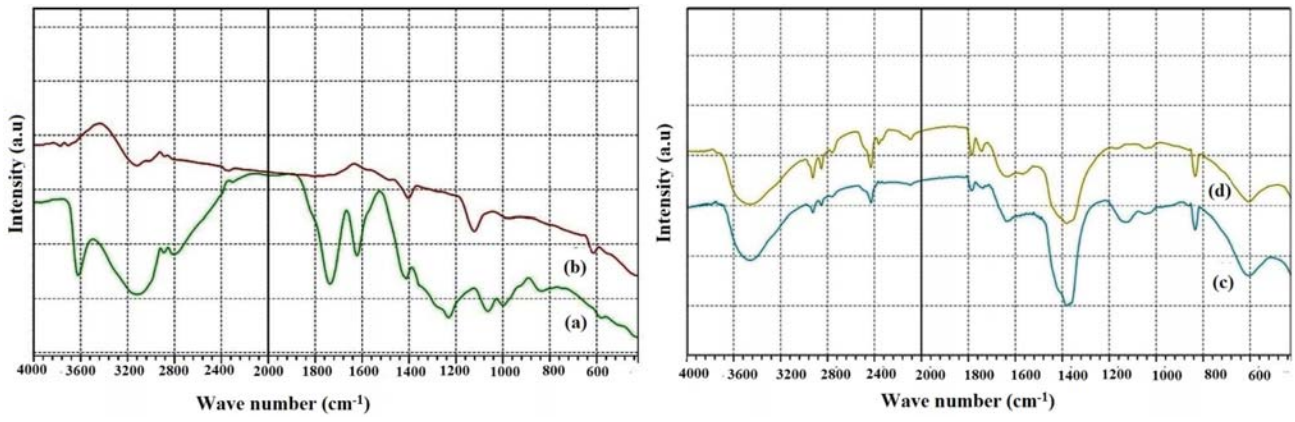

Figure 4. FT-IR spectra of (a) GO (b) NG (c) $NiFe_2O_4$ (d) $NiFe_2O_4$–NG

UV Spectrum of $NiFe_2O_4$–NG. The photocatalytic activities of the as-obtained $NiFe_2O_4$–NG nanocomposite photocatalysts were evaluated by monitoring the degradation of methylene blue (MB) under visible-light irradiation at 25 °C. Figure 5a shows the changes in the absorbance profiles of MB solution (concentration of MB, C = 0.075 M and path length, l = 1cm) in the presence of $NiFe_2O_4$–NG photocatalyst under visible-light irradiated at 25 °C recorded at different time intervals. The adsorption-desorption equilibriated solution of MB and $NiFe_2O_4$–NG was used

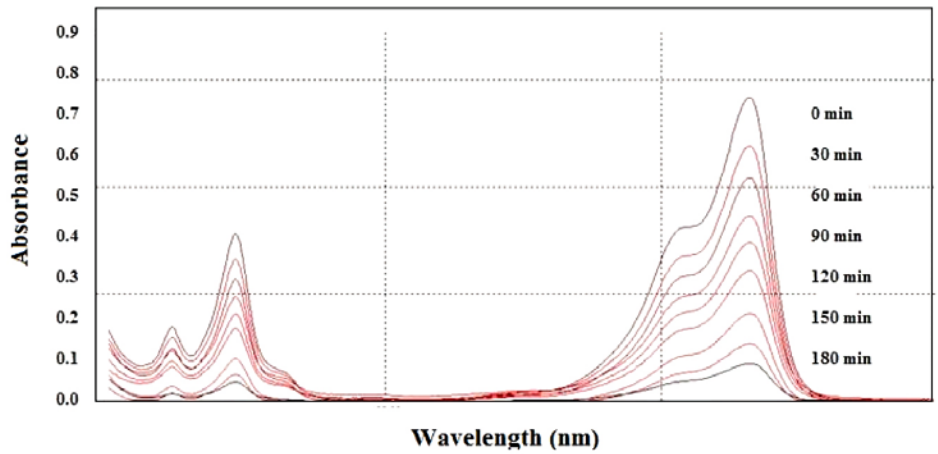

Figure 5a. Absorption spectra of the MB solution (C = 0.075 M and l = 1 cm) taken at different photocatalytic degradation times using Ni-Fe_2O_4–NG.

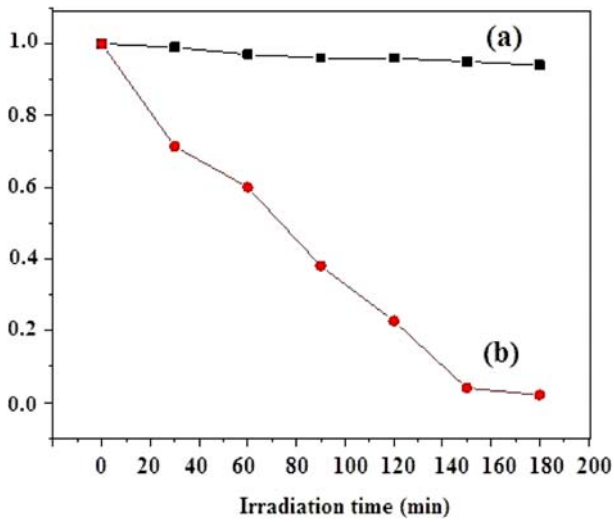

Figure 5b. Kinetics of photodegradation of (a) Pure MB and (b)

as starting solution. In Figure 5b C/C_0 was plotted versus time where C_0 is initial concentration of methylene blue (0.075 M at time t = 0 min. and C is concentration at time t min.). It can be clearly seen that almost all the MB in the solution is decomposed after 180 min in presence of the $NiFe_2O_4$–NG while there is least photodegradation in the pure MB solution. The catalyst acts as magnetic material which gives good performance in magnetic separation for the $NiFe_2O_4$–NG photocatalysts using an external magnet.

3. 4. 1. Mechanism of Photocatalytic Activity Measurements

The photocatalytic activity for MB degradation can be best explained by the following mechanism. The notable increase in photocatalytic activity under visible light exposure can be attributed to exceptional synergistic effect between $NiFe_2O_4$ and the nitrogen-doped graphene sheets causing the effective separation of carriers generated by the light exposure in the $NiFe_2O_4$–NG composite system. A plausible mechanism for enhancement in photocatalysis process is shown as follows:

When the visible-light is irradiated on the surface of $NiFe_2O_4$, the electron-hole pairs are formed (Eq. 2). Then by the percolation mechanism, the electrons generated by the photogeneration process are instantly transfer onto NG sheets (Eq. 3). Superoxide anion radical is produced from oxygen dissolved and activated through nitrogen doped graphene carrying negative charge (Eq. 4). The adsor-

$$NiFe_2O_4 + \text{Visible light} \longrightarrow NiFe_2O_4\,(h+e) \tag{2}$$

$$NiFe_2O_4\,(e) + \text{N-doped graphene} \longrightarrow NiFe_2O_4 + \text{N-doped graphene}\,(e) \tag{3}$$

$$\text{N-doped graphene}\,(e) + O_2 \longrightarrow O_2^{-} + \text{N-doped graphene} \tag{4}$$

$$NiFe_2O_4\,(h) + OH^{-} \longrightarrow NiFe_2O_4 + {}^{\cdot}OH \tag{5}$$

$$NiFe_2O_4\,(h) + {}^{\cdot}OH + O_2^{-} + C_{16}H_{18}ClN_3S(MB) \longrightarrow NiFe_2O_4 + CO_2 + H_2O + SO_4^{2-} + NO_3^{-} + Cl^{-} + NH_4^{+} \tag{6}$$

bed water can react with holes to produce hydroxyl radical (Eq. 5). At the end superoxide anion, and hydroxyl radical cause the oxidation of MB dye adsorbed on the surface of $NiFe_2O_4$–NG composite by electrostatic interaction and π-π interaction between aromatic rings of methylene blue and graphene layer (Eq. 6). In the photocatalytic degradation process, the electrons of the photocatalyst i,e $NiFe_2O_4$–NG nanocomposite are excited from the valence band (VB) to the conduction band (CB) by the visible light irradiation. The photogenerated holes in the VB are scavenged by OH^- of water forming $^{\cdot}OH$ radicals which are responsible for the MB degradation process afterwards. The N-graphene performs two functions; (a) it acts as charge carrier to trap the delocalised electrons thereby restricting the (h–e) recombination. (b) Secondly, it increases the adsorption of MB dye on the catalyst surface thereby increasing the π-π interaction between aromatic rings of methylene blue and graphene layer.[46]

3. 5. Magnetic Characterization

Magnetization hysteresis loops of the as-prepared $NiFe_2O_4$ and $NiFe_2O_4$–NG samples at room temperature were measured using vibrating sample magnetometer as shown in Figure 6(a–b). The magnetic properties of the $NiFe_2O_4$ having inverse spinel structure can be described in terms of cations distribution. The magnetization originates from the Fe^{3+} ions at both tetrahedral and octahedral sites and Ni^{2+} is present only in octahedral sites.[47,48] Coercivity and saturation magnetization of $NiFe_2O_4$–NG are 47.4 G and 10.1 emu/g respectively, whereas that of $NiFe_2O_4$ are 33.5 G and 9.2 emu/g respectively. The values observed for $NiFe_2O_4$–NG are larger than those for $NiFe_2O_4$ which shows that $NiFe_2O_4$–NG is more easily separable than $NiFe_2O_4$. The increase in the saturation magnetization was possibly attributed to the increasing crystallinity and particle size of the nanoparticles.

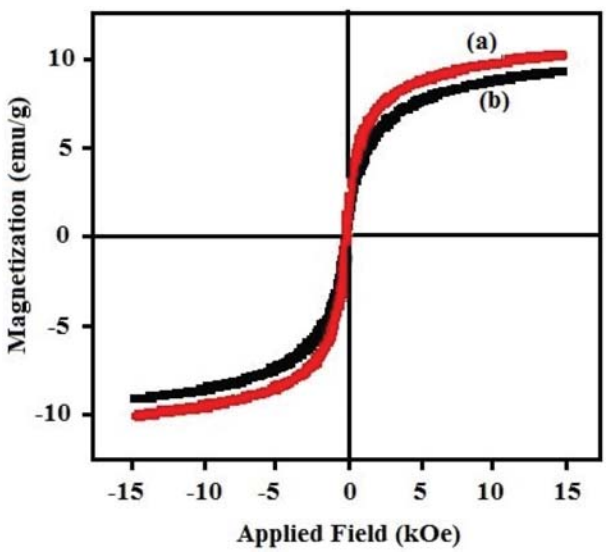

Figure 6. Magnetic hysteresis loop measured at 300 K for (a) $NiFe_2O_4$ (b) $NiFe_2O_4$–NG

4. Conclusions

In the outcome, a magnetic $NiFe_2O_4$–NG photocatalyst has been fabricated through hydrothermal route. The SEM and TEM images show that nitrogen-doped graphene sheets are flaked and furnished with $NiFe_2O_4$ nanoparticles having an average diameter of 80 nm. The photocatalytic activity measurements confirm that the $NiFe_2O_4$ nanoparticles combined with nitrogen-doped graphene sheets lead to exciting conversion of the inactive $NiFe_2O_4$ into very good catalyst for the degradation of methylene blue (MB) under visible light irradiation. The notable increase in photoactivity can be ascribed to the superior conductivity of the reduced NG sheets leading to favourable and efficient separation of photogenerated carriers (hole-electron) in the $NiFe_2O_4$–NG system. Subsequently, there is very large and useful change in photocatalytic activity after coupling nickel ferrite with nitrogen-doped graphene sheets.

5. Acknowledgements

We would like to acknowledge SAIF, Panjab University, Chandigarh and Indian Institute of Technology Guwahati for their technical support. We thank Indian Institute of Technology Mandi for powder X-ray diffraction study.

6. References

1. M. R. Hoffmann, S. T. Martin, W. Choi, D. W. Bahnemann, *Chem. Rev.* **1995**, 95, 69–96. https://doi.org/10.1021/cr00033a004
2. B. Mahrov, G. Boschloo, A. Hagfeldt, L. Dloczik, T. Dittrich, *Appl. Phys. Lett.* **2004**, 84, 5455–5457. https://doi.org/10.1063/1.1767961
3. A. Hattori, Y. Tokihisa, H. Tada, S. Ito, *J. Electrochem. Soc.* **2000**, 147, 2279–2283. https://doi.org/10.1149/1.1393521
4. G. K. Ropidas, M. Bohorquez, P. V. Kamat, *J. Phys. Chem.* **1990**, 94, 6435–6440. https://doi.org/10.1021/j100379a051
5. Z. J. Zhang, W. Z. Wang, W. Z. Yin, M. Shang, L. Wang, S. M. Sun, *Appl. Catal. B* **2010**, 10, 68–73. https://doi.org/10.1016/j.apcatb.2010.09.008
6. B. K. Vijayan, N. M. Dimitrijevic, J. S. Wu, K. A. Gray, *J. Phys. Chem. C* **2010**, 114, 21262–21269. https://doi.org/10.1021/jp108659a
7. X. Shu, J. He, D. Chen, *Ind. Eng. Chem. Res.* **2008**, 47, 4750–4753. https://doi.org/10.1021/ie071619d

8. K. S. Novoselov, A. K. Geim, S. V. Morozov, D. Jiang, Y. Zhang, S. V. Dubonos, I. V. Grigorieva, A. A. Firsov, *Science* **2004**, 306, 666–669. https://doi.org/10.1126/science.1102896
9. A. K. Geim, *Science* **2009**, 324, 1530–1534. https://doi.org/10.1126/science.1158877
10. S. Chen, J. Zhu, X. Wang, *ACS Nano* **2010**, 4, 6212–6218. https://doi.org/10.1021/nn101857y
11. Y. M. Li, X. J. Lv, J. Lu, J. Li, *J. Phys. Chem. C* **2010**, 114, 2177–21774.
12. O. Akhavan, *ACS Nano* **2010**, 4, 4174–4180. https://doi.org/10.1021/nn1007429
13. K. S. Novoselov, A. K. Geim, S. V. Morozov, D. Jiang, M. I. Katsnelson, I. V. Grigorieva, S. V. Dubonos, A. A. Firsov, *Nature* **2005**, 438, 197–200. https://doi.org/10.1038/nature04233
14. J. Sakamoto, J. van Heijst, O. Lukin, A. D. Schluter, *Angew. Chem. Int. Ed.* **2009**, 48, 1030–1069. https://doi.org/10.1002/anie.200801863
15. M. Burghard, H. Klauk, K. Kern, *Adv. Mater.* **2009**, 21, 2586–2600. https://doi.org/10.1002/adma.200803582
16. R. Devi, G. Prabhavathi, R. Yamuna, S. Ramakrishanan, N. K. Kothurkar, *J. Chem. Sci.* **2014**, 126, 75–83. https://doi.org/10.1007/s12039-013-0536-1
17. H. Zhang, X. Lv, Y. Li, Y. Wang, J. Li, *ACS Nano* **2010**, 4, 380–386. https://doi.org/10.1021/nn901221k
18. G. Williams, B. Seger, P. V. Kamat, *ACS Nano* **2008**, 2, 1487–1491. https://doi.org/10.1021/nn800251f
19. Y. Zhang, Z. R. Tang, X. Fu, Y. J. Xu, *ACS Nano* **2010,** 4, 7303–7314. https://doi.org/10.1021/nn1024219
20. D. H. Yoo, V. C. Tran, V. H. Pham, J. S. Chung, N. T. Khoa, E. J. Kim, S. H. Hahn, *Curr. Appl. Phys.* **2011**, 11, 805–808. https://doi.org/10.1016/j.cap.2010.11.077
21. O. Akhavan, *Carbon* **2011**, 49, 11–18. https://doi.org/10.1016/j.carbon.2010.08.030
22. T. G. Xu, L. W. Zhang, H. Y. Cheng, Y. F. Zhu, *Appl. Catal. B* **2011**, 101, 382–387. https://doi.org/10.1016/j.apcatb.2010.10.007
23. S. Shylesh, V. Schunemann, W. R. Thiel, *Angew. Chem. Int. Ed.* **2010**, 49, 3428–3459. https://doi.org/10.1002/anie.200905684
24. H. Zhang, S. Gao, N. Shang, C. Wang, Z. Wang, *RSC Adv.* **2014**, 4, 31328–31332.
25. N. Velinov, K. Koleva, T. Tsoncheva, D. Paneva, E. Manova, K. Tenchev, B. Kunev, I. Genova, I. Mitov, *Cent. Eur. J. Chem.* **2014,** 12, 250–259. https://doi.org/10.2478/s11532-013-0371-8
26. B. I. Kharisov, H. V. R. Dias, O. V. Kharissova, *A. J. Chem.* **2014,** DOI: 10.1016/j.arabjc.2014.10.049. https://doi.org/10.1016/j.arabjc.2014.10.049
27. Y. Fu, Q. Chen, M. He, Y. Wan, X. Sun, H. Xia, X. Wang, *Ind. Eng. Chem. Res.* **2012**, 51, 11700–11709. https://doi.org/10.1021/ie301347j
28. C. U. Aniz, T. D. R. Nair, *OJPC*, **2011**, 1, 124–130. https://doi.org/10.4236/ojpc.2011.13017
29. N. Rezlescu, E. Rezlescu, P. D. Popa, C. Doroftei, M. Ignat, *Romanian Reports in Physics*, **2013,** 65, 1348–1356.
30. Y. Kinemuchi, K. Ishizaka, H. Suematsu, W. H. Jiang, K. Yatsui, *Thin Solid Films* **2002**, 407, 109–113. https://doi.org/10.1016/S0040-6090(02)00021-4
31. Y. S. Chung, S. B. Park, D. W. Kang, *Mater. Chem. Phys.* **2004**, 86, 375–381. https://doi.org/10.1016/j.matchemphys.2004.03.027
32. Rahmayeni, S. Arief, Y. Stiadi, R. Rizal, Zulhadjri, *Indo. J. Chem.* **2012**, 12, 229–234.
33. Y. S. Fu, X. Wang, *Ind. Eng. Chem. Res.* **2011**, 50, 7210–7218. https://doi.org/10.1021/ie200162a
34. H. Guo, Q. Gao, *J. Power Sources* **2009**, 186, 551–556. https://doi.org/10.1016/j.jpowsour.2008.10.024
35. L. Zhao, L. Fan, M. Zhou, H. Guan, S. Qiao, M. Antonietti, M. Titirici, *Adv. Mater.* **2010**, 22, 5202–5206. https://doi.org/10.1002/adma.201002647
36. L. Chen, X. Zhang, H. Liang, M. Kong, Q. Guan, P. Chen, Z. Wu, S. Yu, *ACS Nano* **2012**, 6, 7092–7102. https://doi.org/10.1021/nn302147s
37. J. Xu, G. Dong, C. Jin, M. Huang, L. Guan, *ChemSusChem* **2013**, 6, 493–499. https://doi.org/10.1002/cssc.201200564
38. S. Bag, C. R. Raj, *J. Chem. Sci.* **2016**, 128, 339–347. https://doi.org/10.1007/s12039-016-1034-z
39. W. S. Hummers R. E. Offeman *J. Am. Chem. Soc.* 80 (1958) 1339–1339. https://doi.org/10.1021/ja01539a017
40. A. I. Vogel, A Textbook of Quantitative Inorganic Analysis, forth ed., Longman, London, **1978**.
41. D. C. Marcano, D. V. Kosynkin, J. M. Berlin, A. Sinitskii, Z. Sun, A. Slesarev, L. B. Alemany, W. Lu, J. M. Tour, *ACS Nano* **2010**, 4, 4806–4814. https://doi.org/10.1021/nn1006368
42. Y. Fu, H. Chen, X. Sun, X. Wang, *AIChE J.* **2012**, 58, 3298–3305. https://doi.org/10.1002/aic.13716
43. X. Zheng, Q. Xu, L. He, N. Yu, S. Wang, Z. Chen, *J. Phys. Chem. B* **2011**, 115, 5815–5826. https://doi.org/10.1021/jp2018082
44. M. Acik, C. Mattevi, C. Gong, G. Lee, K. Cho, M. Chhowalla, *ACS Nano* **2010**, 10, 5861–5868. https://doi.org/10.1021/nn101844t
45. D. Du, P. Li, J. Ouyang, *ACS Appl. Mater. Interfaces* **2015**, 7, 26952–26958. https://doi.org/10.1021/acsami.5b07757
46. L. Gan, L. Xu, S. Shang, X. Zhou, L. Meng, *Ceram. Int.* **2016,** 42, 15235–15241. https://doi.org/10.1016/j.ceramint.2016.06.160
47. H. Nathani, S. Gubbala, R. D. K. Misra, *Mater. Sci. Eng. B* **2005,** 121, 126–136. https://doi.org/10.1016/j.mseb.2005.03.016
48. A. B. Nawale, N. S. Kanhe, K. R. Patil, S. V. Bhoraskar, V. L. Mathe, A. K. Das, *J Alloys Compd.* **2011**, 509, 4404–4413. https://doi.org/10.1016/j.jallcom.2011.01.057

Povzetek

Preprost sintezni način smo uporabili za pripravo magnetnega fotokatalizatorja $NiFe_2O_4$ na grafenu, dopiranem z dušikom (NG). Kompozit $NiFe_2O_4$–NG smo pripravili z enostopenjsko hidrotermalno sintezo. Nanokompozitni katalizator smo karakterizirali z naslednjimi metodami: rentgensko praškovno difrakcijo (XRD), vrstično elektronsko mikroskopijo (SEM), presevno elektronsko mikroskopijo (TEM), infrardečo spektroskopijo (FT-IR), UV-Vis spektroskopijo in magnetometrijo z vibrirajočim vzorcem (VSM). Kombinacija nanodelcev $NiFe_2O_4$ in grafena, dopiranega z dušikom pretvori $NiFe_2O_4$ v dober katalizator za fotokatalitični razpad barvila metilen modro (MB). Fotokatalitično aktivnost pod vplivom vidne svetlobe lahko pripišemo obsežnemu premiku vzbujenih elektronov iz $NiFe_2O_4$ v prevodni pas reduciranega grafena (NG). Že sami nanodelci $NiFe_2O_4$ imajo takšne magnetne lastnosti, da jih lahko uporabimo za magnetno separacijo v raztopini brez dodatne uporabe magneta.

Scientific paper

Synthesis, Structures, and Antimicrobial Activities of Two Cobalt(II) Complexes $[Co(L^1)_2(OH_2)_2]$ and $[Co(L^2)_2]$

Yong-Jun Han, Li Wang, Qing-Bin Li and Ling-Wei Xue*

College of Chemistry and Chemical Engineering, Pingdingshan University, Pingdingshan Henan 467000, P.R. China

** Corresponding author: E-mail: pdsuchemistry@163.com*

Received: 27-10-2016

Abstract

A new cobalt(II) complex, $[Co(L^1)_2(OH_2)_2]$ (**1**), was prepared by the reaction of 3-bromo-5-chlorosalicylaldehyde (HL^1) with cobalt nitrate in methanol. Reaction of **1** with cyclopropylamine in methanol afforded the Schiff base cobalt(II) complex, $[Co(L^2)_2]$ (**2**), where L^2 is the deprotonated form of 2-bromo-4-chloro-6-(cyclopropyliminomethyl)phenol (HL^2). The complexes have been characterized by elemental analyses, IR spectroscopy, and single-crystal X-ray diffraction. The L^1 ligand coordinates to the Co atom through the phenolate O and carbonyl O atoms, while the L^2 ligand coordinates to the Co atom through the phenolate O and imino N atoms. The Co atom in complex **1** adopts octahedral coordination and that in complex **2** adopts tetrahedral coordination. The effect of the free ligands and the cobalt complexes on the antimicrobial activities against *Staphylococcus aureus*, *Escherichia coli*, and *Candida albicans* was studied.

Keywords: Synthesis; Crystal structure; Antimicrobial; Schiff base; Cobalt complex

1. Introduction

Schiff bases are a kind of versatile ligands in coordination chemistry.[1–6] In recent years, metal complexes of Schiff bases have attracted considerable attention due to their remarkable biological activity, such as antifungal, antibacterial and antitumor property.[7–9] It has been shown that the Schiff base complexes derived from salicylaldehyde and its derivatives with primary amines, bearing the N_2O, N_2S, NO_2 or NSO donor sets, have interesting biological activity.[9–12] Furthermore, cobalt complexes in its varied oxidation states have become a central theme of current research because of their potentially useful properties in the realm of relevant scientific and technological fields. Recently, we have reported some Schiff base complexes and their application in biological area.[13–15] In the present work, two new cobalt(II) complexes, $[Co(L^1)_2(OH_2)_2]$ (**1**) and $[Co(L^2)_2]$ (**2**), where L^1 and L^2 are the deprotonated forms of 3-bromo-5-chlorosalicylaldehyde (HL^1) and 2-bromo-4-chloro-6-(cyclopropyliminomethyl)phenol (HL^2), respectively, are reported.

2. Experimental

2. 1. Material and Methods

3-Bromo-5-chlorosalicylaldehyde, cyclopropylamine, and cobalt nitrate were purchased from Fluka. Other reagents and solvents were analytical grade and used without further purification. Elemental (C, H and N) analyses were made on a Perkin-Elmer Model 240B automatic analyzer. Cobalt analysis was carried out by EDTA titration. Infrared (IR) spectra were recorded on an IR-408 Shimadzu 568 spectrophotometer.

2. 2. Preparation of $[Co(L^1)_2(OH_2)_2]$ (1)

HL^1 (0.23g g, 1.0 mmol) was dissolved in methanol (20 mL), then a methanol solution (10 mL) of $Co(NO_3)_2 \cdot 6H_2O$ (0.29 g, 1.0 mmol) was added while stirring. The mixture was stirred for 1 h at ambient temperature to give a red solution. Red block-shaped single crystals suitable for X-ray diffraction were formed by slow evaporation of the solution in air for about a week. Yield: 45%. D.p. 173 °C. Elemental analysis found: C, 29.63; H, 1.92; Co, 10.67%. $C_{14}H_{10}Br_2Cl_2CoO_6$ calcd: C, 29.82; H, 1.79; Co, 10.45%. IR data (KBr, cm^{-1}): 3433 (br, m), 1647 (vs), 1505 (m), 1443 (s), 1413 (s), 1313 (w), 1205 (m), 1139 (s), 1080 (s), 989 (m), 926 (w), 864 (m), 747 (s), 693 (w), 543 (m), 409 (w).

2. 3. Preparation of $[Co(L^2)_2]$ (2)

To the methanolic solution (10 mL) of complex **1** (56.4 mg, 0.100 mmol) was added a methanolic solution

(10 mL) of cyclopropylamine (11.5 mg, 0.200 mmol). The mixture was stirred for 1 h at ambient temperature to give a red solution. Red block-shaped single crystals suitable for X-ray diffraction were formed by slow evaporation of the solution in air for three days. Yield: 61%. D.p. 232 °C. Elemental analysis found: C, 39.77; H, 2.58; N, 4.72; Co, 9.9%. $C_{20}H_{16}Br_2Cl_2CoN_2O_2$ calcd: C, 39.64; H, 2.66; N, 4.62; Co, 9.7%. IR data (KBr, cm^{-1}): 1622 (m), 1438 (m), 1360 (m), 1160 (s), 1072 (s), 951 (s), 860 (s), 543 (m), 518 (m), 464 (w).

2. 4. X-ray Diffraction

Data were collected from selected crystals mounted on glass fibers. The diffraction data were collected on a Bruker SMART 1000 CCD with Mo Kα radiation (λ = 0.71073 Å) at 298(2) K. The data for the two complexes were processed with SAINT[16] and corrected for absorption using SADABS.[17] Semi-empirical absorption corrections were applied with ψ-scans.[18] The structures were solved by direct methods using SHELXS-97, and refined by full-matrix least-squares techniques on F^2 using anisotropic displacement parameters.[19] The water hydrogen atoms were located from a difference Fourier map and refined isotropically, with O–H and H···H distances restrained to 0.85(1) and 1.37(2) Å, respectively. The remaining hydrogen atoms were placed at the calculated positions. Idealized H atoms were refined with isotropic displacement parameters set to 1.2 times the equivalent isotropic U values of the parent atoms. The low bond precision on C–C bonds of 0.01614 Å for **1** was caused by the poor quality of the crystal diffraction. The 18 restraints of **1** were generated by the O–H and H···H distances restraints, and the isotropic behavior restraint of C14. The cyclopropane group C18–C19–C20 of **2** was disordered over two sites, with occupancies of 0.352(5) and 0.648(5), respectively. The crystallographic data for the complexes are listed in Table 1.

3. Results and Discussion

3. 1. Chemistry

A new cobalt(II) complex with L^1 as ligand has been prepared. Reaction of this complex with cyclopropylamine afforded a new cobalt(II) complex bearing Schiff base ligand, L^2 (Scheme 1). The results of the elemental analyses are in accord with the calculated composition of these complexes. The air-stable cobalt complexes are soluble in DMF, methanol, ethanol, chloroform, and acetonitrile.

3. 2. Infrared Spectra

The infrared spectrum of complex **1** exhibits strong band at 1647 cm^{-1}, which can be assigned to the C=O stretching frequency of L^1 ligands. When the carbonyl groups form azomethine groups with cyclopropylamine, the band is absent in the spectrum of complex **2**. Instead, a new band indicative of C=N bond is observed at 1622 cm^{-1}.[20,21] When compared with the spectrum of the free Schiff base HL^2, it can be seen that the band is shifted to the lower frequency. This indicates the coordination of the imino N atom to the cobalt center. The medium and broad

Table 1. Crystal and structure refinement data for **1** and **2**

	1	**2**
Empirical formula	$C_{14}H_{10}Br_2Cl_2CoO_6$	$C_{20}H_{16}Br_2Cl_2CoN_2O_2$
Formula weight	563.9	606.0
Temperature (K)	298(2)	298(2)
Crystal system	Monoclinic	Monoclinic
Space group	$P2_1/c$	$P2_1/c$
Unit cell dimensions		
a (Å)	7.590(2)	12.319(2)
b (Å)	27.685(2)	22.916(2)
c (Å)	8.639(2)	7.952(1)
β (°)	101.451(2)	108.83(3)
V (Å^3)	1779.3(5)	2124.6(5)
Z	4	4
Density (g cm^{-3})	2.105	1.895
Absorption coefficient (mm^{-1})	5.784	4.841
Reflections collected	10619	8098
Independent reflections	2778	2979
Data/parameters	1734/238	1478/290
Restraints	18	52
Final R indices [$I > 2\sigma(I)$]	0.0777, 0.1509	0.0355, 0.0500
R indices (all data)	0.1411, 0.1737	0.1024, 0.0615
Goodness-of-fit on F^2	1.054	0.913

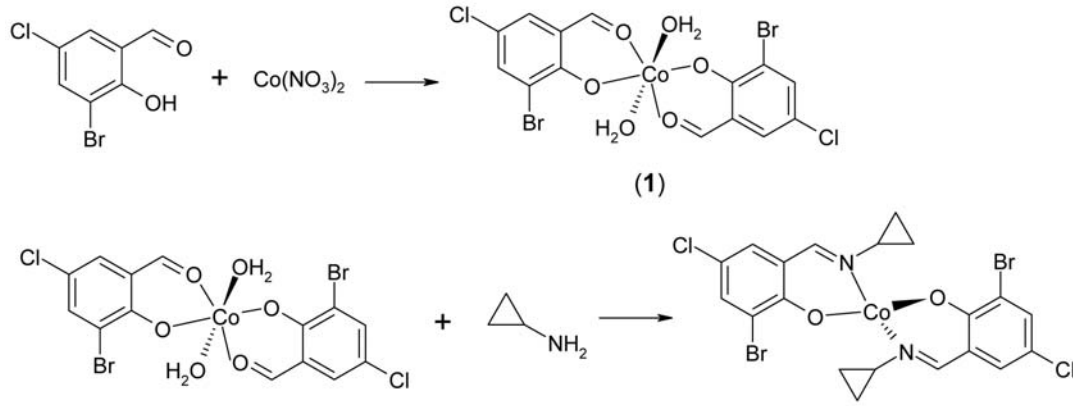

Scheme 1. The synthetic procedure of the complexes

band centered at 3433 cm^{-1} for the spectrum of complex **1** can be attributed to the O–H vibrations of the water ligands. The bands in the region 550–400 cm^{-1} are assigned to the Co–N and Co–O vibrations.[22]

3. 3. Crystal Structure Description of the Complex 1

The molecular structure of the complex **1** is shown in Figure 1. The Co atom has an octahedral geometry and coordinated by two deprotonated 3-bromo-5-chlorobenzaldehyde ligands, and two water molecules. The aldehyde ligands act as bidentate ligands and coordinate to the Co atom through the phenolate O and carbonyl O atoms. For the octahedral coordination, the three *trans* angles are in the range 170.3(3)–177.2(3)°, and the other angles are in the range 84.9(3)–95.5(3)°, indicating a slightly distorted octahedral geometry (Table 2). The distances of the Co–O and Co–N bonds are comparable to the values observed in other cobalt(II) complexes with similar coordination.[23,24] The dihedral angle between the two benzene rings of the ligands is 2.7(3)°. In the crystal structure, the molecules are connected by intermolecular hydrogen bonds O–H···O and O–H···Br, forming a 3D network, as shown by Figure 2. The corresponding hydrogen bonding parameters are listed in Table 3. In addition, there are $\pi\cdots\pi$ stacking interactions (Table 4) among the adjacent benzene rings.[25]

Table 2. Coordinate bond distances (Å) and angles (°) for **1** and **2**

1			
Co1–O1	2.062(7)	Co1–O2	2.069(6)
Co1–O3	2.087(7)	Co1–O4	2.062(7)
Co1–O5	2.096(7)	Co1–O6	2.109(7)
O4–Co1–O1	176.6(3)	O4–Co1–O2	95.5(3)
O1–Co1–O2	87.1(3)	O4–Co1–O3	86.7(3)
O1–Co1–O3	90.7(3)	O2–Co1–O3	177.2(3)
O4–Co1–O5	92.8(3)	O1–Co1–O5	84.9(3)
O2–Co1–O5	94.4(3)	O3–Co1–O5	87.3(3)
O4–Co1–O6	94.5(3)	O1–Co1–O6	87.5(3)
O2–Co1–O6	91.2(3)	O3–Co1–O6	86.8(3)
O5–Co1–O6	170.3(3)		
2			
Co1–O1	1.904(3)	Co1–O2	1.890(3)
Co1–N1	1.995(4)	Co1–N2	1.956(5)
O2–Co1–O1	116.89(14)	O2–Co1–N2	95.83(16)
O1–Co1–N2	115.96(15)	O2–Co1–N1	121.64(14)
O1–Co1–N1	95.18(15)	N2–Co1–N1	112.84(16)

Table 3. Hydrogen bonding parameters for **1** and **2**

D–H···*A*	*d*(*D*–H) (Å)	*d*(H···*A*) (Å)	d(*D*···*A*) (Å)	∠(*D*–H···*A*) (°)
1				
O6–H6B···O4[a]	0.85(1)	1.96(5)	2.766(9)	156(11)
O6–H6A···Br1[a]	0.85(1)	2.72(5)	3.486(7)	151(9)
O6–H6A···O2[a]	0.85(1)	2.26(9)	2.911(11)	133(11)
O5–H5B···Br2[b]	0.85(1)	2.78(5)	3.583(7)	158(11)
O5–H5B···O4[b]	0.85(1)	2.40(10)	3.018(10)	130(11)
O5–H5A···O2[b]	0.85(1)	1.93(5)	2.729(9)	156(12)
2				
C19–H19···Br1[c]	0.97	2.92(3)	3.660(5)	134(6)
C17–H17···Br1[d]	0.93	2.92(3)	3.824(5)	163(6)

Symmetry codes: (a) 1 – *x*, – *y*, – *z*; (b) – *x*, – *y*, – *z*; (c) *x*, *y*, 1 + *z*; (d) 1 – *x*, – *y*, 1 – *z*.

Table 4. Parameters between the planes for **1** and **2**

Cg···*Cg*	*Cg*···*Cg* distance (Å)	Dihedral angle (°)	Perpendi cular distance of *Cg*(I) on *Cg*(J) (Å)	β (°)	γ (°)	Perpendicular distance of *Cg*(J) on *Cg*(I) (Å)
1						
Cg(1)···*Cg*(2)[b]	3.827	2.28	3.562	19.24	21.45	3.613
Cg(1)···*Cg*(2)[a]	3.961	2.28	3.660	21.42	22.48	3.687
Cg(1) and *Cg*(2) are the centroids of the C1–C6 and C8–C13 benzene rings, respectively.						
2						
Cg(3)···*Cg*(3)[b]	3.660	0.00	3.384	22.39	22.39	3.384
Cg(3) is the centroid of the C1-C6 benzene ring.						

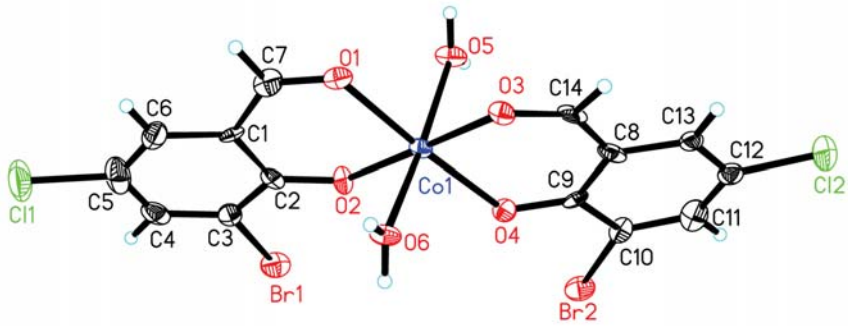

Figure 1. Perspective view of the complex **1** with 30% probability thermal ellipsoids.

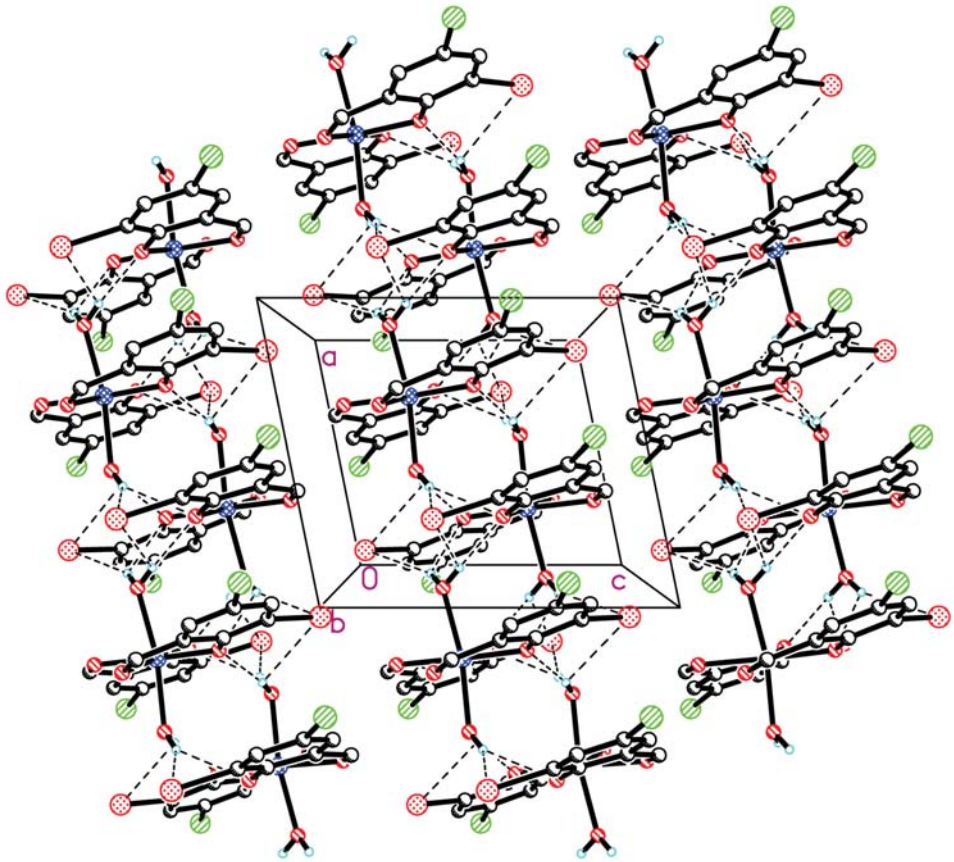

Figure 2. Molecular packing of the complex **1** along the *b* axis.

3. 4. Crystal Structure Description of the Complex 2

The molecular structure of the complex **2** is shown in Figure 3. The Co atom has a tetrahedral geometry and is coordinated by two deprotonated Schiff base ligands 2-bromo-4-chloro-6-(cyclopropyliminomethyl)phenol. The Schiff base ligands act as bidentate ligands and coordinate to the Co atom through the phenolate O and imino N atoms. For the tetrahedral coordination, the angles are in the range 95.18(15)–121.64(14)°, indicating a slightly distorted tetrahedral geometry (Table 2). The distances of the Co–O and Co–N bonds are comparable to the values

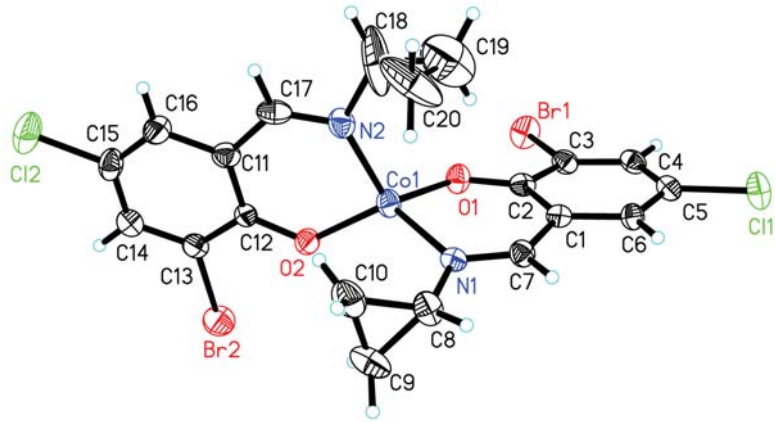

Figure 3. Perspective view of the complex **2** with 30% probability thermal ellipsoids. Only the major component of the disordered cyclohexane group is shown.

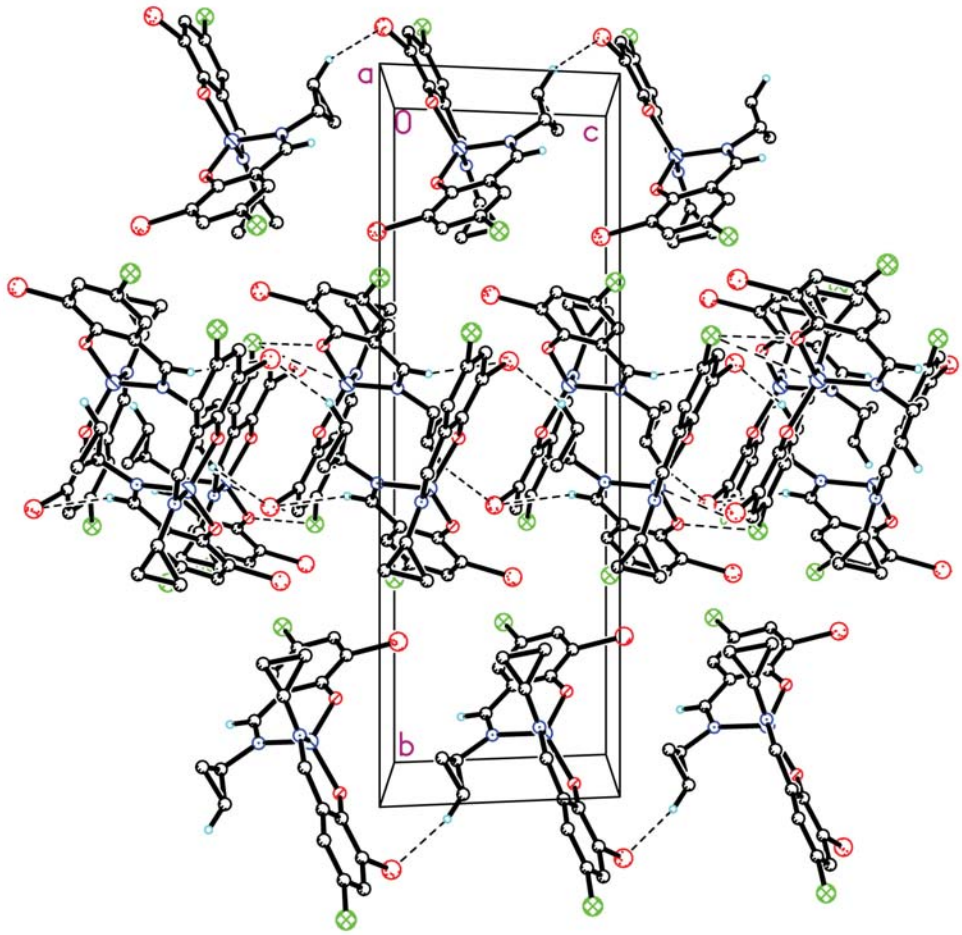

Figure 4. Molecular packing of the complex **2** along the *a* axis.

observed in other cobalt(II) complexes with similar coordination.[26,27] The dihedral angle between the two benzene rings of the ligands is 97.0(3)°. In the crystal structure, the molecules are connected by intermolecular hydrogen bonds C–H···Br, forming 2D layers parallel to the *ac* plane, as shown by Figure 4. The corresponding hydrogen bonding parameters are listed in Table 3. In addition, there are $\pi\cdots\pi$ stacking interactions (Table 4) among the adjacent benzene rings.[25]

3. 5. Antimicrobial Activity

Qualitative determination of antimicrobial activity was done using the disk diffusion method.[28,29] The results are summarized in Table 4. A comparative study of minimum inhibitory concentration (MIC) values of the free ligands and the complexes indicate that the cobalt complexes have better activity than the free ligands. Generally, this is caused by the greater lipophilic nature of the complexes than the ligands. Such increased activity of the metal chelates can be explained on the basis of chelating theory.[30] On chelation, the polarity of the metal atoms will be reduced to a greater extent due to the overlap of the ligand orbital and partial sharing of positive charge of the metal atoms with donor atoms. Further, it increases the delocalization of π-electrons over the whole chelate ring and enhances the lipophilicity of the complexes. This increased lipophilicity enhances the penetration of the complexes into lipid membrane and blocks the metal binding sites on enzymes of microorganisms.

From Table 5, it is obvious that the cobalt complexes show greater antimicrobial and antifungi activities against *Staphylococcus aureus*, *Escherichia coli*, and *Candida albicans* when compared to HL^1 and HL^2. The complex with Schiff base ligand seems to be more active than that with aldehyde ligand. The activity of complex **2** is stronger than **1**. For *Staphylococcus aureus* and *Escherichia coli*, even though the activities of the cobalt complexes are stronger than those of the free ligands, it is still less than the control drug tetracycline. But for *Candida albicans*, both complexes show stronger activity than the free ligands and tetracycline. This trend is in accordance with those reported in literature, that cobalt complexes have stronger activities than the free Schiff bases in the antibacterial fields.[31,32]

Table 5. MIC values (ìg/mL) for the antimicrobial activities of the tested compounds

	Staphylococcus aureus	*Escherichia coli*	*Candida albicans*
HL^1	256	128	> 1024
HL^2	64	64	> 1024
1	16	8.0	256
2	1.0	4.0	128
Tetracycline	0.32	2.12	> 1024

4. Conclusion

Two new cobalt(II) complexes with 3-bromo-5-chlorosalicylaldehyde or 2-bromo-4-chloro-6-(cyclopropyliminomethyl)phenol as ligands have been prepared and characterized. The crystal structures of both complexes were confirmed by X-ray single crystal diffraction. The Co atom in complex **1** is in an octahedral coordination, while in complex **2**, it gives a tetrahedral coordination. The antimicrobial tests show that both complexes have potential activity against *Staphylococcus aureus*, *Escherichia coli* and *Candida albicans*.

5. Acknowledgements

This research was supported by the National Sciences Foundation of China (No. 20676057 and 20877036) and Top-class foundation of Pingdingshan University (No. 2008010).

6. Supplementary Material

The crystallographic data of the structures described in this paper were deposited with the Cambridge Crystallographic Data Centre as supplementary publication no. CCDC-1489222 (**1**) and 1489223 (**2**). Copies of these data are available free of charge from http://www.ccdc.ac.uk/conts/retrieving.html, or from the Cambridge Crystallographic Data Centre, 12 Union Road, Cambridge CB2 1EZ, UK; fax: (+44)1223-336-033; or email: deposit@ccdc.cam.ac.uk.

7. References

1. M. He, Q.-Z. Jiao, X.-F. Chen, J. Li, J. Chen, G.-H. Sheng, Z.-L. You, *Chinese J. Inorg. Chem.* **2016**, *31*, 1590–1596.
2. D. Qu, F. Niu, X. Zhao, K.-X. Yan, Y.-T. Ye, J. Wang, M. Zhang, Z. You, *Bioorg. Med. Chem.* **2015**, *23*, 1944–1949. https://doi.org/10.1016/j.bmc.2015.03.036
3. Y. Zhu, C.-F. Wang, K. Yan, K.-D. Zhao, G.-H. Sheng, Q. Hu, L. Zhang, Z. You, *J. Coord. Chem.* **2016**, *69*, 2493–2499. https://doi.org/10.1080/00958972.2016.1186801
4. J. Qin, Q. Yin, S.-S. Zhao, J.-Z. Wang, S.-S. Qian, *Acta Chim. Slov.* **2016**, *63*, 55–61. https://doi.org/10.17344/acsi.2015.1918
5. D. Barut, N. Korkmaz, S. T. Astley, M. Aygun, *Acta Chim. Slov.* **2015**, *62*, 88–94. https://doi.org/10.17344/acsi.2014.734
6. F.-M. Wang, *Acta Chim. Slov.* **2016**, *63*, 406–410. https://doi.org/10.17344/acsi.2016.2520
7. Z.-C. Liu, B.-D. Wang, Z.-Y. Yang, Y. Li, D.-D. Qin, T.-R. Li, *Eur. J. Med. Chem.* **2009**, *44*, 4477–4484. https://doi.org/10.1016/j.ejmech.2009.06.009

8. D.-D. Qin, Z.-Y. Yang, G.-F. Qi, T.-R. Li, *Transition Met. Chem.* **2009**, *34*, 499–505.
9. Y.-Y. Yu, H.-D. Xian, J.-F. Liu, G.-L. Zhao, *Molecules* **2009**, *14*, 1747–1754. https://doi.org/10.3390/molecules14051747
10. Z. You, M. Liu, C. Wang, G. Sheng, X. Zhao, D. Qu, F. Niu, *RSC Advances* **2016**, *6*, 16679–16690. https://doi.org/10.1039/C6RA00500D
11. Y.-T. Ye, F. Niu, Y. Sun, D. Qu, X.-L. Zhao, J. Wang, D.-M. Xian, H. Jurg, Z.-L. You, *Chinese J. Inorg. Chem.* **2015**, *31*, 1019–1026.
12. C. Jing, C. Wang, K. Yan, K. Zhao, G. Sheng, D. Qu, F. Niu, H. Zhu, Z. You, *Bioorg. Med. Chem.* **2016**, *24*, 270–276. https://doi.org/10.1016/j.bmc.2015.12.013
13. L. Wang, Y.-J. Han, Q.-B. Li, L.-W. Xue, Acta Chim. Slov. **2016**, 63, 822–826. https://doi.org/10.17344/acsi.2016.2699
14. G. P. Cheng, L. W. Xue, C. X. Zhang, *Russ. J. Coord. Chem.* **2014**, *40*, 284–288. https://doi.org/10.1134/S1070328414040022
15. L.-W. Xue, Y.-X. Feng, C.-X. Zhang, *Synth. React. Inorg. Met.-Org. Nano-Met. Chem.* **2014**, *44*, 1541–1544. https://doi.org/10.1080/15533174.2013.802340
16. Bruker, SMART and SAINT. Area Detector Control and Integration Software, Bruker Analytical X-ray Instruments Inc., Madison, WI, USA, 1997.
17. G. M. Sheldrick, SADABS. Program for Empirical Absorption Correction of Area Detector Data. University of Göttingen, Göttingen, Germany, 1997.
18. A. C. T. North, D. C. Phillips, F. S. Mathews, *Acta Crystallogr.* **1968**, *A24*, 351–359. https://doi.org/10.1107/S0567739468000707
19. G. M. Sheldrick, SHELXL-97. *Program for the Refinement of Crystal Structures*, University of Göttingen, Göttingen, Germany, 1997.
20. L. Pan, C. Wang, K. Yan, K. Zhao, G. Sheng, H. Zhu, X. Zhao, D. Qu, F. Niu, Z. You, *J. Inorg. Biochem.* **2016**, *159*, 22–28. https://doi.org/10.1016/j.jinorgbio.2016.02.017
21. F. Niu, K.-X. Yan, L. Pang, D. Qu, X. Zhao, Z. You, *Inorg. Chim. Acta* **2015**, *435*, 299–304. https://doi.org/10.1016/j.ica.2015.07.014
22. S. Chandra, U. Kumar, *Spectrochim. Acta Part A* **2005**, *61*, 219–224. https://doi.org/10.1016/j.saa.2004.03.036
23. R. L. De, K. Samanta, K. Maiti, E. Keller, *Inorg. Chim. Acta* **2001**, 316, 113–116. https://doi.org/10.1016/S0020-1693(01)00369-3
24. Y. Li, Q. Wu, L. Lecren, R. Clerac, *J. Mol. Struct.* **2008**, *890*, 339–345. https://doi.org/10.1016/j.molstruc.2008.05.044
25. A. L. Spek, *Acta Crystallogr.* **2009**, *D65*, 148–155.
26. Z.-L. You, S.-Y. Niu, *Synth. React. Inorg. Met.-Org. Nano-Met. Chem.* **2007**, *37*, 29–33. https://doi.org/10.1080/15533170601172393
27. C. Jing, C. Wang, K. Yan, K. Zhao, G. Sheng, D. Qu, F. Niu, H. Zhu, Z. You, *Bioorg. Med. Chem.* **2016**, *24*, 270–276. https://doi.org/10.1016/j.bmc.2015.12.013
28. A. Barry, Procedures and theoretical considerations for testing antimicrobial agents in agar media. in: Lorian (Ed.), Antibiotics in Laboratory Medicine, 5th ed. Williams and Wilkins, Baltimore, 1991.
29. T. Rosu, M. Negoiu, S. Pasculescu, E. Pahontu, D. Poirier, A. Gulea, *Eur. J. Med. Chem.* **2010**, *45*, 774–781. https://doi.org/10.1016/j.ejmech.2009.10.034
30. J. W. Searl, R. C. Smith, S. Wyard, *J. Proc. Phys. Soc.* **1961**, *78*, 1174–1176. https://doi.org/10.1088/0370-1328/78/6/311
31. T. Yang, F. Niu, L. X. Li, Z. N. Xia, Y. Zhang, Z. L. You, *Russ. J. Coord. Chem.* **2016**, *42*, 402–409. https://doi.org/10.1134/S1070328416050109
32. X. M. Hu, L. W. Xue, G. Q. Zhao, W. C. Yang, *Russ. J. Coord. Chem.* **2015**, *41*, 197–201. https://doi.org/10.1134/S1070328415030045

Povzetek

Pripravili smo nov kobaltov(II) kompleks, $[Co(L^1)_2(OH_2)_2]$ (**1**), z reakcijo 3-bromo-5-klorosalicilaldehida (HL^1) s kobaltovim nitratom v metanolu. Pri reakciji **1** s ciklopropilaminom v metanolu nastane kobaltov(II) kompleks s Schiffovo bazo, $[Co(L^2)_2]$ (**2**), kjer je L^2 deprotonirana oblika 2-bromo-4-kloro-6-(ciklopropiliminometil)phenola (HL^2). Kompleksa sta bila okaratkerizirana z elementno analizo, IR spektroskopijo in monokristalno rentgensko difrakcijo. Ligand L^1 se koordinira na Co atom preko fenolatnega O atoma in karbonilnega O atoma, medtem ko se ligand L^2 koordinira na Co atom preko fenolatnega O atoma in imino N atoma. Co atom v kompleksu **1** ima oktaedrično koordinacijo, v kompleksu **2** pa tetraedrično koordinacijo. Določena je bila tudi antimikrobna aktivnost prostih ligandov in kobaltovih kompleksov na *Staphylococcus aureus*, *Escherichia coli* in *Candida albicans*.

 DOI: 10.17344/acsi.2016.3054 *Acta Chim. Slov.* **2017,** *64,* 186–192

Scientific paper

Monodispersed Gold Nanoparticles as a Probe for the Detection of Hg^{2+} Ions in Water

Bindhu Muthunadar Rajam,[1] Parimaladevi Ramasamy[2] and Umadevi Mahalingam[2,*]

[1] *Department of Physics, Nanjil Catholic College of Arts and Science, Nedumcode, Kaliyakavilai-695502, Tamil Nadu, India*

[2] *Department of Physics, Mother Teresa Women's University, Kodaikanal-624101, Tamil Nadu, India*

* *Corresponding author: E-mail: ums10@yahoo.com*
Tele: 04542241685 (UM and PR)

Received: 08-11-2016

Abstract

Gold nanoparticles were synthesized using *Ananas comosus* as reducing agent. UV-visible spectra show the surface plasmon resonance peak at 544 nm. TEM measurement shows that the formation of monodispersed spherical nanoparticles with average size of 7 nm. Crystalline nature of the nanoparticles was evident from TEM images and peaks in the XRD pattern. FTIR analysis provides the presence of biomolecules responsible for the reduction and capping of the prepared gold nanoparticles. A selective and sensitive method is proposed for detecting mercury based on the SPR change of gold nanoparticles. This mercury sensor based on surface plasmon optical sensor can be used in water analysis.

Keywords: *Ananas comosus.* gold nanoparticles, mercury, optical sensor

1. Introduction

The determination of heavy metal ions in water is of great importance because of their role in the physiological functions of biological systems.[1] Among the heavy metal ions, mercury is an most dangerous metal ions for environment and has most commonly toxic risks for human contacting areas as a result of natural processes, because it is widely distributed in air, water and soil and it is a toxic element that exists in metallic, inorganic, and organic forms.[2] Mercuric ion (Hg^{2+}), exists mostly in surface water due to its high water solubility and it can cause several developmental delays and health problems that can damage the brain, nervous system, kidneys, and endocrine system.[3,4] Therefore, the analysis and measurement of detecting mercury in aqueous media is important. A variety of methods have been developed for quantification of Hg^{2+} concentrations such as atomic absorption spectroscopy, inductive coupled plasma mass spectroscopy, electrochemical impedance spectroscopy, voltammetry and polarography. But, these methods are expensive, complicated sample treatment and mostly take a long measuring period. The selective optical sensor is an alternative method and has been attracted due to the excellent sensitivity, rapid response, the ability to do the detection in a non-destructive manner and cost-effective.

Metal nanoparticles have been received much attention due to their unique optical, electrical and catalytic properties. The size, shape and surface morphology of the particles were crucial in tuning these properties of nanosized metal particles. This was mostly significant for noble metals having strong surface plasmon resonance (SPR) oscillations. There were many synthetic methods have been developed to prepare nanoparticles, including chemical, physical and biological methods, among which green synthesis of metal nanoparticles remains the simplest and environment friendly method. All these synthetic methods vary generally in the way the electrons required for the reduction were provided. Green synthesis of nanoparticles using *D.carota*, *S.lycopersicums*, *Beetroot*, *H.Cannabinus* leaf, *Moringa oliefera* flower, *Avena sativa* and *Hibiscus cannabinus* stem has been reported.[5–11] Among the different metallic nanoparticles, gold nanoparticles have diverse activities and exhibit novel properties such as high surface and variation in electronic and optoelectronic properties; have made them more appropriate for therapeutic use and broad applications in nanobiotechnology. The chemical inertness and resistance to surface oxi-

dation make gold an important material for use in nanoscale technologies and devices. This property is crucial when particle size approaches the nanostructure and the dominance of surface atoms results in an enhanced chemical reactivity.

In this work, gold nanoparticles were synthesized using *Ananas comosus* fruit extract as reducing agent. Since *Ananas comosus* is a readily available fruit and it is a good source of water, carbohydrates, sugars, vitamins A, C and carotene, beta.[12] It contains low amounts of protein, fat, ash and fibre. It is a good source of citric acid, malic acid and ascorbic acid[12,13] and also contain three types of amino acids. Along with this, it also contains bromelain, a protein-digesting enzyme that reduces inflammation. Modified pineapple peel fibre was used to remove heavy metal ions in water through the reaction with succinic acid anhydride.[14,15] Bhosale *et al*. reported the synthesis of nanoparticles using *Ananas comosus* extract as reducing agent with kanamycin A and neomycin as stabilizing agents.[16] They prepared larger nanoparticles with agglomeration.

In the present study, the synthesis and characterization of monodispersed small gold nanoparticles using fruit extract of *Ananas comosus* has been described. Here the size and aggregation of the nanoparticles were controlled without any additional stabilizing agents. The sensing activity of gold nanoparticles obtained by this method has been also described.

2. Experimental Techniques

2. 1. Materials and Methods

Ananas comosus fruit was collected from local supermarket in Kodaikanal, Tamilnadu, India. Chloroauric acid and various heavy metals were obtained from Sigma Aldrich Chemicals. All glasswares were properly washed with distilled water and dried in hot air oven before use.

2. 2. Preparation of Ananas Comosus Extract

Fully riped *Ananas comosus* fruit weighing 100 g cut into fine pieces and were crushed into 100 ml distilled water in a mixer grinder for extraction. The extract was then separated by centrifugation at 1000 rpm for 10 min to remove insoluble fractions and macromolecules. Then the extract obtained was filtered and finally a light yellow extract was collected for further experiments.

2. 3. Synthesis of Gold Nanoparticles

For the synthesis of gold nanoparticles, 5ml of *Ananas comosus* extract was added to aqueous solution of $HAuCl_4$ (3 mM) and stirred continuously for 5min at room temperature. Upon addition of fruit extract, the color of the solution gradually changes from light pink to characteristic dark ruby red upon completion of reaction of the gold colloid (g1). Similarly by adding 10 and 15 ml of fruit extract two more set of samples henceforth called (g2) and (g3) respectively were prepared. UV-visible spectra of these solutions were recorded. Then the solutions were dried. The dried powders were characterized by X- ray diffraction (XRD), Fourier Transform Infrared Radiation (FTIR), Transmission Electron Microscope (TEM) and Energy Dispersive X-ray Spectroscopy (EDX).

2. 4. Characterization Methods and Instruments

The absorption spectra of the prepared nanoparticles were measured using a Shimadzu spectrophotometer (UV 1700) in 300–800 nm range. X- Ray Diffraction analysis of the prepared nanoparticles was done using PANalytical X'pert – PRO diffractometer with Cu Kα radiation operated at 40 kV/30 mA. FTIR measurements were obtained on a Nexus 670 FTIR instrument with the sample as KBr pellets. Transmission Electron Microscopic (TEM) analysis was done using a JEOL JEM 2100 High Resolution Transmission Electron Microscope equipped with an EDX attachment, operating at 200kV.

3. Results and Discussion

3. 1. UV-visible Studies

Noble metals are known to exhibit unique optical properties due to the property of SPR which is the collective oscillation of the conduction electrons in resonance with the wavelength of irradiated light. In the present

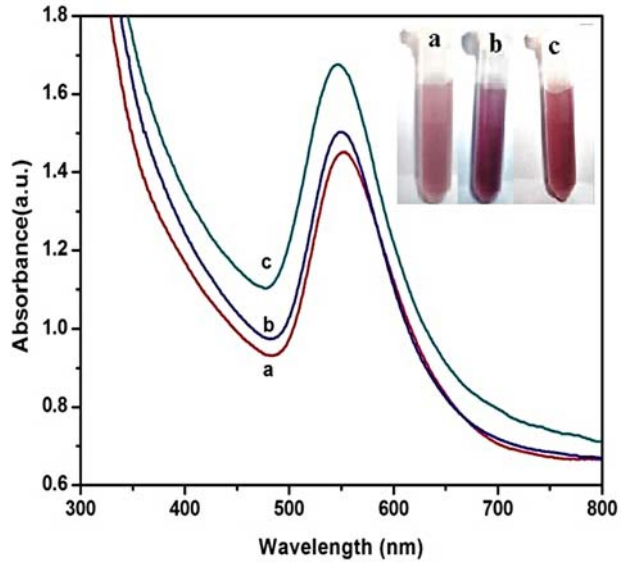

Figure 1. Optical absorption spectra of AuNPs at different concentration of *A.comosus* fruit extract (inset: colour changes of the prepared AuNPs) (a, b and c vs 5, 10 and 15 ml respectively).

study the formation of gold nanoparticles was initially conformed using UV-Visible spectroscopy by measuring Surface Plasmon Resonance (SPR) peaks. Gold nanoparticles exhibit plasmon absorption bands that depend on their size and shape. Fig. 1 shows the absorption spectra obtained for gold nanoparticles with different concentration of fruit extract. The colour variation of the obtained gold nanoparticles for different concentration of *Ananas comosus* fruit extract has been shown in Fig. 1(inset). These characteristic color variations are due to the excitation of the surface plasmon resonance in the metal nanoparticles. As the concentration of fruit extract increases, an fwhm value decreased from 105 nm to 94 nm and blue shift observed from 550 to 544 nm in the reaction medium, indicating the formation of small nanoparticles.

As the particles decrease in size, the absorption peak usually shifts toward the blue wavelengths caused by the donation of electrons to the particles. It has been well established that the maximum wavelength of nanoparticles strongly depends on size, shape, state of aggregation and the dielectric environment. This directly corresponds to a shift of the absorption peak, whereby small gold particle sizes will cause an absorption peak shift to smaller wavelengths, higher frequency and energies.[17] The observed symmetric nature of the SPR indicates the formation of spherical nanoparticles. As the concentration of the extract increases more number of citric, malic and ascorbic acids are available to reduce gold ion and forms large number of very small nanoparticles gives rise to sharp, intense and blue shifted SPR. It was further confirmed by the TEM images shown in Fig. 4 and 5. The symmetric nature of the SPR and the absence of peaks in the longer wavelength region indicate the absence of nanoparticle aggregation. Ascorbate, malate and citrate ions in the fruit extract introduce the negative charge onto the particle surface and thus preventing the particles from aggregation. Thus from the results it can be concluded that the concentration of fruit extract plays an important role in the formation of gold nanoparticles. The obtained nanoparticles were stabilized by physical adsorption of excess negatively charged citrate, malate and ascorbate ions in the solution medium, and thus a repulsive force worked along particles electrostatically and preventing them from aggregation.

3. 2. XRD Studies

The crystalline structure and phase purity of the prepared gold nanoparticles were confirmed with X-ray diffraction (XRD) analysis. Fig. 2(a) shows the XRD pattern for the dried powder of *Ananas comosus*. Three diffraction peaks were observed at 28.5°, 40.8° and 50.9° signify the presence of ascorbic acid (JCPDS 22-1560), citric acid (JCPDS 22-1568) and malic acid (JCPDS 23-1631) in the *Ananas comosus* extract.

Fig. 2(b) shows the XRD pattern for g1 and g3. The broad diffraction peaks were observed at 38.2°, 44.1°,

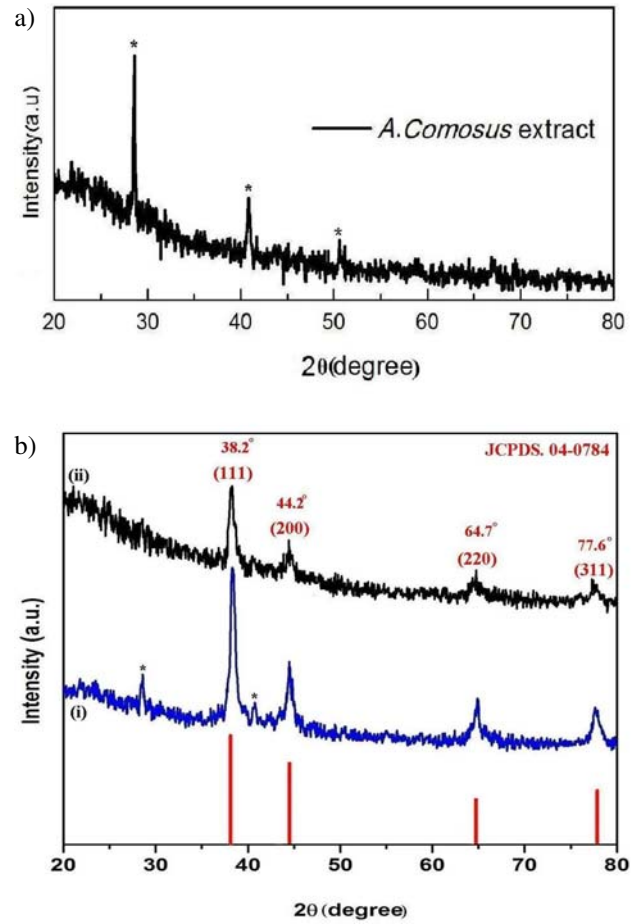

Figure 2. X-ray diffraction pattern of (a) *A.comosus* fruit extract and (b) AuNPs (i) g1 and (ii) g3.

64.8° and 77.6° in the 2θ range and they corresponding to (111), (200), (220) and (311) Bragg's reflections based on the FCC structure of gold nanoparticles with space group of Fm-3m (JCPDS: 04-0784). No peaks of crystallographic impurities in the sample have been found. Generally, the breadth of a specific phase of material is directly proportional to the mean crystallite size of that material. The obtained broader peaks with increasing fruit extract concentration indicating smaller particle size. The XRD line width can be used to estimate the size of the particle by using the Debye–Scherrer formula as $D = k\lambda/\beta \cos\theta$ where D is the particle size (nm), k is a constant equal to 0.94, λ is the wavelength of X-ray radiation (1.5406 Å), β is the full-width at half maximum (FWHM) of the peak (in radians) and 2θ is the Bragg angle (degree). The average particle size, lattice constant, cell volume, surface area to volume (SA: V) ratio, specific surface area (SSA) and Crystallinity index were calculated and tabulated Table.1.

The calculated average particle size for both g1 and g3 indicates that the particle size decreased with the concentration of the fruit extract increased. The calculated lattice constant values are very close to the standard data

Table.1. The average particle size, lattice constant, cell volume, surface area to volume (SA: V) ratio, specific surface area (SSA) and crystallinity index of the prepared nanoparticles.

Prepared AgNPs	Particle Size (nm)	Lattice constant (Å)	Cell volume (Å^3)	SSA (m^2/g)	SA:V ratio	Crystallinity index I*cry*
g1	16	4.0529	66.57	18.46	0.35	~1.0625
g3	7	4.0815	67.99	40.64	0.78	~0.714

(JCPDS File no. 04-0784) and the sample exhibit smaller cell volumes that of bulk. As shown in Table. 1, the observed values of both specific surface area (SSA) and SA:V ratios were increased with decreasing particle size. The SSA has a particular importance in reactivity. It gives the rate at which the reaction will proceed. Because of the large number of atoms available in the reaction medium (g3) makes the reaction faster and hence make them more suitable for broad kind of applications. Crystallinity was evaluated by comparing the crystalline size obtained by XRD to TEM particle size determination. The calculated values of crystallinity index were close to one which indicates the monocrystalline nature of g1 and g3.

3. 3. FTIR Studies

FTIR analysis was carried out to identify the chemical change of the functional groups involved in bioreduction. Fig.3(a) shows the FTIR spectrum of the *Ananas comosus* fruit extract, shows prominent bands at 3417, 2924, 1640, 1019 and 801 cm^{-1} in the 4000 –500 cm^{-1} region. These peaks are assigned to O-H stretching, CH stretching, C=C ring stretching, C-O-C stretching and C-C ring stretching of ascorbic acid, respectively.[18] Fig. 3(b) shows that the FTIR spectrum of g3. The peak at 3417 cm^{-1} was also due to the OH stretching of citric and malic acid.[19,20]

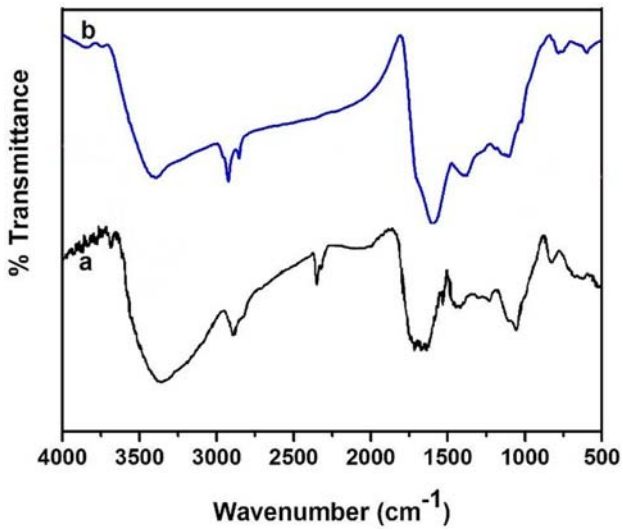

Figure 3. FTIR spectra of (a) *A.comosus* fruit extract and (b) g3.

An interesting peak observed at 2369 cm^{-1} in the spectrum of extract was assigned to NH$^-$ stretching of amines. This vibrational mode was completely reduced in the spectrum of g3. It may the presence of bromelain in the extract. Bromelain is a protein which functions as an enzyme known as proteolytic enzymes. These enzymes have the ability to separate all important peptide bonds. This possibly leads to the absence of this vibrational mode during the synthesis of gold nanoparticles (g3). The interesting peak at 1640 cm^{-1}in the spectrum of extract was assigned to C=C ring stretching of vitamin C, OCO asymmetric stretching of malic acid and C=O stretching of citric acid, was appeared at a sharp peak at 1601 cm^{-1} in the spectrum of g3.

Another interesting broad peak observed at 1414 cm^{-1} in the spectrum of extract was show at a symmetric peak at 1390 cm^{-1} in the spectrum of g3, was due to OCO symmetric stretching of malic acid, COH deformation of citric acid and CH_2 wagging of ascorbic acid. Similarly, the symmetric peak observed at 1115 cm^{-1} was due to C-O-C stretching of ascorbic acid and C-C stretching of malic and citric acid. This indicates that the carboxylic acid groups present in the *Ananas Comosus* fruit extract was responsible for reduction of AuNPs.

3. 4. TEM Studies

The TEM images of the g1 and g3 were shown in Fig. 4 and 5 respectively. The prepared nanoparticles exhibit size dependent morphology. At the TEM image of g1, monodispersed and spherical nanoparticles of average size of 17 nm with diameter ranging from 13 nm to 26 nm (Fig.4). The TEM image of g3, synthesized by higher fruit extract concentration showing the presence of monodispersed spherical nanoparticles of average size of 7 nm ranging from 3 to 15 nm size (Fig. 5). Here, most of the particles observed in the range of 4 nm to 8 nm. As the concentration of fruit extract increases large number of citrate, malate and ascorbate ions are available to reduce gold ion and forms small nanoparticles. The smaller size of g3 was also due to their high specific surface area and its monocrystalline nature. More number of nanoparticles observed in TEM images of g3 in comparison to g1. In both cases, the observed nanoparticles were spherical and homogeneous distribution, which was confirmed from the symmetric nature of SPR shown in Fig. 1(a). Strong interaction between biomolecules in the fruit extract and sur-

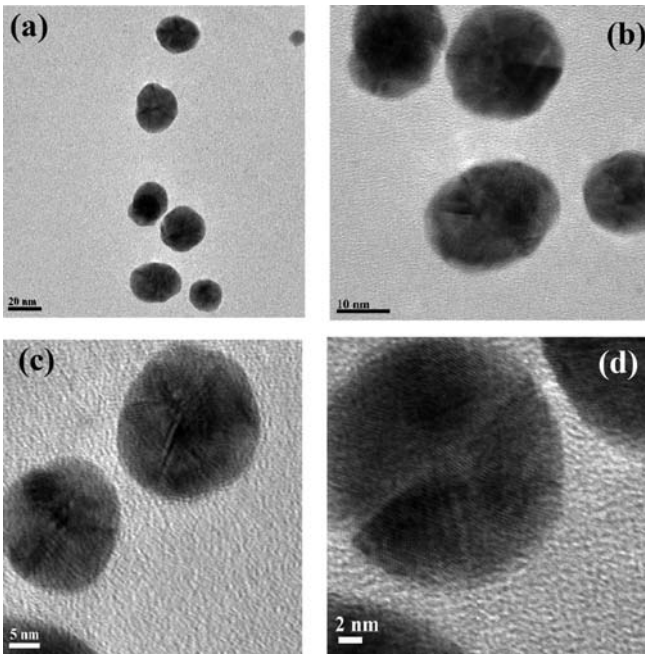

Figure 4. TEM micrograph of the g1.

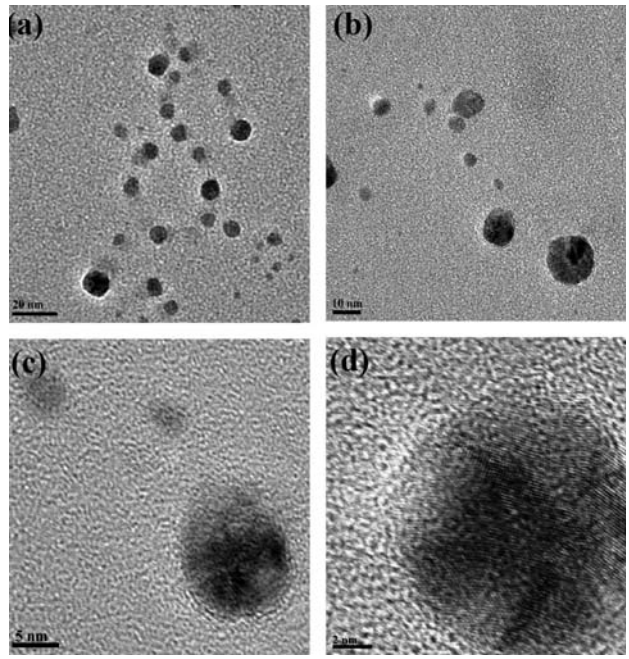

Figure 5. TEM micrograph of the g3**.**

face of nanoparticles was sufficient to the formation of spherical nanoparticles preventing them from sintering.

At lower concentration of fruit extract the citric, ascorbic and malic acid present in fruit extract was insufficient to reduce gold ion, indicating larger size particle. The twined particles observed in Fig. 4(c), 4(d), 5(c) and 5(d) were identified by showing brightness in part of the particles as compared to the other parts. Generally, twinning, the planar defect is observed for face-centered cubic (fcc) structured metallic nanocrystals. Sharing of a common crystallographic plane by two subgrains gives rise to twinning. Face-centered cubic (fcc) structured metallic nanostructures have a tendency to nucleate and grow into twinned particles with their surfaces bounded by lowest energy facets (111)[21]. The formation of gold was further confirmed by the analysis of the energy dispersive spectroscopy shown in Fig. 6.

3. 5. Sensing Activity

Sensing is one of the important applications of nanoparticles. Nanoparticle-based optical surface sensors have received much attention due to their faster response and better resolutions. The interaction between natural biomolecules and the surface of the inorganic nanoparticles paves the way for development of sensing system. The interaction of prepared AuNPs with various alkali metal (Li^+, K^+, Fe^{3+}) and transition metal ions (Ni^{2+}, Mn^{2+}, Cu^{4+},

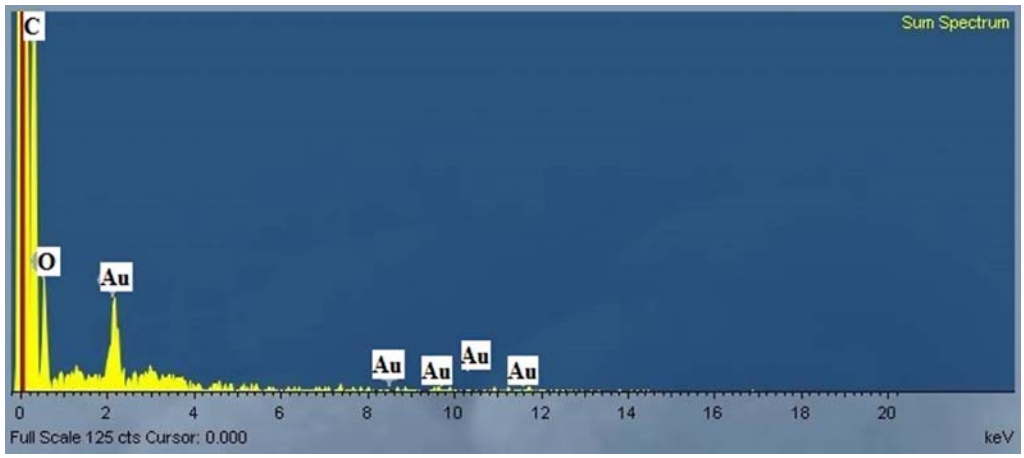

Figure 6. EDX graph of g3.

Zn^{2+}, Hg^{2+}, Cd^{2+}) was examined by adding 1ml of (3mM) salts of these metals into the 2 ml of AuNPs by drop by drop and stirred for 5 min. UV-vis spectra (Fig.6 (a)) of AuNPs were taken immediately after addition of metal ions, after 5 min of interaction. It was observed that except Hg^{2+} no other metal ions exhibited a colour change. UV-vis spectra of these heavy metals interacted with AuNPs were shown in Fig.7 (a). It was observed that the intensity of the SPR bands get reduced for all metal ions as compared to that of the AuNPs. Only mercury got almost quenching of the SPR peak among all the metals, including alkali metal (Li^{+}, K^{+}, Fe^{3+}) and transition metal ions (Ni^{2+}, Mn^{2+}, Cu^{4+}, Zn^{2+}, Hg^{2+}, Cd^{2+}). It was also observed that for Hg^{2+} gave fading of pale pink colour, indicating the prepared AuNPs were sensitive and selective towards Hg^{2+}.

The sensitivity of this method was measured by adding various concentration of aqueous solution of Hg^{2+} ions to the aqueous AuNPs (5 ml) at room temperature. With the increase of Hg^{2+} ions, the color sequentially changed from purple to colorless. The addition of 0.188 mM to 0.653mM Hg^{2+} to the AuNPs solution causes color changes from light purple to colorless were observed shown in Fig. 7 (b) (inset). The UV-vis spectrum correspondingly recorded and shown in Fig. 7(b). With increasing the concentration of Hg^{2+} ion to the AuNPs causes immediate reduction in the intensity of surface plasmon peak at 544 nm. This could be accounted for the slight blue shift of the SPR band of gold nanoparticles. It shows absorbance strength decreases gradually by increasing the concentration of Hg^{2+} ion. With increasing Hg^{2+} ion concentration, blue shift of the SPR peak was also obtained. When Hg^{2+} ion added to the prepared nanoparticles, Hg^{2+} ions interact with the biomolecules (carboxylic acid groups) in the *Ananas comosus* fruit extract on the surface of the nanoparticles form bonds among nanoparticles with Hg^{2+} ions performing as link for binding sites of biomolecules and eliminating it away from the surface of the nanoparticle surface, in that way aggregation of nanoparticles had taken place. This could be accounted for the slight blue shift of the SPR band of gold nanoparticles. There was no SPR peak was observed after the addition of 0.653 mM Hg^{2+}, suggesting the concentration of Hg^{2+} was limited to 0.653 mM. So The linear variation of absorbance (ΔA) changes and the concentration of Hg^{2+} over the range from 0.188 mM to 0.653mM shown in Fig. 7(c). This plot can be fit by a linear equation y = 1.527x-1.0633, R^2 = 0.9889. The sensitivity of the system towards analyte concentration was found to be 1.5273/mM is measured from the plot of absorbance (ΔA) versus concentration of Hg^{2+}. The limit of detection was estimated by defined as the following formula of $C_L = 3S_B/m$, where C_L, S_B, and m are the limit of detection, standard deviation of the sample, and the slope of the calibration curve, respectively. It was found to be 0.1198 mM. Applications of nanoparticle sensors by the aggregation of small particles were useful because aggregates with multiple particles yield large enhancements due to the enormous electromagnetic field that coherently interfere at the junction site between the

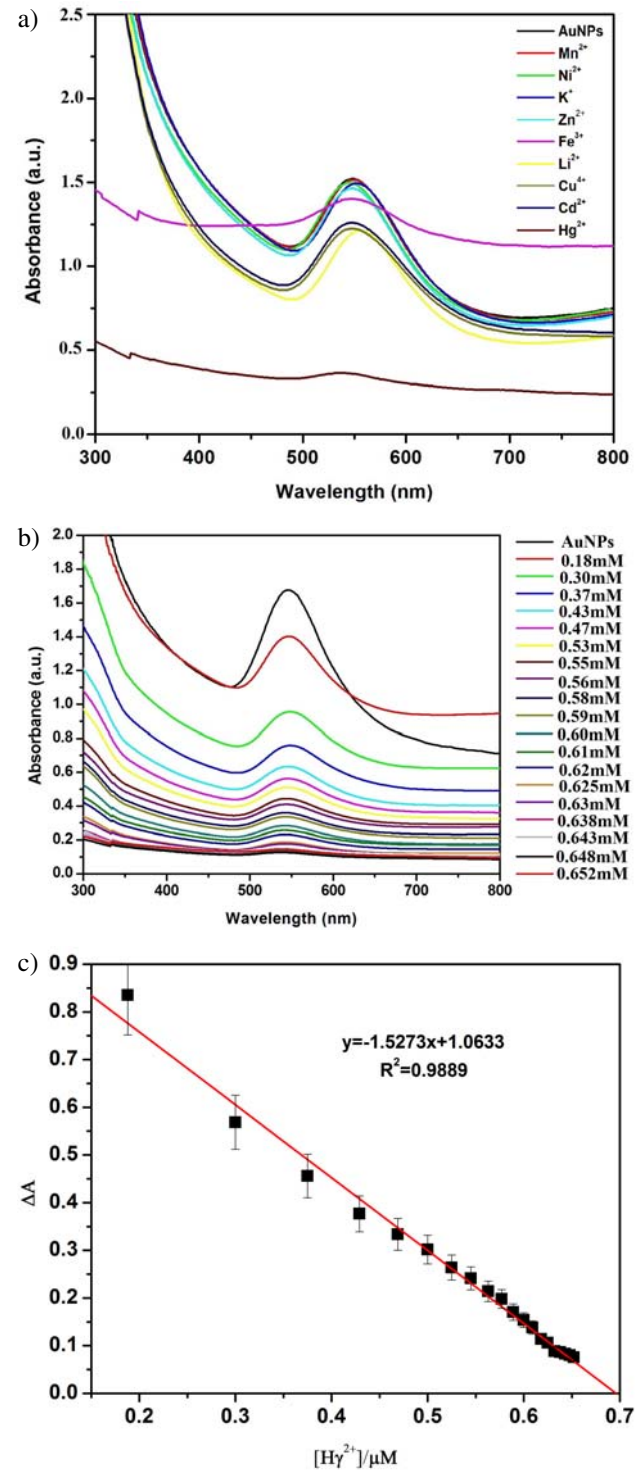

Figure. 7. (a) UV-vis absorption spectrum and photographs (inset) of AuNPs with different heavy metal ions, (b) UV-vis absorption spectrum of AuNPs solution upon addition of Hg^{2+} ions (0.188 mM to 0.653mM) and (c) plot of absorbance (ΔA) intensity at 544 nm versus Hg^{2+} ions concentration.

particles. This mercury sensor based on surface plasmon optical sensor can be used in environmental monitoring especially in water purification.

4. Conclusion

The present simple study was designed to slow reduction of chloroauric acid using fruit extract of *Ananas comosus* as reducing agent. This green synthesis method has formed monodispersed spherical gold nanoparticles with average size of 7 nm. The prepared nanoparticles were characterized by UV-visible, Fourier transform infrared spectroscopy (FTIR), transmission electron microscopy (TEM) and energy dispersive spectroscopy (EDS) technique to identify the size, shape of nanoparticles and biomolecules act as reducing agents. FTIR measurements show that carboxylic acid groups present in *Ananas comosus* fruit extract was used as reducing agent. The prepared gold nanoparticles were stable for one month without aggregation. The surface plasmon resonance of prepared gold nanoparticles was confirmed by UV–visible spectral analysis. As the concentration of *Ananas comosus* fruit extract increases, absorption spectra shows blue shift with decreasing particle size. The prepared AuNPs were sensitive and selective towards Hg^{2+}. This mercury sensor based on surface plasmon optical sensor can be used in water analysis by detecting the concentration of Hg^{2+} ions.

5. Acknowledgements

The authors are thankful to DST-CURIE New Delhi, UGC-DAE CSR Indore for financial assistance.

6. References

1. M. A. Anderson, F. M. M. Morel, *Limnol. Oceanogr.* **1978**, *23,* 283–295. https://doi.org/10.4319/lo.1978.23.2.0283
2. F. A. Cotton, G. Wilkinson, C. A. Murillo, M. Bochmann, *Advanced Inorganic Chemistry, 6th ed.,* John Wiley & Sons, New York, **1999**.
3. T. W. Clarkson, L. Magos, G. J. Myers, *N. Engl. J. Med.* **2003**, *349,* 1731–1737. https://doi.org/10.1056/NEJMra022471
4. Y. Wang, F. Yang, X. Yang, *Biosens. Bioelectron.* **2010,** *25,* 1994–1998. https://doi.org/10.1016/j.bios.2010.01.014
5. M. Umadevi, S. Shalini, M. R. Bindhu, *Adv. Nat. Sci. Nanosci. Nanotechnol.* **2012**, *3 025008,* 1–6.
6. M. Umadevi, M. R. Bindhu, V. Sathe *J. Mater. Sci. Technol.* **2013,** *29,* 317–322. https://doi.org/10.1016/j.jmst.2013.02.002
7. M. R. Bindhu, M. Umadevi, *Spectrochim. Acta A*, **2015**, *135*, 373–378. https://doi.org/10.1016/j.saa.2014.07.045
8. M. R. Bindhu, M. Umadevi, *Spectrochim. Acta A,* **2013**, *101,* 184–190. https://doi.org/10.1016/j.saa.2012.09.031
9. M. R. Bindhu, V. G. Sathe, M. Umadevi, *Spectrochim Acta A,* **2013**, *11, 5*409–415
10. V. Armendariz, I. Herrera, J. R. Peralta-Videa, M. Jose-Yacaman, H. Troiani, P. Santiago, J. L. Gardea-Torresdey, *J. Nanopart. Res.* **2004**, *6,* 377–382. https://doi.org/10.1007/s11051-004-0741-4
11. M.R. Bindhu, P.Vijaya Rekha, T. Umamaheswari, M.Umadevi, *Mater. Lett.* **2014**, *131*, 194–197. https://doi.org/10.1016/j.matlet.2014.05.172
12. J. L. Collins, The Pineapple, Interscience Publishers Inc New York. (**1960**) 250.
13. E. K. Nelson, *J. Am. Chem. Soc.* **1925,** *47,* 1177–1179. https://doi.org/10.1021/ja01681a039
14. X. Hu, M. Zhao, H. Huang, *Water Environ. Res.* **2010,** *8, 2*733–741.
15. X. Hu, M. Zhao, G. Song, H. Huang, *Environ Technol. 32,* **2011**, 739–746. https://doi.org/10.1080/09593330.2010.510853
16. V. Santosh Nalage, V. Sidhanath Bhosale, V. Sheshanath Bhosale, *ONJ* **2011** *5,* 78–82.
17. S. L. Smitha, K. M. Nissamudeen, D. Philip, K. G. Gopchandran, *Spectrochim. Acta A* **2008** *71,* 186–190. https://doi.org/10.1016/j.saa.2007.12.002
18. C. Y. Panicker, H. T. Varghese, D. Philip, *Spectrochim. Acta A,* **2006** *65,* 802–804. https://doi.org/10.1016/j.saa.2005.12.044
19. P. Tarakeshwar, S. Manogaran, *Spectrochim. Acta A* **1994** *50,* 2327–2343. https://doi.org/10.1016/0584-8539(94)E0017-5
20. J. L. Castro, M. R. López-Ramýírez, J. F. Arenas, J. C. Otero, *Vib. Spectrosc.* **2005** *39,* 240–243. https://doi.org/10.1016/j.vibspec.2005.04.007
21. J. G. Allpress, J. V. Sanders, *Surf. Sci*. **1967**, *7,*1–25. https://doi.org/10.1016/0039-6028(67)90062-3

Povzetek

Nanodelce zlata smo pripravili z uporabo *Ananas comosus* kot reducirnega reagenta. UV-Vis spektri kažejo površinsko resonančni plazmonski (SPR) vrh pri 544 nm. Z meritvami s presevnim elektronskim mikroskopom (TEM) pa smo prikazali sintezo monodispergiranih sferičnih nanodelcev s povprečno velikostjo 7 nm. Kristalna narava nanodelcev je razvidna iz TEM slik in vrhov, določenih z rentgensko praškovno difrakcijo (XRD). FTIR spektroskopija kaže na prisotnost biomolekul, ki so odgovorne za redukcijo in ločevanje pripravljenih nanodelcev zlata. Za določanje živega srebra predlagamo selektivno in občutljivo metodo, ki temelji na osnovi SPR sprememb nanodelcev zlata. Takšen senzor bi lahko uporabljali pri analizi voda

Scientific paper

Poly-Dianix Blue/Multi-Walled Carbon Nanotube Modified Electrode for Detection of Levodopa in the Presence of High Concentrations of Ascorbic and Uric Acids

Abdolhamid Hatefi-Mehrjardi,[1,2,*] Mohammad Ali Karimi,[1] Azam Barani[2] and Mahdiyeh Soleymanzadeh[2]

[1] *Department of Chemistry, Payame Noor University, 19395-3697, Tehran, Iran*

[2] *Department of Chemistry & Nanoscience and Nanotechnology Research Laboratory (NNRL), Payame Noor University (PNU), Sirjan, Iran*

* *Corresponding author: E-mail: hhatefy@pnu.ac.ir or hhatefy@Yahoo.com*
Tel: +98-34-423-335-41; Fax: +98-34-423-335-40

Received: 24-11-2016

Abstract

A selective and sensitive electrochemical sensor was studied for determination of levodopa (LD) in the presence of uric acid (UA) and ascorbic acid (AA) using poly-dianix blue and multi-walled carbon nanotubes (PDB/MWCNTs) modified glassy carbon electrode. Cyclic voltammetry, differential pulse voltammetry, and chronoamperometry methods were applied to investigate the electrocatalytic oxidation of LD, UA and AA in aqueous solutions. By DPV technique, LD, UA and AA give oxidation peaks at 0.380, 0.520 and 0.180 V, respectively. Under the optimized experimental conditions LD, UA and AA give a linear response in the range of 0.09-75 μmol L^{-1}, 0.3–110 μmol L^{-1} and 10–160 μmol L^{-1}, respectively. Accordingly, the obtained detection limits were 0.003, 0.002 and 0.023 μmol L^{-1}. The method provides a simple electrochemical sensor for successful determination of LD in human blood serum samples.

Keywords: Dianix Blue; Carbon Nanotubes; Modified Electrode; Levodopa; Uric Acid; Ascorbic Acid.

1. Introduction

Parkinson's disease (PD) is a progressive neurologic disorder that leads to a slowly increasing asthenia in movement. It is caused by a lack of dopamine, a natural substance usually found in the brain. Dopamine cannot be administered directly because it does not cross the blood-brain barrier easily. Levodopa (LD) is one of central nervous system drugs and passes into the brain and is then converted to dopamine by decarboxylase. Then, LD is utilized to increase dopamine levels in the brain.[1] Clearly, the process of LD detection and its concentration determination is an important property in pharmaceutical and clinical procedures. Different analytical methods have been developed in order to measure LD levels in various sample matrices, such as spectrophotometric,[2] high-performance liquid chromatography,[3] and capillary zone electrophoresis.[4,5] All these methods involve complicated techniques and expensive instruments. Compared to other choices, electrochemical methods provide useful alternatives that are faster, cheaper and highly sensitive.[6–10]

Ascorbic acid (AA) is commonly known as vitamin-C.[11] AA plays an important role in several enzymatic reactions and in the defense against oxidative stress.[12] According to these properties, it is utilized for the prevention and treatment of infertility, Alzheimer's disease, atherosclerosis, cancer[13,14] and AIDS.[15,16] However, at higher concentration levels, AA contributes to the formation of kidney stones.

Uric acid (UA) is a nitrogenous compound and the primary major product of purine catabolism.[17] Continuous monitoring of UA in the body fluid is vital since its abnormal concentration levels result in different diseases, such as hyperuricaemia and gout.[18] Several methods for the de-

tection of UA have been explained in papers including enzymatic–spectrophotometry[19] and chemiluminescence.[20] However, most of these methods are complicated because they need derivatization of compound with variety detection methods. Therefore, it is favorable to have a simple, sensitive and fast method for monitoring the concentration of UA in biological fluids such as electrochemical techniques.[21,22]

Whereas LD, UA and AA play the main role in the human body and often coexist in biological fluids, the selective detection of these three compounds has always been the subject of many types of research.[15] As LD, UA and AA are all electroactive, electrochemical methods are often utilized to the determination of these three species.[23,24] However, the direct redox reactions of these species at the bare electrodes take place at very similar potentials[25–28] and often suffer from a pronounced fouling effect, which results in a poor selectivity and reproducibility.[29,30] Also, the voltammetric sensing of neurotransmitter metabolites usually suffers from the interference of AA, which usually coexists in vivo as anion at high concentrations and possesses an oxidation potential close to that of neurotransmitter metabolites at the unmodified electrode.[31] Moreover, one promising approach for minimizing overvoltage effects and facilitating the determination is through the use of an electrocatalytic process at chemically modified electrodes. The most commonly used electrode material is carbon particularly glassy carbon (GC),[32] accordingly the chemical modifications of the inert substrate of glassy carbon electrode with redox active thin films offer significant advantages in the design and development of electrochemical sensors.[33] Modification of GC electrodes can be achieved by numerous ways, and the electropolymerization method has been widely explored.[34] Compared with the conventionally adsorbed layer, the electropolymerized conductive sensing film is more uniform and the thickness is easily controlled by controlling the number of potential sweep cycles. More importantly, the polymeric sensing films on the electrode surface can yield a three-dimensional reaction zone which can provide more active sites for anodic oxidation of LD, UA and AA and greatly increase the sensitivity of the resulting sensor.[35]

Carbon nanotubes (CNTs) are considered to be good supports for polymer-modified GC electrodes, because of their good electric conductivity, small dimensions, high mechanical strength,[36] electric[37,38] and thermal behavior,[39,40] and the property of being polymer carriers.[41,42]

In the previous work, the poly-(Alizarin Red S)-modified glassy carbon electrode was successfully fabricated and used for the electrochemical detection of LD, homovanillic acid, and AA in the presence of the each other.[43] However, modification with new nanocomposite materials offers advanced properties.

In this study, PDB/MWCNTs-modified GC electrode was electrochemically prepared and used as an electrochemical sensor for determination of LD, UA and AA in the presence of the each other. The results have been compared with the bare GCE and PDB/GCE based on electrocatalytic oxidation, and some parameters influencing the performances of this electrode in the determination of the three species are discussed. In fact, the redox active sites shuttle electrons between the analytes and the electrode shows a significant reduction in activation overpotentials.

2. Experimental

2. 1. Chemicals and Solutions

LD, UA and AA were obtained from Alfa Aesar, Fluka (Switzerland) and Merck (Germany), respectively. Dianix blue (4,8-diamino–1,5-dihydroxy-2-(4-hydroxyphenyl)-4a,9a-dihydroanthracene-9,10-dione) with the molecular mass of 362.34 g mol^{-1}, the structural formula of $C_{20}H_{14}N_2O_5$ and the following molecular formula (Scheme 1) was purchased from Dy Star.

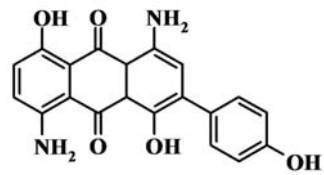

Scheme 1. The structural formula of Dianix blue.

MWCNTs with purity more than 95% were purchased from Research Institute of Petroleum Industry (Iran). MWCNT purification was performed as given in the literature:[44] 0.150 g of MWCNTs were stirred in 12 mL of concentrated HNO_3/H_2SO_4 mixture 3:1 for 24 h. The solid product was filtered using a membrane filter with a pore size of 0.2 m, washed with double distilled water until neutral pH was reached. The filtrate was dried at 80 °C in an oven for 24 h. Other reagents were of analytical grade purchased from Merck and used without further purification. Electrolyte solutions were prepared using Smalley method.[45] The initial pH of the solution 0.10 mol L^{-1} KCl + 0.01 mol L^{-1} H_3PO_4 was *ca.* 2.1. The higher pHs were adjusted by the addition of 0.11 mol L^{-1} NaOH. Ionic strength was constant over the entire range of pH. All electrochemical experiments were carried out in 0.11 mol L^{-1} PBS at pH 3.0. Freshly prepared LD, UA and AA solutions were used for each experiment. All aqueous solutions were made with double-distilled water.

2. 2. Apparatus

A conventional cell with three electrodes including bare GCE or modified GCE with PDB or PDB/MWCNTs

as working electrode, Ag/AgCl (3.0 mol L^{-1} KCl, Metrohm) as reference electrode and platinum bar (Metrohm) as auxiliary electrode, was employed for electrochemical experiments. The cyclic voltammetry and differential pulse voltammetry and chronoamperometry experiments were carried out using an Autolab P/GSTAT 12 (Eco Chemie, The Netherlands) interfaced with a computer and controlled by GPES 4.9 software. The topological imaging of the electrodes was performed by AFM using Nanosurf Easy Scan 2 AFM (Nanosurf AG, Switzerland) and Field Emission Scanning Electron Microscope (FESEM, MIRA, TESCAN, USA). AFM images were taken in the air in the contact/tapping mode and were obtained at least in three different sites in given samples.

2. 3. Electrode Modification

Before electrode modification, the GCE (nominal area of 0.0314 cm^2, Azar electrode Co., Urmia, Iran) was polished using aqueous slurries of alumina (0.05 μm) on polishing cloth. Then it was rinsed with double-distilled water, and sonicated in water/ethanol/water each for 3 min respectively. The suspension of DB/MWCNTs was prepared from at least 2 h ultra-sonication of DB (0.1 mmol L^{-1}) and MWCNTs (1 wt% DB) in PBS.[46] The cleaned electrode was immersed in the suspension of DB/MWCNTs and conditioned out by cyclic potential sweeping between –0.2 to +1.8 V at 0.100 V s^{-1} for 40 scans. After electropolymerization, the modified electrode was rinsed with distilled water and utilized for electrochemical measurements.

3. Results and Discussion

3. 1. Fabrication and Characterization of PDB/MWCNTs Modified GCE

The non-conducting polymer films devoted to developing sensors and biosensors have a very thin thickness (10–100 nm) due to their self-limited growing.[47] The non-conducting films also have favorable perm-selective properties which could be used to reduce possible electrochemical interferences in samples. Therefore, fast response time and high selectivity could also be expected for non-conducting polymers modified GCE. Based on non-covalent interactions such as π-π stacking, van der Waals interaction and strong adsorption, they interact with MWCNTs, increasing the solubility of MWCNT in water and therefore stabilizing the DB/MWCNTs solution. Cyclic voltammetry was used to form electro-polymerized film and the redox behavior of DB in the presence of MWCNTs was investigated between –0.2 and 1.8 V at the clean glassy carbon electrode. The consecutive cyclic voltammograms (the first 10 cycles) are plotted in Figure 1. As the number of cycles increases, the anodic currents increase until a steady state after about 7 cycles. It is an evidence that a polymeric product with the anthraquinone basis formed on the electrode surface.

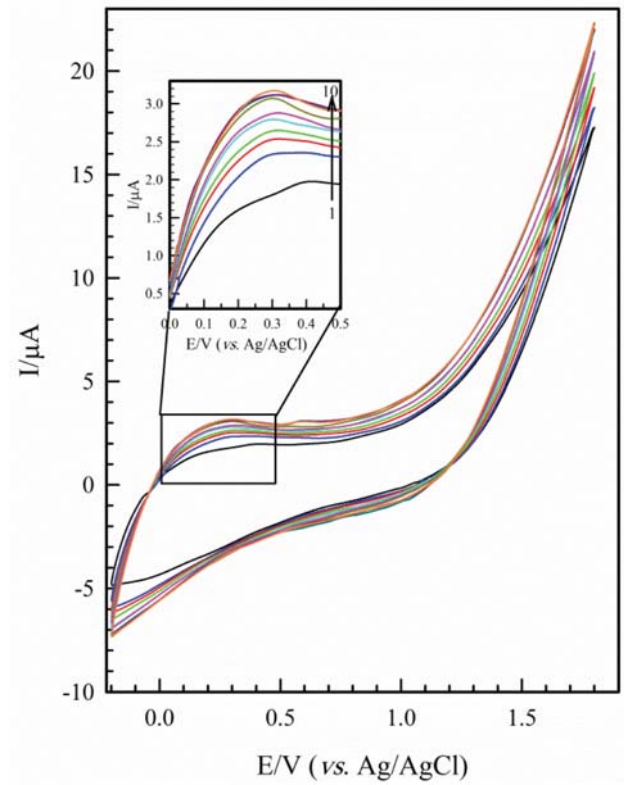

Figure 1. Successive cyclic voltammograms of GCE in 0.11 M PBS (pH 3) containing the suspension of DB/MWCNTs for first 10 cycles. The scan rate was 0.100 V s^{-1}.

The morphological characteristics of the modified electrodes were studied by SEM and AFM. Fig. 2 represents the topography SEM and AFM images acquired from the surface of bare GC, PDB/GC and PDB/MWCNT-GC electrodes.

The SEM images of smooth and homogeneous surface correspond to the unmodified (a) and modified GCE with PDB (b). While the PDB/MWCNTs modified GCE (c) reveal different patterns, this obviously shows that the electrode surface is covered electrochemically by PDB/MWCNTs in three dimensions. The AFM images indicate that the modified electrode surface with PDB/MWCNTs film is throughout rough and in comparison to PDB/GC and bare GC electrode, increases its microscopic area significantly and the resulting currents in voltammetric measurements.

3. 2. Electrochemical Behavior of LD, UA and AA in a Mixture at Modified GCE

In order to study the selectivity of the PDB/MWCNTs-GCE, the cyclic voltammograms of LD, UA and AA in PBS, pH 3, were recorded at the bare and

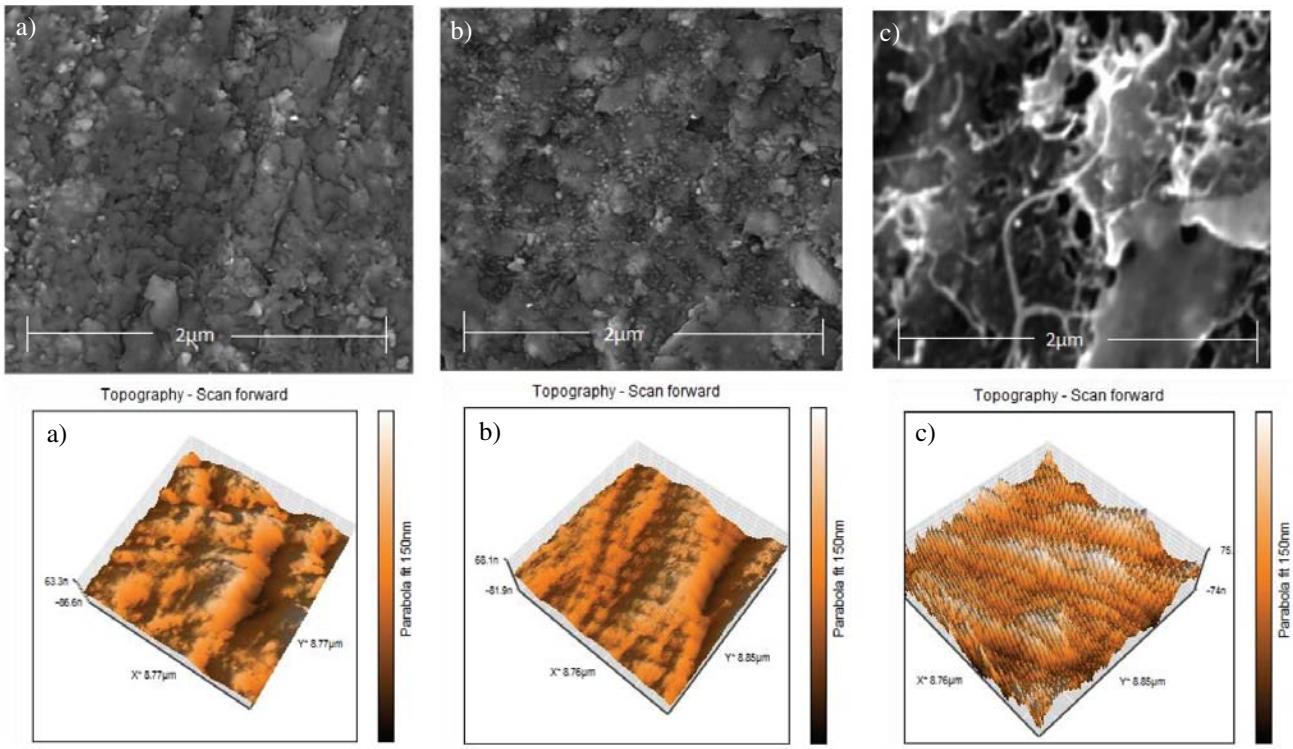

Figure 2. SEM (top) and AFM (down) images of bare GC (a), PDB/GC (b) and PDB/MWCNTs-GC (c) electrodes

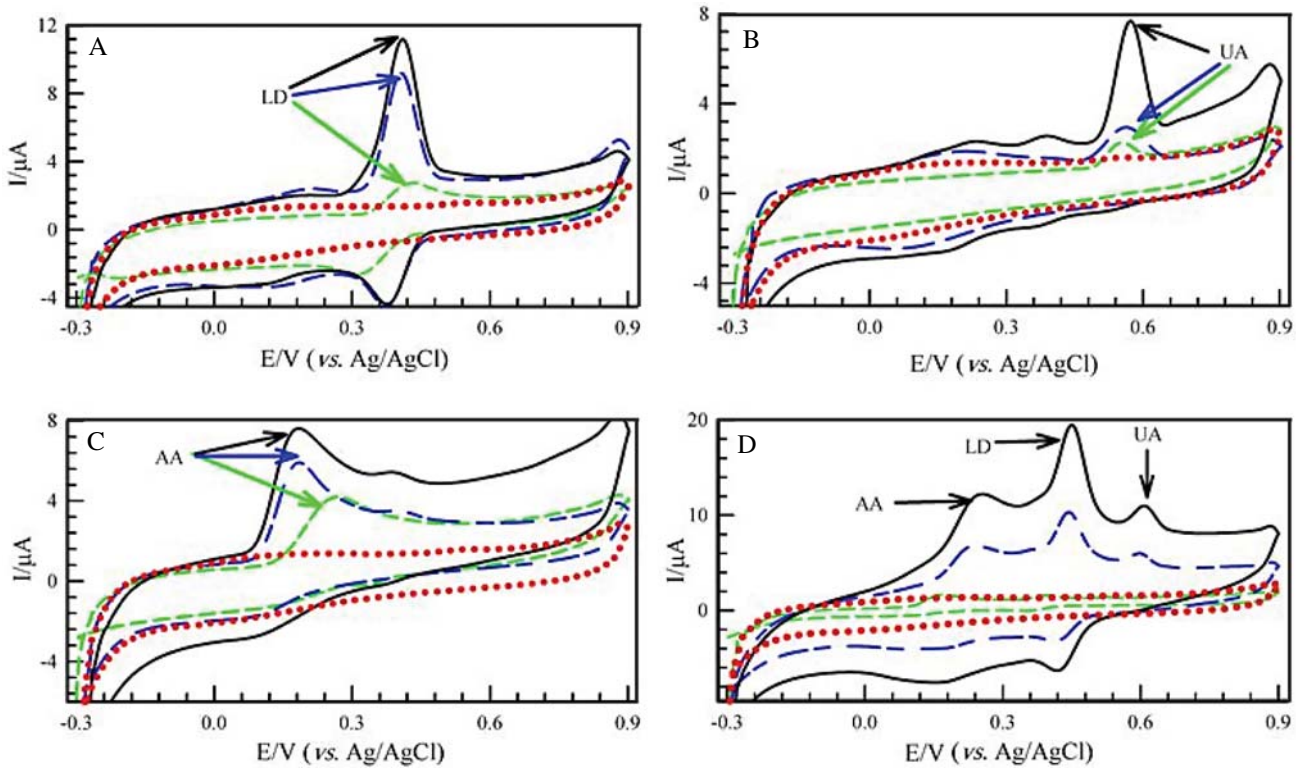

Figure 3. Cyclic voltammograms of blank solution in the absence of any analyte (red dotted lines) and 2 µmol L^{-1} LD (A), 60 µmol L^{-1} UA (B), 100 µmol L^{-1} AA (C) and the mixture of the three analytes (D) obtained on the surface of bare GC (green short dashed lines), modified PDB/GC (blue long dashed lines), and PDB/MWCNTs-GC electrodes (solid black lines). The potential scan rate was 0.100 V s^{-1} and supporting electrolyte was 0.11 mol L^{-1} PBS, pH 3.0.

modified electrodes (Fig. 3). It can be shown that the anodic peak potentials for the LD (A), UA (B), and AA (C) oxidation at the bare GC electrode are about 0.432, 0.554, and 0.268 V, respectively, whereas the respective potentials at the surface of the PDB/MWCNTs modified GC electrode are about 0.411, 0.573, and 0.182 V.

Fig. 3 (D) shows cyclic voltammograms for a mixture of 2 μmol L^{-1}, 60 μmol L^{-1} and 100 μmol $L^{-1}$of LD, UA and AA, respectively in 0.11 mol L^{-1} PBS solution (pH 3.0) at bare GCE, PDB/GCE and PDB/MWCNTs-GCE. As can be seen, at bare GCE the oxidation peaks for LD, UA and AA are overlapped together with low currents and this shows slow electron transfer kinetics. At the PDB/MWCNTs modified GCE, three well-defined oxidation peaks appear at 0.450, 0.607 and 0.255 V for LD, UA and AA, respectively. The oxidation responses of LD, UA and AA show a great enhancement in the peak currents at PDB/MWCNTs-GCE in comparison with PDB-GCE and bare GCE. Also, when we compare the oxidation peak potentials of LD, UA and AA, there is an enhancement of the anodic peak separation at the PDB/MWCNTs-GCE relative to the values specified at the PDB/GCE and bare GCE. So, the LD, UA and AA peaks potential separations are large enough for the determination of these compounds in the presence of each other at PDB/MWCNTs-GCE. The enhancement in the LD, UA and AA oxidation peak current is mainly attributed to the considerable increment in the electroactive area of the electrode due to the presence of MWCNTs. This phenomenon makes possible the determination of all of these compounds with satisfactory separation between their oxidation peak potentials in voltammetry.

3. 3. Effect of pH on the Oxidation of LD

In order to find the optimum pH for determination of LD, the effect of supporting electrolyte pH was studied. In this case, cyclic voltammetry studies were carried out in the pH range of 2.0–9.0 (PBS, 0.11 mol L^{-1}) at the surface of PDB/MWCNTs-GCE. Fig. 4 shows cyclic voltammograms obtained for oxidation of LD at the surface of PDB/MWCNTs-GCE at different pH values. The maximum peak current can be observed at pH 3.0. In addition, all the peak potentials for the oxidation of LD shifted towards negative direction with increasing pH. Therefore, pH 3.0 was selected for further experiments. According to the linear plots of $E_{p,a}$ *vs.* pH concerning the observed slope of –0.057 V/pH for LD (above of the Fig. 4), which is very close to the expected Nernstian value of 0.059 V at 25 °C, where np (number of protons) = ne (number of electrons).

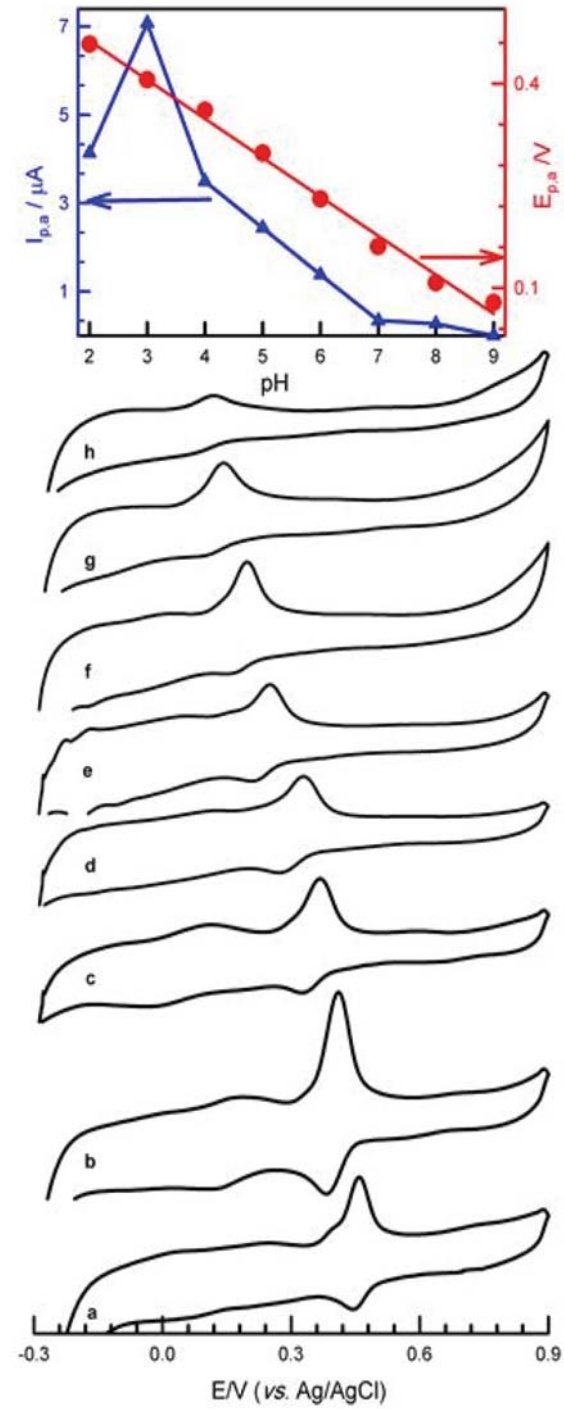

Figure 4. Cyclic voltammograms of 60 μM LD at the PDB/MWCNTs-GCE in 0.11 mol L^{-1} PBS at pH (a) 2.0, (b) 3.0, (c) 4.0, (d) 5.0, (e) 6.0, (f) 7.0, (g) 8.0 and (h) 9.0. The scan rate is 0.100 V s^{-1}. Also, the plots of the extracted $I_{p,a}$ and $E^{0'}$ *vs.* pH are shown above.

3. 4. Chronoamperometry Studies

The catalytic electro-oxidation of LD at the surface of the PDB/MWCNTs-GCE was studied by short time chronoamperometry technique. Fig. 5A indicates the chronoamperograms of the different concentrations of LD in PBS (pH 3.0) obtained on PDB/MWCNTs-GC modified electrode by setting the working electrode potentials to 0.5 V *vs.* Ag/AgCl (KCl 3 mol L^{-1}).

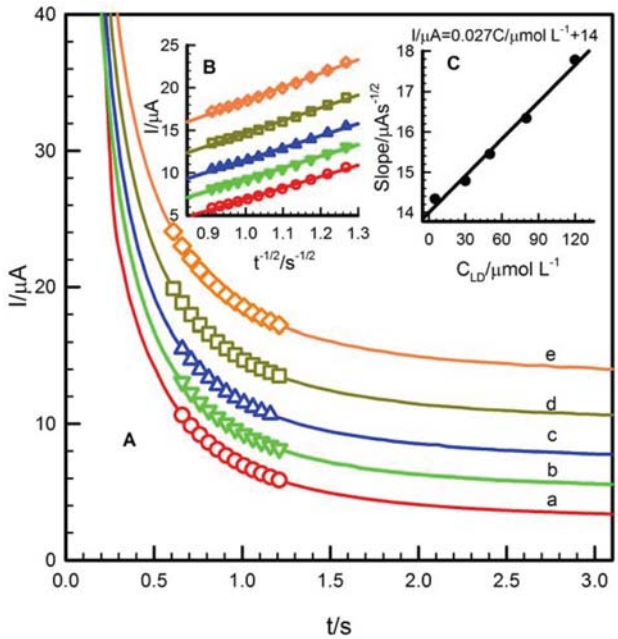

Figure 5. Chronoamperograms of (a) 5.0; (b) 30.0; (c) 50.0; (d) 80.0; (e) 120.0 μmol L^{-1} of LD in PBS (0.11 mol L^{-1}, pH 3.0) obtained on PDB/MWCNTs-GCE, at the initial potential of 0.0 V and step potential of 0.5 V *vs.* Ag/AgCl (KCl 3 mol L^{-1}) (A). The inset shows I as a function of $t^{-1/2}$ (B). The inset shows the slope of lines B as a function of the concentrations of LD (C).

The diffusion coefficient (D) for oxidation of LD at the surface of the modified electrode can be evaluated using Cottrell's equation:

$$I = nFAD^{1/2} C_b \pi^{-1/2} t^{-1/2} \quad (1)$$

Where D and C_b are the diffusion coefficient (cm^2 s^{-1}) and the bulk concentration (mol cm^{-3}), respectively. Under diffusion control conditions, the plots of selected currents versus $t^{-1/2}$ would be linear. The value of D could be evaluated from the slope of these plots, according to the Cottrell equation. Fig. 5B indicates the experimental plots for different concentrations of LD in the range of 5–120 μmol L^{-1}. The mean value of the diffusion coefficients for LD was calculated to be 6.23×10^{-5} cm^2 s^{-1} using the slopes of the resulting straight lines plotted versus the LD concentrations (Fig. 5C).

3. 5. Differential Pulse Voltammetric Determination of LD, UA and AA

Since differential pulse voltammetry (DPV) has a much higher current sensitivity and better resolution than cyclic voltammetry, it was applied for study of LD, UA and AA concentration at PDB/MWCNTs-GCE. Under the optimized solution conditions (0.11 mol L^{-1} PBS, pH 3), the DPVs of various concentrations of LD, UA and AA were separately recorded (Fig. 6). The respective calibration curves of the anodic peak currents for solutions containing different amounts of each analyte were plotted (Fig. 6, inset) and the linear ranges of 0.09–75 μmol L^{-1}, 0.3–110 μmol $L^{-1}$and 10–160 μmol L^{-1}were obtained for LD, UA, and AA, respectively.

The limits of detection (3σ) for determination of LD, UA, and AA on the modified electrode surface, were found to be 3, 2, and 23 nmol L^{-1}, respectively. Also, the modified electrode presented good repeatability. The relative standard deviations (RSDs) for LD at 0.5 μmol L^{-1}, UA at 3 μmol L^{-1}, and AA at 15 μmol L^{-1} were 0.25%, 0.61%, and 2.1%, respectively, for 6 measurements which reveal that the sensor had good repeatability.

3. 6. Simultaneous Determination of LD, UA and AA in the Mixture

The ability of the PDB/MWCNTs modified GC electrode for simultaneous determination of each analyte was

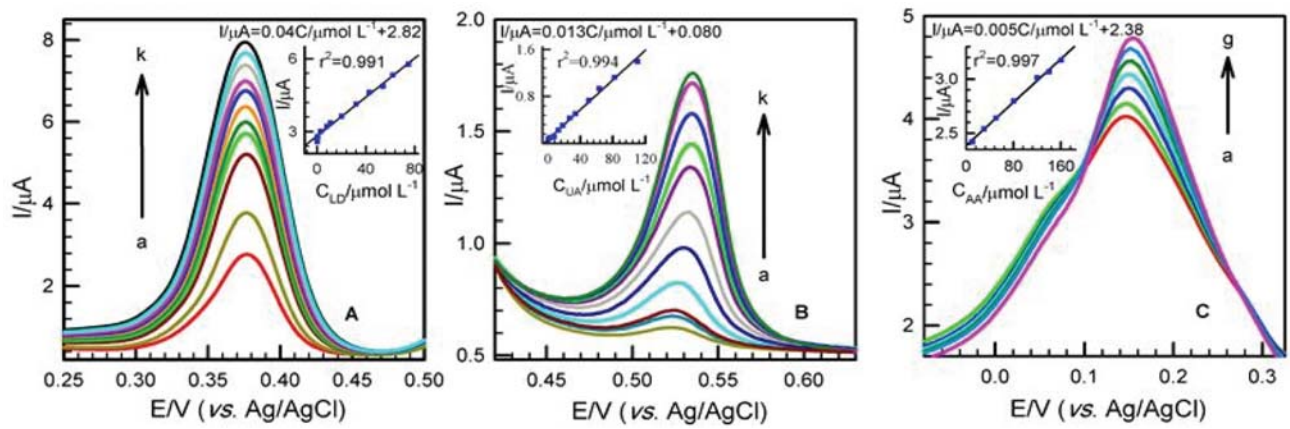

Figure 6. Differential pulse voltammograms of LD (A), UA (B), and AA (C) at PDB/MWCNTs-GCE in 0.11 mol L^{-1} PBS (pH 3). LD concentrations: (a) 0.09, (b) 0.4, (c) 3, (d) 8, (e) 11, (f) 20, (g) 32, (h) 43, (i) 54, (j) 62, (k) 75μmol L^{-1}; UA concentrations: (a) 0.3, (b) 2.5, (c) 7, (d) 12.5, (e) 18, (f) 26.5, (g) 33.5, (h) 50, (i) 63, (j) 82, (k) 110 μmol $L^{-1}$and AA concentrations: (a) 10, (b) 30, (c) 50, (d) 80, (e) 120, (f) 140, (g) 160 μmol L^{-1}. Insets show the calibration lines from the DPVs shown in (A), (B) and (C).

examined by addition of various concentrations of the species in the presence of the constant concentration of the others (Fig. 7). Under the optimal conditions, by increasing of various concentrations of LD, UA and AA, three separated peaks appeared at the potential of about 0.380, 0.520 and 0.180 V, respectively. By increasing the concentration of LD in the presence of 50 μmol L^{-1} UA and 200 μmol L^{-1} AA (Fig. 7A), the peak current of LD increased linearly with increasing LD concentration in the range of 0.8–72 μmol L^{-1} and the related regression calibration is I/μA = 0.10 C/μmol L^{-1}+0.58 (Fig. 7A, inset). It is observable that the oxidation peaks related to UA and AA are approximately constant. Furthermore, different concentrations of UA in the presence of 1.7 μmol L^{-1} LD and 220 μmol L^{-1} AA illustrate excellent DPVs responses (Fig. 7B); the peak current of UA grows linearly by increasing UA concentration in the range of 0.3–110 μmol L^{-1} and the related regression calibration is I/μA = 0.008 C/μmol L^{-1} + 0.11 (Fig. 7B, inset) which shows simultaneous determination of UA in the presence of LD and AA on the surface of PDB/MWCNTs-modified GCE. We also observed oxidation peaks of various amounts of AA in the presence of a constant concentration of LD (2 μmol L^{-1}) and UA (20 μmol L^{-1}) (Fig. 7C). There is no serious variation observed in the peak current of LD and UA, but the peak current of AA in the concentration range of 1–160 μmol L^{-1} increased linearly with calibration regression equation of I/μA = 0.013 C/μmol L^{-1} + 1.0 (Fig. 7C, inset). These results indicate that the electrochemical determination of three analytes in the presence of each other on the PDB/MWCNTs- modified GCE surface is possible independently.

3. 7. Interference Studies

Under the optimal experimental conditions, the influence of various interfering species on the determination of 5.5 μmol L^{-1} LD was investigated. The tolerance limit was taken as the maximum concentration of the foreign compound which caused an approximately ±5% relative error in the determination of the analyte. The experimental results show that neither 500-fold excess concentration of Ni^{2+}, Fe^{3+}, Cu^{2+}, Co^{2+}, Mn^{2+}, Na^{+}, K^{+}, Mg^{2+}, Ca^{2+}, Al^{3+}, Pb^{2+}, Cl^{-}, NO_3^{-}, SO_4^{2-}, PO_4^{3-}, CO_3^{2-}, HCO_3^{-} nor 300-fold excess of glucose, lactose, sucrose, fructose, glycine, L-lysine, and riboflavin did not interfere, but practically equal molar concentrations of dopamine, DOPAC, homovanillic acid, epinephrine, and norepinephrine showed interference on determination of LD.

3. 8. Real Samples Analysis

In order to evaluate the analytical applicability of the proposed sensor, direct determination of LD, UA and AA were applied for two physiological samples (human blood serum). The human blood plasma samples were collected from clinical laboratory and diluted 4 times by 0.11 mol L^{-1} PBS solution (pH 3) without any treatment. The recoveries of these three analytes in blood serum were determined by the standard addition method (Table 1) and satisfactory results were obtained.

These results show that the PDB/MWCNTs-GC modified electrode is an excellent sensitive tool for simultaneous determination of the analytes in physiological samples.

4. Conclusions

In the present work, it was shown that poly-DB/MWCNTs film on the GCE can be considered as a sensitive and selective sensing element in the simultaneous voltammetric determination of LD, UA and AA. The

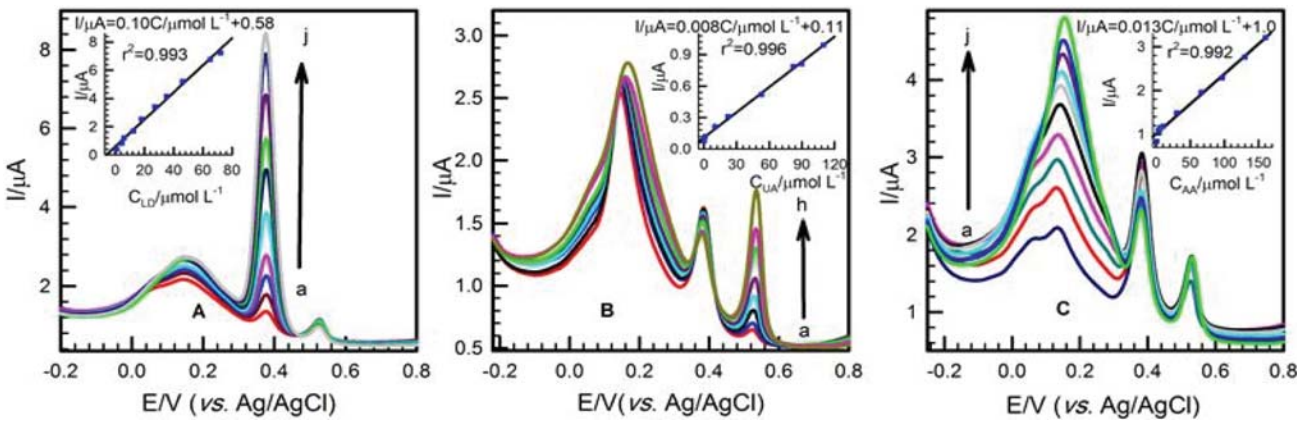

Figure 7. Differential pulse voltammograms of PDB/MWCNTs-GCE in PBS 0.11 mol L^{-1} (pH 3), containing (A) LD concentrations: (a) 0.8, (b) 4.5, (c) 6, (d) 12, (e) 18, (f) 27, (g) 35, (h) 46, (i) 65, (j) 72 μmol L^{-1}in the presence of 50 μmol L^{-1} UA and 200 μmol L^{-1} AA; (B) UA concentrations: (a) 0.3, (b) 1, (c) 10, (d) 22, (e) 53, (f) 82, (g) 90, (h) 110 μmol L^{-1}in the presence of 1.7 μmol L^{-1} LD and 220 μmol L^{-1} AA; (C) AA concentrations: (a) 1, (b) 3, (c) 4.5, (d) 6, (e) 10, (f) 30, (g) 66, (h) 97, (i) 130, (j) 160 μmol L^{-1}in the presence of 2 μmol L^{-1} LD and 20 μmol L^{-1} UA. Insets: The related calibration plots from the DPVs are shown in (A), (B) and (C).

Table 1. Determination and recovery tests of LD, UA and AA in real samples obtained using PDB/MWCNTs-GC modified electrode.

Analyte	Sample	Added(μmol L^{-1})	Found(μmol L^{-1})	Recovery(%)
LD	Serum 1	0	0.112	–
		10	9.909	98.00
	Serum 2	0	0.130	–
		16	16.21	100.5
	Serum 1 [a]	0	0.154	–
		10	10.50	103.5
	Serum 2 [a]	0	0.093	–
		4	3.958	96.70
AA	Serum 1	0	0.297	–
		25	24.60	97.26
	Serum 2	0	0.221	–
		20	20.62	102
UA	Serum 1	0	0.168	–
		20	20.00	99.20
	Serum 2	0	0.087	–
		10	10.52	104.3

[a.] The recovery tests of LD were performed in the presence of 35 μmol L^{-1} AA and 12 μmol L^{-1} UA in real samples

modified electrode showed an effective electrocatalytic activity toward the anodic oxidation of LD, UA and AA, which leads to a significant increase in the peak currents and a decrease in peak over-potentials. The good resolution was observed between the DPV peak potentials of LD, UA and AA, showing this is a very appropriate method for the voltammetric determination of the compounds. This method is financially more reasonable than chromatographic separation methods. Furthermore, sensor production is easy and fast, and there is no need to use complex pretreatment or toxic organic synthetic materials. In other words, they belong to green chemistry.

5. Acknowledgements

The authors gratefully acknowledge the Payame Noor University providing research facilities for this work.

6. References

1. W. J. Weiner, Parkinson's disease: diagnosis and clinical management, Medical Publishing, New York, 2002.
2. T. Madrakian, M. Mohammadnejad, *Chem. Pharm. Bull.* **2007**, *55*, 865–670. https://doi.org/10.1248/cpb.55.865
3. S. F. Li, H. L. Wu, Y. J. Yu, Y. N. Li, J. F. Nie, H. Y. Fu, R. Q. Yu, *Talanta* **2010**, *81*, 805–.812
4. S. Zhao, W. Bai, B. Wang, M. He, *Talanta* **2007**, *73*, 142–146. https://doi.org/10.1016/j.talanta.2007.03.023
5. V. Ladero, N. Martínez, M. C. Martín, M. Fernández, M. A. Alvarez, *Food Res. Int*. **2010**, *43*, 289–295. https://doi.org/10.1016/j.foodres.2009.10.007
6. M. S. M. Quintino, M. Yamashita, L. Angnes, *Electroanalysis* **2006**, *18*, 655–661. https://doi.org/10.1002/elan.200503445
7. C. Zapata-Urzúa, M. Pérez-Ortiz, M. Bravo, A. C. Olivieri, A. Álvarez-Lueje, *Talanta* **2010**, *82*, 962–968. https://doi.org/10.1016/j.talanta.2010.05.071
8. P. Daneshgar, P. Norouzi, M. R. Ganjali, A. Ordikhani-Seyedlar, H. Eshraghi, *Colloids Surf. B* **2009**, *68,* 27–32. https://doi.org/10.1016/j.colsurfb.2008.09.019
9. S. Shahrokhian, E. Asadian, *J. Electroanal. Chem*. **2009**, *636*, 40–46. https://doi.org/10.1016/j.jelechem.2009.09.010
10. H. Beitollahi, J. B. Raoof, R. Hosseinzadeh, *Electroanalysis* **2011**, *23*, 1934–1940. https://doi.org/10.1002/elan.201100242
11. E. Luque-Perez, A. Rios, M. Valcarcel, *Fresenius J .Anal. Chem*. **2000**, *366*, 857–862. https://doi.org/10.1007/s002160051585
12. S. J. Padayatty, A. Katz, Y. H. Wang, P. Eck, O. Kwon, J. H. Lee, S. L. Chen, C. Corpe, A. Dutta, S. K. Dutta, M. Levine, *J. Am. Coll. Nutr.* **2003**, *22*, 18–35. https://doi.org/10.1080/07315724.2003.10719272
13. O. Arrigoni, C. D. Tullio, *Biochim. Biophys. Acta.* **2002**, *1569*, 1–9. https://doi.org/10.1016/S0304-4165(01)00235-5
14. S. Sen, R. Chakraborty, The role of antioxidants in human health, in: S. Andreescu, M. Hepel (Eds.), Oxidative Stress: Diagnostics, Prevention, and Therapy, ACS Symposium Series, Washington, **2011**, Chap. 1, p.1. https://doi.org/10.1021/bk-2011-1083.ch001
15. A. A. Ensafi, M. Taei, T. khayamian, *J. Electroanal. Chem.* **2009**, *633*, 212–220. https://doi.org/10.1016/j.jelechem.2009.06.001
16. S. Shahrokhian, E. Asadin, *Electrochim. Acta* **2010**, *55*, 666–672. https://doi.org/10.1016/j.electacta.2009.08.065

17. E. Popa, Y. Kubota, D. A. Tryk, A. Fujishima, *Anal. Chem.* **2000**, *72*, 1724–1727. https://doi.org/10.1021/ac990862m
18. K. Shi, K. K. Shiu, *Electroanalysis* **2001**, *13*, 1319–1325. https://doi.org/10.1002/1521-4109(200111)13:16<1319::AID-ELAN1319>3.0.CO;2-C
19. A. K. Bhargava, H. Lal, C. S. Pundir, *J. Biochem. Biophys. Methods* **1999**, *39*, 125–192. https://doi.org/10.1016/S0165-022X(99)00007-X
20. D. Yao, A. G. Vlessidis, N. P. Evmriridis, *Anal. Chim. Acta* **2002**, *467*, 133–144. https://doi.org/10.1016/S0003-2670(02)00127-7
21. J. X. Qiao, H. Q. Luo, N. B. Li, *Colloid Surf. B,* **2008**, *62*, 31–35. https://doi.org/10.1016/j.colsurfb.2007.09.012
22. P. Kalimuthu, D. Suresh, S. A. John, *Anal. Biochem.* **2006**, *357*, 188–193. https://doi.org/10.1016/j.ab.2006.07.031
23. X. Yang, J. Kirsch, A. Simonian, *J. Microbiol. Methods* **2013**, *95*, 48–56. https://doi.org/10.1016/j.mimet.2013.06.023
24. X. Yang, J. Kirsch, E. V. Olsen, J.W. Fergus, A.L. Simonian, *Sens. Actuators B* **2013**, *177*, 659–667. https://doi.org/10.1016/j.snb.2012.11.057
25. W. Cai, T. Lai, H. Du, J. Ye, *Sens. Actuators B* **2014**, *193*, 492–500. https://doi.org/10.1016/j.snb.2013.12.004
26. J. B. Raoof, R. Ojani, M. Baghayeri, *Anal. Methods* **2011**, *3*, 2367–2373. https://doi.org/10.1039/c1ay05305a
27. L. M. Niu, K. Q. Lian, H. M. Shi, Y. B. Wu, W. J. Kang, S. Y. Bi, *Sens. Actuators B* **2013**, *178*, 10–18. https://doi.org/10.1016/j.snb.2012.12.015
28. M. Ahn, J. Kim, *J. Electroanal. Chem.* **2012**, *683*, 75–79. https://doi.org/10.1016/j.jelechem.2012.08.012
29. H. R. Zare, N. Rajabzadeh, N. Nasirizadeh, M. Mazloum-Ardakani, *J. Electroanal. Chem.* **2006**, *589,* 60–69. https://doi.org/10.1016/j.jelechem.2006.01.011
30. R. M. Wightman, L. J. May, A. C. Michael, *Anal. Chem.* **1988**, *60*, 769A–793A. https://doi.org/10.1021/ac00164a718
31. T. Selvaraju, R. Ramaraj, *Electrochim. Acta* **2007**, *52*, 2998–3005. https://doi.org/10.1016/j.electacta.2006.09.032
32. R. L. Mc Creery, *Chem. Rev.* **2008**, *108*, 2646–2687. https://doi.org/10.1021/cr068076m
33. M. Mazloum-Ardakani, P. Ebrahimi-Karami, H. Naemi, B. Mirjalili, *Turk. J. Chem.,* **2008**, *32*, 571–584.
34. H. R. Zare, N.N. Nasirizadeh, and M. Mazloum-Ardakani, *J. Electroanal. Chem.***2005**, *577*, 25–33. https://doi.org/10.1016/j.jelechem.2004.11.010
35. X. Chen, F. Wang, Z. Chen, *Anal. Chim. Acta* **2008**, *623*, 213–220. https://doi.org/10.1016/j.aca.2008.06.021
36. A. B. Dalton, S. Collins, E. Munoz, J. M. Razal, V. H. Ebron, J. P. Ferraris, J. N. Coleman, B. G. Kim, R. H. Baughman, *Nature* **2003**, *423*, 703–703. https://doi.org/10.1038/423703a
37. B. E. Kilbride, J. N. Coleman, P. Fournet, M. Cadek, A. Drury, W. J. Blau, *J. Appl. Phys.* **2002**, *92*, 4024–4030. https://doi.org/10.1063/1.1506397
38. J. K. W. Sandler, J. E. Kirk, I. A. Kinloch, M. S. P. Shaffer, A. H. Windle, *Polymer* **2003**, *44*, 5893–5899. https://doi.org/10.1016/S0032-3861(03)00539-1
49. M. J. Biercuk, M. C. Llaguno, M. Radosavljevic, J. K. Hyun, J. E. Fischer, A. T. Johnson, *Appl. Phys. Lett.* **2002**, *80,* 2767–2769. https://doi.org/10.1063/1.1469696
44. C. Wei, K. Srivastava, K. Cho, *Nano Lett.* **2002**, *2*, 647–650. https://doi.org/10.1021/nl025554+
41. M. J. Sims, Q. Li, R. T. Kachoosangi, G. G. Wildgoose, R. G. Compton, *Electrochim. Acta* **2009**, *54*, 5030–5034. https://doi.org/10.1016/j.electacta.2008.10.056
42. R. T. Kachoosangi, G. G. Wildgoose, R. G. Compton, *Anal. Chim. Acta* **2008**, *618*, 54–60. https://doi.org/10.1016/j.aca.2008.04.053
43 . A. Hatefi-Mehrjardi, N. Ghaemi, M.A. Karimi, M. Ghasemi, S. Islami-Ramchahi, *Electroanalysis* **2014**, *26*, 2491–2500. https://doi.org/10.1002/elan.201400302
44. V. Pifferi, G. Cappelletti, C. D. Bari, D. Meroni, F. Spadavecchia, L. Falciola, *Electrochim. Acta* **2014**, *146,* 403–410. https://doi.org/10.1016/j.electacta.2014.09.099
45 J. F. Smalley, K. Chalfant, S. W. Feldberg, T. M. Nahir, E. F. Bowden, *J. Phys. Chem. B* **1999**, *103*, 1676–1685. https://doi.org/10.1021/jp983325z
46. X-L. Xie, Y-W. Mai, X-P. Zhou, *Mater. Sci. Eng. R* **2005**, *49*, 89–112. https://doi.org/10.1016/j.mser.2005.04.002
47. M. Yuqing, C. Jianrong, W. Xiaohua, *Trends Biotechnol.* **2004**, *22*, 227–231. https://doi.org/10.1016/j.tibtech.2004.03.004

Povzetek

Preučevali smo selektiven in občutljiv elektrokemijski senzor na osnovi s poli-dianiks modrim in večstenskimi ogljikovimi nanocevkami (PDB/MWCNT) modificirano elektrodo iz steklastega ogljika za določanje levodope (LD) v prisotnosti sečne kisline (UA) in askorbinske kisline (AA). Za raziskave elektrokatalitske oksidacije LD, UA in AA v vodnih raztopinah smo uporabili metode ciklične voltametrije, diferencialne pulzne voltametrije in kronoamperometrije. Pri tehniki DPV so LD, UA in AA dali oksidacijske vrhove pri 0,380 V, 0,520V in 0,180 V. Pri optimiziranih eksperimentalnih pogojih je bil linearen odgovor za LD v območju 0,09-75 μmol L^{-1}, za UA 0,3–110 μmol L^{-1} in za AA v območju 10–160 μmol L^{-1}. V skladu s tem so bile meje zaznave 0,003, 0,002 in 0,023 μmol L^{-1}. Metoda predstavlja preprost elektrokemijski senzor za uspešno določitev LD v serumskih vzorcih iz humane krvi.

Scientific paper

Mn(II), Zn(II) and Cd(II) Complexes Based on Oxadiazole Backbone Containing Carboxyl Ligand: Synthesis, Crystal Structure, and Photoluminescent Study

Li-Na Wang, Lin Fu, Jia-Wei Zhu, Yu Xu, Meng Zhang, Qi You, Peng Wang and Jie Qin*

School of Life Sciences, Shandong University of Technology, Zibo 255049, P. R. China

** Corresponding author: E-mail: qinjietutu@163.com*
Tel.: 0086-533-2780271; Fax: 0086-533-2781329

Received: 26-11-2016

Abstract

Three coordination polymers, $[Cd(L)_2(H_2O)_2]_n$ (**1**), $[Zn(L)_2(H_2O)_2]_n$ (**2**) and $[Mn(L)_2]_n$ (**3**) were prepared by reacting 5-(3-pyridyl)-1,3,4-oxadiazole-2-thioacetic acid (**HL**) with corresponding metal acetate in DMF/CH_3CN medium under solvothermal condition. The isolated complexes were characterized by elemental analysis and infrared spectroscopy. The X-ray crystallographic analysis revealed double strand structure of **1** and **2**, and 3D framework of **3**. The different structures of these complexes indicate that the configuration of the ligand and the reaction condition play a key role in self-assemble of complexes **1**–**3**. Furthermore, photoluminescent properties of **1** and **2** were also studied in the solid state.

Keywords: Oxadiazole ligand; solvent thermal synthesis; crystal structure; photoluminescent property

1. Introduction

Nowadays, more and more attention has been paid to coordination compounds with various of topological structures and potential promising applications ranging from functional material to therapeutic agent.[1–6] Many factors need to be considered during the self-assembly process of coordination compound, including the nature of the metal ion, the well-designed organic ligand, the auxiliary ligand, the solvent medium, the pH value, the temperature, and so on.[7] Therefore the rational design and precise crystal engineering of coordination compounds with desired structures and specific properties still remain a challenge.[8] According to previously reported work, the choice of organic ligand has been verified as a decisive role in the construction of the overall architectures of coordination polymers, as the organic spacer serves to link metal nodes and to propagate the structural information.[9,10]

Rigid linear organic ligands such as 4,4'-bipyridine and its derivatives are well adopted in generating polymers bearing linear chain,[11] honeycomb-like,[12] square-like,[13] or brick-wall-like structures.[14,15] While the bent organic ligands can offer the possibility of constructing novel polymer network owing to their variable conformation.[15] 1,3,4-Oxadiazole is an intensively investigated class of bent organic bridging moiety due to its convenient synthesis as well as the versatile coordination mode.[9,16–18] Coordination polymers, with structures like helical chain,[19] zeolite-like net,[16] and 3-fold interpenetrated 3D framework,[15] have been reported by Dong group. They are based on symmetric 2,5-diaryl-1,3,4-oxadiazole containing pyridyl, aminophenyl or cyanophenyl groups as terminal coordination sites. Herein we focus on the coordination behavior of 5-(3-pyridyl)-1,3,4-oxadiazole-2-thioacetate (**L**), which is mostly based upon the following considerations. (i) **L** is an unsymmetric ligand bearing both pyridine and carboxyl groups bridged by the oxadiazole backbone. Hence **L** can show diverse coordination modes. Especially the carboxyl group can feature unidentate, chelate or bridging fashions.[20] (ii) **L** is a bent ligand, which can adopt either *gauche*- or *anti*-configuration in the self-assembly reaction (Scheme 1).[8,20] (iii) Heteroatoms such as N, O, and S of **L** could be considered as potential hydrogen bond acceptors to expand polymeric frameworks via hydrogen bonding interactions.[16] Coordination polymers based on **L** and its isomer 5-(4-pyridyl)-1,3,4-oxadiazole-2-thioacetate (**4-pyoa**) were first reported by Du et al. under the layer separation diffusion condition.[20]

Reaction of **HL** and **4-pyoa** with metal salts afforded 1D coordination polymers of $\{[M_2(4\text{-pyoa})_4(H_2O)_2](H_2O)_2\}_n$ (M = Co, Zn), anatase type network of $\{[Pb(4\text{-pyoa})_2](H_2O)\}_n$, 2D layer of $\{[Cu(L)_2(H_2O)](H_2O)_2\}_n$, and 3,6-connected 3D net of $[Cd(L)_2]_n$.[20] Indeed, this demonstrates that **HL** is well-tailored in constructing new polymers with attractive properties.

The aim of the presented work is the construction of complexes derived from **HL** under solvent thermal condition. The reactions of **HL** and $M(CH_3COO)_2$ (M = Cd, Zn, and Mn) in DMF/CH_3CN at 110 °C afford three polymers, $[Cd(L)_2(H_2O)_2]_n$ (**1**), $[Zn(L)_2(H_2O)_2]_n$ (**2**) and $[Mn(L)_2]_n$ (**3**). Herein, the preparation, and crystallographic analyses of these complexes are described. Moreover, luminescent properties of **1** and **2** were investigated in the solid state.

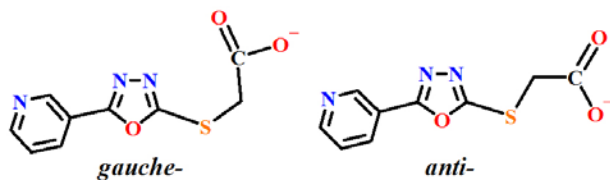

Scheme 1. Two possible configurations of **L**.

2. Experimental

2. 1. Physical Measurements and Materials

Reagents and solvents were purchased commercially from Aladdin Industrial Corporation (China) and used without further purification. The starting compound **HL** was synthesized according to the literature method.[20,21] The IR spectra were taken on a Vector22 Bruker spectrophotometer (400–4000 cm^{-1}) prepared as KBr pellets. Elemental analyses were performed on a Perkin-Elmer model 2400 analyzer. Fluorescence spectra were recorded on Cary Eclipse spectrofluorimeter (Varian, Australia) at room temperature.

2. 2. General Procedure for the Synthesis of Complexes 1–3

HL (0.1 mmol) and metal acetate salts (0.2 mmol) in 10 mL mixed solvent of DMF/CH_3CN (v/v = 1:1) were sealed in a 25 mL Teflon cup. The mixture was heated at 110 °C for 3 days and cooled to room temperature at a rate of 5°C/h. Yellow crystals were obtained.

$[Cd(L)_2(H_2O)_2]_n$ (**1**) Yield: 15.8 mg (51% on the basis of **HL**). The IR (KBr, cm^{-1}): 3446, 3098, 3033, 1607, 1577, 1474, 1462, 1438, 1393, 1222, 1198, 1091, 1049, 1031, 999, 960, 821, 715, 701, 684, 640, 443. Anal. Calcd. for $C_{18}H_{16}CdN_6O_8S_2$: C, 34.82; H, 2.60; N, 13.53. Found: C, 34.92; H, 2.59; N, 13.57%.

$[Zn(L)_2(H_2O)_2]_n$ (**2**) Yield: 13.8 mg (48% on the basis of **HL**). IR (KBr, cm^{-1}): 3468, 3085, 3067, 2985, 1646, 1614, 1459, 1417, 1364, 1326, 1191, 1087, 1052, 1004, 959, 820, 712, 698, 650, 537. Anal. Calcd. for $C_{18}H_{16}ZnN_6O_8S_2$: C, 37.67; H, 2.81; N, 14.64. Found: C, 37.82; H, 2.80; N, 14.69%.

$[Mn(L)_2]_n$ (**3**) Yield: 8.4 mg (32% on the basis of **HL**). IR (KBr, cm^{-1}): 3033, 1574, 1462, 1393, 1196, 1088, 1046, 996, 921, 819, 679, 639, 441. Anal. Calcd. for $C_{18}H_{12}MnN_6O_6S_2$: C, 40.99; H, 2.93; N:15.93. Found: C, 41.12; H, 2.91; N, 15.99%.

Table 1. Crystallographic data for **1–3**.

	1	2	3
Empirical formula	$C_{18}H_{16}CdN_6O_8S_2$	$C_{18}H_{16}ZnN_6O_8S_2$	$C_{18}H_{12}MnN_6O_6S_2$
M_r	620.89	573.86	527.40
Crystal System	triclinic	triclinic	monoclinic
Space group	P–1	P–1	C2/c
a (Å)	7.4145(11)	7.3585(6)	25.302(3)
b (Å)	7.6738(11)	7.4216(7)	10.6816(11)
c (Å)	10.6697(15)	10.7069(9)	7.1462(7)
α (°)	88.064(4)	88.979(3)	90.00
β (°)	82.611(4)	82.757(2)	95.747(3)
γ (°)	74.497(4)	73.709(3)	90.00
V (Å^3)	580.13(14)	556.67(8)	1921.7(3)
Z	1	1	4
ρ_c (g cm^{-3})	1.777	1.712	1.823
F(000)	310	292	1068
T / K	298(2)	298(2)	298(2)
μ(Mo-Kα)/ mm^{-1}	1.179	1.351	0.960
GOF (F^2)	1.131	1.084	1.107
Data / restraints / parameters	2614 / 0 / 160	2531 / 0 / 160	2207 / 0 / 150
R_1[a], wR_2[b] (I>2σ(I))	0.0205, 0.0540	0.0245, 0.0611	0.0248, 0.0662

[a] $R_1 = \sum||Fo| - |Fc||/\sum|Fo|$. [b] $wR_2 = [\sum w(Fo^2 - Fc^2)^2/\sum w(Fo^2)]^{1/2}$

2. 3 Determination of Crystal Structures

X-ray intensity data for crystals **1**–**3** were collected on a Bruker SMART APEX CCD-based diffractometer (Mo Kα radiation, λ = 0.71073 Å) at 298 K. The raw frame data were integrated into SHELX format reflection files and corrected for Lorentz and polarization effects using SAINT.[22] Multi-scan absorption corrections were applied by SADABS.[23] All the structures were solved by direct methods and refined by full-matrix least-square methods applying SHELXL program package.[24] Anisotropic thermal parameters were used to refine all non-hydrogen atoms. H atoms of C–H were geometrically generated and refined with isotropic thermal parameters riding on the parent atoms. The H atoms of water molecules were fixed by difference Fourier maps with O–H = 0.85(2) Å, H···H = 1.44(2) Å and U_{iso}(H) = 1.5U_{eq}(O). Details of crystallographic parameters, data collection, and refinements are summarized in Table 1. Relevant bond distances and bond angles are given in Tables 2, 3 and S1.

3. Results and Discussion

3. 1. Synthesis and General Characterization

The mixing of metal salts and carboxylic ligand solution resulted in precipitation in traditional aqueous reaction system therefore solvothermal synthesis was adopted. By performing parallel experiments, it was found that using $M(NO_3)_2$ or $M(ClO_4)_2$ (M = Cd, Zn, Mn) as the source of metal salts could also isolate these complexes, which indicates that the complexes are independent of the counter-anions of the metal salts. The acetate salts were found to achieve products in a somewhat higher crystal quality and yield.

3. 2. IR Spectra

The IR spectra of complexes **1**–**3** (see Figure S1, Supporting Information) exhibiting the absence of characteristic absorption bands of the carboxyl group (1718 cm^{-1} in **HL**) reveals the complete deprotonation. As a consequence, the antisymmetric (ν_{as}(COO$^-$)) and symmetric (ν_s(COO$^-$)) stretching vibrations of carboxylate groups appear. The separation value $\Delta\nu$ between ν_{as}(COO$^-$) and ν_s(COO$^-$) can be used to identify the coordination mode of the carboxylate ligand.[25,26] The $\Delta\nu$ value is 214 cm^{-1} for **1**, 229 cm^{-1} for **2**, indicating a monodentate coordination mode of carboxylate group. While the $\Delta\nu$ value for **3** is 181 cm^{-1} indicative of bidentate carboxylate coordination. These IR results are in agreement with the crystal structural analyses.

3. 3. Crystal Structures

X-ray single-crystal diffraction reveals that complexes **1** and **2** are isostructural and crystallize in the same triclinic $P\bar{1}$ space group with similar cell parameters. Therefore only the structure of **1** is described here in detail as a representative example. The ORTEP plots of complexes **1** and **2** with atomic numbering scheme are shown in Figures 1 and S2

As drawn in Figure 1, the Cd^{II} ion is located at the inversion center, and the asymmetric unit of compound **1** is composed of one Cd^{II} ion with the occupancy of 0.5, one L^{1-} ligand, and one coordinated water molecule. The central Cd^{II} is six coordinate with two N and two O atoms from four crystallographically independent L^{1-}, and two water O atoms. The coordination geometry of the {CdN_2O_4} can be described as an almost perfect octahe-

Table 2. Selected bond distances (Å) and angles (°) for complex **1**.

Cd1–O4	2.3030(13)	Cd1–O3^{iii}	2.2584(14)
Cd1–N1	2.3703(14)	S1–C7	1.7275(18)
S1–C8	1.8042(19)	O2–C9	1.242(2)
O3–C9	1.251(2)		
N1–Cd1–N1^{i}	180.000(1)	O3^{iii}–Cd1–N1	90.24(6)
O4^{i}–Cd1–N1^{i}	91.59(5)	O3^{iii}–Cd1–O4	91.31(5)
O3^{ii}–Cd1–O4	88.69(5)	O4–Cd1–O4^{i}	180.0
O3^{ii}–Cd1–N1	89.76(6)	O4^{i}–Cd1–N1	88.41(5)
C7–S1–C8	98.83(9)		

Symmetry codes: (i) –x, –y + 1, –z + 2; (ii) –x + 1, –y + 1, –z + 1; (iii) x – 1, y, z + 1

Table 3. Selected bond distances (Å) and angles (°) for complex **3**

Mn1–O2	2.1024(10)	Mn1–O3^{ii}	2.1878(10)
Mn1–N1^{iii}	2.3479(11)	S1–C7	1.7235(14)
S1–C8	1.7969(14)	O2–C9	1.2453(17)
O3–C9	1.2485(17)		
N1^{iii}–Mn1–N1^{i}	94.98(6)	O2–Mn1–O2^{iv}	93.00(6)
O2–Mn1–O3^{v}	103.46(4)	O2^{i}–Mn1–O3^{v}	92.20(4)
O3$^{\#v}$–Mn1–O3$^{\#ii}$	157.28(6)	O2–Mn1–N1^{iii}	176.41(4)
O2^{iv}–Mn1–N1^{iii}	86.11(4)	O3^{v}–Mn1–N1^{iii}	80.06(4)
O3^{ii}–Mn1–N1^{iii}	84.63(4)	C7–S1–C8	98.76(6)

Symmetry codes: (i) –x + 3/2, y – ½, –z + ½; (ii) x, –y + 1, z – ½; (iii) x – ½, y – ½, z; (iv) –x + 1, y, –z + ½; (v) –x + 1, –y + 1, –z + 1

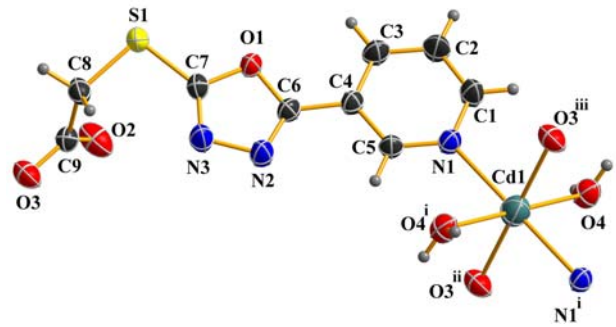

Figure 1. Coordination environment of Cd^{II} in **1**. Symmetry codes: (i) –x, –y + 1, –z + 2; (ii) –x + 1, –y + 1, –z + 1; (iii) x – 1, y, z + 1.

dron, which is reflected by the axial N1–Cd–N1^{i} 180.0°, and the sum of the equatorial bond angels being 360.0°. The *gauche* style of the ligand is observed in complex **1**, which was confirmed by the value of the torsion angle of C7–S1–C8–C9 being –70.94(15)°.

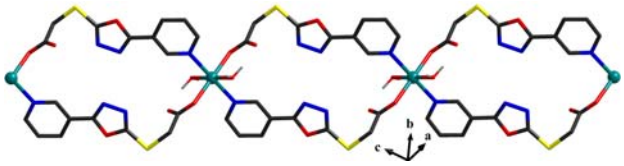

Figure 2. 1D coordination framework of **1**.

Du and coworkers have prepared the complex $[Cd(L)_2]_n$ (**1A**) in CH_3OH/H_2O-NaOH mixed solvent system at room temperature using $Cd(NO_3)_2$ and **HL**.[20] In **1A**, the octahedral coordination sphere of Cd^{II} is provided by four carboxylate O and two pyridyl N atoms coming from six separated ligands. The authors ascribed this coordination geometry to the metal–ligand synergistic effect that the Cd^{II} ion with larger radii is capable of holding six ligands around it. In **1A**, the ligand serves as a 3-connected node resulting in the 3D rutile framework. While in complex **1**, the pyridyl and the carboxylic groups both adopted the monodentate coordination mode acting as 2-connected node. The Cd^{II} ions are bridged by paired **L** ligands. As a consequence, 1-D double-strand coordination array of **1** is formed running along [1 0 –1] direction with Cd···Cd separation of 12.1848(14) Å (Figure 2). The Cd–$N_{pyridyl}$ bond length (2.3703(14) Å) is comparable to that in **1A** (2.373(2) Å), while the Cd–$O_{carboxylic}$ bond length in **1** being 2.2584(14) Å is longer than that in **1A** 2.291(2) Å. The intra-chain hydrogen bond interactions were found between the uncoordinated carboxylic O atoms and the coordinated water molecules (O4–H4B···O2^{iii}, symmetric code: (iii) $x - 1$, y, $z + 1$).

Analysis of the crystal packing of **1** reveals the existence of two types of inter-chain hydrogen bonds, including O4–H4A···O2^{iv} and O4–H4A···S1^{iv} (symmetric code: (iv): $-x$, $-y + 1$, $z + 1$) between the water ligands and the uncoordinated carboxylic O atoms as well as S atoms. Therefore, these 1D chains are connected through these hydrogen bonds, forming a two-dimensional supramolecular layer along the [001] plane, as depicted in Figure 3.

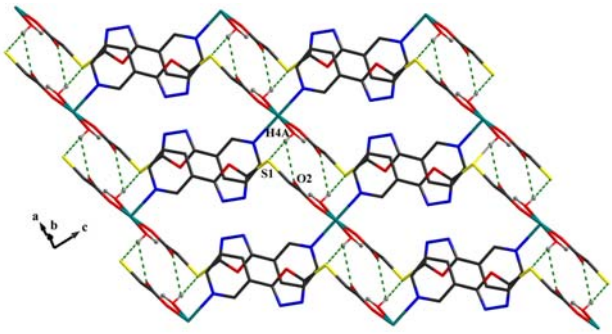

Figure 3. View of the 2D hydrogen-bonding supramolecular layer in **1**.

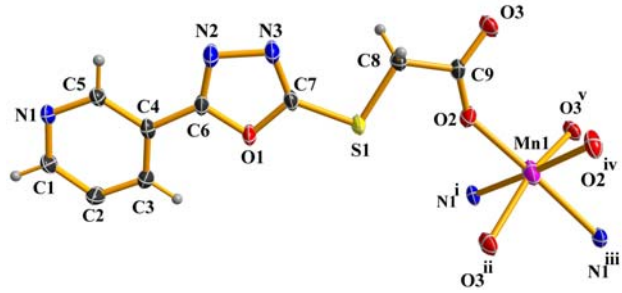

Figure 4. The coordination environment of Mn(II) in **3** at 50% probability displacement. Symmetry codes: (i) $-x + 3/2$, $y - ½$, $-z + ½$; (ii) x, $-y + 1$, $z - ½$; (iii) $x - ½$, $y - ½$, z; (iv) $-x + 1$, y, $-z + ½$; (v) $-x + 1$, $-y + 1$, $-z + 1$.

Polymer **3** crystallized in monoclinic *C*2/*c* space group. As illustrated in Figure. 4, the independent unit of **3** is composed of half Mn(II) cation and one deprotonated ligand L^{1-}. The L^{1-} serves as a μ_3-bridging ligand in **3**, which is identical to that in complex **1A.** The Mn center is hexa-coordinated in distorted octahedron coordination geometry and is bonded by four carboxyl oxygen atoms from four L^{1-} anions [Mn1–O2 = 2.1024(10) Å; Mn1–O3 = 2.1878(10) Å], and two pyridine nitrogen atoms from the other two ligands with Mn–N bond lengths of 2.3479(11) Å. The N1^{i}, O3^{ii}, O2^{iv} and O3^{v} are located in the equatorial plane, while the O2 and N1^{iii} atoms occupy the axial positions. The difference of coordination geometry between Mn^{II} in **3** and Cd^{II} in **1A** lies in that the pyridine N atoms are in the axial positions in **1A**.[20] The Mn–O and Mn–N bond distances are close to other manganese complexes derived from (4-pyridylthio)acetic acid (PTA), such as [(Mn-salen)PTA] and $[Mn(PTA)_2(H_2O)]_n$.[27,28] Compared with complexes **1** and **2**, the ligand adopted *anti*-configuration in **3** as evidenced by the torsion angle of C7–S1–C8–C9 being –167.9°.

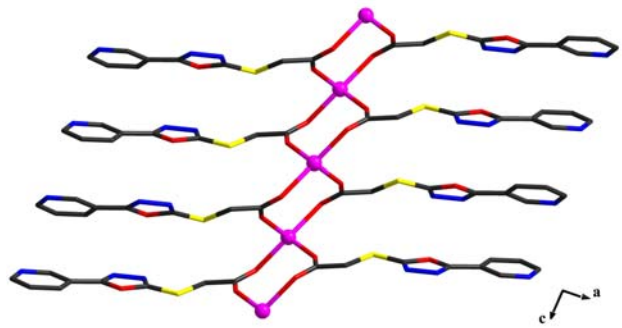

Figure 5. The1D chain structure in **3**.

In **3** the adjacent Mn^{II} centers are doubly bridged by the carboxyl groups of L^{1-}, forming an infinite chain structure along the *c* direction, with a Mn···Mn distance of 4.567(4) Å (Figure 5). In each L^{1-} ligand, the mean plane of the carboxylate group and the plane of the pyridine group are inclined to each other with a dihedral angle of 19.2°. Such 1D chains are aligned side by side in the *ab* plane, and are further linked together by Mn1–N1 linkages, eventually forming the three dimensional network of **3** (Figure 6).

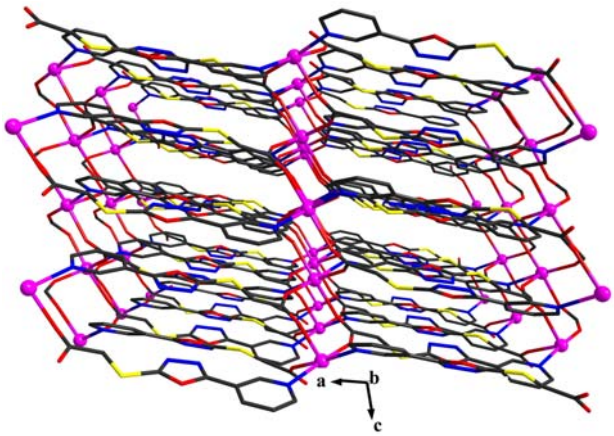

Figure 6. The 3D network of **3**.

3. 4. Photoluminescent Properties

Taking into account that coordination compounds based on d^{10} metal centers are promising candidates for photoactive materials with potential applications,[29,30] the ambient temperature photoluminescent properties of **1** and **2** as well as the free ligand **HL** were measured in the solid state.

As depicted in Figure 7, upon excitation at 290 nm, the free compound **HL** has an emission band maxima at 325 nm. The emission of **HL** can be assigned to the π* to π and π* to n intraligand transitions.[31,32] As Cd^{2+} or Zn^{2+} ions are difficult to oxidize or reduce owning to their d^{10} configuration,[33] the emission spectra of complexes **1** and **2** are similar with that of **HL**. Hence the luminescent emissions of **1** and **2** are attributed to the intraligand transition. Moreover, approximately a three-time increase in the luminescence intensity was observed for complexes compared with the free ligand. The red shifts (10 nm for **1** and 17 nm for **2**) and enhancement of luminescence intensity of the complexes may be ascribed to the deprotonation and coordination to metal ions, which can effectively enhance the rigidity of **HL** and further reduce the loss of energy by radiationless decay of the intraligand emission excited state.[34]

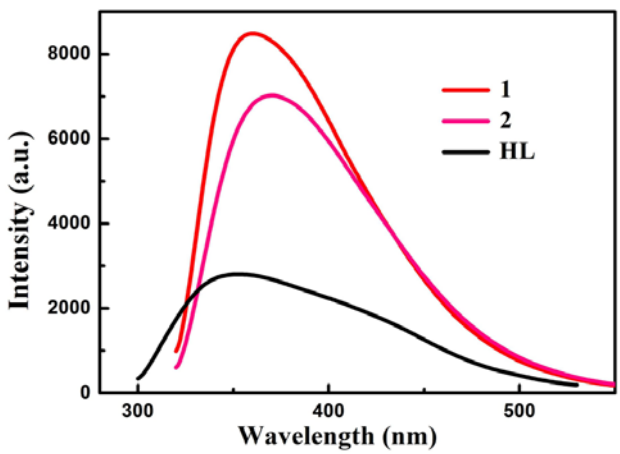

Figure 7. Solid state emission spectra of compounds **HL**, **1** and **2** at room temperature.

4. Conclusions

To sum up, three Cd(II), Zn(II) and Mn(II) coordination polymers based on semirigid asymmetric ligand 5-(3-pyridyl)-1,3,4-oxadiazole-2-thioacetate were successfully prepared. Complexes **1** and **2** are double-strand structures, and two-dimensional supramolecular networks were further observed through O–H···O and O–H···S hydrogen bonding interactions. While **3** features three-dimensional framework. The structural diversity reveals that the configuration of the ligand and the reaction condition play an important role during the self-assembly process of complexes **1**–**3**. In addition, complexes **1** and **2** exhibit intense blue fluorescent emission indicating promising candidates for functional inorganic-organic photoactive materials.

5. Supplementary Material

Crystallographic data (excluding structure factors) for the structural analysis have been deposited with the Cambridge Crystallographic Data Center as supplementary publication Nos. CCDC 1518672 (**1**), 1518673 (**2**), and 1518674 (**3**). Copies of the data can be obtained free of charge *via* www.ccdc.ac.uk/conts/retrieving.html (or from The Director, CCDC, 12 Union Road, Cambridge CB2 1EZ, UK, Fax: +44-1223-336-033. E-mail: deposit@ccdc.cam.ac.uk).

6. Acknowledgment

This work was supported by the National College Students' Innovative and Entrepreneurial Training Plan of China (201510433068) and Natural Science Foundation of Shandong Province (ZR2011HM065).

7. References

1. W. J. Gee, L. K. Cadman, H. A. Hamzah, M. F. Mahon, P. R. Raithby, A. D. Burrows, *Inorg. Chem.* **2016**, *55*, 10839–

10842. https://doi.org/10.1021/acs.inorgchem.6b01917
2. J. Qin, N. Qin, C. H. Geng, J. P. Ma, Q. K. Liu, D. Wu, C. W. Zhao, Y. B. Dong, *CrystEngComm.* **2012**, *14*, 8499–8508. https://doi.org/10.1039/c2ce25561h
3. R. Vafazadeh, A. C. Willis, *Acta Chim. Slov.* **2016**, *63*, 186–192. https://doi.org/10.17344/acsi.2016.2263
4. J. Qin, S. S. Zhao, Y. P. Liu, Z. W. Man, P. Wang, L. N. Wang, Y. Xu, H. L. Zhu, *Bioorg. Med. Chem. Lett.* **2016**, *26*, 4925–4929. https://doi.org/10.1016/j.bmcl.2016.09.015
5. J. Qin, Q. Yin, S. S. Zhao, J. Z. Wang, S. S. Qian, *Acta Chim. Slov.* **2016**, *63*, 55–61. https://doi.org/10.17344/acsi.2015.1918
6. J. X. Qi, S. C. Liang, Y. Gou, Z. L. Zhang, Z. P. Zhou, F. Yang, H. Liang, *Eur. J. Med. Chem.* **2015**, *96*, 360–368. https://doi.org/10.1016/j.ejmech.2015.04.031
7. S. Mohapatra, S. Adhikari, H. Riju, T. K. Maji, *Inorg. Chem.* **2012**, *51*, 4891–4893. https://doi.org/10.1021/ic300237e
8. M. Du, X. J. Zhao, Y. Wang, *Dalton Trans.* **2004**, 2065–2072. https://doi.org/10.1039/B403498H
9. Y. B. Dong, J. P. Ma, M. D. Smith, R. Q. Huang, B. Tang, D. S. Guo, J. S. Wang, H. C. zur Loye, *Solid State Sci.* **2003**, *5*, 601–610. https://doi.org/10.1016/S1293-2558(03)00041-4
10. Y. Bai, J. L. Wang, D. B. Dang, M. M. Li, J. Y. Niu, *CrystEngComm.* **2012**, *14*, 1575–1581. https://doi.org/10.1039/C1CE06030A
11. A. J. Blake, N. R. Champness, P. Hubberstey, W. S. Li, M. A. Withersby, M. Schröder, *Coord. Chem. Rev.* **1999**, *183*, 117–138. https://doi.org/10.1016/S0010-8545(98)00173-8
12. L. R. MacGillivray, S. Subramamian, M. J. Zaworotko, *J. Chem. Soc., Chem. Commun.* **1994**, 1325–1326. https://doi.org/10.1039/c39940001325
13. M. Fujita, Y. J. Kwon, S. Washizu, K. Ogura, *J. Am. Chem. Soc.* **1994**, *116*, 1151–1152. https://doi.org/10.1021/ja00082a055
14. M. Fujita, Y. J. Kwon, O. Sasaki, K. Yamaguchi, K. Ogura, *J. Am. Chem. Soc.* **1995**, *117*, 7287–7288. https://doi.org/10.1021/ja00132a046
15. Y. B. Dong, H. X. Xu, J. P. Ma, R. Q. Huang, *Inorg. Chem.* **2006**, *45*, 3325–3343. https://doi.org/10.1021/ic052158w
16. Y. B. Dong, J. Y. Chen, R. Q. Huang, *Inorg. Chem.* **2003**, *42*, 5699–5706. https://doi.org/10.1021/ic034306t
17. W. Zhang, W. He, X. R. Guo, Y. W. Chen, L. M. Wu, D. C. Guo, *J. Alloy Compd.* **2015**, *620*, 383–389. https://doi.org/10.1016/j.jallcom.2014.09.153
18. C. Köhler, E. Rentschler, *Eur. J. Inorg. Chem.* **2016**, 1955–1960. https://doi.org/10.1002/ejic.201501278
19. J. P. Ma, Y. B. Dong, R. Q. Huang, M. D. Smith, C. Y. Su, *Inorg. Chem.* **2005**, *44*, 6143–6145. https://doi.org/10.1021/ic0505504
20. Z. H. Zhang, M. Du, *CrystEngComm.* **2008**, *10*, 1350–1357. https://doi.org/10.1039/b803736a
21. R. H. Omar, B. A. El-Fattah, *Egypt. J. Pharm. Sci.* **1985**, *24*, 49–56.
22. Bruker, SMART and SAINT. Bruker AXS Inc., Madison, Wisconsin, USA, **2002**.
23. G. M. Sheldrick, SADABS. Program for Empirical Absorption Correction of Area Detector, University of Göttingen, Germany, **1996**.
24. G. M. Sheldrick, *Acta Crystallogr.* **2008**, *A64*, 112–122. https://doi.org/10.1107/S0108767307043930
25. X. H. Bu, M. L. Tong, Y. B. Xie, J. R. Li, H. C. Chang, S. Kitagawa, J. Ribas, *Inorg. Chem.* **2005**, *44*, 9837–9846. https://doi.org/10.1021/ic050886d
26. M. Almáši, Z. Vargová, D. Sabolová, J. Kudláčová, D. Hudecová, J. Kuchár, L.Očenášová, K. Györyová, *J. Coord. Chem.* **2015**, *68*, 4423–4443. https://doi.org/10.1080/00958972.2015.1101074
27. H. Byrd, R. S. Buff, J. M. Butler, G. M. Gray, *J. Chem. Crystallogr.* **2003**, *33*, 515–519. https://doi.org/10.1023/A:1024211021089
28. W. Chiang, D. M. Ho, D. V. Engen, M. E. Thompson, *Inorg. Chem.* **1993**, *32*, 2886–2893. https://doi.org/10.1021/ic00065a015
29. L. Y. Kong, X. H. Lu, Y. Q. Huang, H. Kawaguchi, Q. Chu, H. F. Zhu, W. Y. Sun, *J. Solid State Chem.* **2007**, *180*, 331–338. https://doi.org/10.1016/j.jssc.2006.10.029
30. Y. J. Cui, Y. F. Yue, G. D. Qian, B. L. Chen, *Chem. Rev.* **2012**, *112*, 1126–1162. https://doi.org/10.1021/cr200101d
31. Y. D. Zhang, Z. W. Du, X. G. Luo, *Z. Anorg. Allg. Chem.* **2015**, *641*, 2637–2640. https://doi.org/10.1002/zaac.201500617
32. L. Croitor, E. B. Coropceanu, A. V. Siminel, O. Kulikova, V. I. Zelentsov, T. Datsko, M. S. Fonari, *CrystEngComm.* **2012**, *14*, 3750–3758. https://doi.org/10.1039/c2ce00020b
33. A. Thirumurugan, S. Natarajan, *Dalton Trans.* **2004**, *28*, 2923–2928. https://doi.org/10.1039/b408403a
34. J. F. Fang, J. X. Cheng, S. T. Huang, J. Zhang, C. Q. Ni, Y. J. Xiong, Q. Chen, F. F. Zhu, Y. Li, S. T. Yue, *Z. Anorg. Allg. Chem.* **2015**, *641*, 2657–2663. https://doi.org/10.1002/zaac.201500613

Povzetek

Pripravili smo tri koordinacijske polimere $[Cd(L)_2(H_2O)_2]_n$ (**1**), $[Zn(L)_2(H_2O)_2]_n$ (**2**) in $[Mn(L)_2]_n$ (**3**) z reakcijo med 5-(3-piridil)-1,3,4-oksadiazol-2-tioocetno kislino (**HL**) z ustreznim kovinskim acetatom v mešanici DMF/CH_3CN pri solvotermalnih pogojih. Izolirane komplekse smo okarakterizirali z elementno analizo in infrardečo spektroskopijo. Rentgenska strukturna analiza razkrije strukturo dvojne vijačnice pri spojinah **1** in **2** ter 3D mrežo pri **3**. Različne strukture teh kompleksov kažejo, da imajo konfiguracija liganda in reakcijski pogoji ključno vlogo pri zlaganju v kristalno strukturo. Proučili smo tudi fotoluminiscenčne lastnosti **1** in **2** v trdnem stanju.

 DOI: 10.17344/acsi.2016.3116 *Acta Chim. Slov.* **2017,** *64,* 208–214

Scientific paper

Synthesis and Structure of $[Cu(Hapn)]NO_3]NO_3$, $[Cu(Hapn)(H_2O)_2]SiF_6$, $[Cu(Hapn)(H_2O)BF_4]BF_4 \cdot H_2O$ and $[Cu(Hapn)(NH_2SO_3)_2]$ π-complexes (apn = 3-(prop-2-en-1-ylamino)propanenitrile)

Mykhailo Luk'yanov,[1,*] Evgeny Goreshnik,[2] Vasyl Kinzhybalo,[3] and Marian Mys'kiv[1]

[1] *Department of Inorganic Chemistry, Ivan Franko National University of Lviv, Kyryla i Mefodiya Str., 6, 79005, Lviv, Ukraine*

[2] *Department of Inorganic Chemistry and Technology, Jožef Stefan Institute, Jamova 39, SI-1000 Ljubljana, Slovenia*

[3] *Institute of Low Temperature and Structure Research, Okólna 2, Wrocław, 50-422, Poland*

* *Corresponding author: E-mail: mishalukianov@gmail.com; Tel.: +380 32 23 94 506*

Received: 29-11-2016

Abstract

Four copper(I) π-complexes: $[Cu(Hapn)NO_3]NO_3$ (**1**), $[Cu(Hapn)(H_2O)_2]SiF_6$ (**2**), $[Cu(Hapn)(H_2O)BF_4]BF_4 \cdot H_2O$ (**3**) and $[Cu(Hapn)(NH_2SO_3)_2]$ (**4**) were prepared using alternating-current electrochemical technique, starting from alcohol solutions of 3-(prop-2-en-1-ylamino)propanenitrile (apn) titrated with appropriate acid and copper(II) salts ($Cu(NO_3)_2 \cdot 3H_2O$, $CuSiF_6 \cdot 4H_2O$, $Cu(BF_4)_2 \cdot 6H_2O$ or $Cu(NH_2SO_3)_2 \cdot xH_2O$, respectively). Obtained compounds were characterized by single-crystal X-ray diffraction and partially by IR spectroscopy. In the structures of complexes **1**, **2** and **4** Cu(I) cation possesses a tetrahedral environment formed by the C=C bond of one organic cation Hapn, the N atom of cyano group from another Hapn moiety, and two O atoms (from NO_3^- anions in **1**, from H_2O molecules in **2**) or N atoms ($NH_2SO_3^-$ anions in **4**). In compound **3** strongly pronounced trigonal-pyramidal coordination environment of Cu(I) is formed by a mid-point of C=C-bond of one Hapn cation, nitrogen atom (of cyano group) of another Hapn unit, O atom of H_2O molecule in the basal plane, and F atom of BF_4^- anion at the apical position.

Keywords: Copper(I); π-complex; aminonitrile derivative; crystal structure; coordination polymer

1. Introduction

For almost two centuries the attention of scientists within different branches has been paid to aminonitriles, ranging from α-aminonitriles discovered by A. Strecker as far as in 1850,[1] to various β-, γ-, o-, ω- aminonitriles obtained in our days.[2] Representatives of this class are well-known not only as versatile intermediates in organic synthesis and in many other reactions,[3,4] but also as reagents for synthesis of heterocyclic compounds,[5] inhibitors of enzymes,[6] precursors of peptides,[7] amino-acids,[8] which, in turn, exhibit antibiotic,[9] antifungal,[10] and other important biological and pharmacological properties.[11,12]

The coordination behaviour of aminonitriles in the complexation reactions with Cu(I) salts can be characterized on the basis of only several related,[13,14] or closely related,[15] compounds, though the matter under discussion is still relevant. It has been noticed that atoms of Cl or Br compete for space in coordination polyhedron with allyl groups and cyano group in the halide complexes of Cu(I) with diallylaminopropanenitrile (the tertiary amine N-atom is protonated).[16,17] Still one of the two olefin bonds and halide atoms have a priority, and CN-group (as well as the second C=C-bond) does not coordinate to the metal ion.

Generally speaking, there are few ways for apn-moiety to coordinate with Cu ions. Depending on the status (cation or molecular) of 3-(prop-2-en-1-ylamino)propanenitrile the number of active groups for coordination changes, which, in turn, influences the composition of coordination polyhedron of the Cu ion (other ligand moieties, such as sol-

vent molecules or anions, occupy usually the apical position of the coordination polyhedron) and complexity of the arisen inorganic component in a compound: from $(CuCl)_2$ to $(Cu_2Cl_3)_n^{n-}$.[16] Thus, being in molecular state, apn is coordinated to Cu with allyl- and amino- group and Cl^- in the following sequence (C=C ≥ NH >…), whereas C≡N-group is not coordinated. Cationic form of apn provides these groups the same chance to be coordinated with the metal atom: C=C ≥ C≡N > Hal. In order to study a coordination ability of C=C-bond or C≡N-group to the copper atom, the compounds with ionic copper salts have been studied.

Therefore, we have undertaken the synthesis and crystal structure determination of copper(I)-π-complexes with 3-(prop-2-en-1-ylamino)propanenitrile.

2. Experimental

2. 1. Synthesis of 3-(prop-2-en-1-ylamino) propanenitrile (apn)

A mixture of 0.15 mol allylamine (11.2 mL) and 0.10 mol acrylonitrile (6.8 mL) was continuously stirred and cooled (5 h, 20 °C) preventing the temperature rising higher than 30 °C,[18] then it was heated for 1 h in a water bath with a reflux condenser at 60 °C. The product (orange liquid) was purified by distillation in a vacuum of a water-jet pump (85 °C /40 mm Hg). The yield of apn was 88% (15 mL). IR (KBr) n 3315(w), 3077(m), 2977(m) 2912(s), 2837(s), 2247(s), 1642 (m), 1528(wv), 1465(s), 1419(s), 1118(s), 996(s), 922(vs) cm^{-1}.

2. 2. Preparation of Complexes

Four crystalline copper(I) compounds with 3-(prop-2-en-1-ylamino)propanenitrile were prepared using alternating-current electrochemical syntheses.[19] The density of crystals of **1**–**4** was determined by the flotation method in a chloroform-bromoform mixture (Table 1).

2. 2. 1. Preparation of $[Cu(Hapn)NO_3]NO_3$ (1)

The apn (4.8 mmol) in 2 mL of ethanol titrated by HNO_3 to pH 5.5 was mixed with $Cu(NO_3)_2 \cdot 3H_2O$ (4.3 mmol) in 2 mL of ethanol. The solution was placed into a small test-tube and copper-wire electrodes in cork were inserted. After applying U = 0.50 V of alternating-current tension (frequency 50 Hz, I_{init} = 0.5 mA) for 16 h a starting coloured solution was discoloured and good quality colourless crystals of **1** appeared on the copper electrodes. Yield of complex **1** was 70%.

2. 2. 2. Preparation of $[Cu(Hapn)(H_2O)_2]SiF_6$ (2)

The same synthesis (frequency 50 Hz, U = 0.55 V, I_{init} = 0.54 mA), starting from $CuSiF_6 \cdot 4H_2O$ (3.8 mmol) and 4 mL of methanolic solution of the apn (4.2 mmol), previously titrated with an aqueous solution of 19% H_2SiF_6 to pH 3, resulted in a formation of good quality crystals of **2** in 12 h. Yield of the complex was 95%. IR (Nujol) n 3434(vs), 2953(vs), 2846(vs), 2260(w), 1642 (s), 1458(s), 1376(m), 1019(s), 953(w), 728(s) cm^{-1}.

2. 2. 3. Preparation of $[Cu(Hapn)(H_2O)BF_4]BF_4 \cdot H_2O$ (3)

Good quality crystals of complex **3** were obtained in a similar way (alternating-current, U = 0.65 V, I_{init} = 0.5 mA) starting from 4 mL of propanol solution of the 4 mmol of apn (titrated with HBF_4 to pH = 4) and $Cu(BF_4)_2 \cdot 6H_2O$ (4 mmol). Colourless prismatic crystals of compound **3** appeared on copper wire electrodes after 120 h. The yield was 60%.

2. 2. 4. Preparation of $[Cu(Hapn)(NH_2SO_3)_2]$ (4)

Colourless needle-like crystals of complex **4** appeared from a methanol solution (4 mL) of $Cu(NH_2SO_3)_2 \cdot xH_2O$ (4.1 mmol) and the apn (4.1 mmol) previously titrated with water solution of 50% NH_2SO_3H to pH 6.5 under conditions of the alternating-current electrochemical technique (U = 0.6 V, I_{init} = 0.4 mA) during 7 days. A yield of **4** was 65%. IR (KBr) n 3787(vw), 3264(w), 2923(m), 2361(s), 1662(w), 1249(vs), 1203(vs), 1055(m), 787(w), 643(vw), 593(vw), 560(vw) cm^{-1}.

2. 3. Crystallography

The experimental details, crystallographic parameters and summaries of the data collection for **1**–**4** are presented in Table 1. Single crystals of **1**–**4** were preliminarily studied by the photo-method and then diffraction data were collected on a Rigaku AFC7R (for **1**–**2**) or KUMA-KM4/CCD (for **3**–**4**) diffractometers with graphite monochromated MoK_α radiation (λ = 0.71073 Å). Corrections to the Lorentz and polarization factors were applied to reflection intensities. The X-ray experimental data were processed using the Rigaku Crystal Clear program,[20] for compounds **1** and **2**. The CrysAlisRED program was used for processing the X-ray data for complexes **3** and **4**.[21] An absorption correction was applied by the analytical method.[22] Structures **1**–**4** were solved using direct methods and light atoms were revealed from the difference Fourier syntheses using the SHELX program package.[23] Full-matrix least-squares refinements based on F^2 were carried out for the positional and thermal parameters of all non-hydrogen atoms. Four fluorine atoms of SiF_6^{2-} anion in **2** are split with roughly 50% s.o.f. The hydrogen atoms in structures **1**–**4** were revealed from the difference Fourier syntheses and refined in the riding model along with the non-hydrogen atoms (fixed C–H distances and with U_{iso}(H) equal to 1.2U_{eq}(C)). Hydrogen

Table 1. Crystallographic data and experimental details for structures **1–4**

Compound	1	2	3	4
Empirical formula	$C_6H_{11}CuN_4O_6$	$C_6H_{15}CuN_2O_2F_6Si$	$C_6H_{15}CuN_2O_2B_2F_8$	$C_{12}H_{30}Cu_2N_8O_{12}S_4$
Formula weight	298.73	352.83	384.36	733.76
Temperature (K)	200(2)	200(2)	100(2)	100(2)
Space group	$P2_1/n$	$P2_1/c$	$P2_1/n$	$P\bar{1}$
Unit cell dimensions (Å, °)				
a	8.2341(4)	8.5929(9)	12.351(4)	8.217(2)
b	7.9905(3)	9.7426(8)	12.351(4)	9.018(3)
c	17.4008(8)	15.2109(16)	13.497(4)	17.439(5)
α	90	90	90	91.93(3)
β	98.959(2)	103.448(4)	97.98(3)	92.52(3)
γ	90	90	90	90.21(3)
Volume (Å^3), Z	1130.91(9), 4	1238.5(2), 4	1420.9(7), 4	1290.3(6), 2
D_c (g cm^{-3})	1.755	1.892	1.797	1.889
D_m (g cm^{-3})	1.73	1.88	1.80	1.88
Absorption coefficient (mm^{-1})	1.96	1.93	1.63	2.05
F(000)	608	712	768	752
Measured reflections	4673	5091	14002	11271
Independent reflections	2552	2795	4825	8361
Observed reflections				
[$I > 2\sigma(I)$]	2163	2542	3266	6055
Goodness-of-fit on F^2	1.09	1.12	0.99	1.00
Parameters refined	155	204	226	343
Final R indices	$R1$ = 0.049,	$R1$ = 0.052,	$R1$ = 0.036,	$R1$ = 0.032,
[$I > 2\sigma(I)$]	$wR2$ = 0.134	$wR2$ = 0.145	$wR2$ = 0.087	$wR2$ = 0.073

atoms of amino group and water were refined freely. The figures were prepared using DIAMOND 3.1 software.[24]

3. Results and Discussion

Analysis of the obtained new Cu(I) π-complexes proves that the type of anion influences strongly on a structure formation in these complexes.[25,26]

3. 1. Crystal Structure of [Cu(Hapn)NO$_3$]NO$_3$ Complex (1)

Complex [Cu(Hapn)NO$_3$]NO$_3$ (**1**) is formed with anion NO$_3^-$ which is structurally related to halogenide ones. In this compound due to bridged functions of both Hapn and NO$_3^-$ units the known [Cu(NO$_3$)]$_2$ inorganic fragments[27–30] are interconnected with organic cations Hapn forming goffer chains in the direction [111] (Fig. 1). The

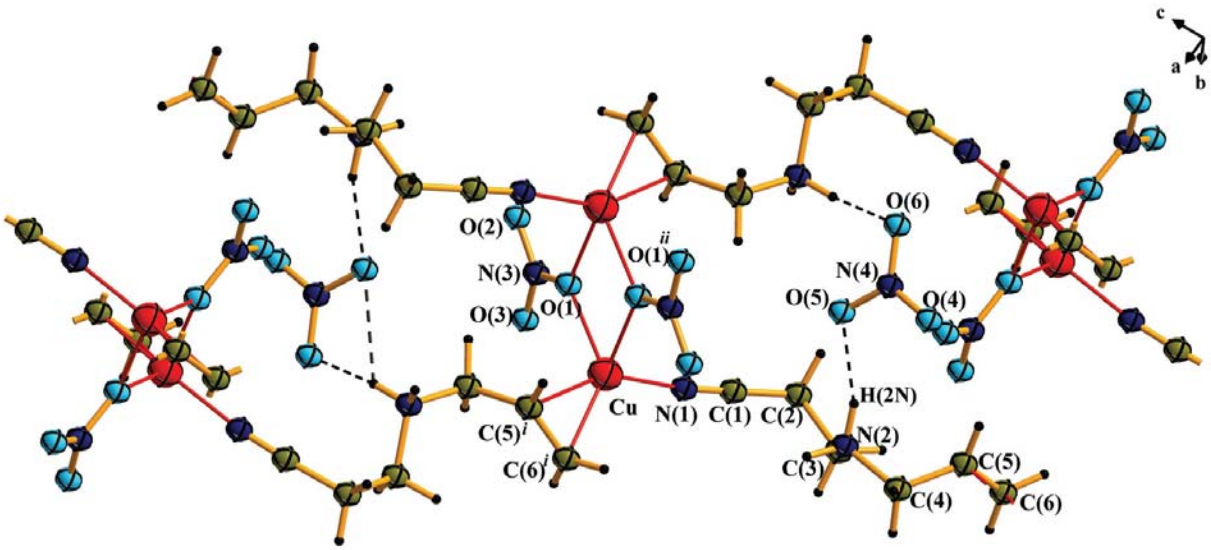

Figure 1. Infinite chains and hydrogen bonding in complex **1**. Symmetry operations: (*i*) x + ½, -y + ½, z + ½; (*ii*) –x + 2, -y, -z + 2.

angle between planes passing through two neighbouring inorganic linkers $[Cu(NO_3)]_2$ of the polymer is 67°. For comparison, the analogous angle between planes passing through two neighbouring inorganic units $[CuCl]_2$ in the halide complex is 65°.[16]

The metal atom possesses a tetrahedral surrounding consisting of the middle (further *m*) of double C(5)=C(6)-bond, N (C≡N-group) and 2 oxygen atoms from two NO_3^- anions. Lengths of the bonds are Cu–*m* 1.933(3), Cu–N 1.939(3), Cu–O(1) 2.102(2) and Cu–O(1)^{ii} 2.202(2) Å (Table 2). The angle formed by three Cu atoms in the chain $[Cu(Hapn)^{2+}]_n$ equals to 152°. The chain is not straight because of an influence of the non-coordinated NO_3^- anion, which forms N–H···O hydrogen bonds (Table 3).[31]

Table 2. Selected bond distances and angles for **1–4**.

Distance	(Å)	Angle	(°)
1[a]			
Cu–N1	1.939(3)	C6^i–Cu–C5^i	38.8(2)
Cu–*m*^{i}	1.933(3)	N1–Cu–O1	104.8(2)
Cu–O1	2.102(2)	N1–C1–C2	177.1(4)
Cu–O1^{ii}	2.202(2)	N1–Cu–O1^{ii}	101.0(2)
N1–C1	1.129(4)	O1–Cu–O1^{ii}	71.9(1)
C5–C6	1.361(4)	*m*^{i}–Cu–N1	132.6(1)
2[b]			
Cu–N1^i	1.987(3)	N1^i–Cu–O1w	107.1(2)
Cu–O1w	2.003(3)	N1^i–Cu–*m*	118.5(9)
Cu–*m*	1.936(3)	N1^i–Cu–O2w	95.9(2)
Cu–O2w	2.239(3)	O1w–Cu–O2w	93.7(1)
C5–C6	1.363(5)	C1–N1–Cu^{ii}	162.9(3)
N1–C1	1.132(5)	N1–C1–C2	178.4(4)
3[c]			
Cu–N1	1.946(2)	N1–Cu–O1w	99.7(7)
Cu–O1w	1.992(2)	O1w–Cu–*m*^{i}	129.1(5)
Cu–*m*^{i}	1.893(5)	C1–N1–Cu	169.7(8)
N1–C1	1.132(2)	N1–C1–C2	177.7(2)
C5–C6	1.364(3)	O1w–Cu–F8^{iii}	89.1(6)
4[d]			
Cu1–N11^i	1.990(2)	N11^i–Cu1–N1	106.2(7)
Cu1–N1	2.061(2)	N11^i–Cu1–N2	92.2(7)
Cu1–*m*1	1.977(7)	N1–Cu1–N2	99.2(7)
Cu1–N2	2.275(9)	N11^i–Cu1–*m*1	117.4(6)
C16–C15	1.352(3)	N2–Cu1–*m*1	110.3(5)
C11–N11	1.134(3)	C11–N11–Cu1^i	176.1(8)
Cu2–N3	2.039(8)	N3–Cu2–N4	104.6(7)
Cu2–N4	2.143(9)	N3–Cu2–N21^{ii}	96.6(7)
Cu2–*m*2	1.971(7)	N21^{ii}–Cu2–N4	93.9(8)
Cu2–N21^{ii}	2.130(2)	N4–Cu2–*m*2	111.1(5)
C26–C25	1.352(3)	N3–Cu2–*m*2	130.5(6)
C21–N21	1.138(3)	C21–N21–Cu2^{ii}	165.8(8)

m – middle point of C5=C6 (in **4**: C15=C16 and C25=C26) double bond. Symmetry codes: [a] (*i*) *x* + ½, -*y* + ½, *z* + ½; (*ii*) –*x* + 2, -*y*, -*z* + 2; [b] (*i*) –*x* + 1, *y* - ½, -*z* - ½; (*ii*) –*x* + 1, *y* + ½, -*z* - ½; [c] (*i*) –*x* + ½, *y* - ½, -*z* + ½; (*iii*) – *x* + 1.5, *y* – ½, –*z* + ½; [d] (*i*) –*x* + 1, -*y* + 1, -*z*; (*ii*) –*x* + 2, -*y*, -*z* + 1.

Table 3. Geometry of selected hydrogen bonds in **1–4**.

Atoms involved D–H···A	Distances, Å D–H	H···A	Angle, deg D···A	D–H···A
1[a]				
N2–H1N···O5^i	0.90	2.48	3.116(4)	128
N2–H1N···O6^i	0.90	1.94	2.798(2)	159
N2–H2N···O5	0.90	1.94	2.807(4)	161
2[b]				
N2–H1N···F1	0.90	1.89	2.784(8)	174
O1w–H2w1···F2^i	0.97	1.70	2.661(1)	170
N2–H2N···F2^{ii}	0.90	1.95	2.812(5)	160
O2w–H2w2···F1	0.96	2.39	3.259(6)	151
3[c]				
O1w–H1w1···F4^i	0.73	1.99	2.710(6)	169
N2–H1N···O2w^{ii}	0.86	1.88	2.725(2)	168
O1w–H2w1···F5^{iii}	0.72	2.01	2.716(1)	169
N2–H2N···F1	0.96	1.96	2.755(1)	139
O2w–H1w2···F7^{iv}	0.92	1.95	2.834(9)	160
O2w–H2w2···F8	0.84	2.09	2.827(3)	146
4[d]				
N1–H1B···O21^i	0.92	2.02	2.919(1)	165
N2–H2A···O31	0.92	1.93	2.820(8)	162
N2–H2B···O12^{ii}	0.92	2.07	2.992(1)	176
N3–H3B···O43^{iii}	0.92	2.01	2.925(2)	173
N22–H2N2···O42^{iv}	0.92	1.81	2.730(3)	178
N4–H4B···O32^{ii}	0.92	2.07	2.992(6)	177

Symmetry codes: [a] (*i*) ½ – *x*, *y* – ½, ½ – *z*; [b] (*i*) –*x*, 1 – *y*, –*z*; (*ii*) 1 – *x*, *y* – ½, –*z*; [c] (*i*) –*x*, –*y*, 1 – *z*; (*ii*) *x* – ½, ½ – *y*, *z*– ½; (*iii*) *x* – 1, *y*, *z*; (*iv*) 1.5 – *x*, ½ + y, ½ – *z*; [d] (*i*) 2 – *x*, –*y*, –*z*; (*ii*) *x* – 1, *y*, *z*; (*iii*) 1 – *x*, 1 – *y*, 1 – *z*; (*iv*) –*x*, 1 – *y*, 1 – *z*.

3. 2. Crystal Structure of $[Cu(Hapn)(H_2O)_2]SiF_6$ Complex (2)

In following two complexes **2** and **3** water molecules act as co-ligands. The structure of the compound **2** consists of infinite metal-organic spiral-like ribbons of $[Cu(Hapn)(H_2O)_2]^{2+}$ composition. The angle between three neighbouring copper atoms is 63°. Located between mentioned ribbons SiF_6^{2-} anions are bound to metal-organic fragment *via* O–H···F and N–H···F hydrogen bonds (Fig. 2). Despite the existence of Cu^I complexes with hexaflourosilicate-anion with the direct Cu^I–F–SiF_5 bond,[32] SiF_6^{2-}-anion does not enter the internal coordination sphere of the metal. Tetrahedral coordination polyhedron of copper(I) ion is formed by a mid-point of C(5) = C(6) bond, one nitrogen (C≡N) and two O (H_2O molecules) atoms. Respective bond lengths are Cu–*m* 1.936(3), Cu–N(1)^i 1.987(3), Cu–O(1w) 2.003(3) and Cu–O(2w) 2.239(3) Å (Table 2). A system of hydrogen bonds is much more developed in the given complex (table 2) in comparison with **1**. This promotes relatively dense packing of metal-organic chains and the inorganic anions.

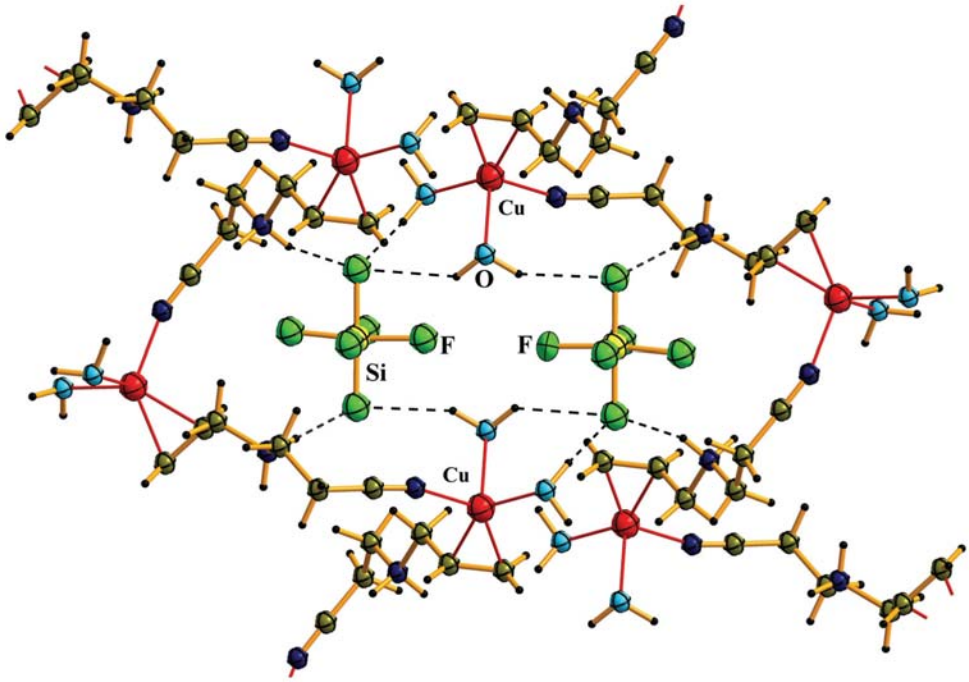

Figure 2. Fragment of molecular structure **2**. Disordered fluorine atoms are omitted for clarity.

3. 3. Crystal Structure of [Cu(Hapn)(H_2O)BF_4]BF_4 · H_2O Complex (3)

In the complex **3** water molecules and BF_4^- anions (apart from the active centers of Hapn) are included in the internal coordination sphere of Cu. The presence of BF_4^- anions promotes transformation of coordination polyhedron of the metal from tetrahedron to trigonal pyramid formed by *m* of (C=C)-bond, N (C≡N-group) and O (H_2O) atoms in the basal plane. Fluorine atom

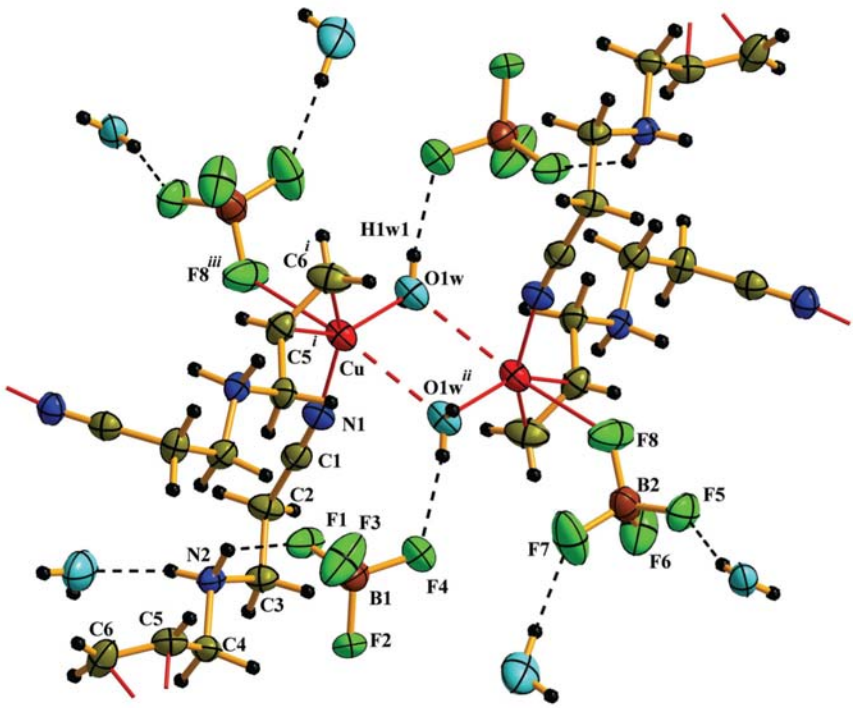

Figure 3. Cu(I) coordination in **3**. Structure fragment of complex **3**. Symmetry operations: (*i*) –*x* + ½, *y* - ½, -*z* + ½; (*ii*) –*x*+ 1, – *y* + 1, -*z*; (*iii*) – *x* + 1.5, *y* – ½, –*z* + ½. (80% probability displacement ellipsoids).

from BF_4^- anion occupies the apical position (Cu–F(8)^{iii} 2.640(2) Å) of coordination polyhedron. Atom of Cu is somewhat (Δ = 0.03 Å) removed from the (*m*, N, O) plane.

Another crystallographically independent H_2O molecule and BF_4^--anion are not coordinated to copper(I) and fixed in a crystal space by relatively strong hydrogen bonds. As one can see from Figure 3, the structure **3** is similar to **2**, but separate fragments of coordination polymer due to the Hapn flexibility demonstrate bulbous chain structure (the angle between three atoms of Cu $[Cu(Hapn)^{2+}]_n$ equals to 59°). Since one distance of Cu–O(1w) equals to 1.992(2) Å, and the other opposite Cu–O(1w)^{ii} is equal to 2.900(2) Å, one may regard from a certain distance $(Cu(H_2O))_2$ moiety as dimeric fragment and Cu(I) polyhedron as a trigonal bipyramid.

3. 4. Crystal Structure of $[Cu(Hapn)(NH_2SO_3)_2]$ Complex (4)

As in complexes **1** and **2**, in the compound **4** coordination polyhedra for both independent Cu(I) ions possess tetrahedral shape. The Cu(1) environment comprises of the mid-point of C(15)=C(16) bond (*m*1), N(11) atom from CN-group and two nitrogen atoms from two $NH_2SO_3^-$ anions. The Cu(2) polyhedron involves *m*2 (C(25) = C(26)), N(21) (C≡N) and N(3) and N(4) ($NH_2SO_3^-$) centers. Bonds lengths: Cu(1)–*m*1 1.977(7), Cu(1)–N(11)^i 1.990(2), Cu(1)–N(1) 2.061(8) and Cu1–N(2) 2.275(9) Å; Cu(2)–*m*2 1.971(7), Cu(2)–N(21)^{ii} 2.130(2), Cu(2)–N(3) 2.039(8) and Cu(2)–N(4) 2.143(9) Å.

The main structural feature of the complex **4** is the appearance of $[Cu(Hapn)]_2$ rings (Fig. 4). Two closest rings are tilted by 72° and linked with H-bonds among inorganic anions and organic cations (N(2)–H(2A)···O(31) 1.93 Å etc. Table. 3).

4. Conclusions

Flexibility of Hapn allows using it as a convenient tool in a construction of coordination compounds. In all the above-mentioned compounds Hapn totally realizes its coordination abilities attaching to the metal atom with (C=C)-bond of allyl- and N atom of cyano-group. The protonated N-amine atom being deprived of its donor ability participates actively in a formation of strong N–H···X hydrogen bonds (Table 2). On the other hand, the combination of Hapn with ionic copper(I) salts ($CuNO_3$, Cu_2SiF_6, $CuBF_4$, $CuSO_3NH_2$) promotes an effective interaction of both π- and σ-ligands with the central atom, which serve to a formation of stable frameworks.

5. Supplementary Material

CCDC 913397 (**1**), 913398 (**2**), 913399 (**3**) and 913400 (**4**) contain the supplementary crystallographic data for this article. These data can be obtained free of charge via http://www.ccdc.cam.ac.uk/conts/retrieving.html (or from the CCDC, 12 Union Road, Cambridge CB2 1EZ, UK; Fax: +44 1223 336033; E-mail: deposit@ccdc.cam.ac.uk).

6. References

1. A. Strecker, *Ann. Chem. Pharm.* **1850**, *75*, 27–45. https://doi.org/10.1002/jlac.18500750103
2. V. Chhiba, M. L. Bode, K. Mathiba, W. Kwezi, D. Brady, *J. Mol. Catal. B: Enz.* **2012**, *76*, 68–74. https://doi.org/10.1016/j.molcatb.2011.12.005
3. D. Enders, J. P. Shilvock, *Chem. Soc. Rev.* **2000**, *29*, 359–373. https://doi.org/10.1039/a908290e
4. E. Rafiee, A. Azad, M. Joshaghani, *Lett. Org. Chem.* **2007**, *4*,

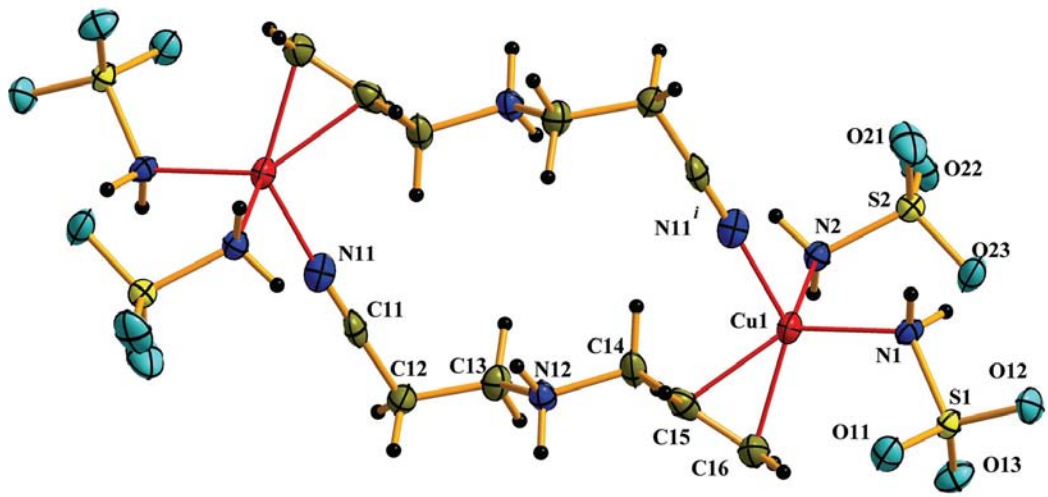

Figure 4. Copper(I) coordination in **4** and $[Cu(Hapn)]_2$. Symmetry operation: (*i*) –*x* + 1, -*y* + 1, -*z*; (80% probability displacement ellipsoids).

60–63. https://doi.org/10.2174/157017807780037478
5. E. C. Taylor, J. G. Berger, *J. Org. Chem.* **1967**, *32*, 2376–2378. https://doi.org/10.1021/jo01283a003
6. S.-S. Tang, P. C. Trackman, H. M. Kagang, *J. Biol. Chem.* **1983**, *258*, 4331–4338.
7. G. Cardillo, C. Tomasini, *Chem. Soc. Rev.* **1996**, *25*, 117–128. https://doi.org/10.1039/CS9962500117
8. M. Preiml, K. Hillmayer, N. Klempier, *Tetrahedron Lett.* **2003**, *44*, 5057–5059. https://doi.org/10.1016/S0040-4039(03)01136-5
9. S. G. Davies, O. Ichihara, I. Lenoir, I. A. S. Walters, *J. Chem. Soc. Perkin Trans. 1* **1994**, *11*, 1411–1415. https://doi.org/10.1039/P19940001411
10. F. Theil, S. Ballschuh, *Tetrahedron Asymmetry* **1996,** *7*, 3565–3572. https://doi.org/10.1016/S0957-4166(96)00465-X
11. D. Steinhuebel, Y. Sun, K. Matsumura, N. Sayo, T. Saito, *J. Am. Chem. Soc.* **2009**, *131*, 11316–11317. https://doi.org/10.1021/ja905143m
12. M. Liu, M.P. Sibi, *Tetrahedron* **2002**, *58*, 7991–8035. https://doi.org/10.1016/S0040-4020(02)00991-2
13. A. Albinati, M. L. Carraro, S. Gross, M. Rancan, S. Rizzato, E. Tondello, A. Venzo, *Eur. J. Inorg. Chem.* **2009**, *35*, 5346–5351. https://doi.org/10.1002/ejic.200900620
14. Y. E. Filinchuk, V. V. Olijnik, V. N. Davydov, *Russ. J. Coord. Chem.* **1997**, *23*, 843–845.
15. E. A.Goreshnik, V. V.Oliinik, *Russ. J. Inorg.Chem.* **1996**, *41*, 206–208.
16. M. Y. Luk'yanov, A. V. Pavlyuk, M. G. Mys'kiv, *Russ. J. Coord. Chem.* **2012**, *38*, 86–91 (*Koord. Khimiya* **2012**, *38*, 92–97).
17. M. Luk'yanov, V. Kinzhybalo, E. Goreshnik, O. Pavlyuk, M. Mys'kiv, *Chem. Met. Alloys.* **2012**, *5*, 66–76.
18. Houben-Weil. *Methoden der organischen Chemie*, Stuttgart: Georg Thieme **1949,** *4*.
19. B. M. Mykhalichko, M. G. Mys'kiv. Ukraine Patent UA25450A, Bull. N. 6 **1998**.
20. *Crystal Clear*. Woodlands (Texas, USA): Rigaku Corporation (**1999**).
21. *CrysAlis RED. Version 1.171.31.8,* Oxford: Oxford Diffraction Ltd. (**2007**).
22. R. C. Clark, J. S. Reid, *Acta Crystallogr., Sect. A: Found. Crystallogr.* **1995**, *51*, 887–897. https://doi.org/10.1107/S0108767395007367
23. G. M. Sheldrick, *Acta Cryst., Sect. A: Found. Crystallogr.* **2008**, *A64*, 112–122. https://doi.org/10.1107/S0108767307043930
24. *DIAMOND v3.1*. Crystal Impact GbR, Bonn, Germany (**2004–2005**).
25. E. Goreshnik, M. Mys'kiv, *J. Chem. Crystallogr*. **2010**, *40*, 381–383.https://doi.org/10.1007/s10870-009-9666-1
26. M.Y. Luk'yanov, A.V. Pavlyuk, E. A. Goreshnik, M. G. Mys'kiv, *Russ. J. Coord. Chem.* **2012**, *38*, 639–645. (*Koord. Khimiya* **2012**, *38*, 663–670).
27. S. P. Neo, Z.-Y. Zhou, T. C. W. Mak, T. S. A. Hor, *J. Chem. Soc., Dalton Trans.* **1994**, *23*, 3451–3458. https://doi.org/10.1039/DT9940003451
28. R. D. Hart, G. A. Bowmaker, J. D. Kildea, E. N. de Silva, B. W. Skelton, A. H. White, *Aust. J. Chem.* **1997,** *50*, 604–620. https://doi.org/10.1071/C96041
29. E. A. Goreshnik, M. G. Mys'kiv, *Acta. Chim. Slov.* **2011**, *58*, 772–775.
30. Y. Slyvka, E. Goreshnik, N. Pokhodylo, O. Pavlyuk, M. Mys'kiv, *Acta. Chim. Slov.* **2016**, *63*, 399–405. https://doi.org/10.17344/acsi.2016.2486
31. G. R. Desiraju, *Angew. Chem. Int. Ed.* **2011**, *50*, 52–59. https://doi.org/10.1002/anie.201002960
32. E. A. Goreshnik, Y. I. Slyvka, M. G. Mys'kiv, *Inorg. Chim. Acta* **2011**, *377*, 177–180. https://doi.org/10.1016/j.ica.2011.08.008

Povzetek

Pripravili smo štiri bakrove(I) π-komplekse: $[Cu(Hapn)NO_3]NO_3$ (**1**), $[Cu(Hapn)(H_2O)_2]SiF_6$ (**2**), $[Cu(Hapn)(H_2O)BF_4]BF_4{\cdot}H_2O$ (**3**) in $[Cu(Hapn)(NH_2SO_3)_2]$ (**4**) z uporabo elektrokemijske tehnike z izmenično napetostjo iz alkoholnih raztopin 3-(prop-2-en-1-ilamino)propannitrila (apn) titriranega z ustrezno kislino ter z bakrovo(II) soljo ($Cu(NO_3)_2 \cdot 3H_2O$, $CuSiF_6 \cdot 4H_2O$, $Cu(BF_4)_2 \cdot 6H_2O$ ali $Cu(NH_2SO_3)_2 \cdot xH_2O$). Pripravljene spojine smo okarakterizirali z monokristalno rentgensko difrakcijo in delno z IR spektroskopijo. Pri strukturah **1**, **2** in **4** ima Cu(I) kation tetraedrično razporeditev ligandov, ki nastane z C=C vezjo enega organskega kationa Hapn, N atoma ciano skupine iz drugega Hapn liganda ter dveh O atomom (iz NO_3^- aniona pri **1**, iz H_2O molekule pri **2**) oziroma N atoma (anion $NH_2SO_3^-$ pri **4**). Pri spojini **3** je prisotna trigonala-piramidalna koordinacija Cu(I) s sredinsko točko C=C-vezi enega Hapn kationa, N atoma (iz ciano skupine) drugega Hapn liganda in O atoma molekule H_2O v osnovni ravnini ter s F atomom iz BF_4^- aniona v navpični legi.

Scientific paper

Three 1D cyanide-bridged M(Ni, Pd, Pt)-Mn(II) Coordination Polymer: Synthesis, Crystal Structure and Magnetic Properties

Jingwen Shi,[1] Chongchong Xue,[1] Lingqian Kong[2] and Daopeng Zhang[1,*]

[1] *College of Chemical Engineering, Shandong University of Technology, Zibo 255049, China*

[2] *Dongchang College, Liaocheng University, Liaocheng 252059, P.R. China*

* *Corresponding author: E-mail: dpzhang73@126.com*

Received: 13-12-2016

Abstract

Abstract: Three tetracyanide-containing building blocks $K_2[M(CN)_4]$ (M = Ni, Pd, Pt) and one semi-closed macrocycle seven-coordinated manganese(II) compound have been employed to assemble cyanide-bridged heterometallic complexes, resulting in three cyanide-bridged M^{II}-Mn^{II} complexes: $[Mn(L)][Ni(CN)_4] \cdot 2H_2O$ (**1**) $[Mn(L)][Pd(CN)_4]$ (**2**) and $[Mn(L)][Pt(CN)_4]$ (**3**) (L = 2,6-bis[1-(2-(*N*-methylamino)ethylimino)ethyl]pyridine). Single-crystal X-ray diffraction analysis shows their similar one-dimensional structure consisting of the alternating $[Mn(L)]^{2+}$ species and $[M(CN)_4]^{2-}$ building blocks, generating a cyanide-bridged neutral polymeric chain. In all three isostructural complexes the coordination geometry of manganese ion is a slightly distorted pentagonal-bipyramidal with the two cyanide nitrogen atoms at the *trans* positions and N5 coordinating mode at the equatorial plane from ligand L. Investigation over magnetic properties of these complexes reveals very weak antiferromagnetic interaction between neighboring Mn(II) ions bridged by the long NC–M–CN unit. A best-fit to the magnetic susceptibility of complexes **1**–**3** leads to the magnetic coupling constant of J = –0.081, –0.103 and –0.14 cm^{-1}, respectively.

Keywords: Cyanide-bridged, heterometallic complex, crystal structure, magnetic property

1. Introduction

In the past several decades, the ultimate goal of crystal engineering is to directional design and construction of molecular crystals with new structures, properties and functions. During which, many effective strategies have been developed to rationally designing and controlling assembly of metal complexes with diversified topological structures and interesting properties. Among the various transition metal coordination systems, the rational design of the cyanide-bridged heterometallic complexes with target structure types have been given intense attention because not only the structures and the nature of the magnetic, optic and electric properties of corresponding complexes can be readily controlled and anticipated, but also the excellent stabilizing ability of cyanide group for many transition metal centers and oxidation states with or without the peripheral ligands.[1–23]

As has been known, except the several factors from the cyanide precursor such as the number and position of cyanide group, number and nature of charge of cyanide-containing building block, and steric effect of reactants that can be used to tune the structure of the cyanide-bridged complexes formed, the ancillary ligands attached to the counterpart assembling cations also play a crucial role for constructing cyanide-bridged complexes with different structures. The polyaza macrocyclic ligands with some rigid character obtained by condensation of 2,6-diacetylpyridine and polyamine, which are usually coordinated to the equatorial plane of metal ions with only two *trans* replaceable sites weakly bonded to other ligands, have proved to be good ancillary ligands to assemble low-dimensional structural cyanide-bridged complexes.[24–31] Interested also in these types of ligands, we have reported many cyanide-bridged bimetallic complexes by using cyanide precursors containing different cyanide groups.[32–36] Here, we investigated the reactions the Mn(II) compound based-on a semi-closed macrocyclic ligand L (L = 2,6-bis[1-(2-(*N*-methylamino)ethylimino)ethyl]pyridine) with three tetra-cyanometallates

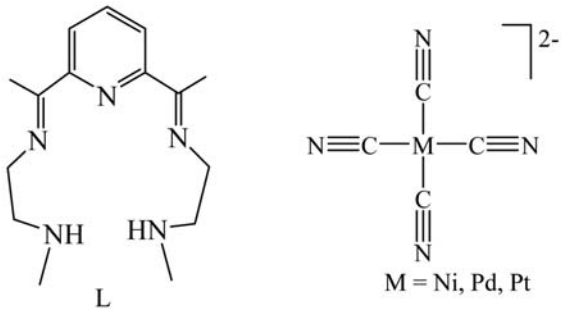

Scheme 1. The semi-closed macrocycle ligand and the cyanide precursors used to synthesize the complexes **1**–**3**.

(Scheme 1), and obtained three one-dimensional cyanide-bridged heterobimetallic complexes with the formula $[Mn(L)][Ni(CN)_4]\cdot 2H_2O$ (**1**) $[Mn(L)][Pd(CN)_4]$ (**2**) and $[Mn(L)][Pt(CN)_4]$ (**3**). It should be mentioned that current complexes are the first one-dimensional example assembled from the semi-closed macrocyclic manganese compound. The synthesis, crystal structure and magnetic properties of all the three complexes are described in this paper.

2. Experimental Section

2. 1. Instruments

Elemental analyses of carbon, hydrogen, and nitrogen were carried out with an Elementary Vario El. The infrared spectroscopy on KBr pellets was performed on a Magna-IR 750 spectrophotometer in the 4000–400 cm^{-1} region. Variable-temperature magnetic susceptibility and field dependence magnetization measurements were performed on a Quantum Design MPMS SQUID magnetometer. The experimental susceptibilities were corrected for the diamagnetism of the constituent atoms (Pascal's tables).

2. 2. General Procedures and Materials

All the reactions were carried out under an air atmosphere and all chemicals and solvents used were reagent grade without further purification. The $[Mn(L)(H_2O)_2]Cl_2$ were prepared by using the reported method for similar manganese macrocycle complex.[33]

Caution! The cyanide compounds are hypertoxic and hazardous and they should be handled in small quantities with care.

2. 3. Preparation of Complexes 1–3

These three complexes were prepared using one similar three layers diffusion procedure, therefore only the synthesis of **1** is reported as a typical representative. A solution containing $K_2[Ni(CN)_4]$ (0.10 mmol, 24.1 mg) dissolved in 5 mL of water was laid in the bottom of a tube, upon which a mixture solvent of water and methanol with a ratio of 1:1 was carefully added. Then, a solution of $[Mn(L)]Cl_2$ (0.10 mmol, 40.1 g) in 5 mL of methanol was carefully added to the top of the mixture solvent layer above formed. About two weeks later, single yellow crystals suitable for X-ray diffraction were obtained from the interface, collected by filtration and dried in air. Yield: 35.5 mg, 67.1%. Anal. Calcd. for $C_{19}H_{29}MnN_9NiO_2$: C, 43.13; H, 5.52; N, 23.82. Found: C, 43.01; H, 5.45; N, 24.01. Main IR bands (cm^{-1}): 3255(s), 2915(m), 2845(m), 2153(s), 2125(s), 1650(m), 1594(m), 1455(m), 1370(m), 1190(m), 965(m).

Complex **2**: Yield: 30.8 mg, 57.1%. Anal. Calcd. for $C_{19}H_{25}MnN_9Pd$: C, 42.20; H, 4.66; N, 23.31. Found: C, 42.10; H, 4.61; N, 23.15. Main IR bands (cm^{-1}): 3257(s), 2910(m), 2850(m), 2150(s), 2120(s), 1652(m), 1590(m), 1458(m), 1377(m), 1197(m), 961(m).

Complex **3**: Yield: 40.1 mg, 63.6%. Anal. Calcd. for $C_{19}H_{25}MnN_9Pt$: C, 36.25; H, 4.00; N, 20.02. Found: C, 36.14; H, 3.85; N, 19.81. Main IR bands (cm^{-1}): 3260(s), 2900(m), 2853(m), 2155 (s), 2123(s), 1658(m), 1597(m), 1452(m), 1375(m), 1191(m), 959(m).

2. 4. X-ray Data Collection and Structure Refinement

Single crystals of all complexes for X-ray diffraction analysis with suitable dimensions were mounted on the glass rod and the crystal data were collected on a Bruker SMART CCD diffractometer with a MoK_α sealed tube (λ = 0.71073 Å) at 293 K using a ω scan mode. The structures were solved by direct method and expanded using Fourier difference techniques with the SHELXTL-97 program package. All the non-hydrogen atoms were refined with anisotropic displacement coefficients. Hydrogen atoms were assigned isotropic displacement coefficients $U(H) = 1.2U(C)$ or $1.5U(C)$ and their coordinates were allowed to ride on their respective carbons using SHELXL97 except some of the H atoms of the solvent molecules that were refined isotropically with fixed U values and the DFIX command was used to rationalize the bond parameter. CCDC 1521398–1521400 for these three complexes contain the supplementary crystallographic data for this paper. These data can be obtained free of charge from the Cambridge Crystallographic Data Centre via . Details of the crystal parameters, data collection, and refinement are summarized in Table 1.

3. Results and Discussion

3. 1. Synthesis and General Characterization

As has been known, the closed macrocycle ligand 3,6-diazaoctane-1,8-diamine and 3,6-dioxaoctano-1,8-

Table 1. Crystallographic data for complexes **1**–**3**.

	1	**2**	**3**
Formula	$C_{19}H_{29}MnN_9NiO_2$	$C_{19}H_{25}MnN_9Pd$	$C_{19}H_{25}MnN_9Pt$
M	529.16	540.82	629.51
Crystal system	Monoclinic	Monoclinic	Monoclinic
Space group	P2(1)/c	C2/c	C2/c
a/Å	18.1273(5)	11.3312(7)	11.3015(6)
b/Å	16.7829(5)	11.2415(6)	11.2472(6)
c/Å	7.7459(2)	17.4718(9)	17.4485(8)
α/°	90	90	90
!*b*/°	93.440(3)	91.187(6)	91.305(4)
γ/°	90	90	90
V/Å^3	2352.28(11)	2225.1(2)	2217.3(2)
Z	4	4	4
F(000)	1100	1092	1220
GOF	1.038	1.049	0.995
$R_1[I>2\sigma(I)]$	0.0350	0.0303	0.0332
wR_2 (all data)	0.0834	0.0751	0.0701

diamine are good auxiliary ligands for assembling cyanide-bridged magnetic complexes by incorporating some paramagnetic metal ions such as Mn(II), Fe(II) and Co(II), etc.[24–31] With comparison to the above two macrocyclic ligands, the semi-closed pentadentate macrocycles ligand used here (Scheme 1) may have more flexibility due to its semi-open nature and the two pendulous methyl groups, which is maybe beneficial to produce single axial magnetic anisotropy for paramagnetic metal ions. As has been known, the Mn(II) ion in some complexes based-on aliphatic amines ligands can be easily oxidized to Mn(III) ion. However, the seven-coordinated Mn(II) species obtained by incorporating Mn(II) ion into these types of macrocyclic ligands are very robust and can be handled in air and in aqueous solution without being oxidized. Furthermore, the large equatorial steric effect from the macrocyclic ligand can effectively lower the dimensionality of the complexes formed, thus far more favoring of constructing functional complexes with low dimensional structure through replacing the two weakly bonded and replaceable ligands at the two trans positions. The reactions between the manganese(II) compound with the semi-closed macrocycle acting as auxiliary ligand and three tetra-cyanidemetallates result in three isostructural one-dimensional cyanide-bridged complexes. In the IR spectra of complexes **1**–**3** two sharp peaks due to the cyanide-stretching vibration were observed at about 2120 and 2150 cm^{-1}, respectively, indicating the presence of bridging and nonbridging cyanide ligands in these complexes.

3. 2. Crystal Structures of Complexes 1–3.

Some important structural parameters for complexes **1**–**3** are collected in Table 2. The neutral binuclear independent unit, one-dimensional structure and the cell packing diagram of compound **1** are shown in Figures 1–3, respectively, and the other compounds show similar structures. The calculated and measured partner of XPRD data for these three complexes is given in Figures S1–S3 (Supporting Information), respectively.

As can be found, complexes **1**–**3** possess similar one dimensional neutral single chain structure comprising of repeating [–NC–M(CN)$_2$–CN–Mn(L)–] (M = Ni, Pd, Pt) unit. In these three complexes, each [M(CN)$_4$]$^{2-}$ unit, acting as a bidentate ligand through it's a pair of *trans* cyanide groups, connects the Mn(II) ion of two independent semi-closed macrocyclic manganese units. The structure of these three complexes is very similar to the reported 1D linear chain complex {[Mn(L^1)][Fe(1-MeIm)(CN)$_5$]}$_n$, but different from {[Mn(L^1)(H$_2$O)][Mn(L^1)][Fe(CN)$_6$]}$_n$ · n(CH$_4$O)·3.5nH$_2$O and {[Mn(L^1)(H$_2$O)][Mn(L^1)][M'(CN)$_8$]}$_n$ · 4nH$_2$O,[36] for the latter which can be structurally characterized as one-dimensional zig-zag chain structure. (L^1 = 2,13-dimethyl-3,6,9,12,18-pentaazabicyclo[12.3.1]octadeca-1(18),2,12,14,16-pentaene), M' = Mo, W). The M–C$_{bridged-CN}$ bond lengths and the M–C≡N$_{bridge}$ bond angles are almost equal to those corresponding parameters found in other non-bridged cyanide groups, demonstrating that the coordination or non-coordination of the N atom to the metal atom has no obvious influence on the geometry of the cyanide precursor.

The Mn(II) ion in complexes **1**–**3** is seven-coordinated forming a slightly distorted pentagonal-bipyramidal coordination geometry in which the five equatorial positions are occupied by N$_5$ unit coming from the semi-closed macrocyclic ligand and the two axial ones coordinated by two N atoms of cyanide groups. The distances between Mn ion and the equatorial N atoms in complexes **1**–**3** are almost equal to each other within the very narrow range 2.322(5)-2.383(2) Å (Table 2). The average Mn–N$_{cyanide}$ bond lengths in all these complexes are 2.257(2), 2.236(3)

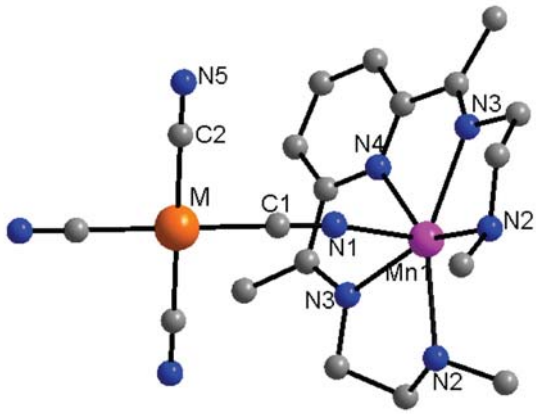

Figure 1. The representative neutral binuclear independent unit of complex **1**. All hydrogen atoms and solvent molecules have been omitted for clarity.

and 2.225(5) Å, respectively, slightly shorter than the Mn–$N_{equatorial}$ bond lengths. As tabulated in Table 2, the bond angle of N1–Mn1–N2 are 176.74(9), 177.42(16) and 177.6(3)°, respectively, indicating the good linear configuration of these three atoms. However, the Mn–C≡N bond angle is somewhat bent with the values about 155°. The intramolecular Mn···Mn separation through the diamagnetic bridging cyanide precursor in **1**–**3** is 9.926, 10.476 and 10.450 Å, respectively.

3. 3. Magnetic Properties of Complexes 1–3.

The temperature dependence of magnetic susceptibility for complex **1** measured in the range of 2–300 K under the external magnetic field of 2000 Oe is showed in Fig. 4. For complexes **2** and **3** their temperature dependen-

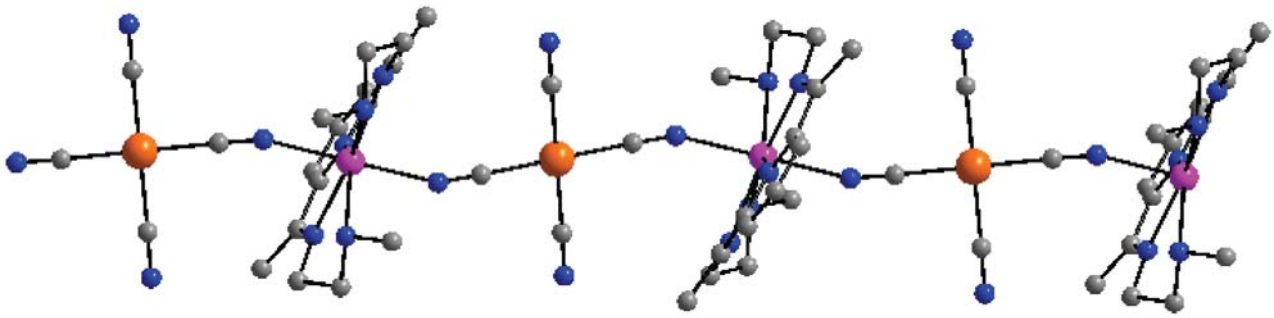

Figure 2. The representative 1D structure of complex **1**. All hydrogen atoms and solvent molecules have been omitted for clarity.

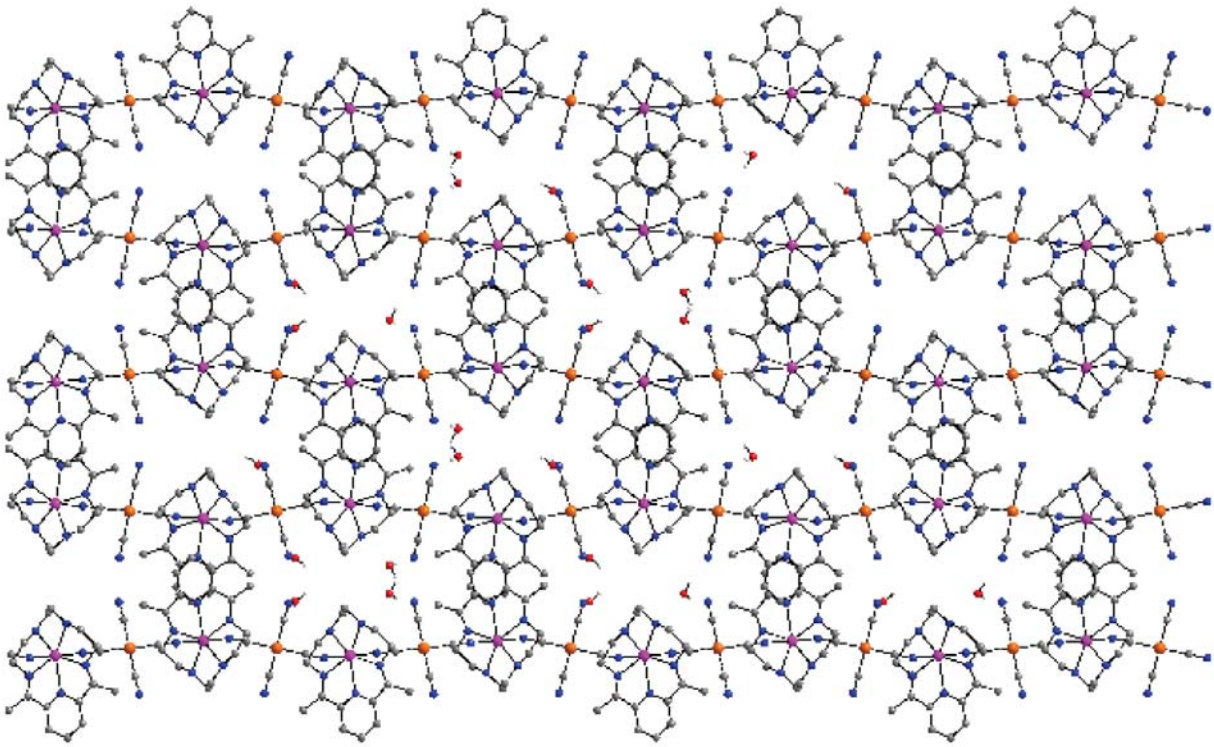

Figure 3. The cell packing diagram along *b* for complex **1.** All the non-solvent hydrogen atoms have been omitted for clarity.

Table 2. Selected bond lengths (Å) and angles (°) for **1**–**3**.

	1 (M = Ni)	2 (M = Pd)	3 (M = Pt)
Mn(1)–N(1)	2.257(2)	2.236(3)	2.225(5)
Mn(1)–N(2)	2.359(2)	2.322(5)	2.367(5)
Mn(1)–N(3)	2.366(2)	2.338(3)	2.342(6)
Mn(1)–N(4)	2.383(2)	2.378(3)	2.325(8)
M(1)–C(1)	1.871(3)	1.989(4)	2.007(6)
M(1)–C(2)	1.858(3)	1.996(5)	1.999(8)
C(1)–N(1)–Mn(1)	156.4(2)	155.2(3)	154.6(5)
N(1)–C(1)–M(1)	178.0(3)	177.6(3)	178.3(6)
N(1)^{i}–Mn(1)–N(1)	176.74(9)	177.42(16)	177.6(3)

Symmetry code: (i) $-x + 3/2, -y + 3/2, -z + 1$.

ce of magnetic susceptibilities is given in Figure S4 (Supporting Information). The changing tendency of $\chi_m T$ for these three complexes is comparatively similar. The $\chi_m T$ value at room temperature is 4.31, 4.30 and 4.29 emu K mol^{-1} for complexes **1**–**3**, respectively, slightly lower than the spin only value of 4.375 emu K mol^{-1} for the isolated high spin Mn(II) (S = 5/2). With the temperature decreasing, the $\chi_m T$ value is with no obvious change from 300 to about 50 K. Below this temperature the $\chi_m T$ begins to decrease rapidly and reaches their lowest value of 1.73 for **1**, 1.85 for **2** and 2.72 for **3** at 2 K, respectively. The magnetic susceptibility for these three complexes conforms well to Curie-Weiss law in a range of 2–300 K (the inset of Fig. 4) and gives the negative Weiss constant $\theta = -3.38$ K and Curie constant $C = 4.17$ emu K mol^{-1} for **1**, $\theta = -4.75$, C = 4.20 emu K mol^{-1} for **2** and $\theta = -1.16$, C = 3.99 emu K mol^{-1} for **3**. These results primarily show the antiferromagnetic magnetic coupling between the two Mn(II) centers bridged by [–NC–M–CN–] unit in these three complexes.

The magnetic data are analyzed by using the Hamiltonian: $\hat{H} = -2\sum J\hat{S}_i\hat{S}_{i+1}$. The temperature dependence of the magnetic susceptibility is given by the equation:[37,38]

$$\chi_M^{chain} = Ng^2\beta^2\{S_{Mn}(S_{Mn}+1)/3KT\}\{(1+\mu)/(1-\mu)\} \quad (1)$$

(Fisher's infinite chain model) with:

$$\mu = \coth[JS_{Mn}(S_{Mn}+1)/KT] - [KT/JS_{Mn}(S_{Mn}+1)] \quad (2)$$

The least-squares fit to the data leads to $J = -0.081$ cm^{-1}, $g = 1.99$, $R = 1.19 \cdot 10^{-5}$ for **1**, $J = -0.103$ cm^{-1}, g = 1.99, $R = 1.23 \cdot 10^{-5}$ for **2** and $J = -0.14$ cm^{-1}, $g = 1.98$, R = $2.12 \cdot 10^{-5}$ for **3**, respectively. These results reveal also the antiferromagnetic coupling between adjacent manganese ion bridged by the cyanide precursor and the small J value can be attributed to the long distance separated by the diamagnetic bridging unit. Both of the thermal magnetic behavior and the theoretical simulation results of the above three complexes are basically consistent with those

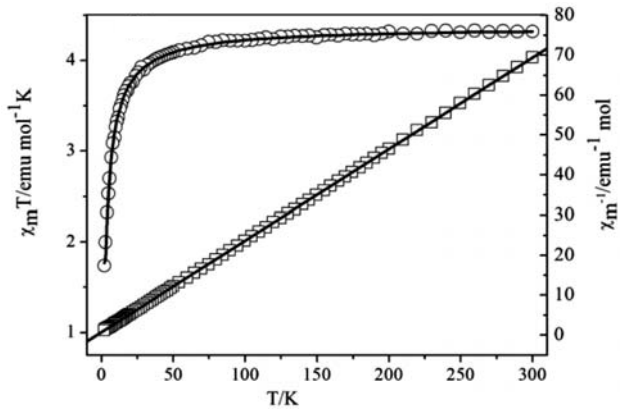

Figure 4. Temperature dependences of $\chi_m T$-T (the solid line represents the best fit based on the parameters discussed in the text) for complex **1**. Inset: Temperature dependences χ_m^{-1}-T (the solid line was calculated from the Curie-Weiss law).

found in the reported complexes assembled from the closed macrocyclic manganese compounds and other diamagnetic cyanometallates.[33,36]

4. Conclusion

In summary, three new cyanide-bridged M(II)-Mn(II) (M = Ni, Pd, Pt) complexes structurally characterized as one-dimensional single chain have been synthesized with tetracyanide-containing precursor $K_2[M(CN)_4]$ as building blocks and semi-closed macrocycle ligand based manganese(II) compound as assemble segment. The magnetic studies demonstrate the weak antiferromagnetic interaction between the Mn(II) ions through [–NC–M–CN–] unit in all the three complexes. The current results and those reported recently[28,29] indicate that the semi-closed macrocycle mangaese(II) compound employed here is good candidate for assembling cyanide-bridged heterometallic complexes with low dimensional structures and sometime interesting magnetic properties.

5. Acknowledgement

This work was supported by the Natural Science Foundation of China (21171107 and 21671121).

6. References:

1. S. Ferlay, T. R. Mallah, P. Ouahès, M. V. Veillet, *Nature* **1995**, *378*, 701–703.
2. W. R. Entley, G. S. Girolami, *Science* **1995**, *268*, 397–400.
3. J. N. Rebilly, T. Mallah, *Struct. Bond*. **2006**, *122*, 103–131.
4. R. Lescouezec, L. M. Toma, J. Vaissermann, M. Verdaguer, F. S. Delgado, C. Ruiz-Perez, F. Lloret, M. Julve, *Coord. Chem. Rev.* **2005**, *249*, 2691–2729.
5. H. Miyasaka, A. Saitoh, S. Abe, *Coord. Chem. Rev.* **2007**, *251*, 2622–2664 and references therein.
6. O. Sato, T. Kawakami, M. Kimura, S. Hishiya, S. Kubo, Y. Einaga, *J. Am. Chem. Soc.* **2004**, *126*, 13176–13177.
7. L. M. Toma, R. Lescouëzec, L. D. Toma, F. Lloret, M. Julve, J. Vaissermann, M. J. Andruh, *J. Chem. Soc., Dalton Trans.* **2002**, 3171–3176.
8. L. M. C. Beltran, J. R. Long, *Acc. Chem. Res.* **2005**, *38*, 325–334.
9. S. S. Kaye, J. R. Long, *J. Am. Chem. Soc.* **2005**, *127*, 6506–6507.
10. K. W. Chapman, P. D. Southon, C. L. Weeks, C. J. Kepert, *Chem. Commun.* **2005**, 3322–3324.
11. L. Jiang, X. L. Feng, T. B. Lu, S. Gao, *Inorg. Chem.* **2006**, *45*, 5018–5026.
12. J. Kim, H. S. Yoo, E. K. Koh, H. C. Kim, C. S. Hong, *Inorg. Chem.* **2007**, *46*, 8481–8483.
13. L. Jiang, H. J. Choi, X. L. Feng, T. B. Lu, J. R. Long, *Inorg. Chem*. **2007**, *46*, 2181–2186.
14. H. Miyasaka, A. Saitoh, S. Abe, *Coord. Chem. Rev.* **2007**, *251*, 2622–2644 and references therein.
15. K. R. Dunbar, R. A. Heintz, *Prog. Inorg. Chem.* **2009**, *56*, 155–334.
16. S. Wang, X. H. Ding, J. L. Zuo, X. Z. You, W. Huang, *Coord. Chem. Rev.* **2011**, *255*, 1713–1732.
17. S. Wang, X. H. Ding, Y. H. Li, W. Huang, *Coord. Chem. Rev.* **2012**, *256*, 439–464.
18. Y. H. Li, W. R. He, X. H. Ding, S. Wang, L. F. Cui, W. Huang, *Coord. Chem. Rev.* **2012**, *256*, 2795–2815.
19. T. Senapati, C. Pichon, R. Ababei, C. Mathoniežre, R. Cleìrac, *Inorg. Chem.* **2012**, *51*, 3796–3812.
20. A. Panja, P. Guionneau, I. R. Jeon, S. M. Holmes, R. Cleìrac, C. Mathoniežre, *Inorg. Chem.* **2012**, *51*, 12350–12359.
21. R. Ababei, C. Pichon, O. Roubeau, Y. G. Li, N. Breìfuel, L. Buisson, P. Guionneau, C. Mathoniežre, R. Cleìrac, *J. Am. Chem. Soc.* **2013**, *135*, 14840–14853.
22. D. P. Zhang, S. P. Zhuo, H. Y. Zhang, P. Wang, J. Z. Jiang, *Dalton Trans.* **2015**, *44*, 4655–4664.
23. D. P. Zhang, L. Q. Kong, H. Y. Zhang, *Acta. Chim. Slov.* **2015**, *62*, 219–224.
24. M. Mousavi, V. Beìreau, C. Desplanches, C. Duhayonab, J. P. Sutter, *Chem. Commun.* **2010**, *46*, 7519-7521.
25. T. S. Venkatakrishnan, S. Sahoo, N. Breìfuel, C. Duhayon, C. Paulsen, A. L. Barra, S. Ramasesha, J. P. Sutter, *J. Am. Chem. Soc.* **2010**, *132*, 6047–6056.
26. C. Paraschiv, M. Andruh, Y. Journaux, Z. ZaČk, N. Kyritsakasd, L. Ricard, *J. Mater. Chem.* **2006**, *16*, 2660–2668.
27. G. Rombaut, S. Golhen, L. Ouahab, C. Mathonière, O. Kahn, *J. Chem. Soc*, *Dalton Trans.* **2000**, 3609–3614.
28. K. Qian, X. C. Huang, C. Zhou, X. Z. You, X. Y. Wang, K. R. Dunbar, *J. Am. Chem. Soc.* **2013**, *135*, 13302–13305.
29. S. L. Zhang, X. H. Zhao, X. Y. Wang, *Dalton Trans.* **2015**, *44*, 15189–15197.
30. F. Bonadio, M. C. Senna, J. Ensling, A. Sieber, A. Neels, H. Stoeckli-Evans, S. Decurtins, *Inorg. Chem.* **2005**, *44*, 969–978.
31. D. P. Zhang, W. J. Si, P. Wang, X. Chen, J. Z. Jiang, *Inorg. Chem.* **2014**, *53*, 3494–3502.
32. D. P. Zhang, H. L. Wang, Y. T. Chen, Z. H. Ni, L. J. Tian, J. Z. Jiang, *Inorg. Chem.* **2009**, *48*, 5488–5496.
33. D. P. Zhang, H. L. Wang, L. J. Tian, J. Z. Jiang, Z. H. Ni, *CryEngComm*. **2009**, *11*, 2447–2451.
34. D. P. Zhang, Z. D.Zhao, P. Wang, X. J. Chen, *J. Coord. Chem*. **2012**, *65*, 2549–2560.
35. D. P. Zhang, Z. D. Zhao, P. Wang, X. Chen, *Bull. Korean Chem. Soc*. **2012**, *33*, 1581–1585.
36. H. Y. Zhang, C. C. Xue, J. W. Shi, H. Liu, Y. H. Dong, Z. D. Zhao, D. P. Zhang, J. Z. Jiang, *Cryst. Growth Des.* **2016**, *16*, 5753–5761.
37. O. Kahn, Molecular Magnetism, VCH, *New York*, **1993**, 258.
38. M. E. Fisher, *Am. J. Phys*. **1964**, *32*, 343–346.

Povzetek

Tri strukturne motive s štirimi ciano skupinami $K_2[M(CN)_4]$ (M = Ni, Pd, Pt) in manganovo(II) spojino s koordinacijskim številom sedem, ki vsebuje polzaprti makrociklični ligand, smo uporabili za pripravo mostovnih ciano heterokovinskih kompleksov in tako pripravili tri M^{II}–Mn^{II} komplekse s mostovno ciano skupino: $[Mn(L)][Ni(CN)_4] \cdot 2H_2O$ (**1**) $[Mn(L)][Pd(CN)_4]$ (**2**) in $[Mn(L)][Pt(CN)_4]$ (**3**) (L = 2,6-bis[1-(2-(*N*-metilamino)etilimino)etil]piridin). Monokristalna rentgenska strukturna analiza razkrije podobno enodimenzionalno strukturo pri vseh treh spojinah zgrajeno iz izmeničnih $[Mn(L)]^{2+}$ in $[M(CN)_4]^{2-}$ strukturnih motivov, ki so povezani preko ciano mostov. Pri vseh treh izostrukturnih kompleksih je koordinacijska geometrija manganovega iona v obliki rahlo popačene pentagonalne bipiramide z dvema ciano dušikovima atomoma v *trans* položaju in z N5 koordinacijo liganda L v ekvatorialni legi. Raziskave magnetnih lastnosti teh kompleksov so razkrile zelo šibko antiferomagnetno interakcijo med sosednjimi Mn(II) ioni, ki so povezani preko daljših NC–M–CN enot. Na podlagi magnetne susceptibilnosti smo določili magnetne sklopitvene konstante za komplekse **1**–**3**, ki so J = –0.081, –0.103 in –0.14 cm^{-1}.

Scientific paper

Phase Equilibria and some Properties of Solid Solutions in The Tl_5Te_3-Tl_9SbTe_6-Tl_9GdTe_6 System

Samira Zakir Imamaliyeva,*[,1] Turan Mirzaly Gasanly,[2] Vagif Akber Gasymov[1] and Mahammad Baba Babanly[1]

[1] *Institute of Catalysis and Inorganic Chemistry named after acad.M.Nagiyev, Azerbaijan National Academy of Sciences, H.Javid ave., 131, Az-1143, Baku, Azerbaijan*

[2] *Baku State University, Z.Khalilov str., 23, Az-1148, Baku, Azerbaijan*

* *Corresponding author: E-mail: samira9597a@gmail.com*

Received: 15-01-2017

Abstract

Phase equilibria in the Tl_5Te_3-Tl_9SbTe_6-Tl_9GdTe_6 system were experimentally studied by thermal analysis, X-ray diffraction and microhardness measurements applied to equilibrated alloys. Some isopleth sections, isothermal section at 760 K, and also projections of the liquidus and solidus surfaces, were constructed. A continuous series of solid solutions was found in this system. Solid solutions crystallize in the tetragonal Tl_5Te_3 structure type.

Keywords: Thallium-antimony tellurides; thallium-gadolinium tellurides; phase equilibria; projections of the liquidus and solidus; solid solutions; crystal structure

1. Introduction

A number of works have illustrated the continuing interests in new multinary chalcogenides of heavy p-elements, including rare earth elements. Due to their important functional properties, they find applications in a wide range of devices such as ion-selective sensors, microbatteries, modern day solar cells, and thermoelectric energy conversion.[1–3] Moreover; some of them have attracted interest as topological insulators.[4,5]

Thallium subtelluride, Tl_5Te_3, thanks to features of crystal structure (Sp.gr.I*4*/mcm, a = 8.930; c = 12.598 Å) has a number of ternary derivatives of $Tl_4A^{IV}Te_3$ and $Tl_9B^{V}Te_6$-type (A^{IV}-Sn, Pb; B^{V}-Sb, Bi).[6–9] These compounds exhibit good thermoelectric properties, and Tl_9BiTe_6 has reported a ZT ~1.2 at 500 K.[10–12] Furthermore, the Dirac-like surface states were observed in $[Tl_4]TlTe_3$ (Tl_5Te_3) and its tin-doped derivative $[Tl_4](Tl_{1-x}Sn_x)Te_3$.[13]

The new ternary compounds of Tl_9LnTe_6- type (Ln-Ce, Nd, Sm, Gd, Tm, Tb) which are a new of substitution derivatives of Tl_5Te_3 were reported in some wokrs.[14–16] Later, H.Kleinke and co-workers have reported the crystal structure as well as magnetic and thermoelectric properties for a number of Tl_9LnTe_6-type compounds.[17–19]

Further studies of phase equilibria in the systems including the Tl_5Te_3 compound or its structural analogs showed that these systems are characterized by the formation of unlimited solid solutions.[20–22]

This study reports a detailed investigation of phase equilibria in the Tl_5Te_3-Tl_9SbTe_6-Tl_9GdTe_6 system.

Tl_5Te_3 and Tl_9SbTe_6 melt congruently at 723 and 790 K while Tl_9GdTe_6 melts with decomposition by the peritectic reaction at 800 K.[7, 23, 24] The lattice parameters of Tl_9SbTe_6 and Tl_9GdTe_6 are following: a = 8.829, c = 13.001 Å, z = 2; a = 8.870; c = 13.027 Å, z = 2.[24, 25]

The Tl_5Te_3-Tl_9SbTe_6 system is characterized by the formation of continuous solid solutions areas based on Tl_5Te_3.[7]

2. Experimental

2. 1. Materials and Syntheses

For the synthesis, we used the high purity thallium, antimony, gadolinium, and tellurium (the purity of the ingredient was better than 99.99 mass. %).

The surface of thallium was coated by a thin oxide film, which was removed before use.

It should be noted that, thallium and its compounds are extremely toxic, and should be handled with great care. Thallium is readily absorbed through the skin and care should be taken to avoid this route of exposure. Therefore, we used protective gloves at all times when working with thallium. However, no respiratory tract covers are required since thallium is not volatile.

The elements were weighed to be about 10 g in total according to the molar ratio of the corresponding binary and ternary compound, were placed in silica tubes of about 20 cm in length and then were sealed under a vacuum of 10^{-2} Pa.

Taking into account the congruent melting of Tl_5Te_3 and Tl_9SbTe_6, their synthesis was carried out by heating of elements in one zone electric furnace at the 750 and 830 K, respectively followed by cooling in the switched-off furnace.

The obtained intermediate ingot of Tl_9GdTe_6 was carefully ground in an agate mortar, pressed into the circular pellet of about 10 mm diameter and annealed at 770 K within ~1000 h as it was done in previous work.[24] The weight losses during the pellet preparation were less than 0.5 mass. %. In order to prevent a reaction between the gadolinium and the quartz during high temperature reactions, quartz tubes coated internally with a thin layer of carbon were used.

The purity of the synthesized compounds was checked by the X-ray diffraction (XRD) and differential thermal analysis (DTA).

Only one thermal effect was observed for Tl_5Te_3 (723 K) and Tl_9SbTe_6 (790 K); whereas two peaks for Tl_9GdTe_6 which were relevant the peritectic reaction at 800 K and its liquidus at 1190 K. These data are in good agreement with the literature references.[7,23,24]

XRD confirmed that synthesized compounds were phase-pure. Powder XRD pattern of the Tl_9SbTe_6 and Tl_9GdTe_6 were similar to that of Tl_5Te_3. The unit cell parameters were practically equal to literature data (Table 1).[24,25]

Synthesized binary and ternary compounds were used for the fabrication of the alloys of the Tl_5Te_3-Tl_9SbTe_6-Tl_9GdTe_6 system. The alloys weighing 1 g were synthesized in quartz tube evacuated to 10^{-2} Pa. Taking into account the fact that an equilibrium state could not be obtained even after the long-time (1000 h) annealing, after synthesis the samples containing more than 60 mol% Tl_9GdTe_6 were powdered, mixed, pressed into circular pellets of about 10 mm diameter and annealed at 700 K for 1 month.

2. 2. Methods

X-ray powder diffraction (XRD), differential thermal analysis (DTA) and also microhardness measurements were employed to check the purity of the synthesized starting compounds and analyze the samples in order to plot the phase diagrams.

DTA was performed using a NETZSCH 404 F1 Pegasus differential scanning calorimeter within room temperature and ~1400 K depending on the composition of the alloys at a heating rate of 10 K min^{-1} and accuracy about ±3°. Temperatures of thermal effects were taken mainly from the heating curves.

The XRD measurements of the powdered specimen were recorded using a Bruker D8 diffractometer utilizing CuK_α radiation within $2\theta = 10 \div 70°$. The unit cell parameters were calculated by indexing of powder patterns using Topas V3.0 software. An accuracy of the crystal lattice parameters is shown in parentheses (Table).

Microhardness measurements were done with a microhardnesmeter PMT-3, the typical loading being 20 g and accuracy about 20 MPa.

3. Results and Discussion

The combined analysis of obtained experimental and literature data [7, 24, 25] allowed us to construct the diagram of the phase equilibria in the Tl_5Te_3-Tl_9SbTe_6-Tl_9GdTe_6 system (Table, Fig.1-6).

The $2Tl_5Te_3$-Tl_9SbTe_6 system is quasi-binary and characterized by the formation of unlimited solid solutions (δ) with Tl_5Te_3-structure.[7]

The $2Tl_5Te_3$-Tl_9GdTe_6 and Tl_9SbTe_6-Tl_9GdTe_6 systems (Table 1, Figs. 1a, 2a) are characterized by the formation of continuous solid solutions (δ) with Tl_5Te_3-structure. However, they are non-quasi-binary sections of the Tl–Gd–Te ternary and Tl-Sb-Gd-Te quaternary systems due to the peritectic melting of the Tl_9GdTe_6 compound. This leads to crystallization infusible X phase in a wide composition interval and formation two-phase L + X and three-phase L + X + δ areas. These areas are not experimentally fixed due to narrow temperature interval and shown by dotted line.

We have assumed that the X phase has a composition $TlGdTe_2$. This assumption is confirmed by the presence of the most intense reflection peaks of $TlGdTe_2$ on diffractograms of the as-cast alloys from the region more than 63 mol% Tl_9GdTe_6.[26]

It should be noted that regardless a very close melting temperature of Tl_9SbTe_6 (790K) and peritectic decomposition of Tl_9GdTe_6 (800 K) compounds, the liquidus and solidus curves have not extremum points and temperature interval of the crystallization of the δ-phase is less than 3 K. Such phenomenon is realized when the enthalpy of mixing during the formation of solid and liquid solutions from starting compounds is practically equal to zero. In other words, in the studied system the Sb → Gd replacement in the solid and liquid states are not accompanied by a significant thermal effect. This fact allows us to characterize the δ-solid solutions as quasi-ideal solution.

Table 1. Some properties of phases in the Tl_5Te_3-Tl_9SbTe_6-Tl_9GdTe_6 system.

Phase	Thermal effects, K (accuracy ±3°)	Microhardness, MPa, (accuracy ±20 MPa)	Parameters of tetragonal lattice, Å	
			a	*c*
Tl_5Te_3	723	1130	8.9303(3)	12.5987(8)
$Tl_{9.8}Gd_{0.2}Te_6$	730–744	1180	8.9184(4)	12.6848(9)
$Tl_{9.6}Gd_{0.4}Te_6$	740–763	1160	8.9064(4)	12.7707(9)
$Tl_{9.5}Gd_{0.5}Te_6$	750–770	–	–	–
$Tl_{9.4}Gd_{0.6}Te_6$	760–773	1150	8.8953(4)	12.8558(8)
$Tl_{9.2}Gd_{0.8}Te_6$	775–788; 1100	1150	8.8824(3)	12.9417(8)
$Tl_{9.1}Gd_{0.9}Te_6$	785–793; 1150	–	–	–
Tl_9GdTe_6	800; 1190	1100	8,8705(4)	13,0277(7)
$Tl_9Sb_{0.2}Gd_{0.8}Te_6$	798; 1100	1150	8.8616(5)	13.0218(8)
$Tl_9Sb_{0.4}Gd_{0.6}Te_6$	795	1130	8.8536(5)	13.0167(9)
$Tl_9Sb_{0.5}Gd_{0.5}Te_6$	794	–	–	–
$Tl_9Sb_{0.6}Gd_{0.4}Te_6$	793	1120	8.8454(4)	13.0115(8)
$Tl_9Sb_{0.8}Gd_{0.2}Te_6$	792	1050	8.8373(3)	13.0066(7)
Tl_9SbTe_6	790	1000	8.8315(4)	13.0017(7)

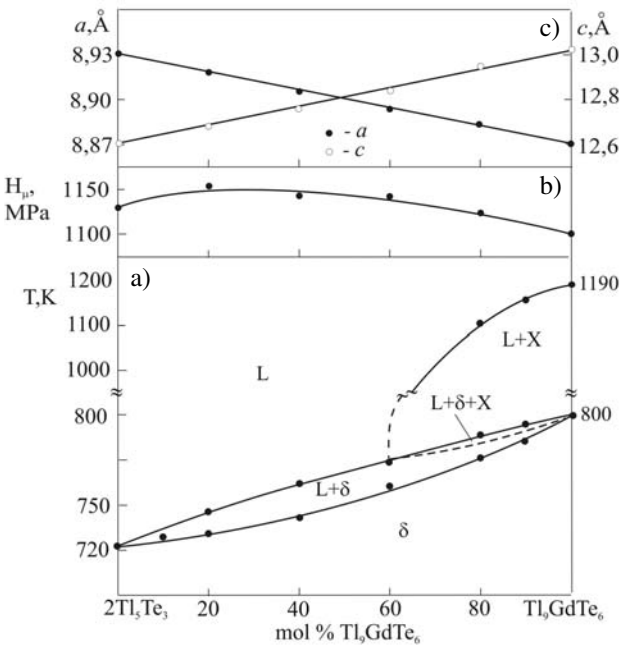

Fig. 1. Polythermal section (a), concentration relations of microhardnesses (b), and lattice parameters (c) for the system $2Tl_5Te_3$-Tl_9GdTe_6

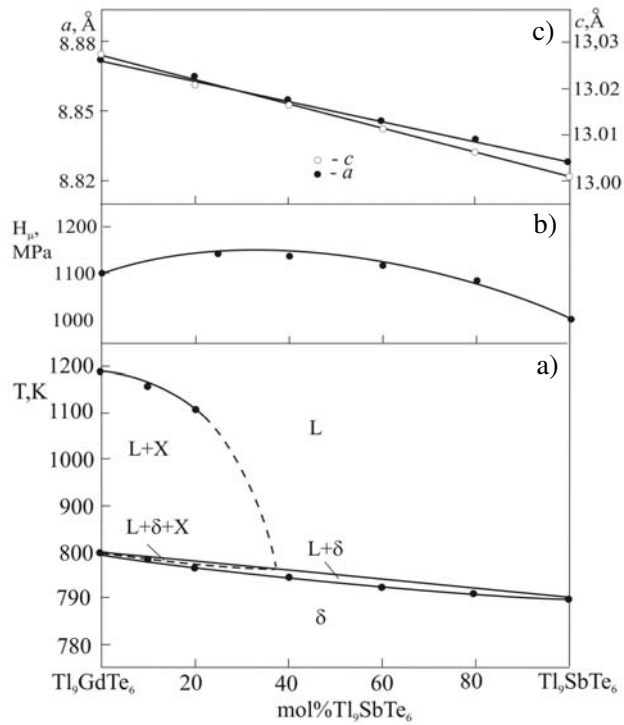

Fig. 2. Polythermal section (a), concentration relations of microhardnesses (b), and lattice parameters (c) for the system Tl_9GdTe_6-Tl_9SbTe_6

The curves of microhardness dependencies have a flat maximum, which is typical for systems with continuous solid solutions (Fig. 1b and 2b).

The XRD patterns obtained are presented in Fig. 3. Powder diffraction patterns of Tl_5Te_3, Tl_9SbTe_6 and Tl_9GdTe_6, and intermediate alloys were very similar to that of Tl_5Te_3 with slight reflections displacement from one compound to another. The lattice parameters of solid solutions depend linearly on the composition, i.e. obey the Vegard's rule.

Projections of the liquidus and solidus surfaces of the Tl_5Te_3-Tl_9SbTe_6-Tl_9GdTe_6 system.

Liquidus of the Tl_5Te_3-Tl_9SbTe_6-Tl_9GdTe_6 system consists of two fields of the primary crystallization of X-phase and δ- solid solutions, limited by the ab curve corresponds to the monovariant peritectic L + X ↔ δ equilibrium (Fig. 4).

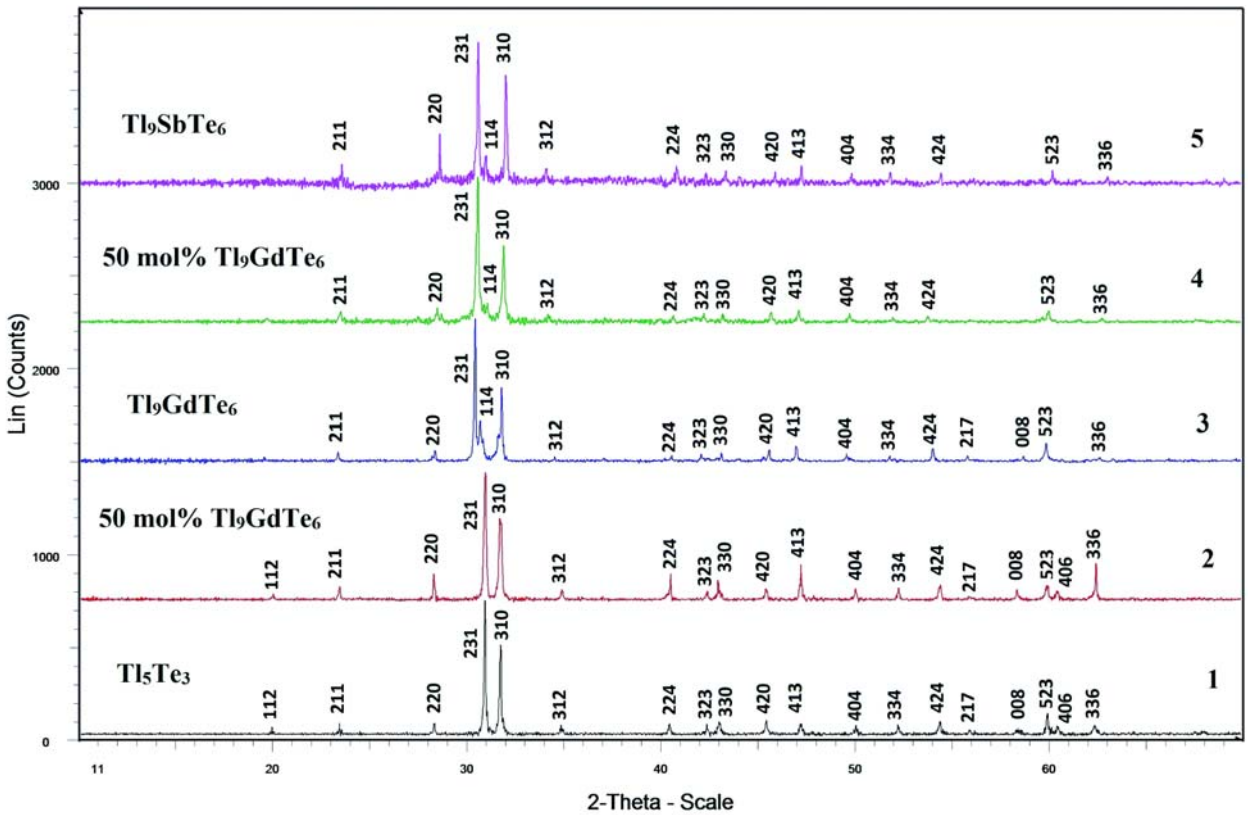

Fig. 3. XRD patterns for different compositions in the Tl_5Te_3-Tl_9GdTe_6 (patterns 1–3) and Tl_9GdTe_6-Tl_9SbTe_6 (patterns 3–5) systems. 1– Tl_5Te_3; 2–50 mol % Tl_9GdTe_6; 3-Tl_9GdTe_6; 4–50 mol % Tl_9GdTe_6; 5-Tl_9SbTe_6.

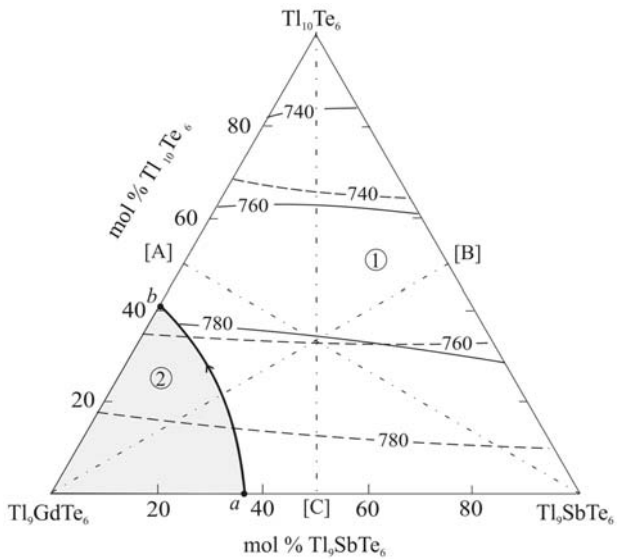

Fig.4. Projections of the liquidus and solidus (dashed lines) surfaces of the Tl_5Te_3-Tl_9GdTe_6-Tl_9SbTe_6 system. Dash-dot lines show the investigated sections. Primary crystallization phases: 1-δ; 2-X phase.

Isopleth sections of the Tl_5Te_3-Tl_9SbTe_6-Tl_9GdTe_6 system (Fig.5).

Figs. 5a–c show the isopleth sections $2Tl_5Te_3$-[C], Tl_9SbTe_6-[A] and Tl_9GdTe_6-[B] of the Tl_5Te_3-Tl_9SbTe_6-Tl_9GdTe_6 system, where A, B and C are equimolar compositions of the boundary systems as shown in Fig. 4.

According to the phase diagram of the Tl_9GdTe_6-[B] cut, the primary crystallization of the δ-phase occurs from the liquid phase in the composition area < 60 mol% Tl_9GdTe_6. In the Tl_9GdTe_6- rich alloys the X-phase first crystallizes, then a monovariant peritectic equilibrium L + X ↔ δ takes place.

As can be seen, over the entire compositions area of the Tl_9SbTe_6-[A] and Tl_5Te_3-[C] cuts only δ-phase crystallizes from the melt.

Comparison between isopleth sections (Fig. 5) with the isothermal section (Fig. 6) shows, that tie-lines positions in two-phase area L + δ do not correspond to the cross section planes and continuously change with temperature. The tie-lines positions at 760 K are shown in Fig. 6.

4. Conclusion

A T-x-y diagram of the Tl_5Te_3-Tl_9SbTe_6-Tl_9GdTe_6 system, including the phase diagrams of boundary systems Tl_5Te_3-Tl_9TbTe_6 and Tl_9SbTe_6-Tl_9TbTe_6, isothermal section at 760 K, some isopleth sections and also the liquidus and solidus surfaces projections, were constructed.

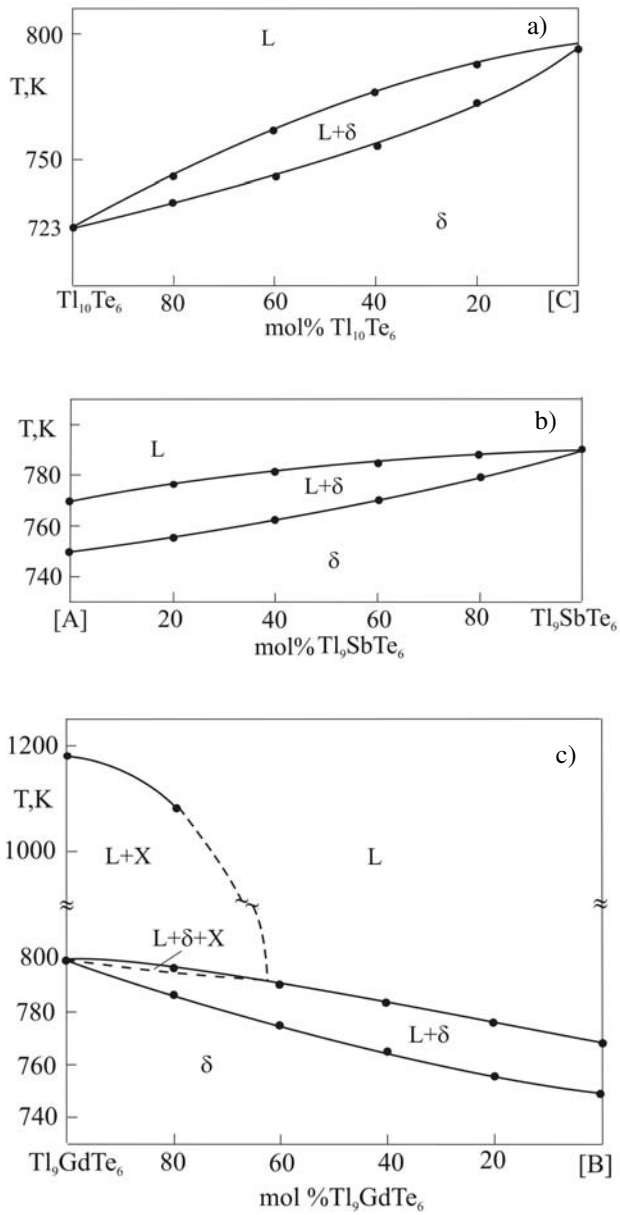

Fig. 5. Polythermal sections $Tl_{10}Te_6$-[C], Tl_9SbTe_6-[A], and Tl_9GdTe_6-[B] of the phase diagram of the Tl_5Te_3 -Tl_9SbTe_6-Tl_9GdTe_6 system.

Components of the system display unlimited solubility in the solid state. Obtained experimental data can be used for choice the composition of solution-melt and for determining of temperature conditions for growing crystals of δ-phase with a given composition.

5. Acknowledgment

This work was done in the international joint research laboratory between Institute of Catalysis and Inorganic Chemistry of ANAS (Azerbaijan) and Donostia International Physics Center (Basque Country, Spain).

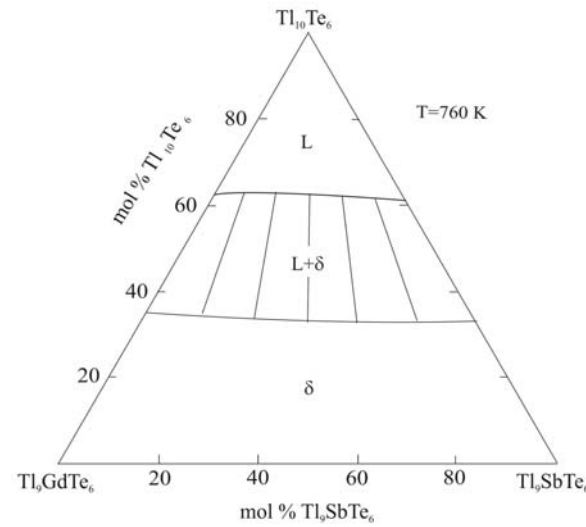

Fig.6. The isothermal section of the phase diagram at 760 K of the Tl_5Te_3-Tl_9GdTe_6-Tl_9SbTe_6 system.

6. References

1. Applications of Chalcogenides: S, Se, and Te, ed. by Gurinder Kaur Ahluwalia, Springer, **2016**.
2. A. R. Jha, Rare Earth Materials: Properties and Applications, CRC Press, United States, **2014**. https://doi.org/10.1201/b17045
3. CRC Handbook of Thermoelectrics, ed. by D. M. Rowe, CRC Press, New York, **1995**.
4. B. Yan, H-J.Zhang, C-X.Liu, X-L. Qi, T. Frauenheim and S-C. Zhang, *Phys. Rev. B*. **2010**, *82*, 161108(R)-7
5. N. Singh and U. Schwingenschlogl, *Phys. Status Solidi RRL*. **2014**, *8*, 805–808. https://doi.org/10.1002/pssr.201409110
6. I. Schewe, P. Böttcher, H. G. Schnering, *Z. Kristallogr.* **1989**, *Bd188*, 287–298. https://doi.org/10.1524/zkri.1989.188.3-4.287
7. M. B. Babanly, A. Azizulla, A. A. Kuliev, *Russ. J. Inorg. Chem*. **1985**, *30*, 1051–1059.
8. M. B. Babanly, A. Azizulla, A. A. Kuliev, *Russ. J. Inorg. Chem*. **1985**, *30*, 2356–2359.
9. A. A. Gotuk, M. B.Babanly, A. A. Kuliev, *Inorg. Mater.* **1979**, *15*, 1062–1067.
10. K. Kurosaki, H. Uneda, H. Muta and S. Yamanaka, *J. Alloys Compd*. **2004**, *376*, 43–48. https://doi.org/10.1016/j.jallcom.2004.01.018
11. Q. Guo, A. Assoud, H. Kleinke. *Adv.Energy Mater.* **2014**, *4*, 1400348/1–8.
12. B. Wolfing, C. Kloc, J. Teubner, E. Bucher, *Phys. Rev. Let*. **2001**, *36*, 4350–4353. https://doi.org/10.1103/PhysRevLett.86.4350
13. K. E. Arpino, D. C.Wallace, Y. F. Nie, T. Birol, P. D. C. King, S. Chatterjee, M. Uchida, S. M. Koohpayeh, J.-J. Wen, K. Page, C. J. Fennie, K. M.Shen, and T. M. McQueen, *Phys. Rev. Lett.* (PRL). **2014**, *112*, 017002-5. https://doi.org/10.1103/PhysRevLett.112.017002

14. S. Z. Imamalieva, F. M. Sadygov, M. B. Babanly, *Inorg. Mater.* **2008**, *44*, 935–938. https://doi.org/10.1134/S0020168508090070
15. M. B. Babanly, S. Z. Imamaliyeva, D. M. Babanly, *Azerb. Chem.* J. **2009**, *2*, 121–125**.**
16. M. B. Babanly, S. Z. Imamaliyeva, F. M. Sadygov, *News of BSU. Nat. Sci. Ser.* **2009**, *4*, 5–10.
17. S. Bangarigadu-Sanasy, C. R. Sankar, P. Schlender, H. Kleinke, *J. Alloys Compd*. **2013**, *549*, 126–134. https://doi.org/10.1016/j.jallcom.2012.09.023
18. S. Bangarigadu-Sanasy, C. R. Sankar, P. A. Dube, J. E. Greedan, H. Kleinke, *J. Alloys. Compd.* **2014**, *589*, 389–392. https://doi.org/10.1016/j.jallcom.2013.11.229
19. Q. Guo, H. Kleinke, *J. Alloys. Compd.* **201**5, *630*, 37–42. https://doi.org/10.1016/j.jallcom.2015.01.025
20. M. B. Babanly, J.-C. Tedenac, S. Z. Imamalieva, F. N. Guseynov, G. B. Dashdieva, *J. Alloys Compd.* **2010**, *491*, 230–236. https://doi.org/10.1016/j.jallcom.2009.08.157
21. S. Z. Imamaliyeva, F. N. Guseynov, M. B. Babanly, *J. Chem. Probl*. **2008**, *4*, 640–646.
22. S. Z. Imamaliyeva, F. N. Guseynov, M. B. Babanly, *Azerb. Chem.J.* **2009**, *1*, 49–53.
23. M. M. Asadov, M. B. Babanly, A. A. Kuliev, *Inorg. Mater.* **1977**, *13*, 1407–1410.
24. S. Z. Imamaliyeva, T. M. Gasanly, I. R. Amiraslanov, M. B. Babanly, *Austr. J. Basic Appl. Sci.* **2015**, *9*, 541.
25. K. Wacker, *Kristallogr. Supple.* **1991**, *3*, 281.
26. C. R. Sankar, S. Bangarigadu-Sanasy, H. Kleinke, *J. El. Mater*. **2012**, *41*, 1662–1266.

Povzetek

V sistemu Tl_5Te_3-Tl_9SbTe_6-Tl_9GdTe_6 smo preučevali fazna ravnotežja s termično analizo, rentgensko praškovno difrakcijo in meritvami mikrotrdote. Pripravili smo nekatere izopletne in izotermične krivulje pri 760 K ter projekcije tekočinsko trdnih površin. V tem sistemu smo našli serijo kontinuirnih trdnih raztopin. Trdne raztopine kristalizirajo v tetragonalnem Tl_5Te_3 kristalnem sistemu.

Scientific paper

Influence of Thermal and Bacterial Pretreatment of Microalgae on Biogas Production in Mesophilic and Thermophilic Conditions

Beti Vidmar,[1] Romana Marinšek Logar,[1] Mario Panjičko[2] and Lijana Fanedl[1,*]

[1] *Chair of Microbiology and Microbial Biotechnology, Department of Animal Science, Biotechnical Faculty, University of Ljubljana, Groblje 3, 1230 Domžale, Slovenia*

[2] *Sustainable Technologies Development Centre Ltd (CROTEH), Dragutina Golika 63, HR-10020 Zagreb, Croatia*

* *Corresponding author: E-mail: Lijana.Fanedl@bf.uni-lj.si*
Tel: 00386 1 3203 835

Received: 23-11-2016

Abstract

Microalgae biomass has a great potential in search for new alternative energy sources. They can be used as a substrate for the biogas production in anaerobic digestion. When using microalgae, the efficiency of this process is hampered due to the resistant cell wall. In order to accelerate the hydrolysis of cell wall and increase the efficiency of biogas production we applied two different pretreatments – biological and thermal under mesophilic and thermophilic conditions. During biological pretreatment we incubated microalgae with anaerobic hydrolytic bacteria *Pseudobutyrivibrio xylanivorans* Mz5^T. In thermal pretreatment we incubated microalgae at 90 °C. We also tested a combined thermal and biological pretreatment in which we incubated *P. xylanivorans* Mz5^T with thermally pretreated microalgae. Thermal pretreatment in mesophilic and thermophilic process has increased methane production by 21% and 6%, respectively. Biological pretreatment of microalgae has increased methane production by 13%, but only under thermophilic conditions (pretreatment under mesophilic conditions showed no effect on methane production). Thermal-biological pretreatment increased methane production by 12% under thermophilic conditions and by 6% under mesophilic conditions.

Keywords: biogas production; anaerobic digestion; microalgae; biological pretreatment; thermal pretreatment; *Pseudobutyrivibrio xylanivorans* Mz5^T

1. Introduction

Global human population growth, rapid technological development, climate changes and depletion of fossil fuels have led to an accelerated search for new renewable energy sources. Renewable energy sources are rapidly evolving area with positive effects on the environment (with little or zero carbon dioxide emissions and substrate low sulfur content) and promising economic aspect.[1] Given alternative energy sources provoked a lot of controversy, despite initial positive expectations.

Renewable energy sources are classified into groups; first generation biofuels (derived exclusively from crops of cultivated plants) and second generation biofuels (derived from lignocellulosic biomass)[2–4] have serious flaws, including a great need for arable land and large amount of consumed water. They are also creating a lot of pressure on agriculture and have a low productivity, since produced biomass cannot cover global demand.[5]

In recent decades we are witnessing increase in interest of exploitation of the algae energy potential. Algae biomass represents the substrate for rapidly developing group of third generation biofuels. This generation offers the perfect solution for solving the above-mentioned drawbacks.[6] The main advantages of using algae are low water consumption (they can be grown in salty, waste and non-potable water), possible production on uncultivated areas with high carbon dioxide concentrations, theoretical high photosynthetic efficiency and high productivity.[7,8]

For a long time technology focused mainly on obtaining biodiesel from algae biomass, which proved to be energy consuming and unbalanced process. More simple process for supplying renewable energy is anaerobic digestion (AD).[9,10] Biogas from AD is an alternative, but

much more economically and energetically-favourable process.[8]

Microbial anaerobic methanogenic process is applied for the multistep decomposition of organic substrates into biogas. Biogas consists of different gases – methane (~65%), carbon dioxide (~35%) and others (nitrogen, nitrogen oxides, hydrogen, ammonia and hydrogen sulfide).[11] Other products in AD, such as heat and digestate can be used in other processes or as a soil conditioner.[8] Efficacy of AD is influenced by various factors such as composition of substrates, carbon and nitrogen ratio (C:N) of digester contents, composition of microbial community, degree of mixing, pH and temperature. It has been shown that among technological parameters temperature and pH have the biggest impact on speed of the biogas production.[12–15] The process of anaerobic degradation can run under psychrophilic (<20 °C), mesophilic (25–40 °C) or thermophilic (50–65 °C) conditions.[16,17] Technically speaking, the industry is only interested in mesophilic and thermophilic process,[18] since the decomposition at lower temperatures is very slow.[19] When speaking about AD of the same substrates the mesophilic and thermophilic processes are distinguished mainly by their composition of microbial community, resulting in biogas production differences from the same substrate.[20,21,22] There are some important microbiological characteristics associated with thermophilic anaerobes, which may affect the biogas production. These characteristics include slow bacterial growth, high cell death, lower bacteria variety, which show an effect on relatively high fatty acids concentration (more than 1 g l^{-1}), reduced substrate degradation etc.[21] Since AD is a multi-step process, it is depending on interactions among bacterial and archaeal microbial communities and their substrate and product specificities. Knowledge about the dynamics of microbial community structure and activity is essential for successful planning of the biogas process, monitoring its parameters and for reaching main goal: process stability and maximum yield.[23] The link between community structure and performance is still not completely clear and more studies are needed.[24,25]

Mesophilic conditions represent the optimum temperature range for larger group of microorganisms (anaerobic bacteria and archaea), as thermophilic conditions. Nevertheless the most important fact is to maintain a stable temperature, irrespective of applied process.[20] Biochemical reactions at higher temperatures are faster therefore the degradation is faster too. Generally, but not always, thermophilic AD is up to 8-times faster and up to 4-times more productive than mesophilic. It allows better organic matter decomposition and increased biogas production (up to 36%), although the actual methane yield in thermophilic AD is dependent on substrate composition and its C:N ratio. Higher temperature also enables thermal destruction of pathogenic bacteria, which is considered as a big advantage over other processes. Disadvantages of thermophilic AD are instability, higher energy inputs and in comparison to the mesophilic process higher temperatures can cause reduced CO_2 solubility, which leads to higher proportion of free ammonium and increase in pH.[20]

Microalgae represent a promising substrate for AD, because they are rich in nutrients, such as carbon, nitrogen and phosphorus, which are essential for the anaerobic microorganisms. Microalgae cells contain a lot of water (78–90%),[26,27] many species have high content of carbohydrates (up to 64% of their dry matter) and lipids (2–75% of their dry matter).[28,29] Carbohydrates occur in the form of starch, cellulose and various sugars,[30] so the substrate is suitable for microbial fermentation. Freshwater microalgae species can contain up to 31% free fatty acids (FFA), but the composition of FFA and lipids is heavily depending on growth conditions (light, temperature, nitrogen level, growth stage at which they are harvested).[31] In comparison to carbohydrates and proteins, lipids have higher theoretical potential for methane production. Nevertheless, when the buffer capacity of the system is low, higher lipid content can result in formation of intermediate products (long chain fatty acids) during AD and consequently process inhibition.[32] Some species of microalgae may contain lignin (<2%),[33] a high level of cellulose (7,1%) and hemicellulose (16,3%).[34] High ash contents are typical for winter months and in early spring. The C:N ratio is around 10:1.[34,35]

Despite the positive aspects of microalgae as substrate for biogas production, we may encounter several problems that also limit their use for anaerobic decomposition. Problems may occur due to low concentration of biodegradable substrate, cell walls resistant to biodegradation, low C:N and sometimes higher lipids concentrations.[32]

Some green algae are covered by multiple layers of intricately sculpted scales while others have crystalline glycoprotein coverings or thick multilaminate fibrillar cell walls. A few taxa though have cell walls with remarkable structural and biochemical similarity to cell walls found in land plants.[36] As an example we can take a known representative of the genus *Scenedesmus*, wherein the rigid cell wall is composed of glucose, mannose and galactose. Individual sugars are otherwise well biodegradable, but in the cell wall they are linked together and form cellulose, hemicellulose and some other polymers (e.g. sporopollenin). These molecules form a strong cell wall, highly resistant to bacterial degradation.[10]

One of the possible solutions to enhance the AD of microalgae biomass are different types of pretreatments, which we use in order to make substrate more susceptible to biodegradation.[37] Pretreatments can be divided into four groups – thermal, mechanical, chemical and biological. Most studied area is thermal pretreatment of microalgae biomass, which shows favourable results and certain industrial processes already run continuously. Mechanical pretreatment generally requires more energy input in

comparison to the chemical, thermal or biological treatments. Chemical pretreatment has proved successful, especially in combination with thermal, but the main disadvantage is contamination and complexity of downstream processes. Biological pretreatment of biomass is also very promising, mainly due to low energy consumption.[38]

In the presented research work the biodegradability of untreated and pretreated microalgae was examined in anaerobic digestion. In order to accelerate the hydrolysis and increase the efficiency of biogas production two different pretreatments were applied – biological (bacterial) and thermal. A combined thermal-biological pretreatment was tested, too. Biogas production was measured in biochemical methane potential assay under mesophilic and thermophilic conditions.

2. Experimental

2. 1. Substrate for Biogas Production

Microalgae biomass was obtained from the open photobioreactor of company Koto d.o.o. Microalgae are produced in digestate (liquid part of the effluent after separation to liquid and solid part) of thermophilic biogas reactor, which converges into 26 m^3 big pool. Microalgae biomass was pumped out of the pool with a peristaltic pump and stored in larger containers, later divided into smaller volumes (up to 1 l) and frozen at –20 °C. Chemical composition of the dry microalgae biomass is shown in Table 1.

Table 1. Chemical composition of the dry microalgae biomass. Legend: TVS (total volatile solids), TOC (total organic carbon), TN (total nitrogen) (Determined by Koto d.o.o.).

Parameters	Content (g kg^{-1})
TVS	796,8
TN	70,7
Ash	203,2
Protein	441,3
TOC	404,8
C:N ratio	5,7

2. 2. Microbial Inoculum for Biogas Production

Two different microbial inoculums were used to test the differences between mesophilic and thermophilic process of biogas production. Mesophilic microbial inoculum was taken from an active CSTR (continuous stirred-tank reactor) operating at 37 °C (biogas plant Petrol d.d., Slovenia). Before the experiment, the microbial inoculum was pre-incubated for eight days at 37 °C. Thermophilic microbial inoculum was taken from CSTR operating at 55 °C (biogas plant Koto d.o.o., Slovenia) and was pre-incubated for eight days at 55 °C.

2. 3. Pretreatment of Microalgae Biomass

The temperature of 90 °C was applied for thermal treatment of microalgae in this experiment. The selected temperature based on previous research reports.[10] Microalgae were first thawed, thoroughly mixed and distributed into glass bottles of 250 ml. The bottles were closed with gas-tight rubber and aluminium stoppers. Thermal pretreatment of microalgae was conducted in water bath for three hours at 90 °C. Occasionally the bottles were mixed and vented.

Bacterial strain *Pseudobutyrivibrio xylanivorans* $Mz5^T$ (DSM 14809) originates from the microbial collection of the Department of Microbiology and Microbial Biotechnology at Biotechnical Faculty and was used for biological pretreatment of microalgae biomass. *P. xylanivorans* $Mz5^T$ holds excellent cellulolytic, xylanolytic, amylolytic and pectinolytic activity.[39,40] Due to these characteristics, *P. xylanivorans* $Mz5^T$ was selected for biological pretreatment of microalgae.

The bacterium was cultured in DSMZ medium M330 (50 ml) and incubated overnight (~20 h) at 37 °C. When the culture reached optical density (λ = 600 nm) 0,5 ± 0,05, it was centrifuged and the precipitate was anaerobically transferred into 1 l batch reactors to pretreat microalgae biomass. Pretreatment was carried out for 24 hours at 37 °C (120 rpm), then microbial inoculum was added to the substrate.

2. 4. Experimental Setup of Biochemical Methane Potential (BMP) Assay

BMP assay was conducted to examine and determine the effect of different microalgae pretreatments on biogas and methane production. On the first day biological and thermal pretreatments were performed, but the BMP assay started the second day. Experimental setup was the same for both processes (mesophilic and thermophilic), as seen on Figure 1.

For biological pretreatment we incubated *P. xylanivorans* $Mz5^T$ together with untreated microalgae (as described in chapter 2.3), for thermal pretreatment only thermally pretreated microalgae (as described in chapter 2.3) were added and for thermal-biological pretreatment we incubated *P. xylanivorans* $Mz5^T$ with thermally pretreated microalgae. All pretreatments lasted for 24 hours, after which methanogenic microbial inoculum was added to the experimental bottles to start the anaerobic digestion.

Before experiments the appropriate loading of the bioreactors was determined by measuring TTS (total solids) and TVS (total volatile solids) for both microbial inoculums and chemical oxygen demand (COD) for microalgae.[41] The microbial inoculum concentration for both experiments was 4 g TVS l^{-1} and microalgae loading was 1,228 g TVS (144 ml).

Phosphate buffer (20 ml) and anoxic tap water were added to all experimental mixtures. Working volume for

all mixtures was 500 ml. Sole microbial inoculum served as a negative control for residual methanogenic activity. For positive control (standard), which represents the internal control for BMP assay, glucose was added as a substrate. Loading for standard mixtures was 0,748 g l^{-1} (0,2 g $COD_{glucose}$). While mixing all ingredients, anaerobic conditions were maintained by sparging gaseous nitrogen.[42] Mixtures with autoclaved culture of *P. xylanivorans* $Mz5^T$ were tested to measure the medium's nutrients and dead cell COD effect (negative control to experimental mixtures with live culture of MZ5) on biogas production. Both experiments were conducted in laboratory bioreactors (1 l) at 37 °C for mesophilic conditions and at 55 °C for thermophilic conditions. The bioreactors were kept in dark at 120 rpm for 46 days (thermophilic process) and 55 days (mesophilic process) with three replicate experimental mixtures.

In order to gain information on the cumulative biogas production in each mixture, after each measurement the volume of produced biogas was added to the sum of previous measurements. In presentation of the final results of biogas production the amount of generated biogas in negative control was also taken into account. To calculate the net quantity of the produced biogas (how much biogas was generated at the expense of the added substrate), the average amount of biogas produced in negative controls was subtracted from the production of the test mixtures. The same was done for cumulative methane production. The resulting methane yields were normalized to standard conditions as described by Hansen et. al (2004).[43]

2. 5. Analytical Methods

TTS and TVS of experimental mixtures were determined at the beginning (t_0) and the end (t_{46} for thermophilic and t_{55} for mesophilic process) of each experiment according to standard methods.[41] COD was also performed, using closed reflux method.[41] The pH-values of mixtures were measured at the beginning (t_0) and the end (t_{46} for thermophilic and t_{55} for mesophilic process) of each experiment.

The quantity and composition of produced biogas was determined 12 times during both processes. Short-chain fatty acids (SCFAs) were monitored 4 times during both processes. The amount of produced biogas was measured manually with a pressure gauge and water column.[43] The proportion of methane, carbon dioxide and nitrogen was monitored by Shimadzu 14A gas chromatograph (GC) equipped with thermal conductivity detector (TCD). The separation of gases was carried out on a steel column (diameter 1/8'') filled with PORAPAK Q (Agilent). He-

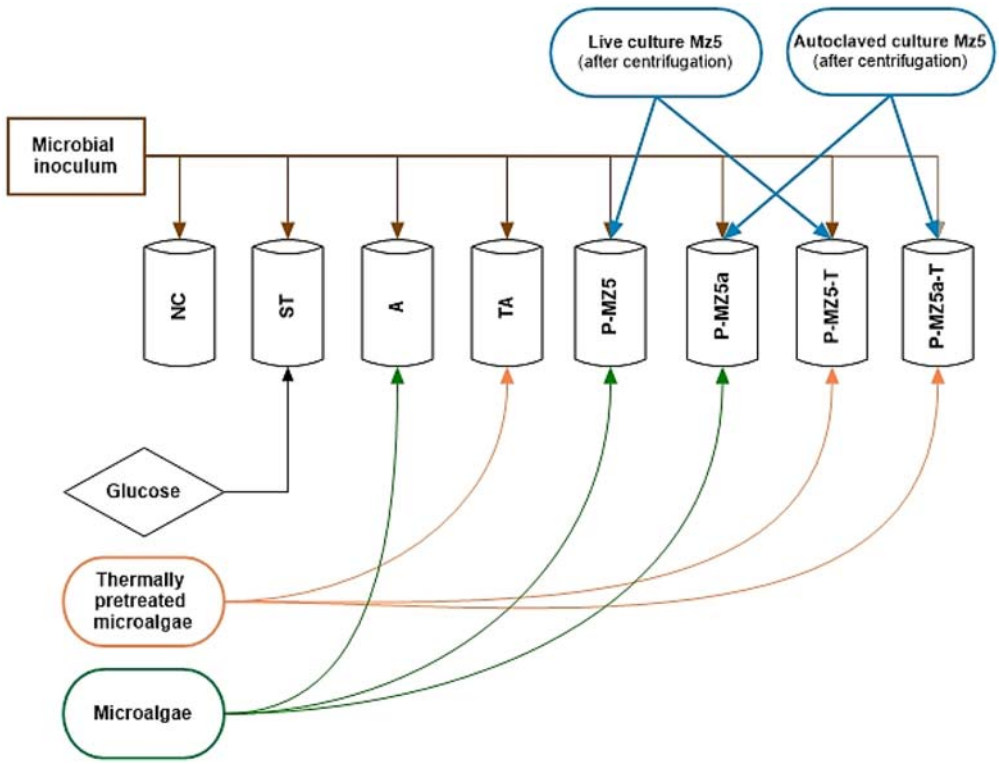

Figure 1. Experimental set-up for BMP assays. NC – negative control (microbial inoculum), ST – standard respectively positive control, A – untreated microalgae, TA – thermally pretreated microalgae, P-MZ5 – biologically pretreated microalgae (Mz5 culture added), P-MZ5a – negative control for biologically pretreated microalgae (autoclaved Mz5 culture added), P-MZ5-T – thermally and biologically pretreated microalgae (Mz5 culture added), P-MZ5a-T – negative control for thermally and biologically pretreated microalgae (autoclaved Mz5 culture added).

lium with flow rate of 25 ml min^{-1} was used as a gas carrier. For analysis, we used the following program: injector temperature was 50 °C, column temperature 30 °C, detector temperature 80 °C, current was 60 mA. Standard mixture of gases (15,7% H_2, 18,7% N_2, 20,5% CH_4 and 45,1% CO_2) was used for calibration performed using the method of surface normalization. The resulting methane yields were normalized to standard conditions and expressed in normalized volume percentage.

Ether extraction of SCFAs was performed according to the adapted method.[44] SCFAs were determined by GC equipped with a flame ionization detector (FID). Helium was used as a gas carrier. For analysis, we used the following program: injector temperature was 250 °C, column initial temperature 80 °C, column final temperature 160 °C, detector temperature 250 °C, time of maintaining the initial column temperature was 2 minutes and time of final temperature maintenance was 4 minutes. Column was heated at a rate of 15 °C per minute. Quantification was performed by an internal standard method (crotonic acid, 100 mg ml^{-1}).

3. Results and Discussion

3. 1. Biogas and Methane Production from Microalgae

3. 1. 1. Mesophilic Process

The highest biogas production under mesophilic conditions resulted from thermal pretreatment of microalgae (TA) with the average production of 452,9 ml per 1 g $TVS_{substrate}$. The lowest production was recorded in case of biological pretreatment of microalgae (P-MZ5), with the average production of 324,5 ml biogas per 1 g $TVS_{substrate}$ (Figure 2, A).

The highest methane production was recorded for mixtures with thermally pretreated microalgae (TA), with the average production of 273,2 ml of methane per 1 g $TVS_{substrate}$. The lowest production of methane was measured in case of untreated microalgae (A), with average production of 217,2 ml of methane per 1 g $TVS_{substrate}$ (Figure 2, B). The average percentage of methane in biogas in mesophilic process on the last day of BMP assay represented 64,1%. The trend showed that each of the pretreatments slightly increased the methane proportion in produced biogas (Table 3).

3. 1. 2. Thermophilic Process

The maximal biogas production under thermophilic conditions was measured in case of microalgae biologically pretreated with bacteria *P. xylanivorans* $Mz5^T$ (P-MZ5), with average biogas production of 406,2 ml per 1 g $TVS_{substrate}$. Mixtures with untreated microalgae (A) and different other pretreatments produced from 317 to 386 ml of biogas per 1 g $TVS_{substrate}$. The lowest production was measured in case of thermally pretreated microalgae (TA), with average production of 317,2 ml of biogas per 1 g $TVS_{substrate}$ (Figure 2, C).

The lowest production of methane was measured in case of untreated microalgae (A), with average production of 176,9 ml of methane per 1 g $TVS_{substrate}$. The highest methane production was recorded for mixtures with biologically pretreated microalgae (P-MZ5), with the average production of 279,9 ml of methane per 1 g $TVS_{substrate}$ (Figure 2, D). The average percentage of methane in biogas in thermophilic process on the last day of BMP assay represented 61,1%. The trend also showed that each of the

Table 2. BMP assay results showing cumulative methane production (at standard conditions) per 1 g $TVS_{substrate}$ (ml) in every experimental mixture for mesophilic and thermophilic anaerobic digestion of untreated, thermally, biologically and thermally-biologically treated microalgae. Legend: A – untreated microalgae, TA – thermally pretreated microalgae, P-MZ5 – biologically pretreated microalgae (Mz5 culture added), P-MZ5a – negative control for biologically pretreated microalgae (autoclaved Mz5 culture added), P-MZ5-T – thermally and biologically pretreated microalgae (Mz5 culture added), P-MZ5a-T – negative control for thermally and biologically pretreated microalgae (autoclaved Mz5 culture added).

	Cumulative methane production per 1 g $TVS_{substrate}$ (ml)	
Bioreactor	**Mesophilic process**	**Thermophilic process**
A	217,2	176,9
TA	273,2	187,1
P-MZ5	230,8	279,9
P-MZ5a	238,6	242,4
P-MZ5-T	254,1	231,7
P-MZ5a-T	240,2	203,8

Table 3. BMP assay results showing increase in biogas and methane production due to different methods of pretreatments in mesophilic and thermophilic anaerobic digestion. Effects of pretreatments were reckoned according to the comparison in pairs (e.g. thermally treated microalgae to untreated microalgae, etc.). Differences of cumulative production of biogas and methane per 1 g $TVS_{substrate}$ due to pretreatment effects between pairs were later expressed in percentages.

	Mesophilic process		Thermophilic process	
	CH_4	Biogas	CH_4	Biogas
Thermal pretreatment	21%	16%	6%	0%
Biological pretreatment	0%	0%	13%	5%
Thermal and biological pretreatment	6%	6%	12%	11%

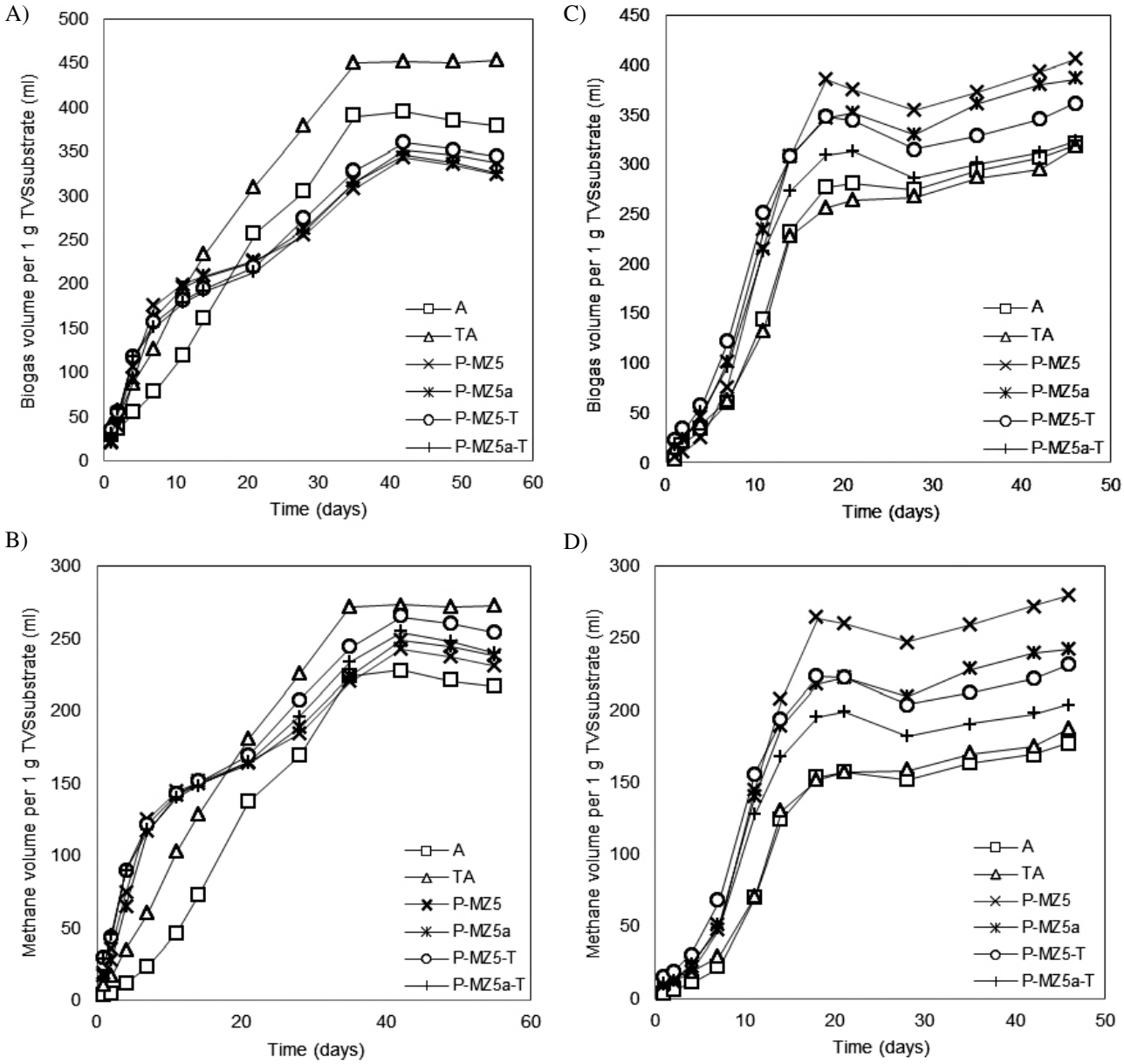

Figure 2. Cumulative biogas and methane production (at standard conditions) in mesophilic and thermophilic anaerobic digestion of untreated, thermally, biologically and thermally-biologically treated microalgae. A) biogas production per 1 g $TVS_{substrate}$ (ml) under mesophilic conditions, B) methane production per 1 g $TVS_{substrate}$ (ml) under mesophilic conditions, C) biogas production per 1 g $TVS_{substrate}$ (ml) under thermophilic conditions, D) methane production per 1 g $TVS_{substrate}$ (ml) under thermophilic conditions. Legend: A – untreated microalgae, TA – thermally pretreated microalgae, P-MZ5 – biologically pretreated microalgae (Mz5 culture added), P-MZ5a – negative control for biologically pretreated microalgae (autoclaved Mz5 culture added), P-MZ5-T – thermally and biologically pretreated microalgae (Mz5 culture added), P-MZ5a-T – negative control for thermally and biologically pretreated microalgae (autoclaved Mz5 culture added).

pretreatments slightly increased the methane percentage in produced biogas (Table 3).

According to the literature, the thermophilic process shows 25–50% higher anaerobic activity compared to mesophilic.[21] The temperature of anaerobic process affects the concentration and presence of individual SCFAs, which indicate that the accumulation of intermediates is in fact different under mesophilic and thermophilic conditions. Research results indicate that this feature depends mainly on the composition of microbial communities.[22,23] For optimal process, the concentration of acetic acid should not be higher than 2 g l^{-1} and concentration of propionic acid higher than 0,9 g l^{-1}. Increased concentration of propionic acid is the most significant indication of process inhibition[45] and occurs following the acetic acid accumulation.

The highest total concentration of SCFAs in this study under mesophilic conditions was 1,4 g l^{-1} (up to 1,3

g l^{-1} of acetic acid and up to 0,17 g l^{-1} of propionic acid). In case of thermophilic BMP assay the highest total concentration of SCFAs was 1,3 g l^{-1} (up to 1 g l^{-1} of acetic acid and up to 0,22 g l^{-1} of propionic acid). Acetic acid was the most abundant in all mixtures. SCFAs were within optimal concentration range during both experiments, with the lowest concentration at the end of BMP assays, demonstrating that anaerobic methanogenic degradation ran smoothly and with no inhibitory effects.

Optimum pH during anaerobic degradation varies between 6 and 8, with optimum value around pH = 7,5 for thermophilic process[46] and pH = 7 for mesophilic process.[47] During our experiments the pH value ranged between 7,9 and 8,1 for mesophilic process and 7,8 and 8,2 for thermophilic process. Results were slightly higher than the optimal value, but still appropriate for stable biogas production.

Important parameter for determining the process activity is the reduction of the organic substance during anaerobic degradation. The content of TVS in thermophilic process has reduced by 22,3% and only by 9,0% in mesophilic process. The results indicate that the thermophilic anaerobic digestion is more efficient in decomposition of organic matter, which confirms the known facts about the thermophilic process.[20]

3. 2. Impact of Microalgae Pretreatments on Biogas and Methane Production

3. 2. 1. Thermal Pretreatment

Thermal pretreatment is recognized as possible and effective hydrolysis treatment for microalgae biomass. Higher temperature conditions stimulate cellulose and hemicellulose hydrolysis of algal cell wall components (mainly cellulose and hemicellulose), followed by formation and release of range of low molecular weight compounds (sugars, acids, etc.).[38,48] Heat also disrupts the hydrogen bonds in crystalline cellulose, causing the biomass to swell.[38] It was found, that bonds between and within the molecules forming the microalgae *Scenedesmus* cell walls were cleaved during the thermal pretreatment at 90 °C, which resulted in increased methane production by 2,2-fold with regard to untreated microalgae.[10] It is also known that time period of pretreatment is less important, as the temperature itself.[49] The same conclusion had the research of Marsolek et al., where culture of *Nannochloropsis oculata* was treated at different temperatures.[50] Temperatures between 30 and 60 °C did not increase decomposition, yet treatment at 90 °C caused partial decomposition, which allowed up to 36% increase in biogas production. High temperatures disintegrate algae cells already after 30 minutes of pretreatment, proving that thermal treatment improves the cellular contents release into extracellular space.[10]

The results of our study show that thermal pretreatment in mesophilic (37 °C) BMP assay increased the biogas production by 16% and methane production by 21% in comparison to untreated microalgae (Table 3). Experimental results show that thermal pretreatment enables more efficient hydrolysis of microalgae cell wall compounds (especially cellulose and hemicellulose) and consequently releases more sugars for further efficient microbial transformation to biogas. The thermal pretreatment of microalgae also increased methane percentage in biogas and finally increased methane yield (Table 3). The results of BMP assay under thermophilic conditions (55 °C) did not show similar trends. Thermal pretreatment has not increased biogas production. Nevertheless, the methane production was increased, but only by 6% (Table 3). We can assume hypothetically, why thermal pretreatment has no significant effect on production in thermophilic process. One of the possible reasons may be the relatively low C:N ratio, which can lead to the release and consequent increase in concentration of free ammonium during the thermal pretreatment of microalgae.[35] Since thermophilic process is performed at higher temperatures than the mesophilic process, the anaerobic degradation of thermally pretreated microalgae can further disintegrate damaged algae cells. That can lead towards ammonium release, too, and thus to partial inhibition of methanogenic activity.[19] Koster et al. have demonstrated the impact of free ammonia on anaerobic microorganisms and discovered that it rapidly penetrates through the cell membrane, causes proton imbalance, lack of potassium (K^+) and enzyme inhibition.[51] From the results we have obtained in our study, we can conclude that thermal pretreatment of microalgae at 90 °C (three hours) for thermophilic process is unnecessary, since the methane yield is not significantly higher than the methane yield from raw and untreated microalgae.

3. 2. 2. Biological Pretreatment

Strains of genus *Butyrivibrio* represent a major proportion (10–30%) of bacteria in the rumen of domestic and wild cattle. Many bacterial species of the genus *Butyrivibrio* contribute to the decomposition of fiber in the rumen. Most strains synthesize xylanase, amylase and cellodextrinase, some also 1,4-β-endoglucanses that can decompose a wide range of polymers.[39] *P. xylanivorans* $Mz5^T$ is a close relative of bacterial species of the genus *Butyrivibrio*. It is a Gram-negative anaerobic bacterium that synthesizes many hydrolytic enzymes and holds excellent enzymatic activities.[39,40]

The results of BMP assay under mesophilic conditions showed that biological pretreatment of microalgae did not affect the production of biogas or methane (Table 3). It may be that during biological pretreatment a part of presented substrate is used for the growth of the microorganism used for the biological treatment itself, resulting in a loss of monomeric organic compounds left for the following methane production. More tests are needed

to explain this phenomenon. The results of BMP assay under thermophilic conditions were somewhat different. Biological pretreatment increased biogas production by 5% and methane production by 13% (Table 3). The results show that bacterium *P. xylanivorans* Mz5^T managed to break down a certain proportion of hemicellulose, cellulose and xylan molecules in microalgae cell walls. This provided easier nutrient access for methanogenic microbial community during the thermophilic process, what consequently influenced the increase in methane production.[20–22]

In the case of biological treatment it is more meaningful if we add live hydrolytic bacteria in to the process, which constantly produce extracellular enzymes and allow the hydrolysis of the substrate (bioaugmentation).[50] The effect of biological pretreatment of microalgae on biogas production is still poorly understood, mainly due to the complexity of the structure of cell walls and species diversity of microalgae. Substrate that was applied for BMP assays contained mixed culture of microalgae in which certain types predominate, but are also changing seasonally. Therefore it is difficult to accelerate the hydrolysis of cell walls with only one bacterial strain. Microalgae are very diverse, thus we should choose an appropriate microorganism for each type or mixed culture and adjust the process of anaerobic degradation accordingly.[50]

3. 2. 3. Thermal-biological Pretreatment

We also tested the influence of the combined pretreatment (thermal-biological) of microalgae on biogas production by BMP assays. The above-mentioned pretreatment showed no significant effect on biogas or methane production in mesophilic process (Table 3). Production of biogas and methane was increased by 6%. Results were similar when the microalgae were only biologically pretreated. Comparing all tested pretreatments (thermal, biological, thermal-biological) of microalgae to produce biogas and methane, we found that only thermal pretreatment maximizes production in mesophilic process. The results of BMP assay under thermophilic conditions showed that thermal-biological pretreatment increases the biogas production by 11% and methane production by 12% (Table 3). According to the results, combined pretreatment of microalgae indicates stronger effect on thermophilic process than individual pretreatments. This result could be explained by the fact that during biological pretreatment a part of substrate presented after thermal pretreatment was used for the growth of the bacteria used for the biological treatment itself, resulting in loss of substrate in the system left for the following methane production. Although it is generally accepted that thermophilic anaerobic digestion is more efficient than mesophilic anaerobic digestion of the same substrate, our results have not proved that for microalgae. It has been calculated from data in Table 2 that the average cumulative biogas production in mesophilic process is more efficient for 2% and the average cumulative methane production for 9% (Table 2) than in thermophilic process. There were also differences in the methane yield, where the average yield of methane in mesophilic process was higher for 9% in comparison to thermophilic process (Table 3).

4. Conclusions

In order to accelerate anaerobic digestion we applied different types of pretreatments of microalgae. Following the obtained results, we can conclude that thermal pretreatment at 90 °C is the most effective method for increasing methane and biogas production under mesophilic conditions. Biogas production was increased by 16% and methane production by 21%. Biological pretreatment with bacterium *P. xylanivorans* Mz5^T is the most effective method for increasing methane and biogas production under thermophilic conditions. Methane production was increased by 13%. Combined (thermal-biological) pretreatment showed the strongest effect in thermophilic process. Biogas production was increased by 11% and methane production by 12%. Further research should be carried out to determine which pretreatments are the most economical for individual biogas plant and which algae species are the best for biofuel production, before we could transfer the research to higher scale.

5. Acknowledgements

The authors would like to thank to the two Slovenian biogas plants Koto d.o.o. and Petrol d.d. for their cooperation during this research.

6. References

1. A. Cadenas, S. Cabezudo, *Technol. Forecast. Soc. Change*. **1998**, *58*, 83–103. http://dx.doi.org/10.1016/S0040-1625(97)00083-8
2. R. E. H. Sims, W. Mabee, J. N. Saddler, *Bioresour. Technol.* **2010**, *101*, 1570–1580. http://dx.doi.org/10.1016/j.biortech.2009.11.046
3. G. Dragone, B. Fernandes, A. Vicente, J. Teixeira, *Curr. Res. Technol. Educ. Top. Appl. Microbiol. Microb. Biotechnol.* **2010**, *Formatex*, 1355–1366.
4. D. Russo, M. Dassisti, V. Lawlor, A. G. Olabi, *Renew. Sustain. Energy Rev.* **2012**, *16*, 4056–4070. http://dx.doi.org/10.1016/j.rser.2012.02.024
5. P. M. Schenk, S. R. Thomas-Hall, E. Stephens, U. C. Marx, J. H. Mussgnug, C. Posten, O. Kruse, B. Hankamer, *BioEnergy Res.* **2008**, *1*, 20–43. http://dx.doi.org/10.1007/s12155-008-9008-8

6. A. Demirbas, *Energy Conversion and Management.* **2009**, *50*, 2239–2249. http://dx.doi.org/10.1016/j.enconman.2009.05.010
7. Y. Li, M. Horsman, N. Wu, C. Q. Lan, N. Dubois-Calero, *Biotechnol. Prog.* **2008**, *24*, 815–820. http://dx.doi.org/10.1021/bp.070371k
8. P. E. Wiley, J. E. Campbell, B. McKuin, *Water Environ. Res.* **2011**, *83*, 326–338.
9. L. Lardon, A. Hélias, B. Sialve, J. – P. Steyer, O. Bernard, *Environ. Sci. Technol.* **2009**, *43*, 6475–6481. http://dx.doi.org/10.1021/es900705j
10. C. González-Fernández, B. Sialve, N. Bernet, J. – P. Steyer, *Biomass and Bioenergy.* **2012**, *40*, 105–111. http://dx.doi.org/10.1016/j.biombioe.2012.02.008
11. I. Angelidaki, W. Sanders, *Rev. Environ. Sci. Biotechnol.* **2004**, *3*, 117–129. http://dx.doi.org/10.1007/s11157-004-2502-3
12. H. M. El-Mashad, G. Zeeman, W. K. P. Van Loon, G. P. A. Bot, G. Lettinga, *Bioresour. Technol.* **2004**, *95*, 191–201. http://dx.doi.org/10.1016/j.biortech.2003.07.013
13. J. S. Zhang, K. W. Sun, M. C. Wu, L. Zhang, *J Environ Sci (China).* **2006**, *18*, 810–815.
14. M. D. Ghatak, P. Mahanta, *Int. J. Adv. Res. Technol.* **2014**, *1*, 1–7.
15. C. Vanegas, J. Bartlett, *Waste and Biomass Valorization,* **2013**, *4*, 509–515. http://dx.doi.org/10.1007/s12649-012-9181-z
16. D. R. Kashyap, K. S. Dadhich, S. K. Sharma, *Bioresour. Technol.* **2003**, *87*, 147–153. http://dx.doi.org/10.1016/S0960-8524(02)00205-5
17. V. Kinnunen, R. Craggs, J. Rintala, *Water Res.* **2014**, *57*, 247–257. http://dx.doi.org/10.1016/j.watres.2014.03.043
18. H. K. Ravuri, *Int. J. Adv. Chem.* **2013**, *1*, 31–38. http://dx.doi.org/10.14419/ijac.v1i2.1318
19. J. L. Chen, R. Ortiz, T. W. J. Steele, D. C. Stuckey, *Biotechnol. Adv.* **2014**, *32*, 1523–1534. http://dx.doi.org/10.1016/j.biotechadv.2014.10.005
20. P. Vindis, B. Mursec, M. Janzekovic, F. Cus, *J. Achiev. Mat. Man. Eng.* **2009**, *36*, 192–198.
21. M. H. Gerardi: The Microbiology of Anaerobic Digesters, John Wiley & Sons, Inc., Hoboken, New Jersey, **2003**, pp. 77–121. http://dx.doi.org/10.1002/0471468967.ch17
22. P. Chaiprasert, S. Bhumiratana, M. Tanticharoen, *Thammasat Int. J. Sc. Tech.* **2001**, *6*, 1–9.
23. M. Čater, L. Fanedl, R. Marinšek Logar, *Acta Chim. Slov.* **2013**, *60*, 243–255.
24. D. Novak, B. Stres, G. Osojnik, I. Škrjanec, R. Marinšek Logar, *Acta Chim. Slov.* **2011**, *58*, 171–175.
25. H. Bouallagui, Y. Touhami, R. Ben Cheikh, M. Hamdi, *Process Biochem.* **2005**, *40*, 989–995. http://dx.doi.org/10.1016/j.procbio.2004.03.007
26. E. Marinho-Soriano, P. C. Fonseca, M. A. A. Carneiro, W. S. C. Moreira, *Bioresour. Technol.* **2006**, *97*, 2402–2406. http://dx.doi.org/10.1016/j.biortech.2005.10.014
27. T. Bruton, H. Lyons, Y. Lerat, M. Stanley, M. B. Rasmussen, A Review of the Potential of Marine Algae as a Source of Biofuel in Ireland, http://www.seai.ie/Publications/Renewables_Publications_/Bioenergy/Algaereport.pdf, (assessed: April 22, 2016)
28. S. M. Renaud, L. – V. Thinh, D. L. Parry, *Aquaculture.* **1999**, *170*, 147–159. http://dx.doi.org/10.1016/S0044-8486(98)00399-8
29. E. W. Becker, *Biotechnol Adv.* **2007**, *25*, 207–210. http://dx.doi.org/10.1016/j.biotechadv.2006.11.002
30. E. Percival, *Br. Phycol. J.* **1979**, *14*, 103–117. http://dx.doi.org/10.1080/00071617900650121
31. L. Yao, J. A. Gerde, S. – L. Lee, T. Wang, K. A. Harrata, *J. Agric. Food Chem.* **2015**, *63*, 1773–1787. http://dx.doi.org/10.1021/jf5050603
32. A. J. Ward, D. M. Lewis, F. B. Green, *Algal Res.* **2014**, *5*, 204–214. http://dx.doi.org/10.1016/j.algal.2014.02.001
33. C. Ververis, K. Georghiou, D. Danielidis, D. G. Hatzinikolaou, P. Santas, R. Santas, V. Corleti, *Bioresour. Technol.* **2007**, *98*, 296–301. http://dx.doi.org/10.1016/j.biortech.2006.01.007
34. X. Briand, P. Morand, *J. Appl. Phycol.* **1997**, *9*, 511–524. http://dx.doi.org/10.1023/A:1007972026328
35. M. E. Montingelli, S. Tedesco, A. G. Olabi, *Renew. Sustain. Energy Rev.* **2015**, *43*, 961–972. http://dx.doi.org/10.1016/j.rser.2014.11.052
36. I. Sorensen, D. Domozych, W. G. T. Willats, *Plant Physiol.* **2010**, *153*, 366–372. http://dx.doi.org/10.1104/pp.110.154427
37. C. – Z. Liu, F. Wang, A. R. Stiles, C. Guo, *Appl. Energy.* **2012**, *92*, 406–414. http://dx.doi.org/10.1016/j.apenergy.2011.11.031
38. C. Rodriguez, A. Alaswad, J. Mooney, T. Prescott, A. G. Olabi, *Fuel Process. Technol.* **2015**, *138*, 765–779. http://dx.doi.org/10.1016/j.fuproc.2015.06.027
39. J. Kopečný, M. Zorec, J. Mrázek, Y. Kobayashi, R. Marinšek Logar, *Int. J. Syst. Evol. Microbiol.* **2003**, *53*, 201–209. http://dx.doi.org/10.1099/ijs.0.02345-0
40. T. Čepeljnik, I. Križaj, R. Marinšek Logar, *Enzyme Microb. Technol.* **2004**, *34*, 219–227. http://dx.doi.org/10.1016/j.enzmictec.2003.10.012
41. APHA/AWWA/WEF, Standard Methods for the Examination of Water and Wasterwater, https://www.standardmethods.org/, (assessed: 2006)
42. M. Čater, L. Fanedl, Š. Malovrh, R. Marinšek Logar, *Bioresour. Technol.* **2015**, *186*, 261–269. http://dx.doi.org/10.1016/j.biortech.2015.03.029
43. T. L. Hansen, J. E. Schmidt, I. Angelidaki, E. Marca, J. C. Jansen, H. Mosbak, T. H. Christensen, *Waste Manag.* **2004**, *24*, 393–400. http://dx.doi.org/10.1016/j.wasman.2003.09.009
44. M. A. T. Adorno, J. S. Hirasawa, M. B. A. Varesche, *Am. J. Anal. Chem.* **2014**, *5*, 406–414. http://dx.doi.org/10.4236/ajac.2014.57049
45. I. H. Franke-Whittle, A. Walter, C. Ebner, H. Insam, *Waste Manag.* **2014**, *34*, 2080–2089. http://dx.doi.org/10.1016/j.wasman.2014.07.020
46. L. Yang, Y. Huang, M. Zhao, Z. Huang, H. Miao, Z. Xu, W.

Ruan, *Int. Biodeterior. Biodegrad.* **2015**, *105*, 153–159. http://dx.doi.org/10.1016/j.ibiod.2015.09.005
47. A. E. Cioabla, I. Ionel, G. – A. Dumitrel, F. Popescu, *Biotechnol. Biofuels*. **2012**, *5*, 39–48. http://dx.doi.org/10.1186/1754-6834-5-39
48. M. Sežun, V. Grilc, G. D. Zupančič, R. Marinšek Logar, *Acta Chim. Slov.* **2011**, *58*, 158–166.
49. R. T. Haug, D. C. Stuckey, J. M. Gossett, P. L. McCarty, *Water Pollut. Control Fed.* **1978**, *50*, 73–85.
50. M. D. Marsolek, E. Kendall, P. L. Thompson, T. R. Shuman, *Bioresour. Technol.* **2014**, *151*, 373–377. http://dx.doi.org/10.1016/j.biortech.2013.09.121
51. I. W. Koster, G. Lettinga, *Agric. Wastes.* **1984**, *9*, 205–216. http://dx.doi.org/10.1016/0141-4607(84)90080-5
52. F. Lü, J. Ji, L. Shao, P. He, *Biotechnol. Biofuels.* **2013**, *6*, 92–103. http://dx.doi.org/10.1186/1754-6834-6-92

Povzetek

Pri iskanju novih alternativnih virov energije ima velik potencial odpadna biomasa. V zadnjem času se pozornost preusmerja tudi na neobičajne vire, na primer mikroalge, ki jih lahko uporabimo kot substrat za proizvodnjo bioplina v anaerobni razgradnji. Mikroalge imajo težko razgradljive celične stene, kar ovira učinkovitost anaerobnega procesa. Za pospešitev hidrolize in povečanje proizvodnje bioplina iz mikroalg smo uporabili dva načina predobdelave – biološko in termično v mezofilnih in termofilnih pogojih. Pri biološkem načinu smo mikroalge pred poskusom inkubirali s hidrolitskimi bakterijami *Pseudobutyrivibrio xylanivorans* Mz5^{T}. Pri termični predobdelavi smo mikroalge inkubirali pri 90 °C. Preizkusili smo tudi kombinirano termično-biološko predobdelavo, kjer smo mikroalge po termični obdelavi inkubirali s *P. xylanivorans* Mz5^{T}. Termična predobdelava je v mezofilnem procesu povečala proizvodnjo metana za 21 %, v termofilnem procesu le za 6%. Biološka predobdelava mikroalg je povečala proizvodnjo metana samo v termofilnih pogojih in sicer za 13% (predobdelava v mezofilnem procesu ni imela večjega vpliva). Termično-biološka predobdelava je v termofilnih pogojih povečala proizvodnjo metana za 12 %, v mezofilnih pogojih pa za 6 %.

Scientific paper

Biosorption of 2,4 dichlorophenol Onto Turkish Sweetgum Bark in a Batch System: Equilibrium and Kinetic Study

Dilek Yıldız,[1,*] Feyyaz Keskin[1] and Ahmet Demirak[2]

[1] *Mugla Sıtkı Kocman University, Research and Application Centre For Research Laboratories, 48000 Mugla, Turkey*

[2] *Mugla Sıtkı Kocman University, Department of Chemistry, 48000 Mugla, Turkey*

* *Corresponding author: E-mail: dilekyildiz2003@hotmail.com*
Tel: +90 0 252 211 1675

Received: 09-12-2016

Abstract

In this study, Turkish Sweetgum bark was used as a new biosorbent to investigate the removal of hazardous 2,4 dichlorophenol (2,4-DCP) from aqueous solutions in batch biosoption experiments. The effective usage of Turkish sweetgum bark is a meaningful work for environmental utilization of agricultural residues. The effects of experimental parameters like solution pH, contact time, initial concentration of adsorbate and amount of bisorbent dosage were investigated in a series of batch studies at 25 °C. Taguchi's Orthogonal Array (OA) analysis was used to find the best experimental parameters for the optimum design process in this study. The functional groups and surface properties of biosorbent were characterized by using Fourier transformer infrared (FTIR) and scanning electron microscopy (SEM) techniques. The experimental data were fitted to Langmuir isotherm and Freundlich isotherm models. There is a good agreement between the parameters and this confirms the monolayer adsorption of 2,4-DCP onto sweetgum bark. As a result of kinetic studies, the pseudo-second-order kinetic model was found to be suitable for all the data. Also, the results of the study show that Turkish Sweetgum bark can be potential as a low-cost alternative commercial adsorbents for removal 2,4 dichlorophenol from aqueous solutions.

Keywords: 2,4 dichlorophenol; Biosorption; Turkish Sweetgum; Equilibrium; Kinetics; Taguchi's Orthogonal Array

1. Introduction

One type of dangerous wastes that are chiefly produced during chemical and many other industrial and agricultural activities is phenols and phenol compounds.[1–6] If the low concentrations of pollutants are harmful to organism, these pollutants are considered as priority pollutants. Many of them have potential to harm human health; therefore, they have been classified as hazardous pollutants.[7] United State Environmental Protection Agency (USEPA) has registered phenolic compounds as priority pollutants. Most of the phenolic compounds are toxic and hardly biodegradable, and it can be really difficult to get rid of them in the environment. Especially chlorophenols (CPs) are believed to create bad taste and odor in drinking water at concentrations below 0.1 g/L and cause adverse impacts on the environment.[8]

Some physicochemical and biological methods including adsorption, extraction by chemical solvents, air stripping, freezing and crystallization, chemical oxidation, wet oxidation, advanced oxidation processes, biological degradation biosorption, coagulation, chlorination and liquid membrane permeation have been developed for the removal of phenolic compounds from aqueous solutions.[6,7,9,10–13] Among these methods, the ones used for the concentration of the chlorinated phenols on the solid phase are adsorption and ion exchange methods but they are not for complete mineralization. The ones used for complete mineralization and combination of chlorophenols are chemical or biological oxidation methods. While one advantage of chemical oxidation methods is their being fast, they might result in undesirable by-products and they are expensive. Mostly preprocessed and rigid solid bisorbent material was investigated for removal hazardous wastes from aqueous solutions. Pretreatment is certainly advantageous

concerning mechanical properties, but it is needed additional resources. Therefore, naturally immobilized biomass in the form of pellets with good biosorption capacities is a type of biosorbent. However, it is a highly porous, soft and mechanically sensitive material, and this might affect the column performance.[14] Biosorption of chlorophenols are more specific and relatively cheap than chemical oxidation methods. Biosorption methods of chlorophenols were also investigated by many researchers.[7–10] According to recent studies, some natural minerals, industrial wastes, agricultural wastes, and forest wastes are low-cost adsorbent materials.[15–18] Agricultural wastes among them are one of the most promising groups of adsorbent materials.

New adsorbents that are locally-easily available, high adsorption capacity and economic materials, or certain waste products from industrial or agricultural operations, may have potential as low-cost sorbents.[19–21] Their unique chemical composition makes these wastes economic and eco-friendly alternatives the removal of chlorophenols.[6,7,22,23] We are interested in bark of Turkish Sweetgum as biosorbent. The sweetgum, which is widely known as Turkish sweetgum. is a deciduous tree native to the eastern Mediterranean region Styrax liquidus obtained from sweetgum have been known since very old times and they are known to have been used to mummify pharoses in ancient Egypt . The volatile oil extracted from Styrax liquidus has been utilized for the production of pharmaceutical and cosmetic products and they are made available in Turkey through export.[24] The barks of sweetgum are a forest wastes to obtain the export goods from sweetgum plant and Styrax liquidus. Processed Turkish sweetgum barks are left in the forest as waste. These can cause forest fires. So it should be cleaned from the forest. Sweetgum bark consists of tannin compounds. Previous studies have reviewed low-cost adsorbents including bark/tannin, lignin, chitin/chitosan, non-living biomass etc.[19] There are main objective of the present study is to explore the ability of sweetgum (Turkish Sweetgum) bark that become forest waste to remove 2,4-DCP from aqueous solutions. For this reason, biosorbent was characterized using Fourier transformer infrared spectroscopy (FTIR) and Scanning Electron Microscopy (SEM). In addition, experimental parameters such as solution pH, contact time, initial concentration of adsorbate and amount of biosorbent dosage were investigated. A statistical optimization was used to determine the optimum biosorption conditions for removal of 2,4-DCP from aqueous solutions in sweetgum bark. Moreover, adsorption isotherm models and kinetics models were studied to understand the biosorption mechanism for theoretical evaluation.

2. Materials and Methods

2. 1. Materials

The bark of sweetgum was obtained from the Mugla Manager ship of Governmental Operation of Forestry, General Directorate of Forestry, Ministry of Environment and Forestry, Republic of Turkey at November, 2015. The 2,4 dichlorophenol, > 99%, (2,4-DCP) was from Sigma-Aldrich (St. Louis, MO, USA). 4-aminoantipyrine and potassium ferricyanid used in this study were obtained from Merck and were of GR grade.

2. 2. Equipment and Analysis

A pH meter (WTW) was used for the measurement of pH. The concentrations of phenol compound were analyzed calorimetrically by using 4-aminoantipyrine and potassium ferriciyanid at pH 7.9 ± 0.1 according to the Standard Methods.[25] All the analyses of this study were performed in the laboratory that has a framework of ISO IEC 17025 Laboratory accreditation

2. 3. Biosorbent

The sweetgum consists of resin alcohols avaiblable free and combined with cinnamic acid, which makes up 30–45 % of the total weight. Detailed chemical composition of TSB was styrene (1.56); a-pinene (1.02); benzaldehyde (0.47); b-pinene (0.15); benzyl alcohol (1.22); acetophenone (0.19); 1-phenyl-1-ethanol (0.17); hydrocinnamyl alcohol (41.13); trans-cinnamyl aldehyde (0.24); trans-cinnamyl alcohol (45.07) and bcaryophyllene (3.60 %).[26] The barks of sweetgum were dried in the oven at 60 °C for 48 h and then passed through a 150 μm size screen to use it in the study.

2. 4. Preparation of Synthetic Sample

It was prepared for a stock solution of 2,4-DCP (1000 mg/l) with distilled water. To obtain all the solutions of varying concentrations, the stock solution was used in the current study. The pH of each solution was adjusted to the desired value using 0.1 M HCl and 0.1 M NaOH.

2. 5. Batch Sorption Experiments

The batch technique was used to conduct the experiments of sorption in a routine manner. The dry biomass (1,0 g) was shaken with 50 ml of 2,4-DCP solution at a concentration of 150 mg/l in a shaker at room temperature (20 ± 0.5 °C) for about 150 minutes. For the separation of the particles of sweetgum barks by filtration, a 0.45 μm membrane filter was used. The amounts of sweetgum barks adsorbed in each case were measured by calculating the difference between the initial and the final concentrations of 2,4-DCP.

By using the difference between the initial concentration and equilibrium (qe) of 2,4-DCP concentration, biosorption capacity at equilibrium time (qe) was calculated as follows:

$$qe = {V(Co - Ce)}/{M} \quad (1)$$

where V is the sample volume (L), Co is the initial concentration of 2,4-DCP (mg/l), Ce is the equilibrium or final concentration of 2,4-DCP (mg/l), M is the dry weight of (0.5 g for this study), and qe is the biomass biosorption capacity of the biomass at equilibrium time.

2. 6. Optimization Study

Taguchi is a simple and effective statistical method, which organizes a systematic experimentation to determine the near to optimum settings of design parameters for performance, quality, and cost. In this method, a large number of variables are studied with a small number of experiments using orthogonal arrays.[27–32] For this reason this study was carried out using Taguchi statistical method.

In the Taguchi approach, an orthogonal arrays and analysis of variance (ANOVA) are used for the analysis of experimentations. By using ANOVA, the effect of factors can be estimated and by orthogonal arrays the minimum number of experiments is needed. In this method variability of parameters is expressed by signal-to-noise (S/N) ratio, which represents the ratio of desirable results (signal) to undesirable results (noise). In this statistical method the S/N ratio is used to measure the quality characteristic derivation from the desired value. The maximum S/N ratio is considered as the optimal condition as the variability is inversely proportional to the S/N ratio.[33]

The Taguchi experimental design method was used to determine optimum removal conditions. The effect of experimental parameters such as pH, amount of biosorbent, initial concentration of adsorbate and contact time were investigated using an L25 (5^5) orthogonal array. One of the main objectives of this research was to apply Taguchi statistical approach to optimize the reaction parameters toward higher adsorption efficiency.

In this work, the effect of four important factors including pH, amount of biosorbent, initial concentration of adsorbate, contact time and each factor at five levels on the adsorption efficiency of 2,4- DCP were studied using Taguchi's method. The used level setting values of the main factors (A–D) and the L25 (55) matrix employed to assign the considered factors are shown in **Tables 1** and **2**, respectively.

Table 1. Factors and levels for experimental parameters used to in sorption capacity test

Levels	A (pH)	B (amount of biosorbent (g)	C (initial concentration of adsorbate (mg/L)	D (contact time (min)
1	2	0,2	25	30
2	4	0,4	50	60
3	6	0,6	100	90
4	8	0,8	150	120
5	10	1,0	200	150

Table 2. L25 Experimental and expected results from Taguchi's Orthogonal Array (OA) analysis

Experiment no.	pH	Amount of biosorbent	Initial concentration of adsorbate	Contact time
1.	1	1	1	1
2.	1	2	2	2
3.	1	3	3	3
4.	1	4	4	4
5.	1	5	5	5
6.	2	1	2	3
7.	2	2	3	4
9.	2	3	4	5
10.	2	4	5	1
11.	2	5	1	2
12.	3	1	3	5
13.	3	2	4	1
14.	3	3	5	2
15.	3	4	1	3
16.	3	5	2	4
17.	4	1	4	2
18.	4	2	5	3
19.	4	3	1	4
20.	4	4	2	5
21.	4	5	3	1
22.	5	1	5	4
23.	5	2	1	5
24.	5	3	2	1
25.	5	4	3	2
26.	5	5	4	3

The experimental data were analyzed using the statistical software MINITAB 15. The data (y_i) and corresponding S/N ratios were calculated on the basis of Taguchi's "larger is better" approach.

2. 7. Scanning Electron Microscopy

Scanning Electron Microscopy with Energy Dispersive Spectroscopy (SEM-EDS) was used to characterize the structures of the samples (JEOL SEM 7700F) in the Research Centre Laboratory at Mugla Sıtkı Koçman University (Turkey).

2. 8. FTIR Analysis

FTIR spectrum of the samples were performed in Perkin Elmer Each spectrum was recorded in a frequency of 400–4000 cm^{-1} using potassium bromide (KBr) disc. The KBr was oven-dired to minimize the interference of water.

2. 9. The Determination of pHpzc

Batch equilibrium experiments were used to estimate zero point charge (pHpzc). 50mL of 0.01M NaCl solu-

tion was poured into several erlenmeyer flasks. The pH of solution for each flask was adjusted to a value between 2 and 12 by addition of 0.1M HCl or 0.1M NaOH solution. Then, 0.10 g of adsorbent was added to the flasks and the dispersion was stirred for 48 h. After this time the final pH was measured.A plot of the final pHf as a function of the initial pHi provides pHpzc of the adsorbents by the plateau of constant pH to the ordinate.[34]

3. Results and Discussion

3. 1. Optimization Study

As the orthogonal array experimental design method was found to be the most appropriate for the conditions under investigation, it was chosen to determine the experimental plan, $L25$ (5^5) (**Table 2**); four parameters each with five values. The data (yi) and corresponding S/N ratios were calculated on the basis of Taguchi's "larger is better" approach using Eq. 2

$$S/N\ Oran_1 = -10.\log[\sum(1/Y2)/n] \quad (2)$$

In order to calculate the effects of parameters, S/N ratio was averaged for each level. The effect of the noise sources on the adsorption process was observed by repeating each experiment twice under the same conditions. The sequence, in which the experiments were carried out, was randomized to avoid any personal or subjective bias. In the proposed method, no interaction between the variables was found in the matrix and the focus was placed on the main effects of the four most important factors. The optimum design for the adsorption of 2,4-DCP by Sweetgum bark is an important aspect in the production of the adsorption process. It can be concluded that the values of optimum experimental parameters for adsorption capacity of 2,4-DCP are as below: contact time (150 min) , amount biosorbent (1 g), initial concentration of adsorbate (150 mg/L) and pH (2) (**figure1**).

Taguchi method predicted that the adsorption efficiency under the optimum conditions will be 90.2371%. Under these optimum conditions, it was determined that the 2,4- DCP adsorption efficiency was 89.2158%.

3. 2. Influence of pH

The previous studies have shown that pH of the solution is a critical parameter affecting biosorption of 2,4-DCP.[7,12,35] The pH ranges of 2–10 were used in this study to ensure the presence of the protonated form of 2,4-DCP and the increase of negative charges at the surface of the particles of bark of sweetgum. The initial pH of the solution was increased with the decrease in the adsorption capacity of 2,4-DCP (figure 2). The figure shows that maximum adsorption capacity of 2,4-DCP was observed at a pH of 2.0. Also it was found the same values of initial pH of the solution using Taguchi's Orthogonal Array (OA) analysis (figure 1).

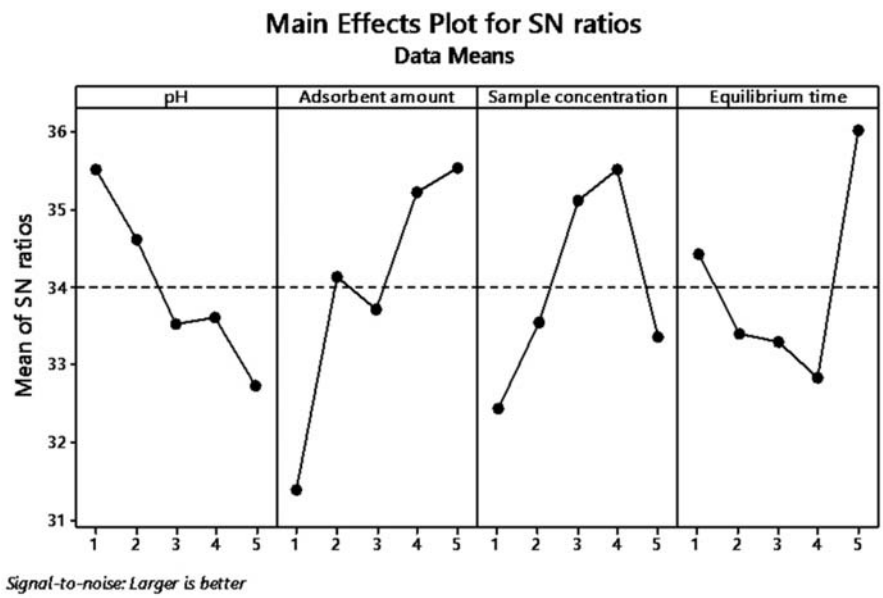

		Factor levels for predictions		Predicted values	
pH	**Amount of**	**Initial concentration of**	**Contact time**	**S/N Ratio**	**Mean**
1	5	4	5	40,6185	90,2371

Figure 1. Main effects plot for SN ratios, Factor levels for predictions, Predicted values

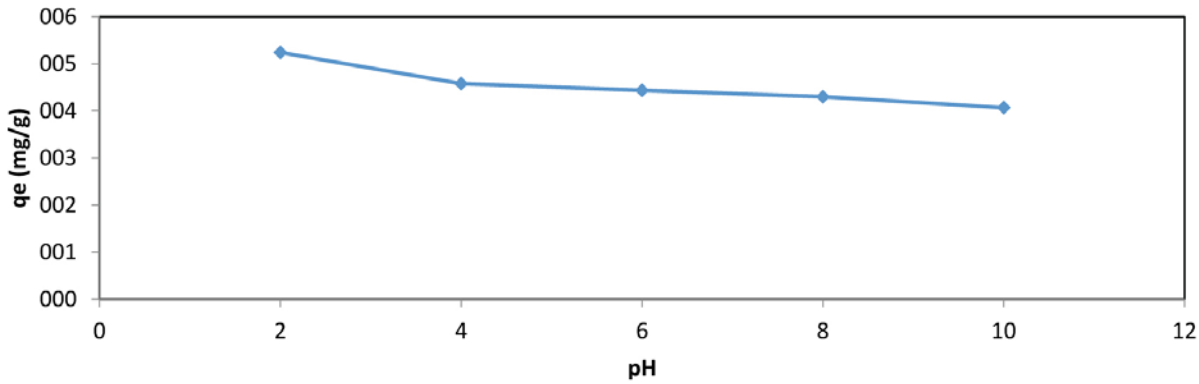

Figure 2. The effect of pH on the equilibrium sorption capacities of sweetgum bark, for 2,4-DCP

The Henderson–Hasselbalch equation

(pH= $pKa + log\,{}^{[A-]}/_{[AH]}$) is useful for estimating the pH of acidic compounds, such as 2.4-DCP. The value of p-Ka for 2,4-DCP which is known to be weak acid is 7.85. The value of pH (2) is lower than p*K*a (7.85), the dissociation degree of 2,4-DCP to form anions increases. The sweetgum bark consists of hydrolyzable tannin compounds.[36] The hydroxyl groups of the carbohydrate in hydrolyzable tannin compounds provide negative charge in surface of the biomass as the pH increases. Consequently, the electrostatic impulse between the identical charged target molecules decreases the adsorption capacity of 2,4-DCP in increasing pH of the 2,4-DCP in aqueous solution.

3. 3. Effect of Contact Time and Initial Concentration

The relationship between contact time and 2,4-DCP sorption on sweetgum bark at different initial 2,4-DCP concentrations is presented in Figure 3. The rate of sorption capacities increased slightly at contact time of 150 min. The sorption was not very rapid and the equilibrium time for 2,4-DCP calculated from this study is more than what is reported for phenols onto different biomass.[1] The initial concentration of aqueous solution ensures an important locomotive strength to accomplish all mass transfer resistances of adsorbate between the aqueous solid phase and therefore increases the rate of adsorbate molecules passing from the solution to the adsorbent surface.[1,37–39] Accordingly, a low initial concentration of 2,4-DCP would decrease the process of adsorption (Figure 3). Also Taguchi's Orthogonal Array (OA) analysis indicates that the optimum of equilibrium time and initial concentration of 2,4-DCP in this study are 150 min and 150 mg/L, respectively (Figure 1).

3. 4. Adsorption Kinetic Models

The pseudo – first-order model and the pseudo – second-order model were performed to the experimental pa-

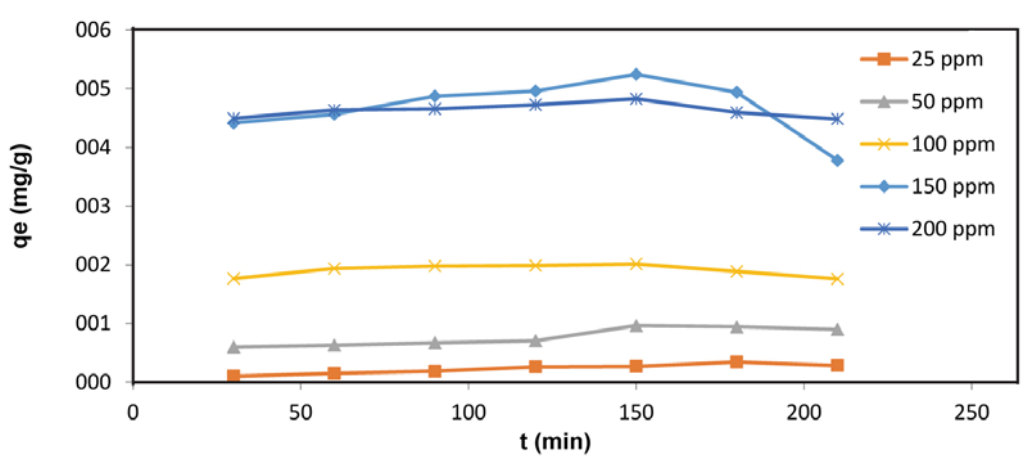

Figure 3. The sorption equilibration time of 2,4-DCP by dried sweetgum bark (biomass: 1 g, 2,4-DCP concentration: 25, 50, 100, 150, 200 mg/I: temperature 20 ± 0.5, agitation rate: 125 rpm)

rameters to evaluate the adsorption kinetics of 2,4-DCP onto sweetgum bark in this study.

3. 4. 1. Pseudo-first-order Model and Pseudo-second-order Model

The kinetic of biosorption by any biological material in an aqueous solution has been tested for the pseudo-first-order model equation given by Lagergren. The pseudo-second-order model may provide a better description of the adsorption kinetics.[7,22]

The pseud-first-order Lagergren equation is:

$$\log(qe - qt) = \log qecal - ({}^{K1}/_{2,303})t \quad (3)$$

where qe and qt are the amount of 2,4-DCP adsorbed per unit of biomass (mg/g) at equilibrium and at time t, t is the contact time (min) and k_1 is the rate constant of this equation (1/min). The values of K_1 and q_{ecal} were calculated from a plot of log (qe-qt) versus t.

The pseudo-second-order kinetic equation is[22,39]

$$ {}^{t}/_{qt} = {}^{1}/_{K_2 \cdot q_{ecal}^2} + {}^{t}/_{q_{ecal}} \qquad h = K_2\, q_{ecal}^2 \quad (4)$$

where h represents the initial adsorption rate (mg/g min), and K_2 is the rate constant in the pseudo-second-order kinetic model (g / mg.min). The values of q_{ecal}, K_2 and h can be obtained by a linear plot of t/qt versus t.

The linear regression correlation coefficient (R^2) values for Lagergren-first order kinetic model ranged from 0.8140 to 0.9922, which was lower than the R^2 values for Pseudo-second order kinetic model which ranged from 0.8140 to 0.9999 (Table 3). The reaction involved in present biosorption system may not be of the Lagergren - first-order kinetic model. The whole range of data might not be sufficiently described by the Lagergren-first order kinetics. Moreover, the q_{ecal} values for pseudo-second-order kinetic model were closer to the experimental qe values than the calculated q_{ecal} values for Lagergren -frist-order kinetic model and, also, calculated q_{ecal} values agreed with experimental qe values for pseudo-second-order kinetic (Table 3). These values show that pseudo-second-order kinetic fits for the biosorption of 2,4- DCP on the sweetgum bark. The Pseudo-second-order kinetic model was suitable for all the data. The process of the Pseudo-first-order kinetic model has been used for adsorption of reversible with an equilibrium being established between

Table 3. Parameters of Lagergren-first order kinetic model Pseudo-second order kinetic model for 2,4- DCP adsorption onto sweetgum bark (pH: 2; biomass: 1 g, temperature 20 ± 0.5, agitation rate: 125 rpm)

(mg/L)	Lagergren-first order kinetic model				Pseudo-second order kinetic model		
2,4 DCP	q_e(mg/g)	K_1(min^{-1})	q_{ecal} (mg/g)	R^2	q_{ecal} (mg/g)	K_2 (gmg^{-1})	R^2
25	0,269	1,74	0,029	0,8124	0,514	0,0187	0,814
50	0,963	2,43	0,004	0,9922	1,049	0,0257	0,8619
100	2,013	1,74	0,029	0,8124	2,077	0,0984	0,9999
150	5,243	1,28	0,013	0,9609	5,482	0,0182	0,9967
200	4,828	2,16	0,012	0,9483	4,900	0,0584	0,9995

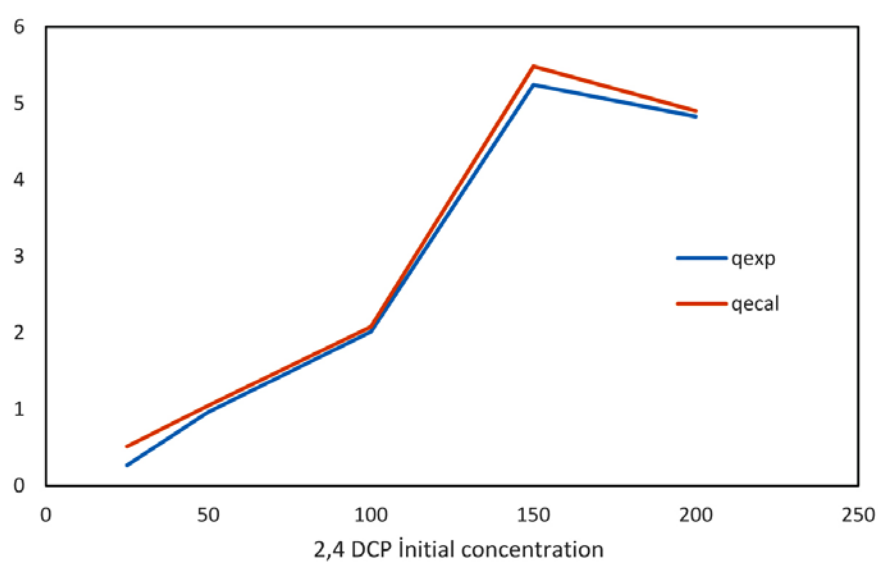

Figure 4. Graphical representation of Pseudo-second order kinetic model

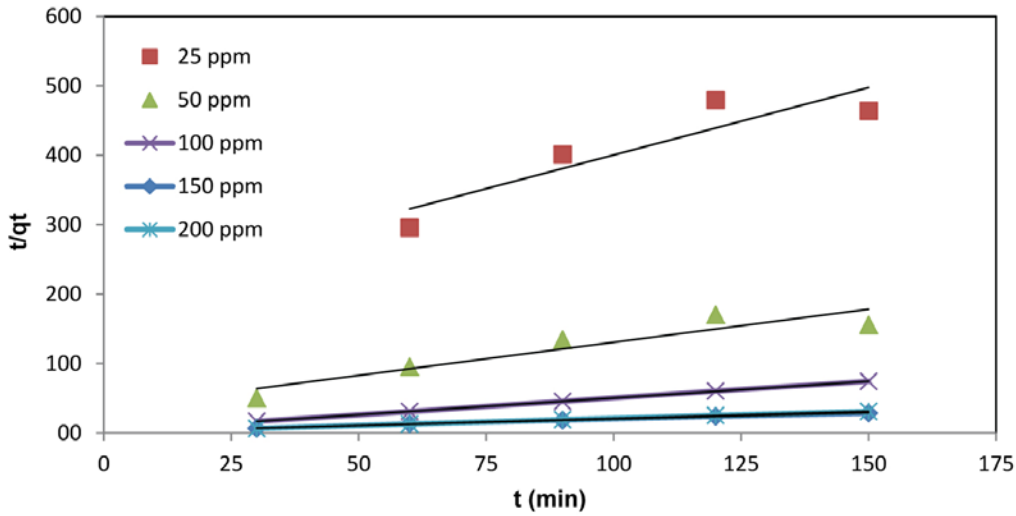

Figure 5. Pseudo-second –order plots at different initial 2.4 DCP concentrations (pH: 2; biomass: 1 g, temperature 20 ± 0.5, agitation rate: 125 rpm)

adsorbate and adsorbent systems although the process of the Pseudo-second-order kinetic model demonstrates chemisorptions which control the adsorption such as Vander Waals, hydrogen bonding, ion exchange etc. [40] The process of 2,4- DCP adsorption in sweetgum bark may be chemisorptions. It is possible to see similar adsorbent performance for each of the three plots in initial concentrations 100, 150 and 200 ppm when they are compared with each other's in Pseudo-second-order plots. However, R^2 values are different. The maximum R^2 value is found at 150 ppm (Table 3, Figure 5). Also, it is possible to say the sorption system reached the final equilibrium plateau after 100 min and it started desorption after 150 minutes for initial concentrations 100, 150 and 200 ppm (Figure 3). This situation may demonstrate that there are surface binding sites on the biomass for the biosortion of 2,4-DCP and a number of biosorption mechanisms that included many factors such as physico-chemical adsorption, complexation, ion-exchange and micro-precipitation.

3. 5. Adsorption Isotherm Models

Adsorption isotherm models are important in order to describe the sorption process. The data of adsorption isotherm models are also important to predict the adsorption capacity and describe the surface properties and affinity of the adsorbent.[22] Two adsorption isotherm models were used to studies in the present study: the Langmuir isotherm model and Freundlich isotherm model. The general Langmuir equation whose linearized form is given as follows:

$$Ce/qe = 1/Qm.b + 1/Qm.Ce \quad (5)$$

where C_e is the equilibrium concentration of the adsorbate (mg/L), q_e is the amount of the adsorbate adsorbed per unit mass of the adsorbent (mg/g), b is the Langmuir adsorption constant (L/mg), and Q_m is the maximum adsorption amount (mg/g). *Qm* and b can be determined from the linear plot of *Ce*/*q*e versus *C*e.[1,22]

The dimensionless separation factor or equilibrium constant (R_L) describes the essential characteristics of Langmuir isotherm. R_L is defined as;

$$R_L = 1/1 + b.Co \quad (6)$$

where Co is the initial concentration (mg/I), and b is the Langmuir constant. Table 4 indicates dimensionless separation factor.

The Freundlich isotherm is an empirical relationship that describes the sorption on a heterogeneous surface. It can be linearized in logarithmic form as follows:

$$\log qe = 1/n \log Ce + \log Kf \quad (7)$$

where C_e is the equilibrium concentration of the adsorbate (mg/L), q_e is the amount of the adsorbate adsorbed per unit mass of the adsorbent (mg/g), K_f and n are the Freundlich constants, whereas K_f and n are indicators of adsorption capacity and adsorption intensity of the sorbents, respectively.[18]

The regression correlation coefficients (R^2) values of Freundlich isotherm model and Langmuir isotherm

Table 4. The dimensionless separation factor.[39]

R_L	> 1	= 1	0<R_L < 1	= 0	0.0001(This study)
Sorption	unfavourable	linear	favourable	irreversible	irreversible

Table 5. Adsorption isotherm constants for 2.4-DCP onto sweetgum bark

	Langmuir model			Freundlich model		
Phenol	Q_m	**b**	R^2	K_f	**n**	R^2
2,4-DCP	8,176	52,36	0,9898	0,0077	0,722	0,9989

model for initial concentration (150 mg/L) of 2,4-DCP are 0.9989 and 0.9898, respectively (Table 4), suggesting that the Freundlich isotherm model provided the best fit and Freundlich isotherm model exhibited a slightly better fit to the biosrption data of 2,4- DCP onto sweetgum bark than the Langmuir isotherm model in the initial concentration (150 mg/).

The adsorption equilibrium of heavy metals on various types of adsorbent was described by Freundlich isotherm and Langmuir isotherm models. However, the descriptions of adsorption equilibrium of organic pollutants such as phenol and chlorophenols were used the Freundlich isotherm model better than Langmuir isotherm model.[1]

The magnitude of Q_m (8, 176) for Langmuir isotherm model shows the amount of 2,4-DCP per unit weight of sorbent to form complete monolayer on the surface of a sample. Langmuir isotherm model was chosen, because of physical meaning of adsorption capacity (Q_m).[41]

The value of adsorption capacity (Q_m) for 2,4-DCP in present study was compared with the adsorption capacity of different adsorbents for 2,4-DCP **(Table 6)**.

According to the equation (5), the value of R_L is 0.0001. This value indicates that sorption of 2,4-DCP on sweetgum bark may be irreversible. On the other hand, a value of correlation coefficient (R^2) for initial concentration of 150 mg/L 2,4-DCP in Langmiur isotherm model is 0.9898. This value indicates that there is a good agreement between the parameters and confirms the monolayer adsorption of 2,4-DCP onto sweetgum bark **(Table 4).**

Table 6. Comparison of adsorption capacity for 2,4-DCP between sweetgum bark and other various adsorbents reported in the literature.

Adsorbent	Q_m (mg/g)	Reference
P.ocenica fibers	1,11	Demirak et al., 2011[7]
Rice Husk	40,5	Vadivelan et al., 2005[42]
Fly ask	5,57	Kumar et al., 2005[43]
Mycelial pellets	4,09	Wu and Yu., 2006[1]
Papermill sludge	4,49	Calace et al., 2002[44]
Sweetgum brk	8.176	This study

The constant values calculated from the Freundlich model for the biosorption equilibrium are given in Table 4. The values of n in this study are less than 1, a favorable adsorption is indicated and chemical rather than physical adsorption is dominant.

In most cases, the kinetic parameters and the equilibrium parameters show good performance in batch.[45] Previous studies show that the models are sensitive to sorption kinetic constants and to the mass transfer coefficient within the biosorbent.[14] Adsorption models showed generally good performance, fitting the experimental data well in this study.

3. 6. Surface Characterization

3. 6. 1. SEM Analysis

SEM was used to observe the surface morphology of sweetgum bark samples and it is shown in Figure 6. SEM

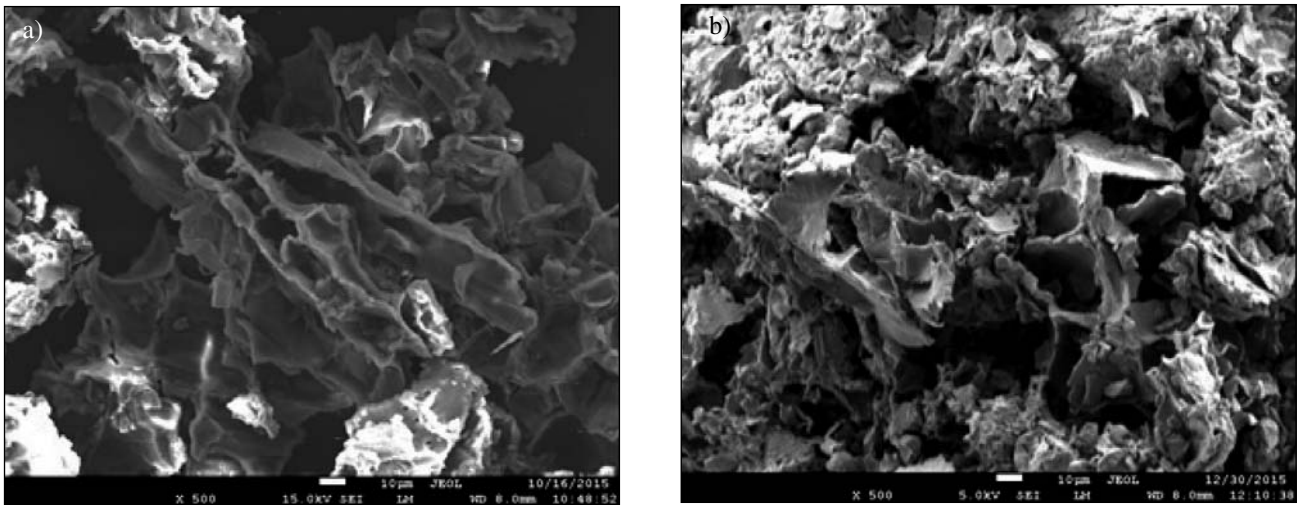

Figure 6. SEM pictures of sweetgum bark samples a) before the sorption of 2,4-DCP b) after the sorption of 2,4-DCP

micrographs were taken at 1 kV accelerating voltage and magnification was fixed according to ×1000. The SEM micrographs show that it was obtained to different from the morphology of the samples. There is clear indicator of sorption of 2,4-DCP on dried sweetgum bark in SEM pictures.

3. 6. 2. FTIR Analysis

FTIR spectroscopy of the extracts showed that the polar extractive spectra were consistent with the hydrolysabletannin compounds isolated during extractions of sweetgum bark.[36] At the center of a hydrolyzabletannin , there is a . Phenolic groups were used to partially or totally esterify the hydroxyl groups of the carbohydrate.[46] The information on the nature of the bonds on biomasses surface allowing the determination of different functional groups is offered by FTIR.

Figure 7 shows the changes of FTIR peaks for raw sweetgum bark compared to those after biosorption with 2,4-DCP Several peaks were observed from the spectra and this indicates that sweetgum bark is composed of various functional groups **(Table 6).**

In the spectra a new band is observed at 1708 cm^{-1}, which can be assigned to ester formation. This peak indicates that he hydroxyl groups of the carbohydrate in sweetgum bark are with 2,4-DCP. These may be because of the interaction between the functional groups of sweetgum bark with 2,4-DCP compounds during the adsorption process.

3. 7. The Determination of pHpzc

pHpzc value (Figure 8) determined for 2,4-DCP is 5.68.

Table 7. The FTIR spectral characteristics of sweetgum bark before and after biosorption of 2,4-DCP

Wavelength Range (cm^{-1})	Before Biosorp.	After Biosorp.	Differences	Assignment
3500–3200	3447	3423	24	Bonded hydroxyl groups (phenolic OH and aliphatic OH
1705–1715		1711	New peak	C=O stretching (unconjugated ketone, carbonyl and ester groups
1670–1500	1635	1623	12	Carboxylic groups
1450–1375	1454	1452	2	Symmetric bending of CH3
1300–1000	1317	1371	0	-SO3 stretching
	1036	1036	0	C-O-C stretching in ethers.

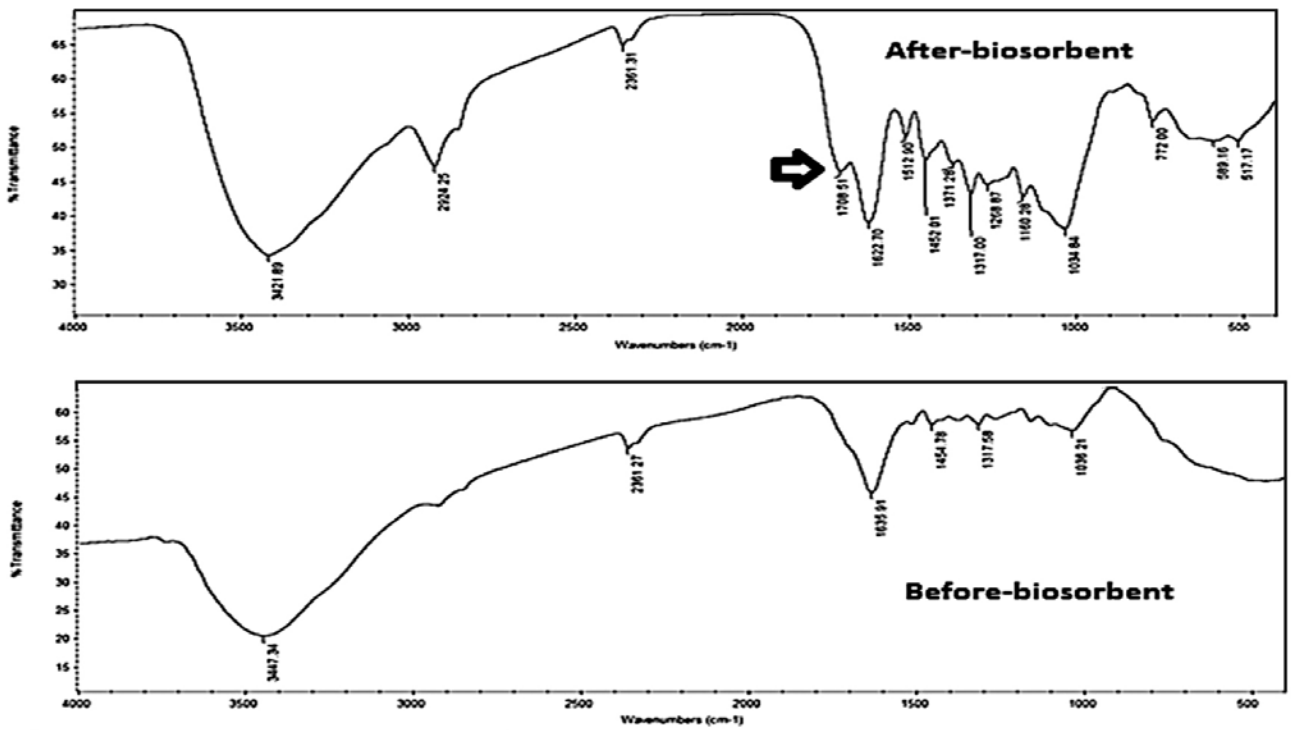

Figure 7. FTIR spectrum of biosorbent (before biosorption and after biosorption)

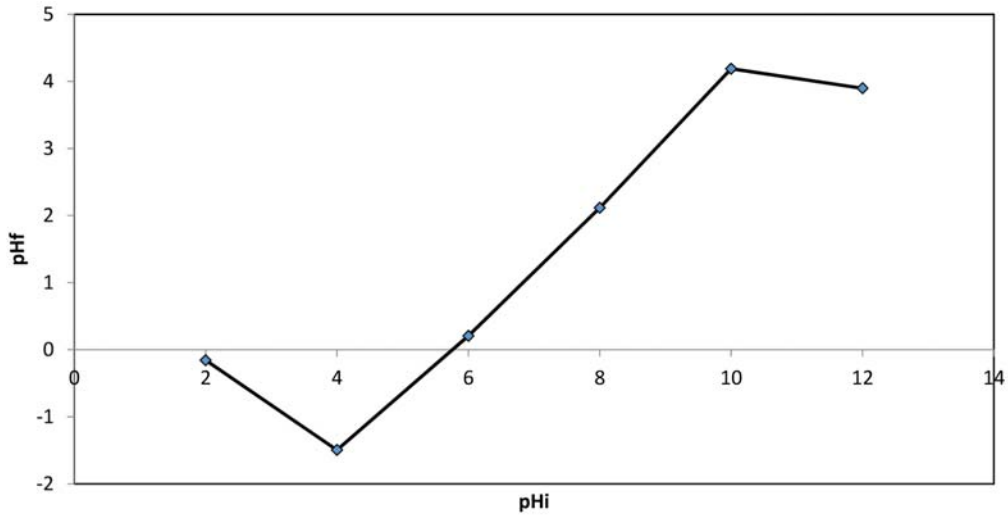

Figure 8. pHpzc value

4. Conclusions

- This study has been performed by using the Turkish sweetgum bark as a potent biosorbent for the removal of 2,4-DCP.
- The choice of the Turkish sweetgum bark was made according to some criteria, including its wastes that are left in the forest.
- The maximum adsorption capacity of 2, 4-DCP was observed at a pH of 2.0.
- The rate of sorption capacities increased slightly at contact time of 150 min.
- Taguchi's Orthogonal Array (OA) analysis was used to determine the values of optimum experimental parameters for adsorption capacity of 2,4-DCP onto Turkish sweetgum bark.
- The values of optimum experimental parameters for adsorption capacity of 2,4-DCP onto Turkish sweetgum bark can be explained clearly by Taguchi's Orthogonal Array (OA) analysis.
- Biosorption was determined by a Pseudo-second-order model predicting a chemisorption process.
- The equilibrium data were well characterized by the Langmuir isotherm model, which confirmed the monolayer coverage.
- The Freundlich isotherm model was found to represent the measured sorption data well.
- A new band is observed at 1708cm^{-1} in FTIR, which can be assigned to ester formation. This peak indicate that hydroxyl groups of the carbohydrate in sweetgum bark are esterified with 2,4-DCP

5. Acknowledgements

This research was supported by Muğla Sıtkı Koçman University (Project no: 15/017)

6. References

1. W. Juan, Y. Han-Qing, *J Hazard Mater B*, **2006**, *137*, 498–508. https://doi.org/10.1016/j.jhazmat.2006.02.026
2. N. S. Kumar, M. V. Subbaiah, A. S. Reddy, A. Krishnaiah, *J Chem Tech Biotechnol* **2009**, *84*, 972–981. https://doi.org/10.1002/jctb.2120
3. V. C. Srivastava, M. M. Swamy, I. D. Mall, B. Prasad and I. M. Mishra, *Colloid Surface A* **2006**, *272*, 89–104.
4. S. P. Kamble, P. A. Mangrulkar, A. K. Bansiwal, S. S. Rayalu, *Chem Eng J* **2008**, *138*, 73–83. https://doi.org/10.1016/j.cej.2007.05.030
5. N. S. Kumar, K. Min, *Chem Eng J* **2011**, *168*, 562–571. https://doi.org/10.1016/j.cej.2011.01.023
6. A.Gholizadeh, M. Kermani, M. Gholami, M. Farzadkia, K. Yaghmaeian *Asian J Chem* **2013**, *25, 7,* 3871–3878.
7. A. Demirak, Ö. Dalman, E. Tilkan, D. Yıldız, E. Yavuz, C. Gökçe, *Microchem. J* **2011**, *99*, 97–102. https://doi.org/10.1016/j.microc.2011.04.002
8. A. S. Ghatbandhea, H. G. Jahagirdara, M. K. N. Yenkieb, and S. D. Deosarkarc, *Russ J Phys Chem A* **2013**, *87*, *8,* 1362–1366.
9. M. W. Jung, K. H. Ahn, Y. Lee, K. P. Kim, *Microchem. J*. **2001**, *70*, 123–131. https://doi.org/10.1016/S0026-265X(01)00109-6
10. F. Kargi, S. Eker, *Process Biochem 40*, *6,* **2005**, 2105–2111.
11. E. Rubin, P. Rodriguez, R. Herrero, M. E. Sastre de Vicente *J Chem Tech Biotechnol* **2006**, *81*, 1093–1099. https://doi.org/10.1002/jctb.1430
12. M. Akhtar, M. I. Bhanger, S. Iqbal, S. M. Hasany, *J. Hazard. Mater. B* **2006**, *128*, 44–52. https://doi.org/10.1016/j.jhazmat.2005.07.025
13. S. K. Nadavala, K. Swayampakula, V. M. Boddu, K. Abburi, *J Hazard Mater* **2009**, *162*, 482–489 https://doi.org/10.1016/j.jhazmat.2008.05.070
14. A.Kogej, B. Likozar, A. Pavko, *Food Technol. Biotechnol*, **2010**, 48,3, 344–351.

15. M. Sathishkumar, A. R. Binupriya, D. Kavitha, S.E. Yun, *Bioresour. Technol*. **2007**, *98*, 866–873. https://doi.org/10.1016/j.biortech.2006.03.002
16. M. Sathishkumar, K. Vijayaraghavan, A. R. Binupriya, A. M. Stephan, J. G. Chai, S. E. Yun, *J Colloid Interface Sci*. **2008**, *320*, *1,* 22–29. https://doi.org/10.1016/j.jcis.2007.12.011
17. M. Sathishkumar, A. R. Binupriya, D. Kavitha, R. Selvakumar, R. Jayabalan, J. G. Choi, S. E. Yun, *Chem. Eng. J.* **2009**, *147*, 265–271. https://doi.org/10.1016/j.cej.2008.07.020
18. A. Bhatnagar, A. K. Minocha, *J. Hazard. Mater.* **2009**, *168*, 1111–1117. https://doi.org/10.1016/j.jhazmat.2009.02.151
19. N. Unlu, M. Ersöz, *J Hazard Mater,* **2006**, 136, 272–280. https://doi.org/10.1016/j.jhazmat.2005.12.013
20. A. Sarı, M. Tüzen, D. Çıtak, M. Soylak, *J Hazard Mater,* **2007**, *148,* 387–394. https://doi.org/10.1016/j.jhazmat.2007.02.052
21. S. Tunalı, T. Akar, A. S. Özcan, İ. Kıran, A. Özcan, *Separ Purif Method,* **2006**, *47,* 105–112. https://doi.org/10.1016/j.seppur.2005.06.009
22. L. Wang, J. Zhang, R. Zhao, C. Zhang, C. Li, Y. Li, *Desalination* **2011**, *266*, 175–181. https://doi.org/10.1016/j.desal.2010.08.022
23. A. Gholizadeh, M. Kermani, M. Gholami and M. Farzadkia, *J. Environ. Health Sci. Eng*. **2013** DOI: 10.1186/2052-336X-11–29 https://doi.org/10.1186/2052-336X-11-29
24. I. Gurbuz, E. Yesilada, B. Demirci, E. Sezik, F. Demirci, K. H. Baser, *J Ethnopharmacol* **2013**, *148*, 332–336. https://doi.org/10.1016/j.jep.2013.03.071
25. Standard Methods for the examination of water and wastewater, Washington, D. C.: APHA-AWWA-WEF, **2005**.
26. Y. S. Lee, J. Kim, S. G. Lee, E. Oh, S. C. Shin, I. Park, **2009**, *Pestic Biochem Physiol, 93,* 138–143. https://doi.org/10.1016/j.pestbp.2009.02.002
27. M. Mahmoodian, A. B. Arya, B. Pourabbas, *Dent. Mater*. **2008**, *24,* 514–521. https://doi.org/10.1016/j.dental.2007.03.011
28. G. Taguchi, Y. Yokoyama, Y. Wu, American Supplier Institute (ASI) Press, Tokyo 1993.
29. S. H. Park, Robust Design and Analysis for Quality Engineering, Chapman & Hall, London 1996.
30. D. R. Cox, N. Reid, , Chapman & Hall/CRC, London 2000.
31. C. Douglas, Montgomery, Design and Analysis of Experiments, Wiley, New York 2001.
32. R. Torkaman, M. Soltanieh, H. Kazemian, *Chem. Eng. Technol*. **2010**, *33,* 902–910. https://doi.org/10.1002/ceat.200900367
33. R. Roy, A Primer on the Taguchi Method, Van Nostrand Reinhold, New York 1990.
34. H. Zaghouane-Boudiaf, M. Boutahala, *Chem Eng J*, **2011**, *170,* 120–126. https://doi.org/10.1016/j.cej.2011.03.039
35. Z. Aksu, J. Yener, *A Waste Manag*. **2001**, *19,* 674–677.
36. L. Thomas, N. L. Eberhardt, C. L. Seok. Kim, K. G. Reed, D. J. Leduc, J. M. Warren, *Trees*, **2015**, *29*, 1735–1747.
37. F. A. Banat, B. Al-Bashir, S. Al-Asheh, O. Hayajneh, *Environ. Pollut* **2000**, *107*, *3,* 391–398. https://doi.org/10.1016/S0269-7491(99)00173-6
38. Z. Aksu, D. Akpinar, *Separation Purif. Technol*. **2000**, *21,* 87–99. https://doi.org/10.1016/S1383-5866(00)00194-5
39. Z. Aksu, *Separation Purif Technol.* **2001**, *21,3,* 285–294. https://doi.org/10.1016/S1383-5866(00)00212-4
40. S Kuppusamy, T Palanisami, M Megharaj, K Venkateswarlu, R Naidu *Rev Envıron Contam T,* **2016**, *236,* 117–192.
41. B. Likozar, D. Senica, A. Pavko, *Braz. J. Chem. Eng,* **2012**, *29,* 635–652Z. https://doi.org/10.1590/S0104-66322012000300020
42. Z. Chen, H. Deng, C. Chen, Y. Yang, H. Xu, *J. Environ. Health Sci. Eng*. **2014**, *12, 63,* 1–10.
43. V. Vadivelan, K. Kumar, *J. Colloid Interf. Sci*. **2005**, *286,* 90–100. https://doi.org/10.1016/j.jcis.2005.01.007
44. K.V. Kumar, V. Ramamurthi, S. Sivanesan, *J. Colloid Interf. Sci.* **2005**, *284,* 14–21. https://doi.org/10.1016/j.jcis.2004.09.063
45. B. Likozar, D. Senica, A. Pavko, *AIChE,* **2012,**58, 99–106. https://doi.org/10.1002/aic.12559
46. N. Calace, E. Nardi, B. M. Petronio, M. Pietroleytti, *Environ. Pollut*. **2002**, *118,* 315–319. https://doi.org/10.1016/S0269-7491(01)00303-7

Povzetek

Proučevane so bile lastnosti odpadnega lesa turškega ambrovca (*Liquidambar styraciflua)* kot biosorbenta za 2,4 diklorofenol (2,4-DCP) iz vodne raztopine. V šaržnih eksperimentih pri 25 °C so bili raziskani vplivi pH-ja kontaktnega časa, začetne koncentracije 2,4-DCP in množine biosorbenta. Za optimiranje procesa je bila uporabljena Taguchijeva ortogonalna metoda. Lastnosti biosorbenta so bile analizirane s pomočjo FTIR in SEM tehnik. Eksperimentalni podatki so bili obdelani z Langmuirjevim in Freundlichovim modelom adsorpcijskih izoterm. Rezultati potrjujejo enoplastno adsorpcijo. Kinetične študije kažejo, da je za opis tega sistema primeren model pseudo drugega reda.

Scientific paper

Separation/preconcentration of Cr(VI) with a Modified Single-drop Microextraction Device and Determination by GFAAS

Sándor Kapitány,[1,]* Erzsébet Sóki,[1] József Posta[2] and Áron Béni[3]

[1] *Institute of Environmental Sciences, University of Nyiregyhaza, Nyiregyhaza, Hungary*

[2] *Department of Inorganic and Analytical Chemistry, University of Debrecen, Debrecen, Hungary*

[3] *Institute of Agricultural Chemistry and Soil Science, University of Debrecen, Debrecen, Hungary*

** Corresponding author: E-mail: kapitany.sandor@nye.hu*
Tel.: +36-42-599-400; Fax: +36-42-402-485

Received: 08-03-2017

Abstract

We have developed a chromium speciation and preconcentration method with the use of the graphite furnace atomic absorption spectrometry (GFAAS) technique. This method is based on single-drop microextraction (SDME) technique. Nowadays the microextractions have become popular, because low amount of organic solvent needs to be used for the separation. The sample was introduced into the extraction cell with a single chloroform droplet. For the separation and enrichment of chromium species, an ion-pair forming compound was used. After the extraction, the chromium content of the droplet was determined by GFAAS. The analytical sensitivity of the standard SDME technique was improved by increasing the volume of organic phase and by sample recirculation. Because of the increased contact area and the developed extraction device, the stability of droplet was markedly increased. As an application we have determined the Cr(VI) content of sea water by the GFAAS technique using these separation/enrichment methods. Under the optimized extraction conditions, the linear range, detection limit ($S/N = 3$) and precision (RSD, $n = 3$) for Cr(VI) were 0.14 – 5.00 μg/L, 0.042 μg/L, and ≤ 3.0%, respectively. The advantages of this method are the following: cost efficiency, the high enrichment of chromium species and easy usage with the GFAAS technique. Therefore the concentration of the chromium species can be determined at the ng/L level.

Keywords: Chromium speciation, GFAAS, sample preparation, SDME

1. Introduction

In analytical chemistry one of the greatest challenges of the 21st century is the development of speciation analysis.[1–4] Speciation analysis means it is not enough to determine the total concentration of the desired element, as the effect of different species of an element on a living organism can be quite different. Hence it is common in speciation analysis for the species to be separated from each other before the quantitative determination of the separated fractions takes place.

Speciation can be divided into two groups: on-line and off-line methods. On-line methods often require expensive chromatographic instruments.[3] They are faster than off-line methods, where the separation and detection is divided in time, although off-line techniques (non-chromatographic methods) are still much cheaper.[4] This is the reason of their popularity even nowadays. Another major challenge of speciation analysis is that some trace elements are below the detection limit of the instruments, thus the enrichment of the species is needed. Enrichment can be carried out easily using extraction techniques.[4,5] Needless to say, the transformation of the different species must be avoided during sample handling.[4,6]

Chromium has two stable valencies in nature. The two species have totally different effect on living forms. Cr(III) is an essential trace element for proper insulin activity, whereas Cr(VI) is toxic and carcinogenic to all living organisms even in trace amounts.

The separation of chromium species can be performed using various separation-enrichment procedures including liquid-liquid extraction[7–12] and solid-phase extraction[13–17]. Pure chromatographic methods involve using liquid extraction for sample preparation to separate and preconcentrate chromium species,[18,19] but oftentimes this results in inadequate sensitivity for the trace concentration of chromium in real samples. These separation techniques combined with flame or graphite furnace atomic absorption spectrometry can be more sensitive than HPLC and UV/VIS methods.[4]

In the case of on-line chromium speciation, the flow injection system can be used for solid phase[20] or liquid extraction.[8] Expensive methods, such as flow-injection coupled to ICP-MS (FI-ICP-MS) have been developed where 74 ng/L and 18 ng/L detection limits can be achieved for Cr(III) and Cr(VI), respectively.[20] To reduce the analysis drawback and cost of the automated chromium speciation, methods were developed with the sequential injection analysis (SIA) system with UV/VIS[21,22] and FAAS[23] or GFAAS[24] detection. Further improvement of these systems was based on the miniaturization of the flow manifolds. The result was a micro sequential injection analysis Lab-On-Valve (μSI-LOV), which alleviated the majority of the drawbacks of FIA methods[25] and it had a small size with a mini spectrometer, which was developed for a field operated chromium speciation method.[26]

Nowadays the current trend is the simplification and miniaturization of sample preparation techniques.[20,27–30] The base of this concept is to preserve the advantages of the original extraction method and to reduce its drawbacks. The possible results of the miniaturized extraction techniques are increased selectivity and enrichment. The methods include reduced organic solvent consumption and waste production to achieve environmentally friendly and inexpensive processes.[27] The microextraction techniques generally are greener,[31] faster and more automatable than the original techniques.

In recent years, the liquid-liquid extraction (LLE) has become popular in miniaturization,[12,30] because it is fast, easy to use, inexpensive and compatible with many analytical instruments. There are three major categories: single-drop microextraction (SDME),[12,32,33] hollow-fiber microextraction (HF-LPME) and cloud-point extraction (CPE).[34] Major advantages of single-drop microextraction are the following: simplicity, a very limited amount of organic solvent, one-step extraction and preconcentration. Major disadvantages of the SDME are that the droplets are unstable and that their volume is limited to 5 μL. Also the reproducibility and extraction efficiency of this method are poor due to the droplet stabilization problems. There were early attempts to increase the volume and stability of the microdroplet by modifying the needle geometry by flared or oval tube.[35,36] The HF-LPME is better and more complex than the SDME, but it has similar problems except for droplet stabilisation. The CPE has overcome the above mentioned problem, but is difficult to automatize and has very limited applicability for complex samples.[30]

Good example of the automation of SDME was a sequential injection (SI) coupled to GFAAS, which was used for the determination of Cd.[37] This method used a modified FIA system with homemade extraction cell. This setup was difficult to adopt for other instruments and had a long idle time for the GFAAS instrument, because sample preparation time was 10 min and the determination approx. 2 min. The on-line speciation is better for FAAS and ICP techniques. For GFAAS exists a direct chromium speciation. The principle of these methods is using β-diketone to make complex ions of chromium species with different volatilization temperature,[38] but it has higher RSD values than other methods. The other approach is using the commercially available multi-purpose samplers (MPS by Gerstel) for determination of organic compounds by GC-MS.[39,40] These methods' advantages are readiness to use, but they are very expensive and available only for gas and liquid chromatograph. The semi-automated approach to the microextraction was suggested for GFAAS.[41]

Our choice for chromium speciation was the SDME, as it is simpler, requires no foreign material (hollow-fiber) and creates a stable redox system for Cr(VI).

Our goal was to reduce the SDME method's disadvantages and to develop a cheap and fast analytical method that would enable us to separate, enrich and determine Cr(VI) species in environmental samples such as tap water, surface water, sea water, etc. Our goal was to develop extraction method using higher volume and stability of the droplet at higher sample flowrate. Another important feature is that the volume of the sample is freely variable, if a higher enrichment needs to be achieved. Finally, there is a possibility to the automatization of the extraction.

2. Experimental

2. 1. Reagents

All solutions were prepared using ultrapure water. Chloroform was HPLC grade, 96% acetic acid and sodium acetate were analytical reagent grade. These chemicals were obtained from VWR International and methyltrioctylammonium chloride (CAS:5137-55-3, purity ≥97%) from Sigma Aldrich were used for the liquid-liquid extraction. Both Cr(III) and Cr(VI) stock standard solutions containing 1000 mg L^{-1} of Cr were obtained from Fluka.

2. 2. Apparatus

To prepare sample solutions ultra-pure water was used, which was made using a Millipore Milli-Q RG apparatus. The pH of the solutions was measured with a pH

Table 1. Heating program I for the determination of total chromium in aqueous phase with Varian AA-20 GFAAS instrument.

Step	Temperature [°C]	Time [s] Ramp	Hold	Argon flow rate [cm^3 min^{-1}]
1	110	1	15	250
2	130	6	10	250
3	1500	8	10	250
4	2300	0	5	0
5	2450	1	3	250

Table 2. Heating program II for the determination of chromium(VI) in chloroform with Varian AA-20 GFAAS instrument.

Step	Temperature [°C]	Time [s] Ramp	Hold	Argon flow rate [cm^3 min^{-1}]
1	45	1	5	250
2	85	6	40	250
3	1000	15	15	250
4	2300	0	5	0
5	2450	1	3	250

meter made by HANNA Instrument. For the chromium analysis a graphite furnace atomic absorption spectrometer (Varian AA-20 + GTA 96) was used. The injected volume of the samples was 20 µL. The temperature program of the furnace was customised for proper determination as seen in Table 1 and Table 2. Chromium measurements were carried out at 357.9 nm wavelength with a spectral bandwidth of 0.5 nm. Argon 99.996% (Linde Hungary) was used as protective gas and integrated absorbance (peak area) was used for the determination.

2. 2. 1. The Modified SDME Cell

The aim of the developed extraction cell was to reduce the disadvantages of the SDME. The procedure is as follows: first, the droplet is sitting, not hanging. This configuration increased the stability of the droplet. The new glass cell is hollowed for the organic droplet (Fig 1). It has two main components: an extraction cell and glass stopper. The extraction procedure is the following: the closed cell is filled with distilled water, and after that the cell is opened so that the organic droplet can be placed in it. Then it is closed. The sample solution is introduced into the extraction cell with a syringe pump. After the extraction the organic droplet can be removed with syringe or pipette. The 10 – 100 µL micropipette (Biohit) was a better solution. The Hamilton syringe for GC was problematic because it had metal parts and the extraction solvent reacted on it. The results were increased blank values for chromium.

The advantages of this cell geometry were the following: first, it stabilised the droplet, increased robustness

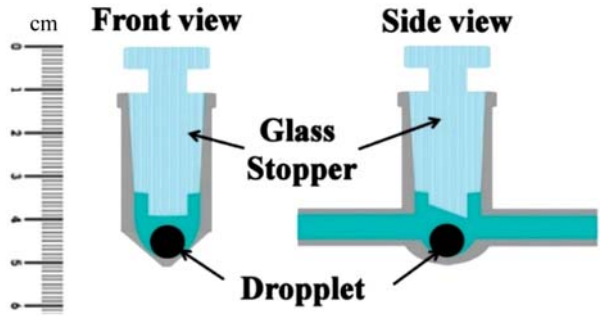

Figure 1. The new extraction cell

of the extraction and ensured a higher flow rate of the sample. Second, the droplet volume was increased to 40 µL to provide a greater contact area between the two phases and a higher extraction efficiency. On the other hand the higher droplet volume was better for GFAAS determination. The droplet could be introduced into the graphite tube or the vials of the autosampler.

At this experiment 40 µL of the chloroform droplet was used and the ion-pair agent was dissolved in chloroform to separate and enrich the Cr(VI) content of the sample.

2. 2. 2. The Recirculating Single-drop Microextraction Device

This system is an upgraded version of the above mentioned system. It is understood that extraction efficiency can be increased by repeating the procedure. Our aim was to construct an extraction system to multiply the single-drop extraction. The result was the recirculating single drop microextraction system shown in Fig. 2. This system consists of a sample reservoir (25 mL beaker), a peristaltic pump (MTA KUTESZ LS-204), an extraction cell, a Hoffmann clamp and a Tygon tube (i.d.: 0.76 mm).

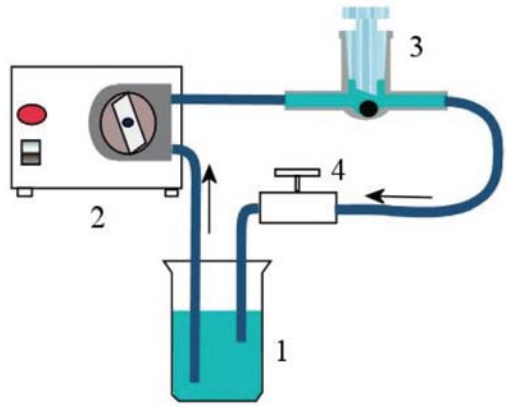

Figure 2. Recirculating single drop micro extraction device with peristaltic pump: 1 sample reservoir, 2 peristaltic pump, 3 extraction chamber, 4 Hoffmann clamp 5 Tygon tube

The Hoffmann clamp was needed to set the back pressure, as the extraction chamber could be fully loaded with the sample solution.

The procedure is as follows: first, the beaker is filled with the sample and the tubes are inserted into the sample solution. After that the whole system is filled using the peristaltic pump and finally, the droplet is ready to be inserted into the extraction cell. The additional advantages of this system over the modified SDME are increased extraction efficiency thanks to the recirculating sample and easier sample changing, as the syringe pump is replaced with peristaltic pump and during the clean-out procedure only the inlet tube has to be put into the distilled water.

3. Results and Discussion

3. 1. Method Development

The principal steps of the method are: adjusting the pH of the water sample, extraction with the new system and finally GFAAS measurement to determine the chromium concentration in the chloroform. Optimal parameters, such as pH, time, reagent concentration and GFAAS heating programme were explored for each step. The aqueous phase volume was set to 10 mL.

3. 1. 1. Optimization of the Extraction

We tested the extraction range of 1.0 – 7.0 pH with 0.5 steps. 1.0 mol/L HCl and 0.1 mol/L NaOH was used to set the pH. The optimum pH range of this extraction was found from 2.0 – 5.0 pH. Thus for all further analyses, we used 4.0 pH, and it was adjusted with acetic acid / sodium acetate buffer (10 mL sample solution + 1 mL buffer). 1 L buffer was prepared from 847 mL 0.1 mol/L acetic acid and 153 mL 0.1 mol/L sodium acetate.

Methyltrioctylammonium chloride concentrations in the chloroform were investigated in the range of 0.1 – 5 % (*w/w*) and the ideal was found at 1 % (*w/w*). Probably at the high methyltrioctylammonium chloride concentration, there is a negative effect on GFAAS determination, because too much organic material was introduced into the graphite tube and at the ashing step chromium losses occurred.

The flow rate of the sample solution was investigated. Previously with the syringe pump the optimal flow rate was 1.0 mL/min with single extraction. The peristaltic pump was used in the range of 2.5 – 14.0 mL/min and the extracted Cr(VI) linearly increased by the flow rate (Fig. 3). At the higher flow rate, the droplet immediately ran out from the extraction cell. The flow rate was reduced to 11.5 mL/min to ensure the stability and repeatability of this method. At this parameter, 10 mL of the sample circulated in the extraction cell 11.5 times in 10 min. This was a remarkable signal increase with GFAAS measurements compared to previous SDME sample preparation.

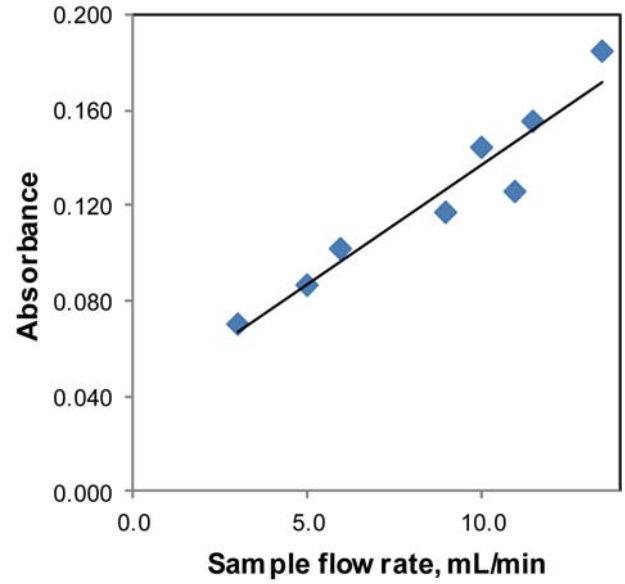

Figure 3. The effect of the flow rate of the sample solution on absorbance. Sample volume was 10 mL, Cr(VI) concentration was 1 µg/L (pH = 4) Extraction time was 10 min (GFAAS, 40 µL droplet volume was diluted to 100 µL)

The extraction time was investigated in the range of 1 – 35 min (Fig. 4). We found that the chromium concentration of the droplet linearly increased in the range of 1 – 15 min.

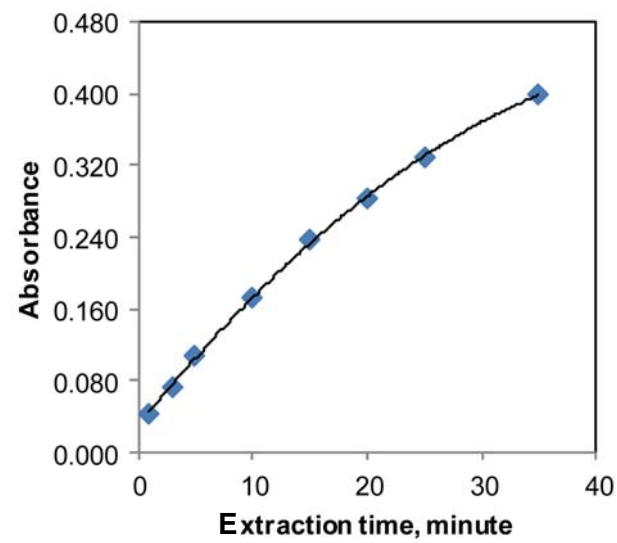

Figure 4. Extraction time effect on the absorbance at 11.5 mL/min flow rate and 10 mL sample volume, concentration of the Cr(VI) was 1 µg/L (pH = 4) (GFAAS, 40 µL droplet was diluted to volume 100 µL, 0.01 mol/L methyltrioctylammonium chloride in droplet)

We limited the extraction time to 10 min to take in account the throughput of this method, and all further measurements were carried out in 10 min.

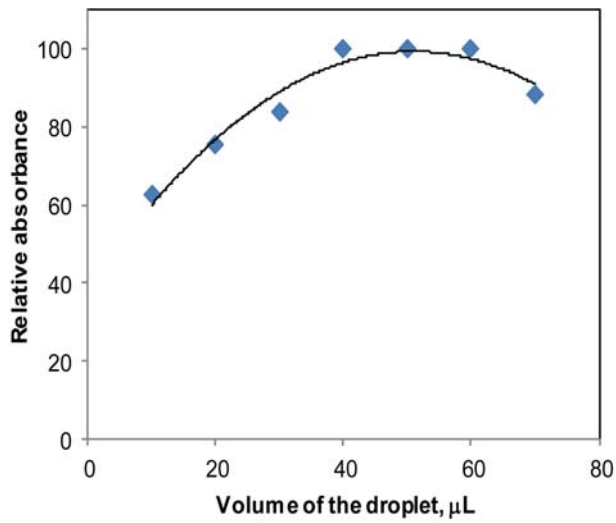

Figure 5. Effect of droplet volume on the relative absorbance (0.25 µg/L pH = 4), flow rate was 11 mL/min (GFAAS, droplet volume was diluted to 100 µL)

The volume of the droplet was investigated between from 10 – 70 µL and the ideal volume was found at 40 µL (Fig 5). At a 70 µL droplet volume, the efficiency of the extraction was decreased.

3. 1. 2. Optimisation of the Heating Programme

The graphite heating was optimized for organic media with a high-concentration of methyltrioctylammonium chloride. The right drying and ashing steps had to be used to maximise the chromium(VI) signal at GFAAS determination. The modified programme is shown in Table 2. Two kinds of calibration standards were prepared. One of them was diluted from the Cr(III) stock standard in water. The other was diluted from the Cr(VI) stock standard in water and was extracted by chloroform with methyltrioctylammonium chloride in 13 mL plastic test tube with screw cap. This liquid-liquid extractions were carried out at an optimum pH and methyltrioctylammonium chloride concentration. The ratio of the phases was 1:1 (3 + 3 mL). Heating programme I was used for the water phase and programme II was used for organic solutions. The results are shown in Fig 6.

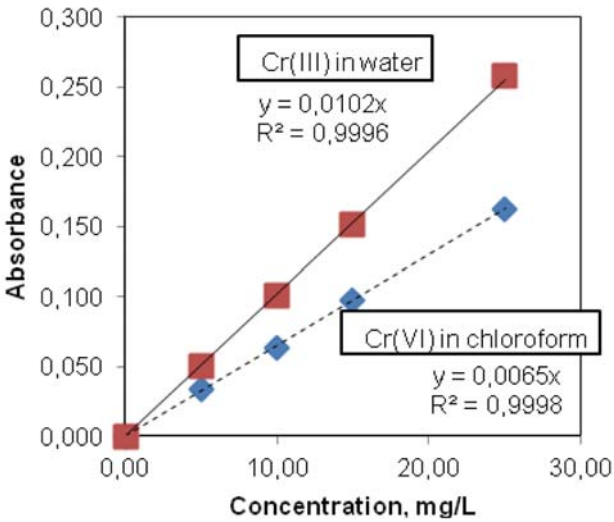

Figure 6. GFAAS calibration curve for Cr(III) in water phase and Cr(VI) in organic phase with 1 % (*w/w*) methyltrioctylammonium chloride in chloroform.

The sensitivity of the chromium determination was decreased in organic media. Therefore, the extraction calibration had to be used for Cr(VI) determination. This calibration method was used for all further measurements at Cr(VI) determination.

3. 2. Method Validation

The 1000 mg/L Cr(VI) stock standard was used and the calibration standards were established by dilution with distilled water. These prepared solutions (10 mL sample + 1 mL buffer) were extracted by this method and the chloroform phase was analysed by the GFAAS.

The recovery analysis was carried out with three different known quantities of Cr(VI). These spiked samples were processed as normal samples. The method was validated for linearity with 0.14 – 5.00 µg/L Cr(VI). The equation of the calibration curve was y = 0.2958x + 0.0395 (R^2 = 0.99), where 'y' is the peak-area and 'x' is the concentration of Cr(VI). The detection limit of the method was 42 ng/L.

The recovery of Cr(VI) in spiked tap water samples ranged from 97% to 101.1% and the precision of the measurements was from 2.38% to 2.81% (Table 3). Regarding the result for the repeatability of this method, 2.53% was observed.

Table 3. Cr(VI) recovery of the developed method (3 replicates)

Sample	Cr(VI) in aqueous phase µg L^{-1}		Recovery, %	RSD %
	Added	Determined		
1	1.00	0.97	97.0	2.53
2	3.00	2.96	98.6	2.81
3	8.00	8.09	101.1	2.38

3. 3. An optimised Method for Cr(VI) Analysis

The optimised procedure was: first, the sample pH was set to 4 with acetic acid and sodium acetate buffer. A 10 mL sample and 1 mL buffer were introduced to the beaker, the flow rate was set to 11.5 mL/min and the extraction time was 10 min. In this procedure, the methyltrioctylammonium chloride concentration in the chloro-

form droplet was 1 % (*w/w*). After the extraction, 40 µL of chloroform was diluted to 100 µL to ensure enough sample volume for the autosampler. Finally 40 µL of the sample was introduced into the graphite tube and the chromium content was determined with the optimized heating programme. At this method the enrichment factor (EF) was 100.

3. 4. Analysis of the Real Samples

The developed method was tested with sea water samples. The water samples were collected from same location at different time. The results were summarized in Table 4.

Table 4. Bulgarian Black Sea water samples 2016 (n = 3, RSD ≤ 3%)

Date	Cr(VI) (µg/L)	Total Cr (µg/L)
I.16.	0.28	0.72
III. 26.	0.24	0.97
V. 28.	0.17	0.28
VI. 29.	0.17	0.66
VII. 20.	0.17	0.45
VIII. 21.	0.21	0.41

The Cr(VI) and total chromium concentrations were determined in sea water samples and the results were in good agreement with other research.[42]

3. 5. Comparison to Other Methods

Our developed method has very good limit of detection compared to other cited methods in Table 5.

The advantage of the developed method is that the sample volume is freely variable. Large amount of water sample can be used to increase the enrichment. The higher volume of the droplet and the recirculation of the sample solution around the droplet leads to higher efficiency of extraction than possible with the normal SDME. This off-line method can be easily adapted to any GFAAS instrument and there is no need to modify the expensive instrument. This SDME technique can be applied to other analytical task, where a high enrichment of the analyte is important.

There are a number of potential drawbacks to the SDME method. Low sample throughput as it takes 10 min, but other SDME methods require the same extraction time. Highly skilled lab worker is needed to set the droplet and this device. The chloroform is volatile, therefore the temperature has to be controlled and before the GFAAS the sample vials have to be sealed to avoid evaporation of the organic solvent. This effect can cause unexpected increase of the chromium concentration. Currently, extraction cell is not commercially available, because it has to be made manually.

Table 5. Comparison of Cr(VI) determination methods for water samples

Extraction method	Analytical method	LOD (µg/L)	Automation approach	Reference
Continuous SDME	GFAAS	0.042		This research
SPE	ICP-AES	0.200	FIA	43
CME	ICP-MS	0.018	FIA	20
SPE	FAAS	0.034	FIA	44
SPE	FAAS	0.8	FIA	45
SPE	FAAS	0.3	SIA	23
SPE	GFAAS	0.02	SIA	24
SPE	FAAS	45		46
SPE	GFAAS	0.027		47
CPE	FAAS	0.18		48
CPE	GFAAS	0.01		49
–	UV/VIS	23	SIA	21
–	UV/VIS	5.6	µSIA-LOV	26
LLE	UV/VIS	7.5	FIA	50
LLME	UV/VIS	0.26	SIA	22
DLLME	FAAS	0.08		51
DLLME	TXRF	0.8		52
Thermal	GFAAS	0.7		38

CME: capillary microextraction, SDME: single drop microextraction, CPE: cloud point extraction, SPE: solid phase extraction, LLE: liquid–liquid extraction, LLME: liquid–liquid microextraction, DLLME: dispersive liquid–liquid microextraction, FAAS: flame atomic absorption spectrometry, GFAAS: graphite furnace atomic absorption spectrometry, TXRF: total reflection X-ray fluorescence spectrometry, ICP-AES, Inductively coupled plasma atomic emission spectroscopy, FIA: flow injection analysis, SIA: sequential injection analysis, LOV: Lab-On-Valve

3. 6. Automatization

Currently, the peristaltic pump had a timer to switch off after 10 min. We are planning to increase the automati-

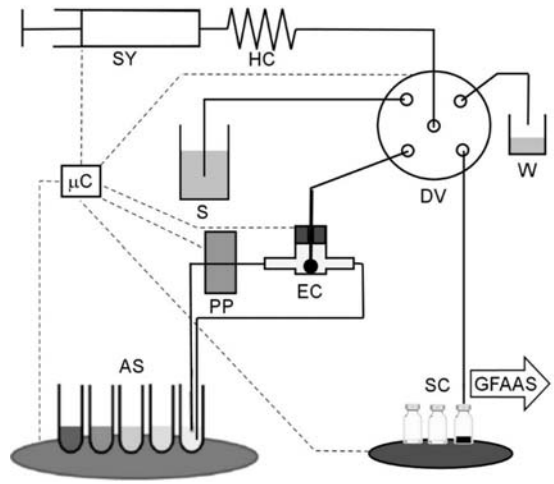

Figure 7. The proposed semi-automatic apparatus for chromium speciation method SY: syringe + steeper motor, HC: holding coil, DV: distribution valve (Hamilton), W: waste, S: organic solvent, PP: peristaltic pump, EC: extraction cell, AS: auto-sampler, SC: sample collector, µC: microcontroller (Arduino)

zation degree of this process. The notion is based on semi-automatic chromium speciation approach with µSIA technique. First, the Arduino microcontroller coordinates the syringe, distribution valve, peristaltic pump and tip of the extraction cell. The next step is to couple the developed device with an autosampler and sample collector (Fig. 7).

This system is containing new and salvaged parts to reduce the cost. The Arduino microcontroller is easily programmable, cheap and easy to connect the display, relay control and motor driver boards.

Further plan is to replace the sample collector (SC) with the autosampler of the GFAAS to achieve the full automatization.

The planned fully automated sample preparation system will be useful to determine the Cr(VI) by GFAAS.

4. Conclusions

In this study a novel single drop microextraction (SDME) technique is presented for chromium speciation. The advantages of this method are, in addition to minimal organic solvent consumption and the need for only one droplet per sample to extract, the higher stability of the drop and the possibility of high enrichment of the analysed elements. The higher volume of the droplet in a modified cell and the recirculation of the sample solution around the droplet leads to higher efficiency of the extraction than is possible with the normal SDME. This simple, easy to make, cheap, effective, rugged and safe extraction method can be used to create fully automated sample preparation system. Finally, this recirculating system can also be used for the extraction and enrichment of other analytes at the ng/L level.

5. References

1. R. Cornelis: Handbook of Elemental Speciation, Weinheim, Germany, Wiley-VCH. **2003**. https://doi.org/10.1002/0470868384
2. S. A. Katz, H. Salem: The Biological and Environmental Chemistry of Chromium, VCH, Weinheim, Germany, **1994**, pp. 155–186.
3. J. A. Caruso, M. Montes-Bayon, *Ecotoxicol. Environ. Saf.*, **2003**, *56*, 148–163. https://doi.org/10.1016/S0147-6513(03)00058-7
4. A. Gonzalvez, M. L. Cervera, S. Armenta, M. d. l. Guardia, *Anal. Chim. Acta* **2009**, *636*, 129–157. https://doi.org/10.1016/j.aca.2009.01.065
5. L. Adlnasab, H. Ebrahimzadeh, Y. Yamini, *Anal. Methods*, **2012**, *4*, 190–195. https://doi.org/10.1039/C1AY05449J
6. M. Pettine, S. Capri, *Anal. Chim. Acta* **2005**, *540*, 231–238. https://doi.org/10.1016/j.aca.2005.03.040
7. S. C. Nielsen, S. Strürup, H. Spliid, E. H. Hansen, *Talanta*, **1999**, *49*, 1027–1044. https://doi.org/10.1016/S0039-9140(99)00044-2
8. S. C. Nielsen, E. H. Hansen, *Anal. Chim. Acta*, **2000**, *422*, 47–62. https://doi.org/10.1016/S0003-2670(00)01051-5
9. A. R. Kumar, P. Riyazuddin, *Microchem. J.*, **2009**, *92*, 145–149. https://doi.org/10.1016/j.microc.2009.03.001
10. Y. Akama, A. Sali, *Talanta*, **2002**, *57*, 681–686. https://doi.org/10.1016/S0039-9140(02)00076-0
11. N. E. El-Hefny, *Separ. Purif. Techn.*, **2009**, *67*, 44–49. https://doi.org/10.1016/j.seppur.2009.03.004
12. B. Hu, M. He, B. Chen, L. Xia, *Spectrochim. Acta B*, **2013**, *86*, 14–30. https://doi.org/10.1016/j.sab.2013.05.025
13. K. O. Saygi, M. Tuzen, M. Soyak, L. Elci, *J. Hazard. Mater.*, **2008**, *153*, 1009–1014. https://doi.org/10.1016/j.jhazmat.2007.09.051
14. M. V. B. Krishna, K. Chandrasekaran, S. V. Rao, D. Karunasagar, J. Arunachalam, *Talanta*, **2005**, *65*, 135–143.
15. M. Korolczuk, M. Grabarczyk, *Talanta*, **2005**, *66*, 1320–1325. https://doi.org/10.1016/j.talanta.2005.01.047
16. S. Morales-Munoz, J. L. Luque-García, M. D. L. Castro, *Anal. Chim. Acta*, **2004**, *515*, 343–348. https://doi.org/10.1016/j.aca.2004.03.092
17. Z. Abbas, B.-M. Steenari, O. Lindqvist, *Waste Manag.*, **2001**, *21*, 725–739. https://doi.org/10.1016/S0956-053X(01)00005-8
18. A. N. Tang, D. Q. Jiang, Y. Jiang, S. W. Wang, X. P. Yan, *J. Chromatogr. A* **2004**, *1036*, 183–188. https://doi.org/10.1016/j.chroma.2004.02.065
19. L.-Y. Ying, H.-L. Jiang, S. C. Zhou, Y. Zhou, *Microchem. J.*, **2011**, *98*, 200–203. https://doi.org/10.1016/j.microc.2011.01.010
20. W. Hu, F. Zheng, B. Hu, *J. Hazard. Mater.*, **2008**, *151*, 58–64. https://doi.org/10.1016/j.jhazmat.2007.05.044
21. L. V. Mulaudzi, J. F. v. Staden, R. I. Stefan, *Anal. Chim. Acta*, **2002**, *467*, 51–60. https://doi.org/10.1016/S0003-2670(02)00188-5
22. M. Alexovič, V. Andruch, Ioseph S. Balogh, J. Šandrejová, *Anal. Methods*, **2013**, *5*, 2497–2502. https://doi.org/10.1039/C3AY40284C
23. S. Şahan, Ş. Saçmacý, Ş. Kartal, M. Saçmacý, U. Şahin, A. Ülgen, *Talanta*, **2014**, *120*, 391–397. https://doi.org/10.1016/j.talanta.2013.12.030
24. A.-M. Zou, X.-Y. Tang, M.-L. Chen, J.-H. Wang, *Spectrochim. Acta B*, **2008**, *63*, 607–611. https://doi.org/10.1016/j.sab.2008.02.008
25. M. M. Grand, P. Chocholous, J. Ruzicka, P. Solich, C. I. Measures, *Anal. Chim. Acta*, **2016**, *923*, 45–54. https://doi.org/10.1016/j.aca.2016.03.056
26. M. Yang, J.-X. Li, J.-H. Wang, *Talanta*, **2007**, *72*, 1710–1716. https://doi.org/10.1016/j.talanta.2007.01.020
27. V. Andruch, L. Kocúrová, I. S. Balogh, J. Škrlíková, *Microchem. J.*, **2012**, *102*, 1–10. https://doi.org/10.1016/j.microc.2011.10.006
28. J. M. Kokosa, *Trends Analyt. Chem.*, **2013**, *43*, 2–13. https://doi.org/10.1016/j.trac.2012.09.020
29. S. Dadfarnia, A. M. H. Shabani, *Anal. Chim. Acta*, **2010**, *658*, 107–119. https://doi.org/10.1016/j.aca.2009.11.022

30. A. Sarafraz-Yazdi, A. Amiri, *Trends Anal. Chem.*, **2010**, *29*, 1–14. https://doi.org/10.1016/j.trac.2009.10.003
31. D. L. Rocha, A. D. Batista, F. R. P. Rocha, G. L. Donati, J. A. Nóbrega, *Trends Analyt. Chem.*, **2013**, *45*, 79–92. https://doi.org/10.1016/j.trac.2012.12.015
32. M. A. Jeannot, A. Przyjazny, J. M. Kokosa, *J. Chromatogr. A*, **2010**, *1217*, 2326–2336. https://doi.org/10.1016/j.chroma.2009.10.089
33. L. Xu, C. Basheer, H. K. Lee, *J. Chromatogr. A*, **2007**, *1152*, 184–192. https://doi.org/10.1016/j.chroma.2006.10.073
34. K. Pytlakowska, V. Kozik, M. Dabioch, *Talanta*, **2013**, *110*, 202–228. https://doi.org/10.1016/j.talanta.2013.02.037
35. H. Yiping, W. Caiyun, *Anal. Chim. Acta*, **2010**, *661*, 161–166. https://doi.org/10.1016/j.aca.2009.12.018
36. X. Wang, J. Cheng, X. Wang, M. Wu, M. Cheng, *Analyst*, **2012**, *137*, 5339–5345. https://doi.org/10.1039/c2an35623f
37. A. N. Anthemidis, I. S. I. Adam, *Anal. Chim. Acta*, **2009**, *632*, 216–220. https://doi.org/10.1016/j.aca.2008.10.078
38. P. Bermejo-Barrera, M. C. Barciela-Alonso, B. Pérez-Fernández, A. Bermejo-Barrera, *Spectrochim. Acta B*, **2003**, *58*, 167–173. https://doi.org/10.1016/S0584-8547(02)00229-X
39. X. Wang, Y. Li, F. Cai, Q. Qing, K. Yuan, B. Chen, T. Luan, *Talanta*, **2017**, *164*, 727–734. https://doi.org/10.1016/j.talanta.2016.06.011
40. X. Wang, K. Yuan, H. Liu, L. Lin, T. Luan, *J. Sep. Sci.*, **2014**, *37*, 1842–1849. https://doi.org/10.1002/jssc.201400198
41. M. Alexovic, B. Horstkotte, I. Srámková, P. Solich, J. Sabo, *Trends Analyt. Chem.*, **2017**, *86*, 39–55. https://doi.org/10.1016/j.trac.2016.10.003
42. T. Shigematsu, S. Gohda, H. Yamazaki, Y. Nishikaw, *Bull. Inst. Chem. Res.*, **1977**, *55*, 429–440.
43. A. G. Cox, I. G. Cook, C. W. McLeod, *Analyst*, **1985**, *110*, 331–333. https://doi.org/10.1039/an9851000331
44. E. Rossi, M. I. Errea, M. M. F. d. Cortalezzi, J. Stripeikis, *Microchem. J.*, **2017**, *130*, 88–92. https://doi.org/10.1016/j.microc.2016.08.004
45. M. Sperling, S. Xu, B. Welz, *Anal. Chem.*, **1992**, *64*, 3101–3108. https://doi.org/10.1021/ac00048a007
46. A. Tunceli, A. R. Türker, *Talanta*, **2002**, *57*, 1199–1204. https://doi.org/10.1016/S0039-9140(02)00237-0
47. A. C. Sahayam, G. Venkateswarlu, S. C. Chaurasia, *Anal. Chim. Acta*, **2005**, *537*, 267–270. https://doi.org/10.1016/j.aca.2005.01.017
48. K. Kiran, K. S. Kumar, B. Prasad, K. Suvardhan, R. B. Lekkala, K. Janardhanam, *J. Hazard. Mater.*, **2008**, *150*, 582–586. https://doi.org/10.1016/j.jhazmat.2007.05.007
49. X. Zhu, B. Hu, Z. Jiang, M. Li, *Water Res.*, **2005**, *39*, 589–595. https://doi.org/10.1016/j.watres.2004.11.006
50. W. Chen, G. Zhong, Z. Zhou, P. Wu, X. Hou, *Anal. Sci.*, **2005**, *21*, 1189–1193. https://doi.org/10.2116/analsci.21.1189
51. P. Hemmatkhah, A. Bidari, S. Jafarvand, M. R. M. Hosseini, Y. Assadi, *Microchim. Acta*, **2009**, *166*, 69–75. https://doi.org/10.1007/s00604-009-0167-x
52. Z. Bahadir, V. N. Bulut, M. Hidalgo, M. Soylak, E. Marguí, *Spectrochim. Acta B*, **2016**, *115*, 46–51. https://doi.org/10.1016/j.sab.2015.11.001

Povzetek

Razvili smo metodo za speciacijo in predkoncentracijo kroma, ki uporablja tehniko atomske absorpcijske spektrometrije z grafitno kiveto (GFAAS). Metoda je osnovana na tehniki mikroekstrakcije v kapljico (SDME). Dandanašnji so mikroekstrakcije postale popularne, saj je za separacijo potrebna majhna količina organskega topila. Vzorec je v ekstrakcijski celici v stiku z eno samo kapljico kloroforma. Za separacijo in obogatitev kromovih zvrsti smo uporabili ionsko-parno spojino. Po ekstrakciji smo vsebnost kroma v kapljici določili z GFAAS. Analizna občutljivost se je izboljšala glede na standardno SDME tehniko zaradi večjega volumna organske faze in zaradi kroženja vzorca. Zaradi večje stične površine in razvite ekstrakcijske naprave je bila tudi stabilnost kaplice znatno večja. Kot primer uporabe smo določili vsebnost Cr(VI) v morski vodi s tehniko GFAAS in razvito separacijsko/ekstrakcijsko metodo. Pri optimiziranih ekstrakcijskih pogojih je bilo za Cr(VI) linearno območje 0,14–5,00 µg/L, meja zaznave (S/N = 3) 0,042 µg/L in natančnost (RSD, n = 3) ≤ 3,0 %. Prednosti metode so naslednje: cenovna učinkovitost, visoka obogatitev kromovih zvrsti in enostavna uporaba v povezavi z GFAAS tehniko. Koncentracijo kromovih zvrsti tako lahko določimo na ng/L nivoju.

Short communication

About the Randić Connectivity, Modify Randić Connectivity and Sum-connectivity Indices of Titania Nanotubes $TiO_2(m,n)$

Wei Gao,[1] Mohammad Reza Farahani[2] and Muhammad Imran[3,4]*

[1] *School of Information Science and Technology, Yunnan Normal University, Kunming 650500, China*

[2] *Department of Applied Mathematics, Iran University of Science and Technology (IUST), Narmak, Tehran 16844, Iran*

[3] *Department of Mathematical Sciences, United Arab Emirates University, P. O. Box 1551, Al Ain, United Arab Emirates*

[4] *School of Natural Sciences, National University of Sciences and Technology, Sector H-12, P.O. 44000, Islamabad, Pakistan*

* *Corresponding author: E-mail: imrandhab@gmail.com*
Phone: +97 137136389, Fax: +971 3 7671291

Received: 28-09-2016

Abstract

The Randić Connectivity Index *R(G)* is one of the oldest connectivity index, introduced by Randić in 1975. Another connectivity indices is the Sum-Connectivity Index *X(G)* introduced in 2008 by Zhou and Trinajstić. Recently in 2011, a modification of the Randić Connectivity Index of a graph *G* was introduced by Dvorak et al. In this paper, we compute these connectivity topological indices for a family of molecular graphs known as titania nanotubes $TiO_2(m,n)$.

Keywords: Molecular graph, Nanotubes, Titania nanotubes $TiO_2(m,n)$, Topological indices, Randić index, Sum-connectivity index, Modify Randić index, Zagreb index, Multiple Zagreb index.

1. Introduction

A graph is a collection of points and lines connecting a subset of them. The points and lines in a graph are respectively called vertices and edges of the graph. An edge in *E(G)* with end vertices *u* and *v* is denoted by *uv*. Two vertices *u* and *v* are said to be adjacent if there is an edge between them. In chemical graph theory, the vertices of molecular graph *G* correspond to the atoms and its edges correspond to the chemical bonds. We denoted the order and size and degree of a vertex/atom *v* of a molecular graph *G* by $|V(G)|$, $|E(G)|$ and dv, respectively. The set of all vertices adjacent to a vertex *v* in *V(G)* is said to be the neighborhood of *v*, denoted as *N(v)*. The number of vertices in *N(v)* is said to be the degree of *v*. The minimum and maximum vertex degrees in a graph *G* denoted by $\delta(G)$ and $\Delta(G)$, respectively and are defined as $min\{dv \mid v\in V(G)\}$ and $max\{dv \mid v\in V(G)\}$, respectively. Our notation is standard and mainly taken from standard books of chemical graph theory.[1–3]

We have many connectivity topological indices, for an arbitrary graph with connected structure in chemical graph theory. The oldest of them is Randić Connectivity Index which has shown to reflect molecular branching, introduced by Milan Randić in 1975,[4] and defined as

$$R(G) = \sum_{uv\in E(G)} \frac{1}{\sqrt{d_u d_v}}, \tag{1}$$

where, d_u and d_v are the degrees of the vertices *u* and *v*, respectively.

Another connectivity indices is the Sum-Connectivity Index that was introduced by Zhou and Trinajstić in 2008.[5,6] The sum-connectivity index *X(G)* is defined as the sum over all edges of the graph of the terms $d_u + d_v)^{-2/2}$ and is equal to

$$X(G) = \sum_{uv\in E(G)} \frac{1}{\sqrt{d_u + d_v}}, \tag{2}$$

Recently in 2011, Dvorak et al. introduced a modification of the Randić Connectivity Index of *G* and is defined as

$$R'(G) = \sum_{uv \in E(G)} \frac{1}{\max\{d_u, d_v\}}, \quad (3)$$

that is more tractable from computational point of view. It is much easier to compute Modify Randić index *R'(G)* than Randić index *R'(G)* (see[7] for more details). Some basic properties of these indices can be found in the recent letters. For more study, see reference.[8–13]

In this paper, we investigate the topological Connectivity indices, and compute some formulas for the Randić, Sum-Connectivity and Modify Randić indices of a family of molecular graphs that called titania nanotubes $TiO_2(m,n)$ for positive integers *n*, *m* (see Figure 1).

2. Main results and Discussion

In this section, we compute the Randić, Sum-connectivity and Modify Randić Indices for the titania nanotubes $TiO_2(m,n)$ ($\forall\ m,n \in \mathbb{N}$). Titania nanotubes were systematically synthesized during the last 10–15 years using different methods and carefully studied as prospective technological materials. Since the growth mechanism for TiO_2 Nanotubes is still not well defined, their comprehensive theoretical studies attract enhanced attention. The TiO_2 sheets with a thickness of a few atomic layers were found to be remarkably stable.[14–17] Molecular graphs titania $TiO_2(m,n)$ is a family of nanotubes, such that the structure of this family of nanotubes consist of the cycles with length four C_4 and eight C_8. Several topological indices of titania nanotubes (TiO_2) have been studied in the literature.[18–20]

Let us denote the number of Octagons or cycles C_8 in the first row and column of the 2- Dimensional lattice of TiO_2 nanotubes (Figure 1) by *m* and *n*, respectively.

Theorem 1. Let $TiO_2(m,n)$ be the titania nanotubes for positive integers *m,n*. Then the following indices are calculated by formulas:

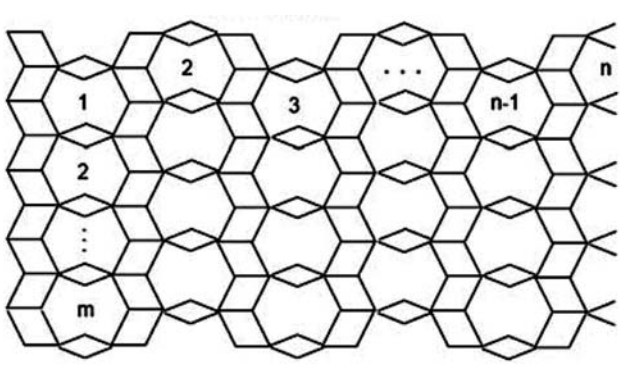

Figure 1. A 2-Dimensional Lattice of the titania nanotubes $TiO_2(m,n)$ ($\forall\ m, n \in \mathbb{N}$).[17]

– The Randić Connectivity index

$$R(TiO_2(m,n)) = \left[\frac{2(\sqrt{15}+\sqrt{10})}{5} m + \left(\frac{45\sqrt{2}+3\sqrt{10}+5\sqrt{3}+2\sqrt{15}}{15}\right)\right] n \quad (4)$$

– The Sum-Connectivity index

$$X(TiO_2(m,n)) = \left[\left(\frac{3\sqrt{2}}{2} + \frac{4\sqrt{7}}{7}\right) m + \left(\sqrt{6} + \frac{4\sqrt{7}}{7} - \frac{\sqrt{2}}{2}\right)\right] n \quad (5)$$

– The Modify Randić index

$$R'(TiO_2(m,n)) = 2n(m+1). \quad (6)$$

Before we prove the main results, let us introduce some definitions.

Definition 1. Consider the graph *G = (V, E)*, then we divide the vertex set *V(G)* and edge set *E(G)* of *G* into several partitions based on the degrees of vertices/atoms in *G* as follows.[9]

$$\begin{aligned}
&\forall k: \delta \le k \le \Delta,\ V_k = \{v \in V(G) | d_v = k\} \\
&\forall i: 2\delta \le i \le 2\Delta,\ E_i = uv \in E(G) | d_u + d_v = i\} \\
&\forall j: \delta^2 \le j \le \Delta^2, E_J{}^* = \{uv \in E(G) | d_u \times d_v = j\}. \\
&\forall f: \delta \le f \le \Delta, E_f{}^+ = \{uv \in E(G) | \mathrm{Max}\{d_u d_v\} = f\} \\
&\forall g: \delta \le g \le \Delta, E_g{}^\times = \{uv \in E(G) | \mathrm{Min}\{d_u d_v\} = g\},
\end{aligned} \quad (7)$$

Where $d_u (1 \le d_v \le n-1)$ be the degrees of $v \in V(G)$ and δ and Δ are the minimum and maximum, respectively.

In particular, let *G* = (*V*, *E*) be a connected molecular graph or nanotubes, then we can divide the vertex set and edge set of *G* in following partitions:

$$V_i = \{v \in V(G) | d_v = i\}, \forall\ i = 1,2,\ldots,5 \quad (8)$$

Since the degree of an atom (or vertex) of the molecular graph is equal to *1, 2,…, 5* and the hydrogen atoms (with degree 1) in *G* are often omitted.

In particular, let $TiO_2(m,n)$ be the titania nanotubes ($\forall m,n \in \mathbb{N}$) with *6n(m+1)* vertices and *10mn+8n* edges, then from its structure, the vertex and edge partitions of

the vertex set $V(TiO_2(m,n))$ and edge set $E(TiO_2(m,n))$ and their order and size are as follow.[17]

$$\begin{aligned} V_2 &= \{v \in V(TiO_2(m,n)) | d_v = 2\}, \\ &|v_2| = 2mn + 4n \\ V_3 &= \{v \in V(TiO_2(m,n)) | d_v = 3\}, \\ &|v_3| = 2mn \\ V_4 &= \{v \in V(TiO_2(m,n)) | d_v = 4\}, \\ &|v_4| = 2n \\ V_5 &= \{v \in V(TiO_2(m,n)) | d_v = 5\}, \\ &|v_5| = 2mn \end{aligned} \tag{9}$$

and

$$\begin{aligned} E_6 &= \{uv \in E(TiO_2(m,n)) | d_u + d_v = 6\}, \\ &|E_6| = 6n \\ E_8{}^* &= \{uv \in E(TiO_2(m,n)) | d_u \times d_v = 8\}, \\ &|E_8{}^*| = 6n \\ E_7 &= \{uv \in E(TiO_2(m,n)) | d_u + d_v = 7\}, \\ &|E_7| = 4n(m+1) \\ E_{10}{}^* &= \{uv \in E(TiO_2(m,n)) | d_u \times d_v = 10\}, \\ &|E_{10}{}^*| = 4mn + 2n \\ E_{12}{}^* &= \{uv \in E(TiO_2(m,n)) | d_u \times d_v = 12\}, \\ &|E_{12}{}^*| = 2n \\ E_8 = E_{15}{}^* &= \{uv \in E(TiO_2(m,n)) | d_u \times d_v = 8\}, \\ &|E_8| = |E_{15}{}^*| = 2n(3m-1) \end{aligned} \tag{10}$$

By above mentioned formulas, one can see that

$$\begin{aligned} |V(TiO_2(m,n))| &= (2mn + 4n) + 2mn + \\ &+ 2n + 2mn = 6n(m+1). \\ |E(TiO_2(m,n))| &= {}^1/_2\,[2 \times (2mn + 4n) + \\ &+ 3 \times 2mn + 4 \times 2n + 5 \times 2mn] = 10mn + 8n. \end{aligned} \tag{11}$$

Now, we have the following computations of the Randić, Sum-connectivity and Modify Randić Indices for the titania nanotubes $TiO_2(m,n)$ $\forall$ $m,n \in \mathbb{N}$.

$$\begin{aligned} R(TiO_2(m,n)) &= \sum_{uv \in E(TiO_2[m,n])} \frac{1}{\sqrt{d_u d_v}} \\ &= \sum\nolimits_{uv \in E_8{}^*} \frac{1}{\sqrt{d_u d_v}} + \sum\nolimits_{uv \in E_{10}{}^*} \frac{1}{\sqrt{d_u d_v}} + \sum\nolimits_{uv \in E_{12}{}^*} \frac{1}{\sqrt{d_u d_v}} + \sum\nolimits_{uv \in E_{15}{}^*} \frac{1}{\sqrt{d_u d_v}} \\ &= (6n) \times \left(\tfrac{1}{\sqrt{2\times4}}\right) + 2n(2m+1) \times \left(\tfrac{1}{\sqrt{2\times5}}\right) + (2n) \times \left(\tfrac{1}{\sqrt{3\times4}}\right) + (6mn - 2n) \times \left(\tfrac{1}{\sqrt{3\times5}}\right) \\ &= 3n\sqrt{2} + \frac{n(2m+1)\sqrt{10}}{5} + \frac{\sqrt{3}}{3}n + \frac{\sqrt{15}}{15}(6mn - 2n) \\ &= \frac{2}{5}\left(\sqrt{15} + \sqrt{10}\right)mn + \left(3\sqrt{2} + \frac{\sqrt{10}}{5} + \frac{\sqrt{3}}{3} + \frac{2\sqrt{15}}{15}\right)n. \end{aligned} \tag{12}$$

Thus the Randić connectivity index of $TiO_2(m,n)$ nanotubes is equal to

$$R(TiO_2(m,n)) = \left(\frac{2\left(\sqrt{15} + \sqrt{10}\right)}{5}m + \left(\frac{45\sqrt{2} + 3\sqrt{10} + 5\sqrt{3} + 2\sqrt{15}}{15}\right)\right)n \tag{13}$$

Also,

$$X(TiO_2(m,n)) = \sum_{uv\in E(TiO_2[m,n])} \frac{1}{\sqrt{d_u+d_v}}$$

$$= \sum_{uv\in E_6} \frac{1}{\sqrt{d_u+d_v}} + \sum_{uv\in E_7} \frac{1}{\sqrt{d_u+d_v}} + \sum_{uv\in E_8} \frac{1}{\sqrt{d_u+d_v}}$$

$$= \frac{6n}{\sqrt{2+4}} + \frac{4mn+2n}{\sqrt{2+5}} + \frac{2n}{\sqrt{3+4}} + \frac{6mn-2n}{\sqrt{3+5}} \tag{14}$$

$$= \sqrt{6n} + \frac{4n(m+1)\sqrt{7}}{7}n + \frac{\sqrt{2}}{2}n(3m-1).$$

Hence the Sum-Connectivity index of $TiO_2(m,n)$ nanotubes is

$$X(TiO_2(m,n)) = \left(\left(\frac{3\sqrt{2}}{2} + \frac{4\sqrt{7}}{7}\right)m + \left(\sqrt{6} + \frac{4\sqrt{7}}{7} - \frac{\sqrt{2}}{2}\right)\right)n. \tag{15}$$

Now, by using Definition 1, we see that there are two modify edges partitions $E_4^+$and E_5^+ for the titania nanotubes $TiO_2(m,n)$ ($\forall m,n\in\mathbb{N}$) as:

$$E_4^+ = \{uv \in E(TiO_2(m,n)) | Max\{2,4\} = Max\{3,4\} = 4\} = E_8^* \cup E_{12}^*$$

$$|E_4^+| = |E_8^*| + |E_{12}^*| = 6n + 2n = 8n \tag{16}$$

$$E_5^+ = \{uv \in E(TiO_2(m,n)) | Max\{2,5\} = Max\{3,5\} = 5\} = E_{10}^* \cup E_{15}^*$$

$$|E_{15}^*| = 4nm + 2n + 2n(3m-1) = 10mn.$$

Therefore the Modify Randić index of $TiO_2(m,n)$ is equal to:

$$R'(TiO_2(m,n)) = \sum_{uv\in E(TiO_2[m,n])} \frac{1}{\max\{d_u, d_v\}}$$

$$= \sum_{uv\in E_4^+} \frac{1}{\max\{d_u, d_v\}} + \sum_{uv\in E_5^+} \frac{1}{\max\{d_u, d_v\}} \tag{17}$$

$$= \frac{8n}{4} + \frac{10mn}{5} = 2mn + 2n = 2n(m+1).$$

Here, we complete the proof of main theorem of this article and all main results are computed.

Corollary 2.1. Consider the titania nanotubes $TiO_2(m,n)$ $\forall m,n\in\mathbb{N}$ (Figure 1), with *6n(m+1)* vertices and *10mn+8n* edges. For enough large integer number *m* and *n*, the Randić, Sum-connectivity and Modify Randić Indices of $TiO_2(m,n)$ are equal to:

(1) The Randić Connectivity index

$$R(TiO_2{}^\wedge[m,n]) \approx (2.814m + 5.9688)n.$$

(2) The Sum-Connectivity index

$$X(TiO_2{}^\wedge[m,n]) \approx (3.6332m + 3.2542)n.$$

(3) The Modify Randić index

$$R(TiO_2(m,n)) = (2m+2)n.$$

Corollary 2. 2. Consider $TiO_2(m,n)$ nanotubes, Corollary 1 implies that for enough large integer number $m,n\in\mathbb{N}$,

$$\mathbf{X(TiO_2(m,n)) > R(TiO_2(m,n)) > R'(TiO_2(m,n)).}$$

3. Discussion

Now we study the change of the values of Randić, Sum-connectivity and Modify Randić Indices of $TiO_2(m,n)$ nanotubes when the parameters m and n are slightly changed. The graphs of these nanotubes corresponding to some small values of m and n are shown in Figure 2. Similarly, the values of the studied topological indices corresponding to small change in the values of *m* and *n* is summarized in Table 1.

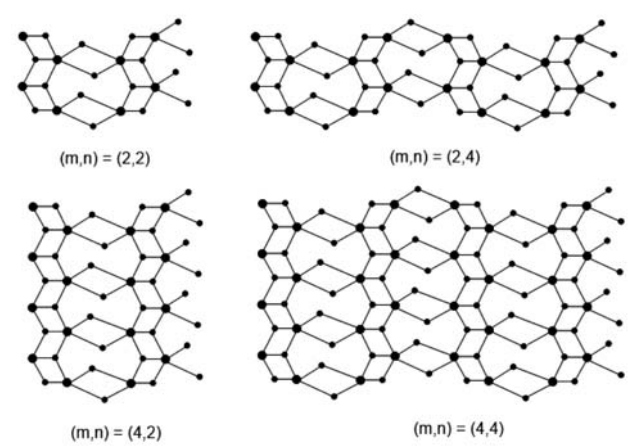

Figure 2. The graph of titania nanotubes $TiO_2(m,n)$ for $m = 2,4$ and $n = 2,4$.

4. Conclusion

In this paper, we considered an infinite class of the titania nanotubes $TiO_2(m,n)$, that were systematically

Table 1. Some values of Randić, Sum-connectivity and Modify Randić Indices of $TiO_2(m,n)$ nanotubes corresponding to the change in m and n.

	(m, n)	$n = 1$	$n = 2$	$n = 3$	$n = 4$
$R(G)$	$m = 3$	14.4112	28.8223	43.2335	57.6446
	$m = 4$	17.225	34.4505	51.6758	68.9010
$X(G)$	$m = 3$	14.1538	28.3076	42.4613	56.6151
	$m = 4$	17.7869	35.5739	53.3609	71.1478
$R'(G)$	$m = 3$	8	16	24	32
	$m = 4$	10	20	30	40

synthesized during the last 10–15 years using different methods and carefully studied as prospective technological materials. We computed its connectivity topological indices including Randić index $R(G) = R(G) = \sum_{uv \in E(G)} (d_u d_v)^{-1/2}$, Sum-Connectivity index $X(G) = X(G) = \sum_{uv \in E(G)} (d_u + d_v)^{-1/2}$ and Modify Randić index $R'(G) = R'(G) = \sum_{uv \in E(G)} \frac{1}{\max\{d_u, d_v\}}$, that d_u and d_v are the degrees of the vertices u and v, respectively.

4. References

1. H. Wiener, *J. Am. Chem. Soc.* **1947**, *69,* 17–20. https://doi.org/10.1021/ja01193a005
2. R. Todeschini, V. Consonni, Handbook of Molecular Descriptors, Wiley-VCH, Weinheim, **2000**. https://doi.org/10.1002/9783527613106
3. N. Trinajstić, Chemical Graph Theory, CRC Press, Boca Raton, FL, **1992**.
4. M. Randić, *J. Am. Chem. Soc*. **1975**, *97*, 6609–6615. https://doi.org/10.1021/ja00856a001
5. B. Zhou, N. Trinajstić, *J. Math. Chem.* **2009**, *46,* 1252–1270. https://doi.org/10.1007/s10910-008-9515-z
6. B. Zhou, N. Trinajstić, *J. Math. Chem.* **2010**, *47,* 210–218. https://doi.org/10.1007/s10910-009-9542-4
7. Z. Dvorak, B. Lidicky, R. Skrekovski, *Eur. J. Comb.* **2011**, *32,* 434–442. https://doi.org/10.1016/j.ejc.2010.12.002
8. F. Ma, H. Deng, *Math. Comput. Model* **2011**, *24,* 497–507. https://doi.org/10.1016/j.mcm.2011.02.040
9. M. R. Farahani, *Acta Chim. Slov.* **2012**, *59*, 779–783.
10. M. R. Farahani, *Adv. Mater. Corrosion* **2012**, *1*, 57–60.
11. M. R. Farahani, M. P. Vlad, *Studia UBB Chemia* **2015**, *60,* 251–258.
12. M. R. Farahani, K. Kato, M. P. Vlad, *Studia UBB Chemia* **2013**, *58*, 127–132.
13. G. Sridhara, M. R. Rajesh Kanna, R. S. Indumathi, *J. Nanomater* **2015**, *16*, 292.
14. R. A. Evarestov, Y. F. Zhukovskii, A. V. Bandura, S. Piskunov, *Cent. Eur. J. Phys.* ***2011****, 9, 492–501.*
15. M. Ramazani, M. Farahmandjou, T. P. Firoozabadi, *Int. J. Nanosci. Nanotechnol.* ***2015****, 11, 115–122.*
16. A. Subramaniyan, R. Ilangovan, *Int. J. Nanosci. Nanotechnol.* ***2015****, 11, 59–62.*
17. M. A. Malik, M. Imran, *Acta Chim. Slov.* **2015***, 62,* 973–976. https://doi.org/10.17344/acsi.2015.1746
18. M. R. Farahani, R. P. Kumar, M. R. R. Kanna, S. Wang, *Int. J. Pharma. Sci. Res.* **2016**, *21*, 3734–3741.
19. J. B. Liu, W. Gao, M. K. Siddiqui, M. R. Farahani, *AKCE Int. J. Graphs Comb.* **2016**, *13*, 255–260.
20. W. Gao, M. R. Farahani, M. K. Jamil, M. K. Siddiqui, *Open Biotechnol. J.* **2016**, *10*, 272–277. https://doi.org/10.2174/1874070701610010272

Povzetek

Randićev indeks povezanosti *R(G)* je eden izmed najstarejših indeksov povezanosti, ki ga je uvedel Randić leta 1975. Drug indeks povezanosti je indeks vsote povezanosti *X(G)*, ki sta ga leta 2008 uvedla Zhou in Trinajstić. Nedavno, leta 2011 so Dvorak in sod. uvedli modificiran Randićev indeks povezanosti grafa *G*. V tem prispevku smo izračunali navedene topološke indekse povezanosti za družino molekulskih grafov znanih kot nanocevke $TiO_2(m,n)$.

Short communication

A Rarely Seen Phenolato and Azido-Bridged Polymeric Cadmium(II) Complex Derived from 2-Bromo-6-[(2-isopropylaminoethylimino)methyl]phenol

Guo-Ping Cheng,[1] Ling-Wei Xue[1,*] and Cai-Xia Zhang[2]

[1] *College of Chemistry and Chemical Engineering, Pingdingshan University, Pingdingshan Henan 467000, P. R. China*

[2] *Coal Chemical Industry Branch of Shenhua Ningxia Coal Group, Yinchuan Ningxia 750411, P. R. China*

* *Corresponding author: E-mail: pdsuchemistry@163.com*

Received: 03-11-2016

Abstract

A rarely seen phenolato and azido-bridged polymeric cadmium(II) complex derived from the Schiff base ligand 2-bromo-6-[(2-isopropylaminoethylimino)methyl]phenol (HL) has been prepared and characterized by elemental analysis, IR spectroscopy, and single crystal X-ray diffraction. The Schiff base ligand coordinates to the Cd atom through the NNO donor set. The Cd atom is hexa-coordinated in an octahedral geometry. Adjacent two Cd atoms are bridged by two phenolato groups generating a dimer with Cd···Cd distance of 3.475(1) Å. The dimers are further linked *via* azido bridges forming 2D sheets parallel to the *bc* plane.

Keywords: Self-assembly; Crystal structure; Schiff base; Cadmium complex; Thermal analysis.

1. Introduction

The self-assembly and construction of metal-organic frameworks is currently a hot research field due to their fascinating structures and potential applications.[1] Schiff bases have long been received much attention for their preparational accessibilities, structural varieties and biological properties.[2] Tri-dentate salen-type Schiff bases are capable of forming complexes with certain metal atoms which can exhibit unusual coordination, high thermodynamic stability and kinetic inertness.[3] Preparation of one-, two- or three-dimensional polymeric network by suitable metal and ligand coordination is the special area of current research because of their interesting properties, such as electrical conductivity, magnetism, host–guest chemistry, molecular separation, gas storage, sensors and catalysis.[4] Among the various transition and non-transition metal atoms cadmium is an extremely toxic element that is naturally present in the environment and also as a result of human activities. The development of chelating agents is essential for the treatment of cadmium intoxication. Schiff bases have been proved to be a kind of interesting chelating agents for cadmium. A number of cadmium complexes with Schiff bases have been reported.[5] Cadmium(II) due to its d^{10} electronic configuration, is particularly suitable for the construction of coordination polymers and networks. The spherical d^{10} configuration is associated with a flexible coordination environment so that geometries of these complexes can vary from tetrahedral to octahedral and severe distortions in the ideal polyhedron occur easily.[6] The terminal or blocking co-ligands, which are usually used along with the bridging ligand to complete the metal coordination sphere, can alter the supramolecular assembly and consequently the type of structure formed taking the advantage of the flexibility of the coordination sphere.[5a] A detailed study of such complexes indicates that thiocyanate ligand is readily coordinate to the Cd atom, either through terminal mode or through bridging modes.[7] As a comparison, azide, a simi-

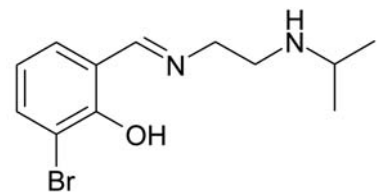

Scheme 1. The Schiff base HL.

lar pseudohalide group to thiocyanate, is rarely seen in the Schiff base cadmium complexes.[8] As a continuation of our work on Schiff base complexes[9] we report herein a rarely seen phenolato and azido-bridged polymeric cadmium(II) complex derived from the Schiff base ligand 2-bromo-6-[(2-isopropylaminoethylimino)methyl]phenol (HL; Scheme 1).

2. Experimental

2. 1. Material and Methods

3-Bromosalicylaldehyde and *N*-ethylethane-1,2-diamine were purchased from Fluka. Cadmium nitrate and other reagents were analytical grade and used without further purification. The Schiff base HL was prepared by the condensation of equimolar quantities of 3-bromosalicylaldehyde with *N*-ethylethane-1,2-diamine in methanol. Elemental (C, H and N) analyses were made on a Perkin-Elmer Model 240B automatic analyser. Infrared spectrum was recorded on an IR-408 Shimadzu 568 spectrophotometer. X-ray diffraction was carried out on a Bruker SMART 1000 CCD diffractometer. Thermal analysis was performed on a Perkin-Elmer Pyris Diamond TG-DTA thermal analyses system.

Caution! Azido compounds of metal ions are potentially explosive especially in presence of organic ligands. Only a small amount of material should be prepared and it must be handled with care.

2. 2. Preparation of the Complex

Schiff base HL (0.271 g, 1.0 mmol) was diluted by methanol (20 mL), to which was added with stirring a methanol solution (10 mL) of cadmium nitrate tetrahydrate (0.309 g, 1.0 mmol) and an aqueous solution (5 mL) of ammonium thiocyanate (0.076 g, 1.0 mmol). The mixture was stirred for 1 h at ambient temperature to give a colorless solution. Colorless block-shaped single crystals suitable for X-ray diffraction were formed by slow evaporation of the solution in air for a week. The crystals were filtered off and washed with cold methanol. Yield 51% (based on HL). Analysis calculated for $C_{12}H_{16}BrCdN_5O$: C, 32.86; H, 3.68; N, 15.97%; found: C, 32.72; H, 3.77; N, 15.83%. Selected IR data (cm^{-1}): 3266 (N–H), 2066 (N_3), 1643 (C=N).

2. 3. X-ray Diffraction

Diffraction intensities for the crystal were collected at 298(2) K using a Bruker Apex II diffractometer with Mo$K\alpha$ radiation (λ = 0.71073 Å). The collected data for the complex was processed with SAINT[10] and corrected for absorption using SADABS.[11] The absorption correction was applied with ψ-scans.[12] Structure of the complex was solved by direct method using the program SHELXS-97, and was refined by full-matrix least-squares techniques on F^2 using anisotropic displacement parameters.[13] All hydrogen atoms were placed at the calculated positions. Idealized H atoms were refined with isotropic displacement parameters set to 1.2 (1.5 for methyl groups) times the equivalent isotropic U values of the parent carbon or nitrogen atoms. The C–H distances for CH_2 and CH_3 are constrained to 0.97 and 0.96 Å, respectively. The remaining C–H distances are constrained to 0.93 Å. The crystallographic data for the complex are listed Table 1.

Table 1. Crystal and structure refinement data for the complex

Empirical formula	$C_{12}H_{16}BrCdN_5O$
Colour; habit	Block, colorless
Formula weight	438.6
Temperature (K)	298(2)
Crystal system	Monoclinic
Space group	$P2_1/c$
Unit cell dimensions	
a (Å)	12.142(1)
b (Å)	12.492(1)
c (Å)	10.385(1)
β (°)	106.649(3)
V (Å^3)	1509.2(3)
Z	4
Density (mg cm^{-3})	1.930
Absorption coefficient (mm^{-1})	4.097
Reflections collected	13740
Independent reflections	2816
Observed reflections [$I > 2\sigma(I)$]	2366
Parameters/restraints	183/0
R_1, wR_2 [$I \geq 2\sigma(I)$][a]	0.0394, 0.0916
R_1, wR_2 (all data)[a]	0.0523, 0.1017
Goodness-of-fit	1.078

[a] $R_1 = \Sigma||F_o|-|F_c||/\Sigma|F_o|$, $wR_2 = [\Sigma w(F_o^2-F_c^2)^2/\Sigma w(F_o^2)^2]^{1/2}$

3. Results and Discussion

3. 1. Description of the Crystal Structure of the Complex

An ORTEP representation of the asymmetric unit of the complex is shown in Figure 1, with selected bond distances and bond angles listed in Table 2. The Schiff base acts as a tridentate ligand and chelates the Cd atoms through phenolate oxygen, imino nitrogen, and amino nitrogen, forming a five-membered chelate ring N1–Cd1–N2 and a six-membered chelate ring O1–Cd1–N1. The coordination mode of the Schiff base ligand is similar to the tridentate Schiff bases we reported recently.[9b,14] The phenolate group of the Schiff base ligand binds two Cd atoms, generating a dinuclear subunit with Cd···Cd distance of 3.475(1) Å. The dinuclear subunits are further linked through end-to-end azido bridges forming two-dimensional sheets parallel to the *bc* plane (Figure 2). The azido-

bridged Cd···Cd distance is 6.559(2) Å. Adjacent four dinuclear subunits are linked *via* end-to-end azido bridges forming a 20-membered ring with dimensions of 10.36 Å × 6.66 Å (Figure 3).

The Cd atoms are all six coordinated with distorted octahedral geometry having N_4O_2 donor set. The equatorial plane of the octahedral geometry is formed by phenolato oxygen (O1), imino nitrogen (N1) and amino nitrogen (N2) of the Schiff base ligand, and terminal nitrogen (N5A) of bridging azido ligand. The two axial positions are occupied by the phenolato oxygen (O1B) and terminal nitrogen (N3) with a *trans* angle, N3–Cd1–O1B, of 164.42(16)°. The distortion of the geometry from regular octahedron is evidenced from the respective *cis*- and *trans*-angles about the metal center. The N–N–N bond angle in the azido ligand is 178.1(6)°, slightly deviated from the linearity. The Cd-O and Cd-N distances are within normal ranges as compared to other Schiff base cadmium complexes.[7,8] As expected, the Cd–N_{imino} is shorter than the Cd–N_{amino}.

Table 2. Coordinate bond distances (Å) and angles (°) for the complex

Bond lengths			
Cd1–O1	2.269(3)	Cd1–N1	2.304(4)
Cd1–N2	2.365(4)	Cd1–N3	2.432(5)
Cd1–N5A	2.210(5)	Cd1–O1B	2.455(3)
Bond angles			
N5–Cd1–O1A	102.24(17)	N5–Cd1–N1A	174.07(18)
O1–Cd1–N1	77.75(15)	N5–Cd1–N2A	105.72(18)
O1–Cd1–N2	150.96(14)	N1–Cd1–N2	75.25(16)
N5–Cd1–N3A	92.05(19)	O1–Cd1–N3	91.63(17)
N1–Cd1–N3	82.04(18)	N2–Cd1–N3	95.04(18)
N5A–Cd1–O1B	103.53(16)	O1–Cd1–O1B	85.37(12)
N1–Cd1–O1B	82.39(14)	N2–Cd1–O1B	80.68(13)
N3–Cd1–O1B	164.42(16)		

Symmetry codes: A) x, ½ – y, –½ + z; B) 2 – x, 1 – y, – z.

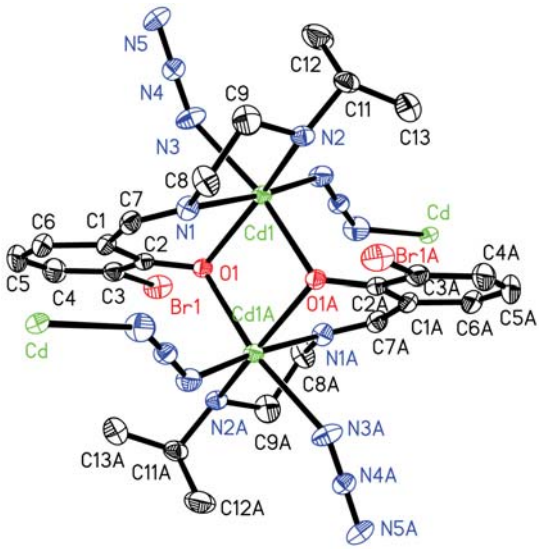

Figure 1. ORTEP view of the complex with atom labels. Displacement ellipsoids are shown at 30% probability level. The carbon hydrogen atoms are omitted for clarity. Atoms labeled with the suffix A are at the symmetry position: x, ½ – y, –½ + z.

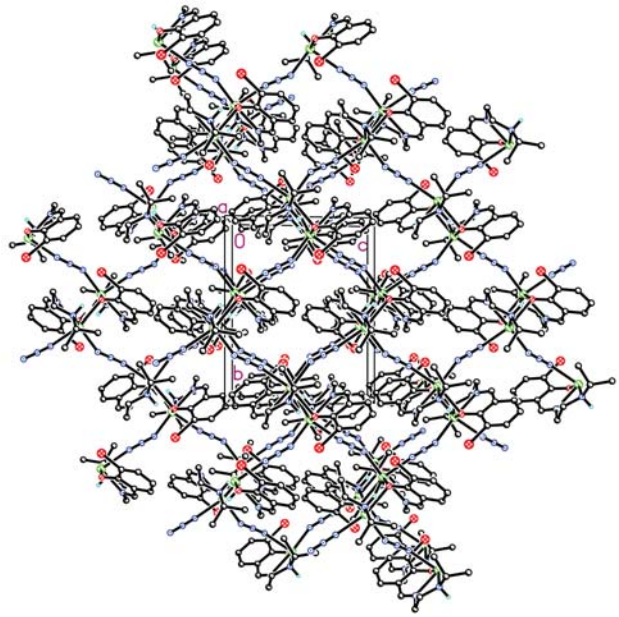

Figure 2. Crystal packing of the complex viewed along the *a* axis.

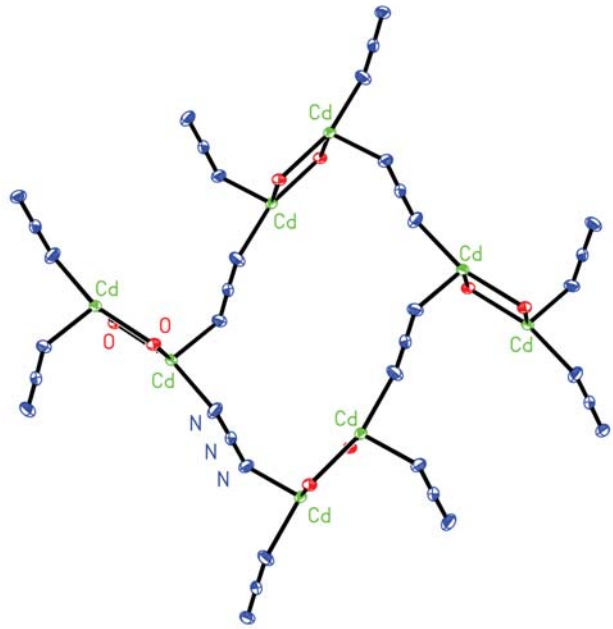

Figure 3. The azido-bridged 20-membered chelate ring.

3. 2. IR Spectrum of the Complex

The solid state infrared spectrum (Figure 4) of the complex is consistent with its crystal structure result. The

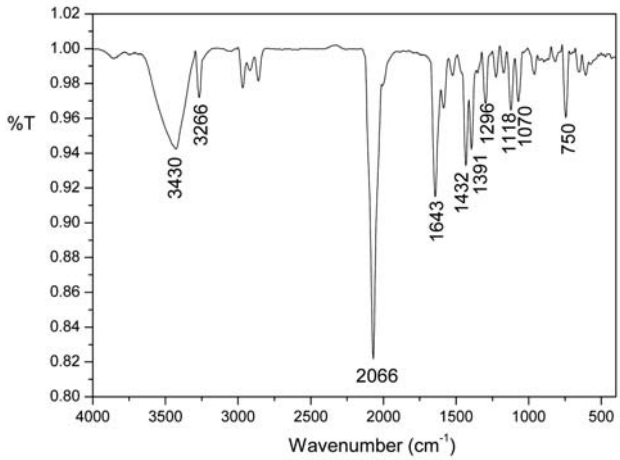

Figure 4. IR spectrum of the complex.

weak and sharp band at 3266 cm^{-1} is assigned to the N–H vibration. The single and intense absorption band at 2066 cm^{-1} is assigned to the stretching vibrations of the azide groups. The strong absorption band centered at 1643 cm^{-1} is assigned to the azomethine group, ν(C=N). The ν(Cd–O) mode is present as a medium band at 1296 cm^{-1}. The vibrations of the Cd–O and Cd–N bonds are located at the low wave numbers of 400–700 cm^{-1}.[7]

4. Conclusion

A rarely seen phenolato and azido-bridged polymeric cadmium(II) complex was obtained by reaction of 2-bromo-6-[(2-isopropylaminoethylimino)methyl]phenol with cadmium nitrate and sodium azide in methanol. The Schiff base ligand coordinates to the Cd atom through the NNO donor set, and the azido ligands bridge Cd atoms, to form a polymeric structure. The complex is stable up to 190 °C.

5. Supplementary Material

CCDC-945893 contains the supplementary crystallographic data for this paper. These data can be obtained free of charge at http://www.ccd.ccam.ac.uk/const/retrieving.html or from the Cambridge Crystallographic Data Centre (CCDC), 12 Union Road, Cambridge CB2 1EZ, UK; fax: +44(0)1223-336033 or e-mail: deposit@ccdc.cam.ac.uk.

6. Acknowledgments

This research was supported by the National Sciences Foundation of China (No. 20676057 and 20877036) and Top-class foundation of Pingdingshan University (No. 2008010).

7. References

1. (a) Z. Hulvey, D.A. Sava, J. Eckert, A. K. Cheetham, *Inorg. Chem.* **2011**, *50*, 403–405; https://doi.org/10.1021/ic101153c
(b) M. Sharma, I. Senkovska, S. Kaskel, P. K. Bharadwaj, *Inorg. Chem.* **2011**, *50*, 539–544. https://doi.org/10.1021/ic101412p
2. (a) A. Valent, M. Melnik, D. Hudecova, B. Dudova, R. Kivekas, M. R. Sundberg, *Inorg. Chim. Acta* **2002**, *340*, 15–20; https://doi.org/10.1016/S0020-1693(02)01062-9
(b) M. T. Raisanen, M. Nieger, A. M. Z. Slawin, M. Leskela, T. Repo, *CryrstEngComm* **2011**, *13*, 4701-4708; https://doi.org/10.1039/c0ce00926a
(c) S. Das, S. A. Maloor, S. Pal, S. Pal, *Cryst. Growth Des.* **2006**, *6*, 2103–2108. https://doi.org/10.1021/cg060305a
3. S. Basak, S. Sen, C. Marschner, J. Baumgartner, S. R. Batten, D. R. Turner, S. Mitra, *Polyhedron* **2008**, *27*, 1193–1200. https://doi.org/10.1016/j.poly.2007.12.005
4. (a) Y. Zhu, C.-F. Wang, K. Yan, K.-D. Zhao, G.-H. Sheng, Q. Hu, L. Zhang, Z. You, *J. Coord. Chem.* **2016**, *69*, 2493–2499; https://doi.org/10.1080/00958972.2016.1186801
(b) H.-H. Li, Z.-L. You, C.-L. Zhang, M. Yang, L.-N. Gao, L. Wang, *Inorg. Chem. Commun.* **2013**, *29*, 118–122; https://doi.org/10.1016/j.inoche.2012.12.023
(c) H. Miyasaka, R. Clerac, T. Ishii, H.-C. Chang, S. Kitagawa, M. Yamashita, *J. Chem. Soc., Dalton Trans.* **2002**, 1528–1534. https://doi.org/10.1039/b111094m
5. (a) S. Shit, J. Chakraborty, B. Samanta, G. Pilet, S. Mitra, *J. Mol. Struct.* **2009**, *919*, 361–365; https://doi.org/10.1016/j.molstruc.2008.10.002
(b) H.-C. Fang, Y.-Y.; Ge, Y. Ying, S.-R. Zheng, Q.-G. Zhan, Z.-Y. Zhou, L. Chen, Y.-P. Cai, *CrystEngComm* **2010**, *12*, 4012–4016; https://doi.org/10.1039/c0ce00177e
(c) W.-K. Lo, W.-K. Wong, W.-Y. Wong, J. Guo, *Eur. J. Inorg. Chem.* **2005**, 3950–3954; https://doi.org/10.1002/ejic.200500362
(d) J. Chakraborty, B. Samanta, G. Pilet, S. Mitra, *Inorg. Chem. Commun.* **2007**, *10*, 40–44; https://doi.org/10.1016/j.inoche.2006.09.002
(e) P. Chakraborty, A. Guha, S. Das, E. Zangrando, D. Das, *Polyhedron* **2013**, *49*, 12–18. https://doi.org/10.1016/j.poly.2012.09.017
6. (a) Y.-H. Liu, H.-P. Fang, P.-C. Jhang, C.-C. Peng, P.-H. Chien, H.-C. Yang, Y.-C. Huang, Y.-L. Lo, *CrystEngComm* **2010**, *12*, 1779–1783; https://doi.org/10.1039/b920419a
(b) M. Martinez-Calvo, A. M. Gonzalez-Noya, R. Pedrido, M. J. Romero, M. I. Fernandez, G. Zaragoza, M. R. Bermejo, *Dalton Trans.* **2010**, *39*, 1191–1194; https://doi.org/10.1039/B915953C
(c) S. H. Rahaman, R. Ghosh, H.-K. Fun, B. K. Ghosh, *Struct. Chem.* **2006**, *17*, 553–559. https://doi.org/10.1007/s11224-006-9024-2
7. (a) J. Chakraborty, S. Thakurta, B. Samanta, A. Ray, G. Pilet, S. R. Batten, P. Jensen, S. Mitra, *Polyhedron* **2007**, *26*, 5139–5149; https://doi.org/10.1016/j.poly.2007.07.038

(b) S. H. Rahaman, R. Ghosh, G. Mostafa, B. K. Ghosh, *Inorg. Chem. Commun.* **2005**, *8*, 1137–1140; https://doi.org/10.1016/j.inoche.2005.09.015
(c) Z.-L. You, H.-L. Zhu, *Z. Anorg. Allg. Chem.* **2006**, *632*, 140–146; https://doi.org/10.1002/zaac.200500308
(d) A. A. Hoser, W. Schilf, A. S. Chelmieniecka, B. Kolodziej, B. Kamienski, E. Grech, K. Wozniak, *Polyhedron* **2012**, *31*, 241–248. https://doi.org/10.1016/j.poly.2011.09.020

8. (a) F. A. Mautner, C. Berger, M. J. Dartez, Q. L. Nguyen, J. Favreau, S. S. Massoud, *Polyhedron* **2014**, *69*, 48–54; F. A. Mautner, C. Berger, R. C. Fischer, S. S. Massoud, *Inorg. Chim. Acta* **2016**, *448*, 34–41; (c) M. A. S. Goher, F. A. Mautner, A. K. Hafez, M. A. M. Abu-Youssef, C. Gspan, A. M.-A. Badr, *Polyhedron* **2003**, *22*, 975–979.
9. (a) L.-W. Xue, Y.-X. Feng, C.-X. Zhang, *Synth. React. Inorg. Met.-Org. Nano-Met. Chem.* **2014**, *44*, 1541–1544; https://doi.org/10.1080/15533174.2013.802340
(b) X. M. Hu, G.Q. Zhao, L. W. Xue, W. C. Yang, *Russ. J. Coord. Chem.* **2016**, *42*, 418–422; https://doi.org/10.1134/S107032841605002X
(c) L. W. Xue, G. Q. Zhao, Y. J. Han, Y. X. Feng, *Russ. J. Coord. Chem.* **2011**, *37*, 262–269; https://doi.org/10.1134/S1070328411030110
(d) F. Xu, L.-W. Xue, C.-X. Zhang, *Synth. React. Inorg. Met.-Org. Nano-Met. Chem.* **2015**, *45*, 1678–1682; https://doi.org/10.1080/15533174.2013.865226
(e) X. M. Hu, L. W. Xue, G. Q. Zhao, W. C. Yang, *Russ. J. Coord. Chem.* **2015**, *41*, 197–201; https://doi.org/10.1134/S1070328415030045
(f) H.-L. Zhu, X.-Z. Zhang, Y. Gu, A. Liu, F. Liu, Z. You, Y. Li, *Acta Chim. Slov.* **2016**, *63*, 721–725.
10. SMART and SAINT, Area Detector Control and Integration Software, Madison (WI, USA): Bruker Analytical X-ray Instruments Inc, 1997.
11. G.M. Sheldrick, SADABS, Program for Empirical Absorption Correction of Area Detector Data. Göttingen (Germany): University of Göttingen, 1997.
12. A.C.T. North, D.C. Phillips, F.S. Mathews, *Acta Crystallogr.* **1968**, *A24*, 351–355. https://doi.org/10.1107/S0567739468000707
13. G.M. Sheldrick, SHELXL-97, Program for the Refinement of Crystal Structures, Göttingen (Germany): University of Göttingen, 1997.
14. (a) X.-M. Hu, L.-W. Xue, C.-X. Zhang, W.-C. Yang, *Synth. React. Inorg. Met.-Org. Nano-Met. Chem.* **2015**, *45*, 1713–1716; https://doi.org/10.1080/15533174.2013.867881
(b) L.-W. Xue, X. Wang, G.-Q. Zhao, *Synth. React. Inorg. Met.-Org. Nano-Met. Chem.* **2012**, *42*, 1334–13

Povzetek

Predstavljamo redek primer polimernega kadmijevega(II) kompleksa z mostovnima fenolato in azido skupinama z uporabo Schiffove baze 2-bromo-6-[(2-izopropilaminoetilimino)metil]fenola (HL) kot liganda. Kompleks smo okarakterizirali z elementno analizo, IR spektroskopijo in monokristalno rentgensko difrakcijo. Schiffova baza je koordinirana na Cd atom preko NNO donorskega seta. Cd atom je heksakoordiniran z oktaedrično geometrijo. Sosednja dva Cd atoma sta mostovno povezana preko dveh fenolatnih skupin, pri čemer tvorita dimer s Cd···Cd razdaljo 3,475(1) Å. Dimeri so nadalje povezani preko azido mostov in tvorijo 2D plasti vzporedne z *bc* ravnino.

DRUŠTVENE VESTI IN DRUGE AKTIVNOSTI
SOCIETY NEWS, ANNOUNCEMENTS, ACTIVITIES

Vsebina

Contents

UNIVERZA V LJUBLJANI
FAKULTETA ZA KEMIJO IN KEMIJSKO TEHNOLOGIJO
1. januar – 31. december 2016

DOKTORATI

DOKTORJI ZNANSOTI

KEMIJA

Nina FRANČIČ
SOL-GEL NANOS Z ENCIMOM His_6-OPH ZA DETEKCIJO ORGANOFOSFATOV
Mentorica: prof. dr. Aleksandra Lobnik
Somentorica: prof. dr. Brigita Lenarčič
Datum zagovora: 6. 4. 2016

Slavko KLOBČAR
IZOLACIJA STRUKTURNO SORODNIH NEČISTOČ ATORVASTATINA S SUPERKRITIČNO TEKOČINSKO KROMATOGRAFIJO
Mentorica: prof. dr. Helena Prosen
Datum zagovora: 7. 7. 2016

Petra ZALAR
TERMODINAMSKE IN TRANSPORTNE LASTNOSTI POLIANETOLSULFONATOV Z RAZLIČNIMI PROTIIONI
Mentor: prof. dr. Ciril Pohar
Datum zagovora: 30. 9. 2016

DOKTORSKI ŠTUDIJSKI PROGRAM KEMIJSKE ZNANOSTI

KEMIJA

Tomaž FAKIN
NAPREDNI GRANULIRANI ZEOLITI S HIERARHIČNO STRUKTURO POR NA POL-INDUSTRIJSKEM NIVOJU
Mentor: prof. dr. Venčeslav Kaučič
Somentor: prof. dr. Anton Meden
Datum zagovora: 11. 3. 2016

Lucija JANEŠ
RAZVOJ ANALIZNIH METOD ZA DOLOČANJE VSEBNOSTI GLUTATIONA IN PREKURZORJEV TIOLOV V GROZDJU IN VINU
Mentorica: izr. prof. dr. Helena Prosen
Somentor: izr. prof. dr. Franc Požgan
Datum zagovora: 21. 4. 2016

Sara SERŠEN
SINTEZA NOVIH RUTENIJEVIH KOORDINACIJSKIH SPOJIN Z MOŽNIMI BIOLOŠKIMI IN KATALITSKIMI UČINKI
Mentor: prof. dr. Iztok Turel
Datum zagovora: 25. 4. 2016

Milena ZORKO
UPORABA DELCEV SILICIJEVEGA DIOKSIDA ZA OPLEMENITENJE TEKSTILIJ IN BATERIJ
Mentor: prof. dr. Miran Gaberšček
Somentor: doc. dr. Ivan Jerman
Datum zagovora: 9. 5. 2016

Sebastijan RIČKO
SINTEZA POTENCIALNIH ORGANOKATALIZATORJEV NA OSNOVI KAFRE
Mentor: doc. dr. Uroš Grošelj
Datum zagovora: 30. 5. 2016

Tomaž MOHORIČ
HIDRATACIJA IN NJEN VPLIV NA KORELACIJO MED MODELNIMI TOPLJENCI
Mentor: prof. dr. Vojeslav Vlachy
Datum zagovora: 2. 6. 2016

Mirjana RODOŠEK
IN SITU IN *EX SITU* PRISTOPI V RAZISKAVAH PROTIKOROZIJSKIH PREVLEK
Mentorica: viš. znan. sod. dr. Angelja Kjara Surca
Somentorica: doc. dr. Romana Cerc Korošec
Datum zagovora: 7. 6. 2016

Jona MIRNIK
SINTEZA NOVIH HETEROCIKLIČNIH SISTEMOV NA OSNOVI 3-PIRAZOLIDINONA
Mentor: prof. dr. Jurij Svete
Datum zagovora: 24. 6. 2016

Primož JOVANOVIČ
ELEKTROKEMIJSKA KARAKTERIZACIJA IN KOROZIJA PLATINSKIH KATALIZATORJEV ZA GORIVNE CELICE
Mentor: prof. dr. Miran Gaberšček
Datum zagovora: 24. 6. 2016

Jernej MARKELJ
ŠTUDIJ MEHANIZMOV TVORBE SEKUNDARNIH ORGANSKIH AEROSOLOV
Mentor: izr. prof. dr. Matevž Pompe
Datum zagovora: 24. 6. 2016

Polonca NEDELJKO
OPTIČNO ZAZNAVANJE BIOGENIH AMINOV
Mentorica: prof. dr. Aleksandra Lobnik
Somentor: izr. prof. dr. Matevž Pompe
Datum zagovora: 26. 7. 2016

Jan BITENC
MATERIALI ZA MAGNEZIJEVE AKUMULATORJE
Mentor: izr. prof. dr. Robert Dominko
Somentor: prof. dr. Anton Meden
Datum zagovora: 7. 10. 2016

Nejc ROZMAN
RAZVOJ NANODIMENZIONIRANEGA TiO_2, FOTOKATALITSKO AKTIVNEGA V VIDNI SVETLOBI
Mentorica: doc. dr. Andrijana Sever Škapin
Somentor: prof. dr. Miran Gaberšček
Datum zagovora: 7. 10. 2016

Simona TUŠAR
MODELIRANJE REAKCIJ RADIKALOV OB PRISOTNOSTI VODE IN KISLIN V ATMOSFERI
Mentorica: viš. znan. sod. dr. Antonija Lesar
Somentor: izr. prof. dr. Tomaž Urbič
Datum zagovora: 21. 10. 2016

Lidija MIRNIK
VPLIV SESTAVE VEZIVNEGA SISTEMA NA LASTNOSTI IZOLACIJSKIH MATERIALOV IZ KAMENE VOLNE
Mentorica: znan. svet. dr. Ema Žagar
Somentor: izr. prof. dr. Drago Kočar
Datum zagovora: 16. 12. 2016

BIOKEMIJA

Katja HROVAT ARNEŽ
STRUKTURNE ZNAČILNOSTI IN VLOGA PROTEINA MLKL PRI CELIČNI SMRTI
Mentor: doc. dr. Gregor Gunčar
Datum zagovora: 20. 1. 2016

Sara DRMOTA PREBIL
STRUCTURAL PROPERTIES AND CONFORMATIONAL CHANGES OF α–ACTININ 1
Mentorica: prof. dr. Kristina Djinović Carugo
Datum zagovora: 24. 6. 2016

KEMIJSKO INŽENIRSTVO

Alen VIŽINTIN
MODIFICIRANE POVRŠINE MATERIALOV ZA LITIJ ŽVEPLOVE AKUMULATORJE
Mentor: izr. prof. dr. Robert Dominko
Somentor: prof. dr. Radovan Stanislav Pejovnik
Datum zagovora: 1. 4. 2016

Maxim ZABILSKIY
CuO-CeO_2 MEŠANI KOVINSKI OKSIDI KOT KATALIZATORJI ZA RAZGRADNJO N_2O: SINTEZA, KARAKTERIZACIJA IN KATALITSKA AKTIVNOST
Mentor: znan. svet. dr. Albin Pintar
Somentor: prof. dr. Igor Plazl
Datum zagovora: 13. 5. 2016

Rok AMBROŽIČ
KOPOLIMERI BENZOKSAZINOV IN EPOKSIDNIH SMOL
Mentor: prof. dr. Matjaž Krajnc
Datum zagovora: 7. 6. 2016

Florian Alexander STRAUSS
INSERCIJSKI KATODNI MATERIALI NA OSNOVI BORATNIH SPOJIN
Mentor: izr. prof. dr. Robert Dominko
Mentor: prof. dr. Jean-Marie Tarascon
Somentor: prof. dr. Radovan Stanislav Pejovnik
Datum zagovora: 25. 11. 2016

MAGISTRSKI ŠTUDIJ

MAGISTRI ZNANOSTI

KEMIJA

Maja OMERZU
UPORABA RAZLIČNIH HPLC DETEKTORJEV ZA DOLOČEVANJE POMOŽNIH SNOVI V FARMACEVTSKIH IZDELKIH
Mentorica: izr. prof. dr. Irena Kralj Cigić
Datum zagovora: 1. 6. 2016

Andrej GLINŠEK
ŠTUDIJ ONESNAŽENOSTI TAL S SVINCEM NA SLOVENSKIH PEHOTNIH STRELIŠČIH
Mentor: prof. dr. Marjan Veber
Datum zagovora: 24. 6. 2016

Hiacinta KLEMENČIČ
PRIPRAVA MERILNIH VIROV ZA SPEKTROMETRIJO ALFA S POUDARKOM NA HOMOGENOSTI NANOSA
Mentorica: prof. dr. Helena Prosen
Somentorica: viš. znan. sod. dr. Ljudmila Benedik
Datum zagovora: 22. 9. 2016

UNIVERZITETNI PODIPLOMSKI ŠTUDIJ VARSTVO OKOLJA

Jasna KOGLOT
DOLOČANJE TEŽKIH KOVIN V ODPADNIH BLATIH ČISTILNIH NAPRAV
Mentor: izr. prof. dr. Matevž Pompe
Datum zagovora: 29. 1. 2016

KEMIJSKA TEHNOLOGIJA

Aleksandra RAČIČ KOZMUS
RAVNANJE Z MULJI V INTEGRIRANI PROIZVODNJI RECIKLIRANIH VLAKNIN IN PAPIRJEV
Mentorica: izr. prof. dr. Andreja Žgajnar Gotvajn
Somentor: izr. prof. dr. Gregor D. Zupančič
Datum zagovora: 11. 3. 2016

Elizabeta MATE
KOROZIJSKA OBSTOJNOST PASIVIRANIH AVSTENITNIH JEKEL AISI 316L IN AISI 321
Mentorica: doc. dr. Klementina Zupan
Datum zagovora: 22. 9. 2016

KEMIJSKO INŽENIRSTVO

Janez RŽEN
UPORABA REVERZNE OSMOZE V PROCESU PROIZVODNJE LIZINOPRILA
Mentor: akademik prof. dr. Janez Levec
Datum zagovora: 22. 9. 2016

MAGISTRSKI ŠTUDIJSKI PROGRAM 2. stopnja – BIOKEMIJA

Sabina KOLAR
DIFERENCIACIJO ČLOVEŠKIH PLURIPOTENTNIH MATIČNIH CELIC SPREMLJA JEDRNA AKUMULACIJA PROTEINA LIN28A
Mentor: izr. prof. dr. Boris Rogelj
Datum zagovora: 23. 9. 2016

Špela PODJED
PRIPRAVA FUZIJSKEGA PROTEINA NANOTELESA M33 Z ALKALNO FOSFATAZO ZA NEPOSREDNO DETEKCIJO MLKL
Mentor: doc. dr. Gregor Gunčar
Datum zagovora: 1. 2. 2016

Tomaž LUTMAN
KAPSULACIJA KURKUMINA IN Cu(II)-KURKUMINSKIH KOMPLEKSOV
Mentorica: prof. dr. Nina Gunde Cimerman
Somentorica: prof. dr. Nataša Poklar Ulrih
Datum zagovora: 19. 1. 2016

Staša KOMLJENOVIĆ
VSTAVITEV GENA V PLAZMIDNI VEKTOR IN PRODUKCIJA NANOTELES, SPECIFIČNIH ZA PROTEINE GLIOBLASTOMA
Mentor: prof. dr. Radovan Komel
Datum zagovora: 21. 12. 2016

Matja ZALAR
VPLIV KATIONOV NA ZVIJANJE OLIGONUKLEOTIDA d(G4C2), NJIHOVA LOKALIZACIJA IN DINAMIKA
Mentor: prof. dr. Janez Plavec
Datum zagovora: 20. 5. 2016

Ana DOLINAR
VNOS SINTETIČNEGA DVOKOMPONENTNEGA SISTEMA SIGNALIZACIJE V SESALSKE CELICE
Mentor: prof. dr. Roman Jerala
Datum zagovora: 30. 8. 2016

Eva KNAPIČ
OPREDELITEV NOVIH ALELOV ZA INZULINSKO REZISTENCO Z ASOCIACIJSKO ANALIZO NA CELOTNEM GENOMU TER UPORABO ZDRUŽENIH VZORCEV DNA PRI DEBELIH MLADOSTNIKIH V SLOVENIJI
Mentor: prof. dr. Simon Horvat
Somentor: doc. dr. Primož Kotnik
Datum zagovora: 16. 9. 2016

Mitja CRČEK
KARAKTERIZACIJA PRVIH ALOSTERIČNIH REGULATORJEV KATEPSINA B
Mentor: doc. dr. Marko Novinec
Datum zagovora: 8. 9. 2016

Eva Lucija KOZAK
KARAKTERIZACIJA INTERAKCIJE EpCAM IN KLAVDINA 7
Mentor: doc. dr. Miha Pavšič
Datum zagovora: 30. 9. 2016

Petra MALAVAŠIČ
FOSFOLIPAZE A2 IN SPREMEMBE V RAZGRADNJI, SINTEZI IN SKLADIŠČENJU LIPIDOV V RAKAVIH CELICAH
Mentor: prof. dr. Igor Križaj
Datum zagovora: 9. 5. 2016

Barbara ŽUŽEK
KARAKTERIZACIJA INTERAKCIJE MED Á-AKTININOM 4 IN CITOSOLNIM DELOM EpCAM in Trop2
Mentor: doc. dr. Miha Pavšič
Datum zagovora: 14. 10. 2016

Tjaša GORIČAN
IDENTIFIKACIJA IN KARAKTERIZACIJA NOVIH ALOSTERIČNIH MODIFIKATORJEV ČLOVEŠKEGA KATEPSINA K
Mentor: doc. dr. Marko Novinec
Datum zagovora: 24. 8. 2016

Jana VERBANČIČ
NEKROPTOZNA AKTIVNOST ČLOVEŠKE MLKL Z MUTACIJAMI NA MESTU Asp 144
Mentor: doc. dr. Gregor Gunčar
Datum zagovora: 30. 9. 2016

Alja ZOTTEL
CILJANJE RAKAVIH GLIOBLASTOMSKIH CELIC Z NANOPROTITELESI
Mentor: prof. dr. Radovan Komel
Datum zagovora: 9. 9. 2016

Klara Tereza NOVOSELC
SPREMEMBE IZRAŽANJA IZBRANIH PROTEINOV V MIŠIČNEM TKIVU PRI MIŠIČNI NEAKTIVNOSTI
Mentor: izr. prof. dr. Boris Rogelj
Datum zagovora: 23. 9. 2016

Maxi SAGMEISTER
POVEZAVA MED NARAVNIMI POLIMORFIZMI ČLOVEŠKEGA GENA CYP51 IN AKTIVNOSTJO ENCIMA LANOSTEROL 14Á-DEMETILAZE
Mentorica: prof. dr. Damjana Rozman
Datum zagovora: 15. 2. 2016

Valter BERGANT
KARAKTERIZACIJA PRISOTNOSTI HETEROGENEGA JEDRNEGA RIBONUKLEOPROTEINA H V CITOPLAZEMSKIH STRESNIH GRANULAH
Mentor: izr. prof. dr. Boris Rogelj
Datum zagovora: 28. 9. 2016

Živa MARSETIČ
PREDNOSTI IN SLABOSTI LOČBE ZDRAVILNE UČINKOVINE TER NJENIH NEČISTOT Z METODO HPLC V PRIMERJAVI Z NAVIDEZNO LOČBO Z METODO NMR (DOSY)
Mentor: prof. dr. Janez Plavec
Somentor: izr. prof. dr. Zdenko Časar
Datum zagovora: 9. 9. 2016

Filip KOLENC
PRIPRAVA OD pH ODVISNEGA PERFRINGOLIZINA O
Mentor: prof. dr. Gregor Anderluh
Datum zagovora: 3. 5. 2016

Sara PRIMEC
ANALIZA PRISOTNOSTI NARAVNIH MUTACIJ V VIRULENTNIH FAKTORJIH LLO, PI-PLC IN PC-PLC BAKTERIJE LISTERIA MONOCYTOGENES
Mentor: prof. dr. Gregor Anderluh
Somentorica: doc. dr. Marjetka Podobnik
Datum zagovora: 12. 10. 2016

Griša Grigorij PRINČIČ
NAČRTOVANJE IN SINTEZA ZA EpCAM SPECIFIČNIH MALIH MOLEKUL
Mentorica: prof. dr. Brigita Lenarčič
Somentor: prof. dr. Jurij Svete
Datum zagovora: 14. 9. 2016

Maša MIRKOVIĆ
MERITVE ZNOTRAJCELIČNE KONCENTRACIJE cAMP V REALNEM ČASU V KULTURI PODGANJIH ASTROCITOV PO DODATKU PROSTIH MAŠČOBNIH KISLIN
Mentorica: doc. dr. Nina Vardjan
Somentor: prof. dr. Robert Zorec
Datum zagovora: 6. 10. 2016

Mirjana MALNAR
KARAKTERIZACIJA PROTEINA L1 ORF1p V SESALSKIH CELICAH
Mentor: izr. prof. dr. Boris Rogelj
Datum zagovora: 13. 9. 2016

Katja LEBEN
VPLIV POVEZAVE LIGANDOV TOLL-U PODOBNIH RECEPTORJEV NA AKTIVACIJO IMUNSKEGA SISTEMA
Mentor: prof. dr. Simon Horvat
Somentorica: doc. dr. Mojca Benčina
Datum zagovora: 13. 9. 2016

Monika BIASIZZO
VPLIV CISTATINA C NA AKTIVACIJO INFLAMASOMA V MIŠJIH MAKROFAGIH, PRIDOBLJENIH IZ KOSTNEGA MOZGA
Mentorica: prof. ddr. Boris Turk
Datum zagovora: 12. 9. 2016

MAGISTRSKI ŠTUDIJSKI PROGRAM 2. stopnja – KEMIJA

Bor ARAH
SPOJINE BAKROVEGA(II) IN MANGANOVEGA(II) KLORIDA Z O-DONORSKIMI LIGANDI
Mentorica: doc. dr. Saša Petriček
Datum zagovora: 21. 12. 2016

Mojca PETERLIN
DOLOČANJE AMINOKISLIN ADSORBIRANIH NA POVRŠINI NANODELCEV ŽELEZOVEGA OKSIDA (Γ-Fe_2O_3)
Mentorica: izr. prof. dr. Irena Kralj Cigić
Somentor: prof. dr. Darko Makovec
Datum zagovora: 6. 6. 2016

Matej KOCEN
SINTEZA IN KARAKTERIZACIJA VOLFRAMA S KARBIDNIMI VKLJUČKI
Mentor: prof. dr. Anton Meden
Datum zagovora: 20. 9. 2016

Nika OSTERMAN
RAZVOJ NIKLJEVEGA KATALIZATORJA NA ZEOLITNEM NOSILCU ZA DEOKSIGENACIJO ODPADNIH OLJ
Mentor: prof. dr. Anton Meden
Datum zagovora: 12. 9. 2016

Silvija BAJUK
FUNKCIONALNI PREMAZI ZA ZAŠČITO HISTORIČNIH MATERIALOV
Mentorica: doc. dr. Romana Cerc Korošec
Somentorica: doc. dr. Andrijana Sever Škapin
Datum zagovora: 28. 10. 2016

Matjaž GRČMAN
DOLOČEVANJE IZBRANIH OGLJIKOVIH HIDRATOV Z UPORABO ANIONSKO IZMENJEVALNE KROMATOGRAFIJE S PULZNO AMPEROMETRIČNO DETEKCIJO
Mentor: izr. prof. dr. Matevž Pompe
Datum zagovora: 25. 11. 2016

Veronika ROVANŠEK
POLIMERNI NOSILCI ZA DOSTAVO RUTENIJEVIH KOMPLEKSOV
Mentor: prof. dr. Iztok Turel
Datum zagovora: 13. 5. 2016

Patricija HRIBERŠEK
SINTEZA IN PRETVORBE ALKIL 5-SUBSTITUIRANIH-4-OKSO-4,5-DIHIDRO-1H-PIROL-3-KARBOKSILATOV
Mentor: doc. dr. Uroš Grošelj
Datum zagovora: 9. 9. 2016

Ana KOVAČIČ
SINTEZA IN DOLOČANJE ANTIOKSIDATIVNE AKTIVNOSTI DERIVATOV RESVERATROLA
Mentor: izr. prof. dr. Franci Kovač
Datum zagovora: 30. 8. 2016

Igor ZELENOVIĆ
FUNKCIONALIZACIJA EPOKSIDOV Z RAZLIČNIMI NUKLEOFILI, VSEBUJOČIMI AZIDNO ALI ALKINSKO SKUPINO
Mentor: prof. dr. Darko Dolenc
Datum zagovora: 17. 10. 2016

Aleš POLOVIČ
SINTEZA POTENCIALNIH NEČISTOT PRI ZDRAVILNI UČINKOVINI
Mentor: izr. prof. dr. Franc Požgan
Datum zagovora: 19. 7. 2016

Jasna DRUŠKOVIČ
ODSTRANITEV ORGANSKIH ONESNAŽEVAL IZ ODPADNE VODE Z UPORABO BIOLOŠKIH IN NAPREDNIH OKSIDACIJSKIH POSTOPKOV ČIŠČENJA
Mentorica: prof. dr. Helena Prosen
Datum zagovora: 27. 6. 2016

Esmira NIKOČEVIĆ
PREUČEVANJE VPLIVOV POSPEŠENEGA STARANJA NA HIDROKSIPROPIL CELULOZO IN ŠKROB
Mentor: doc. dr. Iztok Prislan
Datum zagovora: 22. 12. 2016

Tjaša LUŠINA
OKSIDACIJA α-HIDROKSIKARBOKSILNIH KISLIN Z MOLIBDENOVIMI(V) IN (VI) SPOJINAMI
Mentor: prof. dr. Darko Dolenc
Datum zagovora: 20. 4. 2016

Damjana HRIBERŠEK
SINTEZA IN KARAKTERIZACIJA CINKOVIH KARBOKSILATNIH KOMPLEKSOV
Mentor: prof. dr. Alojz Demšar
Datum zagovora: 16. 9. 2016

Urška LEBAR
KOORDINACIJSKE SPOJINE 3D ELEMENTOV Z 1-HIDROKSIBENZOTRIAZOLOM
Mentor: doc. dr. Bojan Kozlevčar
Datum zagovora: 14. 10. 2016

Janja LAKNER
SINTEZA TRIMETILSILILNIH ESTROV KARBOKSILNIH KISLIN POD REAKCIJSKIMI POGOJI BREZ TOPIL
Mentor: izr. prof. dr. Marjan Jereb
Datum zagovora: 23. 9. 2016

Maruša ŠKALER
DOLOČANJE SORODNIH SUBSTANC NATRIJEVE SOLI NAPROKSENA Z UPORABO SUPERKRITIČNE KROMATOGRAFIJE
Mentorica: izr. prof. dr. Irena Kralj Cigić
Datum zagovora: 15. 9. 2016

Bruno Aleksander MARTEK
PRIKONDENZIRANI PIRAZINI KOT SUBSTRATI V REAKCIJI AKTIVACIJE C–H VEZI
Mentor: izr. prof. dr. Bogdan Štefane
Datum zagovora: 9. 9. 2016

Anja KRISTL
ŠTUDIJ ZADRŽEVANJA ZVRSTI NA KROMATOGRAFSKI KOLONI Z VEČ SEPARACIJSKIMI MEHANIZMI
Mentor: izr. prof. dr. Matevž Pompe
Datum zagovora: 14. 6. 2016

Zala GOMBAČ
KOMPLEKSI KOBALTOVEGA, NIKLJEVEGA IN CINKOVEGA KLORIDA S HIDROKSI DERIVATI PIRIDINA
Mentorica: doc. dr. Saša Petriček
Datum zagovora: 16. 9. 2016

Sandi BRUDAR
UPORABA TEKOČINSKE KALORIMETRIJE IN KROMATOGRAFIJE ZA ANALIZO PROTEOMA ČLOVEŠKE KRVNE plazme
Mentor: doc. dr. Iztok Prislan
Datum zagovora: 9. 9. 2016

Taja VEROVŠEK
DOLOČANJE HLAPNIH SPOJIN V PROPOLISU
Mentorica: prof. dr. Helena Prosen
Datum zagovora: 15. 9. 2016

Tilen ZORE
KOORDINACIJSKE SPOJINE CINKA IN VANADIJA Z DERIVATI PIRIDIN-2,6-DIKARBOKSILNE KISLINE S POTENCIALNIM ANTIDIABETIČNIM DELOVANJEM
Mentor: izr. prof. dr. Franc Perdih
Datum zagovora: 5. 9. 2016

Eva PETKOVŠEK
DOLOČEVANJE AMINOKISLIN IN MAŠČOBNIH KISLIN V PREHRANSKIH IZDELKIH
Mentor: izr. prof. dr. Matevž Pompe
Datum zagovora: 30. 9. 2016

Sarah MERLINI
FUNKCIONALIZACIJA EPOKSI-SUBSTITUIRANIH POLIMERNIH NOSILCEV S KARBOKSILNIMI SKUPINAMI
Mentor: prof. dr. Darko Dolenc
Datum zagovora: 9. 11. 2016

Hermina HUDELJA
NAČRTOVANJE PROCESA KRISTALIZACIJE AKTIVNE FARMACEVTSKE UČINKOVINE Z UPORABO IN-LINE TEHNIK
Mentor: prof. dr. Marijan Kočevar
Somentor: doc. dr. Blaž Likozar
Datum zagovora: 12. 9. 2016

Uroš PRAH
VPLIV DOPIRANJA NA LASTNOSTI PRAHOV IN TANKIH PLASTI TITANOVEGA DIOKSIDA
Mentorica: doc. dr. Irena Kozjek Škofic
Datum zagovora: 2. 9. 2016

MAGISTRSKI ŠTUDIJSKI PROGRAM 2. stopnja – KEMIJSKO INŽENIRSTVO

Nina PETERLIN
MOŽNOSTI RAZGRADNJE BIOPLASTIKE Z LIGNINOLITIČNIMI ENCIMI GLIVE DICHOMITUS SQUALENS
Mentor: prof. dr. Aleksander Pavko
Datum zaključka: 8. 6. 2016

Urban VERBIČ
REAKCIJA VODNEGA PLINA NA Cu-ZnGaOx KATALIZATORJU
Mentor: prof. dr. Janez Levec
Datum zaključka: 17. 6. 2016

Rajko VNUK
VPLIV MAKROOKSIGENACIJE PRI ZORENJU MLADEGA VINA
Mentor: prof. dr. Marin Berovič
Somentorca: prof. dr. Tatjana Košmerl
Datum zaključka: 7. 10. 2016

Katja JURAČ
MATEMATIČNO MODELIRANJE INTERAKCIJE MED BAKTERIJO IN BAKTERIOFAGI
Mentor: doc. dr. Aleš Podgornik
Datum zaključka: 23. 12. 2016

Jasmina SEDMAK
IZBIRA KLJUČNIH VSTOPNIH MATERIALOV V RAZVOJU IN PROIZVODNJI FARMACEVTSKIH UČINKOVIN
Mentor: prof. dr. Aleksander Pavko
Datum zaključka: 19. 5. 2016

Eva UDOVIČ
SUBMERZNA KULTIVACIJA GLIVE HERICIUM ERINACEUS V LABORATORIJSKEM BIOREAKTORJU
Mentor: prof. dr. Marin Berovič (N)
Datum zaključka: 29. 9. 2016

Urban BORŠTNIK
OPTIMIZACIJA PROCESA KONTINUIRNE TER POLŠARŽNE SUSPENZIJSKE POLIMERIZACIJE MIKROSFERNIH AKRILATNIH LEPIL
Mentor: doc. dr. Jernej Kajtna
Datum zaključka: 6. 12. 2016

Kaja JAVORŠEK
GOJENJE GLIVE HERICIUM ERINACEUS NA TRDNEM SUBSTRATU IN DOLOČEVANJE VSEBNOSTI FENOLOV, FENOLSNIH KISLIN IN FLAVONOIDOV
Mentor: prof. dr. Marin Berovič
Datum zaključka: 28. 10. 2016

Katja LOVRIN
RAZVOJ MATEMATIČNEGA MODELA ZA NAPOVED DELOVANJA KOMUNALNIH ČISTILNIH NAPRAV V POREČJU DRAVE – ZGORNJA DRAVA
Mentor: prof. dr. Igor Plazl
Datum zaključka: 21. 10. 2016

Blaž KOMAR
IMOBILIZACIJA Ω-TRANSAMINAZ S POZITIVNO NABITIMI OZNAČEVALCI V MIKROREAKTORJIH
Mentorica: prof. dr. Polona Žnidaršič Plazl
Datum zaključka: 8. 7. 2016

Aljaž PETANČIČ
ZAMENJAVA KOROZIJSKEGA INHIBITORJA V ZAPRTEM HLADILNEM SISTEMU
Mentor: prof. dr. Igor Plazl
Datum zaključka: 10. 6. 2016

Klemen BOGOVIČ
KOROZIJA V UPARJALNIKIH V NUKLEARNI ELEKTRARNI KRŠKO
Mentor: prof. dr. Igor Plazl
Datum zaključka: 14. 7. 2016

Luka NOČ
REOLOŠKA IN APLIKATIVNA KARAKTERIZACIJA DISPERZIJSKIH OMETOV
Mentorica: prof. dr. Urška Šebenik
Datum zaključka: 20. 9. 2016

Nika ŽGAJNAR
EMULZIJSKA POLIMERIZACIJA NA PRITISK OBČUTLJIVIH LEPIL Z DODATKOM NANOGLINE
Mentor: doc. dr. Jernej Kajtna
Datum zaključka: 23. 11. 2016

David BAJEC
KARAKTERIZACIJA SAMOCELJENJA NA OSNOVI DIELS-ALDER REAKCIJE V EPOKSIDNIH SMOLAH
Mentorica: prof. dr. Urška Šebenik
Datum zaključka: 6. 9. 2016

Anže PRAŠNIKAR
SIMULACIJA REAKCIJE IN PRENOSA SNOVI Z MREŽNO BOLTZMANNOVO METODO
Mentor: prof. dr. Igor Plazl
Somentor: izr. prof. dr. Tomaž Urbič
Datum zaključka: 16. 9. 2016

Barbara JOZINOVIĆ
DEGRADACIJA KATALIZATORJEV RuO_2 in IrO_2 Z UPORABO METODE IDENTIČNE LOKACIJE IL-SEM
Mentor: prof. dr. Miran Gaberšček
Datum zaključka: 15. 11. 2016

Filip STRNIŠA
UPORABA MREŽNE BOLTZMANNOVE METODE ZA MODELIRANJE TRANSPORTNIH POJAVOV V MIKROFLUIDNIH NAPRAVAH
Mentor: prof. dr. Igor Plazl
Somentor: izr. prof. dr. Tomaž Urbič
Datum zaključka: 13. 9. 2016

Nina SLAPŠAK
FUNKCIONALIZACIJA NANODELCEV ZA UPORABO V KOZMETIKI
Mentor: doc. dr. Boštjan Genorio
Datum zaključka: 22. 9. 2016

Anja PAJNTAR
KARAKTERIZACIJA MIKROREAKTORJEV S STRNJENIM SLOJEM ZA IZVEDBO ENCIMSKO KATALIZIRANE SINTEZE KRATKOVERIŽNIH ESTROV
Mentorica: prof. dr. Polona Žnidaršič Plazl
Datum zaključka: 2. 12. 2016

MAGISTRSKI ŠTUDIJSKI PROGRAM 2. stopnja – TEHNIŠKA VARNOST

Tine PANJTAR
UGOTAVLJANJE KAKOVOSTI ZRAKA IN ŠKODLJIVOSTI NA DELOVNEM MESTU LAKIRCA
Mentorica: prof. dr. Marija Bešter Rogač
Datum zagovora: 11. 5. 2016

Anja LEŠNJAK
POJAVNOST PSIHOSOCIALNIH TVEGANJ V EVROPSKIH DELOVNIH OKOLJIH
Mentorica: doc. dr. Marija Molan
Datum zagovora: 14. 7. 2016

Nina ČESNIK
ŠIRJENJE PLINOV V MODELU GARAŽE
Mentor: doc. dr. Jože Šrekl
Datum zagovora: 12. 7. 2016

Tomaž VOŠNER
SOCIALNO ZAVAROVANJE ZA PRIMER POŠKODB PRI DELU IN POKLICNIH BOLEZNI ŠTUDENTOV
Mentor: Luka Tičar
Datum zagovora: 8. 1. 2016

Jernej FORSTNER
VPLIV KOMUNIKACIJE V DELOVNIH PROCESIH NA PODROČJE VARNOSTI
Mentor: doc. dr. Mitja Robert Kožuh
Datum zagovora: 14. 7. 2016

Admir BABIĆ
LASERSKA VARNOST NA DELOVNEM MESTU
Mentor: prof. dr. Marjan Bilban
Somentor: pred. dr. Grega Bizjak
Datum zagovora: 13. 1. 2016

Nina JALEN
KARAKTERIZACIJA VZORCEV IZ DIMNIKOV IN PRIMERJAVA NJIHOVE POTENCIALNE NEVARNOSTI ZA POŽAR
Mentor: doc. dr. Saša Petriček
Datum zagovora: 19. 10. 2016

Peter KASTRIN
MERITVE TRDNIH DELCEV IN ČRNEGA OGLJIKA V AVTOMOBILSKIH IZPUHIH IN DOLOČITEV EMISIJSKIH FAKTORJEV
Mentorica: znan. svet. dr. Irena Grgić
Somentorica: prof. dr. Marija Bešter Rogač
Datum zagovora: 18. 11. 2016

DIPLOME – UNIVERZITETNI ŠTUDIJ

KEMIJA

Mirjam PROSENC
KONCENTRACIJE ELEMENTOV NA SUSPENDIRANIH DELCIH PRI POJAVU POVIŠANIH VOD REKE SAVE
Mentor: prof. dr. Marjan Veber
Datum zagovora: 30. 9. 2016

Nataša MEŽNAR
RAZVOJ KROMATOGRAFSKE METODE ZA DOLOČANJE KONCENTRACIJE VIRUSNIH DELCEV INFLUENCE A V LIZATU VERO CELIC
Mentor: izr. prof. dr. Matevž Pompe
Datum zagovora: 19. 9. 2016

Helena LAHOVEC
STRUKTURNO PODPRTO MODELIRANJE INHIBITORJEV KINAZE B-RAF
Mentor: doc. dr. Črtomir Podlipnik
Datum zagovora: 22. 9. 2016

Mateja NOGRAŠEK
RAZVOJ METODE ZA DOLOČANJE KLORIRANIH FENOLOV V VODAH
Mentorica: prof. dr. Helena Prosen
Datum zagovora: 22. 9. 2016

Dren ROLLKA
KVANTITATIVNA IN KVALITATIVNA FAZNA ANALIZA KOMPOZITOV IZ ZEMLJINE STARE CINKARNE CELJE IN PEPELA VIPAP
Mentor: prof. dr. Anton Meden
Datum zagovora: 26. 9. 2016

Uroš LIPOVŠEK
PRIPRAVA IN KARAKTERIZACIJA TANKIH PLASTI TiO_2 FOTOKATALITSKO AKTIVNIH PRI OBSEVANJU Z VIDNO SVETLOBO
Mentorica: doc. dr. Romana Cerc Korošec
Datum zagovora: 28. 9. 2016

Nastja KOTNIK
FLUORIMETRIČNO DOLOČEVANJE TIAMINA PO OKSIDACIJI S HEKSACIANOFERATOM (III)
Mentor: izr. prof. dr. Matevž Pompe
Datum zagovora: 30. 9. 2016

Tomaž KORITNIK
MERJENJE KONTAKTNEGA KOTA TEKOČIN (NA HIDROFOBNIH POVRŠINAH) Z RAČUNALNIŠKO ANALIZO OBLIKE SEDEČE KAPLJICE
Mentor: prof. dr. Ciril Pohar
Datum zagovora: 30. 9. 2016

Tomaž ZORNIK
RAZVOJ POSTOPKA ZA INDUSTRIJSKO SINTEZO CINKOVEGA FOSFATA
Mentor: prof. dr. Iztok Turel
Datum zagovora: 30. 9. 2016

Polona ŠMRGUT
DOLOČEVANJE SINTEZNIH PRODUKTOV MONOBUTIRINA NA PLINSKEM KROMATOGRAFU
Mentor: izr. prof. dr. Matevž Pompe
Datum zagovora: 30. 9. 2016

Tomaž JANŽEKOVIČ
INTERAKCIJE NATRIJEVEGA POLISTIREN SULFONATA Z DEVTERIRANIMI IN/ALI FLUORIRANIMI SURFAKTANTI
Mentorica: prof. dr. Ksenija Kogej
Datum zagovora: 30. 9. 2016

KEMIJA – 1. stopnja

Polona RUDOLF ŽIGON
REAKCIJE SEMIKARBAZIDOV Z NEKATERIMI KOVINSKIMI IONI
Mentor: doc. dr. Andrej Pevec
Datum zagovora: 24. 8. 2016

Mateja HOZJAN
UPORABA POTENCIOMETRIČNIH METOD PRI DOLOČEVANJU STABILNOST KOORDINACIJSKIH SPOJIN
Mentor: izr. prof. dr. Mitja Kolar
Datum zagovora: 25. 11. 2016

Klara KRAPEŽ
VREDNOTENJE V CELOTI TRDNIH ELEKTROD S PVC-MEMBRANO
Mentorica: izr. prof. dr. Nataša Gros
Datum zagovora: 31. 8. 2016

Urh JEVŠOVAR
OPTIMIZACIJA MIKROVALONE EKSTRAKCIJE LOVILCEV SEKUNDARNIH ORGANSKIH AEROSOLOV
Mentor: izr. prof. dr. Matevž Pompe
Datum zagovora: 8. 9. 2016

Uroš KLOPČIČ
MIKROEKSTRAKCIJA ZA DOLOČANJE KLORIRANIH ONESNAŽEVAL V VODI
Mentorica: prof. dr. Helena Prosen
Datum zagovora: 5. 2. 2016

Jakob MAKOVAC
MONTE CARLO SIMULACIJA SISTEMA ELEKTROLIT-MEMBRANA
Mentor: doc. dr. Miha Lukšič
Datum zagovora: 15. 9. 2016

Katja VOVČKO
RAZISKAVA VEZAVE LIGANDA TMPyP4 NA OLIGONUKLEOTID ČLOVEŠKEGA ZAPOREDJA Tel22 Z UPORABO SPEKTROFLUORIMETRA
Mentor: doc. dr. Matjaž Bončina
Datum zagovora: 19. 9. 2016

Miha NOSAN
TITRACIJSKO OBNAŠANJE POLIKARBOKSILNIH KISLIN
Mentorica: prof. dr. Ksenija Kogej
Datum zagovora: 12. 9. 2016

Mitja OVEN
FUGATIVNOSTNI KOEFICIENT RAZLIČNIH PLINOV
Mentor: prof. dr. Andrej Jamnik
Datum zagovora: 13. 9. 2016

Anja DEBELJAK
FAZNA ANALIZA RAZLIČNIH VZORCEV TAL Z RENTGENSKO PRAŠKOVO ANALIZO
Mentorica: izr. prof. dr. Amalija Golobič
Datum zagovora: 4. 2. 2016

Urška ZAPLOTNIK
SINTEZA IN KARAKTERIZACIJA FOTOKATALITSKO AKTIVNIH TANKIH PLASTI TITANOVEGA DIOKSIDA
Mentorica: doc. dr. Romana Cerc Korošec
Datum zagovora: 4. 2. 2016

Robert KRBAVČIČ
ORGANOKATALIZIRANE ADICIJE 1-(TERC-BUTIL) 3-METIL 5-FENIL-4,5-DIHIDRO-4-OKSO-1H-PIROL-1,3-DIKARBOKSILATA NA NITROALKENE
Mentor: doc. dr. Uroš Grošelj
Datum zagovora: 12. 9. 2016

Tjaša GOGNJAVEC
PRETVORBE ORGANSKIH SPOJIN POD KLASIČNIMI IN ZELENIMI POGOJI
Mentor: izr. prof. dr. Marjan Jereb
Datum zagovora: 13. 9. 2016

Jure ZEKIČ
PRETVORBE NEKATERIH ORGANSKIH SPOJIN POD KLASIČNIMI IN ALTERNATIVNIMI POGOJI
Mentor: izr. prof. dr. Marjan Jereb
Datum zagovora: 12. 9. 2016

Anže PAVLIN
SINTEZA IZBRANIH HIDRAZONOFORMAMIDOV
Mentor: prof. dr. Janez Košmrlj
Datum zagovora: 16. 9. 2016

Eva ŽOS
REAKCIJE ETOKSIMETILEN HIDRAZONOV Z DUŠIKOVIMI NUKLEOFILI
Mentor: prof. dr. Janez Košmrlj
Datum zagovora: 16. 9. 2016

Nik RUS
SINTEZE SUBSTITUIRANIH 2H-PIRAN- 2-ONOV S POSEBNIM POUDARKOM NA POIZKUSU SINTEZE DERIVATOV, KI VSEBUJEJO 2-FLUORO- 4-METOKSIFENILNO SKUPINO
Mentor: doc. dr. Krištof Kranjc
Datum zagovora: 13. 9. 2016

Aleš ŠAVRIČ
DEHIDROGENACIJA 5,6-DIFENIL-2,3-DIHIDROPIRAZINA Z UPORABO AKTIVNEGA OGLJA KOT KATALIZATORJA
Mentor: doc. dr. Krištof Kranjc
Datum zagovora: 13. 9. 2016

Bine LEDINEK
KATALITSKO ARILIRANJE C–H VEZI 2-FENILPIRIMIDINA V VODI
Mentor: izr. prof. dr. Franc Požgan
Datum zagovora: 15. 12. 2016

David SMODIŠ
KINAZOLIN KOT USMERJAJOČA SKUPINA V KATALITSKI AKTIVACIJI C–H VEZI
Mentor: izr. prof. dr. Franc Požgan
Datum zagovora: 13. 9. 2016

Blaž HODNIK
UPORABA Cu(0)-GRAFITNEGA KATALIZATORJA V ORGANSKI KEMIJI
Mentor: prof. dr. Jurij Svete
Datum zagovora: 12. 9. 2016

Anže ZUPANC
UPORABA BAKRA NA ŽELEZU KOT KATALIZATORJA V ORGANSKIH REAKCIJAH
Mentor: prof. dr. Jurij Svete
Datum zagovora: 9. 9. 2016

Jana ČIMŽAR
NEKATERE SELEKTIVNE PRETVORBE 8-HIDROKSIKINOLINA
Mentor: izr. prof. dr. Bogdan Štefane
Datum zagovora: 15. 9. 2016

Katarina DOLES
PRIPRAVA FENIL SUBSTITUIRANIH IZOKSAZOLIDINSKIH SISTEMOV
Mentor: izr. prof. dr. Bogdan Štefane
Datum zagovora: 6. 9. 2016

Hana HACE
SUZUKI-MIYAURA REAKCIJA 3-BROMOKINOLINA S HETEROARIL BOROVIMI KISLINAMI
Mentor: izr. prof. dr. Bogdan Štefane
Datum zagovora: 14. 9. 2016

Marija KISILAK
AKTIVACIJA NEREAKTIVNIH C-H VEZI Z ŽELEZOVIMI(II) IN ŽELEZOVIMI(III) KOMPLEKSI
Mentor: izr. prof. dr. Bogdan Štefane
Datum zagovora: 12. 9. 2016

Žan TESTEN
SUZUKI-MIYAURA REAKCIJA 2-BROMOKINOLINA S HETEROARIL BOROVIMI KISLINAMI
Mentor: izr. prof. dr. Bogdan Štefane
Datum zagovora: 14. 9. 2016

Matej REBERC
SINTEZA IN KARAKTERIZACIJA KOVINSKO-ORGANSKIH MATERIALOV Z VGRAJENIMI HIDRANTI LAHKIH KOVIN
Mentor: prof. dr. Anton Meden
Datum zagovora: 15. 9. 2016

Katja VRABEC
SPOJINE NIKLJA S 3-HIDROKSIPIRIDIN-2-ONOM
Mentorica: doc. dr. Saša Petriček
Datum zagovora: 15. 9. 2016

Aja Ana PAVLIČ
VPLIV VSEBNOSTI ŽVEPLA NA FOTOKATALITSKO AKTIVNOST TiO_2
Mentorica: doc. dr. Romana Cerc Korošec
Datum zagovora: 1. 7. 2016

Nina PODJED
SINTEZA IN KAPSULACIJA ORGANORUTENIJEVIH SPOJIN
Mentor: prof. dr. Iztok Turel
Datum zagovora: 15. 9. 2016

Simona GRIČAR
SINTEZA DIKETONOV Z AMINSKIMI SUBSTITUENTI IN NJIHOVIH RUTENIJEVIH KOMPLEKSOV
Mentor: prof. dr. Iztok Turel
Datum zagovora: 15. 9. 2016

Maja TIHOMIROVIĆ
KOORDINACIJSKE SPOJINE BAKRA, CINKA IN KOBALTA Z 1,2,4-TRIAZOLOM
Mentor: doc. dr. Bojan Kozlevčar
Datum zagovora: 15. 9. 2016

Anja SEDMINEK
SINTEZA IN KARAKTERIZACIJA NEKATERIH TIOSEMIKARBAZONOV KOT POTENCIALNIH KELATNIH LIGANDOV
Mentor: doc. dr. Andrej Pevec
Datum zagovora: 16. 9. 2016

Monika HORVAT
KOORDINACIJSKE SPOJINE VANADIJA IN CINKA S 6-SUBSTITUIRANIMI PIRIDIN-2-KARBOKSILATI S POTENCIALNIM ANTIDIABETIČNIM DELOVANJEM
Mentor: izr. prof. dr. Franc Perdih
Datum zagovora: 14. 9. 2016

Nejc BUTALA
SINTEZA VEČVEZNIH LIGANDOV S PIRIDIN-2 - KARBOKSILATNO SKUPINO ZA KOORDINACIJO LANTANOIDNIH IONOV
Mentor: izr. prof. dr. Franc Perdih
Datum zagovora: 15. 9. 2016

Polona ŠKRINJAR
PROUČEVANJE ADSORPCIJSKIH LASTNOSTI BIOOGLJA
Mentorica: doc. dr. Marija Zupančič
Datum zagovora: 16. 9. 2016

Natalija POGORELC
PRODUKTI REAKCIJ SOLI KOVIN ČETRTE PERIODE Z GLICINOM
Mentorica: doc. dr. Nives Kitanovski
Datum zagovora: 14. 9. 2016

Kristina MAGDALENIĆ
VPLIV DEBELINE PLASTI TiO_2 NA RAZGRADNJO BARVILA PLASMOCORINTH B
Mentorica: doc. dr. Irena Kozjek Škofic
Datum zagovora: 10. 11. 2016

Aleksandar DJURDJEVIĆ
VPLIV SILICIJA NA PRETVORBO ANATASA V RUTIL
Mentorica: doc. dr. Irena Kozjek Škofic
Datum zagovora: 16. 9. 2016

Anja KRAMER
UPORABA KONJUGIRANIH POLIMEROV V FOTONAPETOSTNIH CELICAH
Mentor: doc. dr. Janez Cerar
Datum zagovora: 15. 9. 2016

Ema SLEJKO
AKTIVNOSTNI KOEFICIENT PROPANOJSKE KISLINE V ADSORBENTU
Mentorica: prof. dr. Barbara Hribar Lee
Datum zagovora: 14. 9. 2016

Martin KOŠIČEK
DISOCIACIJSKA RAVNOTEŽJA V VODNIH RAZTOPINAH ENOSTAVNIH IN POLIMERNIH KARBOKSILNIH KISLIN
Mentorica: prof. dr. Ksenija Kogej
Datum zagovora: 12. 9. 2016

Anja KOS
STRUKTURNE IN TERMODINAMSKE ZNAČILNOSTI PREPOZNAVANJA IN VEZANJA NETROPSINA NA DNA
Mentor: prof. dr. Jurij Lah
Datum zagovora: 13. 9. 2016

Danijela HODNIK
STRUKTURNE IN TERMODINAMSKE ZNAČILNOSTI PREPOZNAVANJA DNA Z LIGANDOM 360A-Br
Mentor: prof. dr. Jurij Lah
Datum zagovora: 13. 9. 2016

Blaž ZDOVC
KVANTNO – KEMIJSKI PRISTOPI K NAPOVEDI ABSORPCIJSKIH SPEKTROV KONJUGIRANIH BARVIL
Mentor: doc. dr. Miha Lukšič
Datum zagovora: 15. 9. 2016

Tomislav KOSTEVC
ISKANJE INHIBITORJEV VIRUSA ZIKA Z UPORABO METOD MOLEKULSKEGA MODELIRANJA
Mentor: doc. dr. Črtomir Podlipnik
Datum zagovora: 16. 9. 2016

Jaka ŠTIRN
VPLIV PODROBNOSTI MODELOV TETRAMETILAMONIJEVE SOLI POLIANETOLSULFONSKE KISLINE NA RAZREDČILNE ENTALPIJE
Mentor: izr. prof. dr. Jurij Reščič
Datum zagovora: 13. 9. 2016

Klavdija MIRTIČ
INTERAKCIJE MED SURFAKTANTI IN BIOLOŠKIMI MEMBRANAMI
Mentor: Bojan Šarac
Datum zagovora: 16. 9. 2016

Robert KOMAN
SUPERHIDROFOBNE POVRŠINE IN PREMAZI NA TRDNIH MATERIALIH: LASTNOSTI, IZDELAVA IN APLIKACIJE
Mentor: Bojan Šarac
Datum zagovora: 14. 9. 2016

Matjaž SIMONČIČ
KEMIJSKE REAKCIJE V MEDZVEZDNEM PROSTORU
Mentor: izr. prof. dr. Tomaž Urbič
Datum zagovora: 15. 9. 2016

Matjaž DLOUHY
STRUKTURA IN INTERAKCIJA METIL RADIKALA
Mentor: izr. prof. dr. Tomaž Urbič
Datum zagovora: 15. 9. 2016

Petra PAPEŽ
MONTE CARLO SIMULACIJA DVODIMENZIONALNIH MODELOV ALKOHOLOV
Mentor: izr. prof. dr. Tomaž Urbič
Datum zagovora: 13. 9. 2016

Domen KASTELIC
OPTIMIZACIJA INSTRUMENTA ZA MASNO SPEKTROMETRIJO Z INDUKTIVNO SKLOPLJENO PLAZMO
Mentor: prof. dr. Marjan Veber
Datum zagovora: 15. 9. 2016

Ema GRIČAR
POTENCIOMETRIČNE TITRACIJE PRI ŠTUDIJU INTERAKCIJ FITATOV Z IZBRANIMI KOVINSKIMI IONI
Mentor: izr. prof. dr. Mitja Kolar
Datum zagovora: 15. 9. 2016

Jan GAČNIK
DOLOČANJE RADIJEVIH IZOTOPOV V VODI Z METODO TEKOČINSKE SCINTILACIJE
Mentorica: prof. dr. Helena Prosen
Datum zagovora: 12. 9. 2016

Tina GRUBAR
DOLOČANJE TRIAZINSKIH PESTICIDOV V VODI Z DLLME-HPLC
Mentorica: prof. dr. Helena Prosen
Datum zagovora: 12. 9. 2016

Urša KOŠAK
SEKVENČNA INJEKCIJSKA ANALIZA
Mentorica: izr. prof. dr. Nataša Gros
Datum zagovora: 31. 8. 2016

Maja ŠUŠTERŠIČ
DERIVATIVNA SPEKTROMETRIJA
Mentorica: izr. prof. dr. Nataša Gros
Datum zagovora: 9. 9. 2016

Anja PIRC
ŠTUDIJ DEGRADACIJE VITAMINA D2
Mentor: izr. prof. dr. Matevž Pompe
Datum zagovora: 15. 9. 2016

Nika SIMONIČ
UPORABA VISKOZIMETRIJE ZA DOLOČANJE STOPNJE POLIMERIZACIJE CELULOZE V PAPIRJIH Z VISOKO VSEBNOSTJO LIGNINA
Mentorica: izr. prof. dr. Irena Kralj Cigić
Datum zagovora: 12. 9. 2016

KEMIJSKO INŽENIRSTVO

Sara SEVER
PRETVORBA POLŠARŽNEGA PROCESA Z IZMENJAVO MEDIJA V PERFUZIJSKI PROCES NA PRIMERU BIOPROCESA S SESALČJO CELIČNO KULTURO
Mentor: izr. prof. dr. Marjan Marinšek
Datum zagovora: 24. 3. 2016

Jan DEBEVEC
ANOKSIČNI PRETOČNI BIOREAKTOR S STRNJENIM SLOJEM BIOMASE: KINETIČNI MODEL OKSIDACIJE MRAVLJINČNE KISLINE
Mentor: prof. dr. Igor Plazl
Datum zagovora: 16. 9. 2016

Marija OBLAK
PONOVNA UPORABA TEHNOLOŠKEGA ODPADKA ELASTOMEROV
Mentorica: prof. dr. Urška Šebenik
Datum zagovora: 8. 9. 2016

Matej BIRK
PRIMERJAVA GOJENJA CELIČNE LINIJE CHO V RAZLIČNIH BIOREAKTORJIH
Mentor: prof. dr. Aleksander Pavko
Datum zagovora: 13. 9. 2016

Anže DOLINŠEK
OPREDELITEV PRIMERNIH LABORATORIJSKIH METOD ZA DOLOČITEV OPTIMALNIH VOZNIH LASTNOSTI RADIALNE MOTORSKE PNEVMATIKE
Mentorica: prof. dr. Urška Šebenik
Datum zagovora: 7. 9. 2016

Uroš JANIĆIJEVIĆ
PORABA ENERGIJE V KOMUNALNI ČISTILNI NAPRAVI
Mentorica: izr. prof. dr. Andreja Žgajnar Gotvajn
Datum zagovora: 23. 6. 2016

Boris PEKLAR
VPLIV OBRATOVALNIH POGOJEV NA KRISTALIZACIJO DERIVATA PIPERAZINA
Mentor: doc. dr. Aleš Podgornik
Somentor: doc. dr. Blaž Likozar
Datum zagovora: 13. 9. 2016

Ana Tea KOS
RAZVOJ PREVODNIH GRAFENSKIH KOMPONENT ZA FUNKCIONALNE BARVE
Mentor: doc. dr. Boštjan Genorio
Datum zagovora: 23. 9. 2016

Marko VIDIC
OKSIDACIJA LEVULINSKE KISLINE Z UPORABO HETEROGENEGA RUTENIJEVEGA KATALIZATORJA
Mentor: prof. dr. Aleksander Pavko
Somentor: doc. dr. Blaž Likozar
Datum zagovora: 13. 9. 2016

Noel AVBELJ
VREDNOTENJE MORFOLOŠKIH KARAKTERISTIK PRI INDUSTRIJSKI PRIPRAVI VODNE SUSPENZIJE $CaCO_3$
Mentor: izr. prof. dr. Marjan Marinšek
Datum zagovora: 29. 9. 2016

Ana Roza MEDVED
MOKRI POSTOPEK KARBONIZACIJE ELEKTROFILTRSKEGA PEPELA IN KARAKTERIZACIJA PRODUKTOV
Mentorica: doc. dr. Barbara Novosel
Datum zagovora: 6. 5. 2016

Rebeka GREGORČIČ
PRIMERJAVA FIZIKALNO-KEMIJSKIH POSTOPKOV ČIŠČENJA IZCEDNIH VOD KOMUNALNE DEPONIJE
Mentorica: izr. prof. dr. Andreja Žgajnar Gotvajn
Datum zagovora: 19. 5. 2016

Irena IHAN
KINETIKA NASTAJANJA POROZNEGA POLIMETAKRILATA
Mentor: doc. dr. Aleš Podgornik
Datum zagovora: 16. 6. 2016

Rok PUCER
KRIOMACERACIJA GROZDJA
Mentor: prof. dr. Marin Berovič
Somentor: prof. dr. Mojmir Wondra
Datum zagovora: 7. 9. 2016

Tanja BRESKVAR
POLIOLNA SINTEZA AZO SPOJIN Z MIKROVALOVI
Mentor: izr. prof. dr. Marjan Marinšek
Datum zagovora: 8. 9. 2016

Rok KLOBČAR
KINETIKA SINTRANJA KERAMIKE NA OSNOVILANTAN-STRONCIJ-KROM-MANGANMEŠANEGA OKSIDA
Mentor: izr. prof. dr. Marjan Marinšek
Datum zagovora: 8. 9. 2016

Bernarda ANŽELAK
IZLOČANJE PROTEINOV IZ BIOLOŠKIH MEDIJEV Z UPORABO MAGNETNIH NANODELCEV
Mentor: prof. dr. Marin Berovič
Somentor: Darko Makovec
Datum zagovora: 13. 9. 2016

Brina ZUPANČIČ
BIOSINTEZA KORDICEPINA GLIVE *Cordyceps militaris* S KULTIVACIJO NA TRDNEM SUBSTRATU
Mentor: prof. dr. Marin Berovič
Somentor: prof. dr. Samo Kreft
Datum zagovora: 13. 9. 2016

Marko ŠKRILEC
UPORABA OZONA ZA DEZINFEKCIJO ZAPRTIH PROSTOROV
Mentorica: izr. prof. dr. Andreja Žgajnar Gotvajn
Datum zagovora: 16. 9. 2016

Vinko ŠUCUR
VPLIV GLINE NA SINTEZE NANOKOMPOZITNIH UV ZAMREŽLJIVIH AKRILATNIH LEPIL
Mentor: doc. dr. Jernej Kajtna
Datum zagovora: 22. 9. 2016

Jasmina VALENČAK
GRAFTIRANJE POROZNIH METAKRILATNIH NOSILCEV
Mentor: doc. dr. Aleš Podgornik
Datum zagovora: 22. 9. 2016

Borut MLAKAR
IZBOLJŠANJE MEHANSKIH LASTNOSTI ALUMINIJEVE ZLITINE ZA VISOKO TLAČNO LITJE
Mentorica: doc. dr. Klementina Zupan
Datum zagovora: 22. 9. 2016

Irena PRIMC DOLINŠEK
ANALIZA STROŠKOV PROCESA TRANSAMINACIJE Z RAZLIČNIMI OBLIKAMI BIOKATALIZATORJA
Mentorica: prof. dr. Polona Žnidaršič Plazl
Datum zagovora: 23. 9. 2016

Jan ČERNELČ
ENCIMSKO KATALIZIRANA SINTEZA IZOAMIL ACETATA V PRETOČNEM SISTEMU Z INTENZIVNIM KONTAKTIRANJEM DVEH KAPLJEVIN
Mentorica: prof. dr. Polona Žnidaršič Plazl
Datum zagovora: 23. 9. 2016

KEMIJSKO INŽENIRSTVO – 1. stopnja

Anže URANKAR
UTRJEVANJE EPOKSIDNE SMOLE Z RAZLIČNIMI KATALIZATORJI
Mentorica: prof. dr. Urška Šebenik
Datum zagovora: 1. 2. 2016

Miha ŠVAGELJ
VEČANJE PROSOJNOSTI NARAVNO PRESEVNIH MATERIALOV Z UPORABO POLIMEROV KOT POLNILCEV RAZPOK
Mentor: doc. dr. Aleš Podgornik
Datum zagovora: 25. 7. 2016

Rene OBLAK
PRIPRAVA METAKRILATNIH POLYHIPE MONOLITOV
Mentor: doc. dr. Aleš Podgornik
Datum zagovora: 14. 9. 2016

Elizabeta STEKLASA
SPOSOBNOST SAMOCELJENJA POLIMERA
Mentorica: prof. dr. Urška Šebenik
Datum zagovora: 16. 9. 2016

Dejan MIŠIĆ
POLIMERNI MATERIALI S SPOMINSKIM UČINKOM
Mentorica: prof. dr. Urška Šebenik
Datum zagovora: 16. 9. 2016

Klemen ZLATNAR
POLŠARŽNA SUSPENZIJSKA POLIMERIZACIJA MIKROSFERNIH AKRILATNIH LEPIL
Mentor: doc. dr. Jernej Kajtna
Datum zagovora: 20. 9. 2016

Matjaž VELKOVRH
POLŠARŽNA SUSPENZIJSKA POLIMERIZACIJA MIKROSFERNEGA AKRILATNEGA LEPILA
Mentor: doc. dr. Jernej Kajtna
Datum zagovora: 21. 9. 2016

Rok MRAVLJAK
PRODUKCIJA BIODIZLA
Mentor: prof. dr. Marin Berovič
Datum zagovora: 10. 6. 2016

Milena BEVK
IMOBILIZACIJA ENCIMOV NA OSNOVI UPORABE MAGNETNIH NANODELCEV
Mentorica: prof. dr. Polona Žnidaršič Plazl
Datum zagovora: 12. 9. 2016

Kevin JERIČ
UPORABA HOMOGENE IN HETEROGENE FENTONOVE OKSIDACIJE ZA ČIŠČENJE ODPADNIH VOD
Mentorica: izr. prof. dr. Andreja Žgajnar Gotvajn
Datum zagovora: 16. 9. 2016

Monika KRIVEC
ZAKAJ IN KAKO OBLOŽIMO AKTIVNO UČINKOVINO V ZDRAVILU
Mentor: prof. dr. Radovan Stanislav Pejovnik
Datum zagovora: 27. 1. 2016

Katarina SHOAIB
UPORABA TiO_2 v NANOT TEHNOLOGIJI
Mentor: prof. dr. Radovan Stanislav Pejovnik
Datum zagovora: 16. 3. 2016

Maša KLENOVŠEK
STRUKTURE KARAKTERISTIČNIH OKSIDNIH ANODNIH MATERIALOV V KERAMIČNIH GORIVNIH CELICAH
Mentorica: doc. dr. Klementina Zupan
Datum zagovora: 5. 9. 2016

Kevin STOJANOVSKI
ANALIZA MIKROSTRUKTURE KOMPOZITNEGA ANODNEGA MATERIALA ZA SREDNJE-TEMPERATURNE KERAMIČNE GORIVNE CELICE
Mentorica: doc. dr. Klementina Zupan
Datum zagovora: 16. 9. 2016

Dominika ZORMAN
KARAKTERIZACIJA PEROVSKITNEGA ANODNEGA MATERIALA ZA VISOKOTEMPERATURNE GORIVNE CELICE
Mentorica: doc. dr. Klementina Zupan
Datum zagovora: 5. 9. 2016

Marko FIRM
MAGNEZIJEVE ELEKTRODE ZA UPORABO V SEKUNDARNIH BATERIJAH
Mentor: prof. dr. Miran Gaberšček
Datum zagovora: 15. 9. 2016

Katja BALANTIČ
ENCIMSKE REAKCIJE
Mentor: prof. dr. Aleksander Pavko
Datum zagovora: 11. 7. 2016

Matevž PODOBNIK
PRIMERJAVA ŠARŽNIH, POLŠARŽNIH IN KONTINUIRNIH PROCESOV PRI PROIZVODNJI MONOKLONSKIH PROTITELES
Mentor: prof. dr. Aleksander Pavko
Datum zagovora: 11. 7. 2016

Nina KUZMIĆ
MEMBRANSKE SEPARACIJSKE METODE V BIOTEHNOLOGIJI IN FARMACIJI
Mentor: prof. dr. Aleksander Pavko
Datum zagovora: 12. 9. 2016

Tomaž PIRMAN
NIZKOTEMPERATURNI PARNI REFORMING METANOLA ZA PROIZVODNJO VODIKA Z UPORABO Cu-Zn KATALIZATORJEV
Mentor: prof. dr. Igor Plazl
Datum zagovora: 14. 7. 2016

Timotej GALUN
NANOEMULZIJE ZA PROIZVODNJO IZOLACIJSKIH MATERIALOV
Mentor: prof. dr. Igor Plazl
Datum zagovora: 13. 9. 2016

Živa BREČKO
UPORABA DVOFAZNIH VODNIH SISTEMOV Z MICELI ZA ČIŠČENJE PROTEINOV Z MIKROFLUIDNIMI NAPRAVAMI
Mentorica: prof. dr. Polona Žnidaršič Plazl
Datum zagovora: 12. 9. 2016

Ana OBERLINTNER
BIOSENZORJI V MIKROFUIDIKI
Mentorica: prof. dr. Polona Žnidaršič Plazl
Datum zagovora: 16. 9. 2016

Damjan KODER
VPLIV FARMACEVTSKE ODPADNE VODE NA BIOLOŠKO ČISTILNO NAPRAVO
Mentorica: izr. prof. dr. Andreja Žgajnar Gotvajn
Datum zagovora: 7. 9. 2016

Gaja TOMSIČ
KATALITSKA DEPOLIMERIZACIJA NAJLONA 6 S PIROLIZNO METODO
Mentorica: izr. prof. dr. Andreja Žgajnar Gotvajn
Datum zagovora: 7. 9. 2016

Matej ŠADL
KARAKTERIZACIJA DEBELIH PLASTI BIZMUTOVEGA FERITA, PRIPRAVLJENIH Z METODO SITOTISKA, NA PODLAGI IZ KERAMIKE Z NIZKO TEMPERATURO ŽGANJA
Mentor: izr. prof. dr. Marjan Marinšek
Datum zagovora: 22. 9. 2016

Erik STARC
PRIDOBIVANJE IN UPORABA MOLEKULARNO VTISNJENIH POLIMEROV
Mentor: doc. dr. Aleš Podgornik
Datum zagovora: 13. 9. 2016

Tina PALJK
POROZNI PIEZOELEKTRIČNI MATERIALI
Mentor: doc. dr. Aleš Podgornik
Datum zagovora: 14. 9. 2016

Tilen KOPAČ
VPLIV RAZMERJA MONOMEROV TER MOLEKULSKE MASE NA LEPILNE LASTNOSTI PRI POLŠARŽNI SUSPENZIJSKI POLIMERIZACIJI MIKROSFERNIH AKRILATNIH LEPIL
Mentor: doc. dr. Jernej Kajtna
Datum zagovora: 6. 9. 2016

Lorena KUNC
INŽENIRSKI VIDIKI PROIZVODNJE BIOPLINA
Mentor: doc. dr. Aleš Podgornik
Datum zagovora: 12. 9. 2016

Matjaž ŠKEDELJ
TEORETIČNA OBRAVNAVA IN PRISTOP K MODELIRANJU LASTNOSTI POLIMERNIH MATERIALOV S SPOSOBNOSTJO SAMOCELJENJA
Mentor: doc. dr. Aleš Ručigaj
Datum zagovora: 16. 9. 2016

Matej BENEDIK
PERFUZIJSKI BIOREAKTOR ZA GOJENJE SESALSKIH CELIC
Mentor: doc. dr. Aleš Podgornik
Datum zagovora: 16. 9. 2016

BIOKEMIJA

Tjaša KORBAR
VPLIV INVERZIJE POLARNOSTI V DNA ZAPOREDJU NA VEZAVO IN PREMIKANJE KATIONOV
Mentor: prof. dr. Janez Plavec
Datum zagovora: 21. 9. 2016

Irena GRŽINA
STRUKTURNA IN BIOFIZIKALNA ANALIZA CELICO PENETRIRAJOČEGA PEPTIDA TP 10 IN NJEGOVEGA DIMERA
Mentor: prof. dr. Roman Jerala
Somentor: prof. dr. Gregor Anderluh
Datum zagovora: 6. 5. 2016

Jaka CEVC
RAZVOJ LC-MS METODE ZA DOLOČANJE VSEBNOSTI ELAIOFILINA V SALINOMICINU
Mentorica: izr. prof. dr. Irena Kralj Cigić
Datum zagovora: 8. 6. 2016

Maja DEBELJAK
OCENA DIFERENCIACIJE MODELA ČREVESNEGA EPITELIJA NA OSNOVI CELIC CACO-2 S SLEDENJEM IZRAŽANJA GENOV
Mentor: prof. dr. Gregor Anderluh
Datum zagovora: 21. 9. 2016

Uroš JAVORNIK
ANALIZA SUPRAMOLEKULARNIH STRUKTUR DVEH DIASTEREOIZOMEROV MODIFICIRANEGA GVANINSKEGA DINUKLEOTIDA Z NMR-SPEKTROSKOPIJO V RAZTOPINI
Mentor: prof. dr. Janez Plavec
Datum zagovora: 29. 2. 2016

Samo MARINČ
TVORBA G-KVADRUPLEKSOV IZ ZAPOREDJA PROMOTORJA GENA KRAS
Mentor: prof. dr. Janez Plavec
Datum zagovora: 30. 9. 2016

Anja JEŠE
PRIMERJAVA KLASIČNEGA IN MODIFICIRANEGA DROZGANJA V PIVOVARSKI TEHNOLOGIJI
Mentorica: izr. prof. dr. Irena Kralj Cigić
Datum zagovora: 21. 9. 2016

Kristina URBAS
SINTEZA IN PRETVORBE (R)-2-(2,2-DIMETIL-3-METILENCIKLOPENTIL)-ALKILAMINA
Mentor: doc. dr. Uroš Grošelj
Datum zagovora: 17. 2. 2016

Branislav LUKIĆ
SINTEZA 5-AMINOETIL SUBSTITUIRANIH KARBOKSAMIDO PIRAZOLO[1,5-A]PIRIMIDONOV
Mentor: prof. dr. Jurij Svete
Datum zagovora: 9. 5. 2016

Mateja KRŽIŠNIK
PRIPRAVA CISTEINSKIH ANALOGOV TNF-α ZA MESTNOSPECIFIČNO PEGILACIJO
Mentor: prof. dr. Roman Jerala
Datum zagovora: 8. 9. 2016

Nina RAZGORŠEK
ANAEROBNA STRUPENOST IN BIORAZGRADLJIVOST IZCEDNIH VOD KOMUNALNE DEPONIJE
Mentorica: izr. prof. dr. Andreja Žgajnar Gotvajn
Datum zagovora: 8. 9. 2016

Janja ZALETEL
SINTEZA, ALKILIRANJE IN AMIDIRANJE METIL 7-OKDO-4H-PIRAZOLO[1,5-A]PIRIMIDIN-3-KARBOKSILATA
Mentor: prof. dr. Jurij Svete
Datum zagovora: 14. 9. 2016

Staša MATJAŽ
STABILNOST KLOROFILINA V IZBRANIH RAZTOPINAH
Mentorica: izr. prof. dr. Irena Kralj Cigić
Datum zagovora: 14. 9. 2016

Janja REBEC
DOLOČEVANJE SUPEROKSID DISMUTAZNE AKTIVNOSTI KOVINSKIH KSANTURENATOV Z UPORABO METODE NBT
Mentorica: doc. dr. Elizabeta Tratar Pirc
Datum zagovora: 15. 9. 2016

Ajda ŽAGER
VPLIV SULINDAK SULFIDA NA DIMERIZACIJO TUMORSKEGA OZNAČEVALCA EPCAM
Mentor: doc. dr. Miha Pavšič
Datum zagovora: 21. 9. 2016

Gregor MAZOVEC
ŠTUDIJ HIDROFOBNIH INTERAKCIJ OB UKRIVLJENI POVRŠINI Z MERCEDES-BENZ MODELOM VODE
Mentorica: prof. dr. Barbara Hribar Lee
Datum zagovora: 27. 9. 2016

Sonja CIMERMAN
BIOLOŠKA IN KATALITSKA AKTIVNOST TANKIH PLASTI PLATINE
Mentorica: doc. dr. Irena Kozjek Škofic
Datum zagovora: 27. 9. 2016

Aleš KERMELJ
PRIPRAVA TUMORSKIH OZNAČEVALNIH PROTEINOV EpCAM IN Trop2 V KVASOVKI PICHIA PASTORIS
Mentor: doc. dr. Miha Pavšič
Datum zagovora: 27. 9. 2016

Blaž KRŽAN
ŠTUDIJ TERMODINAMSKE STABILNOSTI PRI RAZVOJU UČINKOVINE IFN-α1A
Mentor: prof. dr. Jurij Lah
Datum zagovora: 28. 9. 2016

Gregor MURN
CITOTOKSIČNOST KOMPOZITNIH FIBROINSKIH NOSILCEV IN NJIHOVEGA VPLIVA NA OSTEOGENO DIFERENCIACIJO PRI ZDRAVLJENJU OSTEOHONDRALNIH POŠKODB
Mentor: doc. dr. Miha Pavšič
Datum zagovora: 29. 9. 2016

BIOKEMIJA – 1. stopnja

Rok FERENC
ANALIZA VLOGE KINAZE MKK6 V OBRAMBI KROMPIRJA PROTI VIRUSU PVY Z VIRUSNIM UTIŠANJEM
Mentorica: prof. dr. Kristina Gruden
Datum zagovora: 13. 9. 2016

Primož TIČ
ŠTUDIJE RUTENIJEVIH SPOJIN KOT MOŽNIH INHIBITORJEV ENCIMOV AKR1C
Mentor: prof. dr. Iztok Turel
Datum zagovora: 16. 9. 2016

Sabina ŠTUKELJ
GENOMSKA IN TRANSKRIPTOMSKA ANALIZA ANTIMIKROBNIH PEPTIDOV (AMP) PRI NAJSTAREJŠIH SKUPINAH VRETENČARJEV - NOV POGLED NA NASTANEK IN EVOLUCIJO AMP DRUŽIN PRI VRETENČARJIH
Mentor: izr. prof. dr. Dušan Kordiš
Datum zagovora: 14. 9. 2016

Marija SRNKO
VPLIV FOSFORILACIJE C-KONČNEGA TIROZINSKEGA OSTANKA V PROTEINU FUS NA NJEGOVO CELIČNO RAZPOREDITEV
Mentor: izr. prof. dr. Boris Rogelj
Datum zagovora: 14. 9. 2016

Tomaž ŽAGAR
PRIPRAVA MONOMERNIH MUTANT PROTEINA EpCAM
Mentorica: prof. dr. Brigita Lenarčič
Datum zagovora: 12. 9. 2016

Urška ČERNE
PRIPRAVA FUZIJSKEGA PROTEINA NANOTELESA M33 Z MCHERRY ZA FLUORESCENČNO DETEKCIJO MLKL
Mentor: doc. dr. Gregor Gunčar
Datum zagovora: 15. 9. 2016

Monika PEPELNJAK
IZRAŽANJE ORTOKASPAZ CIANOBAKTERIJE MICROCYSTIS AERUGINOSA PCC 7806 V BAKTERIJI ESCHERICHIA COLI
Mentor: izr. prof. dr. Marko Dolinar
Datum zagovora: 25. 8. 2016

Anja TANŠEK
VPLIV OKOLJSKIH VOD IN KOVINSKIH IONOV NA RAST CIANOBAKTERIJ SYNECHOCYSTIS SP. PCC 6803 TER PREVERJANJE UČINKOVITOSTI SINTEZNOBIOLOŠKIH UBIJALSKIH STIKAL
Mentor: izr. prof. dr. Marko Dolinar
Datum zagovora: 25. 8. 2016

Aneja TAHIROVIĆ
OPTIMIZACIJA IN UPORABA TESTA MTT ZA DOLOČANJE PREŽIVETJA SINTEZNOBIOLOŠKO SPREMENJENIH CIANOBAKTERIJ SYNECHOCYSTIS SP. PCC 6803 PO INDUKCIJI GENOV ZA SPROŽITEV CELIČNE SMRT
Mentor: izr. prof. dr. Marko Dolinar
Datum zagovora: 25. 8. 2016

Tadej ULČNIK
FUNKCIJSKA ANALIZA NEKATERIH MUTANT KATEPSINA K
Mentor: doc. dr. Marko Novinec
Datum zagovora: 15. 9. 2016

Jernej VIDMAR
NAČRTOVANJE IN PRIPRAVA KONSTITUTIVNO MONOMERNE OBLIKE PROTEINA TROP2
Mentor: doc. dr. Miha Pavšič
Datum zagovora: 15. 9. 2016

Katjuša TRIPLAT
PRIMERJAVA SERUMSKIH KONCENTRACIJ TUMORSKEGA OZNAČEVALCA OSTEOPONTINA IN CELOKUPNIH PROTEINOV PRI BOLNICAH Z RAKOM JAJČNIKA OB POSTAVITVI DIAGNOZE IN PO ZDRAVLJENJU
Mentorica: Katarina Černe
Datum zagovora: 12. 9. 2016

Amadeja LAPORNIK
VPELJAVA IN OPTIMIZACIJA VERIŽNE REAKCIJE S POLIMERAZO ZA DOKAZ ALFAVIRUSOV
Mentorica: prof. dr. Tatjana Avšič Zupanc
Datum zagovora: 15. 9. 2016

Jerneja KOCUTAR
UGOTAVLJANJE MIOTOKSIČNOSTI NOVIH OBLIK ANESTETIKOV
Mentor: prof. dr. Tomaž Marš
Datum zagovora: 15. 9. 2016

Inge SOTLAR
TRANSKRIPTOMSKI VIDIK URAVNAVANJA METABOLIZMA GLICEROLA PRI KVASOVKAH RODU AUREOBASIDIUM
Mentorica: Martina Turk
Datum zagovora: 12. 9. 2016

Bine TRŠAVEC
IZRAŽANJE REKOMBINANTNEGA ČLOVEŠKEGA MCSF IN ŠTUDIJA NJEGOVEGA PROTEOLITSKEGA PROCESIRANJA
Mentor: prof. ddr. Boris Turk
Datum zagovora: 15. 9. 2016

Dominik DEKLEVA
VPLIV SREBROVIH NANODELCEV NA SESALSKE CELICE V KULTURI
Mentor: prof. dr. Peter Veranič
Datum zagovora: 12. 9. 2016

Matic KOVAČIČ
STABILIZACIJA G-KVADRUPLEKSA TROMBIN-VEZAVNEGA APTAMERA S PIRENSKIMI SKUPINAMI
Mentor: prof. dr. Janez Plavec
Datum zagovora: 12. 9. 2016

Katja MALOVRH
VPLIV GLUKOZNEGA METABOLIZMA NA NASTANEK LIPIDNIH KAPLJIC V PODGANJIH KORTIKALNIH ASTROCITIH V KULTURI
Mentorica: doc. dr. Nina Vardjan
Datum zagovora: 12. 9. 2016

Enja KOKALJ
VPLIV ADRENERGIČNIH RECEPTORJEV IN RECEPTORJA GPR40 NA TVORBO LIPIDNIH KAPLJIC V PODGANJIH ASTROCITIH V KULTURI
Mentorica: doc. dr. Nina Vardjan
Datum zagovora: 12. 9. 2016

KEMIJSKO IZOBRAŽEVANJE

Lea ZAJEC
OPTIMIZACIJA ANALIZNEGA POSTOPKA ZA DOLOČANJE IZOTOPSKEGA RAZMERJA 87 SR/86 SR V OKOLJSKIH VZORCIH S KVADRUPULNIM ICP-MS
Mentor: prof. dr. Marjan Veber
Datum zagovora: 6. 7. 2016

Doroteja ŠPEC
CIKLOADICIJE DIALKIL AZODIKARBOKSILATOV NA 2H-PIRAN-2-ONE
Mentor: prof. dr. Marijan Kočevar
Datum zagovora: 30. 9. 2016

Marko MERMAL
OKSIDACIJA VINILNIH ETROV Z DIMETILDIOKSIRANOM IN NEKATERE PRETVORBE NASTALIH EPOKSIDOV
Mentor: izr. prof. dr. Franci Kovač
Datum zagovora: 30. 9. 2016

Elma LJUTIĆ
ŠTUDIJ VODNIH RAZTOPIN ATAKTIČNE POLIMETAKRILNE KISLINE Z METODAMI SIPANJA SVETLOBE
Mentorica: prof. dr. Ksenija Kogej
Datum zagovora: 30. 9. 2016

Doris POTOČNIK
ENANTIOSELEKTIVNA REDUKCIJA 2-BENZILIDENCIKLOALKANONOV
Mentor: izr. prof. dr. Bogdan Štefane
Datum zagovora: 30. 9. 2016

TEHNIŠKA VARNOST – 1. stopnja

Nejc JUHART
OKSIDATIVNI STRES V DELOVNEM OKOLJU
Mentor: prof. dr. Marjan Bilban
Datum zagovora: 13. 1. 2016

Mateja KOČEVAR
PROMOCIJA ZDRAVJA V PODJETJU ISKRA IP D. O. O.
Mentor: prof. dr. Marjan Bilban
Datum zagovora: 12. 9. 2016

Klementina RADANOVIČ
STRES IN IZGORELOST V DEJAVNOSTI GOSTINSTVA IN TURIZMA
Mentor: prof. dr. Marjan Bilban
Datum zagovora: 29. 9. 2016

Maruša SVETINA
ERGONOMSKE MERITVE DELOVNEGA MESTA NATAKAR
Mentorica: doc. dr. Klementina Zupan
Datum zagovora: 18. 11. 2016

Tomaž ČRNIGOJ
ERGONOMIJA V ULTRALAHKIH LETALIH
Mentorica: prof. dr. Simona Jevšnik
Datum zagovora: 6. 9. 2016

Nina MONETA
PRIMERJAVA IN MERITVE HRUPA V OKOLICI IZOBRAŽEVALNIH USTANOV
Mentor: doc. dr. Mitja Robert Kožuh
Datum zagovora: 23. 11. 2016

Janja TORI
SPRINKLERSKI SISTEMI V LESENIH OBJEKTIH
Mentor: doc. dr. Domen Kušar
Datum zagovora: 29. 9. 2016

Nastja SMOLNIKAR
VPLIV DODATKOV NA MINIMALNO VŽIGNO ENERGIJO FARMACEVTSKIH AKTIVNIH UČINKOVIN
Mentorica: doc. dr. Barbara Novosel
Datum zagovora: 15. 9. 2016

Polona STARAŠINIČ
UČINKOVITOST DIPHOTERINA ZA NEVTRALIZACIJO JEDKOVIN
Mentorica: doc. dr. Barbara Novosel
Datum zagovora: 15. 9. 2016

Laura BOROŠ
EVAKUACIJA IZ 3C LAMELE NOVE FAKULTETE ZA KEMIJO IN KEMIJSKO TEHNOLOGIJO
Mentorica: doc. dr. Saša Petriček
Datum zagovora: 18. 7. 2016

Luka MAKAROVIČ
ERGONOMSKE MERITVE POLOŽAJEV PACIENTA IN ZDRAVSTVENEGA OSEBJA
Mentorica: doc. dr. Klementina Zupan
Datum zagovora: 4. 2. 2016

Tina ROBNIK
ERGONOMIJA DELA IN ERGONOMSKE MERITVE POLOŽAJEV PRI MOLŽI KRAV
Mentorica: doc. dr. Klementina Zupan
Datum zagovora: 21. 9. 2016

Anže ŠPEHAR
MERITVE UČINKOVITOSTI ZGLOBNIH ODSESOVALNIH ROK
Mentorica: prof. dr. Marija Bešter Rogač
Datum zagovora: 4. 7. 2016

Neja JEKOVEC
PRAVNA UREDITEV VARSTVA PRED HRUPOM
Mentor: Grega Strban
Datum zagovora: 13. 6. 2016

Midhat AHMETOVIĆ
PRAŠNE EKSPLOZIJE V PREHRAMBNI INDUSTRIJI
Mentor: doc. dr. Jože Šrekl
Datum zagovora: 15. 9. 2016

Primož VRBINC
IZBOLJŠANE POŽARNE ODPORNOSTI Z MATERIALI, KI PRI FAZNI PRETVORBI PORABLJAJO TOPLOTO
Mentorica: doc. dr. Klementina Zupan
Datum zagovora: 29. 6. 2016

Ana ŽABJEK
SPECIALNI BETONI ZA DVIG PROTIPOŽARNE VARNOST
Mentor: izr. prof. dr. Marjan Marinšek
Datum zagovora: 15. 9. 2016

Gregor HORVAT
MATERIALI ZA TOPLOTNO ZAŠČITO V OSEBNI VAROVALNI OPREMI
Mentor: izr. prof. dr. Marjan Marinšek
Datum zagovora: 15. 9. 2016

Eva FURLAN
NEVTRALIZACIJSKA SPOSOBNOST DIPHOTERINA, RAZTOPINE KLOROVODIKOVE KISLINE IN NATRIJEVEGA HIDROKSIDA
Mentor: doc. dr. Bojan Kozlevčar
Datum zagovora: 16. 9. 2016

Rok REPINC
HRUP V PAPIRNI INDUSTRIJI
Mentor: doc. dr. Mitja Robert Kožuh
Datum zagovora: 21. 10. 2016

Kaja BERKOPEC
ERGONOMIJA V ZDRAVSTVENI NEGI
Mentor: prof. dr. Marjan Bilban
Datum zagovora: 12. 9. 2016

Urška KOŽELJ
NOČNO DELO IN VPLIV NA ZDRAVJE
Mentor: prof. dr. Marjan Bilban
Datum zagovora: 12. 9. 2016

Maja PORENTA
VPLIV UPORABE MOBILNIH TELEFONOV NA VARNOST V CESTNEM PROMETU
Mentor: prof. dr. Marjan Bilban
Datum zagovora: 12. 9. 2016

Sabina TURK
ZAGOTAVLJANJE VARNOSTI ELEKTRIČNIH DVIGAL
Mentor: doc. dr. Boris Jerman
Datum zagovora: 16. 9. 2016

Valerija PRIMOŽIČ
VPLIV INDUSTRIJE V MESTNIH JEDRIH NA VARNOST LJUDI IN OKOLJA
Mentor: doc. dr. Mitja Robert Kožuh
Datum zagovora: 5. 9. 2016

Martina ČEČ
RAVEN VARNOSTNE KULTURE ŠTUDENTOV RAZLIČNIH FAKULTET
Mentorica: doc. dr. Marija Molan
Datum zagovora: 14. 9. 2016

Karmen KORENIČ
VARNOSTNA KULTURA V RAZLIČNIH EKIPNIH ŠPORTNIH PANOGAH
Mentorica: doc. dr. Marija Molan
Datum zagovora: 14. 9. 2016

Renata MEGLEN
POJAVLJANJE NADURNEGA DELA V KOVINSKI INDUSTRIJI
Mentorica: doc. dr. Marija Molan
Datum zagovora: 14. 9. 2016

Jerneja PAVLIČ
POSREDOVANJE GASILCEV OB NEZGODAH Z NEVARNIMI SNOVMI V PODJETJU ZA PREDELAVO JEKLA
Mentorica: doc. dr. Barbara Novosel
Datum zagovora: 26. 9. 2016

Urška POJE
NEVARNOSTI IN UPORABA PIROTEHNIČNIH IZDELKOV
Mentorica: doc. dr. Barbara Novosel
Datum zagovora: 28. 9. 2016

Karin LAZAR
DOLOČITEV MINIMALNE VŽIGNE ENERGIJE LESNIH PRAHOV SMREKE IN HRASTA
Mentorica: doc. dr. Barbara Novosel
Datum zagovora: 15. 9. 2016

Tajda AHČIN
ZAGOTAVLJANJE POŽARNE VARNOSTI V INDUSTRIJSKEM OBJEKTU STOLARNE
Mentor: prof. dr. Simon Schnabl
Datum zagovora: 5. 9. 2016

Tanja ČERNOŠA
ANALIZA EVAKUACIJSKEGA ČASA V STAVBI OPERE S PROGRAMOM PATHFINDER
Mentor: prof. dr. Simon Schnabl
Datum zagovora: 5. 9. 2016

Rok GREGORIN
ZVOK IN GAŠENJE, ZATIRANJE PLAMENA IN DINAMIKA POŽAROV
Mentor: prof. dr. Simon Schnabl
Datum zagovora: 16. 9. 2016

Tadej LESJAK
OGNJEMETI IN NJIHOV VPLIV NA PRISOTNOST TRDNIH DELCEV V ZRAKU
Mentorica: prof. dr. Marija Bešter Rogač
Datum zagovora: 16. 9. 2016

Miržel COCIĆ
ODPADNE VODE NA FAKULTETI ZA KEMIJO IN KEMIJSKO TEHNOLOGIJO
Mentor: prof. dr. Marjan Veber
Datum zagovora: 20. 9. 2016

DIPLOME – VISOKOŠOLSKI STROKOVNI ŠTUDIJ

KEMIJSKA TEHNOLOGIJA

Vlasta ROZMAN
PREVERJANJE STABILNOSTI PUFRNIH RAZTOPIN IN INDIKATORJEV, KI VSTOPAJO V ANALIZNI PROCES
Mentorica: izr. prof. dr. Nataša Gros
Datum zagovora: 18. 5. 2016

Jernej VARGA
DOLOČANJE VSEBNOSTI VODE V GRANULATIH
Mentorica: izr. prof. dr. Nataša Gros
Datum zagovora: 27. 9. 2016

Jasna DRAGAN
PRIMERJAVA DVEH VIROV KONCENTRATOV ZA PRIPRAVO MEDIJEV ZA RAZTAPLANJE TRDNIH FARMACEVTSKIH OBLIK
Mentor: izr. prof. dr. Matevž Pompe
Datum zagovora: 30. 9. 2016

Anica JOVANDARIĆ
PREGLED OBRATOVANJA KOMUNALNIH ČISTILNIH NAPRAV S PRIMERJAVO DEJANSKIH IN PROJEKTIRANIH VREDNOSTI PARAMETROV NA IZTOKU
Mentorica: izr. prof. dr. Andreja Žgajnar Gotvajn
Datum zagovora: 23. 6. 2016

Ksenja AHČIN
VPLIV INTERFERENC NA POTENCIOMETRIČNE MERITVE
Mentorica: izr. prof. dr. Nataša Gros
Datum zagovora: 30. 9. 2016

Janez ILERŠIČ
REGENERACIJA IZOPROPILACETATA IN METILENKLORIDA
Mentor: prof. dr. Aleksander Pavko
Datum zagovora: 5. 1. 2016

Irena BRODARIČ
OPTIMIZACIJA DELEŽA POSPEŠEVALCA V AKRIALTIVNEM LEPILU
Mentorica: prof. dr. Urška Šebenik
Datum zagovora: 22. 9. 2016

Mitja NOVAK
ŠTUDIJA IZLUŽEVALNIH KARAKTERISTIK FOSFATOV IZ RAZLIČNIH VRST BIOOGLJA
Mentorica: doc. dr. Marija Zupančič
Datum zagovora: 27. 9. 2016

Darja PALATINUS
VPLIV UPORABE NANOCELULOZNIH MATERIALOV NA LASTNOSTI PREMAZANEGA PAPIRJA
Mentor: prof. dr. Igor Plazl
Datum zagovora: 23. 9. 2016

Ema KEMPERLE
LASNOSTI ASFALTNIH ZMESI Z DODANIM HIDRIRANIM APNOM
Mentorica: doc. dr. Klementina Zupan
Datum zagovora: 16. 9. 2016

Denis PUNGERČAR
KVALIFIKACIJA LC/MS SISTEMA ZA POTREBE SPREMLJANJA REAKCIJ
Mentor: prof. dr. Janez Košmrlj
Datum zagovora: 26. 9. 2016

Alenka PAPEŽ
ZNAČILNOSTI SUSPENZIJE ZA PRIPRAVO VEČPLASTNEGA VARISTORJA
Mentorica: doc. dr. Klementina Zupan
Datum zagovora: 28. 9. 2016

Jure ZAJC
POTENCIOMETRIČNE MERITVE Z ELEKTRODAMI V CELOTI V TRDNEM STANJU
Mentorica: izr. prof. dr. Nataša Gros
Datum zagovora: 11. 5. 2016

Elvis DEŽMAN
OPTIMIZACIJA REAKCIJE HIDROGENIRANJA LIPSTATIN OLJA
Mentor: prof. dr. Matjaž Krajnc
Datum zagovora: 16. 5. 2016

Andreja MAVEC
DOLOČANJE VSEBNOSTI MIDAZOLAMIJEVEGA KLORIDA
Mentor: izr. prof. dr. Matevž Pompe
Datum zagovora: 26. 9. 2016

Anja ŠTEBE
PRIPRAVA NEIDEALNIH DVOKOMPONENTNIH RAZTOPIN: VOLUMSKI EFEKTI V MEŠANICAH VODA-ETANOL
Mentor: izr. prof. dr. Jurij Reščič
Datum zagovora: 28. 9. 2016

Ben KRISTAN
NADOMESTEK NONILFENOLNIH ETOKSILATOV
Mentorica: prof. dr. Ksenija Kogej
Datum zagovora: 21. 6. 2016

Simona MATKO
PRIPRAVA IZBRANIH 1,3-DIARILTRIAZENOV
Mentor: prof. dr. Janez Košmrlj
Datum zagovora: 4. 7. 2016

Maja MITROVIĆ
DOLOČITEV UČINKOVITOSTI PRIMARNE SEPARACIJE V BIOPROCESIH S SESALČJO CELIČNO KULTURO
Mentor: prof. dr. Aleksander Pavko
Datum zagovora: 8. 9. 2016

Jernej URH
RAZBARVANJE RAZTOPINE VANKOMICINA Z ALUMINIJEVIM OKSIDOM IN AKTIVNIM OGLJEM
Mentor: prof. dr. Aleksander Pavko
Datum zagovora: 8. 9. 2016

Mojca ŠUTAR
DOLOČEVANJE RIBOFLAVINA Z METODO TEKOČINSKE KROMATOGRAFIJE VISOKE LOČLJIVOSTI V PREHRANSKIH DOPOLNILIH IN BIOLOŠKIH VZORCIH
Mentorica: dr. Tatjana Zupančič
Datum zagovora: 26. 9. 2016

Alisa ĆEHIĆ
VALIDACIJA HPLC METODE ZA DOLOČANJE OSTANKOV HORMONSKEGA PREPARATA NA BRISIH PO ČIŠČENJU PROIZVODNE OPREME
Mentorica: izr. prof. dr. Irena Kralj Cigić
Datum zagovora: 26. 9. 2016

Nataša KOROŠEC
STABILIZACIJA ČRNEGA PIGMENTA V VODNEM PREMAZU Z UPORABO FIZIKALNO-KEMIJSKIH METOD
Mentor: dr. Branko Alič
Datum zagovora: 27. 9. 2016

Mateja FIDERŠEK
OVREDNOTENJE RAZLIČNIH NAČINOV SPEKTROMETRIČNEGA MERJENJA
Mentorica: izr. prof. dr. Nataša Gros
Datum zagovora: 27. 9. 2016

Maja OBERČ
SPREMLJANJE INTERAKCIJ PRI KEMIJSKI STABILIZACIJI ZDRAVILNE UČINKOVINE V FORMULACIJI
Mentor: prof. dr. Janez Plavec
Datum zagovora: 27. 9. 2016

Darja MOHORČIČ
SINTEZA IN KARATKTERIZACIJA PRIRDINSKIH DERIVATOV Z 1H-BENZIMIDAZOL-2-TIOLOM
Mentor: prof. dr. Marijan Kočevar
Datum zagovora: 27. 9. 2016

Anja PLAHUTA
RAZVOJ MIKROSTRUKTURE OKSIDNE ANODE ZA KERAMIČNE GORIVNE CELICE
Mentorica: doc. dr. Klementina Zupan
Datum zagovora: 27. 9. 2016

Mojca MATOH
SINTEZA IN KARAKTERIZACIJA KOMPLEKSOV KOBALTOVEGA IN MANGANOVEGA BROMIDA Z ACETONITRILNIM LIGANDOM
Mentor: prof. dr. Alojz Demšar
Datum zagovora: 28. 9. 2016

Lidija BOŽIĆ MRKONJIĆ
SPREMLJANJE SEKUNDARNIH FAZ V ANODNIH MATERIALIH NA OSNOVI LANTAN STRONCIJ KROM MANGAN OKSIDA ZA KERAMIČNE GORIVNE CELICE
Mentorica: doc. dr. Klementina Zupan
Datum zagovora: 29. 9. 2016

Vladimira OBRANOVIČ
PRIPRAVA KOVINSKIH PRAHOV S TERMIČNIM RAZKROJEM MEŠANIH HIDRAZIN-KARBOKSILATOV
Mentorica: doc. dr. Barbara Novosel
Datum zagovora: 29. 9. 2016

Janez VOLMAJER
PRIMERJAVA DOLOČANJA VLAŽNOSTI PAPIRJA PO STANDARDNI METODI S POMOČJO BLIŽNJE INFRARDEČE SPEKTROMETRIJE
Mentor: izr. prof. dr. Matevž Pompe
Somentorica: Jana Kolar
Datum zagovora: 30. 9. 2016

Matjaž MALAVAŠIČ
IZOLACIJA INHIBITORJEV AMINOPEPTIDAZE N IZ FILTRATA KULTURE STREPTOMYCES RIMOSUS
Mentorica: Metka Renko
Datum zagovora: 30. 9. 2016

Mojca PERPAR
VPLIV STOPENJSKEGA ZNIŽEVANJA pH VREDNOSTI NA PROCES INKAPSULACIJE BUTIL STEARATA Z MELAMINSKO-FORMALDEHIDNO SMOLO
Mentor: dr. Branko Alič
Datum zagovora: 30. 9. 2016

KEMIJSKA TEHNOLOGIJA – 1. stopnja

Blaž ŠPRAJCER
ČIŠČENJE IZCEDNE VODE ZAPRTEGA ODLAGALIŠČA ODPADKOV S FENTONOVO OKSIDACIJO
Mentorica: izr. prof. dr. Andreja Žgajnar Gotvajn
Datum zagovora: 25. 2. 2016

Miha SOLDAT
PRIPRAVA SILIL SUBSTITUIRANIH BENZOJSKIH KISLIN
Mentor: izr. prof. dr. Janez Cerkovnik
Datum zagovora: 16. 9. 2016

Rok PIKON
TVORBA C-C VEZI NA DERIVATU NIKOTINA
Mentor: prof. dr. Janez Košmrlj
Datum zagovora: 14. 9. 2016

Urška TRBOVC
SINTEZA IN NADALJNJA PRETVORBA FENIL-SUBSTITUIRANIH PIRAZINOV IN KINOKSALINOV
Mentor: izr. prof. dr. Franc Požgan
Datum zagovora: 5. 7. 2016

Maja BRINOVEC
SINTEZA IN KARAKTERIZACIJA (3R*,4R*)-4-BENZILOKSIKARBONILAMINO-3-IZOPROPIL-5-OKSOPIRAZOLIDINONA
Mentor: prof. dr. Jurij Svete
Datum zagovora: 6. 7. 2016

Aleš GABER
UV-VIDNI SPEKTRI KROMOVIH(III) KOORDINACIJSKIH SPOJIN
Mentorica: doc. dr. Barbara Modec
Datum zagovora: 4. 3. 2016

Andrej GNIDOVEC
RAZVOJ IN VALIDACIJA METODE ZA DOLOČEVANJE OSTANKOV ANTIBIOTIKA V BRISIH PO ČIŠČENJU PROIZVODNE OPREME
Mentorica: izr. prof. dr. Irena Kralj Cigić
Datum zagovora: 23. 12. 2016

Barbara MENCIN
DOLOČITEV POGOJEV ZA PREVERJANJE KVALITETE VELIKIH KROMATOGRAFSKIH MONOLITOV
Mentor: prof. dr. Marjan Veber
Datum zagovora: 20. 9. 2016

Simon LONČARIČ
VPLIV MLETJA IN RAZKLOPA RAZLIČNIH ILMENITNIH RUD NA PROCES PRIDOBIVANJA TITANOVEGA DIOKSIDA PO SULFATNEM POSTOPKU
Mentorica: doc. dr. Barbara Novosel
Datum zagovora: 21. 1. 2016

Dominika ZORMAN
ANALIZA UV-SUŠEČIH LEPIL ZA UPORABO V ZAŠČITNIH TISKOVINAH
Mentor: prof. dr. Miran Gaberšček
Datum zagovora: 1. 2. 2016

Sanja POPOVIĆ
TEMPERATURNA ODVISNOST GOSTOT ALKOHOLOV IN MEŠANIC ALKOHOLOV TER VODE
Mentor: izr. prof. dr. Tomaž Urbič
Datum zagovora: 15. 9. 2016

Tinkara ČUČNIK BUDIŠA
CINKOVE KOORDINACIJSKE SPOJINE Z INDOL-3-OCETNO IN INDOL-3-PROPANOJSKO KISLINO S POTENCIALNIM ANTIDIABETIČNIM DELOVANJEM
Mentor: izr. prof. dr. Franc Perdih
Datum zagovora: 7. 4. 2016

Anja MODIC
RAZVOJ IN UPORABA ICP-OES METOD ZA DOLOČANJE SREBRA V REALNIH VZORCIH
Mentor: izr. prof. dr. Mitja Kolar
Datum zagovora: 30. 9. 2016

Mirjana BARBORIČ
RAZVOJ ANALIZNE METODE ZA DOLOČEVANJE SORODNIH SUBSTANC KLOPIDOGRELIJEVEGA HIDROGENSULFATA S TANKOPLASTNO KROMATOGRAFIJO
Mentorica: prof. dr. Helena Prosen
Datum zagovora: 21. 10. 2016

Tina KOZJEK
DOLOČEVANJE ORGANSKIH KISLIN V AEROSOLIH S TEKOČINSKO KROMATOGRAFIJO
Mentor: izr. prof. dr. Matevž Pompe
Datum zagovora: 5. 9. 2016

Aleksandra HUDAK
PREVERJANJE ALTERNATIVNIH HPLC KOLON ZA DOLOČANJE DERIVATA BENZIZOKSAZOLA
Mentorica: izr. prof. dr. Irena Kralj Cigić
Datum zagovora: 3. 3. 2016

Eva RIFELJ
IZDELAVA POSTOPKA VREDNOTENJA REFERENČNIH SUBSTANC V FARMACEVTSKI INDUSTRIJI
Mentorica: prof. dr. Helena Prosen
Datum zagovora: 7. 7. 2016

Maja ANTONIĆ
SINTEZA NEČISTOČ DIMETIL AMLODIPINA IN DIETIL AMLODIPINA
Mentor: izr. prof. dr. Franc Požgan
Datum zagovora: 28. 9. 2016

Karmen SIMONČIČ
ADSORPCIJA METANOJSKE, ETANOJSKE, PROPANOJSKE IN BUTANOJSKE KISLINE NA AKTIVNO OGLJE
Mentor: doc. dr. Miha Lukšič
Datum zagovora: 15. 9. 2016

Sabina JENSTERLE
SPREMLJANJE OKOLJSKIH PODATKOV Z RAZVOJNO PLOŠČICO ARDUINO
Mentor: doc. dr. Črtomir Podlipnik
Datum zagovora: 15. 9. 2016

Tanja BIZJAK
VISKOZNOST IN GOSTOTA VODNIH RAZTOPIN 1,2-DIMETILIMIDAZOLIJEVEGA KLORIDA
Mentorica: prof. dr. Marija Bešter Rogač
Datum zagovora: 12. 9. 2016

Katja KERT
TEMPERATURNA ODVISNOST NAVIDEZNIH MOLSKIH VOLUMNOV KOMPLEKSA MED DODECILTRIMETIL AMONIJEVIM KATIONOM IN POLIAKRILATNIM ANIONOM V ETANOLNIH RAZTOPINAH
Mentorica: prof. dr. Ksenija Kogej
Datum zagovora: 23. 9. 2016

Neža BREZOVAR
TEMPERATURNA ODVISNOST NAVIDEZNIH MOLSKIH VOLUMNOV KOMPLEKSA MED KATIONSKIM SURFAKTANTOM IN POLISTIRENSULFONATNIM ANIONOM V ETANOLNIH RAZTOPINAH
Mentorica: prof. dr. Ksenija Kogej
Datum zagovora: 8. 9. 2016

Alen HONSIĆ
POSKUSI PRIPRAVE MODIFICIRANIH DERIVATOV FULERENA C60
Mentor: izr. prof. dr. Janez Cerkovnik
Datum zagovora: 16. 9. 2016

Denis HONSIĆ
POSKUSI PRIPRAVE MODIFICIRANIH DERIVATOV FULERENA
Mentor: izr. prof. dr. Janez Cerkovnik
Datum zagovora: 16. 9. 2016

Domen ŽIGANTE
SINTEZA N-PROPARGILMALEIMIDA
Mentor: prof. dr. Darko Dolenc
Datum zagovora: 30. 6. 2016

Benjamin ODORČIĆ
AMIDIRANJA (S)-(2,2-DIMETIL-3-METILENCIKLOPENTIL) METANAMINA
Mentor: doc. dr. Uroš Grošelj
Datum zagovora: 3. 6. 2016

Katarina ŽAGAR
SINTEZA IN PRETVORBE B-KETO ESTRA PRIPRAVLJENEGA IZ Boc-Aib-OH
Mentor: doc. dr. Uroš Grošelj
Datum zagovora: 5. 9. 2016

Žiga BREGAR
VZDRŽEVANJE IN RAVNANJE Z NMR INŠTRUMENTOM
Mentor: prof. dr. Andrej Petrič
Datum zagovora: 6. 6. 2016

Anže JAKLIČ
SINTEZA IMINOV IZ ALDEHIDOV IN KETONOV
Mentor: izr. prof. dr. Bogdan Štefane
Datum zagovora: 25. 1. 2016

Gregor PAVEC
SINTEZA IN KARAKTERIZACIJA KINOKSALINSKIH DERIVATOV
Mentor: izr. prof. dr. Bogdan Štefane
Datum zagovora: 25. 1. 2016

Tomaž ZUPANČIČ
SINTEZA IN KARAKTERIZACIJA KOORDINACIJSKIH SPOJIN NIKLJA(II) S TIOCIANATNIM LIGANDOM IN 4-PIRIDINOLOM
Mentor: izr. prof. dr. Boris Čeh
Datum zagovora: 27. 9. 2016

Jaka ZEMLJAK
REAKCIJA MANGANOVEGA KLORIDA DIHIDRANTA IN PIPERAZINA
Mentorica: doc. dr. Saša Petriček
Datum zagovora: 29. 1. 2016

Tim KNIFIC
SINTEZA BAKROVIH(II) KOORDINACIJSKIH SPOJIN S KINALDINSKO KISLINO IN PIRIDINSKIMI LIGANDI
Mentorica: doc. dr. Barbara Modec
Datum zagovora: 1. 9. 2016

Pandi BUKLESKI
SINTEZA IN KARATKTERIZACIJA NEKATERIH AMINOMETILPIRIDINIJEVIH HEKSAFLUORIDOTITANATOV
Mentor: doc. dr. Andrej Pevec
Datum zagovora: 2. 9. 2016

Tina ŠIMUNOVIĆ
SPOJINE KOVIN ČETRTE PERIODE Z O-AMINOBENZATOM
Mentorica: doc. dr. Nives Kitanovski
Datum zagovora: 2. 9. 2016

Domen OTOREPEC
DOLOČITEV MINIMALNE VŽIGNE ENERGIJE LESNIH PRAHOV
Mentorica: doc. dr. Barbara Novosel
Datum zagovora: 9. 9. 2016

Martina PETELINC
NEVARNOST PRAŠNIH EKSPLOZIJ V FARMACEVTSKI INDUSTRIJI
Mentorica: doc. dr. Barbara Novosel
Datum zagovora: 9. 9. 2016

Sabrina ČERMELJ
TEMPERATURNA ODVISNOST KRITIČNEMICELNE KONCENTRACIJE SURFAKTANTA N-DODECILPIRIDINIJEVEGA KLORIDA, DOLOČENA S SPEKTROFOTOMETRIČNO METODO
Mentorica: prof. dr. Barbara Hribar Lee
Datum zagovora: 29. 9. 2016

Marko GAŠPERIČ
NOVI KATODNI MATERIALI ZA VISOKOTEMPERATURNE GORIVNE CELICE
Mentorica: doc. dr. Klementina Zupan
Datum zagovora: 29. 6. 2016

Sandi JAKLIČ
OPTIMIZACIJA SINTEZE ORGANSKIH LIGANDOV ZA PRIPRAVO CINKOVIH KOORDINACIJSKIH SPOJIN Z ANTIDIABETIČNIM DELOVANJEM
Mentor: izr. prof. dr. Franc Perdih
Datum zagovora: 15. 11. 2016

Žiga KASTELIC
TRANSFORMACIJE EVGENOLA Z RAZLIČNIMI REAGENTI
Mentor: izr. prof. dr. Franci Kovač
Datum zagovora: 23. 9. 2016

Draženko LONČAR
PRIPRAVA TH-SIMETRIČNIH HEKSASUBSTITUIRANIH DERIVATOV FULERENA C60
Mentor: izr. prof. dr. Janez Cerkovnik
Datum zagovora: 27. 9. 2016

Rok REMŠAK
REAKCIJE MED MODERNIMI MATERIALI ZA VISOKOTEMPERATURNE GORIVNE CELICE PRI POVIŠANIH TEMPERATURAH
Mentor: izr. prof. dr. Marjan Marinšek
Datum zagovora: 18. 5. 2016

Taja VODOPIVEC
PRIPRAVA IN ANALIZA TEHNOLOŠKE VODE
Mentorica: doc. dr. Barbara Novosel
Datum zagovora: 21. 10. 2016

Klemen VRBANČIČ
SINTEZA SREBROVIH KOORDINACIJSKIH SPOJIN Z BENZOATNIM IN 2,6-BIS(TRIFLUOROMETIL) BENZOATNIM LIGANDOM
Mentor: izr. prof. dr. Franc Perdih
Datum zagovora: 6. 10. 2016

Blaž FON
SINTEZA KURKUMINA MODIFICIRANEGA S PROPANOJSKO KISLINO
Mentor: prof. dr. Darko Dolenc
Datum zagovora: 1. 9. 2016

Lenart DEBELAK
ORGANOKATALIZIRANE REAKCIJE 1,3-DIKARBONILNIH SPOJIN Z ORTO-SUBSTITUIRANIMI DERIVATI TRANS-Â-NITROSTIRENA
Mentor: doc. dr. Uroš Grošelj
Datum zagovora: 13. 9. 2016

Janez JAVORNIK
PRIPRAVA NEKATERIH DERIVATOV BENZOTIAZOLA IN IZBRANE PRETVORBE
Mentor: izr. prof. dr. Franci Kovač
Datum zagovora: 9. 9. 2016

Eva ŠTRAKL
SUBSTITUIRANI 3-ACILAMINO-2H-PIRAN-2-ONI KOT DIENI V DIELS–ALDERJEVIH REAKCIJAH
Mentor: doc. dr. Krištof Kranjc
Datum zagovora: 16. 9. 2016

Peter SEBANC
ČIŠČENJE IN SUŠENJE NEKATERIH ORGANSKIH TOPIL
Mentor: prof. dr. Andrej Petrič
Datum zagovora: 5. 9. 2016

Karmen ŽBOGAR
SINTEZA VSEH IZOMEROV DINITROBENZENA
Mentor: prof. dr. Andrej Petrič
Datum zagovora: 19. 9. 2016

Gregor BORDON
UPORABA AZOMETIN IMINOV ZA SINTEZO BICIKLIČNIH HETEROCIKLOV
Mentor: prof. dr. Jurij Svete
Datum zagovora: 6. 9. 2016

Marjana VRHOVEC
SINTEZA CIKLIČNIH AZOMETIN IMINSKIH SUBSTRATOV
Mentor: izr. prof. dr. Bogdan Štefane
Datum zagovora: 16. 9. 2016

Maruša BREGAČ
REAKCIJE CINKOVEGA ALI KROMOVEGA KLORIDA Z MORFOLINOM
Mentorica: doc. dr. Saša Petriček
Datum zagovora: 26. 10. 2016

Daniela MIKIĆ
PRIPRAVA KOORDINACIJSKIH SPOJIN CINKA(II) S KINALDINATOM
Mentorica: doc. dr. Barbara Modec
Datum zagovora: 24. 10. 2016

Jaka ŠTURM
REAKCIJE MOLIDBENA(V) Z N,O-DONORSKIMI LIGANDI
Mentorica: doc. dr. Barbara Modec
Datum zagovora: 30. 11. 2016

Tilen SIMŠIČ
ELEKTROKROMNE LASTNOSTI NIKELJ-OKSIDNIH TANKIH PLASTI
Mentorica: doc. dr. Romana Cerc Korošec
Datum zagovora: 2. 9. 2016

Klavdija KOČNAR
VPLIV PARAMETROV V RAZTOPINI PLASMOCORINTHA B NA UČINKOVITOST NJEGOVE FOTOKATALITSKE RAZGRADNJE S TiO_2
Mentorica: doc. dr. Romana Cerc Korošec
Datum zagovora: 27. 9. 2016

Tina BREC
FAZNA ANALIZA RAZLIČNIH VZORCEV PUDRA Z RENTGENSKO PRAŠKOVNO DIFRAKCIJO
Mentorica: izr. prof. dr. Amalija Golobič
Datum zagovora: 2. 9. 2016

Tina Melisa ŠIMIČ
MANGANOVE SPOJINE Z 1-HIDROKSIBENZOTRIAZOLOM
Mentor: doc. dr. Bojan Kozlevčar
Datum zagovora: 31. 8. 2016

Patricia TANDARA
PIRIDINSKI DERIVATI TIOSECNINE KOT KATIONI V HEKSAFLUORIDOTITANATNIH SOLEH
Mentor: doc. dr. Andrej Pevec
Datum zagovora: 7. 9. 2016

Renata BEVEC
SINTEZE LIGANDOV IZ DIPIKOLINSKE KISLINE ZA VEZAVO NA CINKOVE IN VANADIJEVE IONE
Mentor: izr. prof. dr. Franc Perdih
Datum zagovora: 2. 9. 2016

Neža GARTNAR
RAZISKAVA PIROLIZNIH LASTNOSTI MESNO-KOSTNE MOKE
Mentorica: doc. dr. Marija Zupančič
Datum zagovora: 2. 9. 2016

Natalija PUCIHAR
PRODUKTI SOLVOTERMALNE SINTEZE Z 2-AMINOBENZOJSKO KISLINO
Mentorica: doc. dr. Nives Kitanovski
Datum zagovora: 16. 9. 2016

Nina ZALETEL
VPLIV pH RAZTOPINE BARVILA PLASMOCORINTH B NA NJEGOVO RAZGRADNJO
Mentorica: doc. dr. Irena Kozjek Škofic
Datum zagovora: 2. 9. 2016

Neja LOMBERGAR
ZMRZIŠČE, ZAŠČITA PRED ZMRZOVANJEM IN STRDIŠČE HLADILNIH TEKOČIN
Mentor: dr. Andrej Godec
Datum zagovora: 1. 9. 2016

Kaja PURKAT
LASTNOSTI RAZTOPIN KALCIJEVEGA HIDROKSIDA V RAZLIČNIH TOPILIH
Mentorica: prof. dr. Barbara Hribar Lee
Datum zagovora: 28. 9. 2016

Mojca ZALOKAR
TEMPERATURNA ODVISNOST TOPLOTNE KAPACITETE PLINOV
Mentor: prof. dr. Andrej Jamnik
Datum zagovora: 13. 9. 2016

Simona PUST
PROUČEVANJE INTERAKCIJ LEKTINA FIMH IN RASTLINSKIH POLIFENOLOV Z METODAMI MOLEKULSKEGA MODELIRANJA
Mentor: doc. dr. Črtomir Podlipnik
Datum zagovora: 21. 12. 2016

Urša SEDMAK
DOLOČEVANJE KLORIRANIH SPOJIN Z MIKROEKSTRAKCIJO NA TRDNO FAZO
Mentorica: prof. dr. Helena Prosen
Datum zagovora: 9. 9. 2016

Miha ŠEST
KVANTITATIVNO DOLOČANJE LIMONENA Z IR SPEKTROSKOPIJO
Mentor: izr. prof. dr. Mitja Kolar
Datum zagovora: 14. 9. 2016

Friderik ŠTENDLER
MEŠANJE IN SNOVNI PRENOS KISIKA V BIOREAKTORJIH ZA SUBMERZNO GOJENJE
Mentor: prof. dr. Aleksander Pavko
Datum zagovora: 9. 12. 2016

Evgen ZORC
REGULACIJA NAKLONA LAMEL BRISOLEJA NA NOVI STAVBI FKKT
Mentor: doc. dr. Janez Cerar
Datum zagovora: 25. 11. 2016

VARSTVO PRI DELU IN POŽARNO VARSTVO

Natalija HRASTOVEC
VZROKI NASTANKA VELIKIH KOLIČIN MEŠANIH KOMUNALNIH ODPADKOV V ZDRAVSTVENI USTANOVI
Mentor: doc. dr. Jože Šrekl
Datum zagovora: 28. 9. 2016

Bojan BORIŠEK
OCENA TVEGANJA PRI STRUŽNICI PRVOMAJSKA TN-TNP 250
Mentor: doc. dr. Boris Jerman
Somentor: doc. dr. Mitja Robert Kožuh
Datum zagovora: 23. 9. 2016

Luka ŠKARJA
GAŠENJE POŽAROV V VISOKIH STAVBAH
Mentor: izr. prof. dr. Matija Tomšič
Datum zagovora: 23. 9. 2016

Aleksander ŽAGAR
IZBOR SISTEMA ZA ODKRIVANJE POŽARA GLEDE NA PRIČAKOVANO VRSTO POŽARA IN VRSTO OBJEKTA
Mentor: doc. dr. Tomaž Hozjan
Datum zagovora: 26. 9. 2016

Darko STOLNIK
IZBOLJŠANJE VARNOSTI STROJA ZA PROIZVODNJO VALOVITEGA KARTONA
Mentor: doc. dr. Boris Jerman
Datum zagovora: 30. 9. 2016

Tilen BRECELJ
ERGONOMSKO OBLIKOVANO DELOVNO MESTO OPERATERJA DELOVNIH STROJEV IN KONTROLORJA KAKOVOSTI
Mentorica: prof. dr. Simona Jevšnik
Datum zagovora: 22. 9. 2016

Ivo LOZEJ
MERJENJE IN ZMANJŠEVANJE HRUPA V KOVINSKI PROIZVODNJI
Mentor: doc. dr. Mitja Robert Kožuh
Datum zagovora: 4. 3. 2016

Igor JUSTIN
ANALIZA IZPOSTALJENOSTI HRUPU IN SANACIJSKI UKREPI V PROIZVODNJI PIJAČ
Mentor: doc. dr. Mitja Robert Kožuh
Datum zagovora: 4. 3. 2016

Maja KOŽUH
SAMOSTOJNI PODJETNIK IN OCENA TVEGANJA
Mentor: doc. dr. Mitja Robert Kožuh
Datum zagovora: 26. 9. 2016

Tine MAZALOVIĆ
OCENA PROIZVODNJE IN KORISTNA UPORABA DEPONIJSKEGA PLINA NA DEPONIJI
Mentor: doc. dr. Mitja Robert Kožuh
Datum zagovora: 28. 9. 2016

Primož JAGRIČ
POŽARNA VARNOST V GUMARSKI INDUSTRIJI
Mentor: prof. dr. Simon Schnabl
Datum zagovora: 13. 6. 2016

Aljaž KRIŽMAN
OSEBNA VAROVALNA OPREMA PRI FORENZIČNIH PREISKAVAH POŽAROV
Mentor: izr. prof. dr. Matija Tomšič
Datum zagovora: 26. 9. 2016

Saša BAŽDAR
PROMOCIJA ZDRAVJA PRI DELU V DRUŽBI ELES D. O. O.
Mentor: doc. dr. Mitja Robert Kožuh
Datum zagovora: 21. 7. 2016

Vojko CIGAN
PREVOZ NEVARNEGA BLAGA V CESTNEM PROMETU
Mentorica: doc. dr. Barbara Novosel
Datum zagovora: 13. 6. 2016

Mateja KOCMAN
VARNOSTNI PREGLED DVEH SREDNJEŠOLSKIH LABORATORIJEV
Mentorica: doc. dr. Barbara Novosel
Datum zagovora: 5. 7. 2016

Zdenka PETERLE
NADZOR NAD OGLJIKOVIM MONOKSIDOM V OBJEKTIH - NORMATIVNE ZAHTEVE IN PRAKTIČNE IZVEDBE
Mentor: pred. dr. Aleš Jug
Datum zagovora: 5. 7. 2016

Milena HVALIČ ARHAR
OKVARA HRBTENICE IN GIBALNEGA SISTEMA PRI NEGOVALNEM OSEBJU
Mentor: prof. dr. Marjan Bilban
Datum zagovora: 5. 7. 2016

Lidija KUNŠIČ
MOŽNOST IZRABE BIOPLINA V OBČINI GORJE
Mentor: doc. dr. Mitja Robert Kožuh
Datum zagovora: 9. 9. 2016

Maja MLADENOVIĆ
VPLIV STRESA IN IZGORELOST NA MOTIVACIJO ZAPOSLENIH
Mentor: prof. dr. Marjan Bilban
Datum zagovora: 13. 7. 2016

Stanko MOČNIK
UPORABA ELEKTRIČNIH AGREGATOV V GASILSTVU
Mentor: pred. dr. Aleš Jug
Datum zagovora: 15. 7. 2016

Mojca BAHUN
PRESOJA ZDRAVEGA IN VARNEGA DELA V LABORATORIJU
Mentorica: doc. dr. Barbara Novosel
Datum zagovora: 2. 9. 2016

Blaž RAČNIK
RAVNANJE Z ODPADKI S STRATEGIJO BREZ ODPADKOV V SLOVENIJI
Mentor: doc. dr. Mitja Robert Kožuh
Datum zagovora: 2. 9. 2016

Mladen BJEGOJEVIĆ
NAVODILA ZA VARNO DELO, PREIZKUS ZNANJA, TER UPORABA OVO NA ZNAŠALNO ŠIVALNEM STROJU Müller Martini PRIMA
Mentor: prof. dr. Jože Horvat
Datum zagovora: 2. 9. 2016

Helena FRANK
VARNO DELO V MARKETU
Mentor: doc. dr. Mitja Robert Kožuh
Datum zagovora: 2. 9. 2016

Alan RATNIK
ANALIZA ZDRAVJA IN POČUTJA TAKSI VOZNIKOV ZARADI DELOVNEGA MESTA
Mentor: prof. dr. Marjan Bilban
Datum zagovora: 2. 9. 2016

Janko SEKNE
PRAKTIČNA UPORABA POŽARNIH NAČRTOV PRI GASILCIH V REPUBLIKI SLOVENIJI
Mentor: doc. dr. Jože Šrekl
Datum zagovora: 5. 9. 2016

Igor KRAJNC
OPERATER PREDVAJANJA PROGRAMA
Mentor: doc. dr. Jože Šrekl
Datum zagovora: 5. 9. 2016

Marko RUŽIČ
OBVLADOVANJE TVEGANJA PRI DELU Z NEVARNIMI SNOVMI V TISKARNI
Mentorica: doc. dr. Barbara Novosel
Datum zagovora: 5. 9. 2016

Miha KUKOVICA
SAMOVŽIG LESNE BIOMASE
Mentor: doc. dr. Jože Šrekl
Datum zagovora: 9. 9. 2016

Mateja MALAVAŠIČ
ERGONOMSKO OBLIKOVANJE DELOVNEGA MESTA NATAKARJA
Mentorica: doc. dr. Klementina Zupan
Datum zagovora: 9. 9. 2016

Marinko MAKSIMOVIČ
UPORABA NEVARNIH KEMIKALIJ V GRADBENIŠTVU
Mentorica: doc. dr. Barbara Novosel
Datum zagovora: 9. 9. 2016

Mitja PLANINŠEK
VARNOSTNI UKREPI PRI SKLADIŠČENJU IN DISTRIBUCIJI GORIV
Mentor: doc. dr. Mitja Robert Kožuh
Datum zagovora: 9. 9. 2016

Ivica ĆOSIĆ
ZBIRANJE, ODDAJANJE IN PREDELAVA ELEKTRONSKIH ODPADKOV
Mentor: doc. dr. Mitja Robert Kožuh
Datum zagovora: 15. 9. 2016

Tinka KERN
ZAGOTAVLJANJE VARNOSTI DELOVNE OPREME
Mentor: doc. dr. Boris Jerman
Datum zagovora: 15. 9. 2016

Vesna MARKOVIĆ
VARNOST VODOVODNIH SISTEMOV
Mentor: doc. dr. Mitja Robert Kožuh
Datum zagovora: 15. 9. 2016

Nejc PLEČKO
MIKROPLASTIKA V OKOLJU
Mentor: doc. dr. Mitja Robert Kožuh
Datum zagovora: 16. 9. 2016

Ervin MUJKIĆ
GRADBENO DOVOLJENJE ZA DEPONIJE
Mentor: doc. dr. Mitja Robert Kožuh
Datum zagovora: 16. 9. 2016

Luka BALAS
ANALIZA VŽIGA KOMPRESORJA
Mentorica: doc. dr. Barbara Novosel
Datum zagovora: 21. 9. 2016

Dušan ŠUKLJE
SREDSTVA ZA PASIVIZACIJO V SPECIALNI ENOTI SLOVENSKE POLICIJE
Mentorica: doc. dr. Barbara Novosel
Datum zagovora: 21. 9. 2016

Alenka KOS
IZPOSTAVLJENOST DELAVCA OGLJIKOVEMU OKSIDU MED VARJENJEM
Mentorica: doc. dr. Barbara Novosel
Datum zagovora: 22. 9. 2016

Valentina KOLMAN
ANALIZA INTERVENCIJ PGD ŠKOFJA VAS
Mentor: prof. dr. Simon Schnabl
Datum zagovora: 22. 9. 2016

Tanja VIDMAR
STALIŠČA DO RABE ALKOHOLA NA DELOVNEM MESTU V MIKRO IN MALIH PODJETJIH NA DOLENJSKEM
Mentorica: doc. dr. Marija Molan
Datum zagovora: 22. 9. 2016

Sandi LEPOŠA
OBREMENJENOST SLOVENSKIH POKLICNIH GASILCEV
Mentorica: doc. dr. Marija Molan
Datum zagovora: 22. 9. 2016

Maja ROJC
VPLIV PSIHOSOCIALNIH TVEGANJ NA ZAPOSLENE V PODJETJU KOLEKTOR ETRA
Mentorica: doc. dr. Marija Molan
Datum zagovora: 22. 9. 2016

Zoran MAČKOVIĆ
PSIHOSOCIALNA TVEGANJA IN OBVLADOVANJE LE TEH V KOVINSKI IN ELEKTRO INDUSTRIJI TER V INDUSTRIJI KOVINSKIH MATERIALOV IN LIVARN
Mentorica: doc. dr. Marija Molan
Datum zagovora: 22. 9. 2016

Bojan POLAJŽER
USKLAJENOST OTROŠKIH IGRAL Z VARNOSTNIMI PREDPISI
Mentor: doc. dr. Jože Šrekl
Datum zagovora: 23. 9. 2016

Nuša DROBNAK
OSEBNA VAROVALNA OPREMA V KROVSTVU
Mentor: izr. prof. dr. Matija Tomšič
Datum zagovora: 23. 9. 2016

Miha LEVEC
POŽARNA VARNOST V DOMOVIH STAREJŠIH OBČANOV
Mentor: prof. dr. Simon Schnabl
Datum zagovora: 23. 9. 2016

Rudolf VOLČINI
POŽARNA VARNOST V INDUSTRIJI PREMAZOV
Mentor: prof. dr. Simon Schnabl
Datum zagovora: 23. 9. 2016

Zdenko ZUPAN
POŽARNA VARNOST V PLANINSKIH KOČAH
Mentor: prof. dr. Simon Schnabl
Datum zagovora: 23. 9. 2016

Matej TURK
RAČUNALNIŠKI MODELI ZA IZRAČUN TOKSIČNOSTI KEMIJSKIH SPOJIN
Mentor: doc. dr. Črtomir Podlipnik
Datum zagovora: 26. 9. 2016

Rok SEVER
ZMANŠEVANJE TVEGANJA ZA NASTANEK PRAŠNE EKSPLOZIJE PRI PRAŠNEM LAKIRNJU
Mentorica: doc. dr. Barbara Novosel
Datum zagovora: 26. 9. 2016

Matija GOMILAR
SANACIJA SISTEMA ČIŠČENJA ODPADNIH VOD IZ PROIZVODNJE TEHNIČNE KERAMIKE
Mentor: doc. dr. Mitja Robert Kožuh
Datum zagovora: 26. 9. 2016

Matej PRELEC
OBRATOVANJE KOMUNALNE ČISTILNE NAPRAVE
Mentor: doc. dr. Mitja Robert Kožuh
Datum zagovora: 26. 9. 2016

Robert MIHELČIČ
STATISTIKA NEZGOD PRI DELU V PODJETJU ZA PROIZVODNJO SLAŠČIC IN PEKOVSKEGA PECIVA
Mentor: doc. dr. Jože Šrekl
Datum zagovora: 26. 9. 2016

Gordana DOBRIHA
VARNOST ELEKTRIČNE PEČI ZA TALJENJE STEKLA
Mentor: doc. dr. Boris Jerman
Datum zagovora: 26. 9. 2016

Andraž SLAK
TRDNI DELCI IN NJIHOVI VPLIVI NA OKOLJE IN NA ZDRAVJE LJUDI
Mentorica: prof. dr. Marija Bešter Rogač
Datum zagovora: 27. 9. 2016

Daniel RADONIĆ
ANALIZA IN OPREDELITEV ONESNAŽEVANJA ZRAKA NA PRIMERU LONDONA
Mentor: doc. dr. Mitja Robert Kožuh
Datum zagovora: 28. 9. 2016

Jože DERNAČ
HRUP V PROIZVODNJI PAPIRNATIH VREČK
Mentor: doc. dr. Mitja Robert Kožuh
Datum zagovora: 28. 9. 2016

Igor ŠTEBLAJ
ANALIZA VARNOSTI VERTIKALNIH IN HORIZONTALNIH OPAŽEV VISOKIH OBJEKTOV
Mentor: prof. dr. Simon Schnabl
Datum zagovora: 28. 9. 2016

Miha PEČENIK
NESREČE NA NAFTNIH PLOŠČADIH IN NJIHOV VPLIV NA OKOLJE NA JADRANU
Mentor: doc. dr. Mitja Robert Kožuh
Datum zagovora: 28. 9. 2016

Mateja ŠTEFANČIČ
PREGLED METOD IZOBRAŽEVANJA IN USPOSABLJANJA MLADIH V GASILSTVU
Mentor: prof. dr. Simon Schnabl
Datum zagovora: 28. 9. 2016

Klemen ŠKRJANEC
ANALIZA POŽARNE VARNOSTI OBJEKTA NA MESTNEM TRGU V ŠKOFJI LOKI
Mentor: prof. dr. Simon Schnabl
Datum zagovora: 28. 9. 2016

Jerneja KOZOROG
VARNO IN ZELENO DELOVNO OKOLJE V PISARNI
Mentorica: doc. dr. Klementina Zupan
Datum zagovora: 28. 9. 2016

Aleksander VRABIČ
PROBLEMATIKA HRUPA V LESNI INDUSTRIJI
Mentor: doc. dr. Mitja Robert Kožuh
Datum zagovora: 28. 9. 2016

Igor SAMOTORČAN
VARNOSTNI UKREPI PRI POLNJENJU, TESTIRANJU IN ROKVANJU S TLAČILNIMI POSODAMI
Mentorica: doc. dr. Barbara Novosel
Datum zagovora: 28. 9. 2016

Erika POTRČ HRIBAR
PREGLED PREVENTIVNIH UKREPOV OMEJEVANJA POŽAROV V NARAVNEM OKOLJU
Mentor: prof. dr. Simon Schnabl
Datum zagovora: 29. 9. 2016

Dijana PETKOVIĆ
ANALIZA POŽARNE VARNOSTI V DOMU STAREJŠIH OBČANOV
Mentor: prof. dr. Simon Schnabl
Datum zagovora: 29. 9. 2016

Anita ČUK
POZNAVANJE ZAPOSLENIH GLEDE VARSTVA IN ZDRAVJA PRI DELU V MESTNI OBČINI LJUBLJANA
Mentor: doc. dr. Jože Šrekl
Datum zagovora: 29. 9. 2016

Martina KERMAVNER KOLMAN
PREPREČEVANJE ZDRAVSTVENIH TEŽAV SKOZI CELOTNO POKLICNO ŽIVLJENJE
Mentor: doc. dr. Jože Šrekl
Datum zagovora: 29. 9. 2016

Nina Mirjam MATKOVIČ
OBREMENITVE VZGOJITELJIC NA DELOVNEM MESTU
Mentor: doc. dr. Jože Šrekl
Datum zagovora: 29. 9. 2016

Igor KOSI
VARNOST IN ZDRAVJE PRI DELU PRI MONTAŽI BETONSKIH KONSTRUKCIJSKIH ELEMENTOV
Mentor: doc. dr. Jože Šrekl
Datum zagovora: 29. 9. 2016

Mario MAJKIĆ
VPLIV DELOVNIH POGOJEV NA ZDRAVJE GRADBENIH DELAVCEV
Mentor: doc. dr. Domen Kušar
Datum zagovora: 29. 9. 2016

Nina KOTNIK
VPETOST JEDRSKE ELEKTRARNE V LOKALNO SKUPNOST
Mentor: doc. dr. Mitja Robert Kožuh
Datum zagovora: 29. 9. 2016

Robert TIVADAR
DVIG VARNOSTNE KULTURE PRI ROKOVANJU Z OROŽJEM
Mentor: doc. dr. Jože Šrekl
Datum zagovora: 29. 9. 2016

Mojca BARIČIČ
NIZKOTEMPERATURNI SISTEMI
Mentor: doc. dr. Mitja Robert Kožuh
Datum zagovora: 29. 9. 2016

Brigita BARIČIČ
RAVNANJE Z ODPADKI V OBČINI ILIRSKA BISTRICA
Mentor: doc. dr. Mitja Robert Kožuh
Datum zagovora: 29. 9. 2016

Aleš VOVK
VARNO DELO S KEMIČNIMI SNOVMI V AVTOLIČARSKI DELAVNICI
Mentorica: doc. dr. Barbara Novosel
Datum zagovora: 29. 9. 2016

Barbara PUC
CELOVITO RAVNANJE Z ODPADKI
Mentor: doc. dr. Mitja Robert Kožuh
Datum zagovora: 29. 9. 2016

Barbara DERNAČ
RAVNANJE Z ODPADKI V MANJŠI OBČINI
Mentor: doc. dr. Mitja Robert Kožuh
Datum zagovora: 29. 9. 2016

Blaž FINK
POTENCIALNE NEVARNOSTI PRI MANIPULACIJI IN HRAMBI NAFTNIH DERIVATOV
Mentor: doc. dr. Mitja Robert Kožuh
Datum zagovora: 29. 9. 2016

Ajša TOLA
OBNOVLJIVI VIRI ENERGIJE V SLOVENIJI IN NJIHOVA UPORABA
Mentor: doc. dr. Mitja Robert Kožuh
Datum zagovora: 29. 9. 2016

Anton TEGELJ
ANALIZA SISTEMA RAVNANJA Z OKOLJEM EMAS IN NJEGOVA UPORABA V AVTOKLEPARSKEM PODJETJU
Mentor: doc. dr. Mitja Robert Kožuh
Datum zagovora: 29. 9. 2016

Mateja SAVŠEK
INTERVENCIJSKA TOLERAČNA VREDNOST
Mentorica: doc. dr. Barbara Novosel
Datum zagovora: 30. 9. 2016

Klemen AVBELJ
NEZGODA DEEPWATER HORIZON V MEHIŠKEM ZALIVU
Mentor: doc. dr. Mitja Robert Kožuh
Datum zagovora: 30. 9. 2016

Janez GERČAR
IZVAJANJE VARNOSTNIH MERITEV NA ELEKTRIČNIH STROJIH
Mentor: pred. dr. Grega Bizjak
Datum zagovora: 30. 9. 2016

Herman PEČEVNIK
OBREMENITVE DELOVNEGA OKOLJA NA DELAVCA V KOVINO OBDELOVALNEM OBRATU
Mentor: doc. dr. Mitja Robert Kožuh
Datum zagovora: 30. 9. 2016

Roman KURALT
PROBLEMATIKA PREUREJANJA MANJŠIH NESTANOVANJSKIH KMETIJSKIH STAVB V INDUSTRIJSKE STAVBE Z VIDIKA POŽARNE VARNOSTI
Mentor: doc. dr. Domen Kušar
Datum zagovora: 30. 9. 2016

Iva PERČIĆ
RAVNANJE Z ODPADKI V ZDRAVSTVU
Mentor: doc. dr. Mitja Robert Kožuh
Datum zagovora: 30. 9. 2016

Robert TEŽAK
VOŽNJA VOZIL S PREDNOSTJO
Mentor: pred. dr. Aleš Jug
Datum zagovora: 30. 9. 2016

Branislav ORLIĆ
RAZISKAVE POŽAROV
Mentor: doc. dr. Tomaž Hozjan
Datum zagovora: 30. 9. 2016

UNIVERZA V MARIBORU
FAKULTETA ZA KEMIJO IN KEMIJSKO TEHNOLOGIJO

1. januar – 31. december 2016

DOKTORATI

ENOVIT DOKTORSKI ŠTUDIJ

Gregor FERK
SINTEZA IN KARAKTERIZACIJA MAGNETNIH NANODELCEV ZA UPORABO V SAMOREGULATIVNI MAGNETNI HIPERTERMIJI
Mentor: red. prof. dr. Miha Drofenik
Datum zagovora: 5. 7. 2016

Albin MATAVŽ
VPLIV STARANJA NA MEHANSKE LASTNOSTI SMOLNO VEZANIH BRUSOV S KORUNDNIMI IN SiC ZRNI
Mentor: izr. prof. dr. Darko Goričanec
Somentor: red. prof. dr. Jurij Krope
Datum zagovora: 25. 8. 2016

Nataša SOVIČ
OCENA KAKOVOSTI PODATKOV PRIDOBLJENIH V PROGRAMIH SPREMLJANJA PODZEMNIHVOD IN UPORABA KEMOMETRIJSKIH METOD ZA DOLOČITEV MERILNIH MEST
Mentorica: red. prof. dr. Darinka Brodnjak-Vončina
Somentor: dr. Mitja Kolar
Datum zagovora: 15. 6. 2016

Janez ŽLAK
OKOLJSKO SPREJEMLJIVA ENERGIJSKA IZRABA MULJA KOMUNALNIH ČISTILNIH NAPRAV
Mentor: red. prof. dr. Jurij Krope
Somentor: izr. prof. dr. Darko Goričanec
Datum zagovora: 12. 7. 2016

DOKTORSKI ŠTUDIJ

Marko AGREŽ
SIMULACIJA UPLINJANJA ENERGENTOV ZA PROIZVODNJO ENERGIJE IN SINTETIČNIH GORIV
Mentor: izr. prof. dr. Darko Goričanec
Somentor: red. prof. dr. Jurij Krope
Datum zagovora: 2. 9. 2016

Janja MAJER
SINTEZA IN FUNKCIONALIZACIJA MAKROPOROZNIH POLIAKRILATOV
Mentor: red. prof. dr. Peter Krajnc
Datum zagovora: 27. 9. 2016

DOKTORSKI ŠTUDIJ – 3. stopnja

Darija CÖR
EKSTRAKCIJE BIOLOŠKIH MATERIALOV S SUBKRITIČNIMI IN SUPERKRITIČNIMI FLUIDI
Mentor: red. prof. dr. Željko Knez
Somentorica: red. prof. dr. Mojca Škerget
Datum zagovora: 20. 4. 2016

Urban FEGUŠ
RAZVOJ PILOTNE NAPRAVE ZA ENKAPSULACIJO AROMATIČNIH SUBSTANC V TALINO OGLJIKOVIH HIDRATOV Z UPORABO VISOKOTLAČNEGA HOMOGENIZATORJA
Mentor: red. prof. dr. Željko Knez
Datum zagovora: 15. 7. 2016

Jernej HOSNAR
REKONSTRUKCIJSKI PRINCIPI IN STRATEŠKE ODLOČITVE V OBSTOJEČIH INDUSTRIJSKIH PROCESIH
Mentorica: doc. dr. Anita Kovač Kralj
Somentor: red. prof. dr. Zdravko Kravanja
Datum zagovora: 28. 6. 2016

Maja LEŠNIK
MEHANIZEM DOPIRANJA ULTRAFINEGA RUTILNEGA TiO_2 ZA SPREMINJANJE FOTOKATALITSKE AKTIVNOSTI
Mentor: red. prof. dr. Miha Drofenik
Datum zagovora: 20. 9. 2016

Matej RAVBER
SUBKRITIČNA VODA KOT ZELENI MEDIJ ZA EKSTRAKCIJO IN PROCESIRANJE NARAVNIH MATERIALOV
Mentor: red. prof. dr. Mojca Škerget
Somentor: red. prof. dr. Željko Knez
Datum zagovora: 6. 6. 2016

Jana SIMONOVSKA
OLEORESINI IZ RDEČE PEKOČE PAPRIKE – EKSTRAKCIJA IN UPORABA
Mentor: red. prof. dr. Željko Knez
Somentorica: red. prof. dr. Mojca Škerget
Datum zagovora: 21. 10. 2016

Nina TRUPEJ
TERMODINAMSKE IN TRANSPORTNE LASTNOSTI SISTEMOV POLIMEROV IN BIOLOŠKO AKTIVNIH SPOJIN S SUPERKRITIČNIMI FLUIDI
Mentor: red. prof. dr. Željko Knez
Somentorica: red. prof. dr. Mojca Škerget
Datum zagovora: 20. 5. 2016

MAGISTRSKI ŠTUDIJ

MAGISTRSKI ŠTUDIJ

Andrej CAF
IZKORIŠČANJE NIZKOTEMPERATURNIH VIROV ENERGIJE PLINSKIH KOGENERACIJSKIH MOTORJEV
Mentor: izr. prof. dr. Darko Goričanec
Somentor: red. prof. dr. Jurij Krope
Datum zagovora: 27. 9. 2016

Vanja FORJAN
RAZVOJ, VALIDACIJA IN PRIMERJAVA BIOANALIZNIH METOD HPLC IN LC-MS/MS ZA DOLOČANJE KANDESARTANA V HUMANI PLAZMI
Mentorica: red. prof. dr. Darinka Brodnjak-Vončina
Somentorica: red. prof. dr. Helena Prosen
Datum zagovora: 8. 7. 2016

Dušica IFKO
PRIPRAVA MAGNETNIH ZAMREŽENIH ENCIMSKIH SKUPKOV IZ ENCIMA CELULAZA IN OPTIMIRANJE PARAMETROV
Mentorica: red. prof. dr. Maja Leitgeb
Datum zagovora: 26. 9. 2016

Bojana KRAJNC GALUNDER
KEMIJSKA ANALIZA IN KEMOMETRIJSKA KARAKTERIZACIJA KVALITETE VODE REKE MURE
Mentorica: red. prof. dr. Darinka Brodnjak-Vončina
Somentor: dr. Mitja Kolar
Datum zagovora: 27. 9. 2016

Gorazd PECKO ŠKOF
SINTEZA SEPARACIJSKIH PROCESOV ZA ČIŠČENJE ODPADNIH OLJNIH EMULZIJ
Mentor: red. prof. dr. Zdravko Kravanja
Somentorica: red. prof. dr. Zorka Novak Pintarič
Datum zagovora: 30. 9. 2016

Metka PEŠL
ODZIVNE FUNKCIJE IN TOPLOTNI VPLIV RAZLIČNIH KONFIGURACIJ VERTIKALNIH TOPLOTNIH PRENOSNIKOV V VRTINI V SISTEMIH ZEMELJSKIH TOPLOTNIH ČRPALK
Mentor: izr. prof. dr. Darko Goričanec
Somentor: red. prof. dr. Jurij Krope
Datum zagovora: 12. 7. 2016

Sašo POBERŽNIK
VSEŽIVLJENJSKO VREDNOTENJE STROŠKOV ENERGIJE PRI KLASIČNO IN TRAJNOSTNO NARAVNANI GRADNJI STANOVANJSKEGA OBJEKTA
Mentor: red. prof. dr. Jurij Krope
Somentor: izr. prof. dr. Darko Goričanec
Datum zagovora: 12. 7. 2016

David ŠIROVNIK
SINTEZA SISTEMOV Z MAKSIMIRANJEM TRAJNOSTNE NETO SEDANJE VREDNOSTI
Mentor: red. prof. dr. Zdravko Kravanja
Somentorica: doc. dr. Lidija Čuček
Datum zagovora: 30. 9. 2016

Lidija ŠKODIČ
ČIŠČENJE ODPADNIH TEKSTILNIH VOD Z UV/H_2O_2 POSTOPKOM
Mentorica: red. prof. dr. Darinka Brodnjak-Vončina
Somentorica: red. prof. dr. Alenka Majcen Le Marechal
Datum zagovora: 27. 9. 2016

Andreja ZEMLJIČ
UČINKOVITA RABA ENERGIJE V KLIMATIZACIJSKIH SISTEMIH
Mentor: izr. prof. dr. Darko Goričanec
Somentor: red. prof. dr. Jurij Krope
Datum zagovora: 27. 9. 2016

MAGISTRSKI ŠTUDIJ – 2. stopnja

Filip AMBROŽ
RAZVOJ ELEKTROKEMIJSKEGA ČIPA ZA IN-SITU PROIZVODNJO AKTIVNEGA KLORA
Mentor: doc. dr. Matjaž Finšgar
Somentorica: doc. dr. Irena Ban
Datum zagovora: 1. 9. 2016

Klara BIGEC
FORMULACIJA BIOLOŠKO AKTIVNIH UČINKOVIN S SUPERKRITIČNIMI FLUIDI
Mentor: red. prof. dr. Željko Knez
Somentorica: doc. dr. Maša Knez Hrnčič
Datum zagovora: 21. 9. 2016

Selena BOŠNJAK
OKSALATI IMOBILIZIRANI NA VINILBENZIL KLORIDNI NOSILEC
Mentor: izr. prof. dr. Jernej Iskra
Somentor: red. prof. dr. Peter Krajnc
Datum zagovora: 7. 9. 2016

Mitja BUKOVEC
ANALIZA EMAJLIRANEGA NERJAVNEGA JEKLA
Mentor: doc. dr. Matjaž Finšgar
Somentorica: red. prof. dr. Andreja Goršek
Datum zagovora: 21. 9. 2016

Alja GABOR
IZRAŽANJE GENOV TNFAIP6, S100A8, IL-11, G0S2 IN S100A9 V KRVNIH LIMFOCITIH IN ČREVESNI SLUZNICI BOLNIKOV S CROHNOVO BOLEZNIJO KOT NAPOVEDNI BIOOZNAČEVALEC ODZIVA NA ZDRAVLJENJE Z ADALIMUMABOM
Mentor: red. prof. dr. Uroš Potočnik
Somentor: mag. Peter Skok
Datum zagovora: 1. 9. 2016

Natalija GRAH
ANALIZA AMINOV NA JEKLU
Mentor: doc. dr. Matjaž Finšgar
Somentorica: izr. prof. dr. Regina Fuchs Godec
Datum zagovora: 7. 9. 2016

Kaja GROBELNIK
AKTIVNOST ENCIMOV IZ WALLEMIE ICHTHYOPHAGE PO IZPOSTAVITVI V SC CO2
Mentorica: doc. dr. Mateja Primožič
Somentorica: red. prof. dr. Maja Leitgeb
Datum zagovora: 17. 2. 2016

Jasna GROMAN
RAZVOJ METODE ZA VODENO SPROŠČANJE OGLJIKOVEGA DIOKSIDA MED FERMENTACIJO PROBIOTIČNEGA NAPIKA
Mentorica: red. prof. dr. Andreja Goršek
Somentorica: doc. dr. Darja Pečar
Datum zagovora: 17. 2. 2016

Mateja GRUŠOVNIK
MAKROPOROZNI POLIMERI IZ KROGLIČNIH ŠABLON
Mentor: red. prof. dr. Peter Krajnc
Somentorica: asist. dr. Muzafera Paljevac
Datum zagovora: 23. 2. 2016

Doroteja GSELMAN
GENOTIPIZACIJA SLOVENSKIH BOLNIKOV Z REVMATOIDNIM ARTRITISOM ZA DNA POLIMORFIZME PREDHODNO POVEZANE Z BOLEZNIJO V ASOCIACIJSKIH ŠTUDIJAH V CELOTNEM GENOMU
Mentor: red. prof. dr. Uroš Potočnik
Somentor: izr. prof. dr. Artur Pahor
Datum zagovora: 1. 9. 2016

Ivana HOHNJEC
DOLOČANJE OSTANKOV PESTICIDOV V RIBAH IN ŠKOLJKAH S PLINSKO KROMATOGRAFIJO IN MASNO SPEKTROMETRIJO
Mentorica: red. prof. dr. Darinka Brodnjak-Vončina
Somentor: dr. Mitja Kolar
Datum zagovora: 23. 3. 2016

Neja HROVAT
UPORABA ZEOLITOV IN RAZVOJ ANALIZNIH METOD ZA SPREMLJANJE UČINKOVITOSTI ČIŠČENJA KOMUNALNIH ODPADNIH VOD
Mentor: doc. dr. Matjaž Finšgar
Somentorica: Mojca Poberžnik
Datum zagovora: 21. 9. 2016

Maša IRŠIČ
VPLIV RAZLIČNIH NAČINOV PREDOBDELAVE SUROVE CELULOZE NA UČINKOVITOST ENCIMSKE HIDROLIZE
Mentorica: doc. dr. Darja Pečar
Somentorica: red. prof. dr. Andreja Goršek
Datum zagovora: 13. 7. 2016

Mirjana JEREMIĆ
ODSTRANJEVANJE ATRAZINA IZ PITNE VODE Z VLAKNI IZ AKTIVNEGA OGLJA
Mentorica: izr. prof. dr. Marjana Simonič
Somentorica: red. prof. dr. Andreja Goršek
Datum zagovora: 21. 12. 2016

Gregor JEZERNIK
VPLIV POLIMORFIZMOV V CELOTNEM GENOMU NA PROFILE MAŠČOBNIH KISLIN PRI BOLNIKIH S KRONIČNO VNETNO ČREVESNO BOLEZNIJO
Mentor: red. prof. dr. Uroš Potočnik
Somentorica: doc. dr. Katja Repnik
Datum zagovora: 1. 9. 2016

Kaja KAJZER
VPLIV SC CO_2 NA ODPIRANJE CELIC ČRNE KVASOVKE PHAEOTHECA TRIANGULARIS
Mentorica: doc. dr. Mateja Primožič
Somentorica: red. prof. dr. Maja Leitgeb
Datum zagovora: 23. 3. 2016

Monika KOROŠA
FERMENTACIJA SIROTKE Z NARAVNO STARTER KULTURO
Mentorica: red. prof. dr. Andreja Goršek
Somentorica: doc. dr. Darja Pečar
Datum zagovora: 31. 9. 2016

Alja KOŠTOMAJ
MERJENJE PORAZDELITVE IN VELIKOSTI DELCEV TiO_2 PIGMENTA Z APARATURO MASTERSIZER 3000
Mentorica: doc. dr. Irena Ban
Somentor: doc. dr. Matjaž Kristl
Datum zagovora: 21. 9. 2016

Lucija KRIŽNIK
RAZLIČNE TEHNIKE IMOBILIZACIJE ENCIMA α- GALAKTOZIDAZE
Mentorica: red. prof. dr. Maja Leitgeb
Somentorica: doc. dr. Mateja Primožič
Datum zagovora: 23. 3. 2016

Žiga KVAR
VPLIV NUKLEATORJEV NA LASTNOSTI POLIPROPILENA
Mentorica: red. prof. dr. Andreja Goršek
Somentor: IZTOK ŠVAB
Datum zagovora: 21. 9. 2016

Aleš LORBER
PRIPRAVA ODPADNE VODE ZA PONOVNO UPORABO V TEHNOLOŠKEM PROCESU
Mentorica: izr. prof. dr. Marjana Simonič
Somentorica: red. prof. dr. Zorka Novak Pintarič
Datum zagovora: 21. 12. 2016

Evelina MOHORKO
RAZVOJ IN VALIDACIJA PLINSKIH SENZORJEV ZA MEDICINSKE APLIKACIJE
Mentor: dr. Mitja Kolar
Somentor: Andrej Holobar
Datum zagovora: 20. 1. 2016

Petra NOVINA
IZOLACIJA ANTIOKSIDANTOV IZ JABOLK
Mentor: red. prof. dr. Željko Knez
Somentorica: red. prof. dr. Mojca Škerget
Datum zagovora: 23. 3. 2016

Barbara PETOVAR
ELEKTROKEMIJSKA IN POVRŠINSKA ANALIZA AZOLOV NA JEKLU
Mentor: doc. dr. Matjaž Finšgar
Somentor: izr. prof. dr. Urban Bren
Datum zagovora: 17. 2. 2016

Tjaša PETROVIČ
SIMULACIJE IN OPTIMIZACIJE ODSTRANJEVANJA HLAPNIH ORGANSKIH SNOVI IZ ODPADNIH TOKOV
Mentorica: red. prof. dr. Zorka Novak Pintarič
Somentorica: red. prof. dr. Mojca Škerget
Datum zagovora: 17. 2. 2016

Darja PREDIKAKA
SINTEZA IN KARAKTERIZACIJA BIOOGLJA PRIDOBLJENEGA IZ RAZLIČNIH VRST ODPADNE BIOMASE S SUBKRITIČNO VODO
Mentorica: red. prof. dr. Mojca Škerget
Somentor: red. prof. dr. Željko Knez
Datum zagovora: 22. 6. 2016

Saša PUŠAVER
DOLOČANJE IZBRANIH MONOSAHARIDOV V EKSOPOLISAHARIDIH S PLINSKO KROMATOGRAFIJO IN MASNO SPEKTROMETRIJO
Mentor: doc. dr. Matjaž Finšgar
Somentorica: doc. dr. Maša Islamčević Razboršek
Datum zagovora: 23. 3. 2016

Barbara SITAR
ODSTRANJEVANJE CINKA IN BAKRA IZ VODE Z MODIFICIRANIMI VLAKNI IZ AKTIVNEGA OGLJA
Mentorica: izr. prof. dr. Marjana Simonič
Somentorica: red. prof. dr. Lidija Fras Zemljič
Datum zagovora: 23. 3. 2016

Violeta TRAJKOVSKA
MODELIRANJE ZA HITRO OCENJEVANJE POSLEDIC KEMIJSKIH NESREČ
Mentorica: red. prof. dr. Zorka Novak Pintarič
Somentor: doc. dr. Matjaž Finšgar
Datum zagovora: 23. 11. 2016

Jožica ULČNIK
HIDROLIZA GLIKOZIDNO VEZANIH ANTIOKSIDANTOV V ČEBULNEM EKSTRAKTU S SUBKRITIČNO VODO
Mentorica: red. prof. dr. Mojca Škerget
Somentor: red. prof. dr. Željko Knez
Datum zagovora: 13. 7. 2016

Sabina VERBUČ
SINTEZE KOORDINACIJSKIH SPOJIN Co, Cu, Ni IN NEKATERIH LANTANOIDOV Z MEŠANIMI N-DONORSKIMI LIGANDI: AMINOPIRIDINI IN PIKOLINSKO KISLINO
Mentor: doc. dr. Matjaž Kristl
Somentorica: doc. dr. Irena Ban
Datum zagovora: 17. 2. 2016

Nika VERDELJ
RAZVOJ IN VALIDACIJA SPEKTROFOTOMETRIČNE METODE ZA DOLOČANJE BORA V REALNIH VZORCIH TAL IN RASTLINSKIH TKIV
Mentor: doc. dr. Jože Košir
Somentor: dr. Mitja Kolar
Datum zagovora: 21. 9. 2016

Tadeja VOLAUŠEK
OCENA MOŽNOSTI ONESNAŽENJA TAL IN PODZEMNE VODE NA OBMOČJU NAPRAVE S KEMIČNO NEKOVINSKO PROIZVODNJO
Mentorica: red. prof. dr. Zorka Novak Pintarič
Somentor: doc. dr. Matjaž Finšgar
Datum zagovora: 1. 9. 2016

Marko ŽIŽEK
ANALIZA SISTEMOV ZA DOSTAVO ZDRAVILNIH UČINKOVIN IZ MEDICINSKIH IMPLANTATOV
Mentor: doc. dr. Matjaž Finšgar
Somentor: doc. dr. Uroš Maver
Datum zagovora: 21. 9. 2016

DIPLOME – UNIVERZITETNI ŠTUDIJ

UNIVERZITETNI ŠTUDIJ

Tjaša AHEJ
UPORABA TERMOGRAVIMETRIČNE METODE PRI KARTAKTERIZACIJI KOORDINACIJSKIH SPOJIN
Mentor: doc. dr. Matjaž Kristl
Somentorica: doc. dr. Irena Ban
Datum zagovora: 7. 9. 2016

Simon CEGLAR
IZBIRA NAJPRIMERNEJŠEGA HLADIVA ENOSTOPENJSKE ALI DVOSTOPENJSKE VISOKOTEMPERATURNE TOPLOTNE ČRPALKE
Mentor: izr. prof. dr. Darko Goričanec
Somentor: asist. dr. Peter Trop
Datum zagovora: 20. 4. 2016

Šolasta ČUČEK
REŠEVANJE MEŠANO CELOŠTEVILSKIH NELINEARNIH PROBLEMOV Z DEKOMPOZICIJSKIMI IN RELAKSACIJSKIMI METODAMI
Mentorica: red. prof. dr. Zorka Novak Pintarič
Somentor: red. prof. dr. Zdravko Kravanja
Datum zagovora: 26. 9. 2016

Irena FERLAN
ANALIZA OBDELAVE POLIZDELKOV V GALVANSKEM OBRATU
Mentor: doc. dr. Anita Kovač Kralj
Somentor: doc. dr. Matjaž Kristl
Datum zagovora: 30. 9. 2016

Maja FERLEŽ
BIOINFORMATSKA ANALIZA MOLEKULARNO BIOLOŠKIH POTI RAKA MATERNIČNEGA VRATU
Mentor: red. prof. dr. Uroš Potočnik
Somentorica: doc. dr. Katja Repnik
Datum zagovora: 21. 9. 2016

Mateja FLIS
OPTIMIZACIJA PROCESOV RAZKROJA IN REDUKCIJE V ZAPRTEM SISTEMU ZA DOLOČITEV MASNE KONCENTRACIJE TITANOVEGA DIOKSIDA V REALNIH VZORCIH
Mentor: dr. Mitja Kolar
Somentor: doc. dr. Matjaž Kristl
Datum zagovora: 20. 1. 2016

Kristjan GROBIN
OBDELAVA ODPADNE VODE IZ PROIZVODNJE NITROOKSINA
Mentorica: izr. prof. dr. Marjana Simonič
Somentor: mag. Tomaž Mesar
Datum zagovora: 21. 9. 2016

Estera HABJANIČ
SOČASNO DOLOČANJE IZBRANIH FLAVONOIDOV V RASTLINSKIH EKSTRAKTIH S HPLC
Mentor: doc. dr. Matjaž Finšgar
Somentorica: doc. dr. Maša Islamčević Razboršek
Datum zagovora: 7. 9. 2016

Marjan HORVAT
RAZVOJ METODE ZA DOLOČEVANJE VISKOZNOSTI SUBSTANC V SISTEMIH S SUPERKRITIČNIMI FLUIDI
Mentor: red. prof. dr. Željko Knez
Somentor: doc. dr. Maša Knez Hrnčič
Datum zagovora: 26. 9. 2016

Helena HRIBERNIK
ČIŠČENJE ODPADNE VODE IZ PODJETJA NA KOROŠKEM
Mentorica: izr. prof. dr. Marjana Simonič
Somentorica: asist. dr. Irena Petrinić
Datum zagovora: 21. 9. 2016

Sanja KELBIČ
ČIŠČENJE KOMUNALNE ODPADNE VODE Z MEMBRANSKIM BIOREAKTORJEM
Mentorica: izr. prof. dr. Marjana Simonič
Somentorica: Cimermančič Bernardka, univ. dipl. biol.
Datum zagovora: 21. 9. 2016

Timi KOKOL
ŠTUDIJE MOŽNOSTI TEHNOLOGIJ ZA ZAJEMANJE CO_2
Mentorica: red. prof. dr. Zorka Novak Pintarič
Somentor: red. prof. dr. Zdravko Kravanja
Datum zagovora: 21. 9. 2016

Nataša KORAŽIJA
RAZVOJ IN OPTIMIZACIJA ANALIZNIH METOD PRI SPROŠČANJU KOVIN IZ MATERIALOV NAMENJENIH STIKU Z ŽIVILI
Mentor: dr. Mitja Kolar
Somentorica: red. prof. dr. Karin Stana Kleinschek
Datum zagovora: 20. 1. 2016

Sara KUGLER
PRIMERJAVA NATANČNOSTI DVEH METOD TESTIRANJA ZA PRISOTNOST VIRUSA HEPATITISA C PRI KRVODAJALCIH
Mentorica: izr. prof. dr. Marjana Glaser Kraševac
Somentorica: doc. dr. Špela Stangler Herodež
Datum zagovora: 20. 4. 2016

Tjaša LEMUT
KREIRANJE IN UPORABA INTERAKTIVNEGA MULTIMEDIJSKEGA UČNEGA GRADIVA PRI USVAJANJU NUMERIČNIH METOD
Mentorica: doc. dr. Majda Krajnc
Somentorica: doc. dr. Anita Kovač Kralj
Datum zagovora: 13. 7. 2016

Igor LENKIČ
ANALIZA UPORABE EMAJLA KOT ZAŠČITE ZA BETONSKO JEKLO
Mentorica: red. prof. dr. Andreja Goršek
Somentor: doc. dr. Matjaž Finšgar
Datum zagovora: 21. 9. 2016

Mirjana LUKIĆ
ZNIŽEVANJE VSEBNOSTI KOVIN IZ KOMPOSTNE IZCEDNE VODE Z ZEOLITI
Mentorica: izr. prof. dr. Marjana Simonič
Somentorica: red. prof. dr. Lidija Fras Zemljič
Datum zagovora: 18. 5. 2016

Julija MACUH
PRIDOBIVANJE KLOROFILA IN DERIVATOV KLOROFILA
Mentor: red. prof. dr. Željko Knez
Somentorica: red. prof. dr. Mojca Škerget
Datum zagovora: 26. 9. 2016

Laura MAKSIMOVIĆ
eQTL ANALIZA KROMOSOMSKIH REGIJ 17q21 IN 2q12 TER NJUN VPLIV NA RAZVOJ IN POTEK ASTME PRI SLOVENSKIH OTROCIH
Mentor: red. prof. dr. Uroš Potočnik
Somentorica: doc. dr. Katja Repnik
Datum zagovora: 7. 9. 2016

Matjaž MARKUŠ
ANALIZA VPLIVA ČASA NA VISKOZNOST KOZMETIČNIH POLIZDELKOV
Mentorica: doc. dr. Anita Kovač Kralj
Somentor: doc. dr. Matjaž Kristl
Datum zagovora: 21. 9. 2016

Luka MLINARIČ
POVEZAVA MED POLIMORFIZMI IN IZRAŽANJEM GENOV TRIM35 IN EPHX2 Z OTROŠKO ASTMO
Mentor: red. prof. dr. Uroš Potočnik
Somentor: doc. dr. Vojko Berce
Datum zagovora: 1. 9. 2016

Peter PALLER
SUŠENJE ODPADNEGA KOMUNALNEGA MULJA Z MIKROKOGENERACIJO NA DEPONIJSKI PLIN IN ODPADNA OLJA
Mentor: izr. prof. dr. Darko Goričanec
Somentor: asist. dr. Peter Trop
Datum zagovora: 7. 9. 2016

Lidija PODJAVERŠEK
OBLIKOVANJE POSLOVNEGA MODELA OBSTOJEČEGA IZDELKA ZA ŠIRITEV TRGA
Mentor: doc. dr. Dušan Klinar
Somentor:
Datum zagovora: 21. 9. 2016

Barbara POLANIČ
POVRŠINSKA OBDELAVA SILIKONSKEGA MATERIALA
Mentor: doc. dr. Matjaž Finšgar
Somentorica: red. prof. dr. Lidija Fras Zemljič
Datum zagovora: 21. 9. 2016

Vesna REBIĆ
TERMOGRAVIMETRIČNA ANALIZA SADRE IZ TERMOELEKTRARNE ŠOŠTANJ
Mentorica: red. prof. dr. Andreja Goršek
Somentorica: doc. dr. Darja Pečar
Datum zagovora: 7. 9. 2016

Anita ROGAČ
DOLOČANJE ORTOFOSFATA, AMONIJAKALNEGA DUŠIKA, MBAS INDEKSA IN FENOLNEGA INDEKSA V VODAH, S PRETOČNIM ANALIZATORJEM
Mentor: doc. dr. Matjaž Finšgar
Somentorica: izr. prof. dr. Marjana Simonič
Datum zagovora: 13. 7. 2016

Borut ROŽMAN
IZDELAVA VEZIVA ZA ASFALT - BITUMNA IZ OBNOVLJIVIH VIROV - S POMOČJO PIROLIZE NA LABORATORIJSKI NAPRAVI
Mentor: doc. dr. Dušan Klinar
Somentor: dr. Marjan Tušar
Datum zagovora: 21. 9. 2016

Polona ROŽMAN
INHIBICIJSKE LASTNOSTI NEIONSKEGA SURFAKTANTA POLIOKSIETILEN (40) IZOBUTIL ETER PRI POVIŠANI TEMPERATURI
Mentorica: izr. prof. dr. Regina Fuchs Godec
Somentor: doc. dr. Matjaž Finšgar
Datum zagovora: 21. 9. 2016

Anja SEVER
SONOKEMIJSKA SINTEZA IN KARAKTERIZACIJA INDIJEVIH IN GALIJEVIH SULFIDOV
Mentor: doc. dr. Matjaž Kristl
Somentorica: doc. dr. Irena Ban
Datum zagovora: 14. 9. 2016

Ines ŠPINDLER
SEPARACIJA MONOTERPENOV IZ SEMEN KUMINE (*CARUM CARVI L.*) SEMEN NAVADNEGA KOPRA (*ANETHUM GRAVEOLENS L.*) IN LISTOV ZELENE METE (*MENTHA CORDIFOLIA L.*)
Mentorica: red. prof. dr. Mojca Škerget
Somentor: red. prof. dr. Željko Knez
Datum zagovora: 21. 9. 2016

Žiga ŠUT
PROIZVODNJA BIOPLINA S SOSUBSTRATOM KORUZNO SLAMO
Mentorica: doc. dr. Lidija Čuček
Somentor: red. prof. dr. Zdravko Kravanja
Datum zagovora: 21. 9. 2016

Aleksandra TURK
ENERGETSKA IN EKONOMSKA OCENA SANACIJE STANOVANJSKE STAVBE
Mentor: izr. prof. dr. Darko Goričanec
Somentorica: asist. dr. Danijela Urbancl
Datum zagovora: 23. 3. 2016

Tanja TURK
DOLOČEVANJE BIOMASE ALG IN KLOROFILA V RASTNEM MEDIJU
Mentorica: izr. prof. dr. Marjana Simonič
Somentorica: red. prof. dr. Andreja Goršek
Datum zagovora: 12. 7. 2016

Matej ŽULJAN
UČINEK ČIŠČENJA ODPADNE VODE V SEKVENČNEM BIOLOŠKEM REAKTRORJU PRI RAZLIČNIH TEMPERATURNIH POGOJIH
Mentorica: izr. prof. dr. Marjana Simonič
Somentor: Aljaž Klasinc, univ. dipl. inž. str.
Datum zagovora: 21. 9. 2016

UNIVERZITETNI ŠTUDIJ – 1. stopnja

Nuša CMAGER
SINTEZA ZAMREŽENEGA POLI(4-VINILPIRIDINA)
Mentor: izr. prof. dr. Jernej Iskra
Somentor: red. prof. dr. Peter Krajnc
Datum zagovora: 7. 9. 2016

Suzana CVIJETINOVIĆ
ANALIZA ENERGTSKIH POTREB RASTLINJAKOV
Mentor: izr. prof. dr. Darko Goričanec
Somentorica: asist. dr. Danijela Urbancl
Datum zagovora: 13. 7. 2016

Matej FUREK
SIMULACIJA OBRATOVALNIH KARAKTERISTIK ABSORPCIJSKE TOPLOTNE ČRPALKE
Mentor: izr. prof. dr. Darko Goričanec
Somentor: asist. dr. Peter Trop
Datum zagovora: 7. 9. 2016

Tamara GOVEJŠEK
DOLOČANJE VSEBNOSTI β-GLUKANOV V SLADICI IN PIVU
Mentor: doc. dr. Jože Košir
Somentor: doc. dr. Matjaž Finšgar
Datum zagovora: 1. 9. 2016

Barbara GRABROVEC
DOLOČANJE LOKALNE GENSKE EKSPRESIJE V POSTOPKU CELJENJA RAN
Mentor: red. prof. dr. Uroš Potočnik
Somentor: doc. dr. Uroš Maver
Datum zagovora: 7. 9. 2016

Andreja HORVAT
EKSTRAKCIJA BIOLOŠKO AKTIVNIH SPOJIN IZ RAZLIČNIH VRST GOB DRUŽINE POLYPORACEAE (LUKNJARKE)
Mentor: red. prof. dr. Željko Knez
Somentor: Gregori Andrej
Datum zagovora: 1. 9. 2016

Maša HREN
UPORABA OPLAŠČENEGA ZEOLITA ZA ODSTRANJEVANJE ORGANSKE SNOVI IZ KOMPOSTNE VODE
Mentorica: izr. prof. dr. Marjana Simonič
Somentor: Fakin Tomaž
Datum zagovora: 7. 9. 2016

Žan HRIBAR
VLOGA RECEPTORJEV ENDOKANABINOIDNEGA SISTEMA CB1 IN CB2 PRI INHIBICIJI CITOKINA TNF-α V MONONUKLEARNIH LIMFOIDNIH CELICAH BOLNIKOV S CROHNOVO BOLEZNIJO
Mentor: red. prof. dr. Uroš Potočnik
Somentor: asist. ddr. Matjaž Deželak
Datum zagovora: 7. 9. 2016

Maja IVANOVSKI
KONTROLA ELASTIČNIH LASTNOSTI BETONA Z DODATKOM GUMENIH SEKANCEV
Mentorica: red. prof. dr. Andreja Goršek
Somentor: doc. dr. Samo Lubej
Datum zagovora: 7. 9. 2016

Kaja JEROMEL
PRIPRAVA MAGNETNIH ZAMREŽENIH ENCIMSKIH SKUPKOV (mCLEA) IZ β-GALAKTOZIDAZE
Mentorica: red. prof. dr. Maja Leitgeb
Somentorica: asist. Katja Vasić
Datum zagovora: 7. 9. 2016

Sabina JURAK
VPLIV Br- IN I- IONOV NA INHIBICIJSKO UČINKOVITOST NEIONSKEGA TIPA PAS V KISLEM MEDIJU
Mentorica: izr. prof. dr. Regina Fuchs Godec
Somentor: doc. dr. Matjaž Finšgar
Datum zagovora: 7. 9. 2016

Tina KEGL
MERJENJE FIZIKALNO-KEMIJSKIH IN TRANSPORTNIH LASTNOSTI SISTEMA POLIMER/SCF
Mentor: red. prof. dr. Željko Knez
Somentorica: doc. dr. Maša Knez Hrnčič
Datum zagovora: 1. 9. 2016

Alain KERHE
AKTIVNOST IN STABILNOST PROTEINOV V GELIH ZA KOZMETIČNE IN MEDICINSKE APLIKACIJE
Mentorica: red. prof. dr. Maja Leitgeb
Somentorica: doc. dr. Mateja Primožič
Datum zagovora: 7. 9. 2016

Nika KODBA
VPLIV VELIKOSTI ZRNATOSTI PŠENIČNIH OTROBOV NA RAST GLIVE PLEUROTUS OSTREATUS
Mentorica: red. prof. dr. Maja Leitgeb
Somentorica: doc. dr. Mateja Primožič
Datum zagovora: 22. 6. 2016

Katarina KORES
RAČUNALNIŠKE SIMULACIJE VPLIVA METILACIJE CITOZINA NA VEZAVO AFLATOKSINA B1 V DVOVERIŽNO DNK
Mentor: izr. prof. dr. Urban Bren
Datum zagovora: 9/1/2016

Julij LOZINŠEK
OBSTOJNOST PROTIKOROZIJSKIH HIDROFOBNIH PREVLEK PRI POVIŠANI TEMPERATURI
Mentorica: izr. prof. dr. Regina Fuchs Godec
Somentor: doc. dr. Matjaž Finšgar
Datum zagovora: 13. 7. 2016

Aljaž MARIN
PROJEKTIRANJE IN ZAGON TESTNE PROGE ZA IZVAJANJE MERITVE PRETOKA ODPADNIH VOD
Mentorica: doc. dr. Mateja Primožič
Somentorica: red. prof. dr. Maja Leitgeb
Datum zagovora: 7. 9. 2016

Azra OSMIĆ
OPTIMIZACIJA REAKCIJSKIH POGOJEV ZA KONTROLO POROZNOSTI poli(HEMA-ko-EA) MATERIALOV
Mentor: red. prof. dr. Peter Krajnc
Somentorica: asist. dr. Muzafera Paljevac
Datum zagovora: 7. 9. 2016

Rok PETRIJAN
UČINEK AGONISTOV IN ANTAGONISTOV ENDOKANABINOIDNIH RECEPTORJEV CB1 IN CB2 NA IZRAŽANJE NEKATERIH CITOKINOV V CELIČNIH KULTURAH GOJENIH LIMFOIDNIH CELIC BOLNIKOV Z ASTMO
Mentor: red. prof. dr. Uroš Potočnik
Somentor: asist. ddr. Matjaž Deželak
Datum zagovora: 7. 9. 2016

Tanja POPOVIĆ
REPLIKACIJA DNA POLIMORFIZMOV POVEZANIH Z MULTIPLO SKLEROZO V ASOCIACIJSKIH ŠTUDIJAH V CELOTNEM GENOMU PRI SLOVENSKIH BOLNIKIH
Mentor: red. prof. dr. Uroš Potočnik
Somentorica: izr. prof. dr. Tanja Hojs - Fabjan
Datum zagovora: 21. 9. 2016

Maja PRESKAR
PIROLIZA LESNE BIOMASE
Mentor: izr. prof. dr. Darko Goričanec
Somentorica: asist. dr. Danijela Urbancl
Datum zagovora: 20. 1. 2016

Tina RAJH
SINTEZA IN KARAKTERIZACIJA KOORDINACIJSKIH SPOJIN PREHODNIH KOVIN (Co,Ni,Cu) Z MELAMINOM
Mentor: doc. dr. Matjaž Kristl
Somentorica: doc. dr. Irena Ban
Datum zagovora: 1. 9. 2016

Nina RIBIČ
UPORABA ALGINATNIH NOSILCEV ZA ODSTRANJEVANJE ONESNAŽIL IZ VODE
Mentorica: izr. prof. dr. Marjana Simonič
Somentorica: doc. dr. Irena Ban
Datum zagovora: 21. 9. 2016

Luka ROMANIĆ
EKSTRAKT ROŽMARINA, KOT INHIBITOR KOROZIJSKIH PROCESOV
Mentorica: izr. prof. dr. Regina Fuchs Godec
Somentor: izr. prof. dr. Urban Bren
Datum zagovora: 7. 9. 2016

Barbara SKOK
POLIMERIZACIJA OLIGOMERNIH AKRILATOV V EMULZIJAH
Mentor: red. prof. dr. Peter Krajnc
Somentorica: asist. dr. Muzafera Paljevac
Datum zagovora: 7. 9. 2016

Anita SOVIČ
UPORABA SUROVEGA GLICEROLA ZA PROIZVODNJO BIOPLINA
Mentorica: doc. dr. Lidija Čuček
Somentor: red. prof. dr. Zdravko Kravanja
Datum zagovora: 7. 9. 2016

Rok ŠPINDLER
KRIOGENA AKUMULACIJA ENERGIJE
Mentor: izr. prof. dr. Darko Goričanec
Somentor: asist. dr. Peter Trop
Datum zagovora: 7. 9. 2016

Jadranka ŠVIGELJ
ODPIRANJE CELIC HALOFILNE GLIVE HORTAEA WERNECKII S HOMOGENIZATORJEM IN ZASLEDOVANJE AKTIVNOSTI PRISOTNIH ENCIMOV
Mentorica: red. prof. dr. Maja Leitgeb
Somentorica: asist. Maja Čolnik
Datum zagovora: 7. 9. 2016

Nina URBIČ
TOPNOST ORGANSKIH TOPIL V PLINIH PRI NIZKIH TLAKIH
Mentorica: red. prof. dr. Mojca Škerget
Somentorica: doc. dr. Maša Knez Hrnčič
Datum zagovora: 7. 9. 2016

Sara VOZLIČ
FUNKCIONALIZACIJA POLIAKRILNE KISLINE DO KISLINSKEGA KLORIDA IN ŠTUDIJA STABILNOSTI
Mentor: red. prof. dr. Peter Krajnc
Somentorica: asist. dr. Muzafera Paljevac
Datum zagovora: 7. 9. 2016

Tina ZOREC
STABILNOST KURKUMINOIDOV V SUBKRITIČNI VODI: DOLOČANJE MEHANIZMOV IN HITROST REAKCIJ RAZGRADNJE
Mentorica: red. prof. dr. Mojca Škerget
Somentor: red. prof. dr. Željko Knez
Datum zagovora: 7. 9. 2016

Taja ŽITEK
ANTIOKSIDATIVNE LASTNOSTI EKSTRAKTOV NEKATERIH RASTLINSKIH MATERIALOV
Mentor: red. prof. dr. Željko Knez
Somentorica: red. prof. dr. Mojca Škerget
Datum zagovora: 22. 6. 2016

VISOKOŠOLSKI STROKOVNI ŠTUDIJ

Marjan BALOH
VPLIV PROCESNIH PARAMETROV NA EKSTRAKCIJO MAKROLID LAKTAMOV IZ FERMENTACIJSKE BROZGE S TOLUENOM
Mentorica: red. prof. dr. Mojca Škerget
Somentor: red. prof. dr. Željko Knez
Datum zagovora: 23. 3. 2016

Otmar BEVK
OPTIMIRANJE POSTOPKOV KEMIJSKE PRIPRAVE VODE IN KONDICIONIRANJE TEHNOLOŠKE VODE V TERMOELEKTRARNI TRBOVLJE
Mentorica: red. prof. dr. Andreja Goršek
Somentorica: izr. prof. dr. Marjana Simonič
Datum zagovora: 12. 7. 2016

Dušanka BOHINC
OVREDNOTENJE ENERGIJE RAZTEGOVANJA PmB BITUMNA NA RAZLIČNIH DOLŽINAH RAZTEGA
Mentor: izr. prof. dr. Urban Bren
Somentor: dr. Marjan Tušar
Datum zagovora: 1. 9. 2016

Robert BREMŠAK
IZOLACIJA - REKOMBINANTNEGA FLAGELINA
Mentor: red. prof. dr. Uroš Potočnik
Somentorica: dr. Karolina Ivičak Kocjan
Datum zagovora: 21. 9. 2016

Simona BREŽNIK
ANALIZE LASTNOSTI NANOSA TISKARSKIH BARV
Mentorica: doc. dr. Anita Kovač Kralj
Somentor: doc. dr. Matjaž Kristl
Datum zagovora: 21. 9. 2016

Marjeta BRODAR
PRIPRAVA STANDARDOV PIMEKROLIMUSOVIH NEČISTOČ
Mentor: doc. dr. Matjaž Finšgar
Somentor: dr. Gregor Kopitar
Datum zagovora: 21. 9. 2016

Zlatka CAFUTA PREVOLŠEK
ADSORPCIJA IN DESORPCIJA NEKATERIH NARAVNIH SPOJIN NA RAZLIČNE ADSORBENTE
Mentorica: red. prof. dr. Mojca Škerget
Somentorica: asist. dr. Amra Perva-Uzunalić
Datum zagovora: 21. 9. 2016

Petra DREVENŠEK
VEČKRITERIJSKO OPTIMIRANJE BIOPROCESOV Z UPORABO TRAJNOSTNEGA KAZALCA NA EKONOMSKI RAVNI
Mentorica: doc. dr. Lidija Čuček
Somentor: red. prof. dr. Zdravko Kravanja
Datum zagovora: 21. 9. 2016

Robert FERLINC
UPORABA ANALIZNIH METOD ZA DOLOČANJE UČINKOVITOSTI MALIH KOMUNALNIH ČISTILNIH NAPRAV
Mentor: dr. Mitja Kolar
Somentorica: izr. prof. dr. Marjana Simonič
Datum zagovora: 20. 1. 2016

Jana FERME
MERILNI PROTOKOL TESTIRANJA ULTRAFILTRACIJSKE NAPRAVE
Mentorica: red. prof. dr. Andreja Goršek
Somentor: Boštjan Žigon, univ. dipl. inž. kem. str.
Datum zagovora: 7. 9. 2016

Ksenija FLEISINGER
ENERGETSKA PRENOVA VEČSTANOVANJSKE STAVBE IN NJEN VPLIV NA KVALITETO BIVALNEGA PROSTORA
Mentor: izr. prof. dr. Darko Goričanec
Somentorica: asist. dr. Danijela Urbancl
Datum zagovora: 21. 9. 2016

Klara FRANGEŽ
DOLOČANJE VSEBNOSTI LIGNINA V HMELJU
Mentor: dr. Iztok Jože Košir
Somentor: doc. dr. Matjaž Finšgar
Datum zagovora: 1. 9. 2016

Breda GAŠPAR
VZPOSTAVITEV NOTRANJEGA NADZORA PITNE VODE PO SISTEMU HACCP
Mentorica: red. prof. dr. Andreja Goršek
Somentorica: izr. prof. dr. Marjana Simonič
Datum zagovora: 12. 7. 2016

Marija GOLOB
PRIPRAVA IN TESTIRANJE ODSTRANJEVALCA PREMAZOV NA OSNOVI NADOMESTNIH TOPIL ZA METILENKLORID IN N-METIL-2-PIROLIDON (NMP)
Mentorica: red. prof. dr. Mojca Škerget
Somentorica: mag. Tina Razboršek
Datum zagovora: 1. 9. 2016

Teo IVANČIČ
KOROZIJSKA OBSTOJNOST NANOSA AEROSOLNEGA RAZPRŠILNIKA »PLASTI-DIP« V AGRESIVNEM MEDIJU
Mentorica: izr. prof. dr. Regina Fuchs Godec
Somentor: izr. prof. dr. Urban Bren
Datum zagovora: 27. 9. 2016

Roman JANKOVIČ
PRIMERJAVA UČINKOVITOSTI RAZLIČNIH MAKROZAMREŽENIH POLIMERNIH XAD ADSORBENTOV PRI ADSORPCIJI VANKOMICINA
Mentor: izr. prof. dr. Urban Bren
Somentor: David Senica, univ. dipl. inž. kem. inž.
Datum zagovora: 27. 9. 2016

Darko KERŽAN
RAZVOJ IN VALIDACIJA GC/FID METODE ZA DOLOČEVANJE ALKOHOLOV V VINU
Mentor: doc. dr. Matjaž Finšgar
Somentorica: doc. dr. Maša Islamčević Razboršek
Datum zagovora: 18. 5. 2016

Peter KLADNIK
EPIMERIZACIJA ERGOT ALKALOIDOV IN BROM – ERGOT ALKALOIDOV
Mentor: red. prof. dr. Peter Krajnc
Somentorica: asist. dr. Muzafera Paljevac
Datum zagovora: 7. 9. 2016

Veronika KOLAR
VPLIV OBRATOVALNIH POGOJEV NA HITROST PRENOSA VODE PRI PROCESU OSMOZE
Mentorica: asist. dr. Irena Petrinić
Somentorica: izr. prof. dr. Marjana Simonič
Datum zagovora: 21. 9. 2016

Helena KOTAR
ANALIZE ČIŠČENJA INDUSTRIJSKIH ODPADNIH VOD NA INDUSTRIJSKI ČISTILNI NAPRAVI
Mentorica: doc. dr. Anita Kovač Kralj
Somentorica: izr. prof. dr. Marjana Simonič
Datum zagovora: 21. 9. 2016

Gašper KOZLOVIČ
ANALIZA ŽIVLJENJSKEGA CIKLA PROCESOV PROIZVODNJE BIOETANOLA S PROGRAMSKIM ORODJEM OpenLCA
Mentorica: doc. dr. Lidija Čuček
Somentor: red. prof. dr. Zdravko Kravanja
Datum zagovora: 21. 9. 2016

Martina KŠELA PODGORNIK
UPORABA SIMULATORJA SKL2 ZA KALIBRACIJO MERILNIKOV pH, PREVODNOSTI IN KONCENTRACIJE KISIKA
Mentor: doc. dr. Matjaž Finšgar
Somentorica: doc. dr. Maša Islamčević Razboršek
Datum zagovora: 21. 9. 2016

Tomaž KUMER
VPLIV TEMPERATURE NA PROCES UTRJEVANJA DVOKOMPONENTNIH AKRILNIH PREMAZOV
Mentor: red. prof. dr. Peter Krajnc
Somentorica: asist. dr. Muzafera Paljevac
Datum zagovora: 7. 9. 2016

Marko LAVRIH
POSLOVNI MODEL NOVEGA PROGRAMA IN IZDELKA V OBSTOJEČEM PODJETJU
Mentor: doc. dr. Dušan Klinar
Datum zagovora: 21. 9. 2016

Dejan MENONI
KRISTALIZACIJA NATRIJEVEGA ACETATA TRIHIDRATA
Mentorica: red. prof. dr. Mojca Škerget
Somentor: red. prof. dr. Željko Knez
Datum zagovora: 13. 7. 2016

Robert PERETIN
PRIPRAVA SAMOGASNE MEŠANICENA OSNOVI BLOK KOPOLIMEROV Z NE-HALOGENSKIMI ZAVIRALCI GORLJIVOSTI
Mentorica: red. prof. dr. Andreja Goršek
Somentor: red. prof. dr. Peter Krajnc
Datum zagovora: 7. 9. 2016

David PILINGER
VALIDACIJA HPLC METODE ZA DOLOČEVANJE OSTANKOV AKTIVNE FARMACEVTSKE UČINKOVINE LIDOKAINIJEV HIDROKLORID NA PROIZVODNI OPREMI
Mentor: doc. dr. Matjaž Finšgar
Somentorica: doc. dr. Maša Islamčević Razboršek
Datum zagovora: 1. 9. 2016

Ines POLAK
PRIMERJAVA MERITEV VISKOZNOSTI Z APARATOMA HAAKE VT550 IN HAAKE VISCOTESTER IQ
Mentor: izr. prof. dr. Urban Bren
Somentorica: Tatjana Jambrovič, univ. dipl. inž. kem. tehnol.
Datum zagovora: 27. 9. 2016

Lidija PUNGERŠEK
REŠEVANJE KEMIJSKO – TEHNIŠKIH PROBLEMOV S PROGRAMOM MS EXCEL
Mentorica: doc. dr. Majda Krajnc
Somentorica: izr. prof. dr. Petra Žigert Pleteršek
Datum zagovora: 21. 9. 2016

Tomaž ROZONIČNIK
VPLIV PIROGENEGA SiO_2 IN Al_2O_3 NA REOLOŠKE LASTNOSTI PRAŠKASTEGA LAKA
Mentorica: red. prof. dr. Andreja Goršek
Somentorica: doc. dr. Darja Pečar
Datum zagovora: 7. 9. 2016

Dejan SAKULAC
OPTIMIZACIJA REGENERACIJE CIKLOHEKSANA NA REKTIFIKACIJSKI KOLONI
Mentorica: red. prof. dr. Mojca Škerget
Somentor: red. prof. dr. Željko Knez
Datum zagovora: 26. 9. 2016

Nataša STAROVERŠKI
PREUČEVANJE VSEBNOSTI SNOVI V FLOKULIRANI KOMPOSTNI VODI
Mentorica: izr. prof. dr. Marjana Simonič
Somentor: dr. Karli Udovičič
Datum zagovora: 21. 9. 2016

Sanja STRAH
PRIMERJAVA RAZPRŠEVANJA ZRAKA V AERACIJSKIH BAZENIH KOMUNALNIH ČISTILNIH NAPRAV
Mentor: izr. prof. dr. Darko Goričanec
Somentorica: asist. dr. Danijela Urbancl
Datum zagovora: 21. 9. 2016

Ernest ŠIMON
VARNO DELO S KEMIKALIJAMI IN PRIPRAVA NAVODIL ZA VARNO DELO V KEMIJSKEM LABORATORIJU
Mentorica: red. prof. dr. Zorka Novak Pintarič
Somentorica: doc. dr. Julija Volmajer Valh
Datum zagovora: 21. 9. 2016

Nuša ŠKERLAK
MATEMATIČNI MODEL REZULTATOV ANALIZ V PREHRAMBENI INDUSTRIJI
Mentorica: doc. dr. Anita Kovač Kralj
Somentorica: doc. dr. Irena Ban
Datum zagovora: 21. 9. 2016

Aleksandra TROKŠAR
ANALIZA NEČISTOČ KOVINSKIH ULITKOV
Mentorica: doc. dr. Anita Kovač Kralj
Somentor: doc. dr. Matjaž Kristl
Datum zagovora: 21. 9. 2016

Lucija TURNŠEK
PRIMER MULTIMEDIJSKEGA UČNEGA GRADIVA IN ELEKTRONSKO PREVERJANJE ZNANJA PRI PREDMETU GRADIVA
Mentorica: doc. dr. Majda Krajnc
Somentorica: red. prof. dr. Andreja Goršek
Datum zagovora: 21. 9. 2016

Oliver TUTIĆ
MIKROFILTRACIJA FERMENTACIJSKE BROZGE
Mentorica: red. prof. dr. Mojca Škerget
Somentor: Aljaž Kajtna, univ. dipl. inž. kem. tehnol.
Datum zagovora: 21. 9. 2016

Marjeta UMEK
RAZVOJ IN VALIDACIJA ANALIZNE METODE B PO STANDARDU SIST EN ISO 7887:2012 ZA DOLOČANJE BARVE VODE
Mentor: doc. dr. Matjaž Finšgar
Somentorica: asist. dr. Amra Perva-Uzunalić
Datum zagovora: 13. 7. 2016

Dragica VALEK
DOLOČEVANJE SPOSOBNOSTI DISPERGIRANJA PIGMENTNEGA TITANOVEGA DIOKSIDA V ALKIDNI SMOLI
Mentorica: red. prof. dr. Andreja Goršek
Somentorica: mag. Mojca Pustoslemšek
Datum zagovora: 7. 9. 2016

Stjepan ZAGORŠČAK
SINTEZA IN LASTNOSTI TRIBAZIČNEGA BAKROVEGA SULFATA
Mentorica: red. prof. dr. Andreja Goršek
Somentor: doc. dr. Matjaž Kristl
Datum zagovora: 7. 9. 2016

Mateja ZVER
OD VZORCA DO ANTIBIOGRAMA ENTEROBAKTERIJ V ENEM DNEVU – EVALUACIJA METODE Z VZPOREDNIM KULTIVIRANJEM SEČA V BUJONU V PRIMERJAVI S STANDARDNIM POSTOPKOM
Mentorica: red. prof. dr. Maja Leitgeb
Somentor: mag. Iztok Štrumbelj
Datum zagovora: 21. 9. 2016

VISOKOŠOLSKI STROKOVNI ŠTUDIJ – 1. stopnja

Alenka BAKLAN
ELEKTROKEMIJSKA ANALIZA ALUMINIJEVE ZLITINE 6082 V KLORIDNEM MEDIJU
Mentor: doc. dr. Matjaž Finšgar
Mentorica: izr. prof. dr. Regina Fuchs Godec
Datum zagovora: 21. 9. 2016

Amanda FERLEŽ
VERIŽNI UČINEK ZA POŽAR IN EKSPLOZIJO PRI SKLADIŠČENJU NAFTNIH DERIVATOV
Mentorica: red. prof. dr. Zorka Novak Pintarič
Mentorica: Jasmina Karba
Datum zagovora: 7. 9. 2016

Marijana HITER
VPLIV SKUPNEGA IONA NA VISKOZNOST ELEKTROLITSKIH MEŠANIC
Mentorica: doc. dr. Mojca Slemnik
Mentorica: izr. prof. dr. Marjana Simonič
Datum zagovora: 6. 1. 2016

Špela KOPRIVC
PROGRAMIRANJE V EXCELU VBA IN UPORABA V KEMIJSKI TEHNIKI
Mentorica: red. prof. dr. Zorka Novak Pintarič
Mentor: doc. dr. Miloš Bogataj
Datum zagovora: 21. 12. 2016

Katja LEČNIK
MEHANOKEMIJSKE SINTEZE SULFIDOV PREHODNIH KOVIN 4. PERIODE (MxSy; M = Zn, Ni, Co)
Mentor: doc. dr. Matjaž Kristl
Mentorica: doc. dr. Irena Ban
Datum zagovora: 7. 9. 2016

Maja MAZEJ
INHIBICIJSKE LASTNOSTI MEŠANICE POLIOKSIETILEN (40) IZOBUTILFENIL ETRA Z DODATKOM HALOGENIDNIH IONOV V KLOROVODIKOVI KISLINI
Mentorica: izr. prof. dr. Regina Fuchs Godec
Mentor: izr. prof. dr. Urban Bren
Datum zagovora: 7. 9. 2016

Maja MEŽNAR
IDENTIFIKACIJA NEKATERIH TEHNIČNO POMEMBNIH POLIMEROV NA OSNOVI NJIHOVIH FIZIKALNO-KEMIJSKIH LASTNOSTI
Mentorica: red. prof. dr. Andreja Goršek
Mentorica: doc. dr. Darja Pečar
Datum zagovora: 7. 9. 2016

Tina OPREŠNIK
VSEBNOST FENOLNIH SPOJIN V SADNIH IN ZELIŠČNIH PIJAČAH
Mentorica: red. prof. dr. Mojca Škerget
Mentorica: asist. Tina Perko
Datum zagovora: 7. 9. 2016

Katja RIBIČ
PRIMERJAVA REZULTATOV NATEZNEGA PREIZKUSA ZA PREIZKUŠANCE IZ ZLITINSKIH MATERIALOV
Mentorica: doc. dr. Darja Pečar
Mentorica: red. prof. dr. Andreja Goršek
Datum zagovora: 7. 9. 2016

Mojca SLANC
ODSTRANJEVANJE ŽELEZA IZ PITNE VODE Z UPORABO IMOBILIZIRANIH ALG
Mentorica: izr. prof. dr. Marjana Simonič
Mentorica: red. prof. dr. Andreja Goršek
Datum zagovora: 21. 9. 2016

Peter STRMŠEK
KOROZIJA BIOKOMPATIBILNIH KOVIN IN ZLITIN V UMETNI SLINI
Mentorica: doc. dr. Mojca Slemnik
Mentorica: izr. prof. dr. Regina Fuchs Godec
Datum zagovora: 21. 9. 2016

Anže ŠIMIC
FOTOLUMINISCENČNE IN ELEKTRIČNE LASTNOSTI PLASTOVITIH STANATOV $Sr_{n+1}Sn_nO_{3n+1}$ (n = , 1 in 2) DOPIRANIH Z LANTANOIDI
Mentor: doc. dr. Matjaž Kristl
Mentor: Aivaras Kareiva
Datum zagovora: 23. 11. 2016

Jure ŠKORJA
EKONOMSKE IN OKOLJSKE ANALIZE POSTOPKOV ZA IZRABO ODPADNEGA GLICEROLA
Mentorica: red. prof. dr. Zorka Novak Pintarič
Mentor: red. prof. dr. Peter Krajnc
Datum zagovora: 1. 9. 2016

Tamara ŠUSTER
ŠTUDIJA PRISOTNOSTI MIKROBNIH POPULACIJ V NARAVNIH BAZENIH
Mentorica: red. prof. dr. Maja Leitgeb
Mentorica: izr. prof. dr. Marjana Simonič
Datum zagovora: 7. 9. 2016

Katja VODOPIVEC
SINTEZA IN KARAKTERIZACIJA Bi_2WO_6 NANODELCEV
Mentor: doc. dr. Matjaž Kristl
Mentorica: doc. dr. Irena Ban
Datum zagovora: 7. 9. 2016

Alenka ZADRAVEC
UPORABA METODE DREVO ODPOVEDI V KEMIJSKIH PROCESIH
Mentorica: red. prof. dr. Zorka Novak Pintarič
Mentorica: red. prof. dr. Andreja Goršek
Datum zagovora: 21. 9. 2016

UNIVERZA V NOVI GORICI
FAKULTETA ZA PODIPLOMSKI ŠTUDIJ

1. januar – 31. december 2016

DOKTORATI

PODIPLOMSKI ŠTUDIJSKI PROGRAM ZNANOSTI O OKOLJU

Lucija RASPOR DALL'OLIO
SYMBIOSIS ECOLOGY OF SELECTED SCYPHOZOA
Mentorica: doc. dr. Andreja Ramšak
Somentorica: prof. dr. Alenka Malej
Datum zagovora: 30. 9. 2016

PODIPLOMSKI ŠTUDIJSKI PROGRAM ZNANOSTI O OKOLJU – 3. stopnja

Karmen BIZJAK BAT
CHARACTERIZATION OF SLOVENIAN APPLE JUICE WITH RESPECT TO ITS GEOGRAPHICAL ORIGIN AND AGRICULTURAL PRODUCTION PRACTICE
Mentorica: prof. dr. Branka Mozetič Vodopivec
Somentorica: prof. dr. Nives Ogrinc
Datum zagovora: 2. 6. 2016

Martina JAKLIČ
ECOLOGICAL NICHE RELATIONS OF INDIGENOUS AND INVASIVE CRAYFISH (*ASTACOIDEA*) IN SLOVENIA
Mentor: prof. dr. Anton Brancelj
Datum zagovora: 30. 8. 2016

MAGISTERIJI

PODIPLOMSKI ŠTUDIJSKI PROGRAM ZNANOSTI O OKOLJU

Peter BOHINEC
THE EFFECTS OF MIXED COMMUNAL WASTE RECYCLING MANAGEMENT IN SLOVENIA: A CASE STUDY
Mentor: dr. Marko Vudrag
Datum zagovora: 19. 7. 2016

Renata Janja SLOVŠA
ANALYSIS OF ALTERNATIVE CHANCES FOR SLUDGE TREATMENT OF NEW CENTRAL WASTE WATER TREATMENT PLANT
Mentor: prof. dr. Viktor Grilc
Datum zagovora: 19. 7. 2016

Janez ŠKARJA
THE STUDY OF OPTIMAL TECHNOLOGICAL PROCEDURES OF INTERNAL PLUMBING SYSTEM DISINFECTION FACILITIES IN USE BY THE SENSITIVE HUMAN POPULATIONS
Mentor: doc. dr. Darko Drev
Datum zagovora: 31. 8. 2016

Patrik BAKSA
EVALUATION OF MARINE SEDIMENTS FROM THE PORT OF LUKA KOPER FROM THE ENVIRONMENTAL PERSPECTIVE AND IN TERMS OF THEIR USABILITY IN THE BRICK INDUSTRY
Mentorica: doc. dr. Rebeka Kovačič Lukman
Somentorica: dr. Vilma Ducman
Datum zagovora: 2. 9. 2016

Janez PAGON
FLOODPLAIN FORESTS OF SOČA RIVER BETWEEN KOBARID AND CONFLUENCE WITH RIVER TOLMINKA: CURRENT SITUATION AND DEVELOPMENT
Mentor: prof. dr. Marko Debeljak
Datum zagovora: 15. 9. 2016

Boštjan KEPIC
TIME RESTRICTIONS IN FOREST OPERATIONS PLANNING
Mentor: prof. dr. Janez Krč
Datum zagovora: 15. 9. 2016

Nataša SMREKAR
ASSESSMENT OF EFFECTIVE DOSES BASED ON VARIOUS RADON MEASURING TECHNIQUES
Mentorica: prof. dr. Janja Vaupotič
Datum zagovora: 23. 9. 2016

Sebastijan REP
THE ROLE OF SPECT/CT SCINTIGRAPFY IN LOCALIZATION OF PARATHYROID ADENOMAS
Mentorica: prof. dr. Janja Vaupotič
Somentor: prof. Marko Hočevar
Datum zagovora: 23. 9. 2016

Mojca NOVAK
PREVENTION AND MANAGEMENT OF *LEGIONELLA SPP*. SPREAD IN HOSPITAL WATER SYSTEM (ESTABLISHING AN EFFECTIVE SYSTEM WITHOUT USING CHEMICALS IN UNIVERSITY CLINIC OF RESPIRATORY AND ALLERGIC DISEASES GOLNIK)
Mentorica: doc. dr. Viktorija Tomič
Datum zagovora: 29. 9. 2016

Slavica ILC
ASSESSMENT OF THE DEVELOPMENT POTENTIAL OF FOREST – WOOD PROCESSING CHAIN
Mentor: doc. dr. Henrik Gjerkeš
Datum zagovora: 29. 9. 2016

UNIVERZA V NOVI GORICI
FAKULTETA ZA ZNANOSTI O OKOLJU
1. januar – 31. december 2016

MAGISTERIJI

ŠTUDIJSKI PROGRAM OKOLJE – 2. stopnja

Breda POGLAJEN
OVREDNOTENJE VPLIVA EKSPERIMENTALNIH DEJAVNIKOV NA IZMERJENE VREDNOSTI RESPIRACIJSKE AKTIVNOSTI AT_4
Mentor: doc. dr. Andrej Kržan
Datum zagovora: 21. 6. 2016

Jacopo SEGATO
SYNTHESIS OF NOVEL GROUP 3 AND LANTHANIDE COMPLEXES CONTAINING THE FERROCENYL MOIETY
Mentor: prof. dr. Marco Bertoluzzi
Datum zagovora: 27. 10. 2016

DIPLOME

UNIVERZITETNI ŠTUDIJSKI PROGRAM OKOLJE

Bojan ŠUC
IDENTIFIKACIJA, PORAZDELITEV IN VEZAVNE OBLIKE ŽELEZA V RIŽU (*ORYZA SATIVA L.*) Z RENTGENSKO ABSORPCIJSKO IN EMISIJSKO MIKRO-SPEKTROSKOPIJO
Mentorica: prof. dr. Katarina Vogel Mikuš
Somentor: prof. dr. Iztok Arčon
Datum zagovora: 5. 9. 2016

Vanja KRISTANČIČ
VPLIV KOPALCEV NA BENTOŠKE NEVRETENČARJE V OBALNEM PASU BOHINJSKEGA JEZERA
Mentor: prof. dr. Anton Brancelj
Datum zagovora: 27. 9. 2016

Mateja PETAVS KRISTANČIČ
UGOTAVLJANJE STRUPENOSTI ACETAMIPRIDA NA KOPENSKE ENAKONOŽNE RAKE VRSTE *PORCELLIO SCABER* (*ISOPODA, CRUSTACEA*)
Mentorica: prof. dr. Polonca Trebše
Datum zagovora: 29. 9. 2016

ŠTUDIJSKI PROGRAM OKOLJE – 1. stopnja

Lucija VODIR
VPLIV HIDROLOŠKIH RAZMER NA KAKOVOST KRAŠKIH VODNIH VIROV – PRIMER IZVIRA RIŽANE
Mentorica: prof. dr. Metka Petrič
Datum zagovora: 19. 1. 2016

Tine BIZJAK
OBČUTLJIVOST MODELA ZA DOLOČANJE VIROV AEROSOLIZIRANEGA ČRNEGA OGLJIKA NA IZBRANE VHODNE PARAMETRE
Mentor: doc. dr. Griša Močnik
Datum zagovora: 19. 1. 2016

Tamara GAJŠT
ANALIZA OSTANKOV PLASTIKE V KOMERCIALNEM KOMPOSTU
Mentor: doc. dr. Andrej Kržan
Datum zagovora: 19. 1. 2016

Sara PRIBOVŠEK
VPLIV ONESNAŽIL IZ OKOLJSKIH AEROSOLOV NA TARČNE CELICE V PLJUČIH
Mentorica: doc. dr. Martina Bergant Marušič
Datum zagovora: 8. 3. 2016

Polona PETERNELJ
PREGLED STANJA IN PREDLOG SPREMEMB SISTEMA RAVNANJA Z ODPADNO EMBALAŽO V RS
Mentor: doc. dr. Andrej Kržan
Datum zagovora: 21. 4. 2016

Andrej JERKIČ
DOLOČEVANJE KONCENTRACIJ IN TESTIRANJE BAKTERICIDNEGA DELOVANJA KOLOIDNEGA SREBRA V VODI
Mentorica: doc. dr. Dorota Korte
Datum zagovora: 31. 5. 2016

Jasna GELATI
STABILNOST IN DETEKCIJA ŽELEZOVIH IONOV V VODI IZ OBLAKOV
Mentorica: doc. dr. Dorota Korte
Datum zagovora: 5. 9. 2016

Mojca GRMEK
ITALIJANSKI VRABEC (*PASSER ITALIAE*) V VIPAVSKI DOLINI
Mentor: prof. dr. Davorin Tome
Datum zagovora: 6. 9. 2016

Sandra DUKIĆ
UČINKI HERBICIDA GLIFOSATA V ČISTI OBLIKI IN V PRIPRAVKU NA DEŽEVNIKE (*EISENIA ANDREI*)
Mentorica: doc. dr. Suzana Žižek
Datum zagovora: 14. 9. 2016

Monika FERFOLJA
FIZIKALNA, KEMIJSKA IN BIOLOŠKA ANALIZA REKE IDRIJCE OD IZVIRA DO IZLIVA
Mentorica: izr. prof. dr. Tanja Pipan
Datum zagovora: 28. 9. 2016

Urban ČESNIK
RAZMNOŽEVANJE TIGRASTEGA KOMARJA (*AEDES ALBOPICTUS*) V NOVI GORICI
Mentorica: dr. Jana Laganis
Datum zagovora: 28. 9. 2016

Tjaša STEINMAN
OPTIMIRANJE ZBIRANJA KOMUNALNIH ODPADKOV
Mentor: doc. dr. Andrej Kržan
Datum zagovora: 29. 9. 2016

Aleš GRAHOVAC
DOLOČANJE SREBROVIH ZVRSTI V TEKOČIH VZORCIH
Mentorica: doc. dr. Dorota Korte
Datum zagovora: 29. 9. 2016

Grega SARKA
KAKOVOST TAL V MESTNIH VRTOVIH NA OBMOČJU NOVE GORICE
Mentorica: doc. dr. Suzana Žižek
Datum zagovora: 10. 11. 2016

KOLEDAR VAŽNEJŠIH ZNANSTVENIH SREČANJ S PODROČJA KEMIJE IN KEMIJSKE TEHNOLOGIJE

SCIENTIFIC MEETINGS – CHEMISTRY AND CHEMICAL ENGINEERING

2017

April 2017

3 – 5	SOLUTIONS FOR DRUG-RESISTANT INFECTIONS (SDRI 2017) Brisbane, Australia
Information:	http://www.sdri2017.org/
5 – 6	2ND INTERNATIONAL CONFERENCE ON NANOMATERIALS, NANODEVICES, FABRICATION AND CHARACTERIZATION (ICNNFC'17) Barcelona, Spain
Information:	http://icnnfc.com/
5 – 6	2ND INTERNATIONAL CONFERENCE ON NANOBIOTECHNOLOGY (ICNB'17) Barcelona, Spain
Information:	http://nbconference.com/
5 – 6	2ND INTERNATIONAL CONFERENCE ON NANOTECHNOLOGY MODELING AND SIMULATION (ICNMS'17) Barcelona, Spain
Information:	http://icnms.net/
10 – 13	14TH UNESCO/IUPAC WORKSHOP AND CONFERENCE ON MACROMOLECULES & MATERIALS Stellenbosch, South Africa
Information:	http://academic.sun.ac.za/unesco/
10 – 13	ELECTROSTATICS 2017 Frankfurt am Main, Germany
Information:	http://www.dechema.de/en/electrostatics2017.html
19 – 22	25TH CROATIAN MEETING OF CHEMISTS AND CHEMICAL ENGINEERS Porec, Croatia
Information:	http://25hskiki.org/en/homepage/

May 2017

7 – 11	SETAC EUROPE 27TH ANNUAL MEETING Brussels, Belgium
Information:	http://www.setac.org/events/EventDetails.aspx?id=683532&group=
14 – 17	2ND GREEN AND SUSTAINABLE CHEMISTRY CONFERENCE Berlin, Germany
Information:	http://www.greensuschemconf.com/
16 – 19	ISGC, THE INTERNATIONAL SYMPOSIUM ON GREEN CHEMISTRY La Rochelle, France
Information:	https://www.isgc-symposium.com/welcome/
17 – 18	STAT TEST IN CLINICAL LABORATORY Barcelona, Spain
Information:	http://www.acclc.cat/

17 – 19	FIFTH INTERNATIONAL SYMPOSIUM FRONTIERS IN POLYMER SCIENCE Seville, Spain
Information:	http://www.frontiersinpolymerscience.com/
18 – 21	29TH EUROPEAN SYMPOSIUM ON APPLIED THERMODYNAMICS Bucharest, Romania
Information:	http://jetc2017.hu/
21 – 25	12TH ADVANCED POLYMERS VIA MACROMOLECULAR ENGINEERING (APME 2017) Ghent, Belgium
Information:	http://www.ldorganisation.com/apme2017
23 – 25	14TH JOINT EUROPEAN THERMODYNAMICS CONFERENCE 2017 Budapest, Hungary
Information:	http://jetc2017.hu/
25 – 27	MaCKiE-2017 – INTERNATIONAL CONFERENCE ON MATHEMATICS IN CHEMICAL KINETICS AND ENGINEERING (MaCKiE) Budapest, Hungary
Information:	http://www.mackie-workshops.com/
25 – 27	7TH SLOVENIAN-SERBIAN-CROATIAN SYMPOSIUM ON ZEOLITES Ljubljana, Slovenia
Information:	http://zeo2017.ki.si/
28 – 31	BIOHETEROCYCLES 2017 – XVII INTERNATIONAL CONFERENCE ON HETEROCYCLES IN BIOORGANIC CHEMISTRY Galway, Ireland
Information:	http://www.conference.ie/Conferences/index.asp?Conference=442

June 2017

6 – 10	8TH INTERNATIONAL SYMPOSIUM ON MACRO- AND SUPRAMOLECULAR ARCHITECTURES AND MATERIALS Sochi, Russian Federation
Information:	www.mam-17.org
11 – 15	EUROMEDLAB ATHENS 2017 Athens, Greece
Information:	www.athens2017.org
11 – 16	COLLOQUIUM SPECTROSCOPICUM INTERNATIONALE XL (CSI-XL) Pisa, Italy
Information:	www.csi-conference.org
12 – 14	INORGANIC CHEMISTRY DAYS Nynäshamn, Sweden
Information:	http://www.oorgan.se/
13 – 15	V INTERNATIONAL SYMPOSIUM ON RELIABLE FLOW OF PARTICULATE SOLIDS Skien, Norway
Information:	http://www.relpowflo.no/
18 – 22	16TH INTERNATIONAL CONFERENCE ON CHEMISTRY AND THE ENVIRONMENT (ICCE 2017) Oslo, Norway
Information:	http://icce2017.org/welcome/
19 – 21	6TH EUROPEAN DRYING CONFERENCE Liège, Belgium
Information:	http://efce.info/EuroDrying+2017.html
19 – 23	9TH INTERNATIONAL SYMPOSIUM ON MOLECULAR MOBILITY AND ORDER IN POLYMER SYSTEMS Saint-Petersburg, Russian Federation
Information:	https://iupac.org/event/mmops2017/

25 – 29	INTERNATIONAL SYMPOSIA ON ORGANOMETALLIC CHEMISTRY DIRECTED TOWARDS ORGANIC SYNTHESIS (OMCOS 19) Jeju Island, Republic Of Korea
Information:	https://iupac.org/event/omcos-19/
28	7TH EUROVARIETY – 7TH EUROPEAN VARIETY IN UNIVERSITY CHEMISTRY EDUCATION Belgrade, Serbia
Information:	http://www.chem.bg.ac.rs/eurovariety/
28 – 30	4TH INTERNATIONAL WORKSHOP ON PERICYCLIC REACTIONS AND SYNTHESIS OF HETERO- AND CARBOCYCLIC SYSTEMS Milan, Italy
Information:	http://sites.unimi.it/cirp_workshop/

July 2017

2 – 5	4TH EUCHEMS INORGANIC CHEMISTRY CONFERENCE – EICC-4 Copenhagen, Denmark
Information:	http://www.euchems.eu/events/4th-euchems-inorganic-chemistry-conference-eicc-4/
2 – 6	INTERNATIONAL SYMPOSIUM ON MACROCYCLIC AND SUPRAMOLECULAR CHEMISTRY IN CONJUNCTION WITH ISACS: CHALLENGES IN ORGANIC MATERIALS & SUPRAMOLECULAR CHEMISTRY Cambridge, United Kingdom
Information:	http://www.rsc.org/events/detail/17933/international-symposium-on-macrocyclic-and-supramolecular-chemistry-in-conjunction-with-isacs-challenges-in-organic-materials-and-supramolecular-chemistry
2 – 7	16TH EUROPEAN POLYMER CONGRESS Lyon, France
Information:	http://www.europolyfed.org/home
2 – 8	3RD INTERNATIONAL MASS SPECTROMETRY SCHOOL (IMSS) Dubrovnik, Croatia
Information:	http://www.imss.nl/
3 – 7	ISSNP 2017 – INTERNATIONAL SUMMER SCHOOL ON NATURAL PRODUCTS Naples, Italy
Information:	http://www.issnp.org/
7 – 10	10TH INTERNATIONAL SYMPOSIUM ON CATALYSIS IN MULTIPHASE REACTORS (CAMURE-10) & 9TH INTERNATIONAL SYMPOSIUM ON MULTIFUNCTIONAL REACTORS (ISMR-9) Tsingtao (Qingdao), PR China
Information:	http://camure2017.csp.escience.cn/dct/page/1
9 – 13	16TH INTERNATIONAL MEETING ON BORON CHEMISTRY (IMEBORON XVI) Hong Kong, China
Information:	www.imeboron16.org
9 – 13	EuCOMC 2017 – 22ND EUROPEAN CONFERENCE ON ORGANOMETALLIC CHEMISTRY Amsterdam, The Netherlands
Information:	http://www.eucomc2017.amsterdam/
9 – 14	46TH IUPAC WORLD CHEMISTRY CONGRESS (IUPAC-2017) São Paulo, Brazil
Information:	www.IUPAC2017.org
23 – 29	RACI CENTENARY CONGRESS Melbourne, Australia
Information:	http://www.racicongress.com

24 – 26	5TH INTERNATIONAL CONFERENCE ON GREEN CHEMISTRY AND TECHNOLOGY Rome, Italy
Information:	http://greenchemistry.alliedacademies.com/

August 2017

13 – 17	SE2017 – 200 YEARS OF SELENIUM RESEARCH Stockholm, Sweden
Information:	http://se2017.se/
16 – 18	CHEMICAL IDENTIFIER Bethesda, MD United States
Information:	http://www.inchi-trust.org
20 – 23	GLS-13 – 13TH INTERNATIONAL CONFERENCE ON GAS–LIQUID AND GAS–LIQUID–SOLID REACTOR ENGINEERING (GLS-13) Brussels, Belgium
Information:	http://www.gls13.com/
27 – 30	EUROPACAT 2017 Florence, Italy
Information:	http://www.europacat2017.eu/index.html
28 – 31	17TH IUPAC INTERNATIONAL SYMPOSIUM ON MACROMOLECULAR COMPLEXES (MMC-17) Tokyo, Japan
Information:	http://www.waseda.jp/assoc-mmc17/
28 – Sept. 1	EuroAnalysis 2017 Stockholm, Sweden
Information:	http://euroanalysis2017.se/
28 – Sept. 2	11ICHC – 11TH INTERNATIONAL CONFERENCE ON THE HISTORY OF CHEMISTRY Trondheim, Norway
Information:	http://www.ntnu.edu/11ichc

September 2017

3 – 6	3RD EuGSC – 3RD EuCheMS CONGRESS ON GREEN AND SUSTAINABLE CHEMISTRY York, UK
Information:	http://www.euchems.eu/events/3rd-eugsc-3rd-euchems-congress-on-green-adn-sustainable-chemistry/
3 – 8	21ST EUROPEAN CONFERENCE ON THERMOPHYSICAL PROPERTIES Graz, Austria
Information:	http://ectp2017.tugraz.at/
5 – 8	THERMODYNAMICS 2017 Edinburgh, UK
Information:	http://www.thermodynamics2017.efconference.co.uk/
10 – 13	GDCh SCIENTIFIC FORUM CHEMISTRY 2017 - ANNIVERSARY CONGRESS »GDCh – 150 YEARS Berlin, Germany
Information:	https://veranstaltungen.gdch.de/tms/frontend/index.cfm?l=7210&modus=
17 – 20	BloodSurf2017 Clemson, SC United States
Information:	http://www.ireviakine.net/Bloodsurf/
17 – 22	INTERNATIONAL SYMPOSIUM ON IONIC POLYMERIZATION – IP 2017 Durham, United Kingdom
Information:	https://www.dur.ac.uk/soft.matter/ip2017/

19	CUTTING EDGE 2017 Ljubljana, Slovenia
Information:	http://www.cutting-edge.si/
20 – 22	SLOVENIAN CHEMICAL DAYS 2017 Portorož, Slovenia
Information:	http://chem-soc.si/slovenski-kemijski-dnevi
27 – 29	11TH INTERNATIONAL SYMPOSIUM ON BIOORGANIC CHEMISTRY (ISBOC-11) Konstanz, Germany
Information:	https://www.uni-konstanz.de/isboc-11/about-isboc-11/

October 2017

1 – 5	EPIC 2017 – 6TH EUROPEAN PROCESS INTENSIFICATION CONFERENCE 2017 Barcelona, Spain
Information:	http://www.wcce10.org/index.php/en/
1 – 5	WCCE10 – 10TH WORLD CONGRESS OF CHEMICAL ENGINEERING INCORPORATING THE 11TH EUROPEAN CONGRESS OF CHEMICAL ENGINEERING (ECCE11) Barcelona, Spain
Information:	http://www.wcce10.org/index.php/en/
1 – 5	4TH EUROPEAN CONGRESS OF APPLIED BIOTECHNOLOGY – ECAB3 Barcelona, Spain
Information:	http://www.wcce10.org/index.php/en/
2 – 5	7TH IUPAC INTERNATIONAL CONFERENCE ON GREEN CHEMISTRY Moscow, Russian Federation
Information:	http://greeniupac2017.muctr.ru
4 – 6	XIXTH EUROFOODCHEM CONFERENCE Budapest, Hungary
Information:	http://www.eurofoodchem2017.mke.org.hu/index.php
9 - 12	9TH WORKSHOP ON PROFICIENCY TESTING IN ANALYTICAL CHEMISTRY, MICROBIOLOGY AND LABORATORY MEDICINE Portorož, Slovenia
Information:	http://eurachempt2017.eu/
9 – 13	POLYCHAR 25 – 25TH ANNUAL WORLD FORUM ON ADVANCED MATERIALS Kuala Lumpur, Malaysia
Information:	http://www.25POLYCHAR.org.my
11 – 13	IUPAC-FAPS 2017 POLYMER CONGRESS ON SMART MATERIALS FOR EMERGING TECHNOLOGY Jeju Island, Republic of Korea
Information:	http://www.faps2017.org
12 – 14	EWCC 2017 – EAST-WEST CHEMISTRY CONFERENCE 2017 Skopje, Macedonia
Information:	http://ewcc2017.org/

November 2017

5 – 9	HPLC 2017 – THE 46TH INTERNATIONAL SYMPOSIUM ON HIGH PERFORMANCE LIQUID PHASE SEPARATIONS AND RELATED TECHNIQUES Jeju Island, Republic Of Korea
Information:	http://www.hplc2017-jeju.org

2018

February 2018

21 – 23	ChemCYS 2018 – 14TH CHEMISTRY CONFERENCE FOR YOUNG SCIENTISTS Blankenberge, Belgium
Information:	http://chemcys.be/

June 2018

4 – 6	IIS PRAGUE 2018 – 13TH INTERNATIONAL SYMPOSIUM ON THE SYNTHESIS AND APPLICATIONS OF ISOTOPES AND ISOTOPICALLY LABELLED COMPOUNDS Prague, Czech Republic
Information:	http://www.iis-prague2018.cz/

September 2018

16 – 19	DISTILLATION & ABSORPTION CONFERENCE 2018 Firenze, Italy
Information:	http://www.aidic.it/da2018/

October 2018

14 – 18	14TH IUPAC INTERNATIONAL CONGRESS OF PESTICIDE CHEMISTRY Rio de Janeiro, Brazil
Information:	https://iupac.org/event/14th-iupac-international-congress-of-pesticide-chemistry/

Acta Chimica Slovenica

Author Guidelines

Submissions

Submission to ACSi is made with the implicit understanding that neither the manuscript nor the essence of its content has been published in whole or in part and that it is not being considered for publication elsewhere. All the listed authors should have agreed on the content and the corresponding (submitting) author is responsible for having ensured that this agreement has been reached. The acceptance of an article is based entirely on its scientific merit, as judged by peer review. There are no page charges for publishing articles in ACSi.

Submission material

Typical submission consists of:

- full manuscript (Word file, with title, authors, abstract, keywords, figures and tables embedded, and references);
- supplementary files:
  - ***Statement of novelty*** (Word file),
  - ***List of suggested reviewers*** (Word file),
  - ZIP file containing ***graphics*** (figures, illustrations, images, photographs),
  - ***Graphical abstract*** (single graphics file),
  - ***Proposed cover picture*** (optional, single graphics file),
  - ***Appendices*** (optional, Word files, graphics files).

Submission process

Submission process consists of 5 steps. Before submission, authors should go through the checklist at the bottom of these guidelines page and prepare for submission:

Step 1: Starting the submission

- Choose one of the journal sections.
- Confirm all the requirements of the ***checklist.***
- Additional plain text comments for the editor can be provided in the relevant text field.

Step 2: Upload submission

- Upload full manuscript in the form of a Word file (with title, authors, abstract, keywords, figures and tables embedded, and references).

Step 3: Enter metadata

- First name, last name, contact email and affiliation for all authors, in relevant order, must be provided. Corresponding author has to be selected. Full postal address and phone number of the corresponding author has to be provided.
- ***Title and abstract*** must be provided in plain text.
- Keywords must be provided (max. 6, separated by semicolons).
- Data about contributors and supporting agencies may be entered.
- ***References*** in plain text must be provided in the relevant text filed.

Step 4: Upload supplementary files

- ***Statement of novelty*** in a Word file must be uploaded
- ***List of suggested reviewers*** with at least three reviewers must be uploaded as a Word file.
- All ***graphics*** have to be uploaded in a single ZIP file. Graphics should be named Figure 1.jpg, Figure 2.eps, etc.
- ***Graphical abstract image*** must be uploaded separately.
- ***Proposed cover picture*** (optional) should be uploaded separately.
- Any additional ***appendices*** (optional) to the paper may be uploaded. Appendices may be published as a supplementary material to the paper, if accepted.
- For each uploaded file the author is asked for additional metadata which may be provided. Depending of the type of the file please provide the relevant title (Statement of novelty, List of suggested reviewers, Figures, Graphical abstract, Proposed cover picture, Appendix).

Step 5: Confirmation

- Final confirmation is required.

Article Types

Review articles are welcome in any area of chemistry and may cover a wider or a more specialized area, if a high impact is expected. Manuscripts normally should not exceed 40 pages of one column format (letter size 12, 33 lines per page). Authors should consult the ACSi editor prior to preparation of a review article.

Scientific articles should have the following structure:

1. Title (max. 150 characters),
2. Authors and affiliations,
3. Abstract (max. 1000 characters),
4. Keywords (max. 6),
5. Introduction,
6. Experimental (Results and Discussion),
7. Results and Discussion (Experimental),
8. Conclusions,
9. Acknowledgements (if any),
10. References.

The sections should be arranged in the sequence generally accepted for publications in the respective fields. Scientific articles should report significant

and innovative achievements and exhibit a high level of originality.

Short communications generally follow the same order of sections, but should be short (max. 2500 words) and report a significant aspect of research work meriting separate publication.

Technical articles report applications of an already described innovation. Typically, technical articles are not based on new experiments.

Preparation of Submissions

Text of the submitted articles must be prepared with Word for Windows. Normal style set to single column, 1.5 line spacing, and 12 pt Times New Roman font is recommended. Line numbering (continuous, for the whole document) must be enabled to simplify the reviewing process. For any other format, please consult the editor. Articles should be written preferably in English. Correct spelling and grammar are the sole responsibility of the author(s). Papers should be written in a concise and succinct manner. The authors shall respect the ISO 80000 standard, and IUPAC Green Book rules on the names and symbols of quantities and units.The Systčme International d'Unités (SI) must be used for all dimensional quantities.

Graphics (figures, graphs, illustrations, digital images, photographs) should be inserted in the text where appropriate. The captions should be self-explanatory. Lettering should be readable (suggested 8 point Arial font) with equal size in all figures. Use common programs such as Word Excel to prepare figures (graphs) and ChemDraw to prepare structures in their final size (8 cm for single column width or 17 cm for double column width) so that neither reduction nor enlargement is required. In **graphs**, only the graph area determined by both axes should be in the frame, while a frame around the whole graph should be omitted. The graph area should be white. The legend should be inside the graph area. The style of all graphs should be the same. **Figures and illustrations** should be of sufficient quality for the printed version, i.e. 300 dpi minimum. **Digital images and photographs** should be of high quality (minimum 250 dpi resolution). On submission, figures should be of good enough resolution to be assessed by the referees, ideally as JPEGs. High-resolution figures (in JPEG, TIFF, or EPS format) might be required if the paper is accepted for publication.

Tables should be prepared in the Word file of the paper as usual Word tables. The captions should above the table and self-explanatory.

References should be numbered and ordered sequentially as they appear in the text, likewiise methods, tables, figure captions. When cited in the text, reference numbers should be superscripted, following punctuation marks. It is the sole responsibility of authors to cite articles that have been submitted to a journal or were in print at the time of submission to ACSi. Formatting of references to published work should follow the journal style; please also consult a recent issue:

1. J. W. Smith, A. G. White, *Acta Chim. Slov.* **2008**, *55*, 1055–1059.
2. M. F. Kemmere, T. F. Keurentjes, in: S. P. Nunes, K. V. Peinemann (Ed.): Membrane Technology in the Chemical Industry, Wiley-VCH, Weinheim, Germany, **2008**, pp. 229–255.
3. J. Levec, Arrangement and process for oxidizing an aqueous medium, US Patent Number 5,928,521, date of patent July 27, **1999**.
4. L. A. Bursill, J. M. Thomas, in: R. Sersale, C. Collela, R. Aiello (Eds.), Recent Progress Report and Discussions: 5th International Zeolite Conference, Naples, Italy, 1980, Gianini, Naples, **1981**, pp. 25–30.
5. J. Szegezdi, F. Csizmadia, Prediction of dissociation constant using microconstants, http://www.chemaxon.com/conf/Prediction_of_dissociation_constant_using_microco nstants.pdf, (assessed: March 31, 2008)

Titles of journals shoud be abbreviated according to Chemical Abstracts Service Source Index (CASSI).

Special Notes

- Complete characterization, **including crystal structure**, should be given when the synthesis of new compounds in crystal form is reported.
- Numerical **data should be reported with the number of significant digits corresponding to the magnitude** of experimental uncertainty.
- **The SI system of units and IUPAC recommendations** for nomenclature, symbols and abbreviations should be followed closely. Additionally, the authors should follow the general guidelines when citing spectral and analytical data, and depositing crystallographic data.
- **Characters** should be correctly represented throughout the manuscript: for example, 1 (one) and l (ell), 0 (zero) and O (oh), x (ex), D7 (times sign), B0 (degree sign). Use Symbol font for all Greek letters and mathematical symbols.
- The rules and recommendations of the **IUBMB** and the **International Union of Pure and Applied Chemistry (IUPAC)** should be used for abbreviation of chemical names, nomenclature of chemical compounds, enzyme nomenclature, isotopic compounds, optically active isomers, and spectroscopic data.
- **A conflict of interest** occurs when an individual (author, reviewer, editor) or its organization is involved in multiple interests, one of which could possibly corrupt the motivation for an act in the other. Financial relationships are the most easily identifiable conflicts of interest, while conflicts can occur also as personal relationships, academic competition, etc. **The Edi-**

tors will make effort to ensure that conflicts of interest will not compromise the evaluation process; potential editors and reviewers will be asked to exempt themselves from review process when such conflict of interest exists. When the manuscript is submitted for publication, **the authors** are expected to disclose any relationships that might pose potential conflict of interest with respect to results reported in that manuscript. In the Acknowledgement section the source of funding support should be mentioned. The statement of disclosure must be provided as Comments to Editor during the submission process.

- **Published statement of Informed Consent.** Research described in papers submitted to ACSi must adhere to the principles of the Declaration of Helsinki (***http://www.wma.net/e/policy/b3.htm***). These studies must be approved by an appropriate institutional review board or committee, and informed consent must be obtained from subjects. The Methods section of the paper must include: 1) a statement of protocol approval from an institutional review board or committee and 2), a statement that informed consent was obtained from the human subjects or their representatives.
- **Published Statement of Human and Animal Rights.** When reporting experiments on human subjects, authors should indicate whether the procedures followed were in accordance with the ethical standards of the responsible committee on human experimentation (institutional and national) and with the Helsinki Declaration of 1975, as revised in 2008. If doubt exists whether the research was conducted in accordance with the Helsinki Declaration, the authors must explain the rationale for their approach and demonstrate that the institutional review body explicitly approved the doubtful aspects of the study. When reporting experiments on animals, authors should indicate whether the institutional and national guide for the care and use of laboratory animals was followed.
- Contributions authored by **Slovenian scientists** are evaluated by non-Slovenian referees.
- Papers describing **microwave-assisted reactions** performed in domestic microwave ovens are not considered for publication in *Acta Chimica Slovenica*.
- *Manuscripts that are **not prepared and submitted** in accord with the instructions for authors are not considered for publication.*

Appendices

Authors are encouraged to make use of supporting information for publication, which is supplementary material (appendices) that is submitted at the same time as the manuscript. It is made available on the Journal's web site and is linked to the article in the Journal's Web edition. The use of supporting information is particularly appropriate for presenting additional graphs, spectra, tables and discussion and is more likely to be of interest to specialists than to general readers. When preparing supporting information, authors should keep in mind that the supporting information files will not be edited by the editorial staff. In addition, the files should be not too large (upper limit 10 MB) and should be provided in common widely known file formats so as to be accessible to readers without difficulty. All files of supplementary materials are loaded separatly during the submission process as supplementary files.

Proposed Cover Picture and Graphical Abstract Image

Authors are encouraged to submit illustrations as candidates for the journal Cover Picture as well as graphical abstracts. Graphical abstract contains an image that appears as a part of the entry in the table of contents in both online and printed edition. The pictures may be the same. The illustrations must be related to the subject matter of the paper. Usually both proposed cover picture and picture for graphical abstract are the same, but authors may provide different pictures as well.

Graphical content: an ideally full-colour illustration of resolution 300 dpi from the manuscript must be proposed with the submission. Graphical abstract pictures are printed in size 6.5 × 4 cm (hence minimal resolution of 770 × 470 pixels). Cover picture is printed in size 11 × 9.5 cm (hence minimal resolution of 1300 × 1130 pixels).

Statement of novelty

Statement of novelty is provided in a Word file and submitted as a supplementary file in step 4 of submission process. Authors should in no more then 100 words emphasize the scientific novelty of the presented research. Do not repeat for this purpose the content of your abstract.

List of suggested reviewers

List of suggested reviewers is a Word file submitted as a supplementary file in step 4 of submission process. Authors should propose the names, full affiliation (department, institution, city and country) and e-mail addresses of three potential referees. For each reviewer at least one reference relevant to the scientific field should be provided as well. Appropriate referees should be knowledgeable about the subject but have no close connection with any of the authors. In addition, referees should be from institutions other than (and preferably countries other than) those of any of the authors.

How to Submit

Users registred in the role of author can start submission by choosing USER HOME link on the top of

the page, then choosing the role of the Author and follow the relevant link for start of submission. Prior to submission we strongly recommend that you familiarize yourself with ACSi style by browsing the journal, either in print or online, particularly if you have not submitted to the ACSi before or recently.

Correspondence

All correspondence with the ACSi editor regarding the paper goes through this web site and emails. Emails are sent and recorded in the web site database. All emails you receive from the system contain relevant links. **Please do not answer the emails directly but use the embedded links in the emails for carrying out relevant actions**. Alternatively, you can carry out all the actions and correspondence through the online system by logging in and selecting relevant options.

Proofs

Proofs will be dispatched via e-mail and corrections should be returned to the editor by e-mail as quickly as possible, normally within 48 hours of receipt. Typing errors should be corrected; other changes of contents will be treated as new submissions.

Submission Preparation Checklist

As part of the submission process, authors are required to check off their submission's compliance with all of the following items, and submissions may be returned to authors that do not adhere to these guidelines.

1. The submission has not been previously published, nor is it under consideration for publication in any other journal (or an explanation has been provided in Comments to the Editor).
2. All the listed authors have agreed on the content and the corresponding (submitting) author is responsible for having ensured that this agreement has been reached.
3. The submission files are in the correct format: manuscript in MS Word; diagrams and graphs are created in Excel and saved in one of the file formats: TIFF, EPS or JPG; illustrations are also saved in one of these formats (See ***Author guidelines*** for details).
4. The manuscript has been examined for spelling and grammar (spell checked).
5. The ***title*** (maximum 150 characters) briefly explains the contents of the manuscript.
6. Full names (first and last) of all authors together with the affiliation address are provided. Name of author(s) denoted as the corresponding author(s), together with their e-mail address, full postal address and telephone/fax numbers are given.
7. The ***abstract*** states the objective and conclusions of the research concisely in no more than 150 words.
8. Keywords (maximum six) are provided.
9. ***Statement of novelty*** is prepared as a Word file.
10. The text adheres to the stylistic and bibliographic requirements outlined in the ***Author guidelines***.
11. Text in normal style is set to single column, 1.5 line spacing, and 12 pt. Times New Roman font is recommended. All tables, figures and illustrations have appropriate captions and are placed within the text at the appropriate points.
12. Mathematical and chemical equations are provided in separate lines and numbered (Arabic numbers) consecutively in parenthesis at the end of the line. All equation numbers are (if necessary) appropriately included in the text. Corresponding numbers are checked.
13. Tables, Figures, illustrations, are prepared in correct format and resolution (see ***Author guidelines***).
14. The lettering used in the figures and graphs do not vary greatly in size. The recommended lettering size is 8 point Arial.
15. Separate files for each figure and illistration are prepared. The names (numbers) of the separate files are the same as they appear in the text. All the figure files are packed for uploading in a single ZIP file.
16. Authors have read ***special notes*** and have accordingly prepared their manuscript (if necessary).
17. References in the text and in the References are correctly cited. (see ***Author guidelines***). All references mentioned in the Reference list are cited in the text, and *vice versa.*
18. Permission has been obtained for use of copyrighted material from other sources (including the Web).
19. The names, full affiliation (department, institution, city and country), e-mail addresses and references of three potential referees from institutions other than (and preferably countries other than) those of any of the authors are prepared in the word file.
20. Full-colour illustration or graph from the manuscript is proposed for graphical abstract.
21. ***Appendices*** (if appropriate) as supplementary material are prepared and will be submitted at the same time as the manuscript.

Privacy Statement

The names and email addresses entered in this journal site will be used exclusively for the stated purposes of this journal and will not be made available for any other purpose or to any other party.

ISSN: 1580-3155

Koristni naslovi

Slovensko kemijsko društvo
www.chem-soc.si
e-mail: chem.soc@ki.si

Wessex Institute of Technology
www.wessex.ac.uk

SETAC
www.setac.org

European Water Association
http://www.ewa-online.eu/

European Science Foundation
www.esf.org

European Federation of Chemical Engineering
https://efce.info/

International Union of Pure and Applied Chemistry
https://iupac.org/

Novice europske zveze kemijskih društev (EuCheMS) najdete na:

EuCheMS: Brussels News Updates
http://www.euchems.eu/newsletters/

DONAU LAB Ljubljana
Member of LPPgroup

Donau Lab d.o.o., Ljubljana
Tbilisijska 85
SI-1000 Ljubljana
www.donaulab.si
office-si@donaulab.com

TINYCLAVE

Kovinska posoda 10 ml
Do 100 bar
-20 do +300 °C

€ 2.310+DDV

MINICLAVE

Kovinska posoda 100 ml
Do 100 bar
-20 do +300 °C

€ 2.708+DDV

- Izmenljiva reaktorska posoda, dobavljiva v stekleni ali kovinski izvedbi (nerjaveče jeklo s PTFE insertom oz. Hastelloy). Vse posode so izmenljive in kompatibilne z osnovnim pokrovom.
- Prostornina modela Tinyclave: 10 do 25 ml
  Prostornina modela Miniclave: 100 do 300 ml

büchiglasuster® Pilot Plant and Reactor Systems
switzerland

Vaš um v vrhunski formi.

www.bilobil.si

Izboljšana prekrvitev za večjo moč uma.

Redna uporaba Bilobila:

- razširi krvne žile in izboljša pretok krvi v možganih,
- krepi delovanje možganskih celic, saj izboljša izrabo kisika in glukoze,
- varuje možganske celice pred škodljivimi vplivi radikalov.

Bilobil vsebuje izvleček iz listov *Ginkga bilobe*.

Bilobil®

KRKA

Naša inovativnost in znanje za učinkovite in varne izdelke vrhunske kakovosti.

Pred uporabo natančno preberite navodilo!

O tveganju in neželenih učinkih se posvetujte z zdravnikom ali s farmacevtom.

Acta Chimica Slovenica
Acta Chimica Slovenica

The figure showed that MnO_2 submircoparticles arrayed densely on the eggshell membrane along with the fiber-like protein (scale bar: 20 μm). The size of the spherical particles was about 710 nm, which was a good consistency with the microstructured biotemplate. See more details on page 55

Year 2017, Vol. 64, No. 1